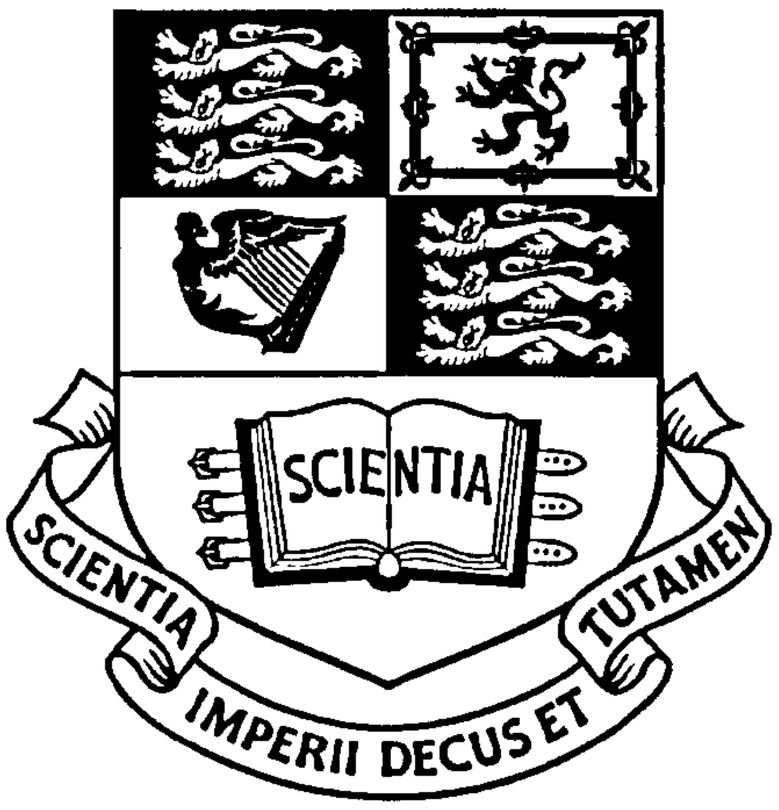
ANALYSIS OF NATURAL FRACTURE NETWORKS IN MASSIVE AND WELL-BEDDED CARBONATES AND THE IMPACT OF THESE NETWORKS ON FLUID FLOW IN DUAL POROSITY MODELLING

By

Mandefro WA Belayneh



A thesis submitted for fulfilment of the requirements of the University of London for the degree of Doctor of Philosophy

Department of Earth Science and Engineering,
Royal School of Mines,
Imperial College of Science Technology and Medicine,
Prince Consort Road,
London, SW7 2BP.

February 2003

ABSTRACT

The geometry of natural fracture networks have been studied in massive to well-bedded Lower Carboniferous limestones in the Pennines of North Yorkshire and in the Lower Lias succession on the southern margin of the Bristol Channel Basin, which is made up of alternating limestone and shales. The work involved three stages: (i) field observations and gathering of 1D and 2D data sets (ii) detailed statistical and mechanical analyses of the field data and (iii) the use of numerical code to study fluid flow in these fracture networks and thus to assess the impact of these fractures in localising flow within the Earth's crust.

Field observations and numerical analyses show that when the two beds on either side of a bedding interface are identical, fractures are able propagate easily across the interface to form composite or through-going joints. Excellent examples are found in the Pennines of the North Yorkshire. The study shows that the presence of identical competent beds with no intervening weak layers, combined with the formation of stylolites along the bedding surface and a large overburden stress, all promoted the propagation of through-going joints. In contrast, if two competent fractured limestone beds are separated by intervening shale, fracture propagation will be arrested at the limestone/shale bedding interface and fracturing of the two limestone beds occur independently. This lack of mechanical communication between adjacent fractured beds during the propagation of Alpine joints is confirmed by the occurrence of different fracture patterns in adjacent limestone beds which can be observed in the southern margin of the Bristol Channel coast. Although the systematic variation is difficult to establish, the horizontal offset of joints in adjacent limestone beds increases with increasing the thickness of the intervening shale.

Abstract

An attempt has also been made in the Bristol Channel study area to determine the palaeo-stress orientations based on fractographic features, in particular plumose structures and twist hackle fringes of the joints. The plumose structures observed on Alpine joints of the Bristol Channel indicate that they initiated in the middle of the limestone beds and propagated parallel to the bedding. The plumose structure is bounded by twist hackle fringes at the top and bottom of the bed. These fringes initiated from the plane of the parent joint and twisted away from it as they approached the boundary of the bed. Analysis of the above fractographic features in the Bristol Channel area shows the remote stress (σ_H) was N-S and horizontal at the time of joint propagation.

Finite element/finite volume numerical modelling has been used to examine fluid flow through the natural fracture networks measured and recorded from the limestone beds in the Pennines and the Bristol Channel coast. This numerical modelling has enabled the partitioning of flow through the fractures and matrix in a realistic fracture network in porous rocks to be quantified. The results are displayed as pressure distribution maps and contours, normalised fluid velocity histograms for the fractures and for the surrounding matrix. The parameters that influence the partitioning have been identified and the detailed geometry of the flow velocity histograms used to understand the influence of fracture network geometry and orientation with respect to the fluid pressure gradient on fluid flow. The results of numerical modelling show that in the majority of the fracture networks, the histogram of fluid flow through the joints is skewed to the left whereas through the matrix, it is skewed to the right. This is considered to be the result of hydraulic communication between the fractures and the matrix.

Acknowledgments

In an undertaking such a breathtaking project, it is inevitable to become indebted to a large number of people and a mention in the acknowledgments barely seems credit for the assistance they have kindly given me. First of all I thank God for paving the ways for me by giving me the opportunities to be a geologist and getting involved in such exciting work. I am very grateful to my supervisor Dr. John Cosgrove for his relentless help during the entire postgraduate study at Imperial College. His guidance and has been tremendous. I am very proud to work with him and to have had the opportunity on several stimulating discussions during the course of this project. I would like to give special thanks to Dr. Stephan Matthäi, without whom this work would not have been in the present shape. His contribution has enormous in the cerebral part of my work by allowing me to use CSP numerical code and for his tremendous and unreserved support at all stages of my study period at Imperial College. Dr. Richard Jolly is thanked for his help in designing the project at the initial stages.

Special thanks to Mrs. Chloë Thomas, to whom I dedicate my work, for funding this project and without whose support, endless effort and time, nothing would be possible. Some people are born to make this world a better place for others and she is definitely one of them. I owe her a lot.

I thank my friend Dr. Ian Mac Lennan, for his constant support and encouragement without whose patience, help and understanding, this research would have been difficult, or if not impossible. Members of the Earth Science and Engineering Department at Imperial College are thanked for their considerable cooperation and

support in time of need and friendly atmosphere. Dr. Richard Jolly from BP, Prof. David Sanderson and Catherine Greenfields both from IC are thanked for allowing me to use their numerical code. I would like to record my gratitude to Professor Andrew W. Woods at the BP Institute for Multiphase Flow in Cambridge University for allowing me to attend training on '*Flows in Porous Media*'. I would like to record my gratitude to Dr. Chris Halls kindly offered me proof reading most of the thesis. The discussion on fractured rock masses related to quarry industry on several occasions with Dr. J-P Latham has been very useful. Ella NG Chieng and Hin Ken Davis are among many nice, friendly and helpful people I met at Imperial College.

Many thanks to my friends: Jorge Acosta, Salim Al-Mahruqui, Mohammad Sepehr and Matthew Brown at structural geology for enjoyable time during this period and sharing common interest and understanding on many topics. They are all very special friends! Little Kimiya (the youngest student at IC?) has been great entertainer during the whole period especially at the writing up stage.

I express my gratitude to my parents, my brothers and sisters for their respect and encouragement at all levels in my life. I am unfortunate that my mother could not see her endless efforts bearing fruit at last and her loss has been tremendous that made huge pain and disappointment in my life. May her soul be resting in peace in Heaven.

I finally thank all my friends in the Trinity Association, whose names have not been mentioned here and who expressed their support in some way or another.

Dedication

It is a great honour to dedicate this work to Mrs. Chloe Thomas for her generous and unreserved support, encouragement and for making dream come true. To my-beloved deceased mother who taught me courage and determination. I wish you were with me to share my joy and the fruition of all these years of hard work. I miss you dearly.

CONTENTS

	Page
Abstract	I
Acknowledgements	III
Dedication	V
Contents	VI
List of figures	XIII
List of tables	XXVI
CHAPTER ONE	1
1 INTRODUCTION	1
1.1 Title of the thesis	3
1.2 Problems addressed in the research	4
1.3 Aims and objectives of this work	5
1.4 Methodology	6
1.4.1 Scan line sampling	7
1.4.2 Area/window sampling	10
1.4.3 Simulation of fluid flow along and across joints	13
1.5 Data presentation and analysis	13
1.5.1 Joint strike and dip	13
1.5.2 Joint spacing versus frequency	14
1.5.3 Joint spacing versus bed thicknesses	14
1.5.4 2D joint trace maps	14

1.5.5 Fluid flow maps 14

1.6 Limitations 15

1.7 Thesis layout 16

CHAPTER TWO REGIONAL GEOLOGICAL SETTING 18

2.1 Summary of previous structural investigations in the Pennines 18

2.2 Detail geology of the study area 24

2.3 Fractures 25

2.4 Summary of the geology and structures at the southern margin of the Bristol Channel Basin 28

2.4.1 Introduction 28

2.4.1.1 Basin extension 28

2.4.1.2 Basin inversion 31

2.4.2 Structures 36

2.4.2.1 Structures associated with the opening of the Bristol Channel Basin 36

2.4.2.2 Structures associated with Alpine Orogeny 46

2.4.2.2.1 Folds 46

2.4.2.2.2 Thrust faults 48

2.4.2.2.3 Joints in the Bristol Channel 52

(i) Burial joints 52

(ii) Alpine joints 53

(iii) Post-Alpine joints 53

2.4.2.2.4 Strike-slip faults 53

2.5 Summary 54

2.5.1 Pennines 54

2.5.2 The Bristol Channel Basin 54

CHAPTER THREE CONTROLS ON JOINT SPACING AND THE RELATIONSHIPS BETWEEN JOINTS AND OTHER STRUCTURES 56

3.1 Introduction 56

3.2 Controls on fracture spacing 56

3.3 Joint initiation and propagation 59

3.3.1 Mid-point bisection process 66

3.3.2 Semi-random process 66

3.3.3 Random process 68

3.3.4 Interaction process 68

3.4 Joint spacing evolution 71

3.5 Relationships between joint spacing and bed thickness 71

3.5.1 Linear 71

3.5.2 Non-linear and complex 74

3.6 The relationship between joints and other structures 76

3.6.1 Faults 76

3.6.2 Folds 82

3.6.3 Joints 92

3.6.4 Burial and uplift 93

CHAPTER FOUR FIELD OBSERVATION AND ANALYSIS

OF JOINT SPACING, ORIENTATION AND DENSITY 95

4.1 Introduction 95

4.2 Review of previous work 96

4.3 Joints of the Pennines 97

4.3.1. Malham Cove and surrounding area 2 97

4.3.2 Langcliffe, Settle and Giggleswick 102

4.3.3 Ingleton 110

4.3.3.1 Scan line sampling 110

4.3.3.2 Window sampling 112

4.3.3.2.1 The influence of window shape and size on fracture density 114

(i) square window 115

(ii) rectangular window 115

(iii) circular windows 116

4.3.4 Horton-in-Ribblesdale 117

4.4 Joints from the southern margin of the Bristol Channel Basin 118

4.4.1 Introduction 118

(i) Burial joints 119

(ii) Joints formed during the Alpine inversion of the Bristol Channel Basin 124

4.4.2 Joints from East of Lilstock 125

4.4.3 Lilstock 130

4.4.3.1 Bed 1 131

4.4.3.2 Bed 2 133

4.4.3.3 Bed 3 137

4.4.3.4 Bed 4 138

4.4.4 Joints on the moderately dipping south limb of the Lilstock anticline 141

4.4.5 Joints around the hinge zone of Lilstock rollover anticline 145

4.4.6 Kilve 147

4.4.7 East Quantoxhead and Blue Ben 154

4.5 Post-Alpine joints 159

4.6 Statistical analysis of joint spacing from the two study areas 161

4.6.1 Analysis of joint spacing from the Pennines area 162

4.6.2 Results of the analysis of joint spacing from the Bristol Channel 164

4.7 Summary 166

CHAPTER FIVE FRACTURE MECHANICS AND FRACTOGRAPHY 171

5.1 Introduction 171

5.2 Fracture mechanics 176

5.2.1 Fracture initiation 176

5.2.1.1 Griffith energy balance theory 178

5.2.1.2 Griffith fracture stress criterion 180

5.3 Factors controlling crack paths 182

5.4 Fractography 189

5.4.1 Introduction 189

5.4.2 Types of fracture surface morphology 192

5.5 Present work 196

5.6 Summary 203

CHAPTER SIX MODELS OF FLUID FLOW IN LIMESTONE USING REALISTIC JOINT NETWORKS 209

6.1 Introduction 209

6.2 Overview of flow in porous and fractured media 209

6.2.1 The role of fluids during deformation: effective stress 211

6.3 Evidence of high fluid pressure in the Lower Lias of the Bristol Channel 216

6.4 Numerical modelling 219

6.4.1 Methodology 221

6.4.1.1 Run a GeometryPreprocessor.exe program 225

6.4.1.2 triangleMesher (window) 225

6.4.1.3 Run CSP3D_Mesh_to_VTK.exe 226

6.4.1.4 Run CSP3D_linear_flow_analysis.exe 229

6.5 Validation of FE/FV numerical models 231

6.6 Results of the simulation 232

6.6.1 North Yorkshire 232

6.6.2 East of Lilstock 238

6.6.3 Lilstock 244

6.6.4 Kilve, East Quantoxhead and Blue Ben 254

6.7 Discussion 267

CHAPTER SEVEN DISCUSSION AND CONCLUSION 272

7.1 The study area in the Pennines 273

7.2 The Bristol Channel study area 276

7.2.1The role of the normal faults 277

7.2.2 The relationship between joints and folds 278

7.2.3 Reverse faults 279

7.2.4 Strike-slip faults 279

7.2.5 Joint spacing and bed thicknesses 280

7.2.6 Joint spacing as a function of structural position 280

7.2.7 Fractographic evidence seen on joint faces 282

7.2.8 Fluid flow modelling 282

7.3 Conclusions 285

7.4 Recommendations for future work 287

REFERENCES 296

ENCLOSURE

LIST OF FIGURES

1.1 Schematic layout of a jointed rock illustrating the principle of scan line. 9

1.2 (a) Photograph and (b) line drawing of window sample made in a metre square grid on a jointed limestone bed from the Bristol Channel. 12

2.1 Dinantian palaeo-geography and major structures that influenced sedimentation through much of Carboniferous (From Guion *et al.*, 2000). 19

2.2 Structure map of the Pennines and the surrounding area (from Edwards *et al.*, 1954). 21

2.3 (a) Photograph (b) and line drawing of right-stepping *en-echelon* fractures striking WNW-ESE from east of Langcliffe. 27

2.4 (a) Rectangular and (b) rhombohedral joint patterns on the bedding planes at Malham Cove. 28

2.5 Sedimentary basin fault models: (a) to (c) listric normal fault model and (d) rotated block fault model 29

2.6 Seismic section showing reactivated Variscan thrust north of the Devon coast (from Brooks *et al.*, 1988). 32

2.7 Geology and major structures in the Lilstock-Kilve areas of the southern margin of the Bristol Channel Basin (modified from 1:50,000 scale geological maps of England and Wales sheets 263, 279 and part of 295). 33

2.8 Mud volcano at Kilve. 38

2.9 Planar view of micro-veins exposed on a bedding surface and enhanced by differential weathering. 38

2.10 Lower hemisphere stereographic projection of normal faults from the

study area on the southern margin of the Bristol Channel Basin. 40

2.11 (a) Photograph and (b) line drawing of veins formed during basin opening. 41

2.12 (a) Photograph and (b) line drawing of tightly folded vertical calcite vein within 30cm thick limestone bed from Kilve beach. Note how the calcite vein tapers on both ends approaching the bedding interface. 42

2.13 (a) Photograph and (b) line drawing of shortened calcite vein within shale beds on the hanging-wall of normal fault from Kilve Beach. 44

2.14 (a) Photograph and (b) line drawing that show how subtle changes in lithology affect the response of the shale during basin opening. Note the development of pull-aparts within an apparently homogeneous shale bed. 45

2.15 Gently folded alternating limestone and shale beds at Kilve. 47

2.16 Block diagrams showing the stress regimes associated with the formation of (a)normal, (b) reverse and (c) strike-slip faults. 49

2.17 (a) Photograph and (b) line drawing of ESE-WNW striking pre-inversion normal fault at East Quantoxhead that was probably reactivated later as a high-angle reverse fault from. 51

2.18 Photograph of bed-parallel thrust within gently north-dipping shale beds at East Quantoxhead. The direction of tectonic transport is SSW. 52

3.1 (a) Negative exponential, (b) log-normal and (c) normal distributions (Rives *et al.*, 1992) (d) Gamma distribution (Huang and Angelier, 1989). 67

3.2 (a) Relationships between bed thicknesses and joint spacing and (b) shows early formed fracture preventing the formation of new in the

proximity except at distance d (from Ladiera and Price, 1981). 73

3.3 Three-fold classification of faults (Anderson, 1951*)*. 77

3.4 (a) Block diagram of horizontally bedded sediments and possible joint orientation that form at various settings: F_{1-2} form during thrusting, F_{3-6} form during normal faulting and F_{7-8} during wrench faulting, (b) stereographic projection of faults, and (c) stereographic projection of joints (Price, 1966). 78

3.5 Schematic illustration of the fractures in the vicinity of normal faults (from Stearns, 1967). 79

3.6 Small faults and fractures that may develop around a fault (a) normal, (b) reverse and (c) strike-slip faults (from Blés and Feuga, 1986). 80

3.7 Schematic diagram illustrating the temporal relationships between joints and faults (from Peacock, 2001). 81

3.8 Relationship between a fold and joints: (a) block diagram folds and fractures, (b) stereographic plot of (a), (c) fractures in the trailing and leading lime of anticline, (d) and (e) stereo plot of (c) (Price, 1966). 83

3.9 Joints associated with (a) and (b) anticlines and (c) synclines (Price, 1966). 84

3.10 Main joint sets found in folded rocks and their relation to folds (from Stearns, 1967). 85

3.11 Strain distribution in flexural flow fold models (Ramsay, 1967). 87

3.12 Strain distributions in a tangential longitudinal strainfolds (Ramsay, 1967). 88

3.13 Flexural-slip folding (from Price and Cosgrove, 1990). 89

3.14 Stress trajectories of a flexed homogeneous and isotropic layer (from Couples *et al.*, 1998). 89

3.15 Fracture patterns predicted from buckle folds (a) 2 orthogonal joints where the minimum stress remains parallel to bedding (b) typical orientation of thin bedded unit and (c) shear fractures and joints patterns expected in tangential longitudinal strain folds (Price and Cosgrove, 1990). 90

3.16 Fracture distribution predicted around (a) reverse faults and (b) normal faults (from Cosgrove and Ameen, 2000). 92

3.17 Map view of two ways in which the state of stress may rotate a free surface at a through-going joint (Dyer, 1988). 93

3.18 Joint orientations predicted during (a) downwarp and (b) uplift (from Price and Cosgrove, 1990). 94

4.1 (a) Simplified geological map of the study area in the Pennines, (b) index map and (c) layout of scan lines at Malham Cove 98

4.2 Rose diagrams for joint orientation in Cove Limestone. 99

4.3 Extensional veins striking ESE-WNW (110°) locally observed in the area. 101

4.4 Rose diagrams for area 2, Langcliffe and Giggleswick. 103

4.5 (a) Photograph and (b) line drawing of bedding-parallel stylolite indicating vertical compression caused by the overburden pressure at Giggleswick quarry. 104

4.6 Medium- to coarse-grained limestone after blasting at Giggleswick quarry. 107

4.7 (a) Photograph and (b) line drawing of vertical calcite vein filled joints at Giggleswick quarry crosscutting several bedding. 107

4.8 '*Through-going*' joints in Cove Limestone at Giggleswick quarry crosscuts several bedding planes. Note that joints terminate at arbitrary position. 108

4.9 Rose diagram showing joint strike along scan lines from Gordale limestone at Giggleswick. 109

4.10 ENE-WSW striking joints in (a) Gigleswick quarry and (b) Victoria cave. 110

4.11 Rose diagram of joint striking NW-SE and NE-SW at Ingleton. 111

4.12 2D joint trace map of a square window (l = 15m) from Ingleton. 114

4.13 Fluctuation of joint density in a square window of various sizes. 115

4.14 Joint density determined from Fig. 4.12 using rectangular windows. 116

4.15 Layout of circular windows in cubic packing superposed on 2D joint traces from Ingleton. 117

4.16 Variation of joint density determined for circular window. 117

4.17 Rose diagrams showing the strike of joints from Horton-in-Ribblesdale. 118

4.18 Zones of high-density veins (micro-veins) contained within the limestone beds from Kilve view towards ESE. Coin is for scale. 120

4.19 WNW-ESE striking extensional veins and later barren joints crosscutting micro-veins. 121

4.20 Pull-apart structures in southward tilted limestone-shale beds from Lilstock. 122

4.21 Lower hemisphere stereographic projection of the bedding plane and extensional joint that form the pull-apart at Lilstock. 123

4.22 Some of the calcite fibres are oblique to the main joint surfaces indicating sinistral transtenssional sense of opening. 123

4.23. Injected shale-limestone mixture crosscut by extensional veins indicating soft-sediment deformation. 124

4.24 A prominent joint set propagating either vertically up or down

without significant offset to form composite or through-going joints. 126

4.25 Joint trace maps around the hinge zone of the fold comprising 7cm, 30cm and 24cm limestone beds from east of Lilstock. 127

4.26 Joint trace maps of two limestone beds from east of Lilstock on the hanging-wall of a normal fault. 129

4.27 Simplified structural map of Lilstock (from Rawnsley *et al.*, 1998). 130

4.28 Joint pattern in the lower bed (*i.e.* bed 1) on the gently dipping northern limb of the Lilstock anticline. 131

4.29 Joint propagated in perturbed stress field around inverted normal fault at Lilstock. 132

4.30 Variation of joint density as a function of window size and shape. 133

4.31 Joint patterns in bed 2 from gently dipping northern limb at Lilstock. 134

4.32 Joint produced by bending of the PVC plate coated with brittle varnish during non-cylindrical folding (from Rives and Petit, 1990). 136

4.33 Joints pattern in bed 3 from gently dipping northern limb of Lilstock fold. 138

4.34 Joint trace maps in bed 4 on the trailing limb of Lilstock anticline. 139

4.35 Strike of the joints measured along three scan lines in bed 2, 3 and 4. 140

4.36 Stereographic projection of dominant joint sets on moderately southern dipping limb of Lilstock anticline. 142

4.37 An aerial view of joint patterns on the moderately south dipping limb of the Lilstock rollover fold. 143

4.38 (a) and (b) show ladder patterns observed on moderately dipping southern limb of the Lilstock anticline. 144

4.39 Grid patterns formed by two mutually crosscutting orthogonal joint sets. 144

4.40 Oblique ladder and ladder-within-ladder patterns observed in moderately-dipping southern limb of Lilstock anticline. 145

4.41 Oblique photograph of joints from a 5cm thick limestone in the hinge zone of the Lilstock anticline. 146

4.42 The joint pattern commonly observed at the hinge zone of the fold (similar to irregular ladder pattern of Rives *et al.*, 1994). 147

4.43 Joints around the hinge zone of the Kilve anticline viewed looking ESE. 148

4.44 Plan view of the relationship between Kilve fold, strike-slip fault and joints and the position of the scan line and window sample. 149

4.45 Map of joint traces from the hinge region of the Kilve fold. 150

4.46 Joint strike variations around the hinge of the asymmetric Kilve fold. 150

4.47 Joint spacing in the hinge zone of Kilve fold. 152

4.48 Strike versus number of joints along 5 beds in the vicinity of a fault. 153

4.49 Map of joint traces on a 25cm thick limestone bed from East Quantoxhead. 154

4.50 Photograph of joints on either side of the NE-SW striking fault from East Quantoxhead. 156

4.51 Joint traces from 33cm thick limestone bed dipping gently towards NNW. Note the fault displacing the joints. 157

4.52 Joint traces on 25cm thick limestone bed west of Blue Ben fault. Early joints strike E-W and non-crosscutting joints extending between them to form ladder patterns. 158

4.53 Joint spacing from the Gordale Limestone at Langcliffe that fits

negative exponential distribution. 163

4.54 Joint spacing showing a best-fit to log-normal distribution from. 163

4.55 Joint spacing from Malham Cove showing a best-fit to power-law. 164

4.56 Alpine joint spacing at Lilstock (*i.e.* joint set 2 in bed 2) showing a negative exponential distribution. 165

4.57 Graph of spacing of the post-Alpine joints at Lilstock which shows a log-normal distribution. 165

5.1 The three basic modes of crack displacement (after Lawn, 1975). 175

5.2 Joint propagation in mixed mode loadings (Younes and Engelder, 1999). 175

5.3 Stress magnification around (a) circular pore and (b) elliptical crack. 177

5.4 Crack path of vertical *en-echelon* cracks at various spacing and differential stress. S_x and S_y denote crack parallel and perpendicular stresses. 185

5.5 (a) Inhomogeneities in rocks deviates straight crack paths (b) and interaction between neighboring joints (Renshaw and Pollard, 1994). 186

5.6 (a) Photograph and (b) line drawing of right-stepping closely spaced *en-echelon* joints from the leading limb of Lilstock buttress anticline. 188

5.7 Variation in joint propagation paths East Lilstock caused by local heterogeneity and interaction with the adjacent joints of the same set. 189

5.8 Surface features typical of a joint surface (from Hodgson, 1961). 191

5.9 Plumose structures indicating the initiation of a joint from a point source in the middle of 17cm thick limestone bed at Kilve. 197

5.10 Photograph of multiple initiation points showing complex propagation direction on joint faces at Lilstock. 197

5.11 (a) Photograph and (b) line drawing showing a plan view of twist hackle fringe observed at Lilstock. 199

5.12 Asymmetrical twist hackle fringe from Kilve. Note the width of the fringe zone at the top and bottom of the bed. 200

5.13 Photograph of plumose structure with symmetrical twist hackle fringe from Blue Ben. 201

5.14 Twist hackle fringe extending from either side of the bedding plane to the other in a thin limestone bed. 203

5.15 (a) Planar view and (b) section view of twist hackle fringes on a 16cm thick limestone at Lilstock. 206

5.16 Pressure solution cleavage striking approximately E-W and post-dating joint development in the area is evidence that the remote stress was N-S during Alpine inversion. 208

6.1 The influence of an increase of fluid pressure on stable stress states represented by circles (i), (ii) and (iii). 213

6.2 7cm thick horizontal vein of vertical calcite fibres growing normal to the bedding plane at Kilve suggesting build up of high fluid pressure during the inversion of the basin. 218

6.3 The joint trace map from the lowest bed on the trailing limb of Lilstock rollover anticline. Red lines are double lines showing apertures of 0.003 and 0.005 for Alpine and post Alpine joints respectively. Blue squares represent material points defined by fracture bounded blocks. In this model 1369 material points, 1375 curves and 23579 curve points are represented. 224

6.4 Example of triangular mesh of fractured limestone at Kilve anticline. Meshing in the smallest regions of the model can have good representation unlike the finite grid difference method where it assumes uniform grids. 227

6.5 An enlargement of the lower right hand corner of Figure 6.3. The two lines represent joint traces projected on a horizontal plane. The highly variable size of triangles inside the fractures and the surrounding matrix enables the fractures to be represented with adequate resolution. 227

6.6 Interconnected networks of joints from the hinge zone of Kilve fold viewed by 'PermeabilityViewer'. Red colour shows conductive and blue represents relatively low permeability matrix. 228

6.7 Pressure distribution map in a model of fractured Carboniferous limestone from Ingleton. Note that the pressure contours are highly perturbed around long and systematic joints. Pressure distribution shown in rainbow colour to indicate red for high and blue for low. 235

6.8 Histogram of normalised fluid velocity within the fractures and matrix from massive bedded limestone beds at Ingleton shown in Fig. 6.7. 236

6.9 The Craven Faults and the distribution of mineralized veins in the region compiled from 1:50,000 scale maps of sheets 50 and 60. 238

6.10 Pressure distribution map for approximately uniformly distributed joint network. The coloured lines are the isobars. 240

6.11 Normalised velocity histogram of fluid flow through the joints and matrix obtained from numerical simulation illustrated in Fig. 6.10. 240

6.12 Linear pressure distribution obtained from a numerical simulation of a fractured limestone bed east of Lilstock. 241

6.13 Normalised velocity histogram of fluid flow within the joints and matrix obtained from the numerical simulation. 242

6.14 Linear pressure map of jointed limestone bed from East Lilstock. 243

6.15 Normalised velocity histogram of flow in the joints and matrix shown in Fig. 6.14 obtained by numerical simulation. 243

6.16 Linear pressure distribution map of fractured limestone from the lowest exposed trailing limb of Lilstock rollover anticline. 245

6.17 Flow velocity histogram for the joints and matrix of the lowest exposed limestone bed of the Lilstock anticline (Fig. 6.16). 245

6.18 Linear pressure distribution map of fractured limestone containing six joint sets from the trailing limb of Lilstock rollover anticline. 247

6.19 Velocity histogram of the joints and matrix obtained from the numerical simulations in the fracture network shown in Fig. 6.18. 248

6.20 The trajectory of the fluid pressure gradient expressed as a rainbow colour scheme is strongly perturbed by the oblique pattern of connected fractures. 249

6.21 Velocity histogram of fluid flow within the joints and the matrix in the fracture networks shown in Fig. 6.20. 249

6.22 Pressure field strongly perturbed by oblique fracture distribution in a limestone bed from the Lilstock anticline. 250

6.23 Normalised velocity histogram of flow through the joints and the surrounding matrix. 250

6.24 This model shows how the pressure is distributed when the pressure gradient from the lower boundary of the model. 252

6.25 Normalised velocity histogram of fluid flow within the joints and matrix for the fractured network shown in Fig. 6.24. 252

6.26 Linear pressure map of fractured limestone from the gently-dipping limb of of the Lilstock anticline. The joints are oblique to the pressure gradient. 253

6.27 Velocity histogram of flow through the matrix and the joints shown in Fig. 6.26. Note that some joints with low velocity have the same flow velocity as the matrix. 254

6.28 (a) Pressure distribution map of fracture network in limestone from the hinge zone of the Kilve fold and (b) enlargement of the highlighted area showing communication between the joint and the matrix. 255

6.29 Velocity histogram of fluid flow through the joints and matrix of the limestone. 256

6.30 The same model as shown in Fig. 6.28 but with the fluid pressure applied normal to the strike of the dominant joint set. 257

6.31 Left skewed velocity histogram of fluid flow through joints and a normal through the matrix. 257

6.32 Pressure distribution map in the model based on the joint network in the 32cm thick limestone bed west of the sinistral strike-slip fault at East Quantoxhead. 258

6.33 Histogram of fluid flow velocity through the matrix and through the joints on west side of the fault. 259

6.34 Pressure distribution map for the model based on fracture pattern in the 32cm thick limestone bed east of the fault. 259

6.35. Fluid velocity histogram for the joints and matrix east of the fault. 260

6.36 Pressure distribution map of fractured limestone underlying the beds shown in Figs 6.30 and 6.32. 261

6.37 Right skewed histogram of velocity within the matrix and left skewed histogram of velocity for the joints. 261

6.38 (a) Plot of stress ratio R, magma pressure and the angle between minimum principal stress and joint wall (from Delaney *et al.*, 1986) and (b) range of orientations of joints that are likely to dilate for different stress ratios arrows indicate the direction of opening of the joint and/or dyke (from Jolly and Sanderson, 1995). 263

6.39 Pressure map of well connected and approximately uniform distribution of joints from East Quantoxhead. 264

6.40 Fluid velocity histogram obtained from numerical models for the joints and matrix from East Quantoxhead. 265

6.41 Pressure distribution map of joint networks from Blue Ben. 266

6.42 Velocity histogram for the joints and the matrix from Blue Ben. 267

7.1 Pressursed 2D window model gradient released after 2 hours. 290

7.2 After 5.2 hours the non-wetting front advances at approximately the same speed along most fractures. 292

7.3 Shows advancing front of the non-wetting phase along some fractures. 293

7.4 Sweeping of oil from the matrix and from the fractures after 9.8 hours. 294

7.5 Snapshot of the model showing the advance of the waterfront after running the numerical analysis for 21.6 hours. 295

7.6 Snapshot of the lower left section of the model simulations showing water breakthrough in the fractured system. 295

LIST OF TABLES

4.1 Summary of scan line sampling of joints on gently dipping northern limb of Lilstock anticline. 140

5.1 Twist hackles measured on joints from Lilstock. 199

5.2 Thickness of the plumose structure and twist hackle fringe. 202

6.1 Range of intrinsic permeability and hydraulic conductivity for unconsolidated sediments. 210

6.2 Material points assigned to joints and joint bounded blocks (matrix). 223

6.3 Configuration file for the linear flow analysis in CSP3D.

'*my file.I*' model configuration file for CSP3D example file set. 229

CHAPTER ONE

1 INTRODUCTION

As a result of early lithification, carbonate rocks are particularly susceptible to brittle deformation (*i.e.* fracturing), which may take place in multiple stages throughout their history. Where such fractures are present, the permeability contrast between the fracture and the matrix can cause very heterogeneous flow patterns that result in a complex distribution of saturation (Nelson, 1985). Nelson argues that efficient hydrocarbon production from fractured reservoirs depends on a good understanding of the mechanisms controlling fracture development and the distribution of the fracture network. Extensive research over the last century has greatly improved our understanding of joints, in particular the processes related to joint/fracture development and distribution. It is well known that fractures/joints significantly affect the hydrological and mechanical properties of the fractured rock masses. Dual porosity modelling (discussed in Chapter 6) in which the modelled rock mass contains fractures and a primary porosity, shows that fluid flow occurs dominantly through fractures, following either a single dominant fracture or a coherent and interconnected fracture network. Therefore, understanding the hydrological properties of fractured rock masses is essential for workers in the oil, waste management and rock engineering industries. The literature on joints/fractures and fluid flow in the crust is substantial and only specific aspects will be discussed in this thesis. This research focuses on detailed analysis of fractures in well-bedded and massive-bedded limestones and the way in which these fractures govern and localise the flow of fluids. In the following section, the aims and objectives of the research are outlined and the methods used to collect, analyse and present the data are explained. The chapter ends with a critical discussion of the research methodology and the results obtained.

A fracture is a discrete break within a rock mass across which cohesion is lost. Fractures may be classified using various criteria as follows: joints, shear fractures (faults), hybrid extension/shear fractures (Hancock, 1985; Price and Cosgrove, 1990; Hancock, 1994) and as mode I, II and III based on the sense of displacement of one side of the joint with respect to the other (Lawn, 1975). In a broad sense, fractures that are characterised by opening mode (extension without lateral displacement) are termed joints (Pollard and Aydin, 1988). Joints are also classified on the basis of their geometry and spatial organization. For example (Hodgson, 1961) defined a joint as a planar or approximately planar fracture that forms regularly oriented sets known as *systematic joint sets*. However *non-systematic* joints are generally curved, conchoidal and non-parallel are common in nature particularly when earlier joint sets occur which locally disturb the stress field in which the new joints are forming. Geological examples include polygonal cracks produced by desiccation and by thermal contraction. Wu and Pollard (1995) use the ratio of joint length to joint spacing to distinguish between well- and poorly-developed joint sets. They suggest that if the average joint length is greater than the average spacing, the joints should be classified as 'well-developed'. Alternatively, if the average spacing is greater than the length of fractures, they propose the term 'poorly-developed' joints. Joints often exhibit very distinctive surface morphology such as plumose structures and twist hackle fringes (Woodworth, 1896; Corte and Higashi, 1960; Hodgson, 1961; Kulander *et al.*, 1979, Bahat and Engelder, 1984; Pollard and Aydin, 1988; Bahat, 1991; Kulander and Dean, 1995; Ameen, 1995; Younes and Engelder; 1999; Belayneh, in prep.). Fracture surfaces decorated with fractographic features occur in most rock types but, because of the susceptibility of limestones to chemical solution by groundwater, these marks are often eroded from joint surfaces in carbonate rocks.

A single crack in a brittle bed may behave as a mode I fracture in the middle of the fracture (the result of plane strain conditions which will be discussed in Chapter 5), showing mixed mode I and II fracturing as the edges of the fractures are approached, and mode I and III at the crack fronts (usually at their terminations). Natural fractures in rocks can be extremely complex, particularly when made up of the several joint sets which form a fracture network. The fracture network may be made up of several genetic classes of fractures that cannot be easily distinguished in the field. The author has therefore used the term fracture and joint are used synonymously in this work to refer to a discontinuity in the rock mass.

Because of the abundance of joints compared to other structures in rocks, and because of their practical importance in controlling rock strength, permeability, porosity and various processes within the Earth's crust, such as the location of mineralization and hydrocarbon accumulations, joints have been the subject of study by a large group of geoscientists. The collection of data concerning joint properties and their analysis has however proved to be notoriously difficult (Loosveld and Fransen, 1992).

1.1 Title of the thesis

The title of this thesis is '*Analysis of natural fracture networks in massive and well-bedded carbonates and the impact of these networks on fluid flow in dual porosity modelling*'. In order to achieve this, I have carried out field mapping, mechanical and statistical analysis and has used the best numerical code available to study flow in a dual porosity medium. Dual porosity is defined in this work as a rock containing primary pores and fractures. Attempts have been made to rationalise the distribution patterns and to relate their relationship to the mechanical processes governing the formation of joints.

1.2 Problems addressed in the research

The problems addressed in this thesis are the definition and comparison of the geometry of natural fracture networks that form in well-bedded and poorly-bedded or massive limestones and the assessment of the impact of these fracture networks on the flow of fluids through the rocks that contain them.

Factors influencing joint orientation and spacing are considered, and the field data collected from the two study areas, (the Pennines in North Yorkshire and from the southern margin of the Bristol Channel Basin) are analysed. This is to determine whether the joint spacing is controlled by a deterministic or stochastic process or combination of the two.

The problem of fracture propagation across an interface between two beds is also examined. A bedding plane may be an interface between different lithologies, as in the limestone-shale alternations that characterise the Liassic rocks of the Bristol Channel coast, or between two beds of the same rock, as in the case of adjacent thick limestones in the Pennines. Particular attention is paid to the effects of the interface properties and the depth of burial. The role of decoupling of fracturing between two adjacent fractured competent beds by an intervening incompetent bed is considered. The procedures for determining various fracture parameters from the field data, *e.g.*, fracture density, are examined and the effects of the size and shape of the measured scan lines and windows on these parameters is discussed. Having established the geometries of the fracture networks, their influence on fluid movement through the rock mass is examined using a numerical code (Matthäi *et al.*, 2001) suitable for the analysis of such dual porosity systems.

1.3 Aims and objectives of this work

Joint orientation, spacing and density from the massive- and thickly-bedded Carboniferous limestone beds of the Pennines and from the rapidly alternating limestone and shale beds of Liassic age on the southern margin of Bristol Channel Basin have been studied. In addition the spacing and orientation of the fractures in adjacent competent beds, sometimes separated by thin incompetent beds, has been studied in detail in an attempt to determine the role of a mechanical layer boundary and/or layer on fracture propagation.

The main objectives of this work are:

(i) To use the scan line measurements to determine the evolution of joint spacing and an area sampling method to examine fracture density and to see how large an area is needed to obtain an acceptable (*i.e.* consistent) value of fracture density.

(ii) To review and assess the factors that determines joint spacing and density.

(iii) To understand the complex joint patterns at Kilve and Lilstock (on the southern margin of the Bristol Channel coast), firstly so that the great variation of joint patterns in adjacent competent limestone layers can be explained, and secondly to assess the effect of the intervening shale on fracture propagation and stress transmission.

(iv) To assess the role of major structures (folds and faults) on fracture development.

(v) To determine the reliability of palaeo-stress analysis based on joint orientations using examples from the Bristol Channel area.

(vi) To examine the use of fractographic features on the joint surfaces in unravelling the tectonic history of the areas.

(vii) To examine the hydrological properties of fractured rock masses using a numerical analysis and to determine the effects of different joint patterns on the localisation of flow through fractured limestone.

1.4 Methodology

In order to achieve the aims and objectives of the research, the work has involved three stages: (i) field observation and measurement (ii) statistical and mechanical analyses and (iii) numerical modelling.

In the Pennine area, four sites on the southern shoulder of the Askrigg block were mapped, namely Malham Cove, Langcliffe-Settle, Ingelton and Horton-in-Ribblesdale and a total of 49 scan lines were measured. The length and orientation of the scan lines depended entirely on the availability of the outcrop. Because of the excellent exposure of fractured beds at Ingleton, a window sample covering an area of 225m^2 was analysed using a rectified field photograph.

The area of study in the Bristol Channel is located between Hinkley Point Power Station in the east and Blue Ben Fault in the west. Fieldwork was restricted to the beach sections where the wave cut platform provides excellent exposures for the study of various structures in the basin. On the moderate- to steep-south-dipping limbs of the rollover folds that formed against E-W striking antithetic normal faults along the southern margin of the Bristol Channel Basin, scan lines were run approximately parallel to the strike of the beds that coincides with the axis of the E-W trending folds. Joint patterns were studied around folds and faults to establish whether or not they post-date these structures and if so what effect these structures had on the joints. A total of 25 scan lines were measured. Using suitable exposures, 18 windows

in the area were mapped. In areas where neither the scan line measurements nor window sampling were possible, field photographs were used to compare fracture networks on successive bedding planes and to determine the degree of continuity of fractures from one brittle limestone bed to the next. Finally the joint trace maps constructed from the field data were used in the numerical code (as discussed in Chapter 6) to study the hydraulic properties and the likely impact of these fractures on fluid flow.

1.4.1 Scan line sampling

The *scan line method* (Fig. 1.1) was used to measure the spacing of joints and their orientations. Spacing was measured along a scan line perpendicular to the average strike of a major joint set, either in a cross-section through the layer(s) or on a bedding surface. The technique was applied directly on an outcrop rather than using photographs. It can also be used in boreholes, tunnels and on aerial photographs provided that any distortions are corrected. A series of scan line surveys were made on sub-horizontal to gently dipping bedding planes in the Pennines (see Chapter 4). In both field areas (the Pennines and the Bristol Channel), the length and sometimes the strike of the scan line depended on the availability and size of the exposures. The average spacing (S) of the joint data (Hudson and Priest, 1983; La Pointe and Hudson, 1985) is given by:

$$S = \frac{L}{N} \qquad (1.1)$$

where L is the length of the scan line and N is the number of the discontinuities. Wu and Pollard (1995) express this in the general form:

$$S = \frac{1}{n+1}\sum_{i=1}^{n} li \qquad (1.2)$$

where l_i is the spacing between neighbouring joints. Wu and Pollard (1995) have also developed a technique of determining of joint spacing using windows rather than scan line sampling.

The frequency of joint spacing (λ) is the reciprocal of joint spacing:

$$\lambda = \frac{N}{L} \qquad (1.3)$$

Using this technique it is possible to quantify the frequency of joint data after the necessary trigonometric corrections have been made. If more than one set of joint is present in the rock mass, the frequency of all joints along the scan line is given by the sum of all joint sets λ_s:

$$\lambda_s = \sum_{i=1}^{n} \lambda_i \cos\theta_i \qquad (1.4)$$

where λ_i and θ_i are the fundamental set frequency and the angle between the joint normal and the scan line for the i^{th} set, and n is the number of the discontinuity sets. The number of joint traces intersected along the scan line depends on the orientation of the scan line relative to the joint traces (Terzaghi, 1965; La Pointe and Hudson 1985). To eliminate the orientation bias, a *weighting* (w) is used which is given by:

$$w = 1/\cos\theta \qquad \theta < 90 \qquad (1.5)$$

where θ is the angle between scan line and the discontinuity normal. Weighting is a means of artificially correcting the spacing of fractures when the scan line is oriented at low angles to the average strike of the joints. For a large sample size this weighting will serve to balance the bias caused by the orientation of the scan line. When θ approaches 90°, w becomes very large and great care should be taken during analysis and interpretation of the data. Conversely, this weighting can be ignored if the scan line is oriented normal to the average strike of joints.

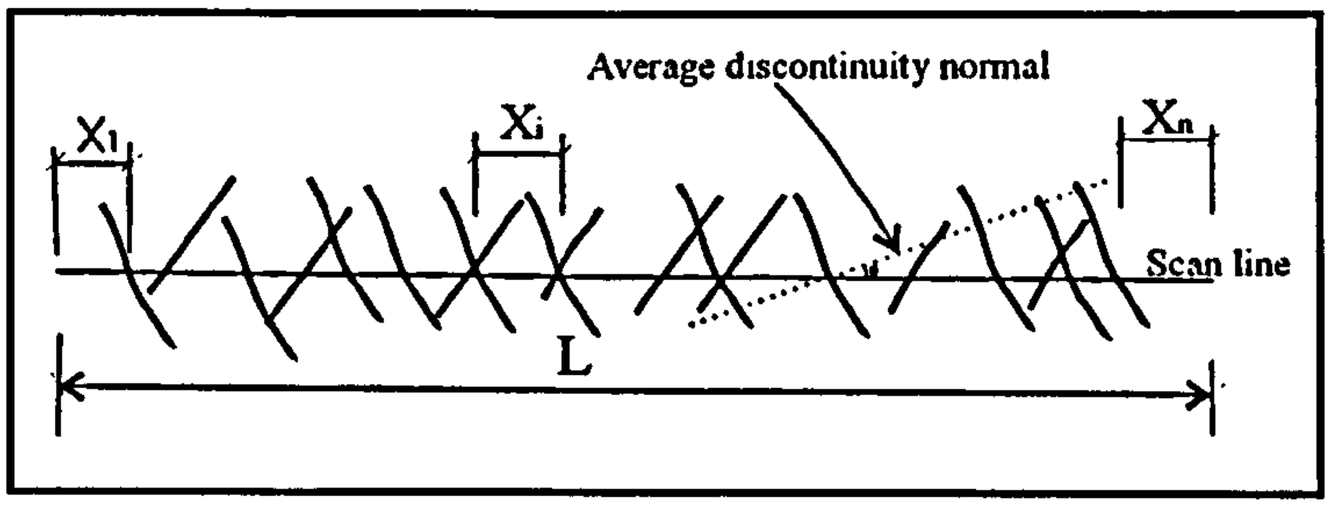


***Figure 1.1** Schematic layout of a jointed rock illustrating the principle of scan line sampling. In this example two sets of joints intersect the scan line.*

Where possible the vertical continuity of fractures was recorded (*e.g.* on the quarry faces and cliff sections). Unlike the joints in alternating limestone and shale beds of the Lias of the Bristol Channel, fractures in the Pennines limestones of north Yorkshire are through-going fractures that do not generally terminate at the bedding planes.

Two techniques have been used to describe natural fracture systems: (i) a statistical analysis of various attributes of the joints and (ii) an interpretation of individual outcrop data with respect to the mode of origin of the joints. When analysing these data, joint spacing was compared with normal (Gaussian), log-normal, negative exponential and a power-law distribution to determine the best-fit. Cumulative frequency plots provide a graphical representation of the data in a form suitable to estimate the best-fit distributions. The distribution determined for these data and the implications of these various distributions are described and discussed in section 4.6 of Chapter 4.

Because the geometric relationship between joints and the causative stress field is known, the direction of the palaeo-stress responsible for the fracturing can be

inferred. The consistent orientation of joints relative to other structures such as folds, faults and joints is commonly taken to be indicative of a genetic relationship (*e.g.* Twiss and Moores, 1992). The orientation is the parameter most diagnostic for identifying joint sets. However, interpretation that relies too heavily on orientation data may result in significant error in interpretation particularly in areas where the rocks contain early joints sets. In such an event more than one orientation of fracture may be associated with a single fracturing event. Segmentation and twisting of the fracture plane may occur as well as curving of a fracture plane and the reorientation of the fracture into parallelism with or normal to existing fracture or planes of weakness and branching of the fractures at their termination.

1.4.2 Area/window sampling

Fractures are not directly observable in complete 3D sets or networks, but rather as traces viewed on the surface of an outcrop or a map (*e.g.* Mauldon, 2001). It is therefore important to consider how best to analyse fracture phenomena by observation of their traces. To understand the spatial organisation of fractures, an *area (window) sampling* method was used. The area method of sampling can also be carried out using photographs, aerial photographs and satellite imagery. In the two field areas, photographs of exposed surfaces in outcrops (mainly bedding planes) were used.

Field mapping of joints involved taking photographs of areas on carbonate platforms (usually bedding planes) marked with a grid. The procedure starts by the marking of the four corners of a square. The size of window depends on the number of joint sets and/or the number of joints in the area of interest. If the number of joints per unit area is low, large window sizes up to 2 metres can be used. Otherwise a grid spacing of

about a metre was chosen as the optimum for computer restoration of the photographs. First, all the photographs taken of the grids were scanned and the joint traces redrawn in CorelDraw (or any graphic package) as shown in Fig. 1.2. This is saved in CorelDraw version 4.0 in which the software compatible with that used to manipulate the data. The traced joint maps have to be saved as *.plt files (version 4.0).

Three programs are used in the analyses of the fractures on the photographs namely *Weild*, *OBLIQUE* and *Weildbak*. *Weild* is a file conversion program for the joint trace maps obtained from a field photograph. This program converts the *.plt files from CorelDraw 4.0 version into *.lin files, in which each tip of a fracture on a joint trace map or vector is given a coordinate value. For curving joints, the program creates a series of vectors, the tips of which are represented by x-y coordinates. The *.lin files are user readable using notepad. The co-ordinates of the four corners of the window are also given in ascending order at the start of the file.

OBLIQUE (version 1.3) was written by Dr. Richard J. H. Jolly and Professor David J. Sanderson at Imperial College, and it converts oblique photographs into a normalised orientation and shows joint frequency distribution in the form of rose diagrams. Oblique opens *.lin files and then saves them as *.pl3, which can be opened by the *Weildbak* program. *Weildbak*, written by Dr. Richard J. H. Jolly at Imperial College, can convert *.pl3 files into the *.plt which can be opened by commercial software or graphic packages such as CorelDraw. *Weild* and *Weildbak* programs are file conversions. For large areas it is possible to make a mosaic of joint trace maps by fitting the corrected *.plt files from *Weildbak* with the adjacent window. The method continues until all the windows are normalised and a complete map is constructed.

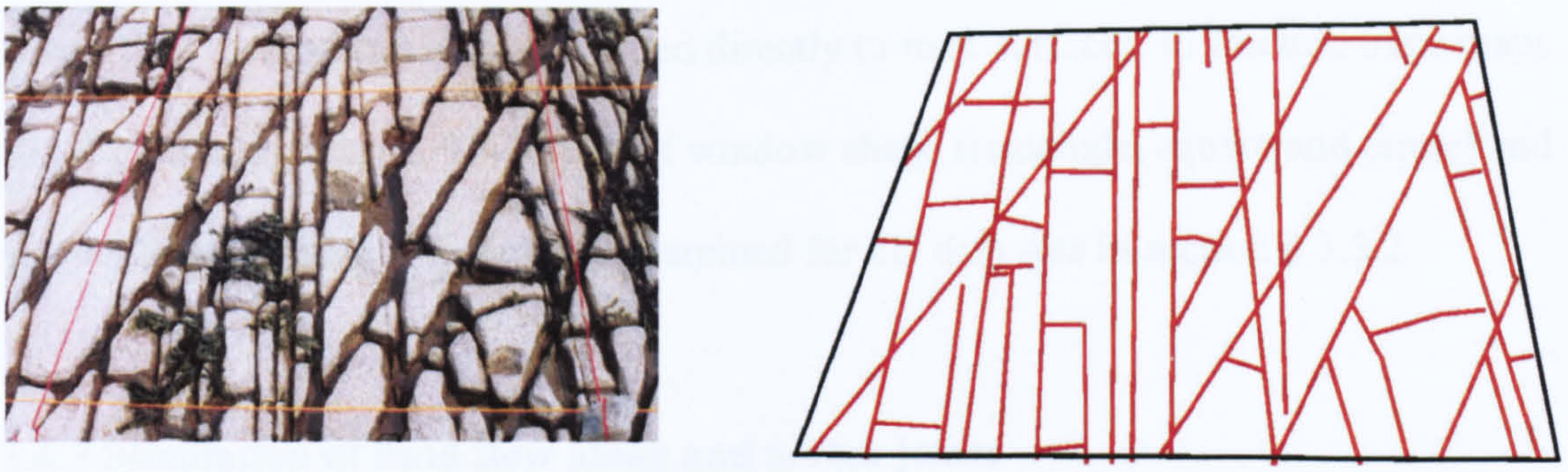


Figure 1.2 *(a) Photograph and (b) line drawing of a window sample made in a metre square grid on a jointed limestone bed from the Bristol Channel. Note that photographic distortion causes the square grid on the photograph to appear as a rhombohedron.*

The sensitivity of joint density to various window shapes and sizes has also been investigated using *Densityinfo* version 2.0, developed by Catherine Greenfields at Imperial College. *Densityinfo* was developed in Visual Basic for the NT/Windows platform. The input is a joint trace map saved as a plotter file that needs scaling. Circular windows may be arranged in '*cubic*' or '*rhombic*' packing. Cubic close packing has a higher proportion of voids, therefore, more fracture length falls outside the analysed area than in the case of rhombic packing. Data are stored as (x, y) coordinates of the beginning and end of segments that make up a line. Fracture length within circles is calculated by equating the equation of the circle with the equation of a line for each fracture segment to determine points of intersection. Then the total fracture length inside the circle can be determined.

Joint lengths within boxes are calculated by measuring from the point where a fracture trace enters the box to the point where it exits. Fracture lengths within each box or circle are saved as a comma separated file with extension *.dat that can be imported into a spreadsheet program such as Microsoft Excel. The fracture density can then be obtained using the total length of fractures in the window divided by the respective

areas. This method can also be applied directly to rock surfaces, to fracture trace maps and digital image maps. The effect of window shape (rectangle, square and circle) and size on fracture density have been examined for 2D data sets in section 4.3.3.2.

1.4.3 Simulation of fluid flow along and across joints

In this study finite element method (FEM) and finite volume (FV) are used to investigate the hydrological properties of fractured rocks. The discussion on the FEM/FV methods goes beyond the scope of the present work and interested reader is referred to Matthäi *et al.* (2001). The finite element method is used to compute partial differential equations that describe the distribution of a field variable such as fluid pressure across the domain of interest which is discretized into a finite number of regions/sub-regions each represented by a finite element (Matthäi *et al.*, 2001). The finite element program computes the dependent variable as a function of independent variables integrated to obtain the desired results. The finite volume (FV) method is a complementary approach to the FEM. For the purpose of studying the responses of joints to a far-field applied fluid pressure, commercial software and a Complex Systems Platforms (CSP) code written and compiled by Matthäi *et al.* (2001) were combined. '*Rhinoceros*' is a commercial software package (R. McNeel and Associates) which is used to create triangle meshes from NURBS curves (*i.e.* joint trace maps). The procedures for using these are discussed in Chapter 6.

1.5 Data presentation and analysis

1.5.1 Joint strike and dip

The most common methods of graphical representation of joint/fracture orientation are stereographic projections and rose diagrams. Rose diagrams are mostly used for vertical or high-angle fractures. This circular histogram is usually divided into 10°

intervals. The data are plotted into class interval as wedges that are radial and the length of the wedge is proportional to the number of readings. The data can also be plotted on x and y axes. For joints dipping at low angles, stereographic (hemispherical projection) techniques can be used. The data can be plotted either as planes or as poles.

1.5.2 Joint spacing versus frequency

Joint spacing was plotted on the frequency versus spacing axis for both north Yorkshire and the southern margin of the Bristol Channel. The field measurements of joint spacing were compared with standard statistical curves.

1.5.3 Joint spacing versus bed thicknesses

Assuming other parameters and loading conditions to be the same, thinner beds tend to contain more fractures of the same set compared to thicker beds (Bogdanov, 1947; Novikova, 1947; Kirillova, 1949; Ladeira and Price, 1981; Narr and Suppe, 1991) and this relationship has now become widely accepted. As a general rule, fracture spacing increases with an increase in bed thickness of the fractured layer; however, the quantitative relationship between these two parameters is still uncertain.

1.5.4 2D joint trace maps

As discussed in section 1.4.2, joint trace maps were prepared for each window. The field relationship between the different fracture networks in each window is explained in detail.

1.5.5 Fluid flow maps

The results of numerical modelling of fluid flow in fractured beds are presented as

pressure distribution maps shown in rainbow colour schemes and by contours. The velocities of fluid flow through the matrix and the joints are plotted as histograms.

1.6 Limitations

Scan line sampling provides a one dimensional survey an area of interest and the method can be used on a bedding plane, a cliff section or in a borehole. The intersection between the scan line and each of the structural features such as joints/fractures, together with their strikes and dips are recorded. The exposed surface along which the scan line is measured should be large compared to the spacing of joints. Priest (1993) suggests that such exposures should contain between 150 to 350 fractures. Scan line measurement is an extremely useful technique and provides a very fast and efficient way of gathering data. An inherent problem with this technique is that biases are introduced as a result of the orientation of the scan line with respect to the joint strike (La Pointe and Hudson, 1985).

Bed thickness and joint spacing relationships have limitations. For example, bedding planes may not be clearly defined. They can be imperceptible and may only locally be apparent when they are defined by stylolites (such as in the Cove limestone in north Yorkshire). The second limitation is that the joint sets in adjacent limestone beds in the Bristol Channel area have a different orientation. This makes it difficult to compare joints in one bed with those of the next adjacent limestone bed.

Biases are very common as joints commonly show clusters. The scales at which the joints are sampled, whether on the large- or small-scale, can govern whether the fracture data are represented or not. Fluid flow modelling is based mainly on 2D fracture trace maps that are sometimes too small to give reliable values of parameters

or patterns of fluid flow characteristic of the network. In addition, the fracture pattern observed in nature probably experienced boundary conditions different to those incorporated in the numerical models. For example Odling (1992) obtained higher permeability values for smaller areas, mainly because of the presence of fractures that traverse the whole area thus allowing high flow in specific directions. Alpine and exhumation joints in the Bristol Channel area are assigned uniform apertures of 0.003 and 0.005m respectively. These values are a little too high because of the stress relaxation of the rocks at the surface. In reality, fracture apertures are variable and dependent on surface roughness and the effective normal stress across the fracture surface.

1.7 Thesis layout

The thesis is divided into seven chapters. A brief introduction to define the problem, the aims of the research, the methodology used, the limitations of the research and the highlights and scope of each chapter in the thesis is given in Chapter 1. The regional geological setting of the two areas investigated is presented in Chapter 2. In Chapter 3 a critical review of (i) the controls on joint spacing, (ii) the various processes governing the initiation and propagation of joints based on field study, analogue simulation, and numerical modelling, (iii) the evolution of joint spacing, (iv) bed thickness and joint spacing relationships, (v) the relationship between joints and other structures such as folds, faults and pre-existing joints is presented. Joint orientation and spacing in the two field areas based on 1D and 2D data sets and their best-fit statistical curves are presented in Chapter 4. A brief introduction to fracture mechanics relevant to the study of fractographic surface features and field data from the southern margin of the Bristol Channel is given in Chapter 5. Fluid flow modelling in geologically realistic joint networks using the combined finite

element/finite volume method is examined in Chapter 6. The steps of the numerical analysis, the basic principles of flow in porous and fractured media and the results of the flow simulation using 2D joint trace maps generated from the field data are also reviewed in Chapter 6. The extent to which the results of this research can be used to model the interplay between natural fracture networks, geological stress and fluid flow in the crust and how far the numerical simulation used is able to cope with the complexity of natural fracture networks will be discussed in Chapter 6. The uniqueness of sub-seismic features for studying flow through realistic fracture networks is addressed in the same chapter. Discussion and conclusions are presented in Chapter 7, which ends with recommendations for future work on micro-veins and the 3D modelling of fluid flow through fracture networks.

CHAPTER TWO

REGIONAL GEOLOGICAL SETTING

Two areas have been selected for the purpose of studying joint spacing, orientation and density in limestones. The first is located in Yorkshire, North England, and the second on the southern margin of the Bristol Channel coast, southwest England between longitudes 3°7' and 3°16' W (Fig. 2.1).

2.1 Summary of previous structural investigations in the Pennines

The area of investigation in the Pennines, north Yorkshire, is depicted partly on the Hawes and partly on the Settle 1: 50,000 scale British Geological Survey sheets numbers 50 and 60. The Pennines constitute a dominant physiographic feature lying between the Irish Sea to the west and the North Sea to the east (Edwards *et al.*, 1954). Back-arc extension (N-S directed) north of the Variscan subduction zone during Late Devonian to Early Carboniferous time produced a series of fault-bounded half grabens striking E-W in the Pennines province (Guion *et al.*, 2000) (Fig. 2.1). In the Early Carboniferous, a seaway opened around the Lake District-Pennines region striking E-W to WNW-ESE between the granite-cored stable blocks of Askrigg and Alston (as identified from the low Bouger gravity anomaly and drilling). The two blocks are separated by the Cotherstone trough (Dunham and Wilson, 1985). This was followed by the deposition of limestone on the floor of a shallow tropical sea. The Carboniferous in the British Isles is divided into two major successions: one linked to the deposition in the Lower Carboniferous (Dinantian) and the other to the Variscan Orogeny in the Upper Carboniferous (Silesian) (Guion *et al.*, 2001).

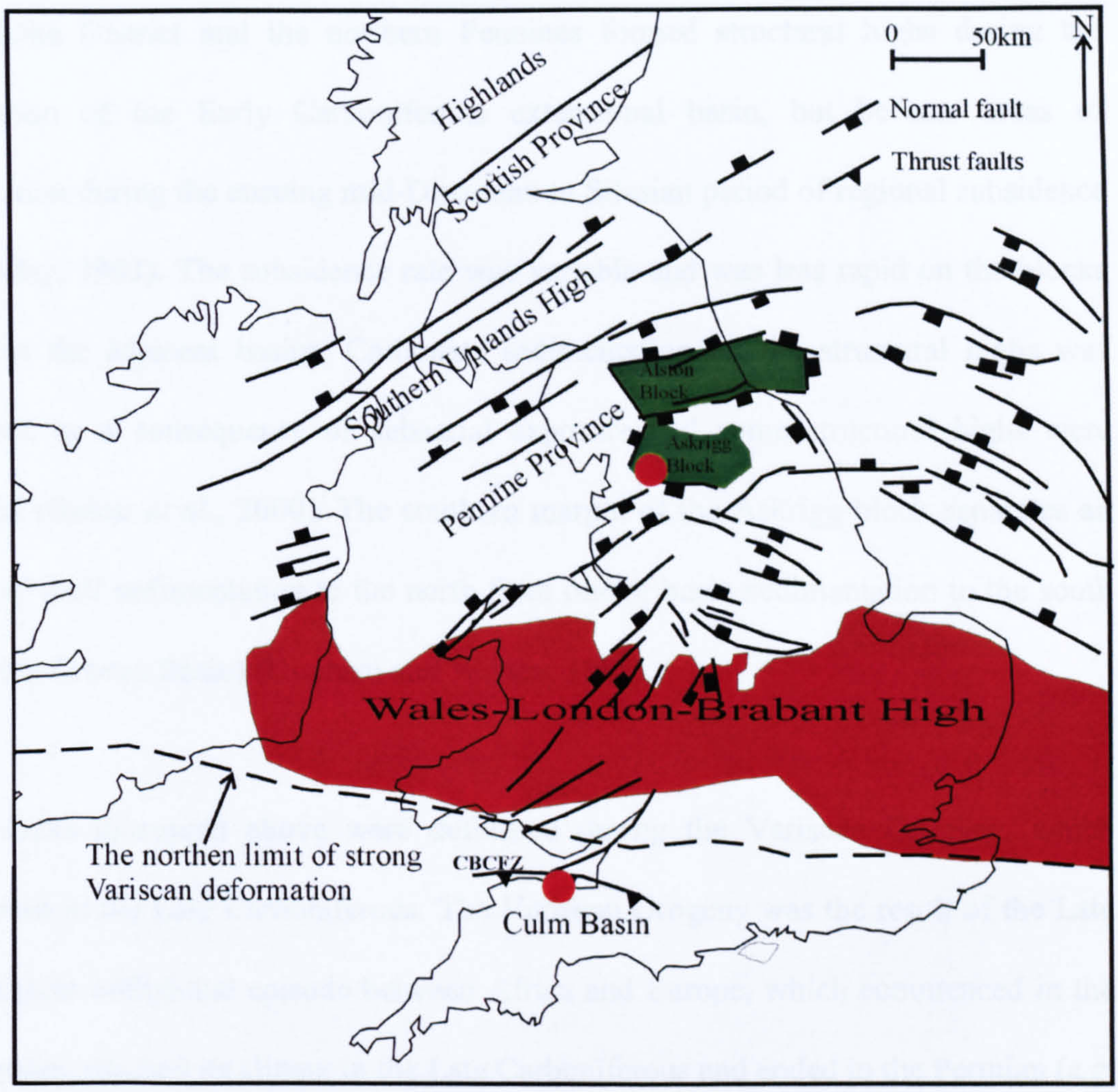


Figure 2.1 *Dinantian palaeogeography and major structures that influenced sedimentation through much of the Carboniferous. Note that the basins have very strong Caledonian trend (modified from Guion et al., 2001). CBCFZ - Central Bristol Channel Fault Zone. The locations of the two study areas is indicated by the red circle.*

The Lake District and the northern Pennines formed structural highs during the formation of the Early Carboniferous extensional basin, but became areas of deposition during the ensuing mid-Dinantian to Silesian period of regional subsidence (Holliday, 1993). The subsidence rate was variable and was less rapid on the blocks than in the adjacent basins. Carbonate sedimentation on the structural highs was reduced as a consequence of subaerial exposure and some structural highs were eroded (Guion *et al.*, 2000). The southern margin of the Askrigg block separates an area of shelf sedimentation to the north from one of basin sedimentation to the south (*e.g.* the Craven Basin) (Dunham and Wilson, 1985).

The rocks discussed above were deformed during the Variscan Orogeny, which occurred in the Late Carboniferous. The Variscan Orogeny was the result of the Late Palaeozoic collisional episode between Africa and Europe, which commenced in the Devonian, reached its climax in the Late Carboniferous and ended in the Permian (*e.g.* Warr, 2000). The Variscan Orogeny is considered to be the last strong crustal shortening event that affected northwest Europe (Woodcock and Strachan, 2000). In the Pennines-Lake District region, the Variscan movements resulted in regional uplift and inversion of the basins and the removal of much of the Carboniferous cover on the former structural highs (Holliday, 1993). The Askrigg and Alston blocks behaved as rigid structural plateaux during the Variscan deformation. The shelf sediments in the Craven Basin to the south of the study area have been strongly folded, whereas the limestone capping of the Askrigg block shows no sign of folding (Fig. 2.2). The study area is located at the southern margin of the Askrigg block, bounded to the west by the Dent Fault and to the south by the North- and Middle-Craven Faults.

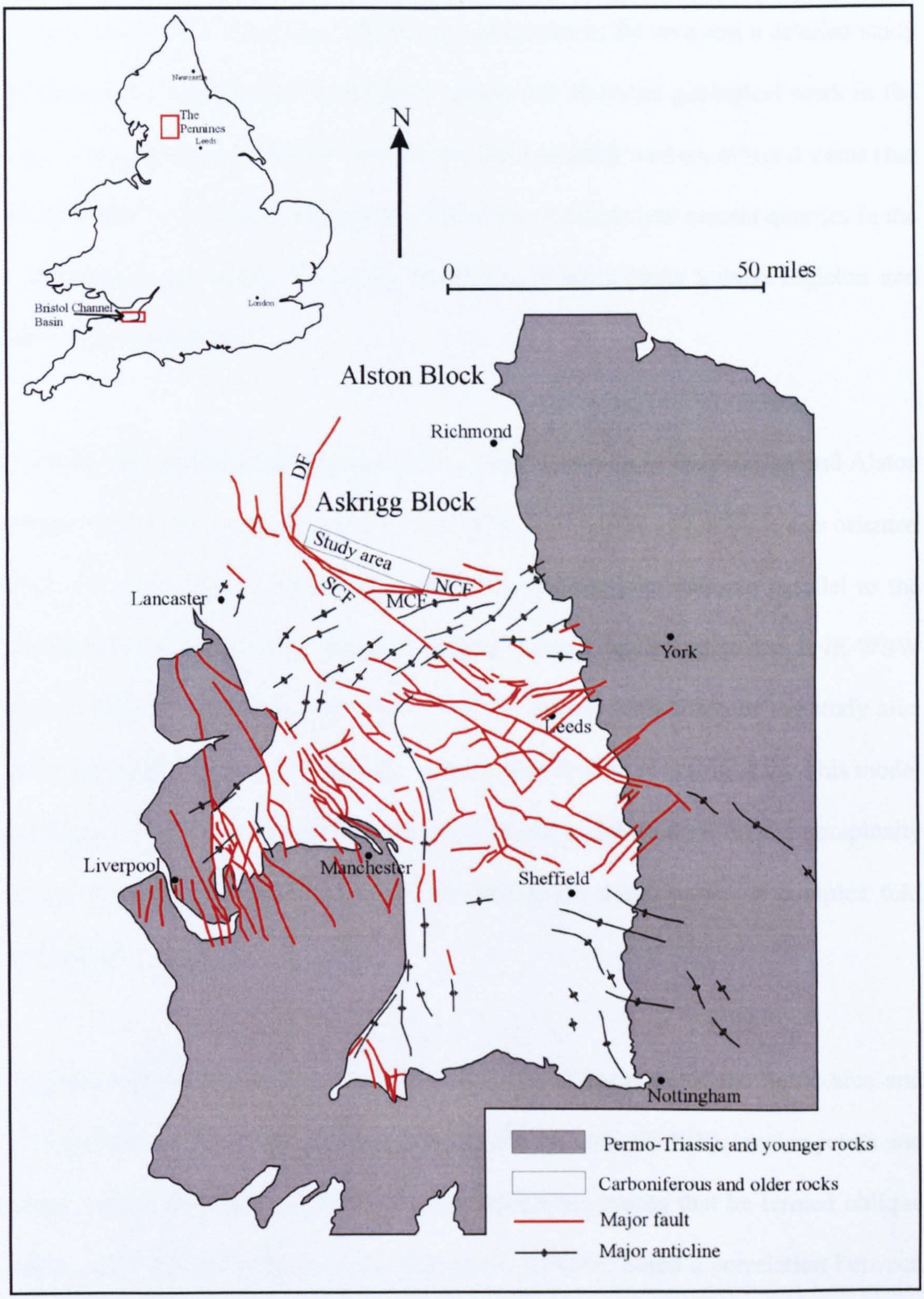


Figure 2.2 *Structural map of the Pennines and the surrounding area. The position of the study areas is shown. NCF – North Craven Fault, MCF – Middle Craven Fault, SCF – South Craven Fault, DF – Dent Fault (modified from Edwards et al., 1954). Inset map shows the position of the two study areas.*

Joints are the most abundant of all tectonic structures in the area and a detailed study of these joints has not previously been carried out. Previous geological work in the area is limited to, and mainly focused on, the coalfields and on mineral veins that contain Ba, Cu, F, Pb and Zn deposits. There are roadstone and cement quarries in the Carboniferous limestone and in the underlying Silurian rocks around Ingleton and Horton-in-Ribblesdale.

Moseley and Ahmed (1967) described two major joint sets in the Askrigg and Alston blocks, one striking NW-SE and the other ENE-WSW, with subordinate sets oriented N-S and E-W. They considered that the Carboniferous joint sets ran parallel to the Caledonian NW-SE dextral and N-S sinistral wrench faults and to the ENE-WSW Caledonian cleavage. They point out that the Variscan folds south of the study area are extremely variable in orientation, ranging from E-W to N-S (Fig. 2.2). This model of relatively weak basins separated by rigid blocks could account for the complexity of the Late Variscan stress fields that resulted in the development of complex fold orientations.

Doughty (1968) described joints in the Great Scar Limestone of the Settle area and recognised a conjugate set of joints (striking NW-SE and NE-SW), tension joints and joints with a low angle of dip relative to the bedding planes that he termed oblique joints. The NW-SE set is the most developed. Doughty noted a correlation between high joint density and coarse-grained limestone and between low joint density and carbonate mudstones. Doughty also suggested that joint density was unrelated to the thickness of the beds.

Dunham and Wilson (1985) gave a comprehensive account of the geology and mineralisation in the Pennines and adjacent areas. They proposed that the main factor controlling mineralisation in the region during the Upper Carboniferous was the permeability related to the formation of fractures that governed the circulation of mineralising fluids. They concluded that fractures with small displacements provided the most effective channels. A detailed account of the geology, structure and mineralisation in the Pennines Orefield (Stainmore to Craven) and the adjacent areas is beyond the scope of the present work and the reader is referred to Dunham and Wilson (1985).

Soper (2001) described the inliers of Ordovician and Silurian rocks at Ingleton, which are mainly sandstones, shale and siltstones. Soper sub-divided the rocks into three lithofacies, namely: (i) thick-bedded sand-grade turbidite greywackes commonly with delayed grading picked out by the cleaved silty tops of the beds; (ii) thinly-bedded green siltstones, mudstones and sandstones with cross lamination, flute casts, slump structures and intraformational breccias and; (iii) coarse-grained quartz-feldspar lithic wackes. The greywacke is largely massive, with no uniform bedding and a tendency to fissuring. In places, these rocks contain important fracture sets comparable in orientation to those in the Carboniferous beds that overlie the Silurian and Ordovician rocks with a marked angular unconformity.

The major structures in the area include the North-, Middle- and South-Craven Faults (Fig. 2.2) and joints. Dunham and Wilson (1985) argued that fresh scarps associated with the Middle Craven Fault at Giggleswick, near Settle, and the Skipton earthquake of 1944 provide evidence of relatively recent geological activity. The Middle and

North Craven Faults coincide approximately with the boundary between the Craven Basin to the south and the Askrigg block to the north. Knoll and patch reefs of the Craven reef belt occur along this basin-bounding fault zone that governed the sedimentary patterns. They crop out in Malham Cove and provide evidence that this zone marked the boundary between deep and shallow marine conditions.

Whether a significant thickness of the Mesozoic rocks covered the structural highs of the Lake District and the Northern Pennines has long been a subject of debate. The Lake District-Pennines island was emergent for all or much of the Mesozoic except perhaps during the Cretaceous. The lack of unequivocal evidence in the form of preserved outliers of Mesozoic strata (*i.e.* the general absence of any pre-Quaternary beds younger than Early Jurassic) has lead to a wide range of opinions regarding the amount of Mesozoic sediment deposited on these palaeo-highs. The greatest thickness has been proposed by Holliday (1993) based on apatite fission track analysis (AFTA). Holliday suggested that a Mesozoic cover of between 1200 to 1750m was present on the highs prior to erosion during the Cenozoic. Holliday argued that even if sedimentation had been continuous over the old Palaeozoic horsts of Northern England throughout Mesozoic times, the cumulative thickness need not have been great, and must have been significantly less than in the adjacent basins.

2.2 Detailed geology of the study area

Early in the Carboniferous, a clear tropical sea invaded the study area in North Yorkshire. The Carboniferous limestone rocks in the study area have been subdivided into the Cove and Gordale Limestones that together form the Malham Formation. The remains of calcareous animals such as molluscs, corals and crinoids form the massive

beds of the Cove Limestone, also known as the Great Scar Limestone, which is a sequence of massive, light grey, pure packstones and grainstones, now forming the lower part of the Malham Formation. The Gordale Limestone is made up mainly of well-bedded packstone, wackstone and subordinate grainstones. The Cove Limestone overlies the Chapel House Limestone and Kilsney beds which consist of limestone and mudstone. The rocks at the boundary are marginal reef limestone that defines the transition between shelf and basin environments. Dunham and Wilson (1985) noted that the Middle and North Craven Faults mark the site of rapid facies change across the marginal reef belt.

The major structures in the area are the Dent Fault in the west and the Craven Faults (North-, Middle- and South). These faults were formed as early as Silurian-Devonian time (*e.g.* Soper, 2001) and were active towards the end of the Dinantian when they controlled Lower Carboniferous sedimentation. Soper argues that they were also active possibly as strike-slip faults during the Upper Carboniferous (Variscan) contraction, causing en-echelon folding of the overlying rocks which now make up the Ribblesdale fold belt.

2.3 Fractures

The present author studied joint spacing in the Cove- and Gordale- Limestones. Joints in the area are generally vertical, normal to the bedding and show ENE-WSW to NE-SW and NNW-SSE strikes with subordinate E-W and N-S orientations. According to previous workers in the area (*e.g.* Doughty, 1968), the ENE-WSW (050° to 060°) and NNW-SSE (320° to 330°) joints form a conjugate set although the acute angle between them is considerably greater than the calculated 60° of most rock types. In

places the WNW-ESE joints are organised in a right-stepping manner (Fig. 2.3) whereas the ENE-WSW ones locally show a left-stepping *en-echelon* arrangement. An *en-echelon* arrangement is defined as any stepped arrangement of two or more overlapping or underlapping structural elements (see *e.g.* Biddle and Christie-Blick, 1985). The *en- echelon* array may be overlapping, underlapping or neutral. The *en-echelon* fracture in the Pennines, where exposed, shows a large overlap and close spacing with no deflection of the straight crack paths. The joint networks show rectangular and rhomboidal patterns that characterise the limestone pavement (Fig. 2.4a and b).

The NNW-SSE fractures, when plotted on a rose diagram show only a small spread around the mean strike and are mostly made up of long and continuous fractures that can be traced over a few tens of metres. The ENE-WSW joints are less continuous and less regular. These Late Carboniferous structures may have developed in a stress field associated with the Variscan deformation in which the principal compressive stress (σ_1) trended E-W to WNW-ESE. Moseley and Ahmed (1967) argued that fractures in the limestones have lineament equivalents in the Lower Palaeozoic basement that may have propagated upwards into the Carboniferous Limestone. I agree that the joints in the Carboniferous beds formed during the Variscan deformation with σ_1 consistently in a WNW-ESE to E-W direction. However observation shows that the joints do not always propagate from the contact with the basement rocks (defined by an angular unconformity) into the overlying younger beds.

The joint sets in the Pennines described in this section show consistent strikes throughout the region.

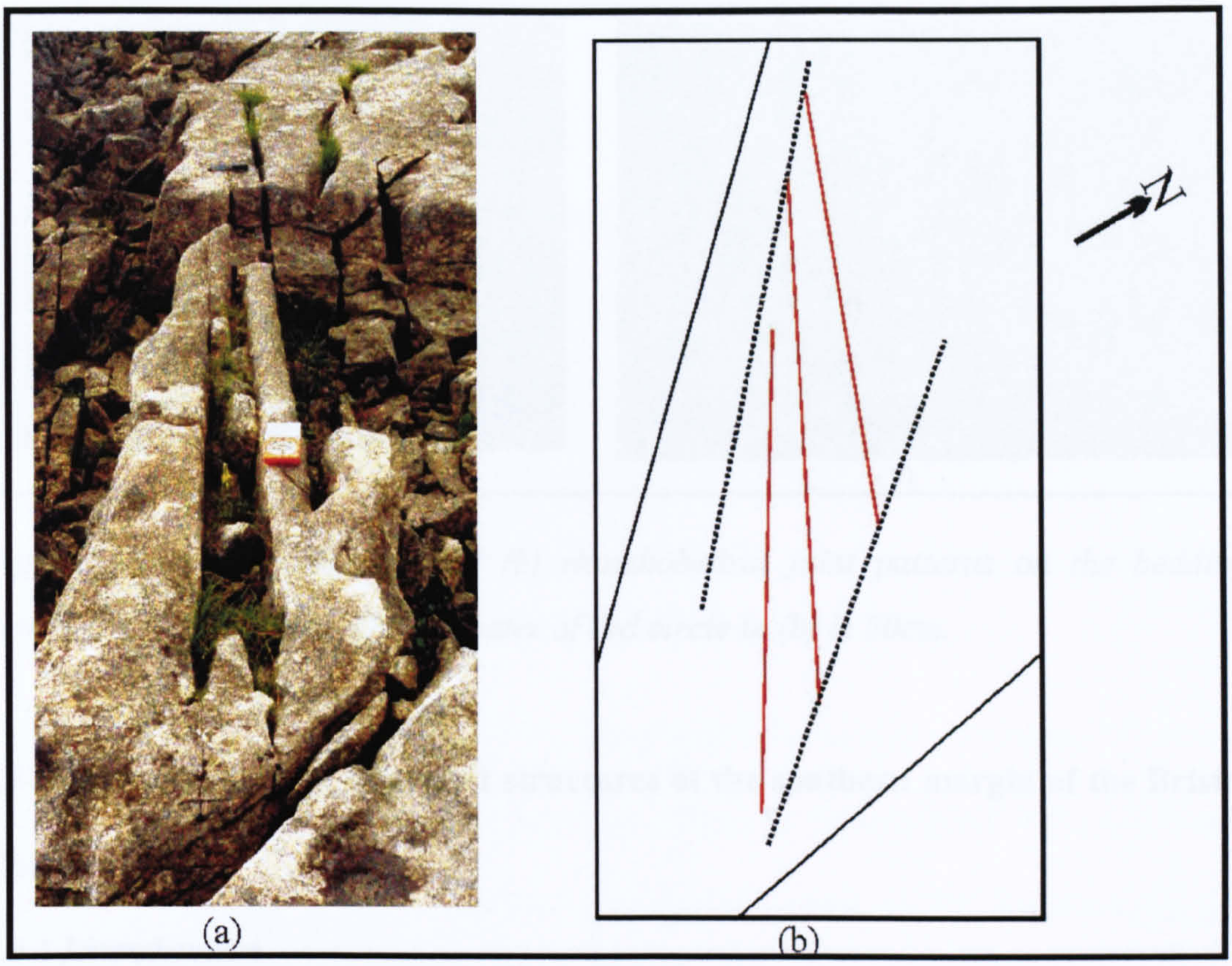


Figure 2.3 *(a) Photograph and (b) line drawing of right-stepping en-echelon joints from east of Langcliffe striking WNW-ESE. Compass at the centre of the photograph is for scale.*

In places the joints are 20 to 30cm wide and it is thought that dissolution during glaciokarst activity (the combined effect of glaciation and karst activity) was the main mechanism in this widening. The process continued with limestone weathered by acids in rain and groundwater, leading to the enlargement of the pre-existing joints. As a result of this dissolution, kinematic indicators and joint surface features have been destroyed. Drainage is now mostly underground along solution channels giving rise to many caves and sink holes in the region.



Figure 2.4 *(a) Rectangular and (b) rhombohedral joint patterns on the bedding planes at Malham Cove. The diameter of red circle in (b) is 50cm.*

2.4 Summary of the geology and structures at the southern margin of the Bristol Channel Basin

2.4.1 Introduction

The area of study on the southern margin of the Bristol Channel Basin has been the subject of many stratigraphic, palaeontological and structural investigations. The excellent cliff and foreshore exposures allow almost complete 3D visualisation of the bedding and structures in the successions of the Upper Permian to Trias and Lower Lias. The area is a world-class natural analogue to study evolution of a sedimentary basin and typically fractured and faulted reservoirs. Before describing the geology and structures within the southern margin of the Bristol Channel Basin, it is apposite to review the formation and deformation of extensional sedimentary basins in order to understand the structures that are likely to form during extension and inversion.

2.4.1.1 Basin extension

Extensional (rift) basins form in the upper levels of the crust. As the lithosphere is stretched, the upper, most brittle part of the crust tends to respond to this extension by

brittle fracturing and major normal faults are formed. These define the basin boundaries creating the typical graben geometry. As the graben grows, the sequence of sediments accumulating within it is cut by new normal faults as the regional extension continues. The faults can penetrate down to considerable depths, either retaining high dip angles or displaying a gradual decrease in dip with depth until the fault plane approaches the horizontal (*i.e.* parallel to bedding) and detaches along a weak bedding plane, defining detachment level. These curved faults are termed listric normal faults.

Models for the formation of rift basins have been discussed in great detail by several authors (*e.g.* McKenzie, 1978; Royden *et al.*, 1980; Le Pichon, 1981; Xiao and Suppe, 1982; Gibbs, 1984 among many others). Two basic models: *i.e.* the listric normal fault model (Fig. 2.5a-c) and the rotated block model (Fig. 2.5d) have been proposed.

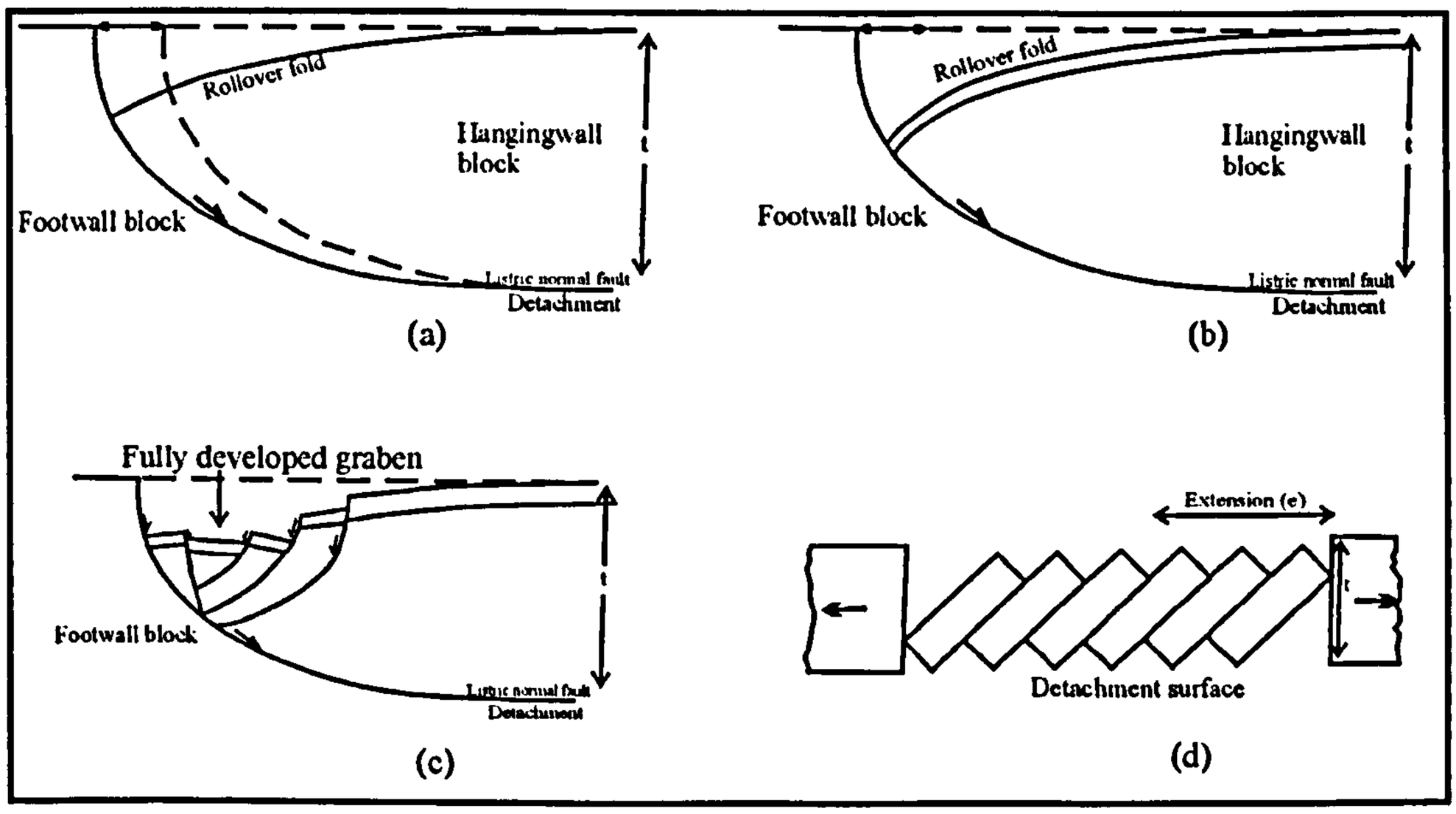


Figure 2.5 *Sedimentary Basin Fault Models: (a) to (c) Listric Normal Fault Model and (d) Rotated Block Fault Model. Note the progressive development from rift initiation to fully developed graben through rollover folds basins (after Gibbs, 1984).*

In the listric normal fault model the fault initiates at a high angle to the surface (dip of approximately 60°) and flattens out to near horizontal at depth, showing an overall concave upward profile (Fig. 2.5a). For large-scale basins, the depth at which the fracture flattens out is the '*brittle ductile*' transition zone in the crust, for smaller faults flattening out occurs along a suitable weak detachment horizons such as a shale or evaporite bed. In general however, the listric normal faults flatten out along some *'detachment horizon'*.

In the rotated fault block model, the basin boundary faults lie parallel to one another and have an originally uniform dip of approximately 60°. The fractures divide the crust into a series of sub-parallel blocks or dominoes (Fig. 2.5d) which, under the influence of subsequent regional extension, rotate, thus reducing the dip of the faults. This type of fracturing requires much greater extension to form a sedimentary basin than the listric fault model. A geometric problem with the rotated block fault model is that a '*space*' is created at the base of the rotated blocks. This is assumed to be infilled with ductile material such as weak sediments or, for deeper detachments, a more ductile crustal rock.

Unlike the rotated block fault model, the listric normal fault model does not suffer from the space problem at the base of the block but, as the crust is extended, the hanging-wall will tend to pull away from the footwall leaving a gap (Fig. 2.5a). This gap may be filled either by ductile bending of the beds of the hanging-wall to form a '*rollover*' anticline (Fig. 2.5b) or by brittle deformation of the hanging-wall (Fig. 2.5c) or a combination of the two. Both processes produce a wedge shaped basin profile with a convex upward base. The formation of a rollover structure causes intense

strains to build up in the hanging-wall.

According to Xiao and Suppe (1992) the shape of the rollover folds depends on many factors including: (i) the shape of the fault (ii) total slip on the fault (iii) the direction of the motion of the fault (*i.e.* dip-slip or oblique dip-slip), (iv) the history of sedimentation relative to fault slip-rate and (v) the amount of compaction.

The strains in the hanging-wall may be accommodated by the formation of secondary fractures, for example a series of smaller antithetic faults. The displacements on these secondary faults, which are conjugate to the basin-bounding normal faults, accommodate displacement on the major fault. The second method of strain accommodation requires the ductile thinning of the beds adjacent to the fault. As noted above, rollover folds and antithetic faulting frequently occur together. If movement on the main fault continues and the hanging-wall rotates by more than 30°, then some of the early formed antithetic normal faults in the hanging-wall will become overturned and appear as reverse faults (see *e.g.* Jackson *et al.*, 1982).

2.4.1.2 Basin inversion

Basin inversion is a process whereby an extensional basin is shortened as a result of a reversal of the tectonic stress regime. Some of the shortening was accommodated by reverse movement along the pre-existing normal faults. This leads to uplift. The Permo-Triassic E-W trending Bristol Channel Basin was inverted during the N-S Alpine compression. The basin was formed during the break up of Pangaea in the Permian as a result of a regional N-S extension. This extension commonly exploited early (*i.e.* Variscan) E-W striking south dipping thrusts so that they become the basin

bounding faults for the new extensional basin. Down-dip reactivation of these ideally oriented low-dipping structures required lower energy than that required for the formation of new south-dipping normal faults with the same strike. Seismic reflection data from the Bristol Channel Basin (Brooks *et al.*, 1988) provides direct evidence of a reactivated major Variscan thrust deeper in the Palaeozoic basement (Fig. 2.6). The resulting extensional basins include the Bristol Channel Basin, the Wessex Basin and basins of the English Channel.

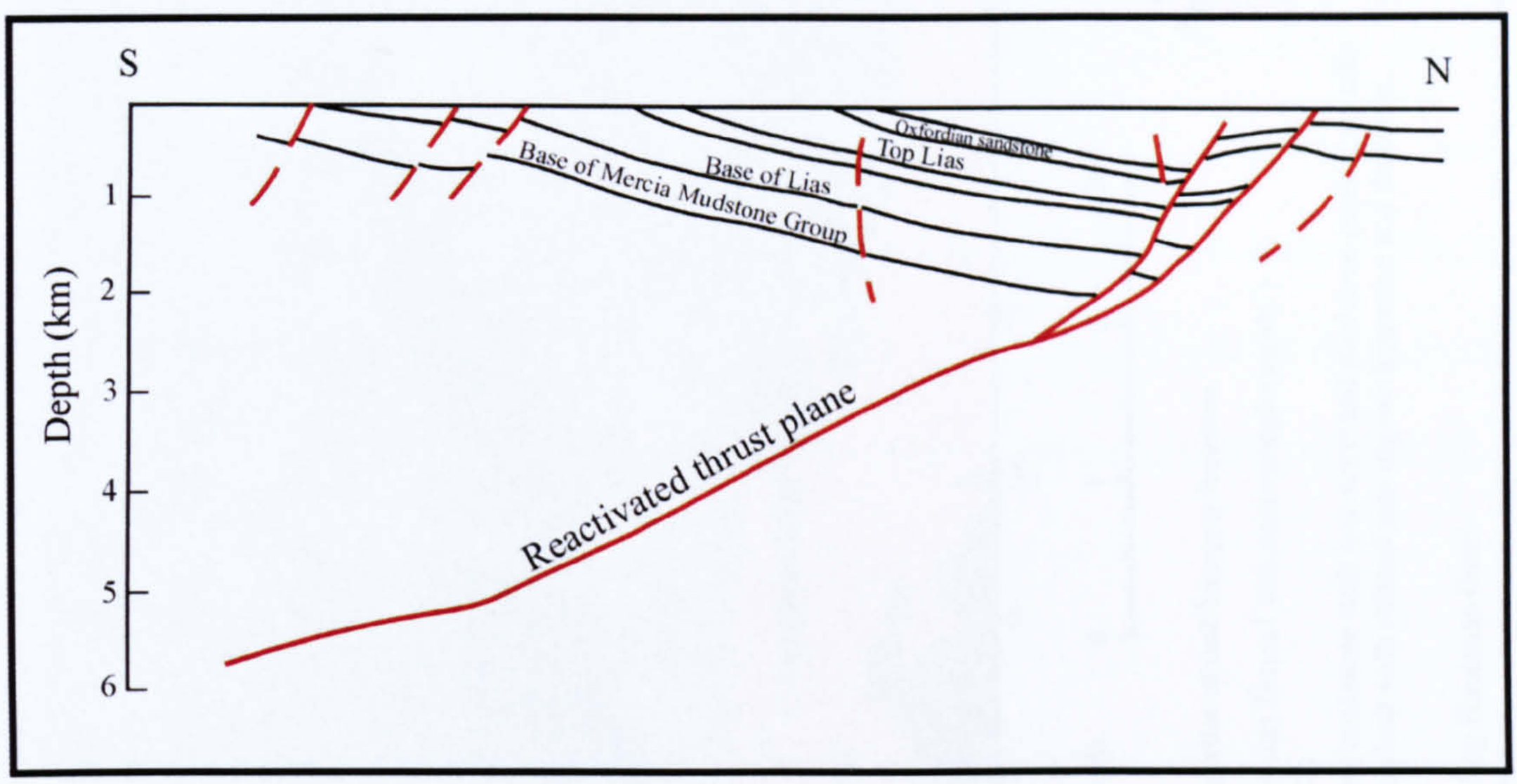


Figure 2.6 *Seismic section showing reactivated Variscan thrust north of the Devon coast (from Brooks et al., 1988).*

The Bristol Channel Basin (Fig. 2.7) was formed in a Palaeozoic basement that consisted of Devonian sandstones and slates, and Carboniferous Limestones that had been deformed during the Variscan Orogeny as a result the N-S closing of the Variscan Ocean (Dart *et al.*, 1995). To the north and south the basin is bordered by major E-W striking Variscan structures in the Palaeozoic basement, notably the

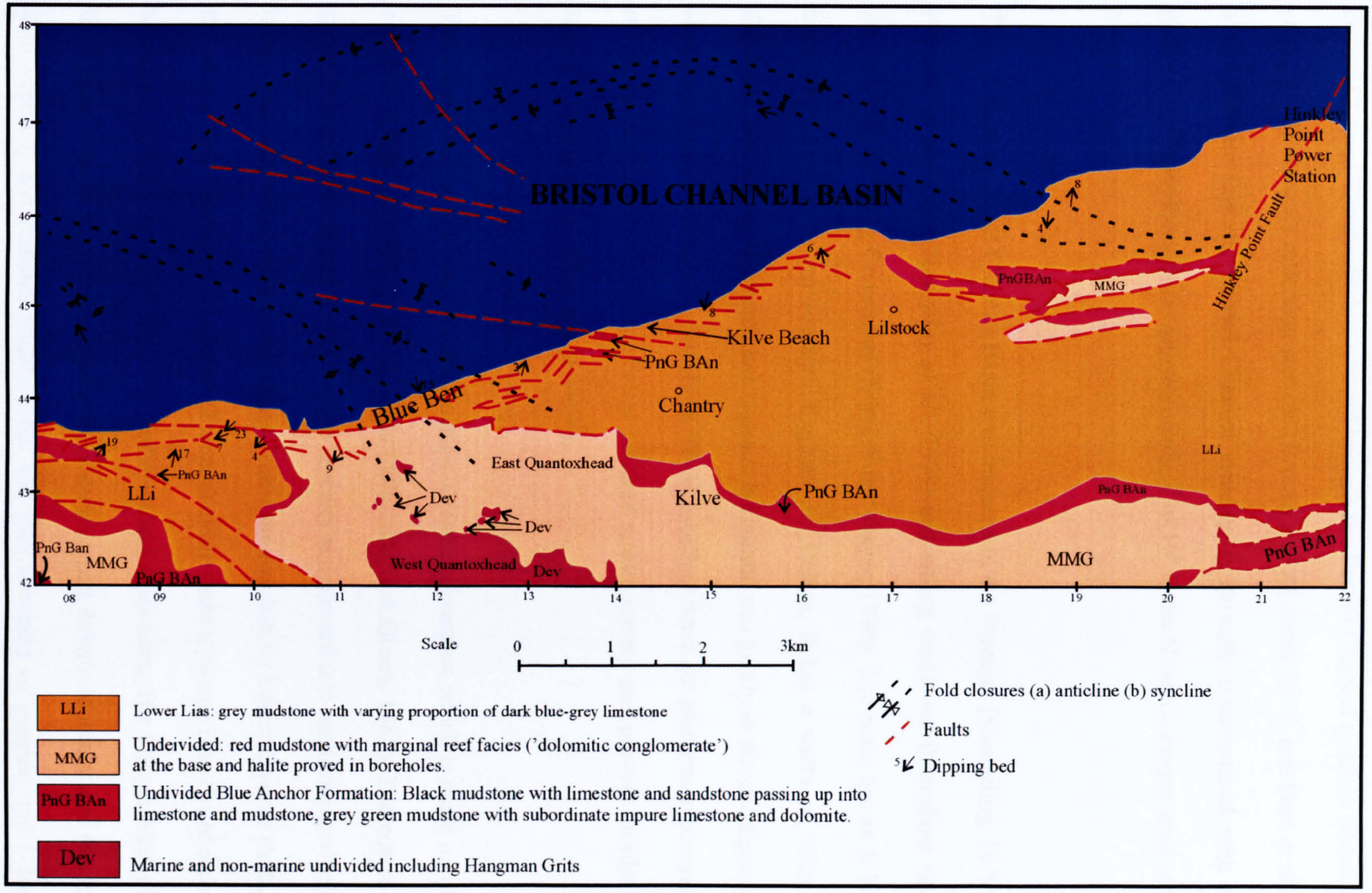


Figure 2.7 *Geology and major structures in the Lilstock-Kilve areas on the southern margin of the Bristol Channel Basin (modified from 1: 50,000 scale geological maps of England & Wales sheets 263, 279 and part of 295).*

Bristol Channel Thrust which is situated beneath the Bristol Channel syncline (Brooks *et al.*, 1988). Seismic reflection surveys (Brooks and Al-Saadi 1977; and Dart *et al.*, 1995) indicate that the Bristol Channel syncline is strongly asymmetrical with a gently-dipping southern limb (approximately 5° to 10° to the N) and a steeper northern limb (20° to the S).

The rift-related Bristol Channel Basin was initiated in the Permian (Kamerling, 1979; Nemčok *et al.*, 1995; Rawnsley *et al.*, 1998) and rifting continued throughout the Jurassic into the Early Cretaceous (Nemčok and Gayer, 1996). The basin has an E-W trend and stretches across southern England for 155km. It has a width of 30km. Extensive recent coastal erosion has exposed horizontal and gently to steeply-dipping stratigraphic sequences on the foreshore. These excellent wave cut platform exposures of Liassic carbonates are up to several hundred square metres and provide an ideal location for the study of fracture networks.

The oldest beds in the basin are the Permian-Triassic succession which is made up of continental red beds/alluvial fan deposits (Whittaker and Green, 1983). The coarse-grained conglomerates and breccias grade laterally and upward into sandstones, which in turn pass into siltstones and mudstones. These are overlain by Lower Triassic strata, the arenaceous Sherwood Sandstone Group, which passes upwards into the Mercia Mudstone which consists of siltstone, mudstone and evaporites. The Keuper Marl of the Upper Triassic is made up mainly of calcareous and dolomitic mudstones (up to 85m exposed) and contains nodular beds and vein networks of gypsum and 1-2m thick isolated intraformational conglomerate and sandstone lenses with gypsum cement. Toward the top, the red marls become inter-bedded with grey/green marls

which increase in frequency and grade up into the marine Blue Anchor Formation (Carnian to Lower Rhaetian) which consists of alternating green, grey and dark grey mudstone/siltstones (26 to 31m) which are also rich in nodules and networks of fibrous gypsum veins. Nodular gypsum is abundant at outcrop forming laterally impersistent horizons in the lower part of the Blue Anchor Formation. The underlying red mudstones are generally unfossiliferous, poorly bedded and contain few sedimentary structures although current ripples and shrinkage cracks are common. The abundance of silt-sized grains led Leslie *et al.* (1993) to conclude that significant volumes of aeolian sediment was supplied to the Triassic basins. The Blue Anchor Formation is conformably overlain by the Westbury Formation (6-7m thick) of Rhaetian age which comprises inter-bedded light grey limestone, sandstone and dark grey shales, the base of this formation being marked by the first appearance of the limestone beds. The black shales of the Westbury Formation mark the stratigraphic contact between the Trias and Lias. Hesselbo (2000) suggests that this transition from non-marine 'red-bed' deposition through to organic-rich marine strata was not the result of gradual drowning of the region instead he considers that the movement occurred in pulses. The Westbury Formation is followed by interbedded grey mudstones, siltstone and limestone of the Lilstock Formation.

The major facies change which occurred at the end of the Triassic was the result of arid continental conditions giving way to marine conditions as isolated continental rifts became linked to each other and to the sea as Pangaea became progressively more fractured. Dart *et al.* (1995) suggest a shallow marine lagoon/embayment for the environment of deposition of the Westbury and Lilstock Formations. The Lilstock Formation is overlain by rocks of the Lower Lias consisting of rapidly alternating beds

of grey mudstones (or grey/black bituminous shales) and light grey limestones of Lower Jurassic age (Hettangian and Sinemurian) known locally as the Blue Lias (Waters *et al.*, 1987). Ammonites, thin shell bivalves, fish remains and bioclastic debris are very common (Dart *et al.*, 1995; this work). Dart *et al.* (1995) argued that black shale deposition was probably linked to planktonic blooms that led to the creation of anoxic bottom waters.

2.4.2 Structures

The structures observed along the southern shore of the Bristol Channel Basin are described in this section. In the western half of the study area, the junction between the Uppermost Triassic and Lower Lias horizons occurs along the coastline. Because of their differing rheological properties, the response of these two units to tectonic stress is distinctly different. The Triassic marls behave as an isotropic material because of the poorly-defined bedding planes and relatively homogeneous composition. The faults that occur in these zones are generally diffuse. The rapidly alternating micritic limestones and marly shales of the overlying Lower Lias have a marked mechanical anisotropy. Faults within the Lias are more localised than in the Triassic. They form discrete, sharp fault planes and these frequently occur in dense fault zones (*e.g.* at Kilve). In the following sections a detailed description of some of the structures (folds, faults and joints) along the coast will be given. The structures are discussed in chronological order.

2.4.2.1 Structures associated with the opening of the Bristol Channel Basin

The earliest structure in the study area is a circular domal feature within a mixture of shale and limestone (Fig. 2.8). This is probably a mud volcano formed as a result of

the over-pressuring of the sediments during burial and diagenesis.

Micro-veins (high-density veins of Rawnsley *et al.*, 1998) are systematic extensional veins 1mm or less in thickness filled by fine-grained sparry calcite. They take the form of numerous closely-spaced veins (Fig. 2.9) and are linked to the initial stages of basin opening. They are mostly sub-parallel or slightly oblique to the later, vein-filled extensional joints that were formed during the main phase of rifting. The micro-veins strike approximately WNW-ESE (*i.e.* sub-parallel to the basin margin) and are sometimes traceable for tens of metres along strike. The vertical extent of the micro-veins is controlled by the thickness of the brittle limestone beds containing them, and they taper at the limestone-shale contacts, indicating a contrast in mechanical properties. Caputo and Hancock (1999) argue that they were formed by the '*crack-jump*' mechanism. This process is governed by the contrast in strength between the host micritic limestone and the sparry calcite vein filling. If the sparry calcite vein has lower strength than the surrounding micrite, the next rupture will occur inside the vein and the process of crack-seal will occur, but if the sparry calcite is stronger than the surrounding micrite, the next fracture will form at a discrete distance away in the host rock. This is the process of crack-jump. They argue that in this process cracks dilate, fill and seal in a series of rupturing increments and that the remote stress shows cyclic behaviour.



Figure 2.8 *Mud volcano at Kilve. The WNW-ESE striking micro-veins, are taken to be the manifestations of earliest extensional structures linked to the opening of the Bristol Channel. These cut across the mud volcano and are in turn cut by Alpine and post-Alpine joints linked to basin inversion and uplift.*

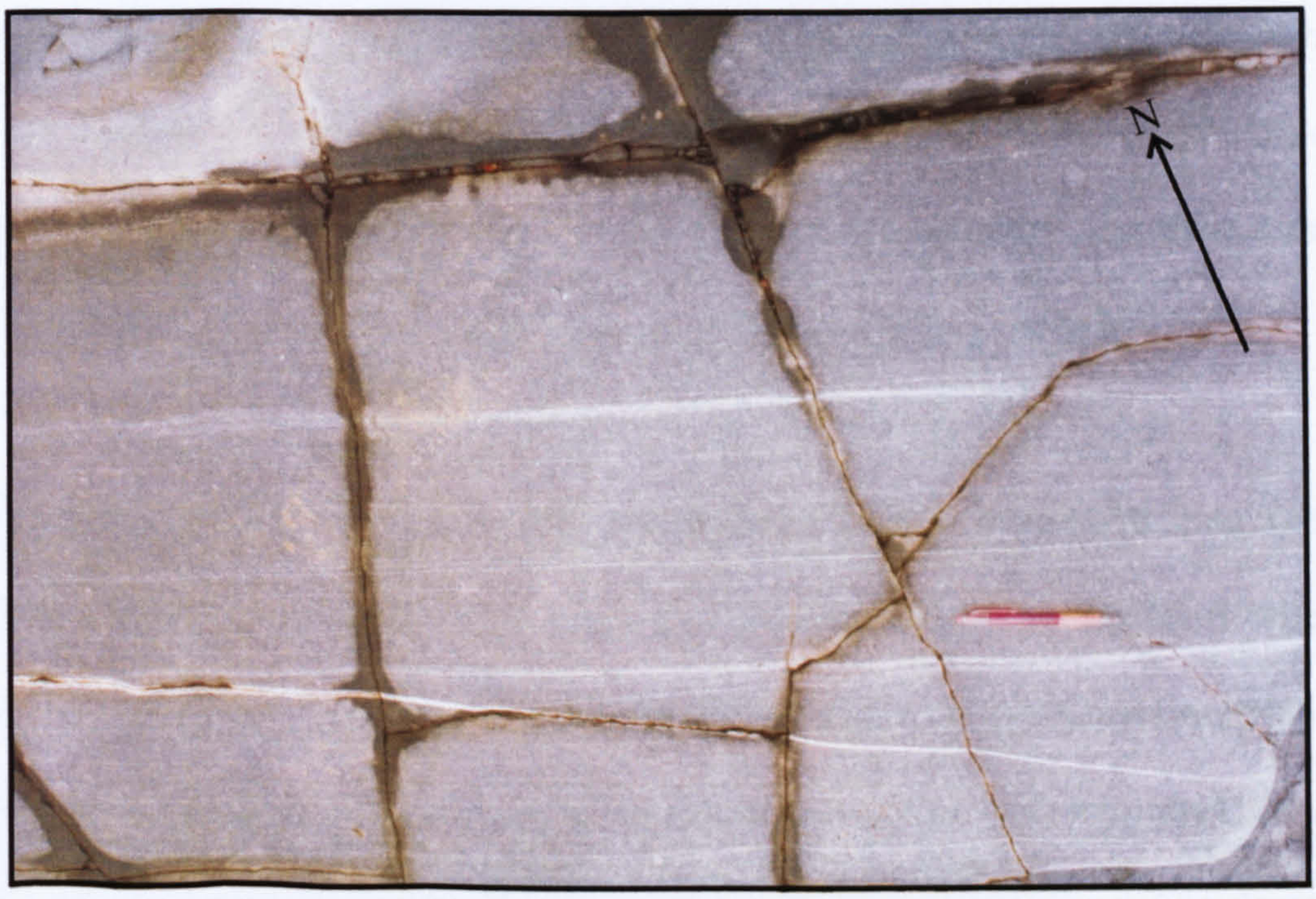


Figure 2.9 *Plan view of micro-veins exposed on a bedding surface and enhanced by differential weathering. When viewed in a vertical section, the veins can be seen to taper out as they approach the limestone-shale interfaces.*

The synthetic faults in the area which define the basin margin are north-dipping normal faults. South-dipping antithetic faults have affected the Lias rocks. Normal faults within the Lias mostly have a listric profile. Some of the north-dipping faults show accommodation structures such as drag folds in the hanging-wall and footwall (synclines and anticlines respectively), as seen at grid reference 148445. Most north-dipping normal faults occur as narrow zones and some faults show brecciation and other evidence of shearing.

As noted above the limestone beds accommodated deformation by brittle fracturing which divides the rocks into discrete blocks, the spaces between which have become infilled with vein material. The shale beds behave in a ductile manner and in most places veining terminates at the limestone-shale contacts. The overall dip of the faults generally depends on the ratio between the thickness of the competent limestone beds and that of the incompetent shale beds (growth ratio) as can be clearly seen on the cliff exposures. There is overwhelming field evidence to suggest that the normal faults were formed by the oblique linkage of veins in adjacent limestone beds.

Measurements of 12 major normal faults were made along the southern margin of the Bristol Channel. Synthetic faults now dip between 48°-57° to the NNE whereas antithetic faults dip between 49°-75° to the SSW (Fig. 2.10). As noted briefly above, the location of some major normal faults appears to coincide with important Variscan thrust faults and it is thought that these thrust faults were reactivated as down-dip faults during the extension associated with basin formation (Dart *et al.*, 1995). The extension direction of the basin, deduced from the calcite fibres that grew normal to the joint walls, indicates an opening direction between 5° and 20°. However, some of

the calcite fibres are oblique to the joint walls, suggesting a sinistral transtensional sense of opening (Fig. 2.11).

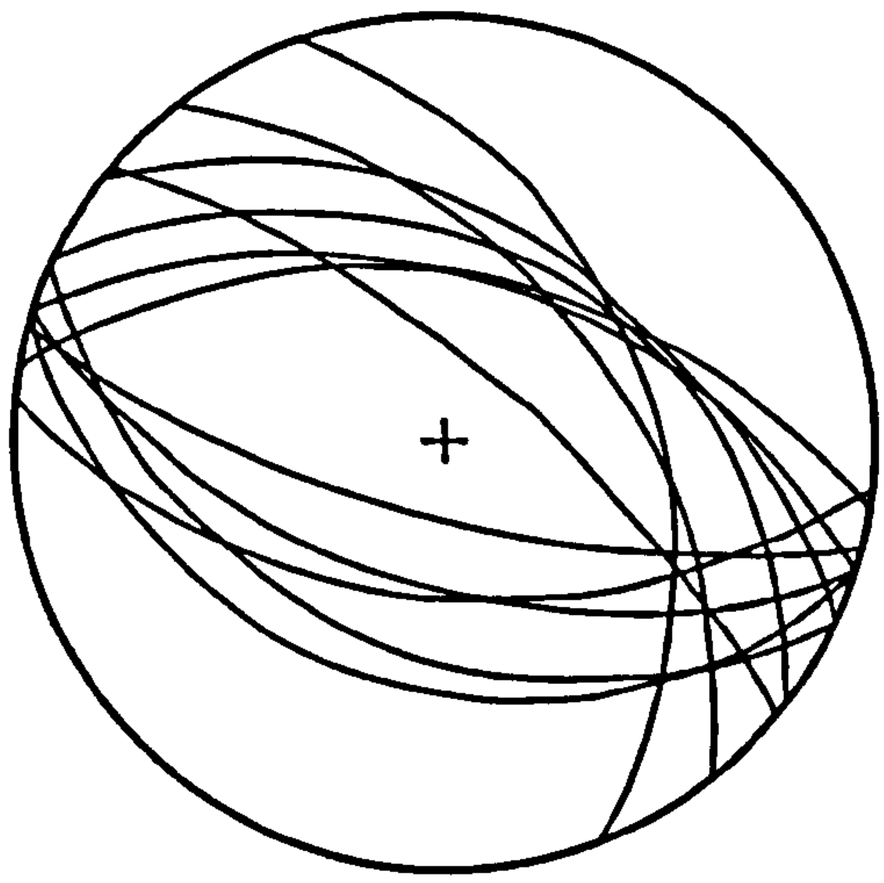
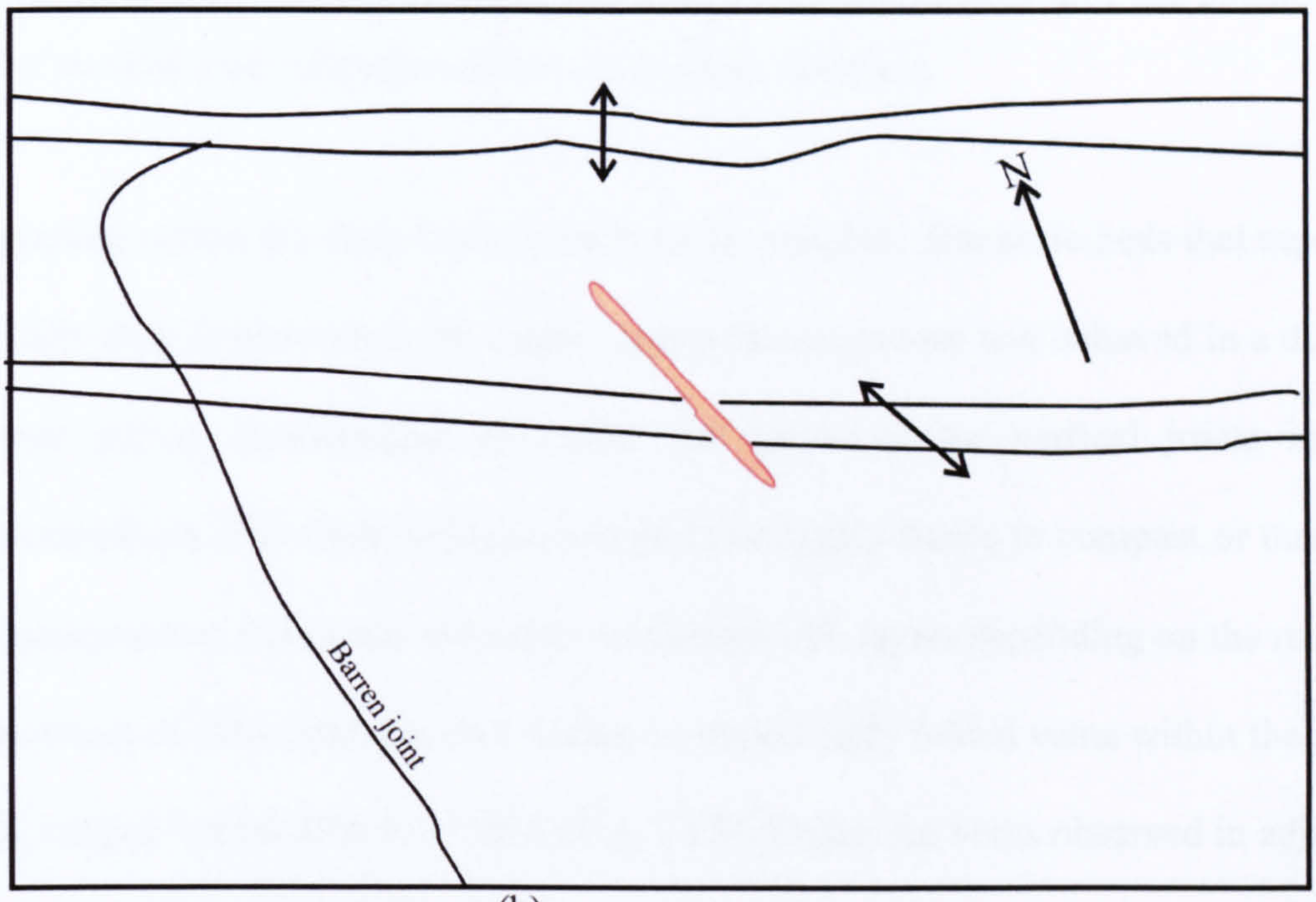


***Figure 2.10** Lower hemisphere stereographic projection of the normal faults from the southern margin of the Bristol Channel Basin. Note that the antithetic faults have a steeper dip than the north dipping, synthetic basin- bounding faults.*

At Kilve Beach, folded extensional veins occur in the hanging-walls of the normal faults. The folds have sub-horizontal axes and they were formed as a result of vertical compaction of the sediments subsequent to vein formation. A vertical shortening within the micritic limestones in the hanging-wall of these normal faults as deduced from these folds ranges from 6.9% to 10.15%. This value may have been slightly affected by the removal of limestone along bed-parallel fractures (strylolites) because of overburden pressure (Fig. 2.12). Nemčok and Gayer (1996), working in a different locality on the northern margin of the Bristol Channel Basin, calculated shortening using folded calcite veins and obtained values between 50% and 75%. Flattening of the competent limestone beds during this event took place partly by pressure solution (Fig. 2.12).

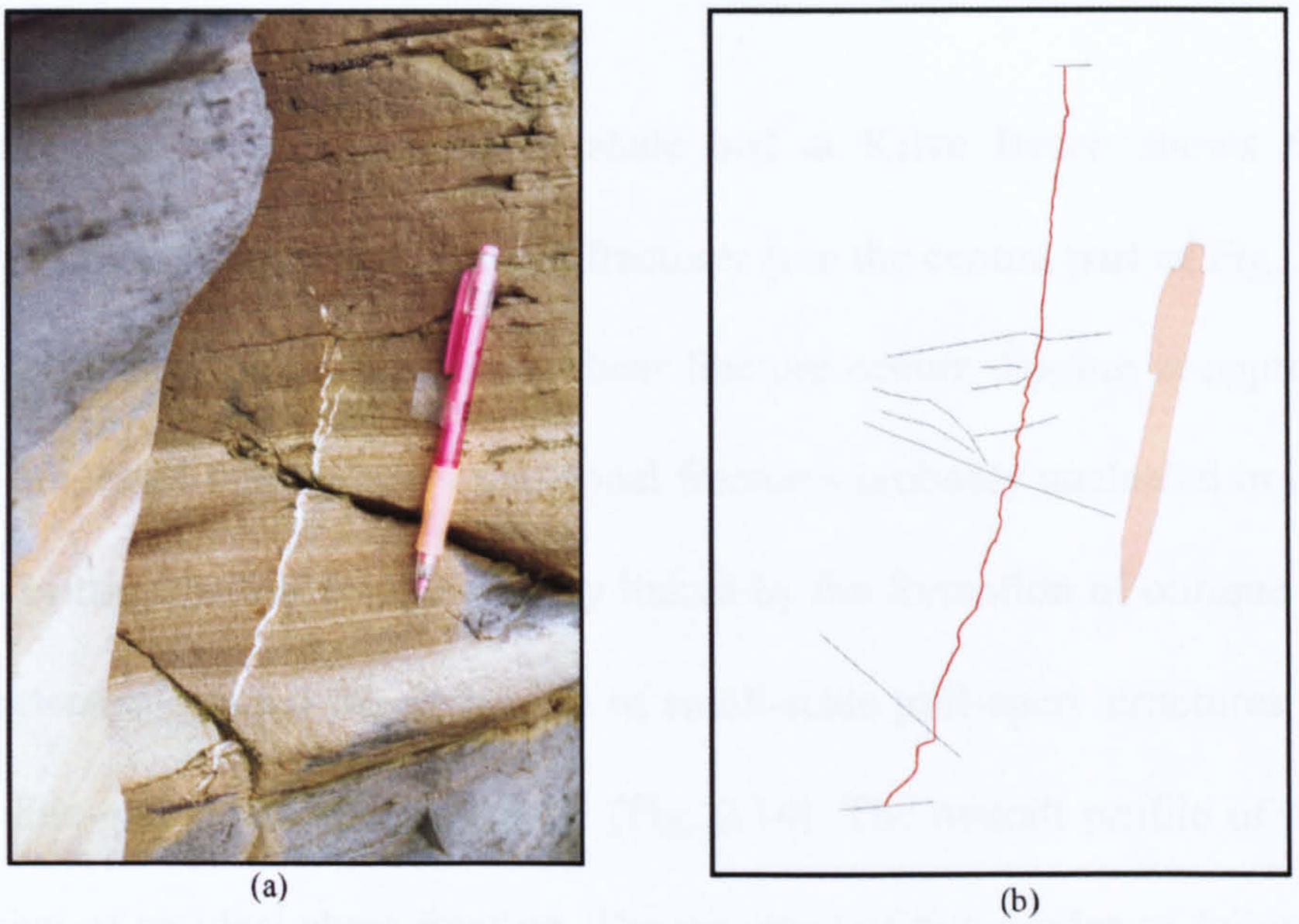


(a)



(b)

Figure 2.11 *(a) Photograph and (b) line drawing of veins formed during basin opening. Arrows in the line drawing which are parallel to the calcite fibres of the vein infill indicate pure extension during the formation of the upper vein and sinistral transtensional opening during the formation of the lower vein.*



(a) (b)

Figure 2.12 *(a) Photograph and (b) line drawing of tightly folded vertical calcite vein within 30cm thick calcareous shale bed from Kilve beach. Note how the calcite vein tapers on both ends as it approaches the bedding interface.*

Shortening within the shale beds is much more complex. The shale beds that separate the individual limestones in the region appear homogeneous and behaved in a ductile manner during layer-parallel extension that produced the vertical joints in the limestone beds. The shale varies in texture from highly fissile to compact or massive and composition from mud and silt to calcareous rich layers depending on the relative proportions of carbonate and clay. Using asymmetrically folded veins within the shale beds, ranged from 6.45% to 12.26% (Fig. 2.13). Unlike the veins observed in adjacent competent limestone beds, which are normal to the bedding, veins in shale beds are oblique. These veins may have formed by the linkage of vertical extension joints in two adjacent limestone beds by the formation of oblique fractures within the shale beds that separated them. During vertical compaction of the sediments these inclined veins which were oblique to the vertical overburden stress shorten by forming asymmetric folds (Fig. 2.13).

Close inspection of one 80cm thick shale bed at Kilve Beach shows failure by extension and the formation of vertical fractures (see the central part of Fig. 2.14). On the right hand side the photograph, a shear fracture occurs dipping at approximately 60°. It is suggested that vertical extensional fractures probably nucleated in individual relatively brittle layers and subsequently linked by the formation of oblique fractures. Further extension caused the formation of small-scale pull-apart structures that were filled by fine-grained crystalline calcite (Fig. 2.14). The overall profile of the failure plane is that of an ideal shear fracture. The presence of two modes of failure, namely failure by extension and by shear, require, that the differential stress was less than 4 times the tensile strength of the rock in the first case, and in the second case that the differential stress was greater than four times the tensile strength (Cosgrove, 1997). If as suggested, the initial extensional fractures form in slightly more calcareous horizon within the shale then it can be argued that the differential stress was less than four times the tensile strength of the horizon but more than four times that of the intervening weaker less carbonate rich parts of the shale. The links between extensional and shear failure are beyond the scope of this discussion and the reader is referred to Cosgrove (1997).



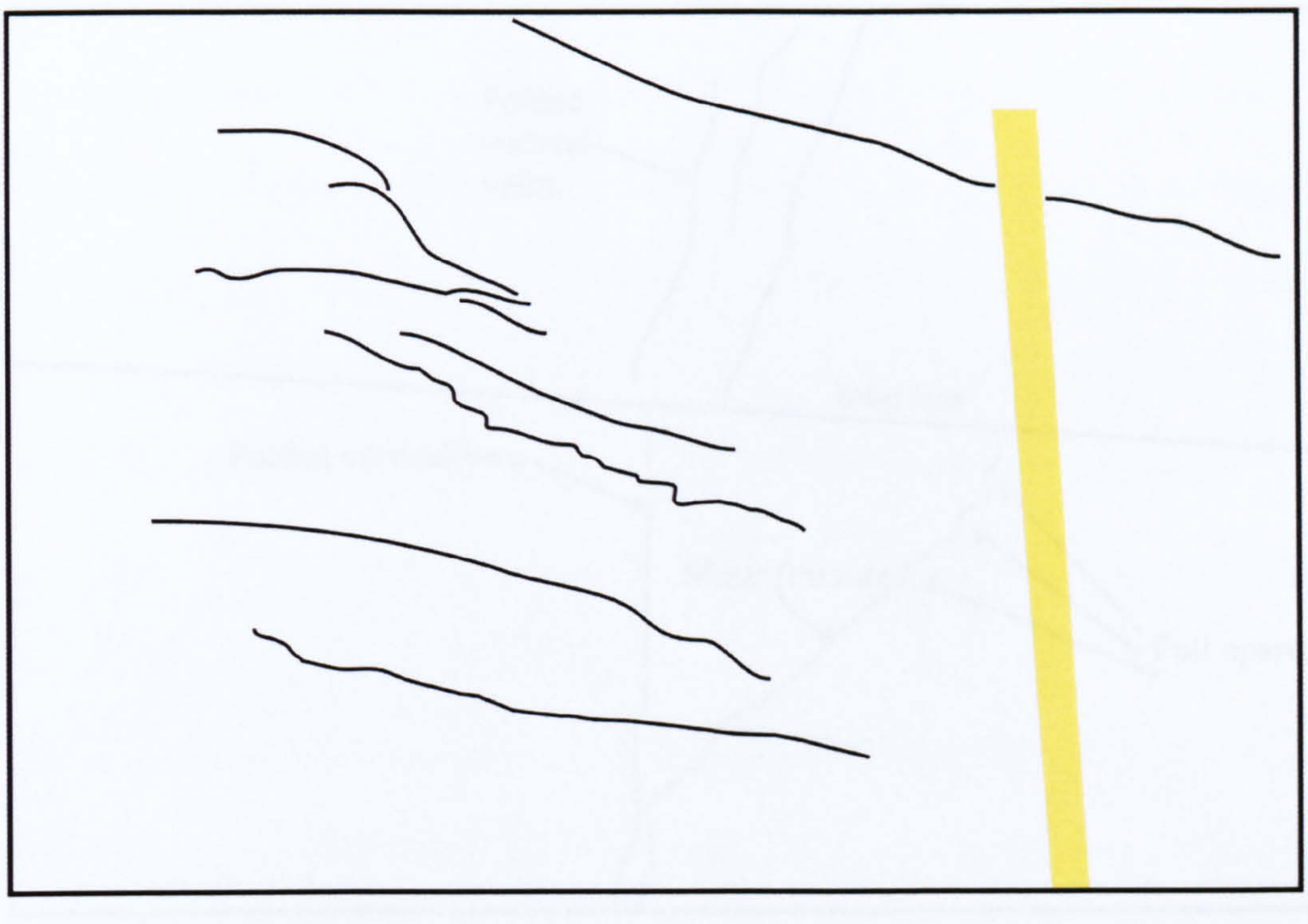
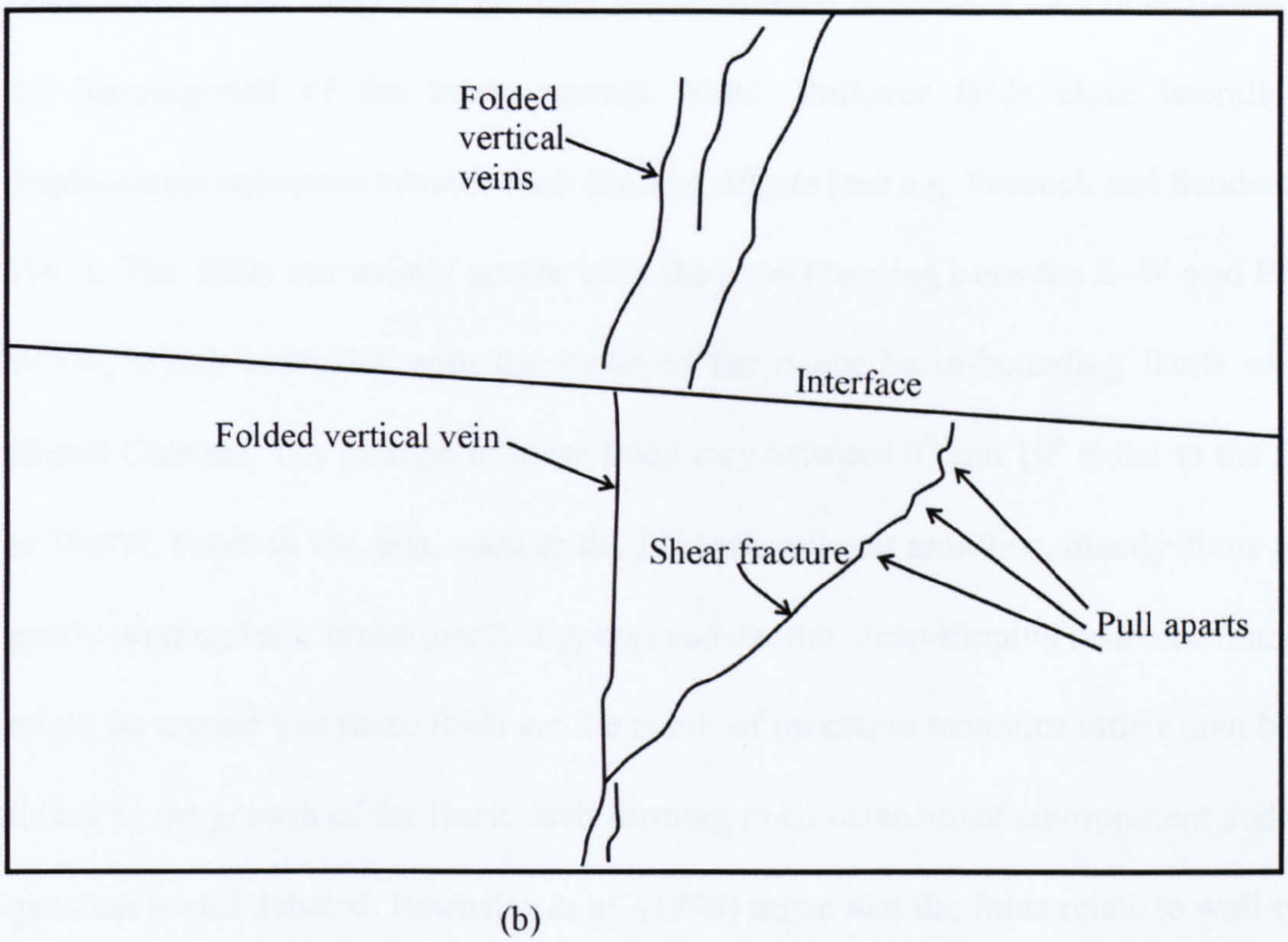


Figure 2.13 *(a) Photograph and (b) line drawing of calcite vein within shale beds on the hanging-wall of a normal fault from Kilve Beach. Note that the veins are oblique to the bedding planes and to the vertical overburden stress which caused these to fold. As a result the folds are asymmetric. Scale bar on the right is 30cm long.*



(a)



(b)

Figure 2.14 *(a) Photograph and (b) line drawing that show how subtle changes in lithology affect the response of the shale to the overburden stress during basin opening. Note the development of pull-aparts within an apparently homogeneous shale bed.*

2.4.2.2 Structures associated with the Alpine Orogeny

By the end of the Cretaceous and Early Tertiary, the Bristol Channel Basin had been inverted as a result of N-S directed compression linked to the Alpine Orogeny. The tectonic history of the Kilve and Watchet areas has been discussed by Dart *et al.* (1995) who argue that all faults in the area operated as a coherent system both during the extension and the subsequent compression. A few of the E-W trending faults show evidence of multiple slip direction (*i.e.* dip-slip to strike-slip through oblique-slip orientations) indicating that they were re-utilised by different stress fields at different times.

2.4.2.2.1 Folds

Folds occur in the study area and they are interpreted as rollover anticlines formed in the hanging-wall of the listric normal faults. Rollover folds close laterally as displacement decreases towards fault tips and offsets (see *e.g.* Peacock and Sanderson, 1991). The folds are mostly gentle with the axes trending between E-W and ESE-WNW, which coincides with the strike of the major basin-bounding faults of the Bristol Channel. The plunges of these folds vary between 0° and 10° either to the ESE or WNW. Folds in the area, such as the Lilstock rollover anticline, mostly show long gently-dipping back limbs (north-dipping) and shorter steep-dipping southern limbs. It might be argued that these folds are the result of inversion tectonics rather than being linked to the growth of the listric fault forming in an extensional environment and this question is still debated. Rawnsley *et al.* (1998) argue that the folds relate to wall-rock deformation around E-W striking normal faults (*i.e.* that they are rollover folds), but were tightened during the N-S Alpine compression. One of the best-exposed anticlines opposing limbs dipping to the NNE and SSW occurs at Kilve (Fig. 2.15). The fold is gentle with a horizontal fold axis trending 100°. The fold has a wavelength of about

50m and a strike length of over 80m. The joints in the hinge zone are parallel to the fold axis and surface features on these joints indicate that they were propagated by mode I failure (*i.e.* they are extensional joints). However such fold geometry and fractures could have been formed in association with a rollover fold or a buckle fold linked to inversion. The present author notes that the fact that the northern limb of the fold dips significantly indicate that even if the fold was originally a rollover fold, it has subsequently been amplified by the Alpine inversion. Rollover fold geometry is characterised by sub-horizontal limbs and an inclined limb that dips towards the normal fault.



Figure 2.15 *Gently folded alternating limestone and shale beds at Kilve. Note that the joints strike parallel to the fold axis indicating that they are fold-related. View is looking towards ESE.*

2.4.2.2.2 Thrust faults

Thrust faults usually propagate along, or at a low angle to, the bedding. Sometimes they cut across the bedding, the fault plane dipping at approximately 30° and forming a '*ramp.*' Dewey (1982) argued that the lower parts of listric normal faults are convenient zones of weakness for the nucleation of thrust faults during an episode of basin inversion. The lower parts of listric normal faults at depth that dip at around 30° act as the perfect zone upon which thrust faults can initiate. The condition required for reshear occurs when the shear stress (τ) acting along the fault is sufficiently large to overcome the frictional resistance to sliding and the cohesive strength across the fault. If this cohesion is negligible then the condition for reshear is given by (Amonton's Law):

$$\tau = \mu\sigma_n \qquad (2.1)$$

where μ is the coefficient of sliding friction and σ_n is the normal stress acting on the plane. For failure to occur in an intact piece of rock, the shear stress on the potential shear plane has to satisfy the Navier-Coulomb criterion for shear failure as given by the equation:

$$\tau = C_o + \mu\sigma_n \qquad (2.2)$$

where C_o is the cohesion.

According to the Navier-Coulomb criterion of failure, faults develop at approximately 30° to the maximum principal stress (σ_1). Therefore ideal normal and thrust faults will have a dips of 60° and 30° respectively (Fig. 2.16a and b). It is possible for listric normal faults to reactivate as reverse faults or 'thrusts' as long as the condition represented by equation 2.1 are reached before those represented by equation 2.2. The

condition for the reactivation of old fault in preference to the generation of a new fault has been discussed by Sibson (1985).

In the study area, the pre-existing listric normal faults were reactivated as reverse faults and some new reverse faults (thrusts) may have formed during Cretaceous-Tertiary inversion. Normal faults in the area show reverse and strike-slip reactivation caused by the Cretaceous to Tertiary compression (Peacock and Sanderson, 1991; Nemčok *et al.*, 1995; Nemčok and Gayer, 1996; Engelder and Peacock, 2001).

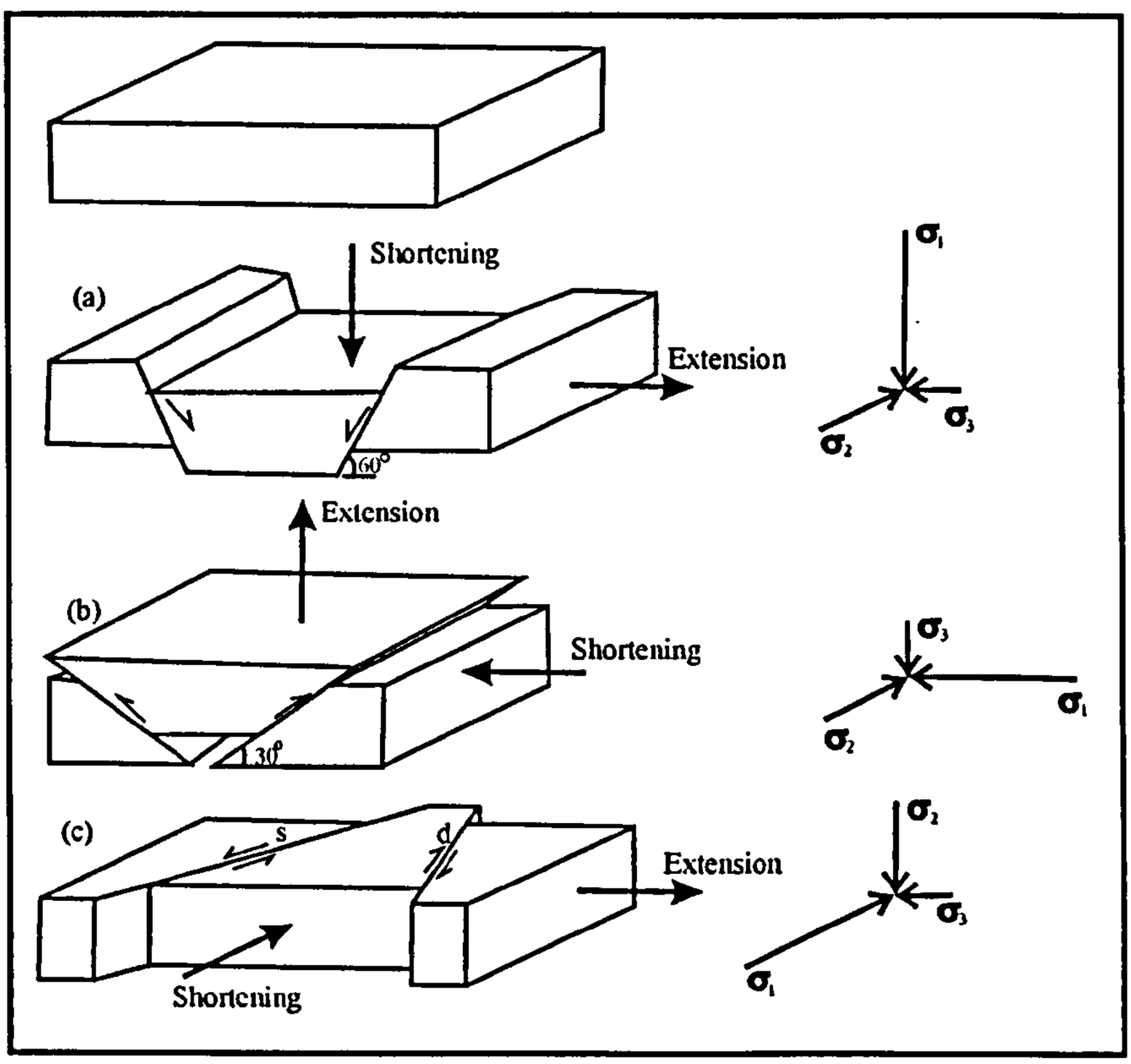


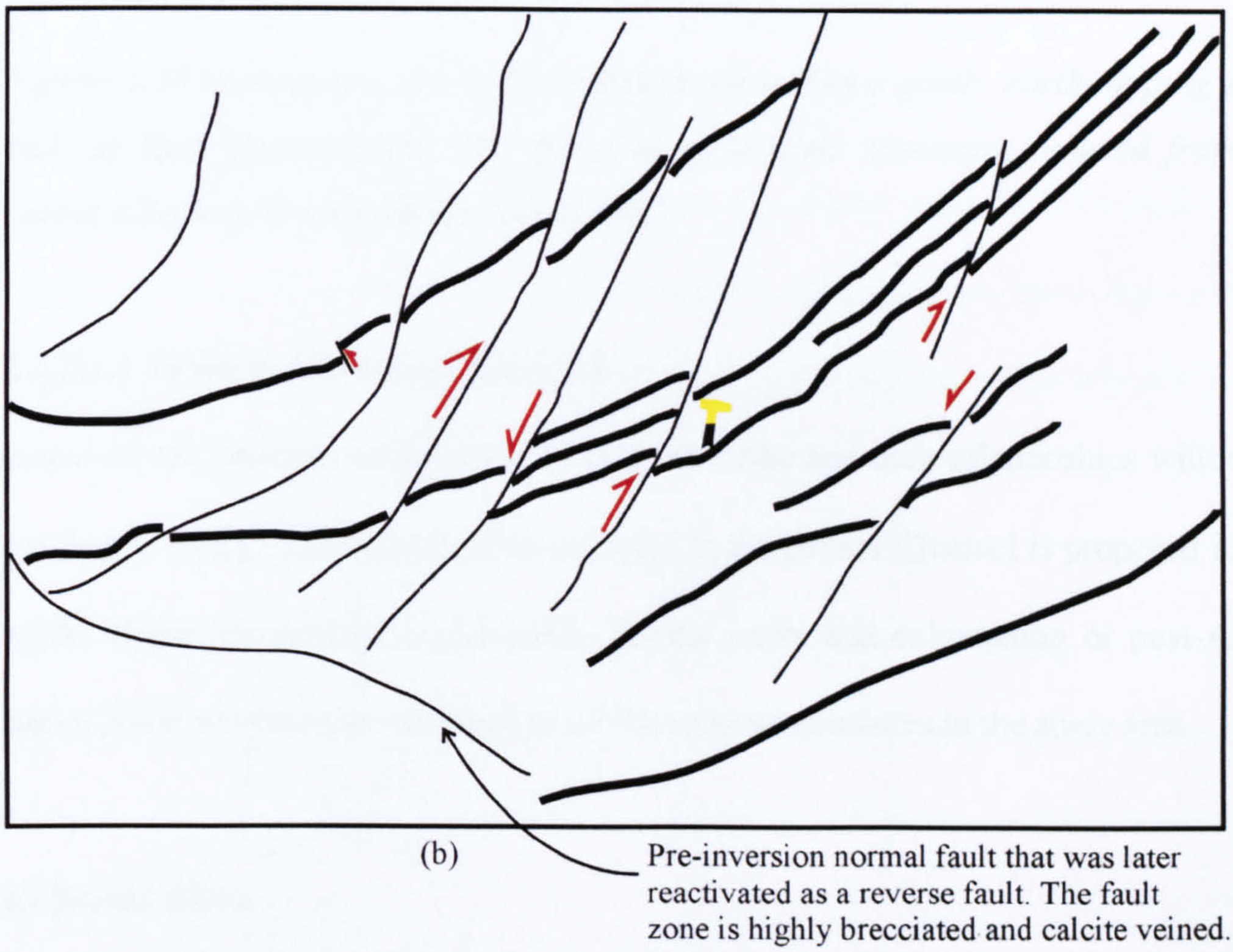
Figure 2.16 *Block diagrams showing the stress regimes associated with the formation of (a) normal (dip approximately 60°) (b) reverse (dip approximately 30°) and (c) strike-slip faults. Note that d and s denote right and left handed sense of displacement (modified from Blés and Feuga, 1986).*

The author has also observed evidence for reactivation of a normal fault at East Quantoxhead (GR 136443) shown in Fig. 2.17. This is an antithetic fault dipping 49° to the SSW beneath the headland. The cliff provides exposures of Lias and the full extent of the hanging-wall and footwall of this major fault is exposed. Beds in the footwall are relatively undeformed and show a slight antiformal flexure near the fault. In the hanging-wall, a number of meso-scale structures occur. The beds are folded into an open syncline with an axial plane sub-parallel to the fault. These features are compatible with normal movement on the fault. However there is also clear evidence for inversion. For example, a series of small-scale synthetic faults occur in the hanging-wall. Some of these have been partially inverted as can be seen from the displaced marker horizon. Inspection of the Fig. 2.17 shows that the shale beds are thicker in the hanging-wall of the inverted normal faults. The bedding in the hanging-wall defines a box fold. This geometry is not characteristic of a rollover fold and was probably generated by subsequent inversion. Small-scale accommodation structures commonly observed in the hinges of these box folds include small-scale thrusts. It can be noted from Fig. 2.17 inversion occurred on the pre-existing normal faults developed as back thrusts during Alpine compression on the hanging-wall of the pre-existing antithetic normal fault.

In some cases the thrust faults have exploited the pre-existing planes of weakness such as the fissility within the shale beds. These incompetent beds are the ideal rock within which to propagate thrust faults. An example is shown in Fig. 2.18. The shale bed is gently-dipping to the north. From calcite striations on the thrust plane, a general southward-direction of tectonic transport can be inferred.



(a)



(b)

Figure 2.17 *(a) Photograph and (b) line drawing of ESE-WNW striking pre-inversion normal fault at East Quantoxhead that was probably reactivated later as a high-angle reverse fault (see text for explanation). Note the hammer at the centre for scale.*



Figure 2.18 *Photograph of a bed-parallel thrust within a gently north-dipping shale beds at East Quantoxhead. The direction of tectonic transport deduced from the calcite striations is towards the SSE (170°).*

2.4.2.2.3 Joints in the Bristol Channel

Based on the presence or absence of infill, the strike and their relationships with other structures, a three-fold classification of joints in the Bristol Channel is proposed in this work. These are namely: burial joints, Alpine joints and exhumation or post-Alpine joints. Joints are the most abundant of all the tectonic structures in the study area.

(i) Burial joints

Bahat (1991) suggested that the history of burial includes sedimentation, downwarping and diagenesis and that the surface morphology of the joints may preserve features of the burial history which are distinct from subsequent tectonic events. Bahat (1999) proposed a method of distinguishing between single layer burial

joints and single layer uplift joints based on his work on the Beer Sheva syncline in Israel. Bahat points out that older beds fracture first during the burial history, and that the resulting joints tend to be closed and are commonly aligned parallel to fold axes. They also occur in orthogonal cross-fold sets. In contrast, uplift joints tend to open during exhumation. Burial joints in the Bristol Channel can be distinguished from the Alpine and post-Alpine joints (*i.e.* uplift joints) by being closed and healed or filled with calcite veins or injections of calcite and mud mixtures. In addition, they are mostly found in the vicinity of normal faults and along the axis of the anticline.

(ii) Alpine joints

Alpine joints in the Bristol Channel Basin are not mineralised and clearly formed after the normal faults that contain mineralization. This implies that fluid pressure was less important during Alpine jointing than during the earlier faulting (Rawnsley *et al.*, 1998). Inversion of the basin amplified the rollover anticlines and reactivated some of the pre-existing normal faults to create reverse, oblique-slip and strike-slip faults.

(iii) Post-Alpine

Joints of this age are the most abundant of all geologic structures in the Bristol Channel Basin and they are discussed in Chapter 4. They mark the last event in the Bristol Channel, namely the uplift and inversion that followed the Alpine Orogeny.

2.4.2.2.4 Strike-slip faults

NW-SE dextral strike-slip faults were formed in the basement during the later stages of the Variscan Orogeny (Whittaker, 1972; Holloway and Chadwick, 1986; Chadwick, 1993; Dart *et al.*, 1995). The sediments of the Bristol Channel Basin are

also cut by such faults and by their conjugate member. They may represent the result of the activity of Variscan transfer faults within the basement during both the Mesozoic and Tertiary (Brooks *et al.*, 1988; Chadwick, 1993). Al-mahruqi (2001) reported extensional fractures oriented N-S to NNE-SSW associated with the strike-slip faults displaces the alpine joints. These are commonly filled with coarse-grained calcite veins at Kilve Beach and East Quantoxhead (this work).

2.5 Summary

2.5.1 Pennines

The exposures in the Pennines field area, North Yorkshire, are located inland. The exposures are monotonous and tend to be located in the vicinity of faults. These limestone outcrops have been subjected to a long period of erosion and dissolution. Joints were further opened wide by subaerial karstic solution and the rounding of blocks and the development of runnels confuse the angular resolution of the fractures which is also disturbed by physical breakdown and vegetated potholes. For these reasons, it was only possible to find a limited number of sites suitable for measuring scan lines and window samples. Nevertheless, it proved possible to gather some useful information regarding the evolution of joint spacing in the massive- to thickly-bedded limestone beds in the area. It has been shown that the pattern of their formation is compatible with the Variscan stress field that governed their formation.

2.5.2 The Bristol Channel Basin

Based on field studies by the author and those of Dart *et al.* (1995), the chronology of events linked to the evolution of the Bristol Channel Basin can be divided into three stages:

1. The development of an E-W trending normal fault system in response to N-S directed extension which started in the Permian and continued until the Cretaceous. Some of the features formed during this period of basin opening were linked to the local development of high fluid overpressures. They include mud volcanoes, micro-veins (Caputo and Hancock, 1999) or high-density veins (Rawnsley *et al.*, 1998) and vein-filled joints (*i.e.* burial joints or veins) in the vicinity of the faults and in the outer arcs of rollover folds.

2a. N-S oriented Alpine compression led to the amplification of the pre-existing rollover folds, partial reactivation of the pre-existing normal faults as reverse faults, the nucleation of thrusts in the deeper, low-angle segments of listric faults and the propagation of fold related Alpine joints (discussed in Chapter 4).

2b. The formation of NW-SE striking dextral and NE-SW striking sinistral strike-slip faults (as a result of continued N-S compression at the late stage of Alpine inversion) and the subsequent uplift, and the formation of post-Alpine joints.

CHAPTER THREE

CONTROLS ON JOINT SPACING AND THE RELATIONSHIPS BETWEEN JOINTS AND OTHER STRUCTURES

3.1 Introduction

In this chapter, the literature on the current understanding of the controls governing joint spacing and, in particular, the relationships between joint spacing and bed thickness, and the mechanisms of joint initiation and propagation are reviewed. Joints are intimately associated with the formation of various structures in the Earth's crust such as folds and faults and the development of folds is often dominated by fracturing and faulting (Couples *et al.*, 1998). Joints are between 10^2 to 10^5 times more abundant than faults (Hancock, 1994; Caputo and Hancock, 1999). Because of the abundance of joints compared to other structures and their practical importance in controlling rock strength, permeability and secondary porosity, the localising of mineral deposition and accumulation of hydrocarbons, joints have been and remain a subject of fundamental interest for a large group of geoscientists. Joints are particularly important palaeo-stress indicators because they have a definite geometric relationship to the stress fields that form them.

3.2 Controls on fracture spacing

Layer normal joints that form as a result of layer normal compression have been discussed by numerous workers (*e.g.*, Ramberg, 1955; Kidan, 1982; Kidan and Cosgrove, 1996). The process may be associated entirely with brittle deformation or, as in the example of boudins, where relatively competent beds are sandwiched between two less competent beds, a combination of both brittle and ductile behaviour may be involved. Ramberg (1955) was the first to produce boudins experimentally

using putty to simulate the incompetent layers and modelling clay, plasticine and cheese to simulate the competent layers. He argued that fracturing of a competent layer between two relatively incompetent layers is the result of stress transfer from the matrix to the competent unit. In his work on boudinage he argues that the basic reason for boudinage is the difference in competency between the layer and the surrounding rocks. The elastic displacements of the layer and matrix are different because of the difference in material properties. Hobbs (1967) suggested that because of the differences in material properties the displacements in the jointed rock and the neighbouring matrix will be different. The stress-strain curve for the incompetent unit has a lower gradient (*i.e.* lower Young's Modulus) than the competent layer and the matrix will therefore show greater displacements (Lloyd *et al.*, 1982). For layers under an applied normal load, '*stress transfer*' theory predicts that the tensile stress increases from the minimum at the end of the segment to a maximum at the centre (Hobbs, 1967; Lloyd *et al.*, 1982; Ji and Saruwatari, 1998). According to the theory, this process of mid-point failure will continue until the layer is reduced to segments (boudins) all of which are shorter than some critical length (for which the tensile strength of the layer is equal to the tensile stress at the mid point).

In practice, although successive mid-point fracturing is controlled by material properties (tensile strength, elastic moduli), it is also influenced by local variations in lithology and major pre-deformation flaws that control the starting length of the layer segments (Lloyd *et al.*, 1982). The stress transfer theory implies that the fractures which define boudins occur sequentially so that inter-boudin gap width will be unequal (Lloyd *et al.*, 1982). Boudin width is a measure of the spacing of fractures and can be used synonymously with joint/fracture spacing.

In interbedded sedimentary sequences, it is commonly observed that joints are confined to the competent layers, whereas the incompetent bounding matrix is unfractured and acts as a mechanical layer boundary (Narr and Suppe, 1991; Gross, 1993). It has been argued that this indicates differences in mechanical properties between competent layer and the adjacent incompetent matrix. However, Teufel and Clark (1984) argue that fracture containment may be the result of low shear strength of the layer interface rather than any difference in material properties on either side of the interface. Narr (1996) has described fractured massive carbonates in which the fractures are generally through-going joints and do not appear to terminate at mechanical layer boundaries. These fractures typically terminate by the gradual tapering of their aperture which reaches zero towards their upper and lower terminations which generally do not coincide with any change in lithology or with any planes of weakness. In contrast, Ji and Saruwatari (1998) suggest that joints terminate at the contacts with the adjacent incompetent layers because the competent layer fails at much lower magnitudes of extensional strain compared to the incompetent layers.

Field observations, however, have shown that some fractures do continue from competent layers into the incompetent matrix and the fractures experience a change in strike and dip as they cross this interface. Lack of understanding of the factors controlling fracture initiation and propagation and of the variables involved during their evolution hinder our ability to predict the connectivity/permeability of fractured rocks. In this section it is therefore apposite to review literature on fracture initiation and propagation and the relationship between joint spacing and bed thickness. Because of the intimate relationship between joints and other structures, some of the

literature in which these relationships are described is discussed at the end of this chapter.

3.3 Joint initiation and propagation

Fracture initiation is defined as a failure process by which the pre-existing cracks in a material start to grow whilst fracture propagation is a failure process by which the pre-existing cracks grow subsequent to fracture initiation (Whittaker *et al.*, 1992). In an attempt to determine the point of initiation of joints in rocks several workers have used natural analogues such as polygonal cooling cracks in basalts (DeGraff and Aydin, 1987; Aydin and DeGraff, 1988), fractured permafrost, natural mud cracks, and crevasses in glaciers (Lachenbruch, 1961), analogue modelling (Ramberg, 1955; Kidan, 1982; Rives *et al.*, 1992; Kidan and Cosgrove; 1996), starch desiccation (Müller, 1998 and 2001, Müller and Dahm, 2000), theoretical studies (Hobbs, 1967) and numerical analyses. The literature on the numerical modelling of crack initiation and propagation goes beyond the scope of this work.

Mud cracks have generally been envisaged as downward propagating fractures that nucleate from the surface and terminate at a depth where the horizontal stress acting within the sediments becomes compressive. The result of laboratory experiments using a uniform mud layer on either glass or wooden substrates (Corte and Higashi, 1960) show that cracking starts from the centre of the desiccated layer and propagates either upward to the surface or downward to the bottom with non-uniform speed. These experiments were carried out on a single desiccated layer with a uniform grain size. In nature clastic sediments tend to be sorted by gravity and show stratification and fining upwards. Corte and Higashi's experimental result is contrary to the field

observation on natural mud cracks by Weinberger (1999) in the Dead Sea region, Israel, who used plumose structures to deduce initiation points and direction of propagation of the cracks. His study showed that cracking began at the bottom of the layers and propagates upwards until the plume axis branches into horizontal axes.

Analogues for modelling fracture initiation and propagation include the simulation of basalt cooling joints by the desiccation of mixtures of starch and water (Müller, 1998 and 2001, Müller and Dahm, 2000). Their experiments clearly indicate that the cracks develop from the surface and propagate into the interior. Müller (2001) found a remarkable similarity between cracks in starch-water mixtures (Poisson ratio approximately 0.5) and burial joints that form in the early stages of lithification when sediments still have significant water content. Despite the geometrical similarities, they argued that the mechanisms of joint formation in basalts, desiccation-related contraction in starch and also in sediments are different.

Surface features on joints in outcrops indicate a point origin for the site of fracture initiation and propagation parallel to the bedding (*e.g.* Hodgson, 1961; Bahat and Engelder, 1984; DeGraff and Aydin, 1987; Pollard and Aydin, 1988; Helgeson and Aydin, 1991; Wu and Pollard, 1995; Weinberger, 2001; Belayneh and Cosgrove, in prep.). Field observations in the Appalachian Plateau (Bahat and Engelder, 1984; Helgeson and Aydin, 1991) show that initiation points on joint surfaces in siltstone and shale turbidite sequences are almost always at the bedding interface. Bahat and Engelder (1984) suggested initiation of joints in siltstones mostly occurs at the bottom of the layer in contrast to the shale beds where cracks initiate at the top. Although this is in agreement with field observations made by Weinberger (1999) in the Dead Sea, it

is contrary to earlier suggestions by Hobbs (1967), Corte and Higashi (1960) and the observations by the present investigator from observations of outcrops of limestone beds on the southern margin of the Bristol Channel Basin (see Fig. 5.9 in Chapter 5) which indicate that most joints originate from the middle of the layer and propagate parallel to the beds. It has been proposed that initiation of fractures at the layer edges may occur as a result of some local inhomogeneity such as an elliptical cavity, a fossil, a mineral inclusion, burrows along bedding interfaces and sole marks with sharp cusps which act as sites of stress concentration at which joint initiation can occur (Pollard and Aydin, 1988; Helgeson and Aydin, 1991). These flaws are more abundant towards the bottom of a bed as a result of natural gravitational sorting of the grains (Weinberger, 1999).

Weinberger (2001), in his detailed field investigation of the dolomites of the Judea Group in the Dead Sea region in Israel, studied the distribution of cavities. He showed how the size, shape, orientation and distribution of cavities within a rock mass determined fracture initiation. Fracture initiation points for joints were found to be relatively large, isolated cavities near or at the top of a layer. It was found that for fracture initiation from cavities, it is necessary for them to be above a *'critical size'*. In the absence of macroscopic cavities, joint initiation points were located along bedding interfaces and other irregularities (mentioned above). He also noted that joint propagation was impeded by the bedding planes between the dolomite layers.

Helgeson and Aydin (1991) point out that in layered sedimentary rocks the interfaces between dissimilar layers play a fundamental role during joint propagation, limiting the vertical extent and physical continuity of joints. They suggest that there is

mechanical communication between adjacent fractured layers when no intervening incompetent layer is present and that the presence of thin shale layers inhibits fracture propagation. If the shale layer is relatively thick compared to the thickness of the fractured layer, the communication between joints in the fractured layers may be absent and the two layers may fracture quite independently of each other. Field observation of rocks in the Genesee Group in the Appalachian Mountains led them to conclude that the amount of stress transfer taking place without dissipation depends on the strength of the interface and, the stiffness and the thickness of the shale layer.

In this section the distribution of joints in 2D is now discussed. The distribution data *e.g.* joint spacing, joint length, joint density and joint apertures can be plotted as histograms. Each of these sets of data have certain characteristics such as the position of their mid-point, median and mode, the amount of spread and the symmetry of distribution (*i.e.* the data may have a positive or negative skew). Measurements of large samples drawn from a population produce a characteristic frequency distribution. Most values are clustered around the central value or the mean and the frequency declines symmetrically away from this point. A graph of such a distribution has a bell-shape and is called a normal or Gaussian distribution. It is assumed that random variables (perturbations) are statistically normally distributed and analyses of field data by geoscientists working on various aspects of joints such as joint length, joint number, joint spacing and joint apertures are based on this assumption. Some results from field observations and analogue modelling are presented below.

Hudson and Priest (1979) studied the intersections of joints along a 1D transect (a scan line) through a rock mass. They showed that for a limited number of sets of

discontinuity, the discontinuity frequency is a function of the scan line orientation. The scan line method was later extended to 2D and 3D to generate fracture trace maps by making the assumption that the fractures encountered along the scan line are persistent. The results were also used for plotting frequency distribution curves and for calculating block areas and block volume in quarries and mines (*e.g.* Hudson and Priest, 1979; Wang *et al.*, 1991; Wang, 1992; Wang *et al.*, 1992).

Segall and Pollard (1983) made detailed field maps of single, steeply dipping joint sets in granitoid rocks of the Sierra Nevada, California. The joint lengths vary from 1cm to nearly 70m. The joints were filled by epidote and chlorite almost immediately after their formation. Segall and Pollard argued negative exponential function adequately represents the length mapped joints. However, the exponential function predicts only 10^2 cracks with lengths in the range between 0.01m to 1.0m. Extrapolating the result to the power-law, they predicted $4*10^4$ cracks. Thus, they concluded that the power-law provides a better fits to the length distribution of the data.

Power-law distribution can be written as:

$$f(l) = c.\, l^n \qquad (3.1)$$

Where l is the joint length, $f(l)$ is the number of joints with a length l, and n is the power-law exponent often termed the fractal dimension of the distribution. Gillespie *et al.* (1993) argue that *fractal* geometry does not depend on scale. If this is so, then at all scales between the upper and lower fractal limit the geometry will be *'self similar'* *i.e.* any portion of the system is a scaled down version of the whole. They also argue that a feature of such geometry is that the relative numbers of large and small

elements within it remains the same at all scales. As a result the size-frequency distribution of a portion or elements of such a system obeys a power-law and this scaling relationship is defined by its fractal dimension.

Van Dijk *et al.* (2000) studying joints from Monte Alpi region of southern Italy demonstrated a consistent power-law distribution when plotting fracture frequency versus length. These measurements range in scale from thin sections, through core, rock slabs, vertical sections and walls, geological maps and 3D seismic maps.

In order to understand the evolution of the different distribution patterns shown by joint spacing (negative exponential, Gamma, log-normal, normal and power law distributions) (Fig. 3.1) attempts have been made to relate these patterns to specific geometric features or some mechanism of formation. Rives *et al.* (1992) have used analogue models and numerical simulation to explore this problem. The analogue models involved the bending of a polystyrene plate while maintaining a constant radius of curvature. The extension of the outer surface under conditions of plane strain thus model those of cylindrical folding. Their study showed that joint spacing generally evolves from an initially negative exponential to log-normal and finally to normal distribution with increasing joint development and/or deformation. Negative exponential, log-normal, normal and Gamma distributions are shown in Figs. 3.1(a) to (d).

Huang and Angelier (1989), in their study of tectonic extension joints and shear fractures from the Gulf of Suez and southeastern France, suggest that the distribution fits a Gamma distribution. They argue that the apparent fit with negative exponential distribution obtained by photo interpretation is caused by the limits of resolution (*i.e.*

the minimum size that can be observed). The probability density function for Gamma distribution is given by (equation 3.2):

$$f(x) = \frac{1}{\Gamma(\alpha+1)\beta^{\alpha+1}} x^{\alpha}\exp(-x/\beta) \qquad (3.2)$$

where Γ is the Gamma function, β controls the decrease of f value when $x > \alpha\beta$. According to these authors $x = \alpha\beta$ corresponds to the maximum value of f. When $\alpha =$ 0, the above equation reduces to a negative exponential distribution. It is interesting here to note that as α increases and β decreases, the distribution changes from Gamma to negative exponential distribution then to log-normal (Fig. 3.1d).

Ramberg (1955), in his pioneer experimental work, used layered cakes of putty, plasticine and cheese to simulate boudinage and pinch and swell structures. One dimensional compression was imposed, allowing compensating elongation in the other two dimensions. Ramberg demonstrated that the structures produced are strikingly similar to natural boudins and give information about the relative strength and ductility of the different layers. Ramberg noted that the tension created by plastic flowage in the weak layers not only forms boudins and pinch and swell structures, but is also an important factor localizing the growth of new minerals in inter-boudin necks and voids. Later, theoretical analysis by Hobbs (1967) showed that the frequency of occurrence of joints depends on the thickness and physical property of the layer, the physical property of the surrounding matrix and degree of tectonic deformation.

In the following section the distribution of data gathered by various geoscientists from fractured outcrops and analogue models will be considered. These distributions show a variety of patterns and, ideally, it would be useful to know what determines these

patterns, particularly if they relate to specific mechanism of joint formation or to the various stages in the build up (evolution) of a particular fracture set. The mechanisms that have been suggested for joint initiation and propagation are (i) mid-point bisection, (ii) semi-random bisection, (iii) random mechanisms and (iv) interaction processes (Rives *et al.*, 1992). These are discussed briefly in the following section.

3.3.1 Mid-point bisection process: Price (1966) proposed that in a bed subjected to extension and containing randomly positioned joints, the next fracture will form at the mid-point along the distance corresponding to the greatest spacing between already existing joints (theoretically subjected to greatest extensional stress). Narr and Suppe (1991) argue that although the tensile stress reaches its maximum value mid-way between the existing joints, the next joint commonly forms at an existing flaw which controls its position. Rives *et al.* (1992) argue that distribution of spacing resulting from a mid-point bisection process does not fit any theoretical uni-modal laws and pointed out that this process cannot produce realistic joint spacing distributions. They concluded that mid-point fracturing probably does not represent real joint development.

3.3.2 Semi-random process: As noted by Rives *et al.* (1992) this process is similar to mid-point bisection except that after random fracturing has been initiated, the largest spacing is selected for the next fracture but fracturing occurs randomly along that interval. Large spaces are quickly broken down and the population of spaces becomes

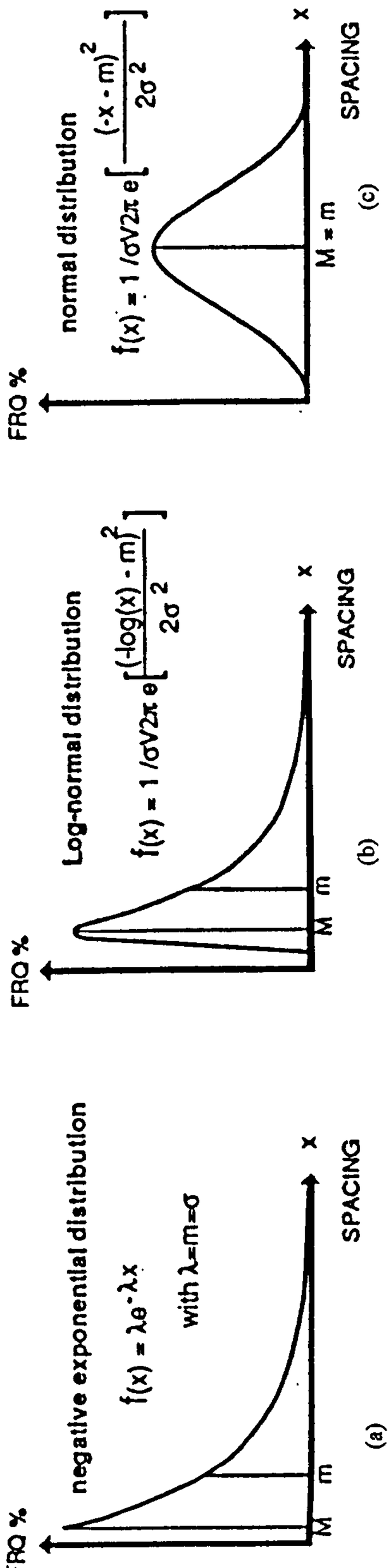


Figure 3.1 (a) Negative exponential, (b)log-normal and (c) normal (from Rives et al., 1992) and (d) Gamma distribution (from Huang and Angelier, 1989).

uniformly distributed between zero and the greatest value. This semi-random process does not give rise to distributions comparable to real (*i.e.* geological) situations and it is also unlikely that this process is a realistic representation of natural joint formation.

3.3.3 Random process: Random initiation of fractures gives rise to a negative exponential population distribution for fracture spacing with a mean close to the standard deviation throughout the whole process. It cannot therefore produce the log-normal and normal distributions frequently observed in natural fracture sets.

3.3.4 Interaction process: Rives *et al.* (1992) propose that fractures initiate at random and propagate according to an interaction process. They argue that the criteria for initiation and propagation processes are entirely different. Once the fracture initiates, it propagates until it enters the interaction zone of another joint or the driving stress (P_f-σ_3) becomes insufficient for continued propagation. The spacing distribution generated by this process is initially negative exponential. It then changes progressively to a log-normal and finally to a normal distributions as more and more fractures are formed (see Fig. 3.1).

They conclude that fracture initiation is at first governed by a random process but with increasing fracture density the shadow or interaction zones around each fracture prevent new fractures growing in the immediate vicinity of the existing fractures. Thus, as the fractures become more numerous, they reach a near constant spacing (at saturation). Their work showed that with increasing strain, fracture spacing evolves from a negative exponential through a log-normal to a normal distribution. They proposed that the ratio of mode (the most frequently occurring value of joint spacing)

to mean, which varies between 0 and 1, can be used as a good indicator of joint set development with the values close to 0 and 1 indicating poorly- and well-developed states respectively. Joint spacing is defined as being at a poorly- or well-developed stage when typical joint lengths are respectively less and greater than inter joint spacing (Wu and Pollard, 1995).

At saturation, fractures are present in all the spaces available and no more fractures of the same set can form (Wu and Pollard, 1995). Their work indicates that when the applied strain reaches a certain value, fracture spacing reaches a critical minimum value. During the development of a fracture set, the mean spacing of the fractures decreases hyperbolically with increasing strain. Wu and Pollard (*op. cit.*) argue that fracture spacing at saturation is a function of layer thickness and is independent of strain, whereas spacing before saturation varies strongly with applied strain. The strain associated with the formation of a joint is generally low because joints, by definition, lack significant displacements compared to faults (Odling *et al.*, 1999).

Cobbold and Ferguson (1979) proposed two models for the spacing of fractures. Firstly the *propagation model* in which early forming structures nucleate at sites of heterogeneity. Each of these early structures triggers the appearance of new neighbours at fixed spatial intervals. The process continues, producing spreading zones of wave-like disturbance. Secondly they propose the *saturation model* in which individual structures nucleate at various points throughout a deforming material at various times. No structure can nucleate at less than a certain limiting distance from any other structure already in existence. The process continues until all the available space is occupied. Thus the interval between neighbouring structures has limited

range of values. The results of the experimental work of Rives *et al.* (1992) indicate that the initiation of one fracture does not trigger the formation of another *i.e.* the propagation model of Cobbold and Ferguson (1979) does not apply. Of the two models presented by Cobbold and Ferguson, it is argued that the saturation model of fracture propagation appears to be more realistic.

Theoretically, under conditions of layer normal compression, a competent layer sandwiched between two incompetent layers will have a maximum layer parallel tensile stress at the centre of the layer and this will decreases off towards layer ends. Thus, any section of a layer bounded by two adjacent joints will also have the maximum tensile stress mid-way between the two joints (Hobbs, 1967) and this will give rise to joint formation by the process of mid-point bisection (see section 3.3.1).

Masuda and Kuriyama (1988), in a study of micro-boudinage of piedmontite grains during plastic flowage of quartz in quartz schist, proposed a mechanism of mid-point fracturing and subsequent pulling apart for their formation. They found that the spacing of fractures on a best-fit frequency plot showed a log-normal to quasi-normal distribution. Rives *et al.* (1992) showed that if the controlling mechanism was mid-point fracture the resulting distribution pattern did not fit any of the theoretical unimodal laws *i.e.* negative exponential, log-normal and normal distributions. In contrast, Mandal *et al.* (1994) studied boudin formation using analogue modelling of bilaminates and showed that none of the fractures occurred by mid-point failure. A possible explanation was suggested by Rives *et al.* (1992). They point out that joints initiate from flaws (randomly distributed defects) and that they are therefore not constrained to form at the mid-point between two joints. The flaws are sites where the

tensile strength of the rock is reduced and they are therefore sites of likely failure. Narr and Suppe (1991) suggest that joints form whenever the tensile stress equals the local tensile rock strength and that this does not necessarily coincide with the point of maximum tensile stress.

3.4 Joint spacing evolution

Joint spacing distribution laws remain a controversial topic in the literature. Statistical analysis of joint spacing shows several different distributions: negative exponential (Priest and Hudson, 1976), log-normal (Sen and Kazi, 1984; Narr and Suppe, 1991, Rives *et al.*, 1992) and normal distributions. Priest and Hudson (1976) argued that unless the fractures are distributed uniformly, a combination of clustered, uniform and randomly positioned joints will lead to a negative exponential distribution. Based on the data from the Gulf of Suez and the South of France, Huang and Angelier (1989) suggested that the negative exponential distribution resulted from a limited resolution and did not properly describe joint spacing whereas log-normal and gamma distributions represent realistic models. They noted that normal distribution in fracture spacing is rarely observed from natural fracture populations.

3.5 Relationships between joint spacing and bed thickness

3.5.1 Linear

Joint spacing is defined as the perpendicular distance between neighbouring systematic joints of the same set. Many workers have noted that joint spacing is linearly dependent on the thickness of the mechanical layer containing the joints (*e.g.* Bogdanov, 1947; Novikova, 1947; Kirillova, 1949; Hobbs, 1967; Ladeira and Price, 1981; Price and Cosgrove, 1990; Narr and Suppe, 1991; Gross, 1993; Gross *et al.*,

1995 and Bai and Pollard, 2000a and b). This relationship is defined by the following equation:

$$S = K.\, b \qquad (3.3)$$

Where S is joint spacing, K is a constant related to the lithology and b is the bed thickness. From this relation one can conclude that the slope of a line, K in this expression, does not change with thickness, but must be a function of lithology and, by inference, mechanical properties such as tensile strength.

Many of the above observations demonstrating a linear relationship were made in rocks with bed thicknesses generally less than 1.5 metres. Some authors (*e.g.* Ladeira and Price, 1981) have argued that a different relationship exists when the beds are thicker than ≈ 1.5m. They indicated that the bed thickness/joint spacing curve defines a bilinear relationship for thicknesses greater than 1.5m. They argue that joint spacing in thin layers is influenced by traction at the interfaces between the competent and incompetent layers and that the mechanism of hydraulic fracturing plays only a secondary role. In contrast, joint spacing in thick layers is independent of bed thickness and is the result of hydraulic fracturing.

The curve defining the bilinear relationship (Fig. 3.2a) can be split into two segments. The first segment of the curve defines the bed thickness range where bedding traction along the boundary between the competent layer and the adjacent matrix controls joint spacing. The second segment of the curve defines the range of thickness over which hydraulic fracturing determines the fracture spacing.

Bai and Pollard (2000b) suggested that, at saturation, the critical fracture spacing/fractured layer thickness ratio varies between 0.8 and 1.2 depending on the material properties of the fractured medium and the neighbouring incompetent beds. It can therefore be argued that for layer thicknesses of less than 1.5 metre, fracture spacing at saturation approaches that for which the coefficient of the slope, K, will be approximately one (Ladeira and Price, 1981) (Fig. 3.2a).

Thus in multilayers of contrasting lithologies and thicknesses fracture development is likely to be the result of bedding traction, hydraulic fracturing and the combined effects of both bedding traction and hydraulic fracture mechanisms. They suggest that fracture spacing in thick layers is related to the gradient of fluid pressure which in turn depends on permeability, rate of propagation of fractures and strain-rates all which depend on lithology (Fig 3.2b).

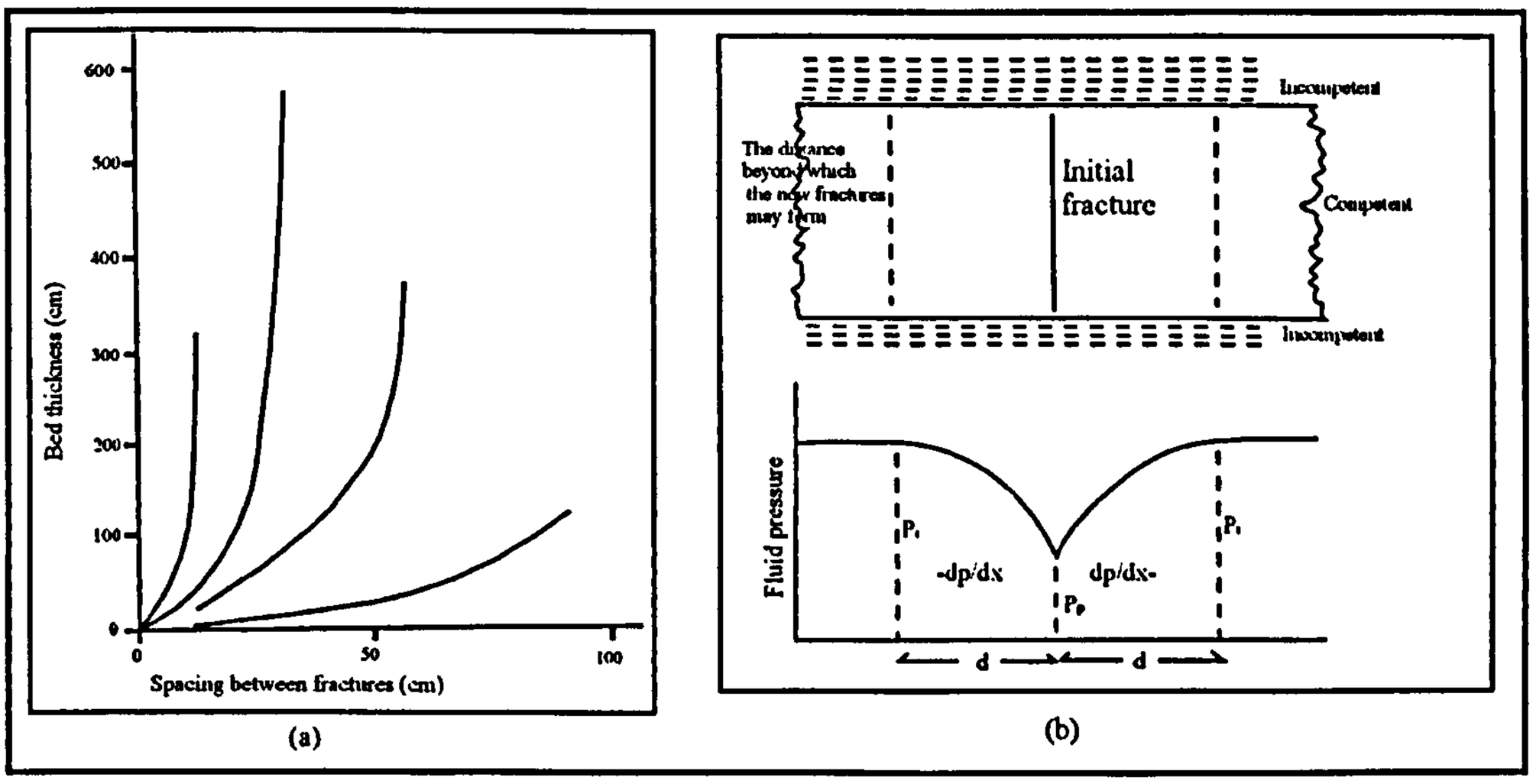


***Figure 3.2** (a) Relationships between bed thickness and joint spacing and (b) shows decreasing fluid pressure (dp/dx) in the vicinity of early formed joint. This prevents the formation of new fractures in the proximity (from Ladeira and Price, 1981).*

Bai and Pollard (*op. cit.*) show that when fracture spacing to layer thickness ratio changes from greater than to less than the critical value ($0.8 < S/T_f < 1.2$), the normal stress acting perpendicular to the fractures changes from tensile to compressive. They argue that this transition in stress state precludes further '*infilling*' by new fractures, unless these are initiated by mechanisms other than pure tension such as hydraulic fracturing mechanisms or from pre-existing flaws. They suggest that the critical spacing of fractures, which is approximately the same as the thickness of the fractured layer, marks the lower limit for fractures that are driven by tension in the material without significant influence from flaws or high fluid pressures and that this corresponds to the condition of fracture saturation as proposed by Rives *et al.* (1992) and Wu and Pollard (1995).

The results of 2D finite element analysis by Bai and Pollard (2000a) show that when the fracture spacing to layer thickness ratio attains the critical value, *i.e.* $0.8 < S/T_f < 1.2$, a flaw between two fractures would tend to propagate from the tip that is furthest away from the centre of the two existing fractures and where the flaws are positioned at the edge rather than in the middle of the fractured layer. The numerical models show that if the flaw is located at the centre of the existing fractures, the fracture spacing to layer thickness ratio (S/T_f) has to be greater than the critical value in order for the flaw to propagate.

3.5.2 Non-linear and complex

Norris (1966) expressed doubts about the linear relationship described above and noted that the spacing of joints of a given set in coal-bearing strata in the Eastern Cordillera of Canada was unpredictable. Although the increase in fracture spacing

with layer thickness is well documented and widely accepted, the quantitative relationship between layer thickness and spacing of fractures is not well established (Mandal *et al.*, 1994; Ji and Saruwatari, 1998). Using theoretical and experimental results Mandal *et al.* (1994), argued that under conditions of layer-parallel extension, fractures will develop more or less simultaneously at mechanically most-favoured sites *i.e.* sites where the resistance of the rigid layer to the bulk extension is minimum. This produces fracture spacing which will have a *non-linear* relationship to bed thickness.

Ji and Saruwatari (1998) showed analytically a non-linear decay of shear stress from the interface and the effects of the surrounding incompetent matrix. The model of Hobbs (1967) is based on the assumption that the shear stress in the bounding incompetent layer decreases from a maximum value at the interface to zero at a distance from the interface equal to the thickness of the competent layer. For a competent layer sandwiched between two incompetent layers of identical thickness, their analytical result showed that:

$$S = \eta\sqrt{t.d} \qquad (3.4)$$

where S is joint spacing in the competent layer, t and d are thicknesses of the competent and incompetent layers respectively and η is a constant which depends on the material properties of both layers (*e.g.* Young's Modulus, tensile strength and fracture saturation strain of the competent layer, and shear modulus of the incompetent layer) and decay modes of the shear stress in the bounding layers. They argue that if the ratio of d to t is constant, the relationship between joint spacing and bed thickness is linear. Conversely, if the thickness of the incompetent layer is constant, joint spacing increases as a function of the square root of the competent

layer. They noted that complex t-d variations in the Cambrian flysch sediments at Plage Victor in the Saint-Jean-Port of the Quebec Appalachians statistically showed a linear relationship between joint spacing and bed thickness.

Based on the study of the Asmari Limestone in the foothills of the Zagros Mountains, McQuillan (1973) proposed an inverse logarithmic relationship between fracture density (the reciprocal of joint spacing) and bed thickness. He rejected a genetic relationship between the fractures and the folding process in the area. Nemčok *et al.* (1995) also found an inverse logarithmic relationship (linear regression) between joint density and bed thickness in the north part of the Bristol Channel Basin when studying extensional veins that developed during the extensional phase of basin evolution.

3.6 The relationship between joints and other structures

3.6.1 Faults

Anderson (1951) proposed the possibility of three arrangements of the principal stresses. Each arrangement illustrates the stresses operating during the formation of one of the three major types of faulting and the concept of the *'standard state'* is introduced. He classified faults with respect to the orientation of the principal stress axes as follows: normal when σ_1 acts vertically, strike-slip when σ_2 is vertical and reverse when σ_3 is vertical (Fig. 3.3). Anderson argued that the principal stresses will act either normal or parallel to the Earth's surface, particularly near the Earth's surface, because this is a free surface and unable to sustain a shear stress.

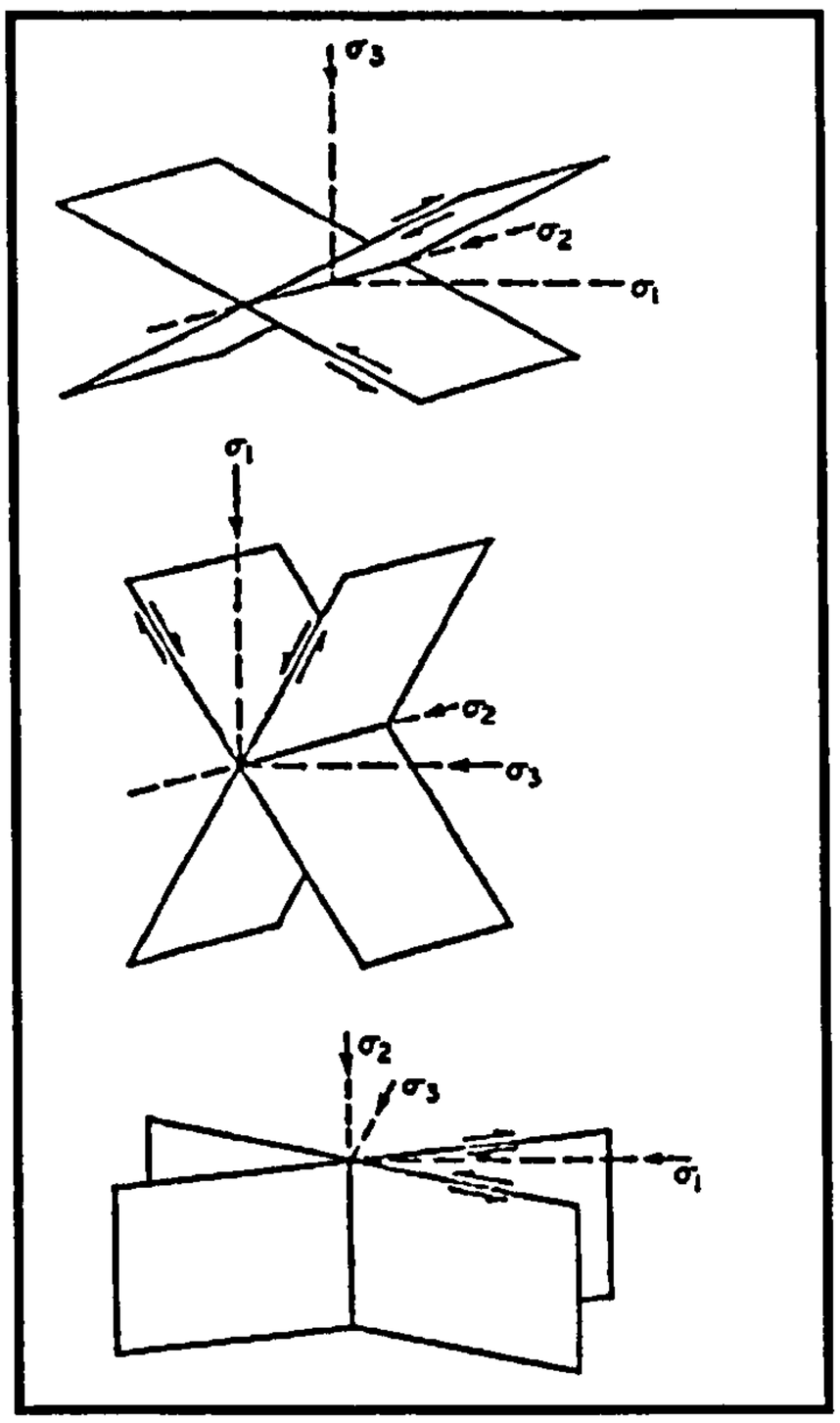


Figure 3.3 Three-fold classifications of faults (Anderson, 1951).

Price (1966) defines a fault as *'a plane of fracture which exhibits obvious signs of differential movement of the rock mass on either side of the plane.'* Price extended Anderson's classification by considering the direction of displacement vector *i.e.* dip-slip, strike-slip or oblique-slip. Price noted that the relationship of systematic joints to folds and faults had been widely studied and well established. However, in any specific example, one or more of the predicted sets of joints may fail to develop. He summarised the fracture sets associated with the various types of faults as shown in Fig. 3.4.

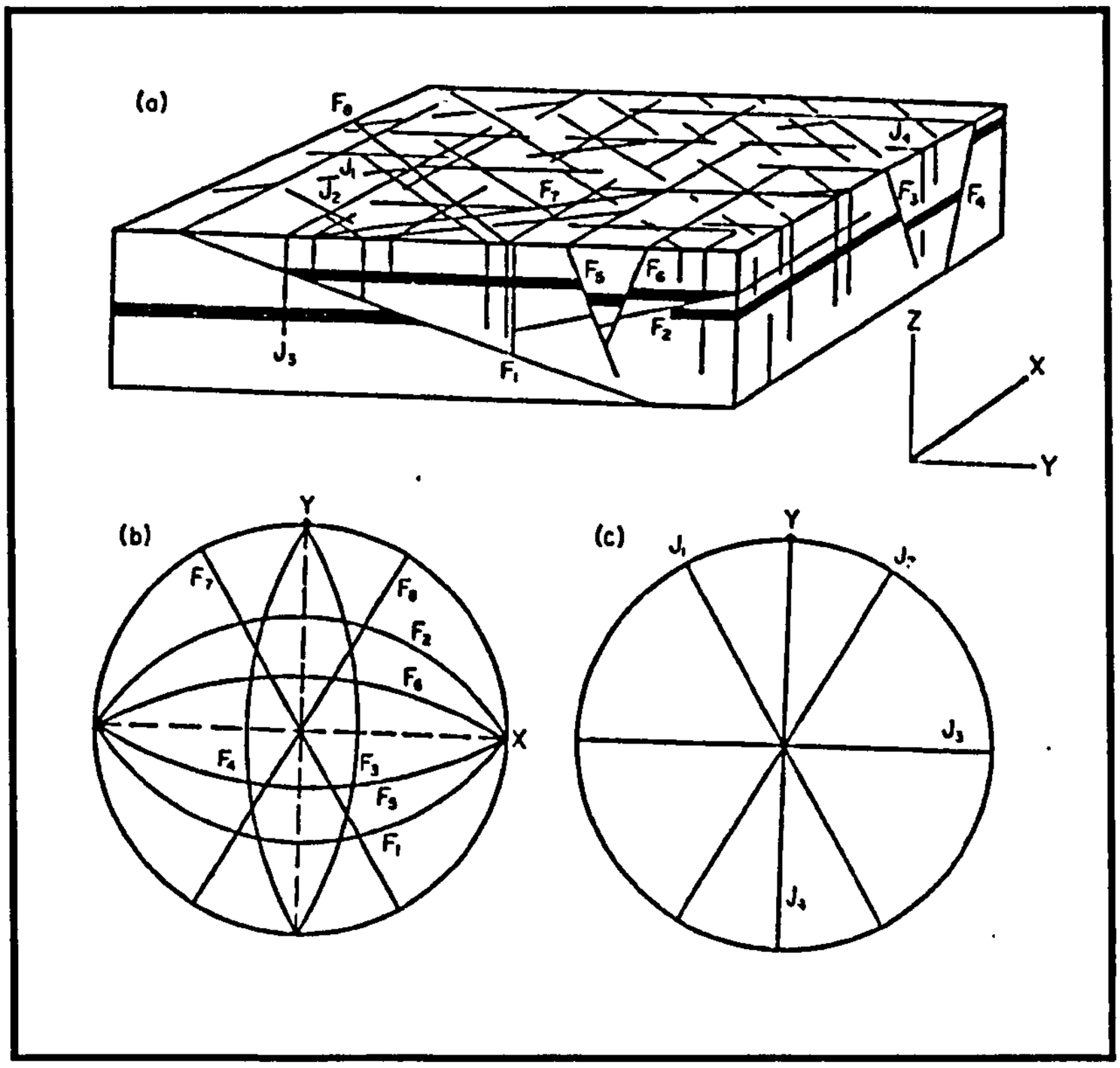


***Figure 3.4** (a) Block diagram of horizontally bedded sediments showing the possible orientation of joints that form during thrusting, F_{1-2}, during normal faulting, F_{3-6} and during wrench faulting, F_{7-8}, (b) stereographic projection of fault planes and (c) stereographic projection of joint planes (from Price, 1966).*

Hancock (1969), in his work on jointing of the Jurassic limestone beds in the Cotswold Hills, observed identical fracture patterns to those predicted by Price (1966) except that fractures associated with thrusting are not present because the area has not been affected by thrusting. Hancock identified two systems of normal faults striking N-S and E-W with six associated sets of fractures. Two sets of joints strike NE-SW (dextral) and NW-SE (sinistral) with the acute angle bisector striking E-W. Two other sets strike N-S and E-W and are vertical extensional joints. Although the joints show a generally consistent orientation, locally they show a strike variation of up to 25° on either side of the mean.

Stearns (1967) pointed out that fractures in the vicinity of a fault can be used to deduce the stress field responsible for the fault. He argued that there are two potential shear and extension fractures for every arrangement of σ_1, σ_2 and σ_3. He noted that fracture intensity or frequency increases in the vicinity of a fault (Fig. 3.5) and that such an increase in fracture intensity can be used to predict the proximity of faults and also that the fractures are associated with faulting. In some examples however, the fractured layers rotate as a result of drag on the fault to form synclines in the hanging-wall and anticlines in the footwall. If the rotated fractures were the only evidences available, then one would conclude that the associated fault was either an abnormally steep or abnormally low-angle normal fault (Stearns, 1967).

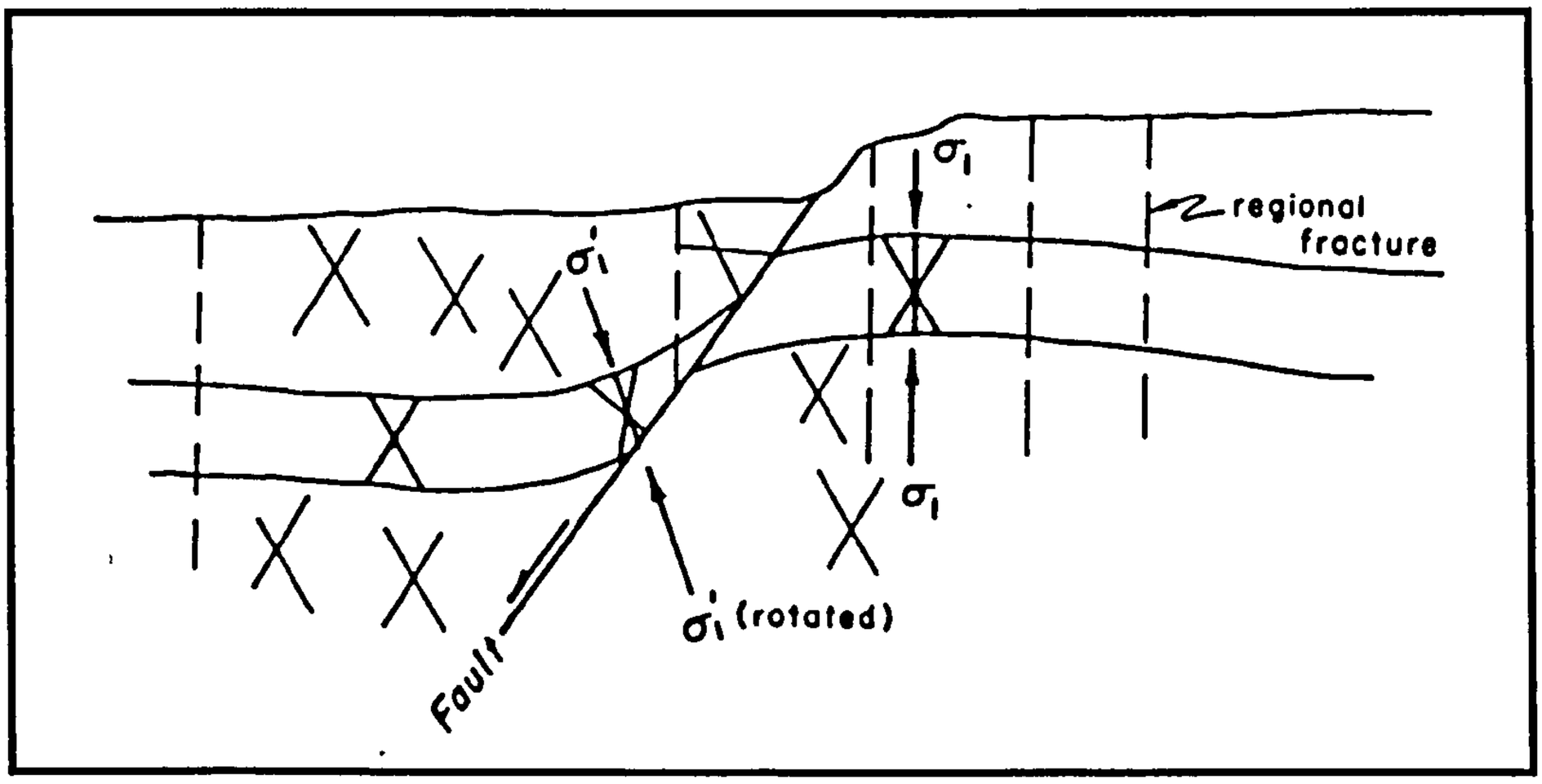


***Figure 3.5** Schematic illustrations of the fractures in the vicinity of normal faults (from Stearns, 1967).*

Blés and Feuga (1986) gave a broad classification of the small-scale faults and fractures associated with large-scale normal faults, reverse faults and strike-slip faults (Fig. 3.6). They argue that the joint/fracture networks form both parallel to the fault with the same direction of displacement and parallel to the conjugate fault. With

continued deformation however, these discontinuities merge breaking the bridges between them and growing into faults.

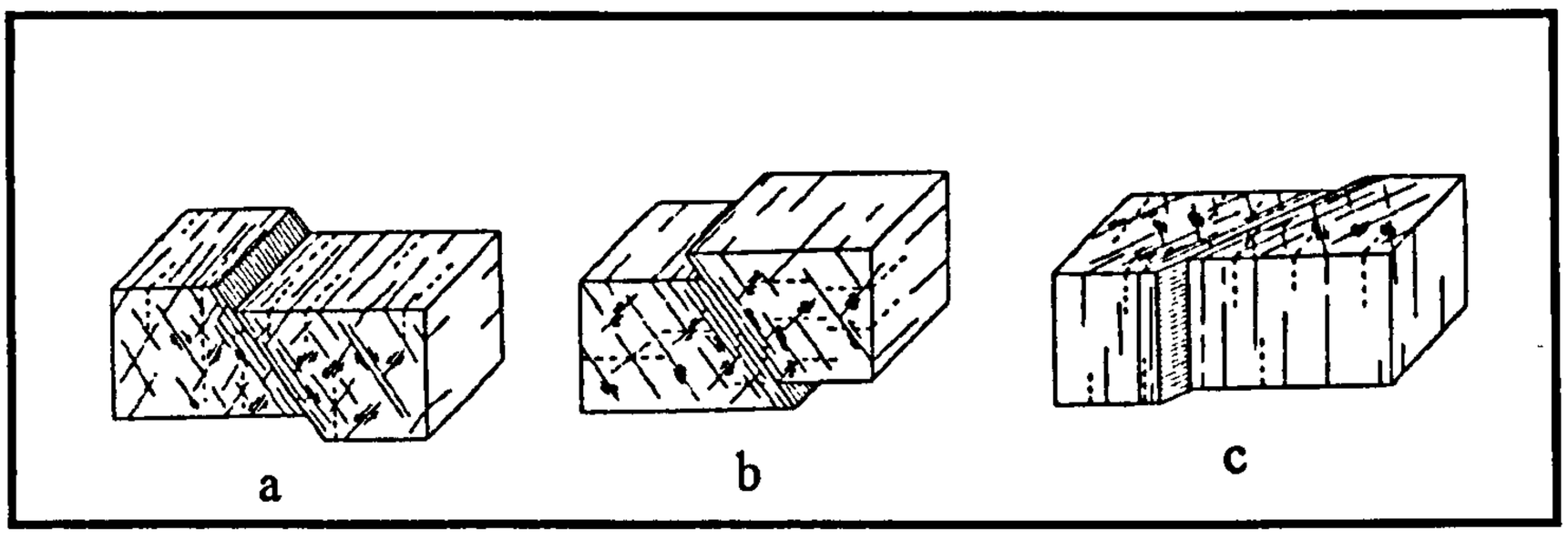


***Figure 3.6** Small faults and fractures that may develop around a large fault. (a) normal fault, (b) reverse fault and (c) strike-slip faults (from Blés and Feuga, 1986).*

Rawnsley *et al.* (1992) discussed complex spatial and temporal perturbations in the orientation of joints around faults. The local deviation of joint patterns is explained with reference to two models: the '*point of stress concentration model*' and the '*free surface model.*' The first model arises because of the roughness of natural discontinuities including faults and the consequent inability of the two surfaces to meet exactly under an applied normal stress. Increased normal stress across the fault causes stress concentration at local points of contact along the fracture. Joints follow the stress trajectories and will therefore converge towards the points of contact. In the second model it is argued that the reorientation of joints close to a fault can be explained by the fact that the fault behaves mechanically as a free surface. This causes the principal stresses to rotate so that they become parallel or perpendicular to the fault.

Peacock (2001) discussed the geometric features that can be used to establish temporal relations between joints and faults, so that joints that predate, are

synchronous with, and postdate faults can be distinguished (Fig. 3.7). Depending on the orientation of the applied stress system with respect to joints that predate the faults, the joints can become dilated, sheared, or affected by pressure solution during faulting. Joints that are synchronous with faulting have an orientation compatible with the stress system that generated the fault and tend to increase in frequency towards the fault. Pre- and post-fault joints do not increase in frequency. Post-fault joints may crosscut or abut the fault without being displaced by it. Syn- and post-fault joints may curve as they approach the fault as discussed above, indicating perturbation of stresses around the fault. A change in orientation of jointing across the fault plane may also occur.

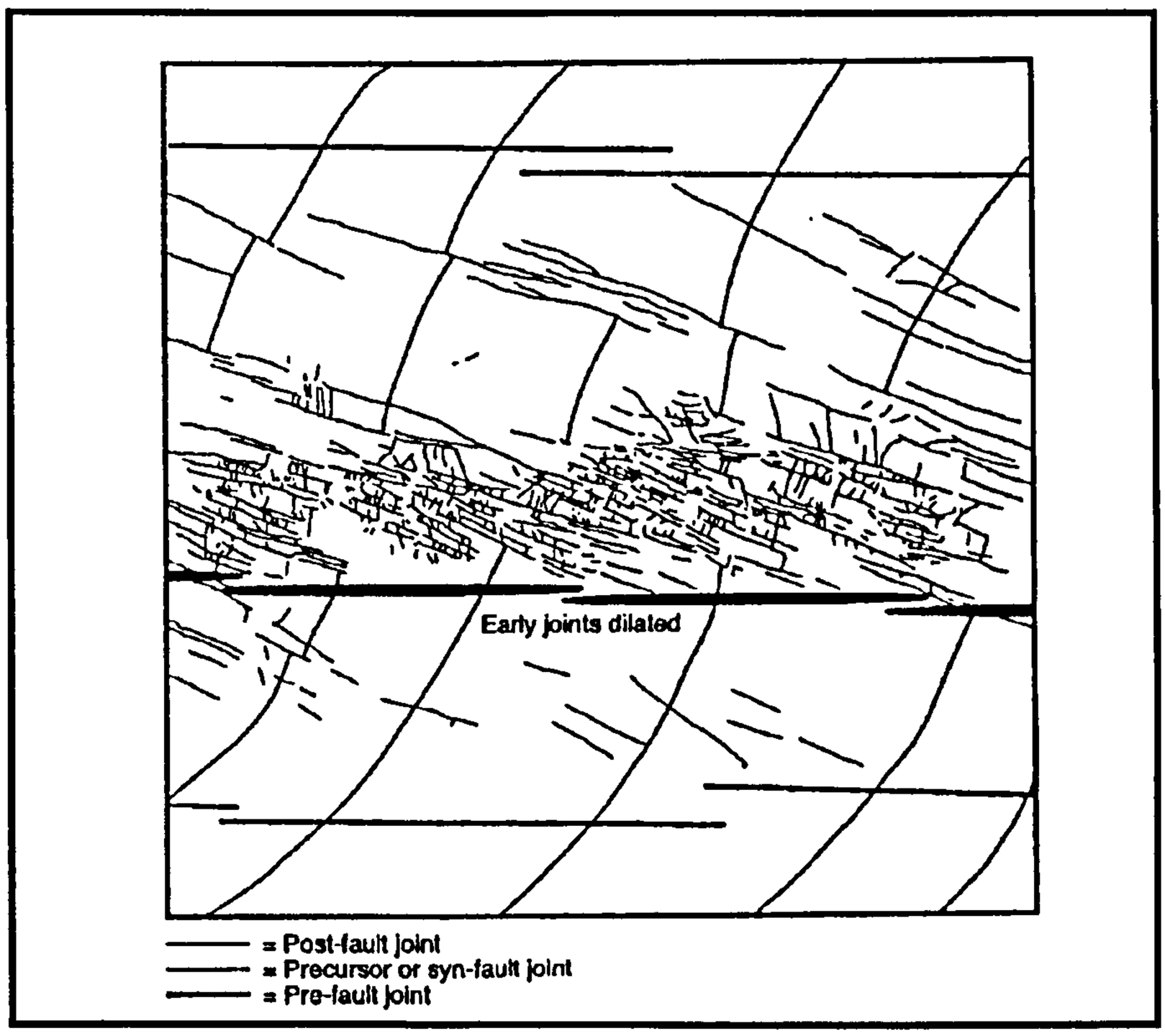


Figure 3.7 Schematic diagram illustrating the temporal relationships between joints and faults (from Peacock, 2001).

3.6.2 Folds

Hodgson (1961) discussed the spatial relationships of joints and folds that Hodgson observed in the study area at part of the Colorado Plateau in northern Arizona and southeast Utah. From the spatial relations of systematic joints, he argues that the joints formed at or near the surface of the earth in a uniform stress field. Joint trends cross several fold axes of considerable magnitude maintaining a consistent direction and do not swing to maintain a regular angular relationship with the fold axes when these axes change their strike. He thus rejects the idea that the joints in the area are genetically related to the folding process.

Nickelsen and Hough (1967) studied joints in coal beds and shales from the folded Appalachians to the Central Stable Interior. They described a *fundamental jointing system* made up of approximately orthogonal systematic and non-systematic joints and *complex systems* which overprint two or more fundamental systems. They noted differences in the styles of joints in the coal and shale beds and concluded that systematic joints in the area formed early and are independent of folds and faults.

A synthesis of joint orientations related to the folds has been presented in the pioneering work of Price (1966). He suggested that the orientation of the joint sets relative to folds depend upon size of the fractures, the type of fold and the thickness and competency contrast between beds (Figs. 3.8). He argued that the orientation and type of joints on the crests and troughs of folds depend upon the thickness of the competent unit and degree of deformation. He classified joints related to the process of folding as *bc* or *longitudinal* and *ac* or *cross joints* that strike parallel and perpendicular to the fold axis respectively (Fig. 3.8). He termed joints that are oblique

to the fold shear joints. He pointed out that joint orientations that are far from the hinge regions of folds are strongly influenced by the orientation of the layer containing the joints and pointed out that in asymmetric folds the joint orientation on the steep and gently inclined limbs would be different (Fig. 3.8c). Joints that could develop in the leading and trailing limbs of an anticline are shown in Fig. 3.8(c), (d) and (e).

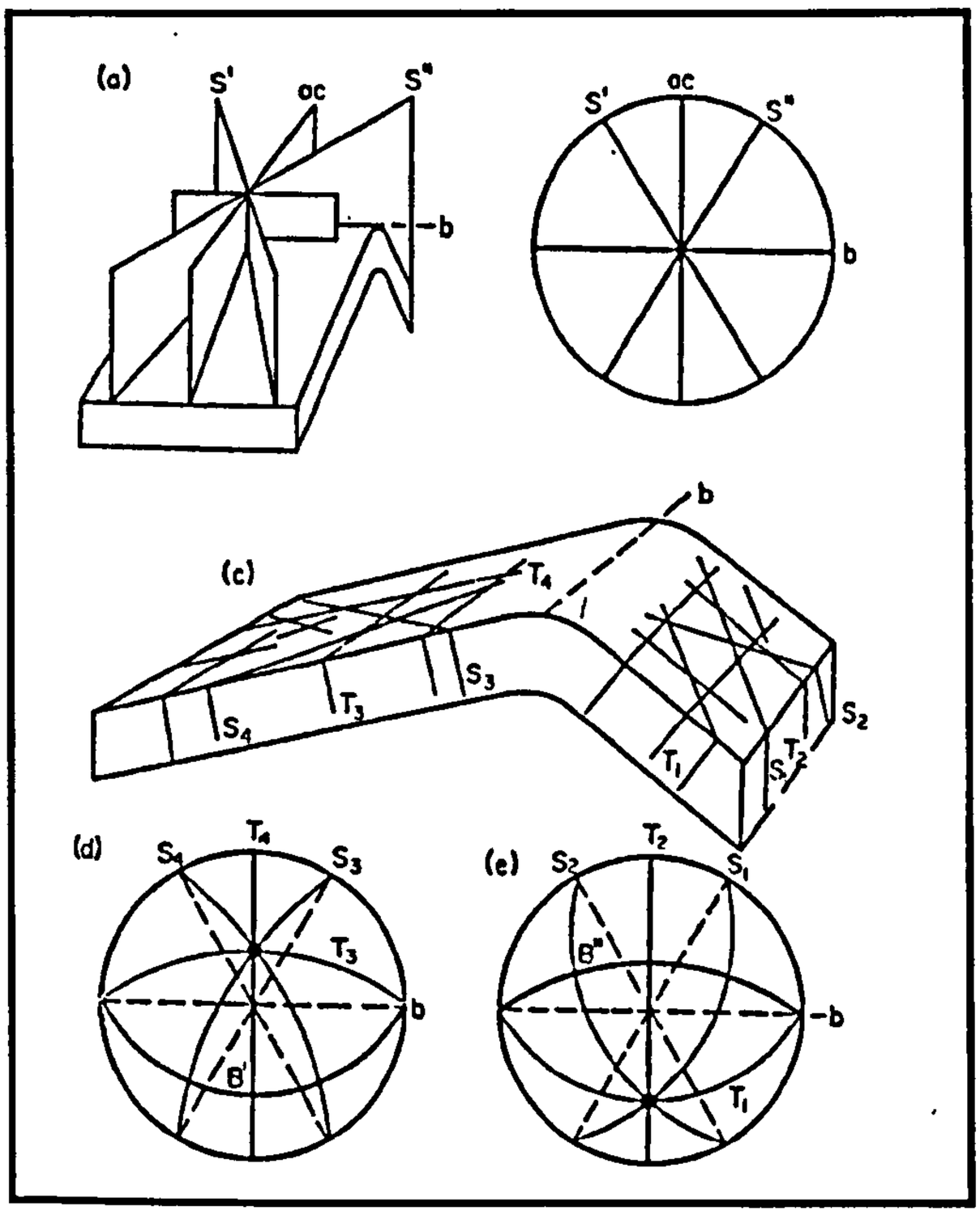


Figure 3.8 *Relationship between a fold and associated joints: (a) block diagram between folds and fractures, (b) stereographic plot of (a), (c) fracture distribution in the trailing and leading limb of an anticline, (d) and (e) stereographic plot of (c) (from Price, 1966).*

Price (1966) argues that the type and orientation of joints in the hinge region of folds depend on the thickness of the fractured unit and the degree of deformation expressed by the tightness (interlimb angle) of the fold (Fig. 3.9). With increasing degree of deformation, he suggests that fractures will open up and may become filled with quartz or carbonate material.

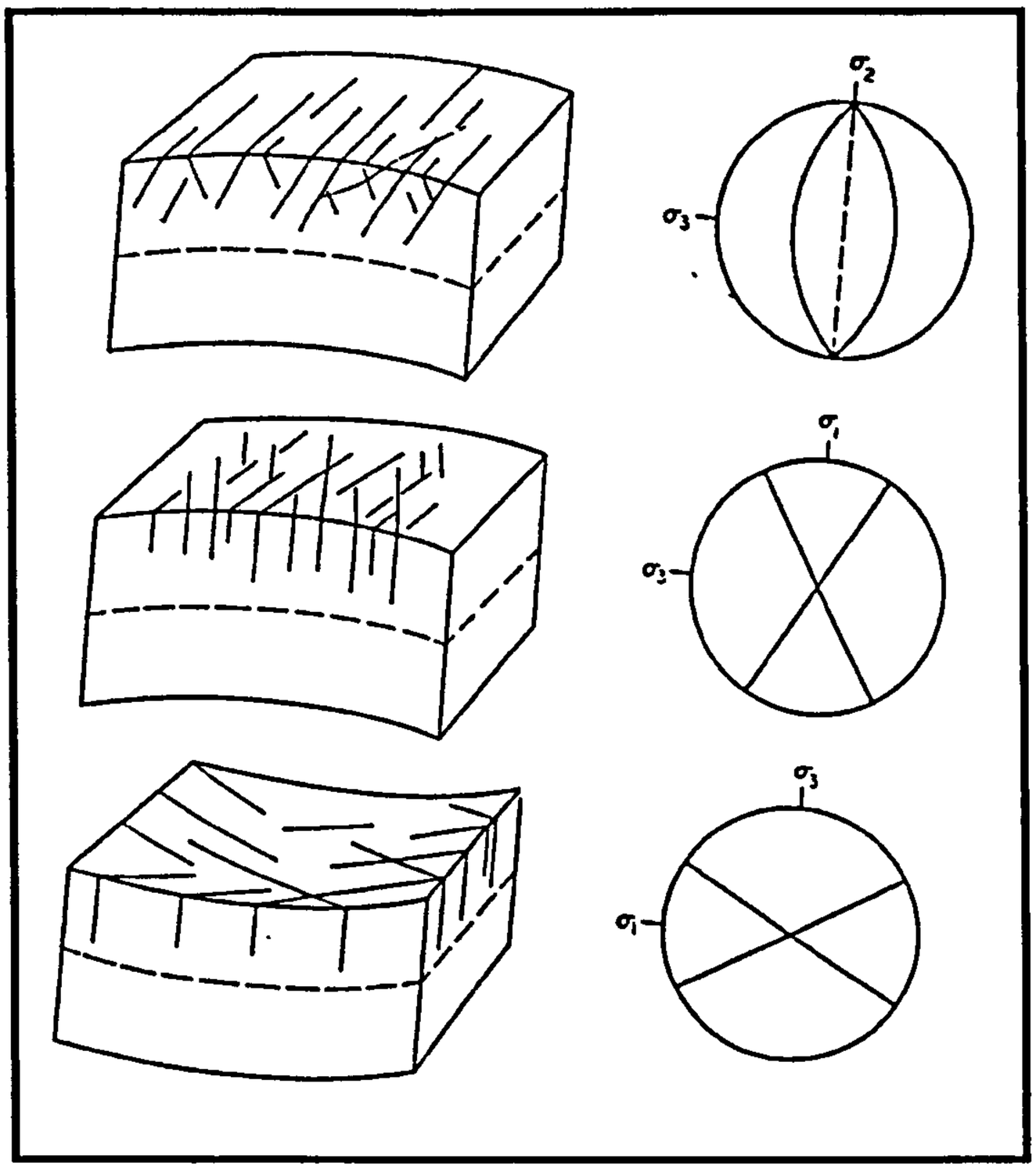


***Figure 3.9** (a) and (b) Show joints associated with the anticlines and (c) shows syncline (after Price, 1966). Note the variation in strike of the joints.*

Based on his work on naturally fractured rocks of the Teton anticline in the eastern front of the Saw-tooth Range, northwest Montana, Stearns (1967) argues that '*most fractures do not reflect the regional stress field, but rather, are genetically related to the folding process.*' It can be seen that the folds contain varying orientation of fractures because the fractures are related to locally developed compressional and extensional regimes within the folded layer. He proposed four different possibilities for fracturing related to folding. They form when: (i) σ_1 and σ_3 are parallel to the bedding and σ_1 parallel to the dip direction (Fig. 3.10a) (ii) σ_1 and σ_3 parallel to bedding plane and σ_1 parallel to the strike (Fig. 3.10b) (iii) σ_2 parallel to the strike of the beds with σ_1 normal to the bedding (Fig. 3.10c) and (iv) σ_2 parallel to the strike of the beds with σ_3 oriented normal to the beds (Fig. 3.10d). These four orientations give rise to 12 potential

fracture planes (*i.e.* two shear and one extension fractures for each). The potential extension fracture in (ii) and (iii) are identical and the potential extension fracture in (iv) is parallel to the bedding effectively reducing the possible sets of joints to 10 (Fig. 3.10e). In addition, when bedding plane slip occurs, bedding is a shear plane and conjugate shear fractures may form along with it (Stearns, 1967).

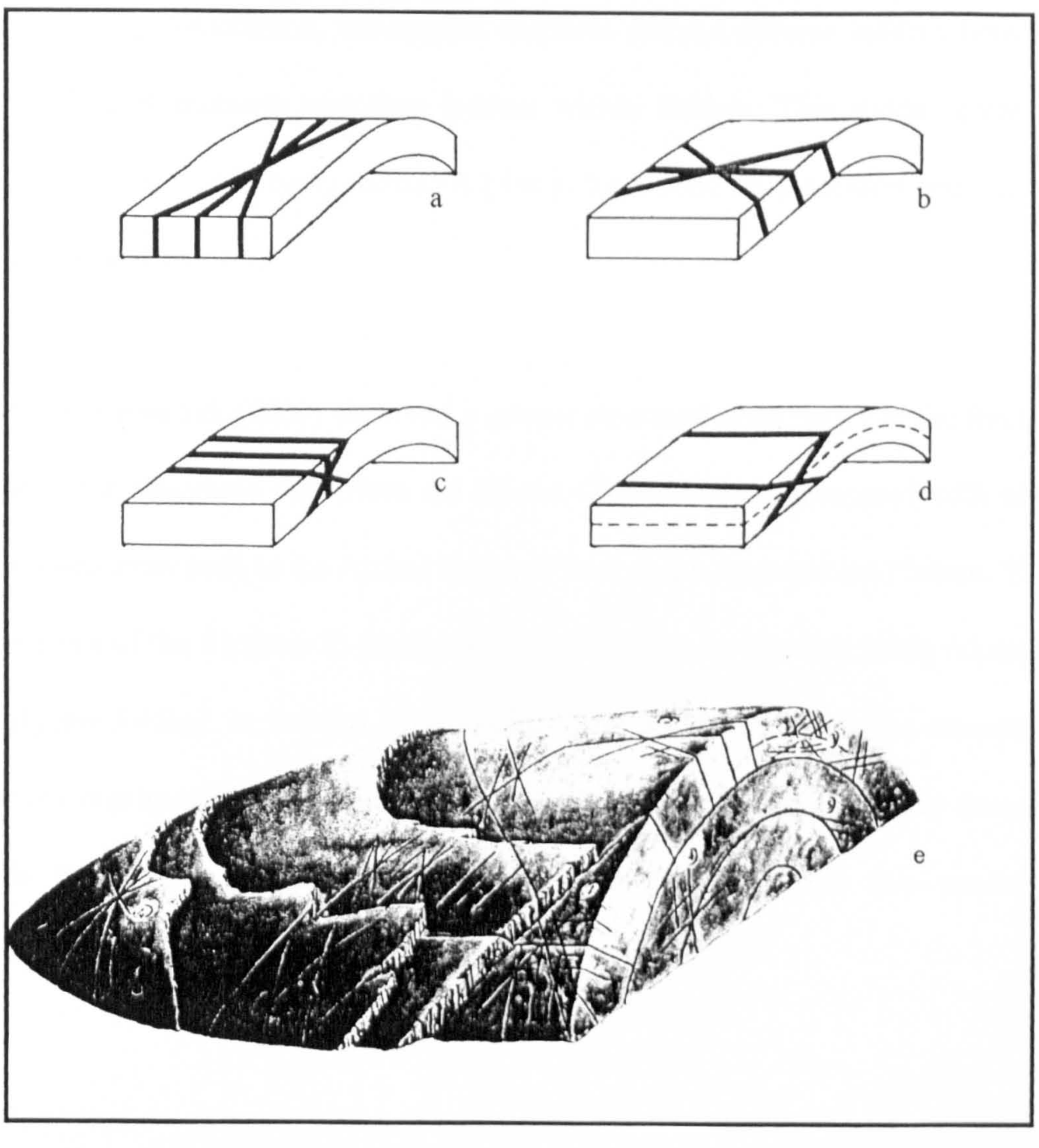


Figure 3.10 *Main joint sets found in folded rocks and their relation to folds, (from Stearns, 1967).*

In order to understand the origin of joint patterns linked to folding, Rives *et al.* (1990) conducted experiments on PVC plates coated with brittle varnish submitted to a cylindrical and non-cylindrical folding. During cylindrical folding, the fractures developed parallel to the fold axis and orthogonal fractures developed during unloading. During non-cylindrical folding (*i.e.* the layer was subjected to torsion before shortening), subsequent fractures formed oblique to the main compression. With increasing deformation, subsequent fractures formed oblique ladders between the early-formed fractures and then ladders within ladders. This model gives an insight into some of the early-formed Alpine joints found in limestone beds of the Bristol Channel Basin.

Engelder and Peacock (2001) observed a greater structural complexity in the fracture spacing in the limestone beds from the Bristol Channel Basin compared with other well exposed areas such as the Arches National Park or the Appalachian Plateau. They explain some of the fractures in the Bristol Channel Basin as possibly being related to *flexural flow folding*. In flexural flow folding (Fig. 3.11), the maximum amount of slip or the maximum strain occurs on the limbs at the inflection point and decrease towards the hinges (Ramsay, 1967). The strain distribution in this model is characteristic of folds that form in well-bedded successions.

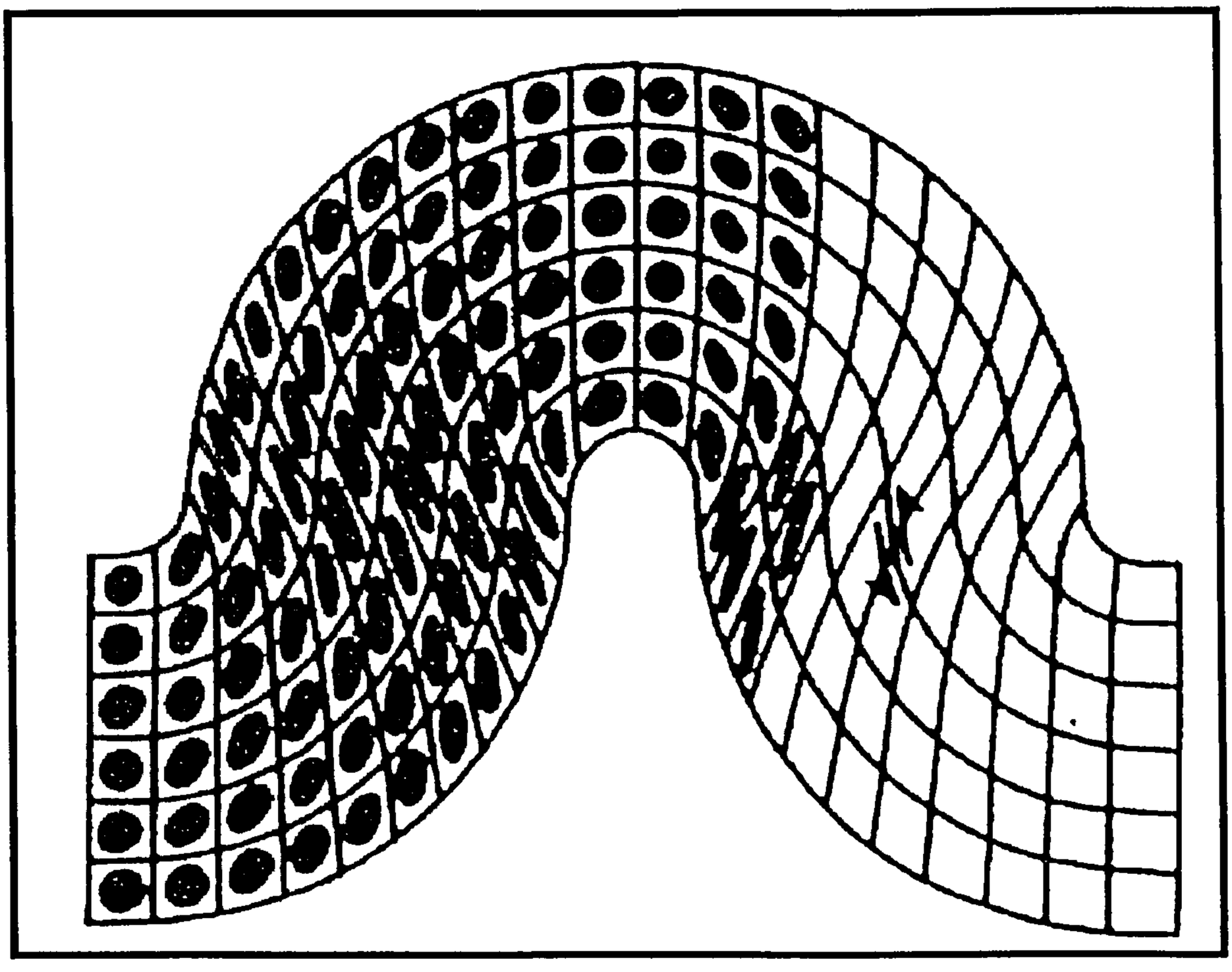


Figure 3.11 Strain distribution in a flexural flow fold models (after Ramsay, 1967).

The second model of strain distribution within a fold is that of *tangential longitudinal strain.* These folds develop when in a homogeneous, isotropic layer. In contrast to the flexural flow folds where the maximum strain occurs at the inflection point and zero strain at the hinges, in tangential longitudinal strain folds the maximum strain occurs at the hinges and no strain at the inflection point (Fig. 3.12). The outer and the inner arcs of the hinge experience extension and compression respectively, the two being separated by the neutral line or surface (in 3D) along which there is no strain.

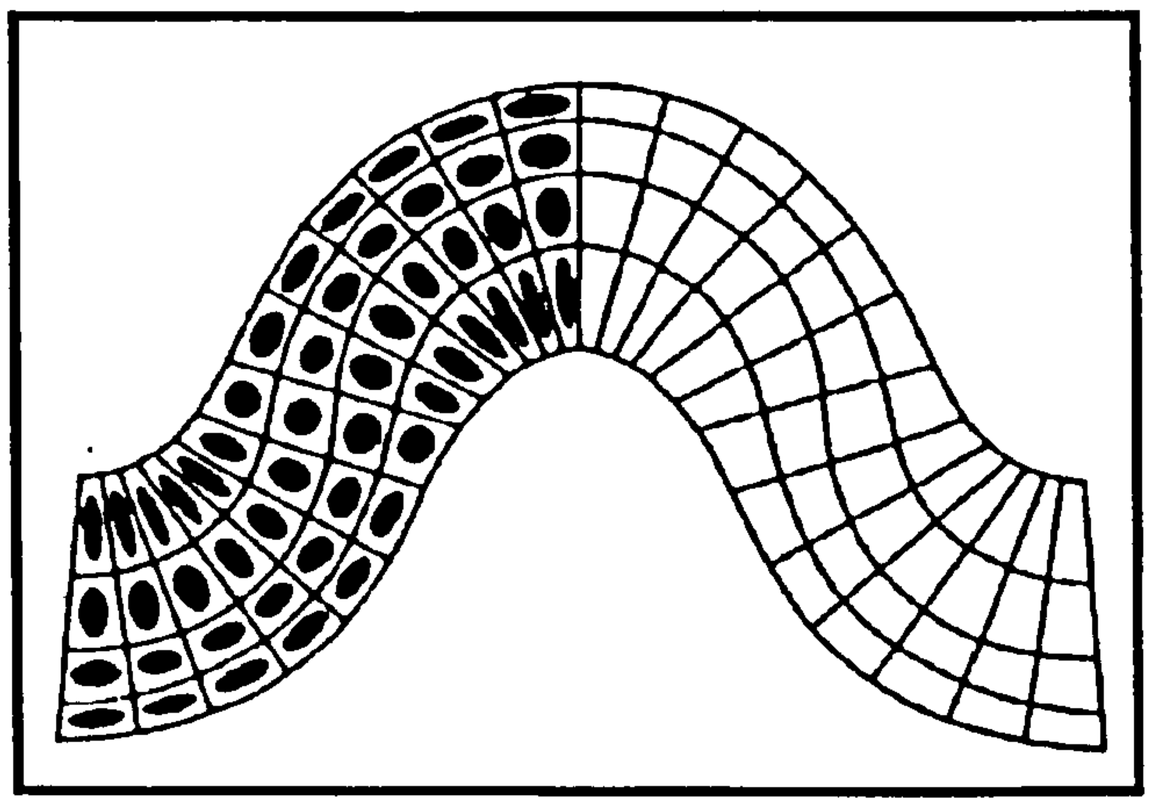


Figure 3.12 Strain distributions in a tangential longitudinal fold (Ramsay, 1967).

In real systems such as a multilayer made up of competent and incompetent beds combination of the two types of folding occurs. This folding is termed *flexural-slip fold* model and in this model, the slip planes are more widely spaced than in the flexural flow model (Fig. 3.13) where layer-parallel shear would be uniformly distributed throughout the layer. In flexural-slip folding bedding parallel shear is concentrated along the bedding planes (Price and Cosgrove, 1990).

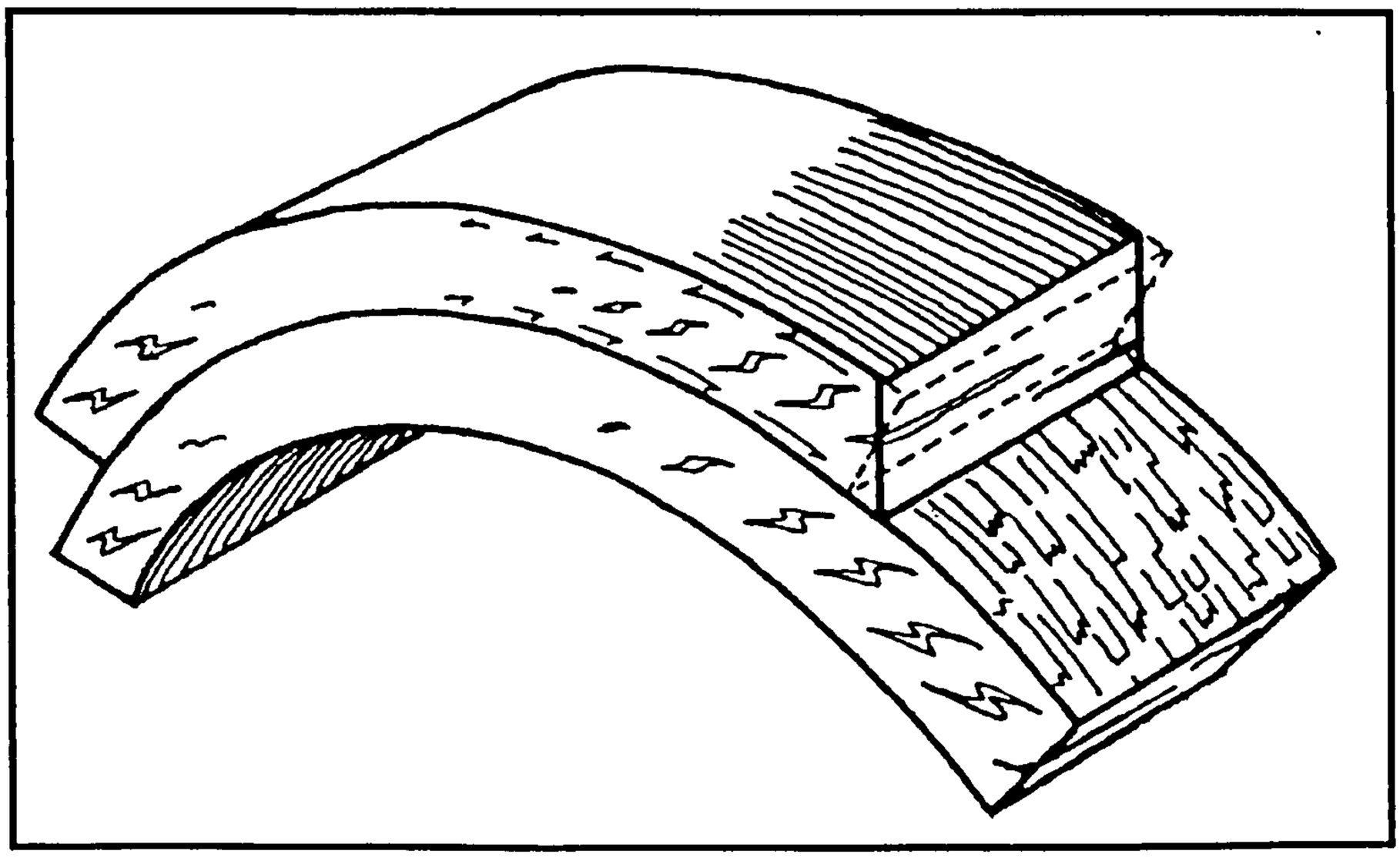


Figure 3.13 Flexural-slip folding (from Price and Cosgrove, 1990).

Folding by flexural slip leads to the partitioning and ordering of strains that are commonly expressed by means of faults, fractures and joints (Couples *et al.*, 1998). In a layered sequence such as a sedimentary succession, bedding plane slip occurs during folding along numerous bed-to-bed contacts and these slip surfaces partition the succession into mechanical units each of which deforms as though it were a single beam. Couples *et al.* (1998) argued that during flexural slip folding, the principal stress trajectories are only normal or parallel to the layering in limited areas and throughout the remainder of the folds they are inclined to the layer boundaries (Fig. 3.14). Nearly everywhere in the flexure, the stress trajectories are curved. Lack of distinct curvature and evidences of slip on the beds makes it difficult to demonstrate the association of joints with flexural-slip folding. Couples *et al.* (1998) argued that bedding plane slip develops in a sequential and hierarchical fashion and that the distribution of the resulting strains (expressed as joints or fractures) is complex.

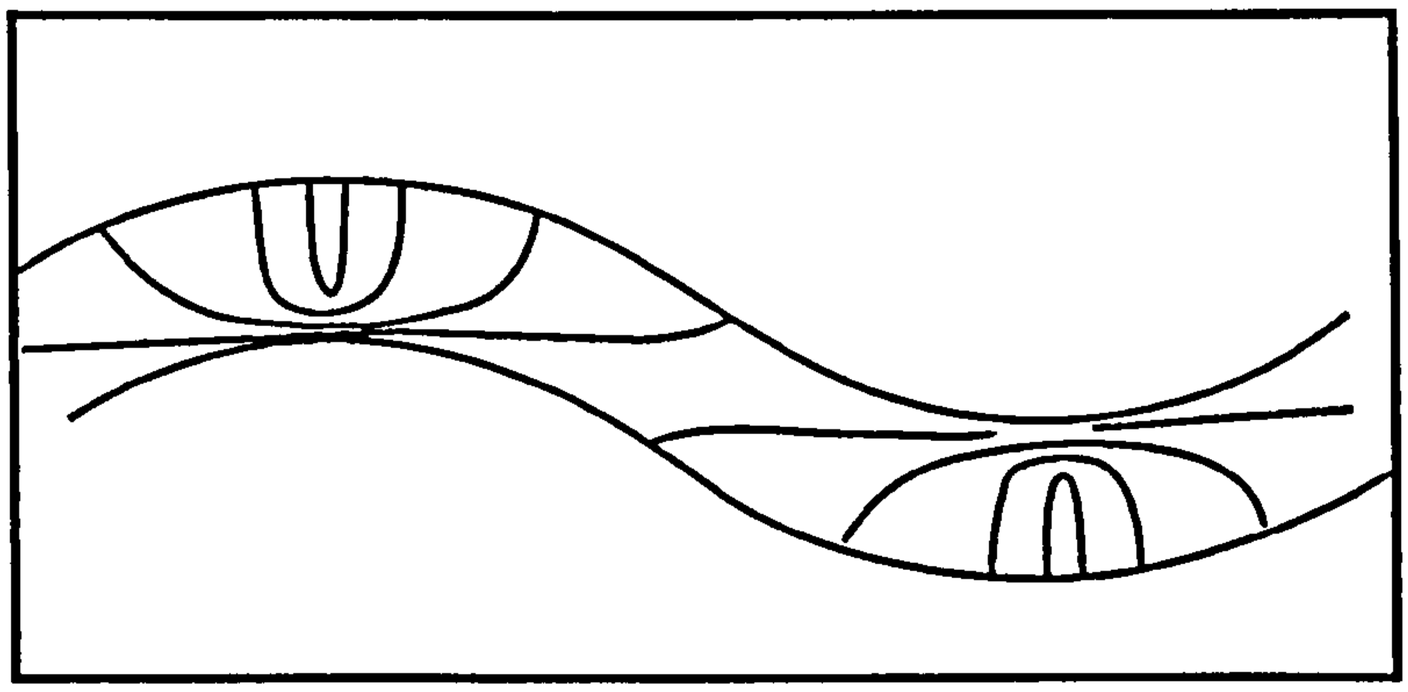


Figure 3.14 2D stress trajectories of a flexed homogeneous isotropic layer. The lines represent σ_1 trajectory (from Couples et al., 1998).

Price and Cosgrove (1990) discussed the relationship between folds and fractures. They argue that extensional joints, which are parallel and perpendicular to the fold axes, form at a high angle to the bedding (Fig. 3.15a). If the folded structures have a

rounded outline, they argue that the fractures will form a fan. These fractures may often be filled with calcite or quartz to form tension gashes. In both orientations, it is interesting here to note that during the formation of extension fractures in folded rocks, the minimum principal stress remains parallel to the bedding. The relationships between fold geometry and shear fractures that are commonly observed in nature are summarised in Figs. 3.15(b) and (c).

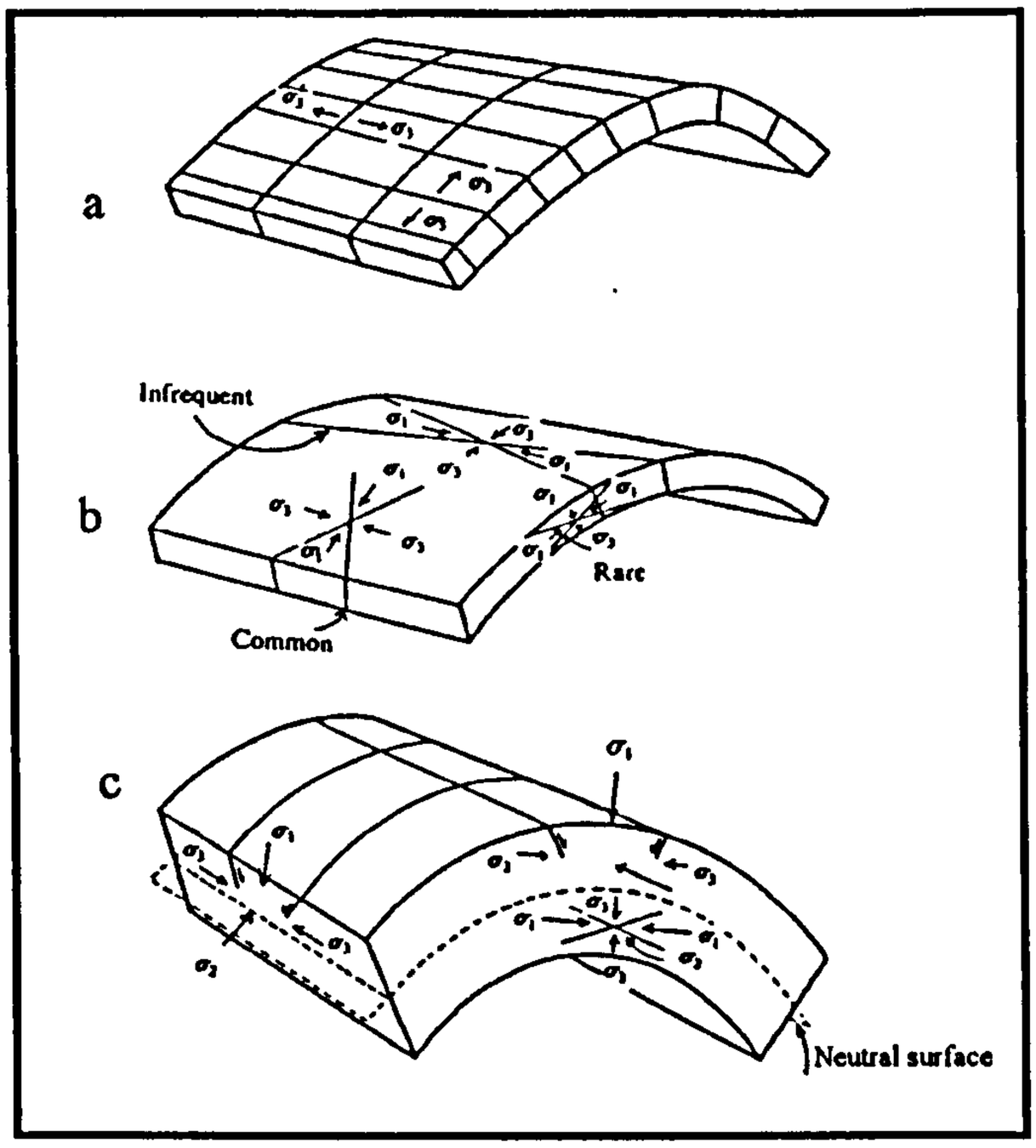


***Figure 3.15** Fracture patterns predicted from buckle folds (a) two orthogonal joints where the minimum principal stress remains parallel to bedding, (b) typical orientation of a shear fractures in a thin-bedded unit and (c) joints patterns expected to form in beds that deform by tangential longitudinal strain (from Price and Cosgrove, 1990).*

Based on numerical analysis, Hudleston *et al.* (1996) argued that strain patterns produced by flexural flow folding have not been documented in nature and suggest that the anisotropies required to produce the geometries and strains predicted by

flexural flow folds is unlikely in natural materials. Despite the fact that the distinction between *tangential longitudinal strain*, *flexural-slip* and *flexural flow folds* is clearly defined in the literature, their application in the field remains vague. Flexural flow folds are most likely to develop in rocks with high anisotropy such as those rich in aligned micas. Conversely rocks rich in quartz, feldspars and carbonates are unlikely to be highly anisotropic and by deform by flexural flow folding. Tangential longitudinal strain and flexural flow folds may be regarded as two ends of a complete spectrum. With increasing the thickness of the competent unit tangential longitudinal strain fold is progressively more favoured.

Cosgrove and Ameen (2000) make the comparison of the geometry, spatial organization and fracture patterns associated with forced folds and buckle folds. They suggested a way of predicting fracture patterns from folds where the exposures are very poor. They argue that once the fold geometry is deduced from various sources such as interpretation of seismic sections, it is possible to predict the fracture geometries. The fracture distribution around forced folds formed above reverse faults and normal faults is shown in Figs. 3.16(a) and (b). Analogue modelling of fracturing and forced folding in layers above basement oblique-slip faults has also been carried out (*e.g.* Richard, 1990). In those experiments different ratios of dip-slip and strike-slip movement on the "basement" fault were used. A discussion of the range of fracture patterns linked to these structures is beyond the scope of this work and the interested reader is referred to the original work.

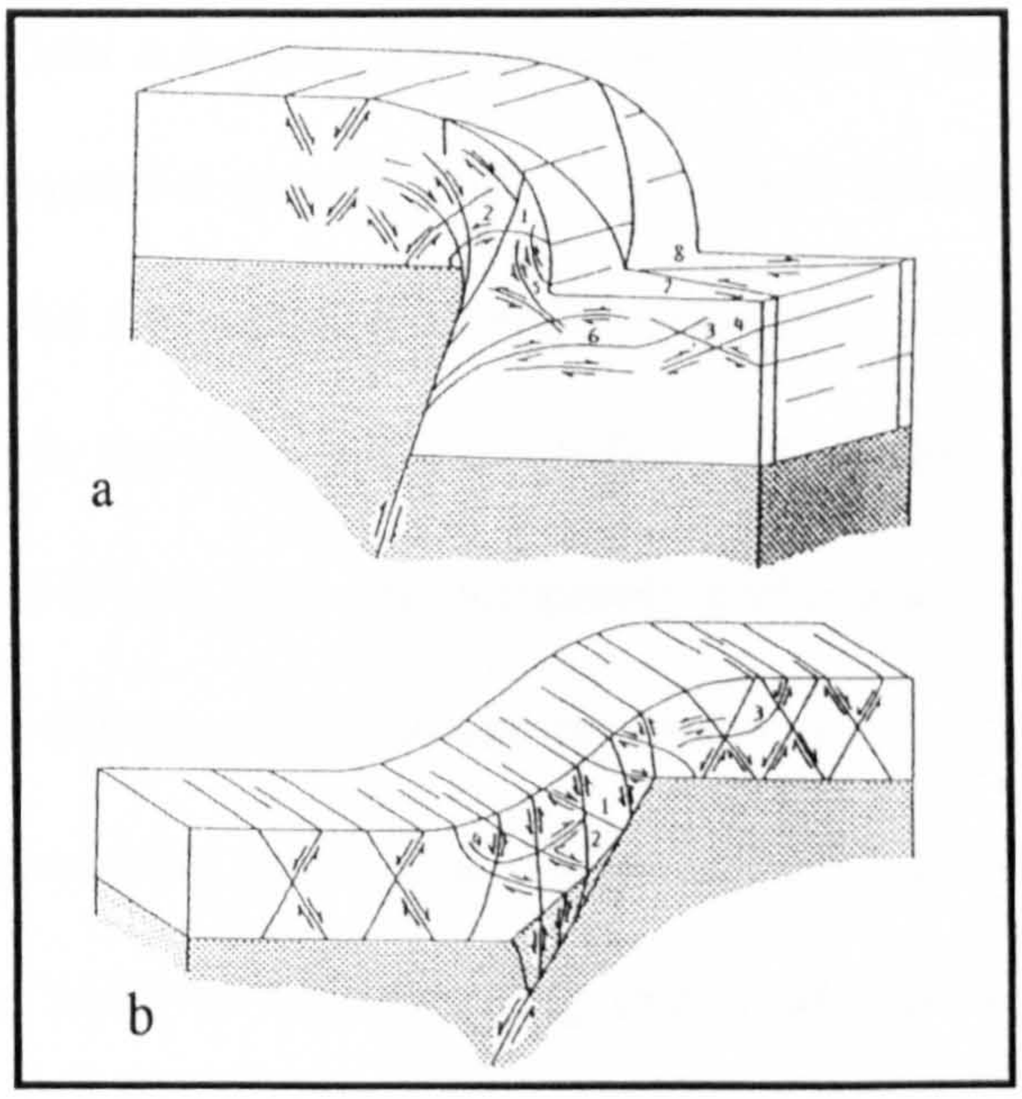


Figure 3.16 *(a) Fracture distribution predicted around reverse faults and (b) normal faults (from Cosgrove and Ameen, 2000).*

3.6.3 Joints

Investigations by Dyer (1988) showed that younger joints may show a systematic change in orientation as they approach older through-going joints. This change in orientation reflects a change in the stress field as the younger joint set is growing. If the later joints are not parallel to the pre-existing through-going joint, and they initiate at a distance and propagate toward the through-going joint, the stress field in which the new joint grows will change systematically because of the presence of the pre-existing joint (Fig. 3.17). He argued that the systematic change in orientation of younger joints reflects the change in the principal stresses near the through-going joint and can be used to estimate the ratio of the far-field horizontal stresses. Dyer shows that the sense of rotation and change in the magnitude of the principal stresses near an existing joint are functions of the orientation and the ratio of magnitudes of the far-field principal stresses and the coefficient of friction across the joint. He combined field studies in the Salt Valley Anticline of the Arches National Park, southern Utah

with analytic stress field solutions. The field observations and theoretical analyses showed that a curving parallel geometry of younger joints is indicative of a stress field in which the ratio of the maximum (σ^{∞}_{H}) and the minimum (σ^{∞}_{h}) principal horizontal far-field stresses lies in the range $-3 < \sigma^{\infty}_{H}/\sigma^{\infty}_{h} < -1/3$. In this case a large negative number means that the σ^{∞}_{H} is large and compressive whereas σ^{∞}_{h} is effectively tensile (Engelder, 1993). For curving perpendicular joints the ratio must lie in the range $-1/3 < \sigma^{\infty}_{H}/\sigma^{\infty}_{h} < 1$. To summarise, curving parallel younger joints indicate a compressive stress parallel to the walls of through-going joints, whereas curving perpendicular geometry indicates an effective tension parallel to the walls of the through-going joints.

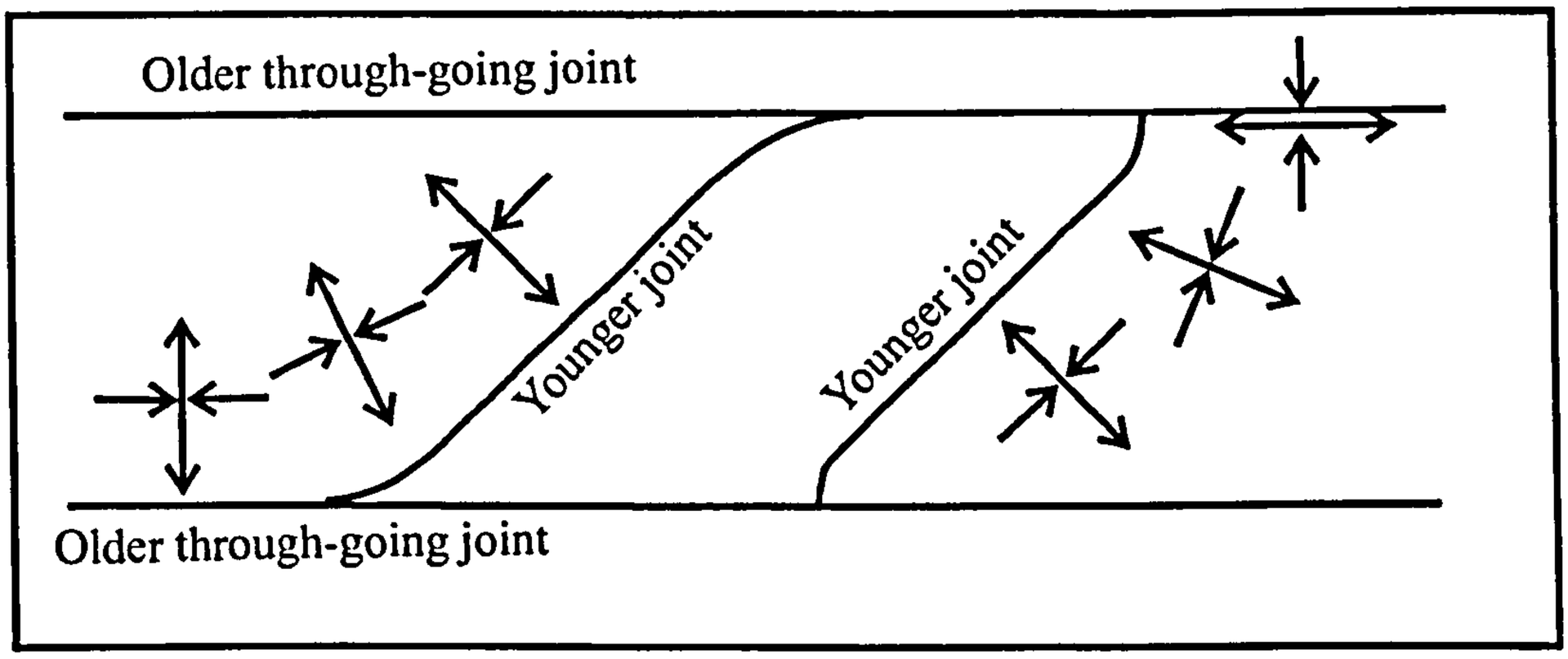


***Figure 3.17** Map view of the two ways in which the state of stress may rotate to accommodate a free surface at a through-going joint. Orientation and magnitude of principal stress in mid-region between the through-going joint approximates the remote stress during the propagation of younger joints (from Dyer, 1988).*

3.6.4 Burial and uplift

Price and Cosgrove (1990) analyse the stresses developed in a sedimentary layer within an elliptical basin such as thermal subsidence basin and make predictions regarding the trends of the fractures that may develop (Fig. 3.18). Fractures associated

with burial and increase in overburden stress is shown in Fig. 3.18(a) and fractures associated with subsequent uplift are shown in Fig. 3.18(b). The detailed description of this analysis is beyond the scope of this work and the interested reader is referred to Price and Cosgrove (1991). Attempts have been made to distinguish between these burial and uplift joints. For example Bahat (1999) based on his field study of the Lower Eocene Chalks in Beer Sheva, Israel discusses ways of distinguishing single layer burial joints (in Lower Eocene chalk) from single layer uplift joints (in the Middle Eocene chalk). He argues that single-layer burial joints tend to form early in the rock history, are limited to one layer and often tend to be arrested at the interface between two beds. Uplift joints develop at a late stage in the geological history of a rock, have a wider opening and are more irregularly spaced than burial joints. He notes that the distinction between single-layer uplift and single-layer burial joints can often be very difficult.

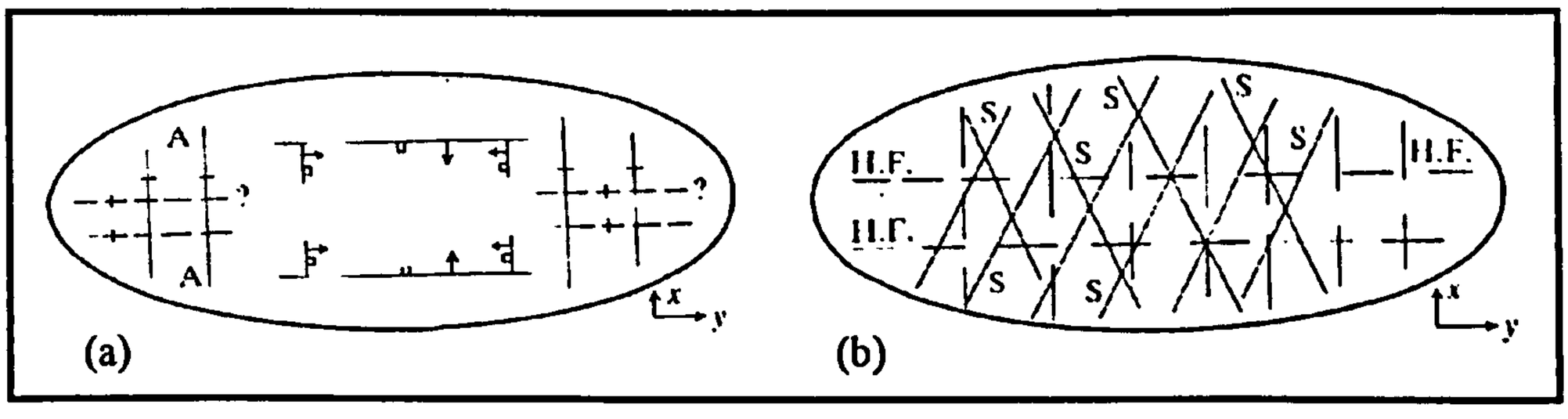


***Figure 3.18** Joint orientations predicted during (a) down-warp and (b) uplift (from Price and Cosgrove, 1990).*

CHAPTER FOUR

FIELD OBSERVATION AND ANALYSIS OF JOINT SPACING, ORIENTATION AND DENSITY

4.1 Introduction

Patterns of orientation and spacing of joints have been studied in two field areas, namely in the Pennines of North Yorkshire and on the southern shore of the Bristol Channel Basin. Joints in the Pennines are generally *through-going* fractures whereas in the Bristol Channel Basin they are confined largely to individual beds (*layer-bound*). The classification of joints into *layer-bound* and *through-going or composite* has implications for fluid flow in fractured rock masses (Odling *et al.*, 1999). They argue that in the former case, the absence of joints that penetrate across the layer boundaries (*i.e.* bedding) tend to inhibit cross-bed flow and bulk rock permeability is therefore directed mainly parallel to the bedding. Through-going joints, on the other hand, facilitate cross-bed flow and the contrast in bulk rock permeability parallel and perpendicular to the bedding is less marked. Whether or not the joints form as layer-bound or through-going depends, in part, on the nature of the bedding interface and on the applied normal load across the interface.

The terms (i) *layer-bound* and (ii) *through-going* joints are used in this thesis. The former term describes joints that are confined to a single mechanical layer and the second describes vertically persistent joints that do not terminate at the bedding interfaces. Odling *et al.* (1999) describe them as strata-bound and non-strata-bound joints and propose the two as end members in a spectrum of possible joint types. Gillespie *et al.* (2001) define a persistence ratio that indicates the proportion of joints that cross the bedding interface relative to the total number of joints contained in each bed.

Joint density is defined by Odling (1992) as the number of joints per unit length along a scan line or the total joint length per unit area or the total joint surface area per unit volume in 3D. Some previous workers (*e.g.* La Pointe, 1988; USNRC, 1996; Mauldon *et al.*, 2001; Al-Mahruqi, 2001) define joint density as the number of joints per unit area. This definition has shortcomings arising from variations in the lengths of joints in a particular area. In 2D, the longest and the shortest joints in a given sample are given equal importance. In this study the *number* of joints has not been used to calculate density in 2D.

For joints showing *en-echelon* arrangements, the *array length* to *spacing* is defined in this study as a ratio of the total length of *en-echelon* joints to the mean perpendicular distance within an *en-echelon* array.

4.2 Review of previous work

No recent and systematic study of joint spacing in the Pennines is available. Joint density and its relationship to lithology in the Great Scar Limestone was studied by Doughty (1968) and Carboniferous joints in the North of England and their relations to other structures are highlighted in a study by Moseley and Ahmed (1967). A detailed description of the geology, major structures and mineralization in the region has been presented by Dunham and Wilson (1985).

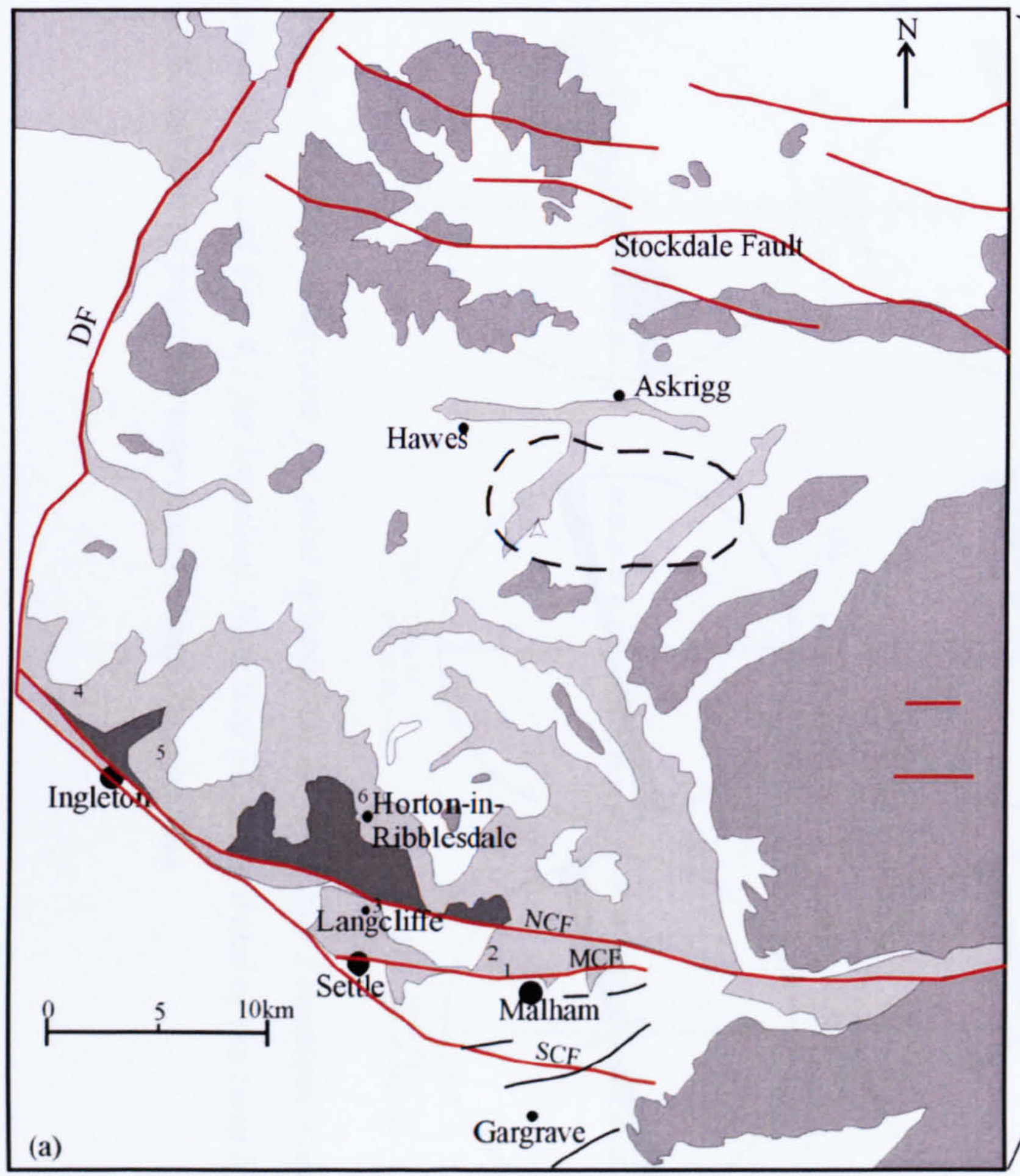
In the Bristol Channel Basin, Kamerling (1979) and Whittaker and Green (1983) give a detailed description of the stratigraphy. The region has been used to study various structures such as normal faults (Peacock and Sanderson, 1991; Nemčcok and Gayer, 1996), inverted normal faults and thrust faults (Brooks *et al.*, 1988; Chadwick, 1993;

Dart *et al.*, 1995; Nemčok, *et al.*, 1995), strike-slip faults (Peacock and Sanderson, 1995), veins (Caputo and Hancock, 1999; Cosgrove, 2001) and joints (Loosveld and Franssen, 1992; Rawnsley *et al.*, 1992 and 1998; Engelder and Peacock 2001; Al-Mahruqi, 2001; Belayneh, in prep.). The deformation history of the region have been considered by Dart *et al.* (1995).

4.3 Joints of the Pennines

4.3.1. Malham Cove and surrounding area 2

Massive bedded, grey limestones consisting of packstones and grainstones of Lower Carboniferous age are exposed at Malham Cove. The first area of exposure that was studied lies at grid reference 897641. As described in section 2.2 of Chapter 2, the Cove Limestone is light grey and massive, consisting of packstones and grainstones. The dip/dip direction of the limestone bed is 10°/040°. There are two main joint sets in the area. These are the NNW-SSE and ENE-WSW to NE-SW sets. Most of the joints do not terminate at bedding planes and propagate vertically upwards or downwards across the bedding interface. 20 scan lines were measured at Malham Cove (see Figs. 4.1(a) and (b) for location) and the trend of each scan line is shown in Fig. 4.1(c). Joint strike is plotted on rose diagrams (Fig. 4.2). The rose diagrams show that the joints strike predominantly in ENE-WSW and NNW-SSE directions with subordinate joints striking N-S and E-W. As illustrated in Fig. 4.2, the majority of rose diagrams show a predominant fracture set striking ENE-WSW. This is because the scan lines are orientated NNW-SSE *i.e.* are sub-parallel or at very low angles to another important fracture set (see Fig. 4.1c).



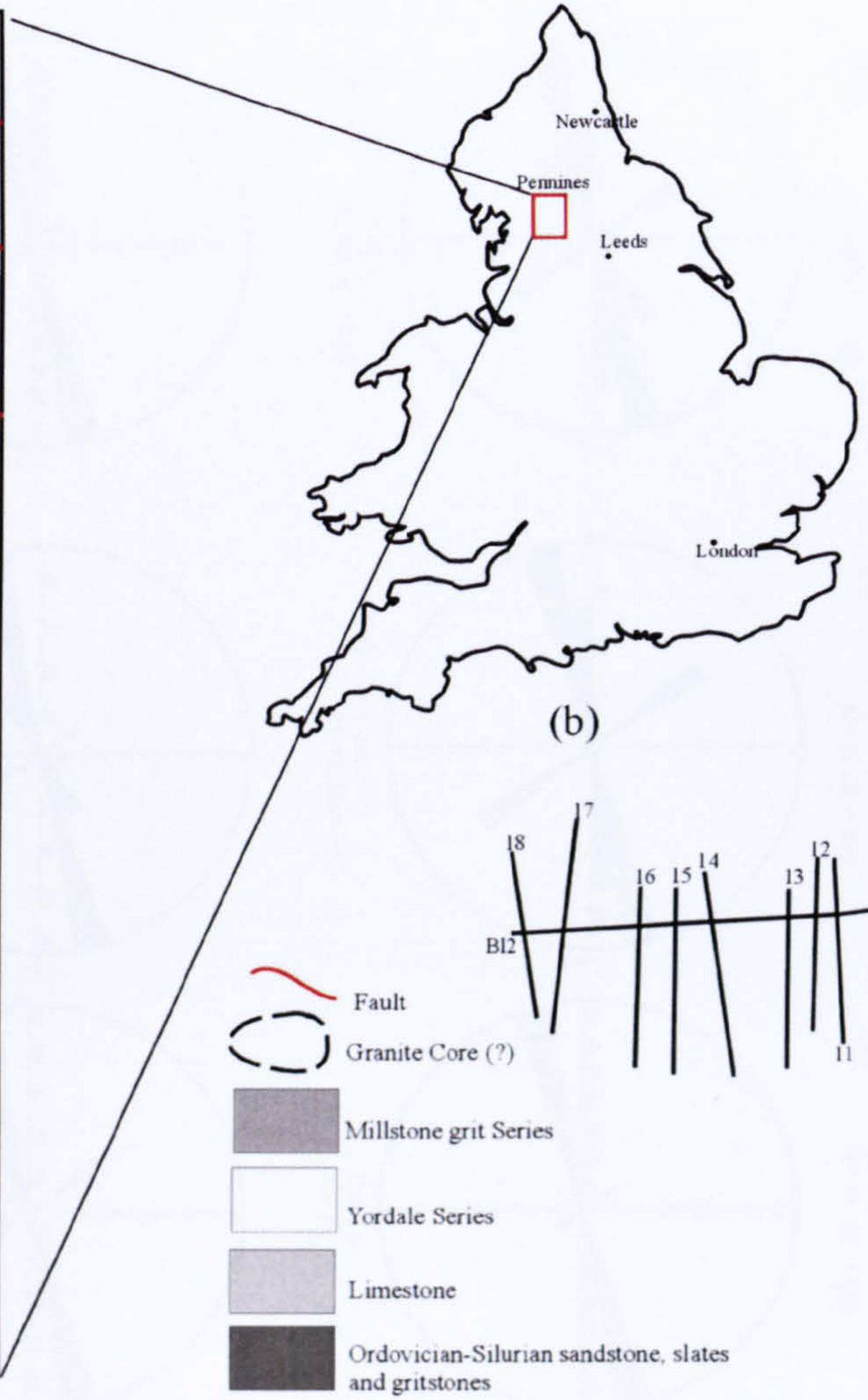
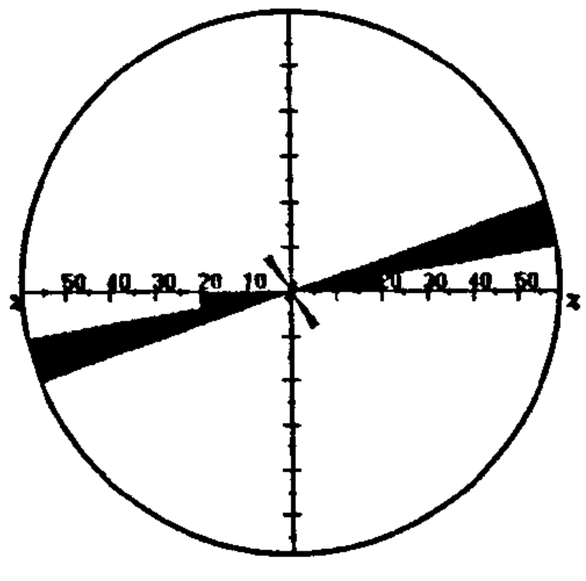
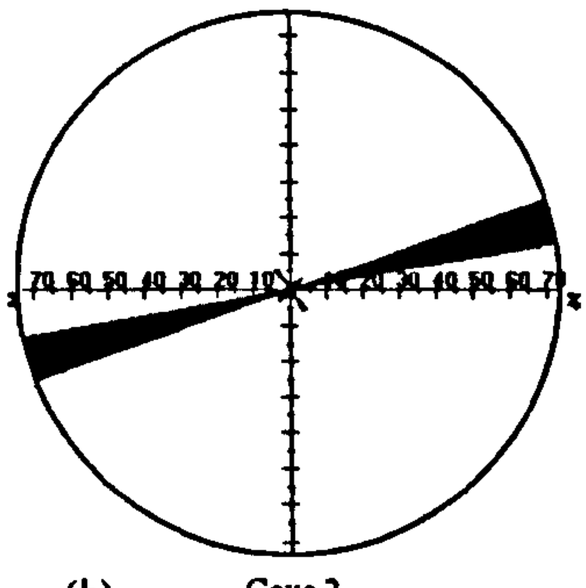


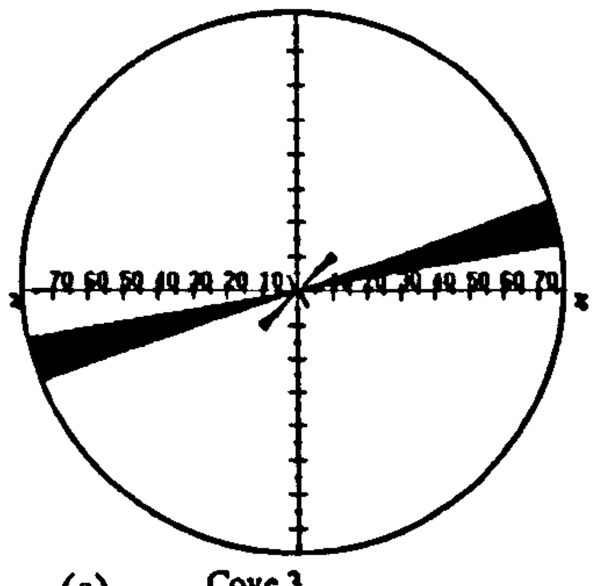
Figure 4.1 *(a) Simplified geological map of the study area in the Pennines, North Yorkshire, (b)index map and (c) lay out of scan line at Malham Cove.NCF-North Craven Fault; MCF-Middle Craven Fault; SCF-South Craven Fault; DF-Dent Fault (Taken and modified from Wilson, 1997). (1) Malham Cove, (2) area 2, (3) NE Langcliffe, (4) NW Ingleton, (5) NE Ingleton and (6) Horton-in-Ribblesdale (see text for details).*



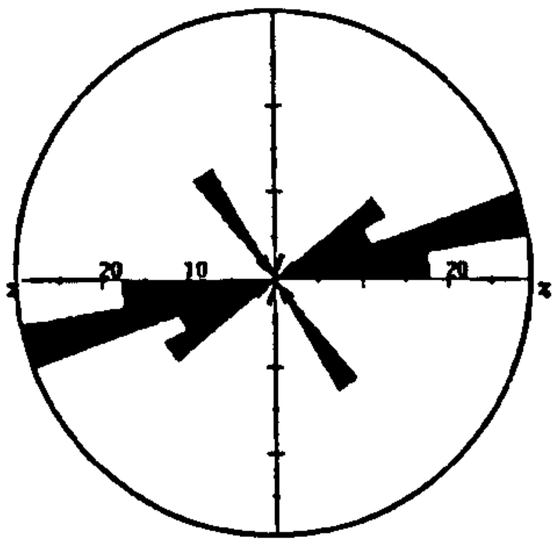
(a) Cove 1
N=44, SL = 340



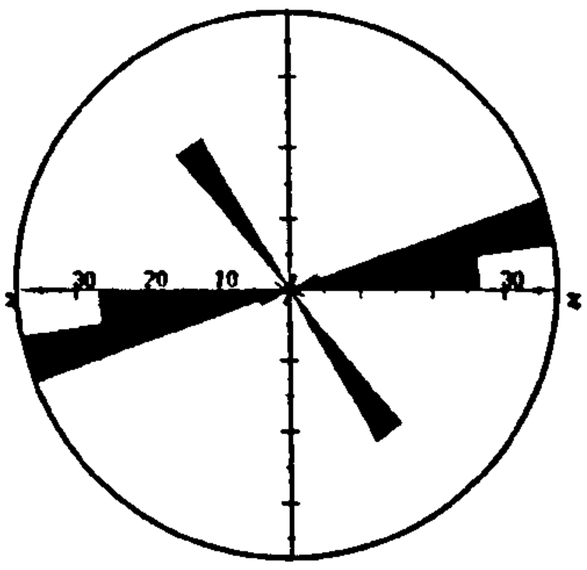
(b) Cove 2
N=45, SL = 350



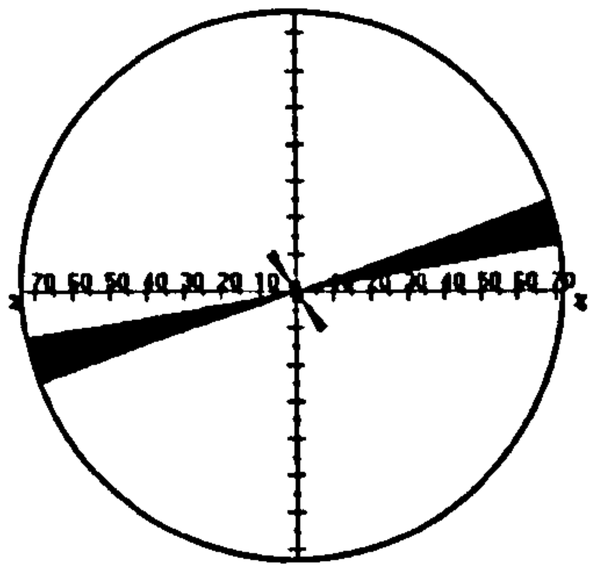
(c) Cove 3
N= 41, SL = 350



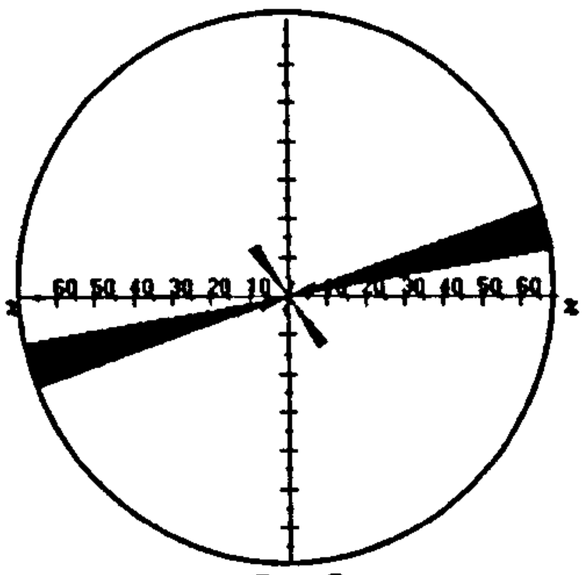
(d) Cove 4
N=34, SL = 345



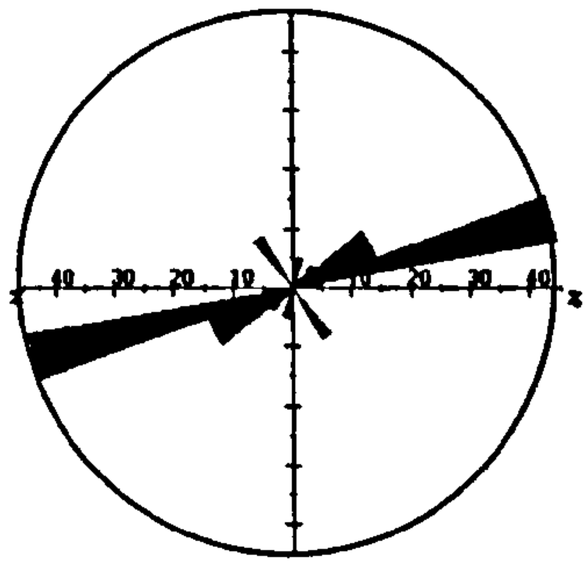
(e) Cove 5
N=45, SL = 355



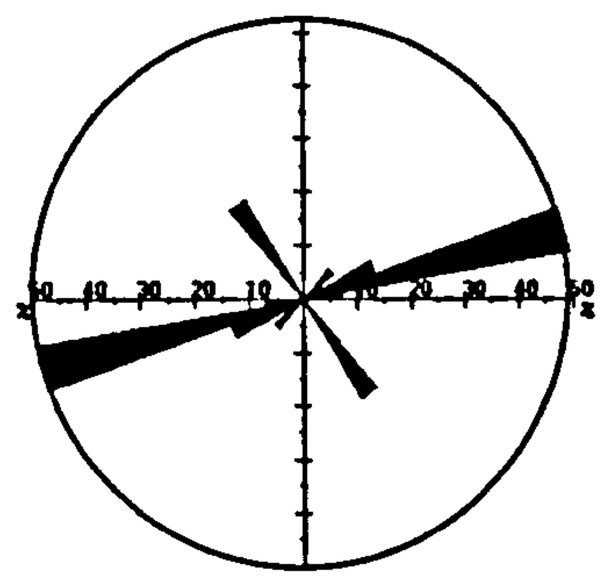
(f) Cove 6
N= 33, SL = 355



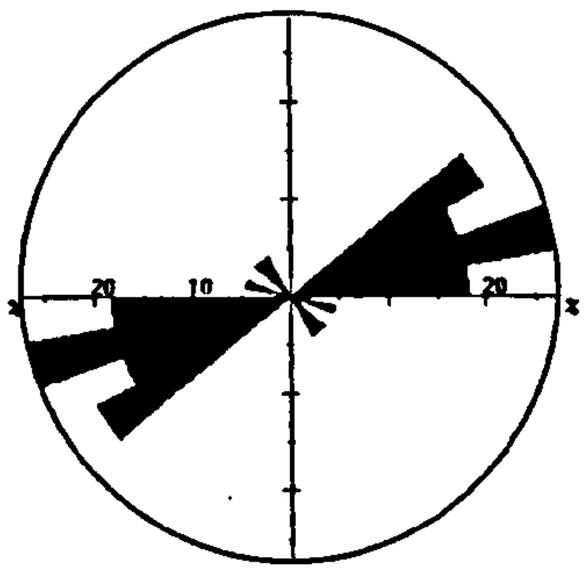
(g) Cove 7
N= 26, SL = N-S



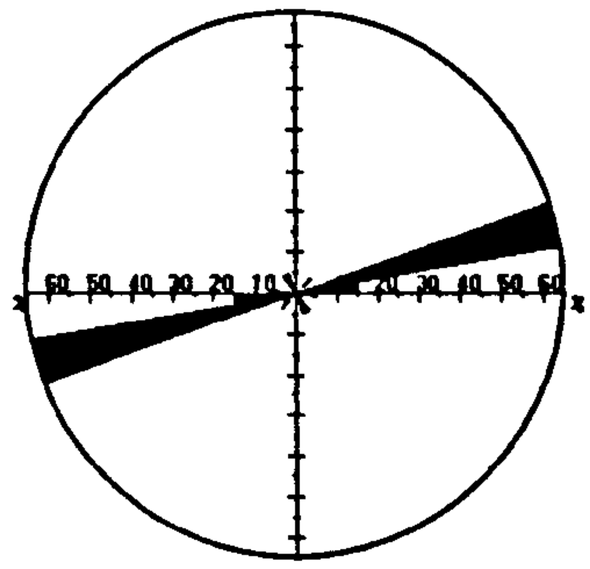
(h) Cove 8
N= 20, SL = 355



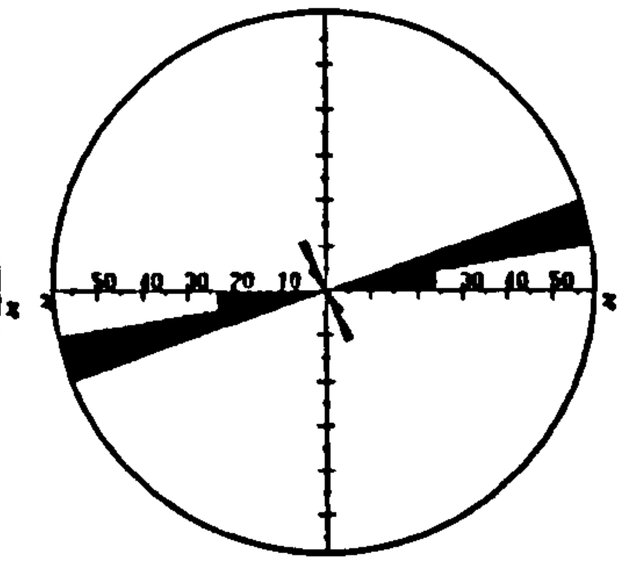
(i) Cove 9
N= 14 . SL. = 350



(j) Cove 10
N= 22, SL = 358

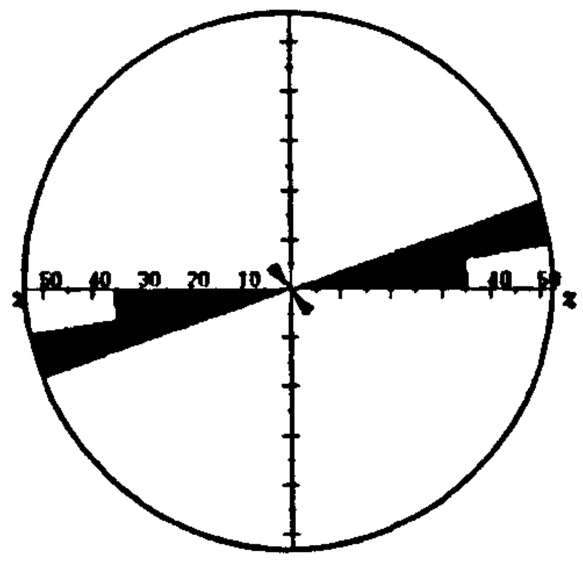


(k) Cove 11
N= 20, SL = 355

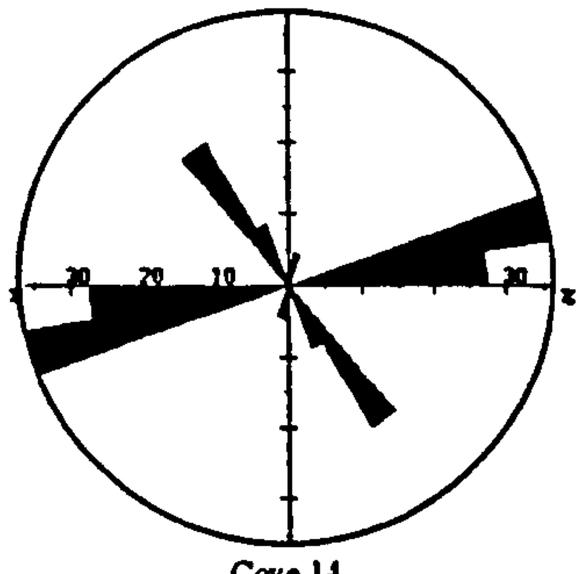


(l) Cove 12
N= 17, SL = 10

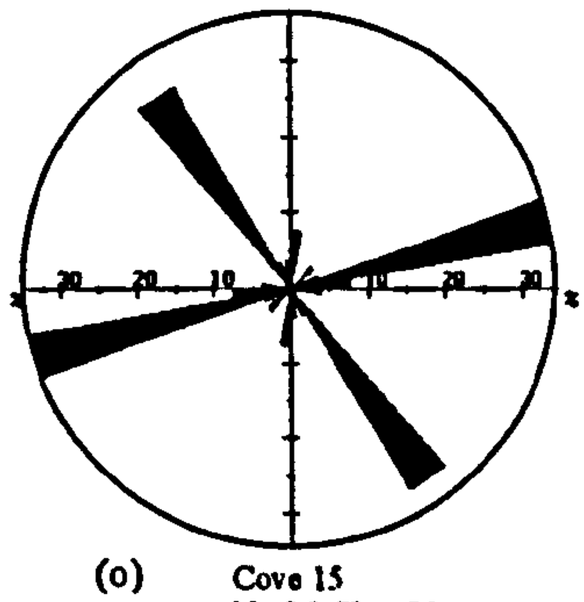
Figure 4.2 *Rose diagrams for joint orientation in the Cove Limestone (see text for explanation and Fig. 4.1 for location). Note that SL is the trend of the scan line and N is the number of fractures intercepted along the scan line.*



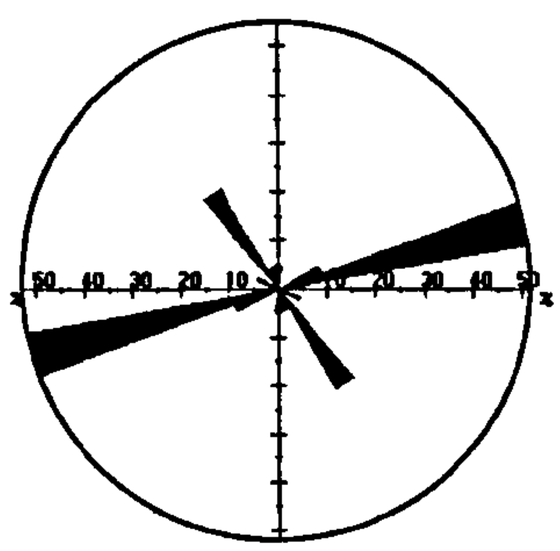
(m) Cove 13
N= 17, SL = 10



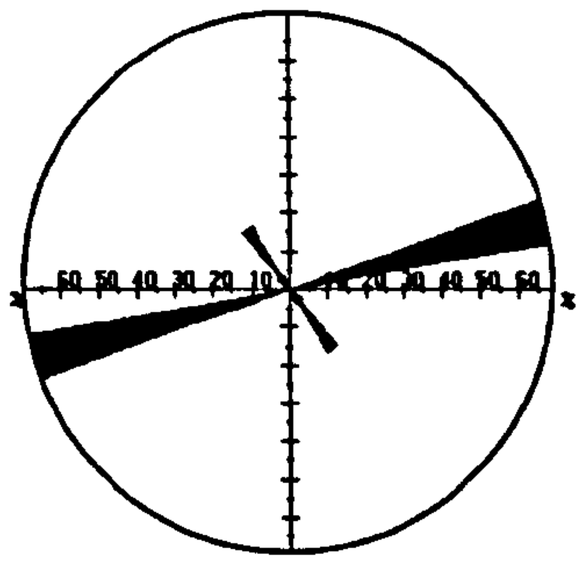
(n) Cove 14
N= 22, SL = N-S



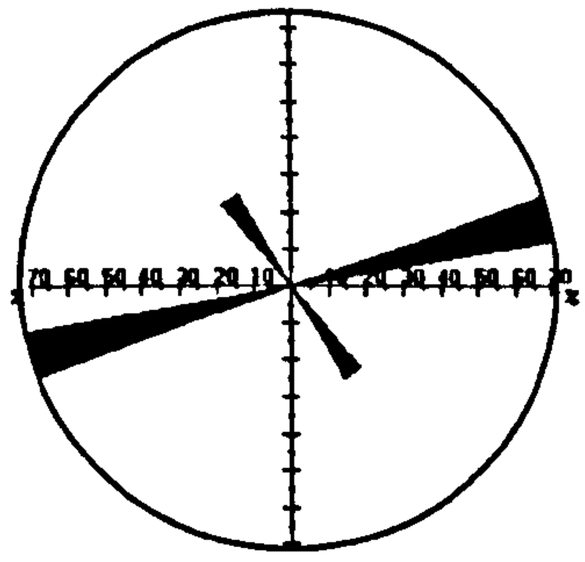
(o) Cove 15
N= 26, SL = 20



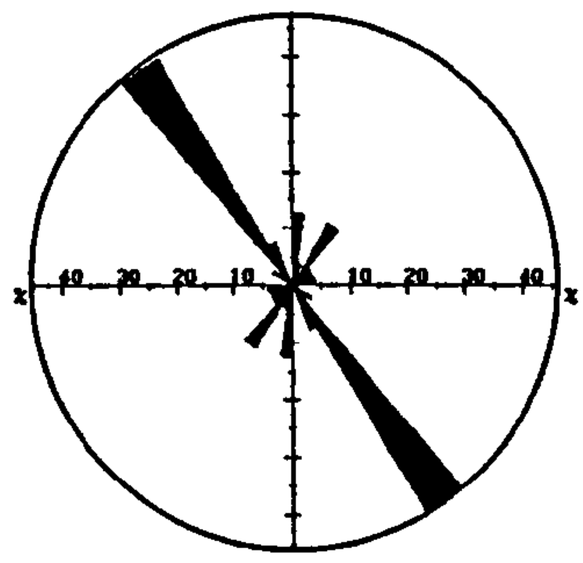
(p) Cove 16
N= 21, SL = 201



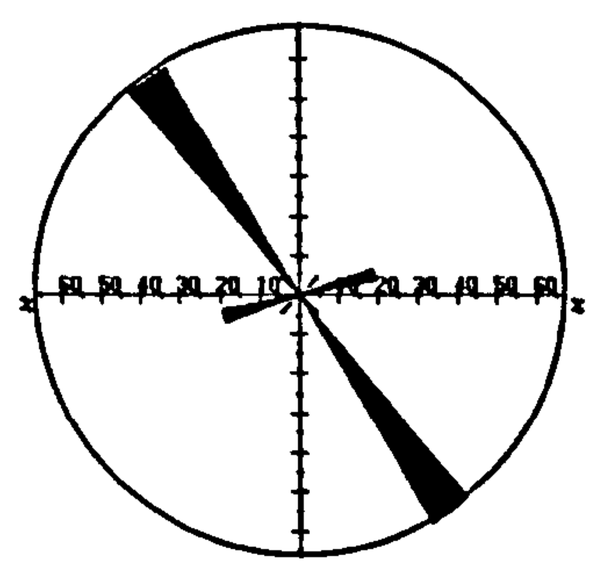
(q) Cove 17
N= 26, SL = 25



Cove 18
N= 21, SL = 10



(s) B11
N= 24, SL = 80



(t) B12
N= 15. SL = 85

***Figure 4.2** (continued) Rose diagrams for joint orientation from Malham Cove. Note that SL shows the orientation of the scan line and N represents the number of fractures intercepted along the scan line.*

Some of the ENE-WSW joints show a closely spaced, left-stepping *en-echelon* arrangement. The propagation path for these joints is roughly straight, even for those with a very small spacing. According to Olson and Pollard (1988 and 1989) this organization of joints probably indicates that they propagated under the influence of a high, remote horizontal differential stress. The NNW-SSE set consists of long straight joints and commonly shows right-stepping closely spaced *en-echelon* arrangements.

Based on earlier investigations in the region (*e.g.* Moseley and Ahmed, 1967; Doughty, 1968) and on my field observations, it is deduced that the NE-SW and NNW-SSE joint sets are a conjugate pair. The acute angle between the joint sets (2θ) varies between 65° and 70°. Of the scan lines measured at Malham Cove, 75% show the bisector of the acute angle (which is the direction of the maximum principal stress (σ_H) to be oriented 115°. The remaining 25% of the data indicates that σ_1 lies within ± 5° of 115°. In addition, joints striking 110° were observed locally filled by calcite veins (Fig. 4.3) and provide further evidence of the orientation of σ_1 during the formation of joints in the area.



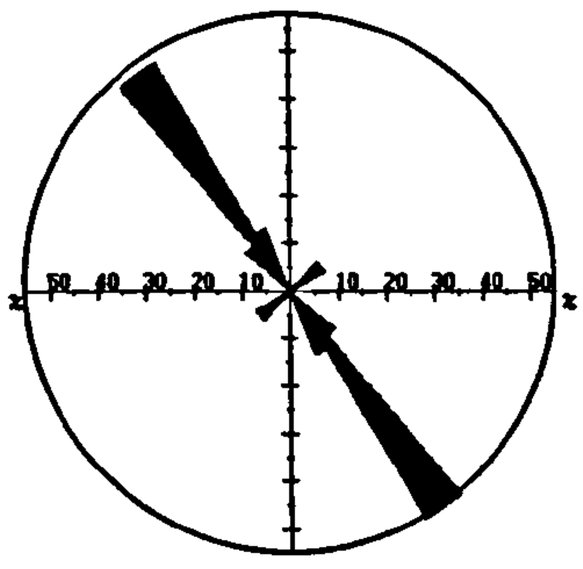
Figure 4.3 *Veins striking ESE-WNW (110°) locally observed in the area.*

The second study area (area 2) is situated 1km NW of the previous site at grid reference 894645 (see site 2 in Fig. 4.1) on the same rock types, *i.e.* packstones and grainstones. One E-W and four N-S scan lines spaced 3metres apart were measured. Two additional scan lines were run in the 030° and 060° directions. Rose diagrams show the strike of joints sampled along the scan lines (Figs. 4.4a-g). Apart from minor local variations in strike, the joints are regionally consistent from Malham Cove in the east to Ingleton in the west. As described above, the ENE-WSW and NNW-SSE joints in the Malham Cove area are considered to be conjugate sets with an acute angle of ≤90° (Fig. 4.4a-g). In places it exceeds the theoretically predicted angle of maximum

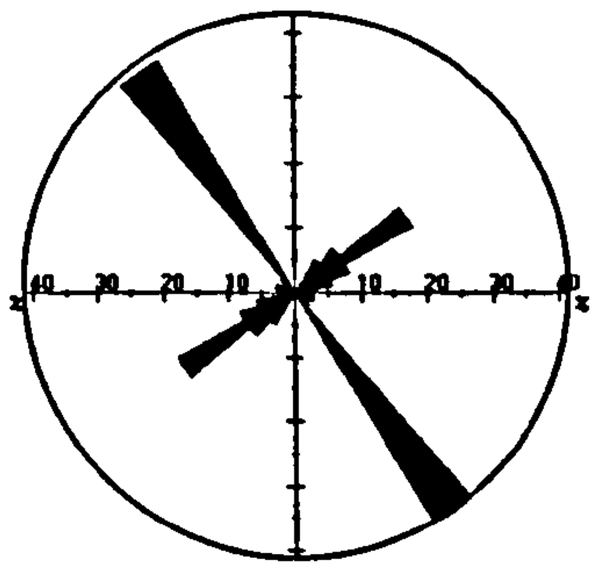
shear stress (τ_{max}). The variation of the acute angle from 60° to 70° in Malham Cove to 90° or slightly higher in area 2 may be caused by pressure solution. Continued compression causes the limestone along the joints to be removed by pressure solution and this results in opening of the acute angle. This process is similar to the negative dilational model of Ramsay and Huber (1987, p.629). Ramsay and Huber argue that the acute angle (2θ) is facing the direction of bulk shortening. Where the veining is developed, the acute angle between the zones may reach or even exceed the predicted angle of maximum shear stress (τ_{max}).

4.3.2 Langcliffe, Settle and Giggleswick

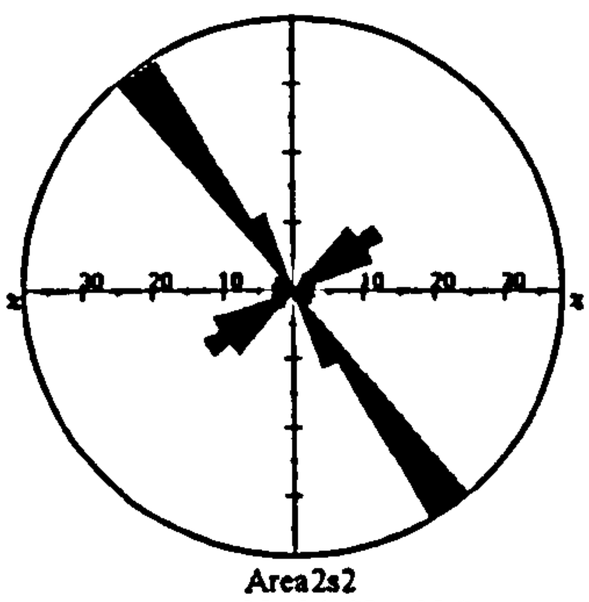
Because of the lack of well-exposed outcrop for scan line and window sampling in the study area of north Yorkshire, the author carried out measurements over a large area, especially around the Middle and Craven faults, where the cover has been removed by erosion. Two scan lines were run east of Langcliffe (grid reference 830655) (see location 3 in Fig. 4.1). The rock type exposed in the area is Cove Limestone consisting of patches of monotonous packstones and grainstones. The dip/dip direction of bedding is 10°/300°. The bedding planes are mostly defined by stylolites. The first scan line trends 020° and the rose diagram shows joints striking 150° with a subordinate population in a direction 055° (Fig. 4.4h). The second scan line trends 035° and the strike of joints on the rose diagram shows a single maximum at 150° (Fig. 4.4i). Joints observed in this area have the same strike observed elsewhere in the region and, in addition, the NW-SE joints show a right-stepping *en-echelon* arrangement. This indicates that the maximum horizontal compression during the propagation of the joints was in an ESE-WNW direction.



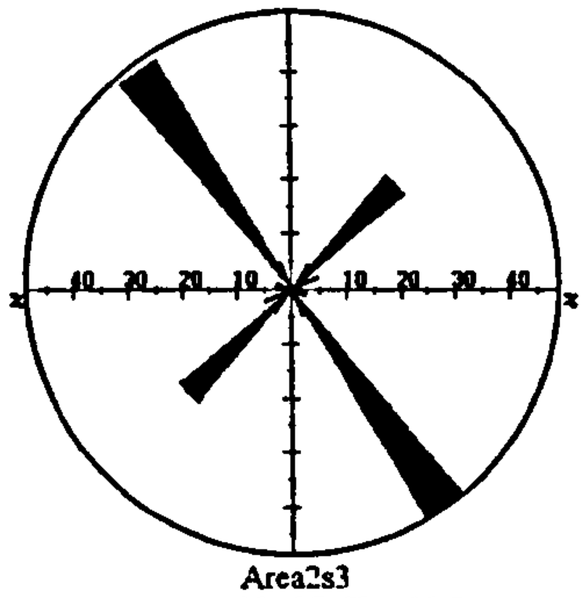
(a) Area2b1
N= 49, SL = 90



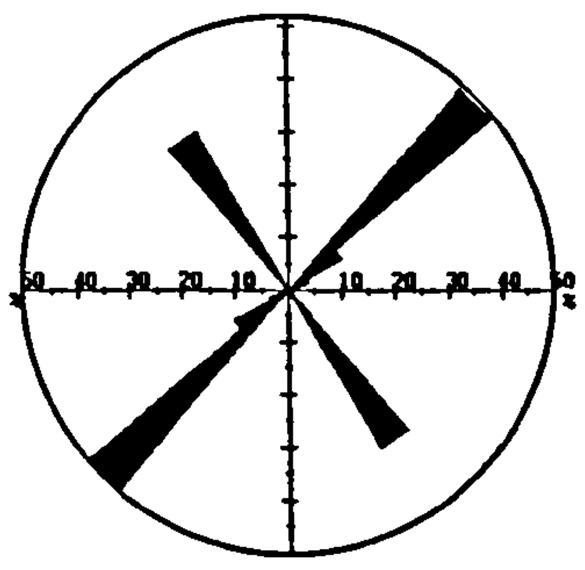
(b) Area2s1
N= 34, SL = N-S



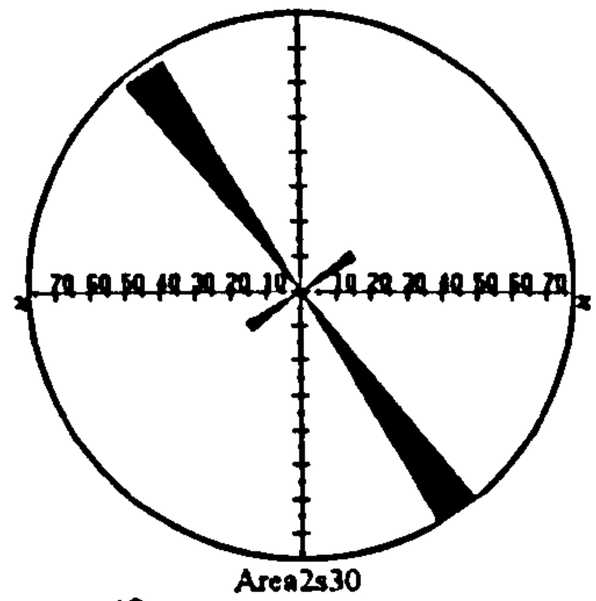
(c) Area2s2
N= 34, SL = N-S



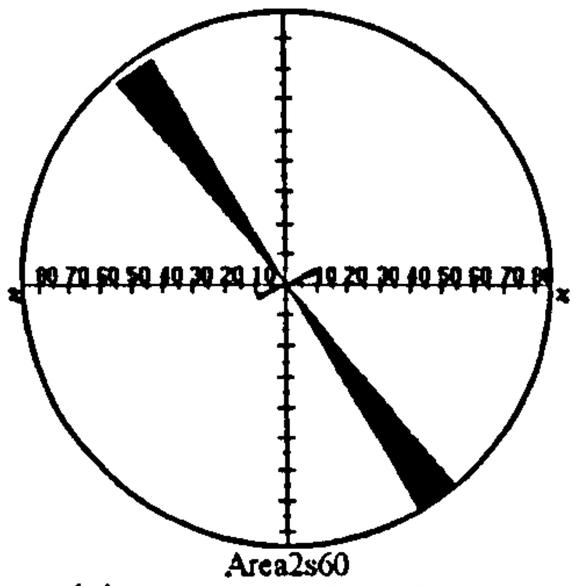
(d) Area2s3
N= 37, SL = N-S



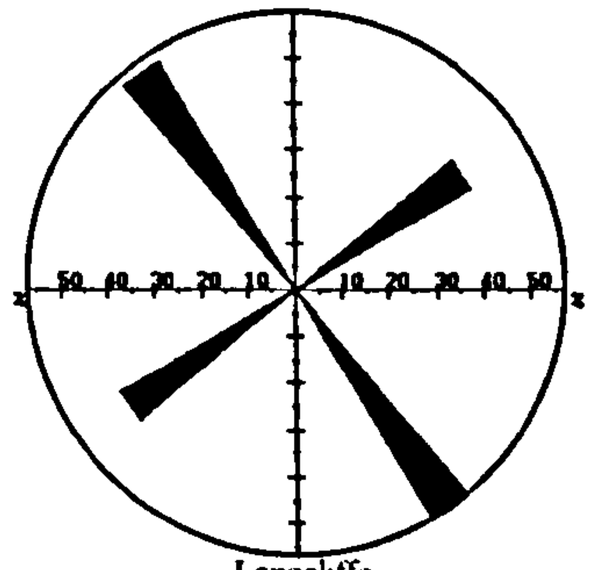
(e) Area2s4
N= 26, SL = N-S



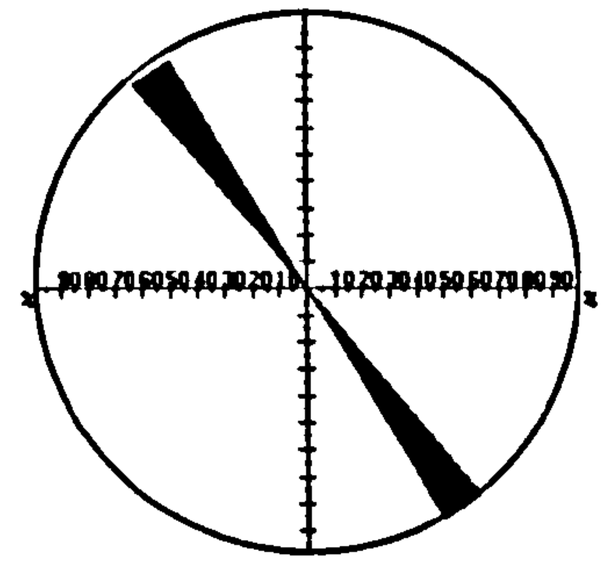
(f) Area2s30
N= 51, SL = 30



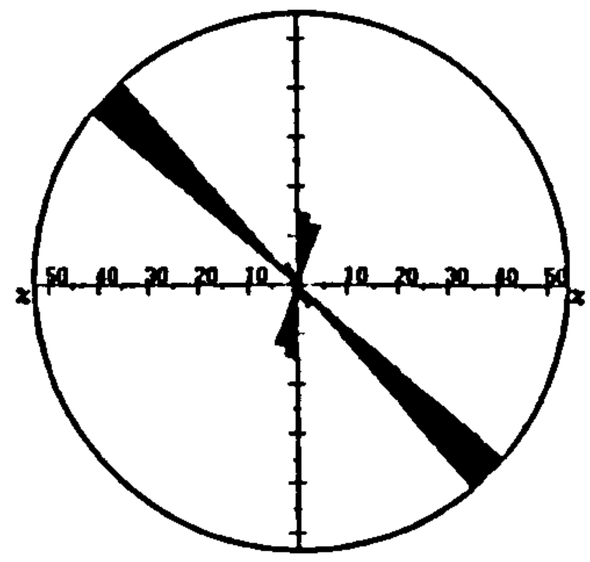
(g) Area2s60
N= 52, SL = 60.



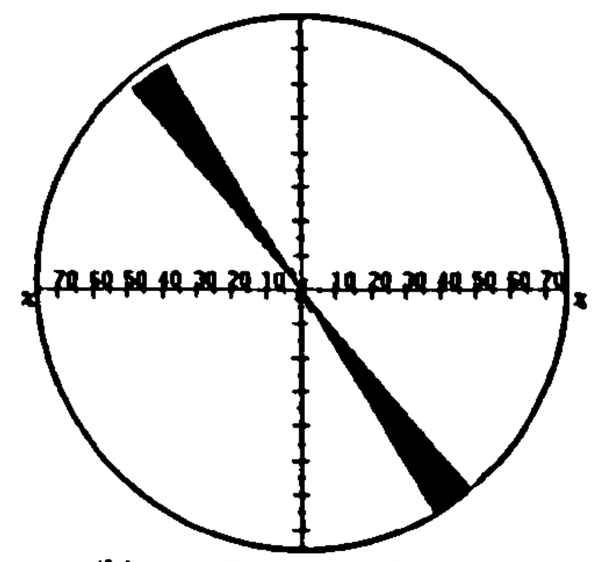
(h) Langcliffe
N= 37, SL = 20



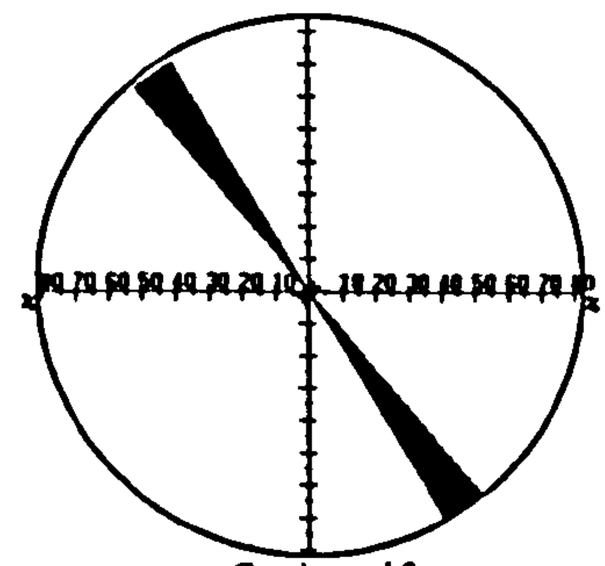
(i) NE of Langcliffe
N= 77, SL = 35



(j) Giggleswick1
N= 62, SL = 70



(k) Giggleswick2
N= 58, SL = 25



(l) Giggleswick3
N= 54, SL = 30

***Figure 4.4** Rose diagrams for area 2, Langcliffe and Giggelswick (see Fig. 4.1a for location of the areas). Note that SL is the scan line orientation and N is the number of joints along the scan line.*

The bedding planes are mostly defined by rough stylolites (Fig. 4.5). Stylolites are one of the most common features in calcareous rocks. The surfaces have a castellated appearance and the amplitude of the castellation range from a few mms to a few cm. The bedding-parallel stylolites were formed during burial (*i.e.* during diagenesis) when σ_1 was vertical and caused by the mass of the overburden. Stylolites have been classified as (i) wave like, (ii) sutured type, (iii) up-peak, (iv) down-peak, (v) sharp peak or conical and (vi) seismogram type. Stylolites can be used as palaeo-stress indicators with the apex of the 'saw teeth' indicating the direction of shortening. Stylolites form in rocks under the influence of compressive stress. They usually form along pre-existing discontinuities such as bedding planes and fractures. However, they can also form in rocks containing no discontinuities when they are initiated from irregularities or heterogeneities in the rock matrix. The two sides of the stylolite interpenetrate as a result of dissolution of rock at the boundary. In places they are coated by thin film of clay residues, carbonaceous matter, iron oxides or other insoluble minerals.

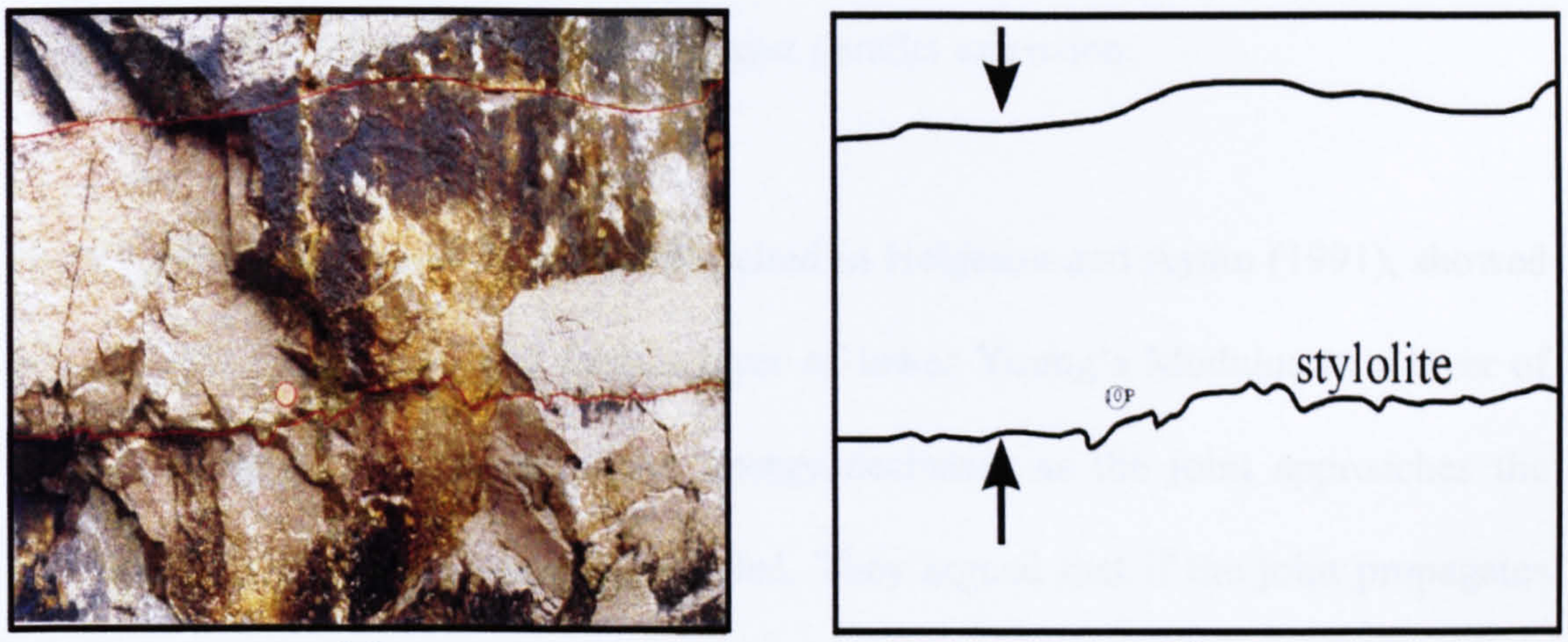


Figure 4.5 *(a) photograph and line drawing of (b) bedding-parallel stylolite indicating vertical shortening caused by the overburden pressure at Giggleswick quarry. Arrows indicate direction of maximum compressive stress. Coin in the left centre is 2.5cm in diameter.*

Previous studies of joint propagation (*e.g.* Renshaw and Pollard, 1995 and references therein) present that in an environment with modest compression acting perpendicular to the bedding, slip and opening along the interface as a joint tip approaches the bedding interface reduces the degree of stress concentration at the tip of the joint and propagation ceases. However, if bonding exists across the bedding and/or the compressive stress acting normal to the interface is sufficiently high, any opening and slip along the interface will be inhibited and thus the propagation of joints across the bedding will be facilitated and multilayer rather than single layer joints will form. Finite element models (Al-Mahruqi, 2001) confirm that when interfacial slip is not allowed (*i.e.* the contact is welded) fractures are able to propagate across the interface. In addition, Al-Mahruqi showed that when the elastic properties are the same on either side of the interface, the fractures were able to propagate across several interfaces. Al-Mahruqi concludes that, at depths in excess of 2km, the vertical stress generated by the overburden pressure is sufficient to ensure that the fractures would propagate across the layer without any significant layer parallel extension.

Erdogan and Birickoglu's (1973) work, cited in Helgeson and Aydin (1991), showed that, when a joint propagates from a layer of lower Young's Modulus to a layer of higher Young's Modulus, the strain energy decreases as the joint approaches the interface and joint propagation is impeded. They argued that if the joint propagates from a layer of higher to one of lower Young's Modulus, the propagation will be enhanced. If the moduli are the same on both sides of the interface, there is no effect on joint propagation. Gillespie *et al.* (2001), in their study of vein formation in the Carboniferous Burren Limestone in County Clare, Ireland, inferred depth of formation of >1.25km. This is compatible with the depth required to propagate through-going

joints predicted by numerical models (*e.g.* Renshaw and Pollard, 1994; Al-Mahruqi, 2001). The study of Teufel and Clark (1984) also indicates that for each rock type and surface roughness, there is a critical interfacial normal stress that has to be exceeded in order for the fracture to cross the interface.

Even after the limestone in Giggleswick quarry (grid reference 810650) has been blasted, it retains coherence across the stylolite surfaces (Fig. 4.6) indicating that the strength of the rock along the stylolite planes is actually higher than the intact rock. The stylolites effectively weld the bedding planes together, creating cohesion and facilitating the propagation of joints across the interface. In addition, the stylolitic surfaces prevent slippage along the bedding. As the propagation of fractures continued, the 'driving pressure' was sufficiently large to cause the propagation of the fractures across the interface, resulting in the development of through-going joints. Irregularities such as stylolites may indeed have served as important sites for stress magnification/concentration for initiation (and propagation) of fractures.

Joint orientations and spacings were studied at Giggleswick quarry, which is situated approximately 1km WNW of Langcliffe (see number 3 in Fig. 4.1). The North Craven Fault, described in section 2.1, passes through the quarry. Very good examples of vertical veins striking 060° and 325° and in places filled by coarse-grained calcite veins can be seen cut across several bedding planes in the quarry (Fig. 4.7). Two sets of vertical calcite veins trending NW-SE and E-W occur. From the vertical continuity of these fractures and veins, it can be inferred that the stratigraphic layering did not impede crack propagation from one bed to the next.

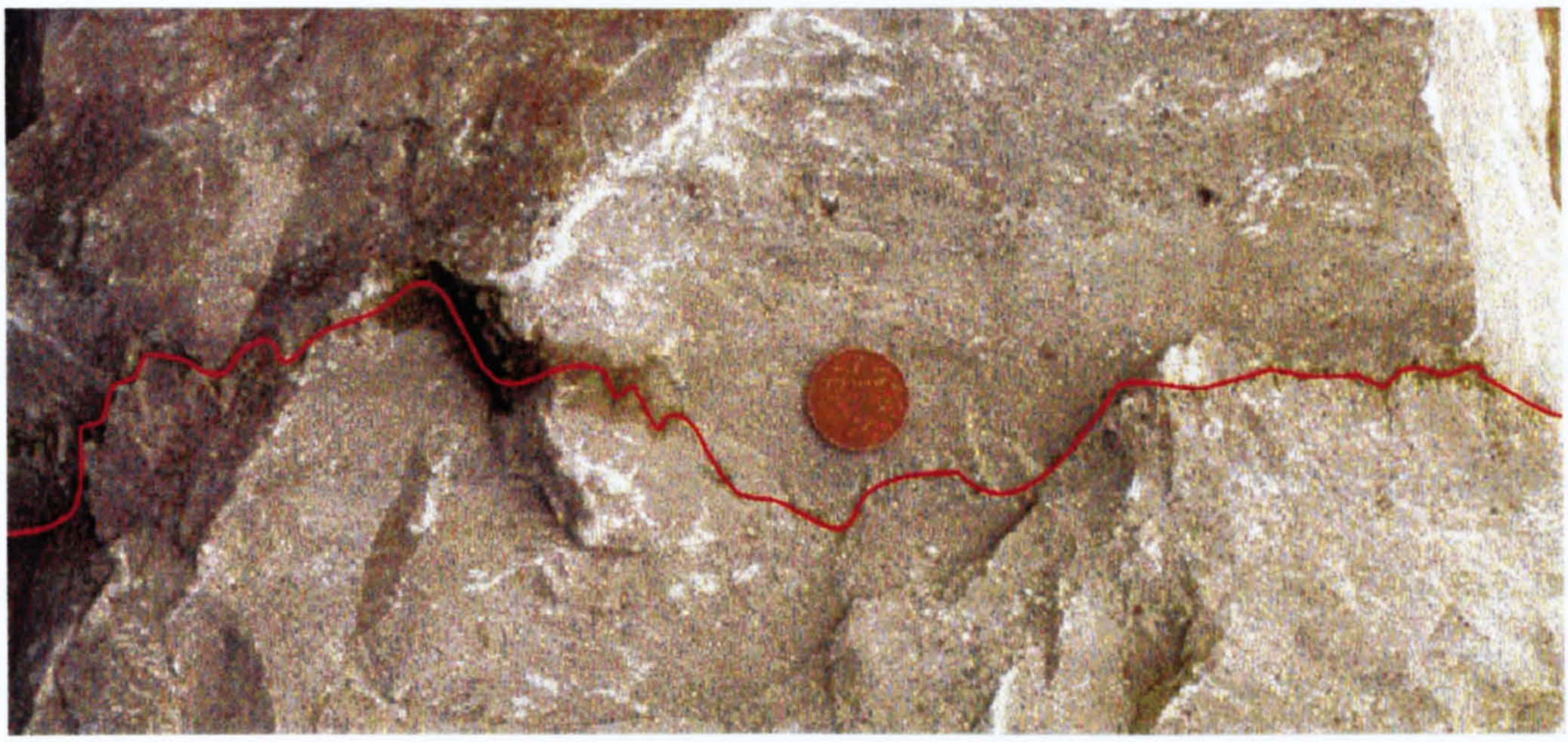
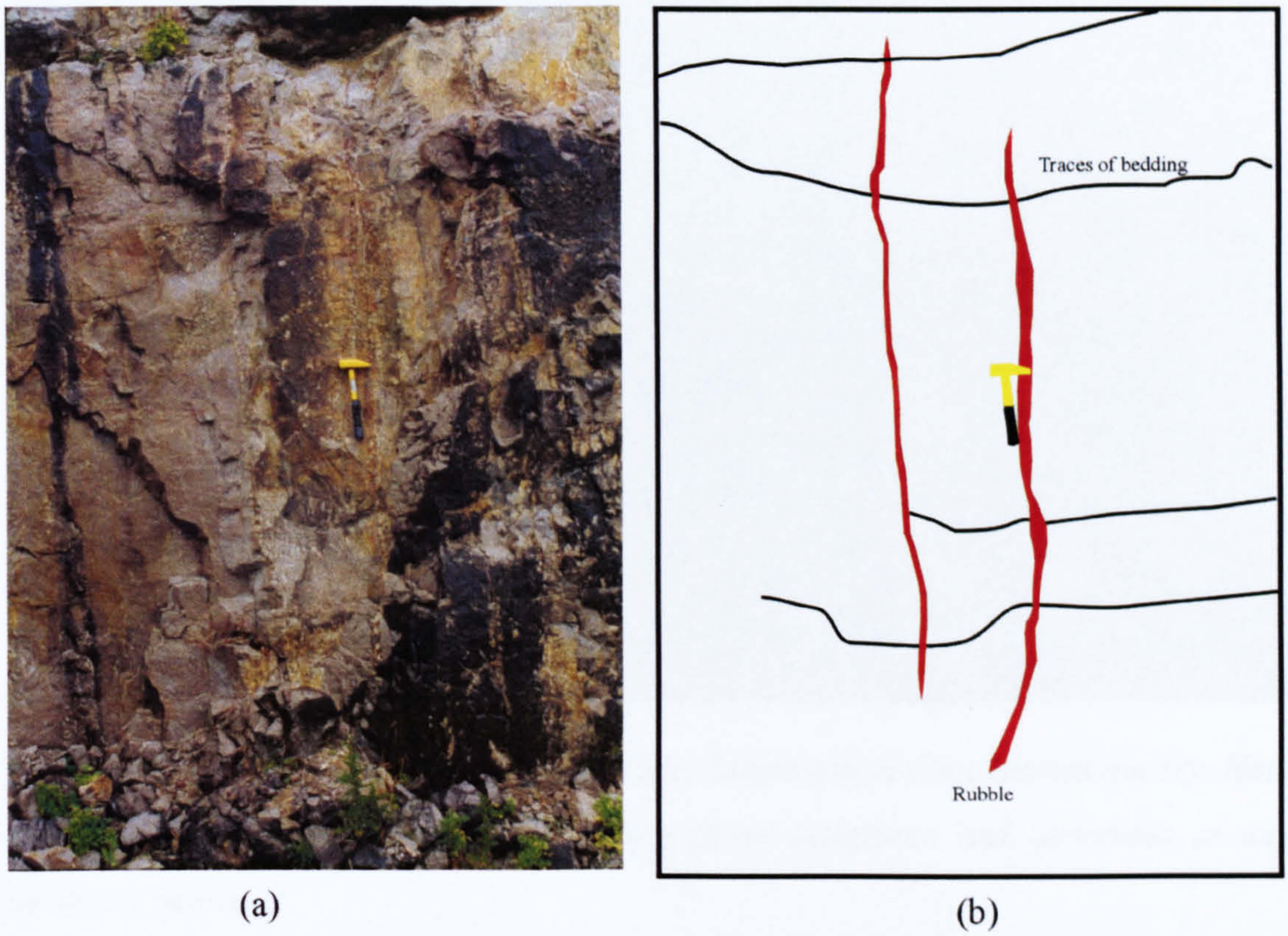


Figure 4.6 *Medium- to coarse-grained limestone after blasting in Giggleswick quarry. Note that the rock remained intact along the irregular stylolite implying higher strength across the discontinuity than in the intact rock.*



(a) (b)

Figure 4.7 *(a) photograph and (b) line drawing of ENE-WSW striking vertical veins with calcite vein fill cutting across several bedding planes at Giggleswick quarry. Hammer is for scale.*

3 horizontal scan lines oriented 070°, 025° and 030° were measured in the Cove Limestone north of Giggleswick quarry. Rose diagrams showing the strike of the joints are shown in Figs. 4.4(j to l). As can be seen from the rose diagrams, the dominant joint sets in the area strike NW-SE and ENE-WSW. Where these joints are seen on cliffs and quarry faces, they show vertical continuity to form through-going joints (Fig. 4.8). The joints terminate at arbitrary positions on the quarry face (*i.e.* not necessarily at a bedding plane). Joint arrest at bedding interfaces is generally low.



Figure 4.8 *'Through-going' joints in the Cove Limestone at Giggleswick quarry. Note that the joints cut across several bedding plane interfaces and terminate at any arbitrary position.*

The Gordale Limestone overlies the Cove Limestone and consists of well-bedded packstones, wackstones and subordinate grainstones. Scan-line sampling has been used to measure joint spacing in this limestone to the north of Giggleswick quarry.

Scan line trends are 020°, 040°, 055°, 090°, 110° and 340°. In common with other sites in the study area, the strike of joints is dominantly NW-SE and ENE-WSW and the direction of shortening inferred from the joints is approximately E-W (Fig. 4.9).

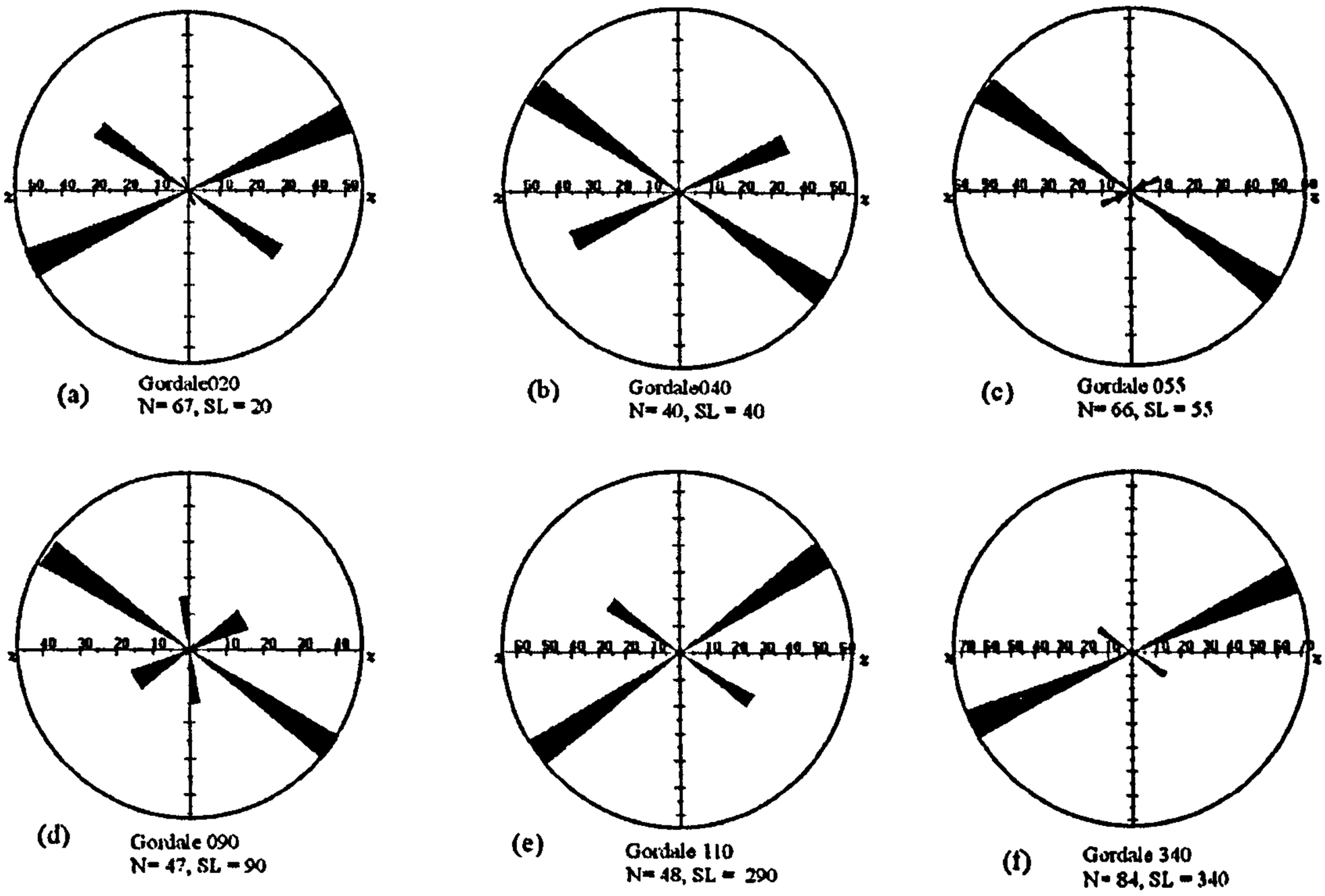


***Figure 4.9** Rose diagrams showing joint strike along the scan line in the Gordale limestone at Giggleswick.*

Two small caves, one at Malham, and the Victoria Cave east of Langcliffe, occur in the region. These and other caves in the region were probably formed as a result of solution along the pre-existing zones of closely spaced joints by underground drainage. These zones of localised regions that have a very small joint spacing are called *fracture corridors* (Peter Connolly, personal communication) (Fig. 4.10). These highly localised clusters of closely spaced fractures are common on quarry faces and cliff sections, but the process by which these fractures form is poorly understood. It is thought that 5-10% extension is needed for the formation of fracture corridors and that they are the result of

strain localisation (Peter Connolly, personal communication). Another explanation is that the stress intensities at the tips of the cracks increase with increasing length. In front of long propagating fractures elevated driving stresses can be achieved and this promotes the growth of smaller fractures. As smaller fractures are passed by rapidly propagating long fracture, they will fall into the stress shadow of this large fracture and propagation stops. This process is called crack-tip shielding (Olson, 1993 and references there in) and is thought to be responsible for the clustering of veins in the Burren limestone in County Clare (Gillespie *et al.*, 2001).

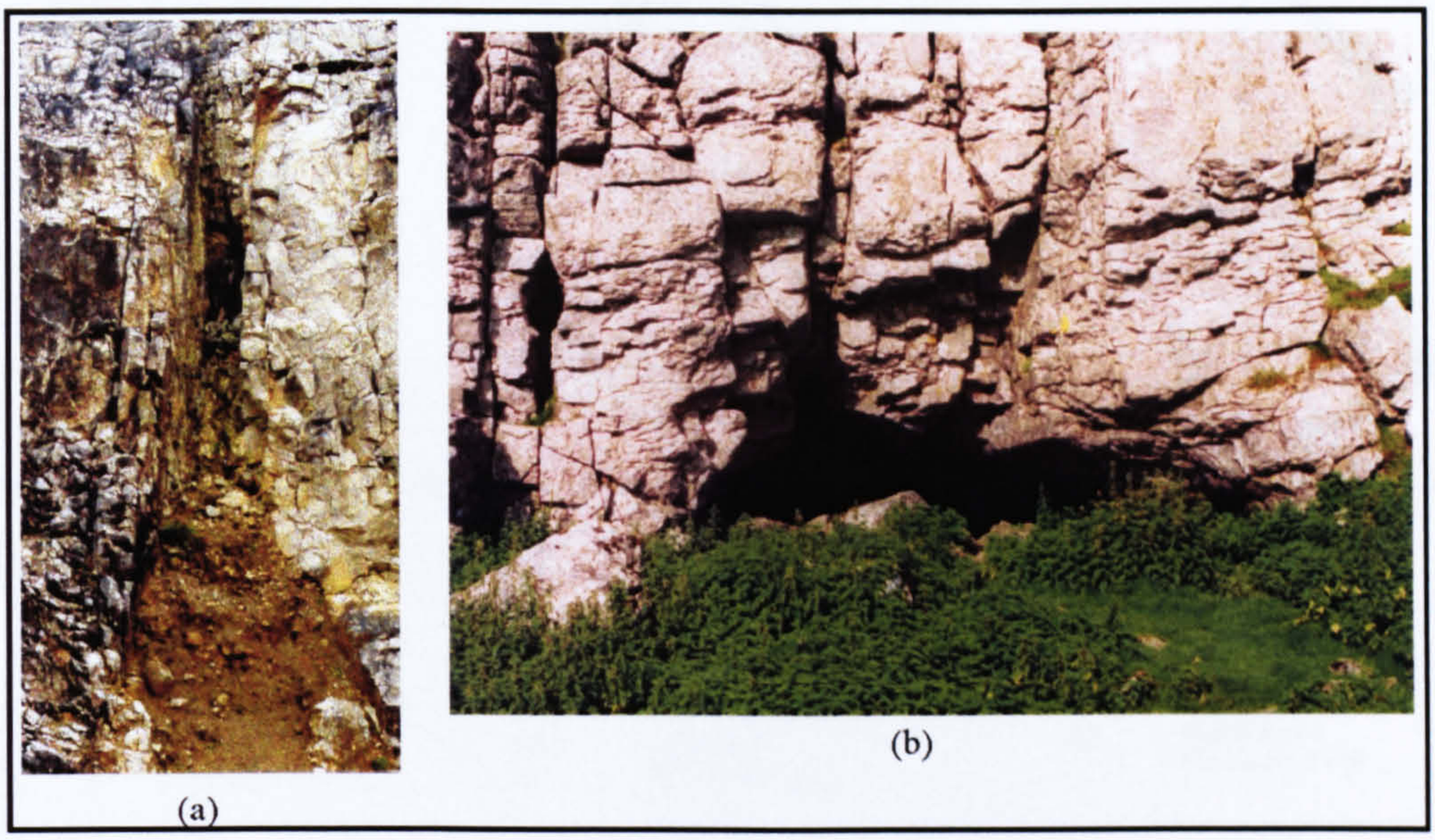


Figure 4.10 *ENE-WSW striking joints in (a) Giggleswick quarry and (b) at Victoria Cave. Note that the caves are formed along zones of closely spaced joints (fracture corridors) which were later enhanced by solution along the fractures.*

4.3.3 Ingleton

4.3.3.1 Scan-line sampling

Scan line sampling has been carried out on the Gordale Limestone at Ingleton at grid reference 715745 (see locality 5 in Fig. 4.1a). The limestone in this area is mostly flat-

lying and in places dips 05° to ENE. Joints strike mainly NE-SW and NW-SE (Fig. 4.11). The acute angle between the conjugate set is ≤ 90°. Compared to the joints in the limestone beds at the southern margin of the Bristol Channel, which will be described in section 4.4, joints in the Cove and Gordale Limestones show a fairly consistent strike over a large area.

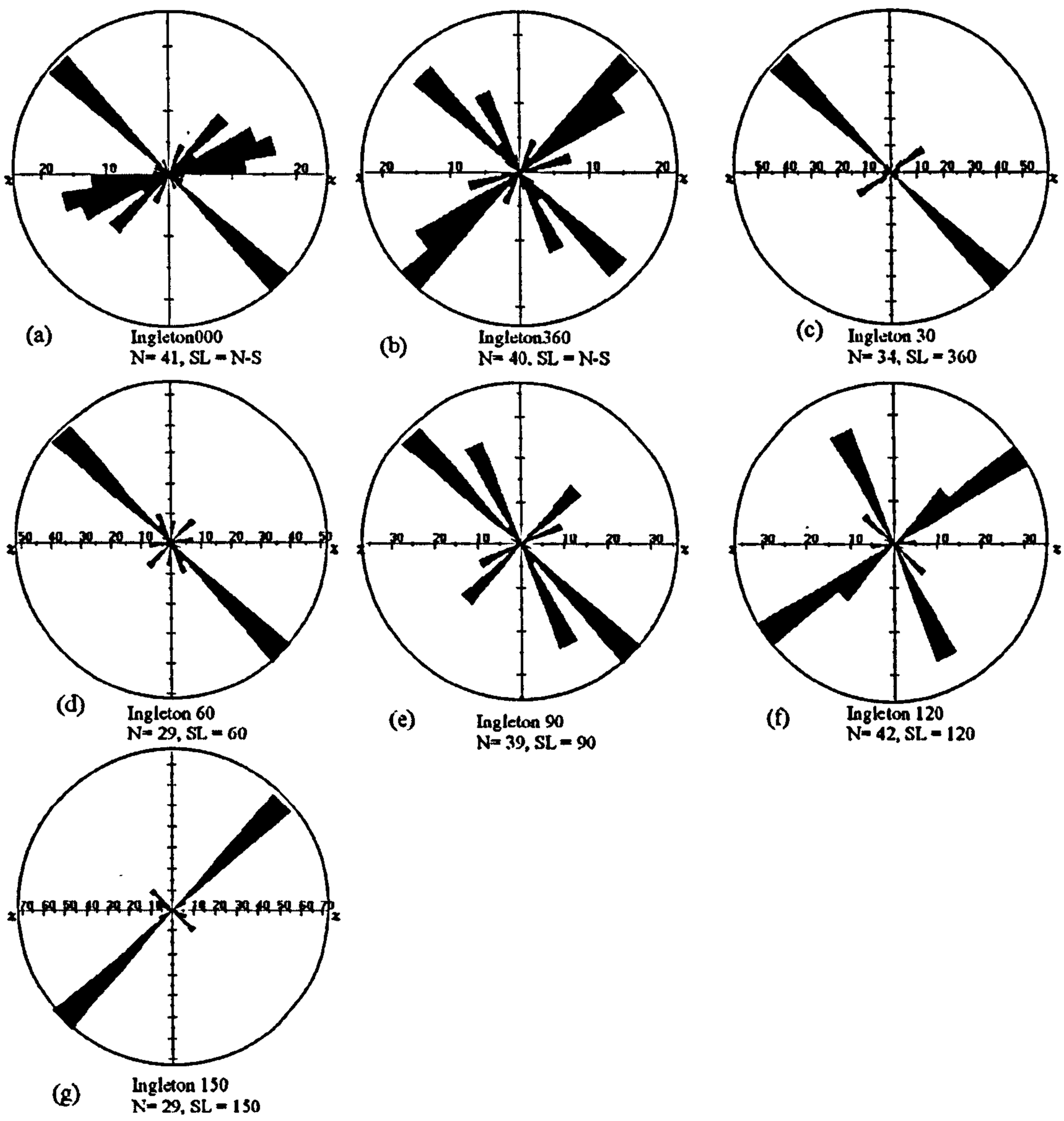


Figure 4.11 *Rose diagram of joint strike from Ingleton. Note that SL is the direction of each scan line and N is the number of fractures intersected.*

Joints striking NNW-SSE (150°) and ENE-WSW (060°) were observed in the Twiss River in the Silurian grits underlying the Cove Limestone. This led previous workers (*e.g.* Moseley and Ahmed, 1967; Doughty, 1968) to conclude that jointing in the Carboniferous Limestone in the area resulted from the inheritance of older structures. The present work shows that although some joints in the limestone extend down to the unconformity surface between the Silurian-Devonian and the overlying Carboniferous Limestone, it is very difficult to conclude that all the joints were inherited from the underlying formations.

4.3.3.2 Window sampling

The fieldwork described above relates to scan line analysis. However, because of the excellent exposures of fractured beds in Ingleton, window sampling was undertaken at grid reference 705753 (see locality 4 in Fig. 4.1a). The following section describes an investigation by the author to determine the sensitivity of fracture density on the shape and size of the sampling window. In window sampling, joint density is defined as the total length of joints in a geometrically defined window that may be a square, rectangle or circle. Joint density does not take into account fracture orientation and spatial distribution. In window sampling, fracture density is measured in units of m/m^2 or simply m^{-1}.

Fracture density was examined using various window shapes and sizes using *Densityinfo* version 2.0, a program developed by Catherine Greenfields at Imperial College. Densityinfo is developed in visual basic for an NT/Windows platform. Input is a joint trace map saved as a plotter file in vector format, which requires scaling along the x-axis of the joint network window. The user can overlay circles of any radius. If the circle or rectangle does not fit completely within the mapped area, it is

excluded for the purpose of the calculation. Circles may be arranged on the fracture trace map in '*cubic*' or '*rhombic*' packing. A cubic close-packed arrangement has a higher proportion of voids, and therefore, misses more fractures than rhombic packing. Data are stored as (x, y) coordinates at the beginning and end of segments that make up a line. Knowing the co-ordinates of the fracture tips and the position and size of the circle, the fracture length within circles can be calculated. From this, the total fracture length within each circle is determined.

In a similar way, fracture/joint lengths within boxes (rectangular windows) are calculated by determining the point where a fracture trace enters a box and where it exits. The user can then save fracture lengths within each box or circle as a comma or tab delimited file with extension *.dat. This can be imported into a spreadsheet program such as Microsoft Excel™ or notepad. The fracture density is then obtained by dividing the total length of fractures by the areas of the respective windows. Both of these methods can also be applied directly to rock surfaces as well to fracture trace maps and digital images.

The joint trace map of the limestone pavement made on the field photographs from Ingleton were rectified by the process described in section 1.3.2 and is shown in Fig. 4.12. Assuming that the joints are uniformly distributed (*i.e.* statistically homogenous) throughout the window, the average joint density (*i.e.* the length of joints per unit area) is $2.1m^{-1}$. This assumption of uniform distribution has also been checked using the coefficient of variation (C_v) method. The coefficient of variation is a measure of spatial distribution of variation from the mean and is given by the standard deviation divided by the mean (Cox and Lewis, 1966; Gillespie *et al.*, 1999; Odling *et al.*, 1999).

These authors propose that clustered, random and anti-clustered distributions have C_v values generally greater than, equal to and less than one respectively. $C_v = 0$ corresponds to periodic (equally spaced) joints (Gillespie *et al.*, 1999). The distribution of joints has been checked for every square metre within the entire window using the C_v and it is found that the distribution is anti-clustered (C_v of 0.4731).

4.3.3.2.1 The influence of window shape and size on fracture density

In this section, fracture density in the joint trace map is determined using rectangular, square and circular windows.



Figure 4.12 *2D joint trace map for a square window (l = 15m) from Ingleton. Two sets of fractures in the NW-SE direction are defined by long joints and ENE-WSW by short unconnected fractures showing typical joint pattern in the region.*

(i) square windows of various sizes were selected with x-y axes of the sampling window being kept parallel to the axes of the main window and joint density determined for square windows of areas 1, 4, 9, 16, 25 and 100m^2. The graph shown in Fig. 4.13 relates to joint density within square windows. Fracture density for one m^2 is found to vary between 0 (no joints) and 6m^{-1}. With increasing window size, the joint density decreases and approaches a mean value (Fig. 4.13). If we consider an area of 100m^2, fracture density variation from the mean is only ±14%.

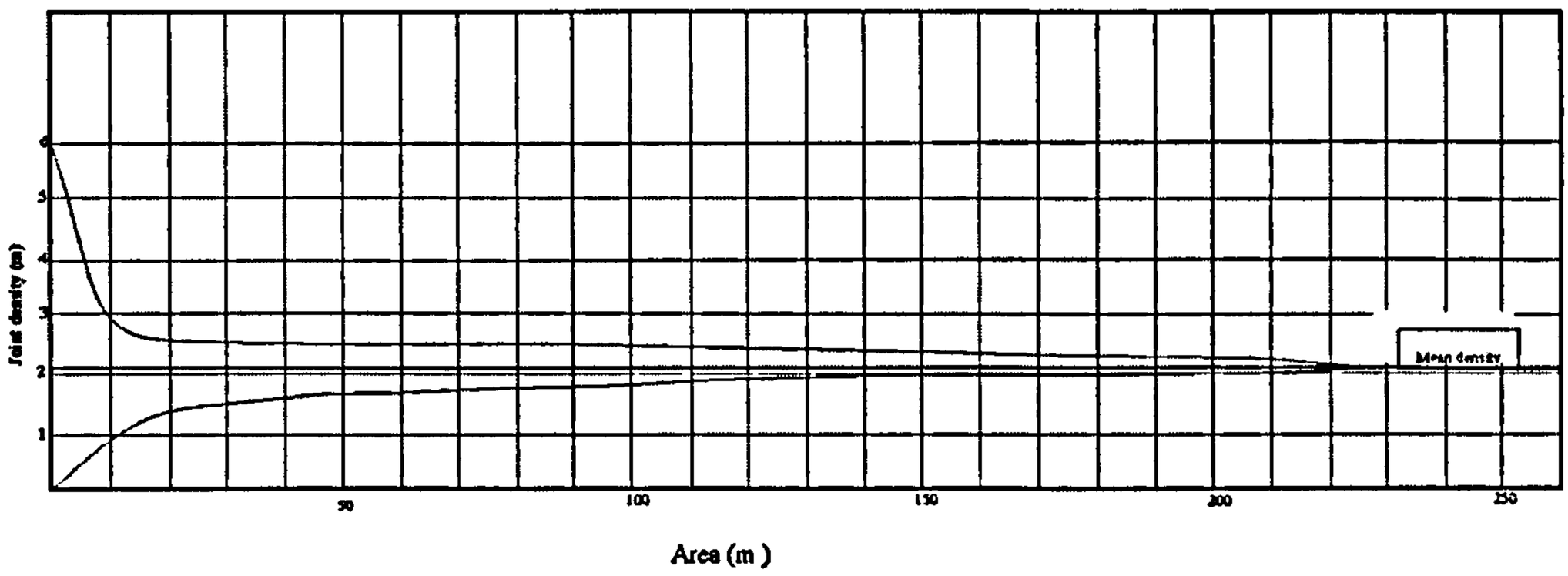


***Figure 4.13** Fluctuation of joint density in Fig. 4.12 determined from various sizes of square windows. The red line indicates the mean joint density for the entire window. The curves on both sides enclose joint density variations and converge towards the mean as the area of sampling is increased. Note the fluctuation gets smaller as the area of sampling increases.*

(ii) rectangular windows: Joint density variation when using sampling windows of rectangular shape has also been examined. In rectangular windows the greatest variation is seen when the longest side of the window is parallel to the dominant joint set (Fig. 4.14a). When the longest side of the rectangular window is perpendicular to the dominant set the fluctuation is minimum (Fig.4.14b).

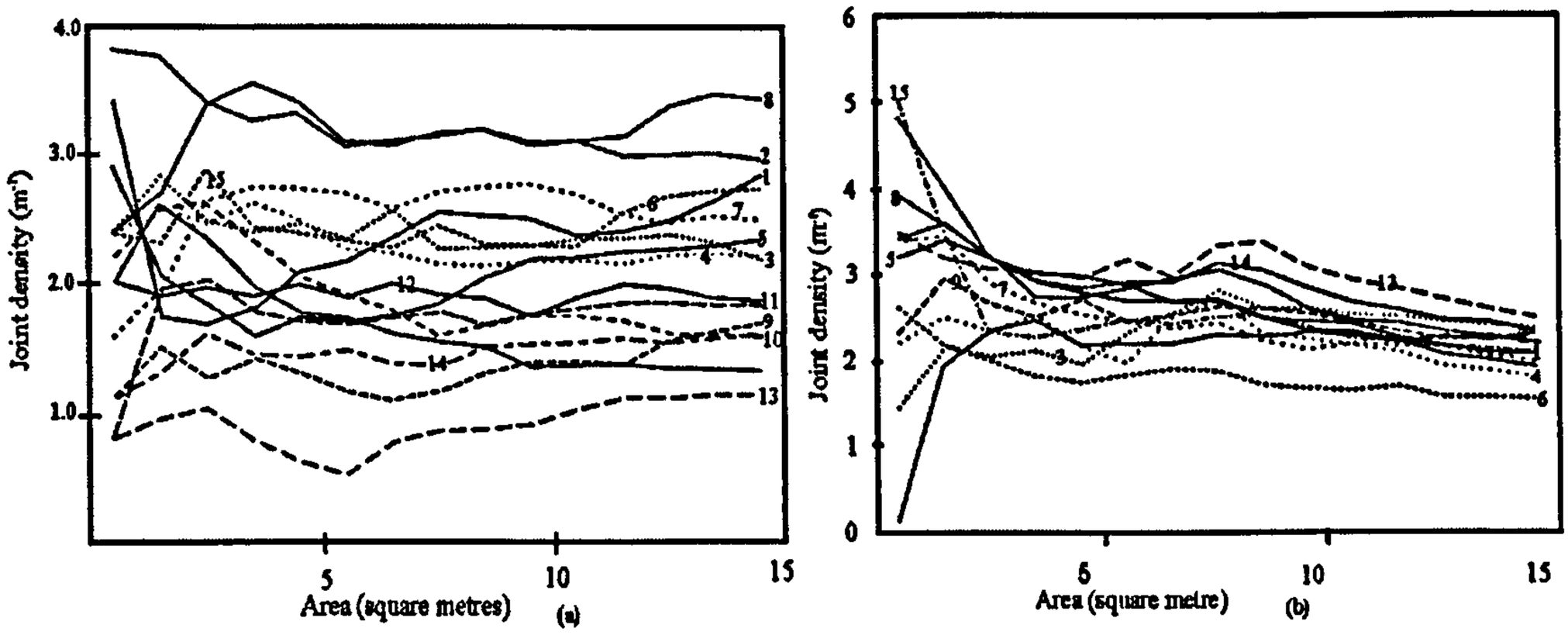


Figure 4.14 Joint density variations determined from Fig. 4.12 using rectangular windows (a) when the longest side is parallel to and (b) perpendicular to the dominant joint.

(iii) circular windows: Determination of joint density using circular windows has been carried out using the *densityinfo* computer program mentioned earlier. A circular window is the region enclosed by a circular scan line (Mauldon *et al.*, 2001). Fig. 4.15 shows circular windows imposed in cubic packing on the joint trace map is shown in Fig. 4.12. The joint density variation for different sized circular windows is shown in Fig. 4.16. When 5625 circular windows are generated using a radius of 10cm, 59.66% of the windows do not intersect joints. If the arrangement of the circular windows is changed to rhombic packing with the same radius gives 6364 circles, of which 3826 (*i.e.* 60.12%) do not intersect any joints. A circular window of 7m radius results in a joint density of $2.17m^{-1}$(or 3.85% error from the mean fracture density). The largest circle that can be inscribed in the square gives a joint density of $2.1m^{-1}$.

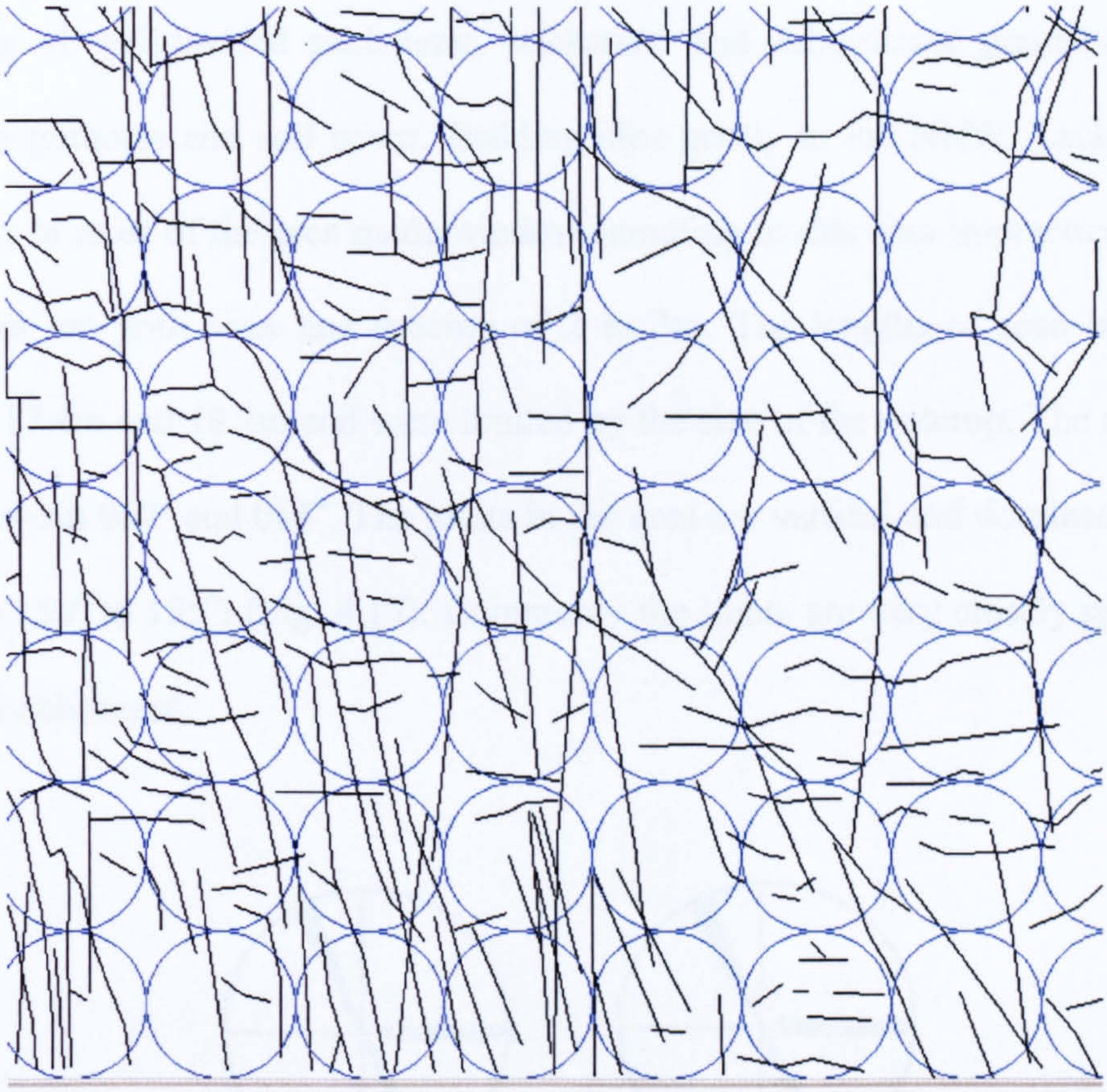


Figure 4.15 *Layout of circular windows in cubic packing superimposed on the 2D joint trace map from Ingleton.*

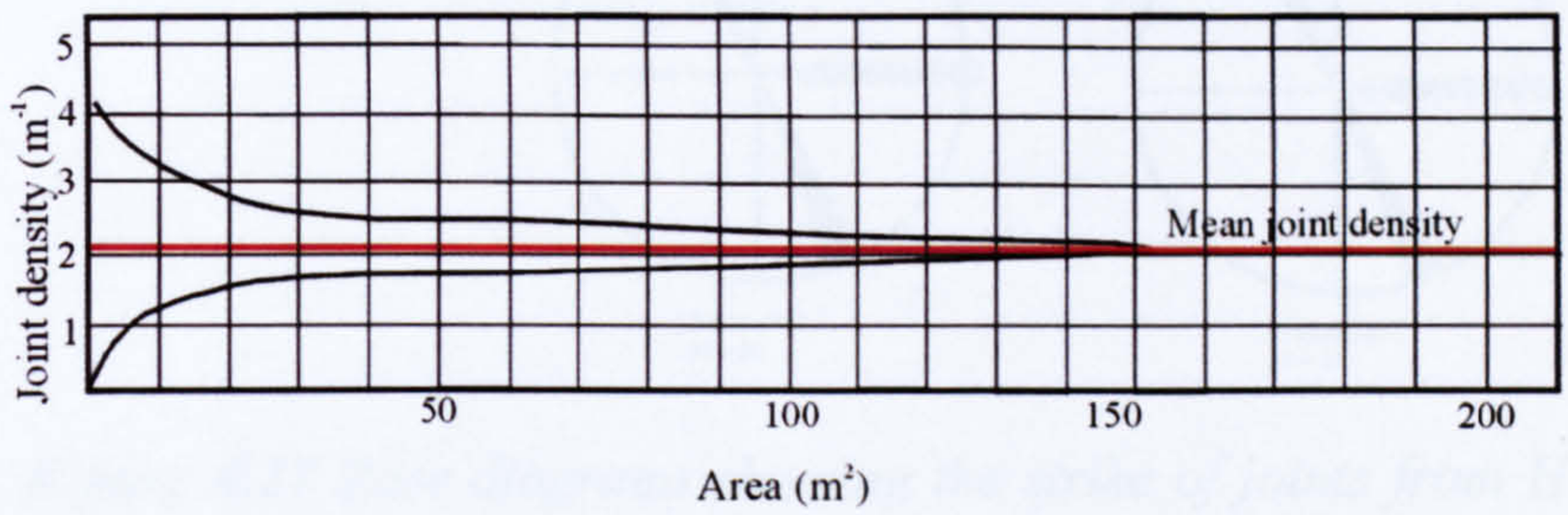


Figure 4.16 *Variation of joint density determined for Fig. 4.12 using circular windows of different sizes. The fluctuation decreases and approaches the mean as the area of the circle is increased.*

4.3.4 Horton-in-Ribblesdale

The last area studied in North Yorkshire was Horton-in-Ribblesdale (see locality 6 in Fig. 4.1a and b). The limestone in this area is strongly weathered Gordale Limestone

consisting of well-bedded packstone, wackstone and subordinate grainstones with numerous potholes and soil cover. Bedding dips gently to the NNW. Lack of good exposures in most of the area made window sampling in this area impractical. 4 scan lines were run with scan line spacing of 2 to 3m. The lengths of scan lines were between 17.4m and 18.2m and were limited by the size of the outcrop. The scan lines trend between 062° and 065°. The joints in the area are vertical and dominantly strike NW-SE (150° to 155°) (Fig. 4.17). Commonly the joints are very closely spaced and are locally clustered.

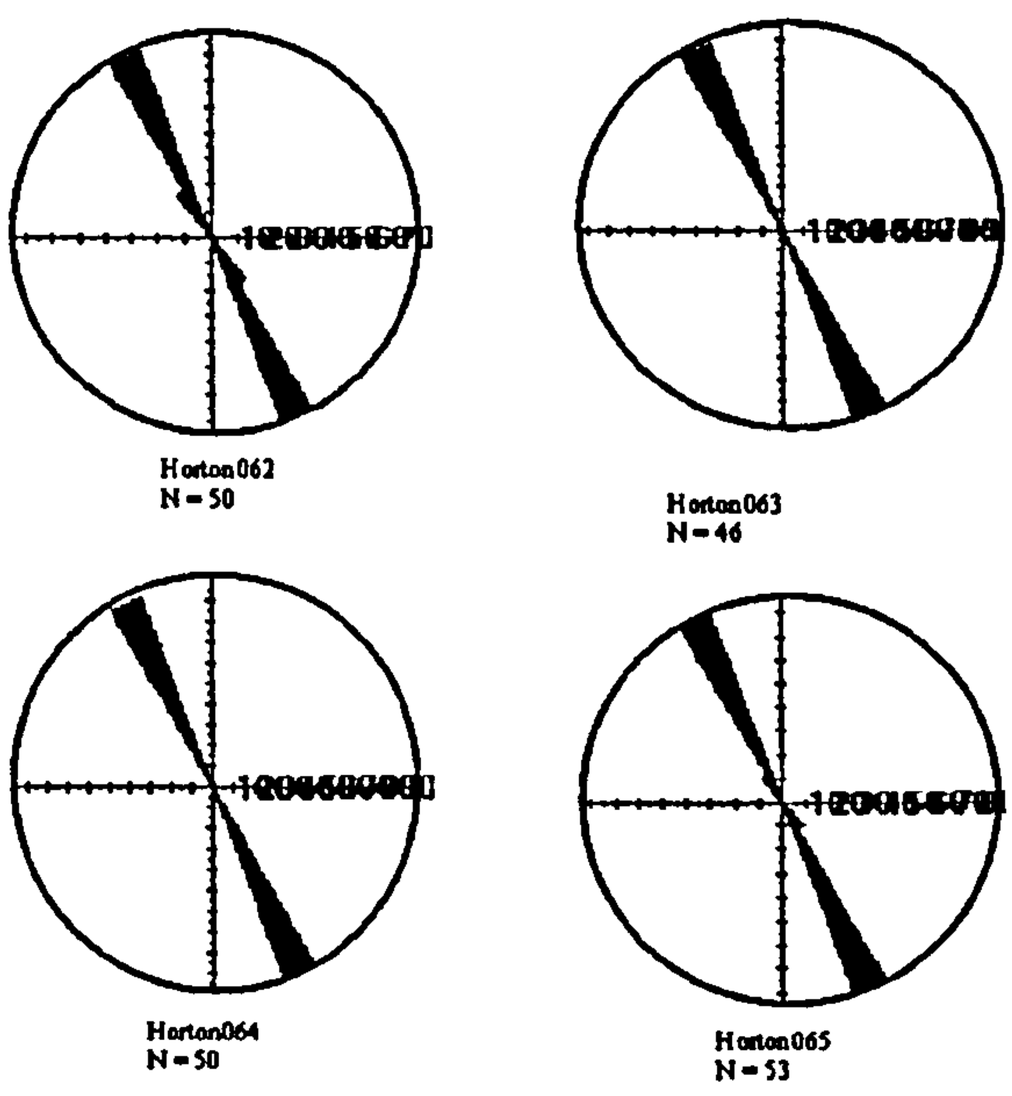


***Figure 4.17** Rose diagrams showing the strike of joints from Horton-in-Ribblesdale. Note that fractures in all rose diagrams strike NW-SE.*

4.4 Joints from the southern margin of the Bristol Channel Basin

4.4.1 Introduction

A study of the fracture patterns in micritic limestone beds of the Lower Lias which crop out along the southern margin of the Bristol Channel from the Hinkley Power Point in the east to Blue Ben in the west was undertaken (see Fig. 2.7 and section

2.4.1). In this section, 2D joint trace maps, and joint density calculations (*i.e.* from window samples), joint spacing and orientation data are presented. In exposures too limited to get statistically meaningful results, *i.e.* where window and scan line sampling was not possible, field photographs and brief descriptions are used to compare the fracture patterns contained in each bed. In this area joints are described from East Lilstock, Lilstock, Kilve, East Quantoxhead and Blue Ben. Based on this field study a three-fold classification of joints is proposed.

(i) **Burial joints:** These are joints that have been either 'healed' or filled by calcite veins. They are mostly sub-parallel to the strike of major basin-bounding faults and the fold axes of the rollover folds. The earliest expression of extensional structures within the micritic limestone beds is the formation of closely-spaced sub-vertical micro-veins with a general E-W strike and these are common structures between Kilve and Lilstock. Micro-veins (Caputo and Hancock, 1999) or high density veins (Rawnsley *et al.*, 1998) form zones 1-2cm in thickness consisting of tens of micro-veins that taper as they approach the bedding plane interface with the underlying and overlying shales suggesting marked lithological controls (Fig. 4.18). The height of the micro-veins is determined by the thickness of the limestone beds containing them. They are often visible where erosion has exploited the contrast between the micro-veins and the country rock. I accept the view of previous investigators who consider the micro-veins to represent the earliest manifestation of a relatively diffuse extension, during which deformation took place throughout the bed before the onset of focussed displacement along discrete localised fault planes. The micro-veins formed in a sequence of rupturing and sealing events. They are commonly oblique to, or are cut by, veins that were formed during major basin opening and also by some barren joints

(Fig. 4.19). Caputo and Hancock (1999) argue that they were formed by a '*crack-jump'* mechanism and inferred a cyclic evolution of the stress tensor during their formation. Vertical compaction ranging between 7% and 12% has been determined in the hanging-wall of the normal faults by using folded, originally sub-vertical calcite veins at Kilve Beach as strain markers. This is thought to relate to post micro-vein compaction during the stage of basin opening.

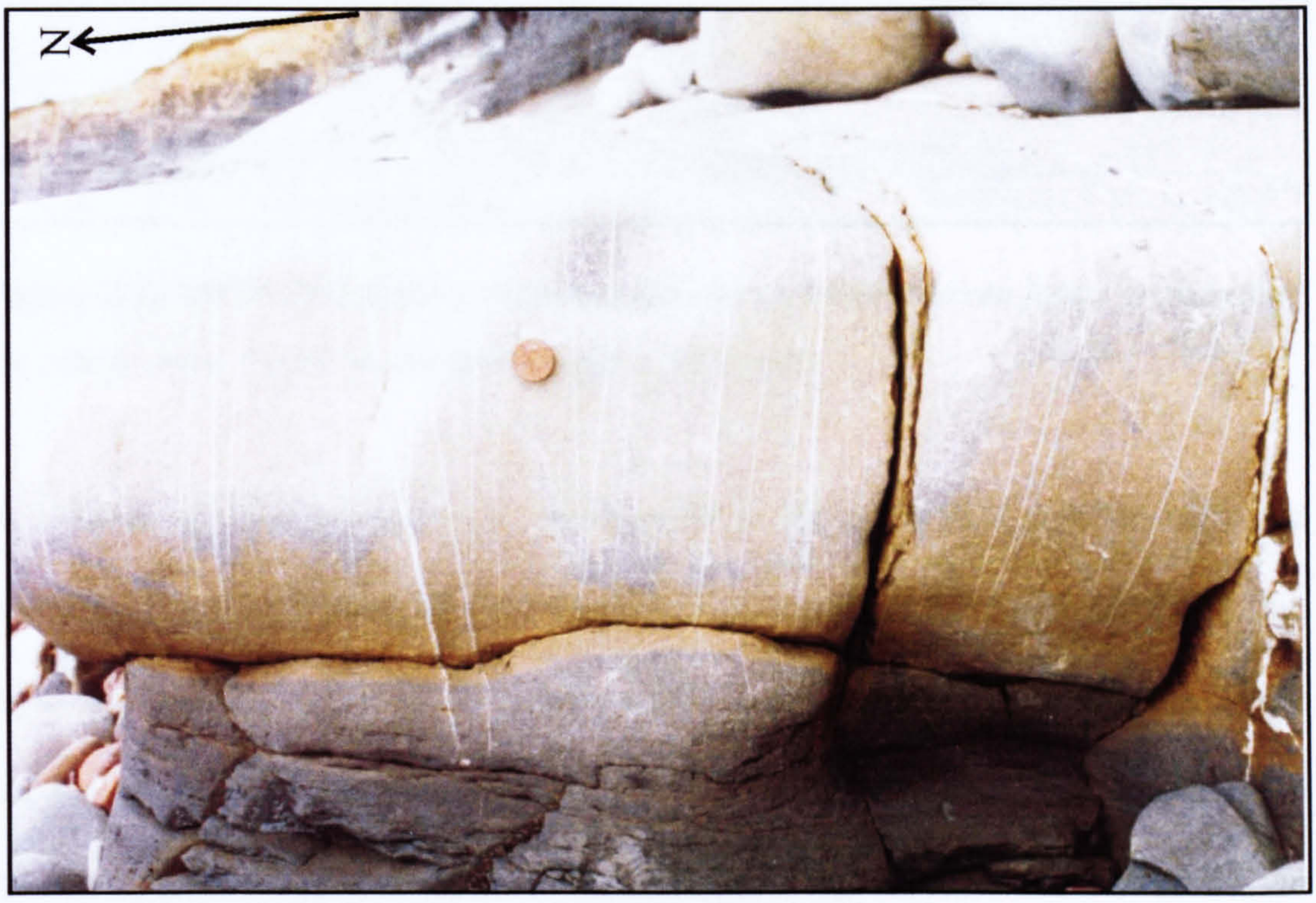


Figure 4.18 *Zones of high-density veins (micro-veins) contained within the limestone beds from Kilve looking towards ESE. Coin in the centre of the photograph is for scale and has a diameter of 2cm.*

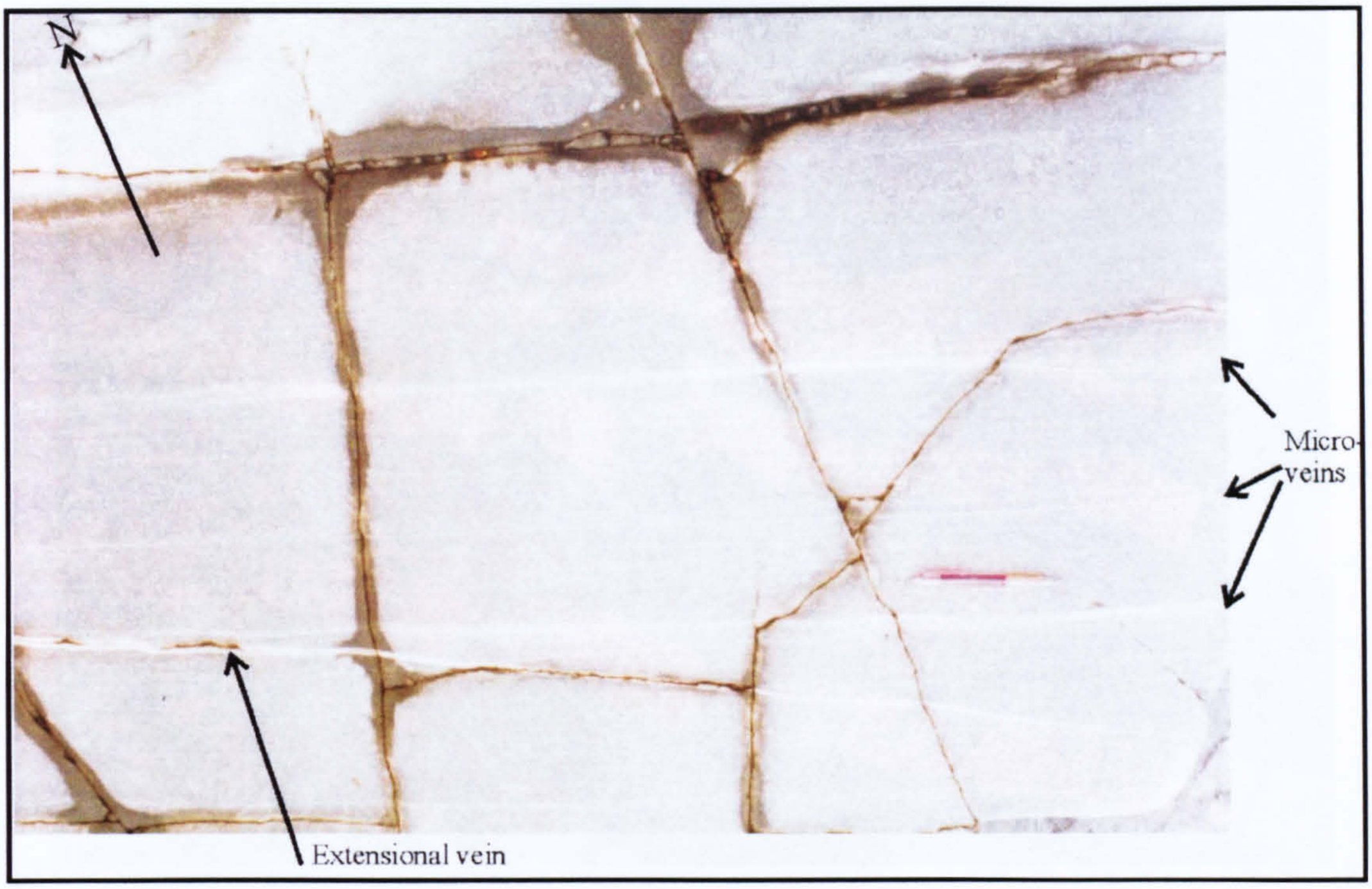


Figure 4.19 *WNW-ESE striking extensional veins and later barren joints crosscutting the micro-veins. Pencil on the lower right is for scale.*

At Lilstock, the bedding planes dip between 30° to 35° to the SSW (190° to 195°) and the veins containing the pull-apart (discussed in section 2.4.2.1 and shown in Fig. 2.14) dip from 52° to 58° to NNE (Fig. 4.20). These veins, which are normal to the bedding plane, probably initiated randomly in the limestone beds. Further extension caused oblique linking of these extensional joints by shear fractures which form approximately 30° to the maximum principal compressive (*i.e.* overburden) stress. Further extension caused slip on these composite fractures resulting in the formation of openings in the limestone beds (pull-apart structures) and oblique fractures in the shales (*e.g.* Peacock and Sanderson, 1991) (Fig. 4.20). The fault is seen cutting the succession and calcite mineralisation has occurred in the pull-apart gaps. Similar structures were also observed at Kilve Beach (section 2.4.2.1 and Fig. 2.14).



Figure 4.20 *Pull-apart structures in southward tilted alternating limestone and shale beds at Lilstock. Note the open vugs at the centre that probably indicate the calcite grew in pre-existing open space created when the extension joints formed. Compass at the centre of the photograph for scale.*

When the bedding planes shown in Fig. 4.20 are restored to the horizontal, the veins in the limestone beds dip vertically or very steeply to the NNE. The majority of the calcite fibres in the area grow normal to the joint planes and indicate a consistent N-S to NNE-SSW extension (Fig. 4.21). Palaeo-stress analysis (Nemčok *et al.*, 1996) also indicates that the least principal stress (σ_3) was oriented NE-SW during basin opening. In some cases however, a sinistral transtensional sense of opening is deduced from the calcite fibres that grew oblique to the joint walls (Figs.4.22). Some extensional veins are arranged in a left stepping *en-echelon* fashion when viewed in plan.

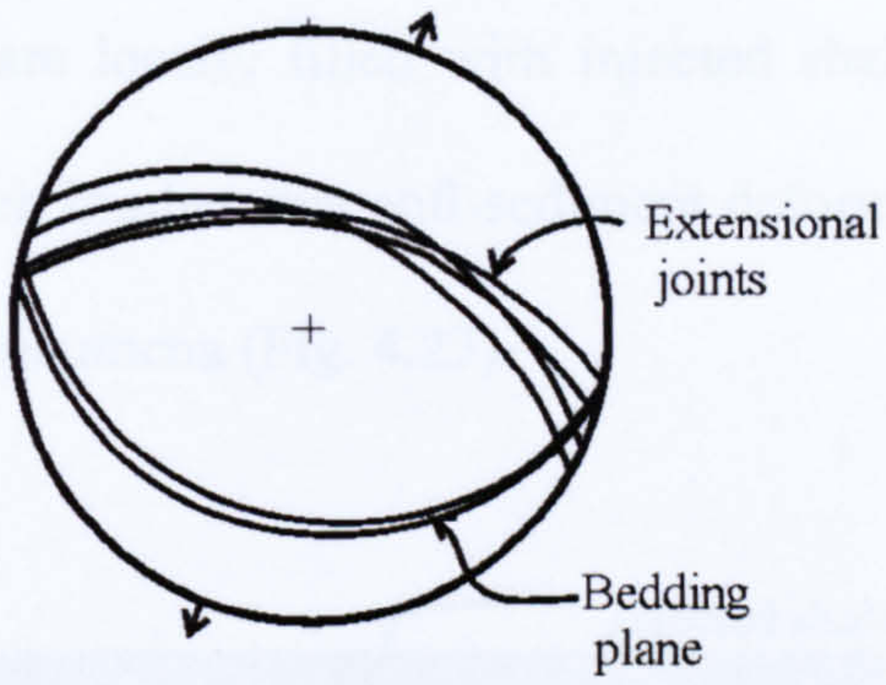


Figure 4.21 *Lower hemisphere stereographic projection of the bedding planes and extensional joints that form the pull-aparts at Lilstock. Arrows indicate the direction of opening of the basin.*



Figure 4.22 *Some of the calcite fibres east of Lilstock are oblique to the main joint planes indicating a dextral transtensional sense of opening. The hammer is 45cm long for scale.*

There is considerable evidence for the development of high fluid pressures during the formation of the early veins (Cosgrove, 2001), probably related to rapid sediment burial and the reduction in porosity of the low permeability shales. Some veins of the

same age, or older, are locally filled with injected shale-calcite mixtures from the underlying beds, which implies that soft-sediment deformation and fluid overpressure were simultaneous phenomena (Fig. 4.23).

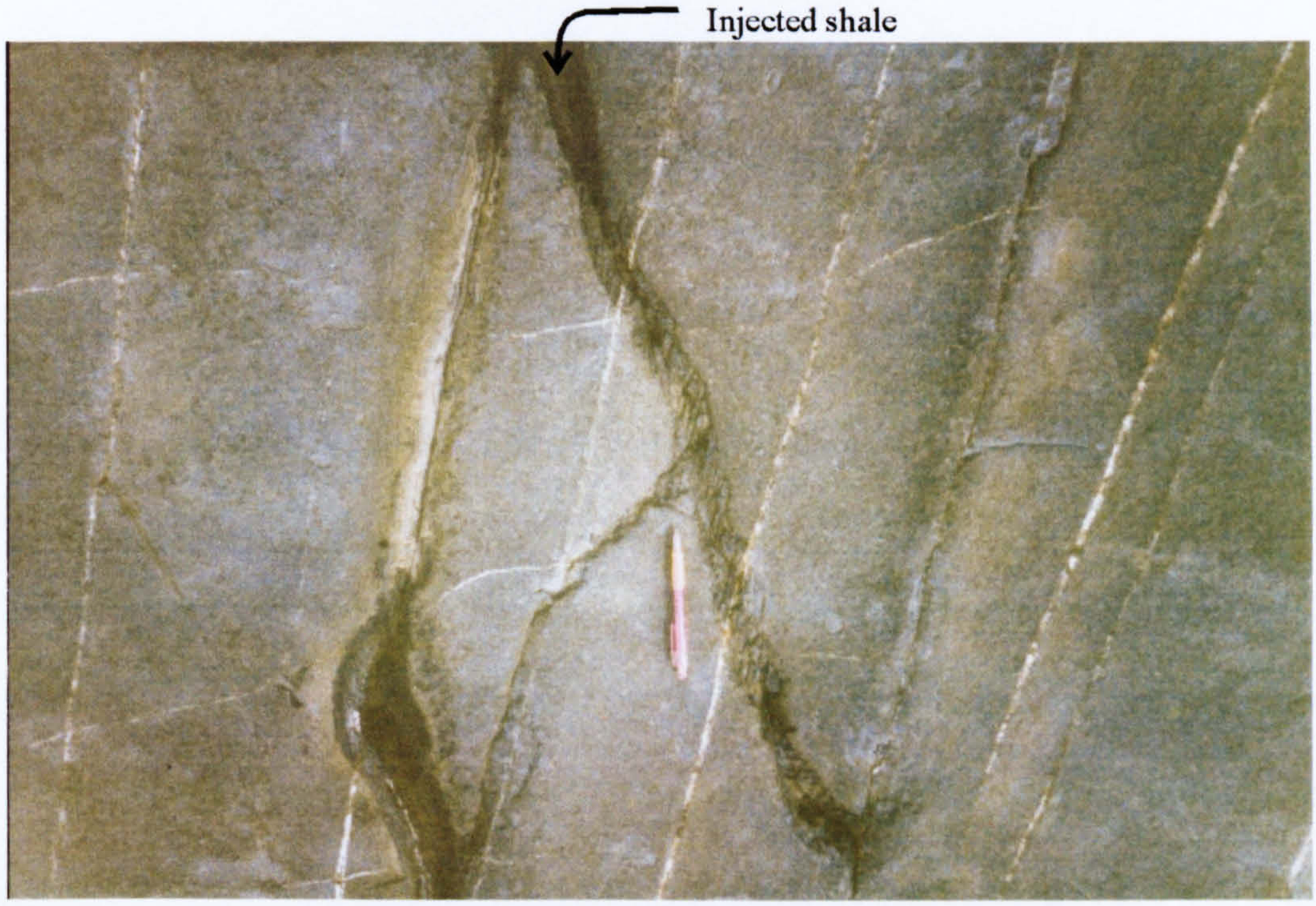


Figure 4.23 *Injected shale-limestone mixtures indicative of soft-sediment deformation cut by veins. E-W aligned pencil on lower centre is for scale.*

(ii) Joints formed during the Alpine inversion of the Bristol Channel Basin

Joints in this group are the most abundant in the area and form the main subject of the present investigation in the Bristol Channel area. Due to the containment of joints within the micritic limestone, they are generally blade-shaped with their length exceeding their height.

As discussed above, fracture density is defined as the total length of joints per unit area (section 4.3.3.2). In the following sections, joint density will be examined in

fractured limestone beds mapped at Lilstock. Joint spacing (*i.e.* the perpendicular distance between neighbouring joints of the same set) have also been examined. When the scan line does not trend perpendicular to the average strike of the joints in the set, the average joint spacing was determined using the method of Hudson and Priest (1983) and La Pointe and Hudson (1985), as discussed in section 1.3.1.

4.4.2 Joints from east of Lilstock

West of Hinkley Point Power Station (grid reference 190463 to 204463 see Fig. 2.7) the earliest Alpine joints in some beds have a NW-SE strike, though these are not common. E-W striking joint set that have a strike length over 1.5km was observed along the coast. One of the 20cm thick limestone beds has dip/dip direction of 7°/325° and an average joint spacing of 20cm (Fig. 4.24). E-W striking joints tend to link with one another by forming hook junctions (tip-to-plane). The ratio of average joint spacing to the fractured limestone thickness is 1 and this, according to Bai and Pollard (2000b), corresponds to the joint 'saturation' stage. As can be seen in Fig. 4.24, there are two identical limestone beds into which the joints have propagated without any significant offset from one bed to another. The shale separating the two limestone beds is very thin and almost imperceptible to the naked eye. However most of the limestone beds in the area are bounded top and bottom by ductile shale layers at least as thick as the limestone beds and these inhibit the direct propagation of joints from one limestone to the next. Although a systematic variation is difficult to establish, the vertical offset of joints in adjacent limestone beds in the sequence increases with increasing thickness of the shale separating two adjacent brittle limestone layers. This indicates the effect of the shale beds in the decoupling of strain between the limestone beds during jointing.



Figure 4.24 *A prominent joint set propagating vertically without significant offset between adjacent limestone beds thus forming composite or through-going joints. Hammer is for scale.*

Three adjacent limestone beds were studied at grid reference 178453, with thicknesses of 7cm, 30cm and 24cm for the upper, middle and lower beds respectively. 2D joint trace maps of these beds have been constructed around the hinge zone of a gentle syncline with an axis plunging 10^{o} to 290^{o} (Fig. 4.25). The intersection lineation formed by bedding and faintly developed cleavage in the shale beds is approximately parallel to the fold axis. The first set of Alpine joints in all beds is either parallel to the axis of the fold or deviates from it by a very small angle. Some joints in the upper limestone bed tend to curve towards joints of the same set to form hook junctions (tip-to-plane). On the upper bed using scan line measurements, the average joint spacing of the earliest formed joints which trend 100^{o} was found to be 37cm. The total length of all joints within the window (Fig. 4.25a) is 54.6m, giving an average joint density

(*i.e.* total length of joints in the window divided by the area of the window) of 5.6m^{-1}.

A 40cm of shale separates the upper and middle limestone bed.

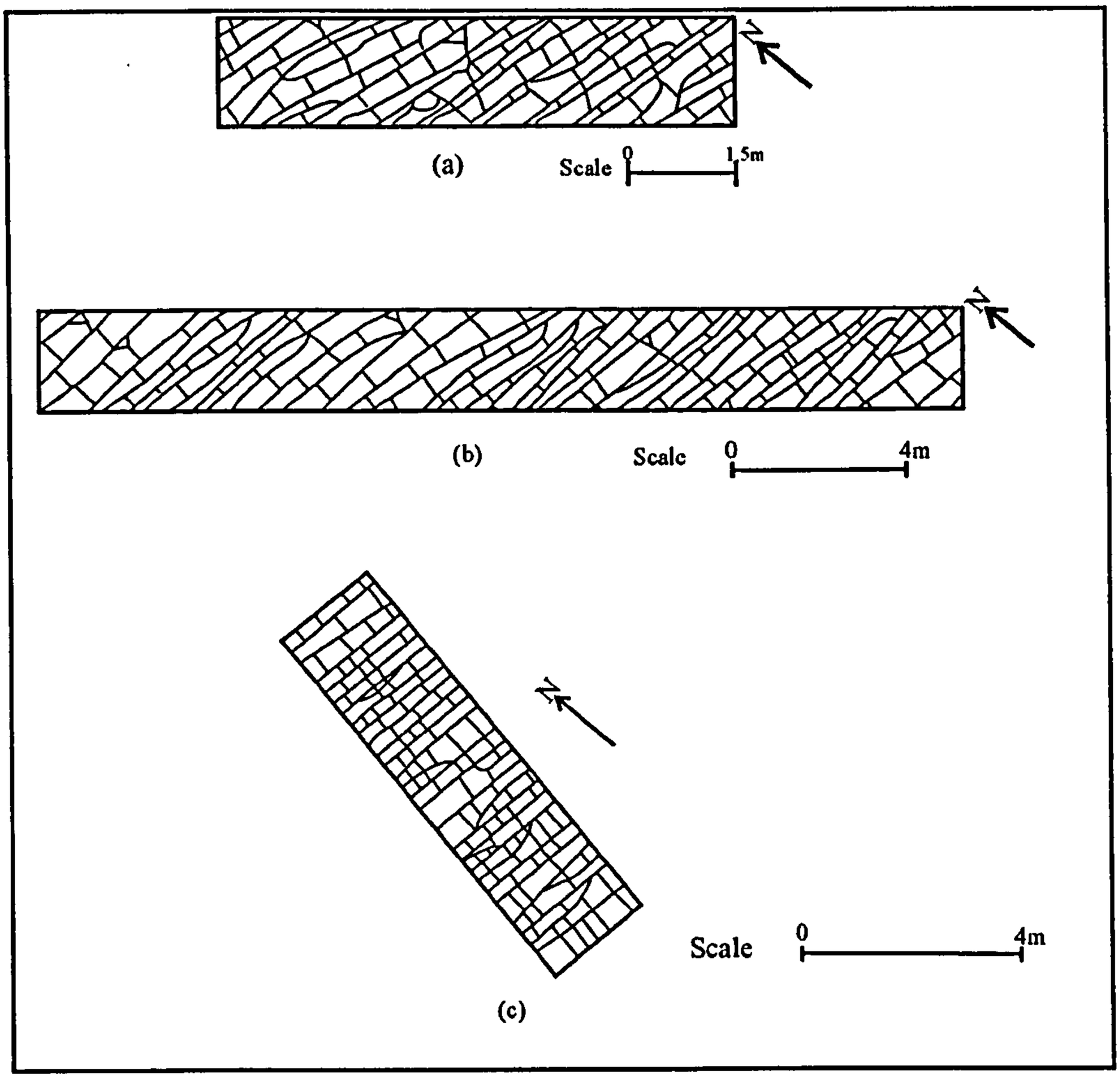


***Figure 4.25** Joint trace maps around the hinge zone of the fold from (a) 7cm (b) 30cm and (c) 24cm thick limestone beds at East of Lilstock.*

The middle limestone bed is 30cm thick and the average joint spacing of the first formed joint set is 60cm. This set strikes at 100° and the second set, which abuts against the first set, is approximately normal to the first set with which it forms a ladder pattern (Fig.4.25b). The total length of fractures within this window is 146m giving a mean joint density of 8.11m^{-1}.

The lowest of the three beds is 24cm thick and the mean joint spacing of the first set is 27cm. The first joint set (J_1) strikes 100° and the second set (J_2) is normal to J_1 forming ladder patterns (Fig. 4.25c). The total length of joints within the measured window is 74.52m and the average joint density of 9.86m^{-1}.

As can be seen from the above discussion, joint spacing and bed thicknesses in this locality are poorly correlated. The values of the proportionality constant (K) that relates joint spacing to bed thicknesses for the three adjacent limestone beds are 5.23, 2 and 1.1 for the upper, middle and lower beds. In addition to bed thickness and lithology, K is also influenced by the degree of deformation (see *e.g.* Ladeira and Price, 1981). However, at this particular locality the difference in K values is not related to the difference in degree of deformation as the three beds are in the same structural position *i.e.* in the hinge of a gentle fold. The variation of K in this work is thought to be related to the variation in lithology and the effect of the surrounding shale beds.

A study of joint density and patterns was carried out on two limestone beds of different thickness separated by 50cm of shale in the vicinity of a normal fault at east of Lilstock (grid reference 179454). This was done to examine the role of pre-existing major structures, such as the normal faults, on fracture development during Alpine inversion of the Bristol Channel Basin. A 2D joint trace map was constructed on the hanging-wall 2m from a normal fault, which has a strike of 095°. The upper bed is 15cm thick with a dip/dip direction of 05°/290°. The earliest formed joint set in the upper bed strikes 020° and the second set strikes 090° (Fig. 4.26a). 80% of the second (J_2) joints in this bed abut the early set and sometimes curve into an orientation perpendicular to the first (J_1) as they approach the earlier formed joints. The total

length of joints in this measured window is 128.8m and there is an average fracture density of $4.1m^{-1}$.

The lower bed is 33cm thick and has a dip/dip direction of 7°/340°. The first joint (J_1) and the second joint set (J_2) in this bed strike 020° and 095° respectively (Fig 4.26b). The second set of joints abuts the earlier set. The total length of the joints in this window is 102.4m and the average density is $4.3m^{-1}$. In both beds, unsystematic and non-crosscutting joints are very common and these are probably related to later uplift. Joint orientations, the number of joint sets and joint density in the two beds is identical and these parameters illustrate independent of bed thickness. In addition, the influence (if any) of the proximity of the measured windows to the adjacent normal fault seems to be the same for both beds. It might therefore be concluded that the mechanical properties of the fractured beds and the adjacent shale controlled the degree of fracturing.

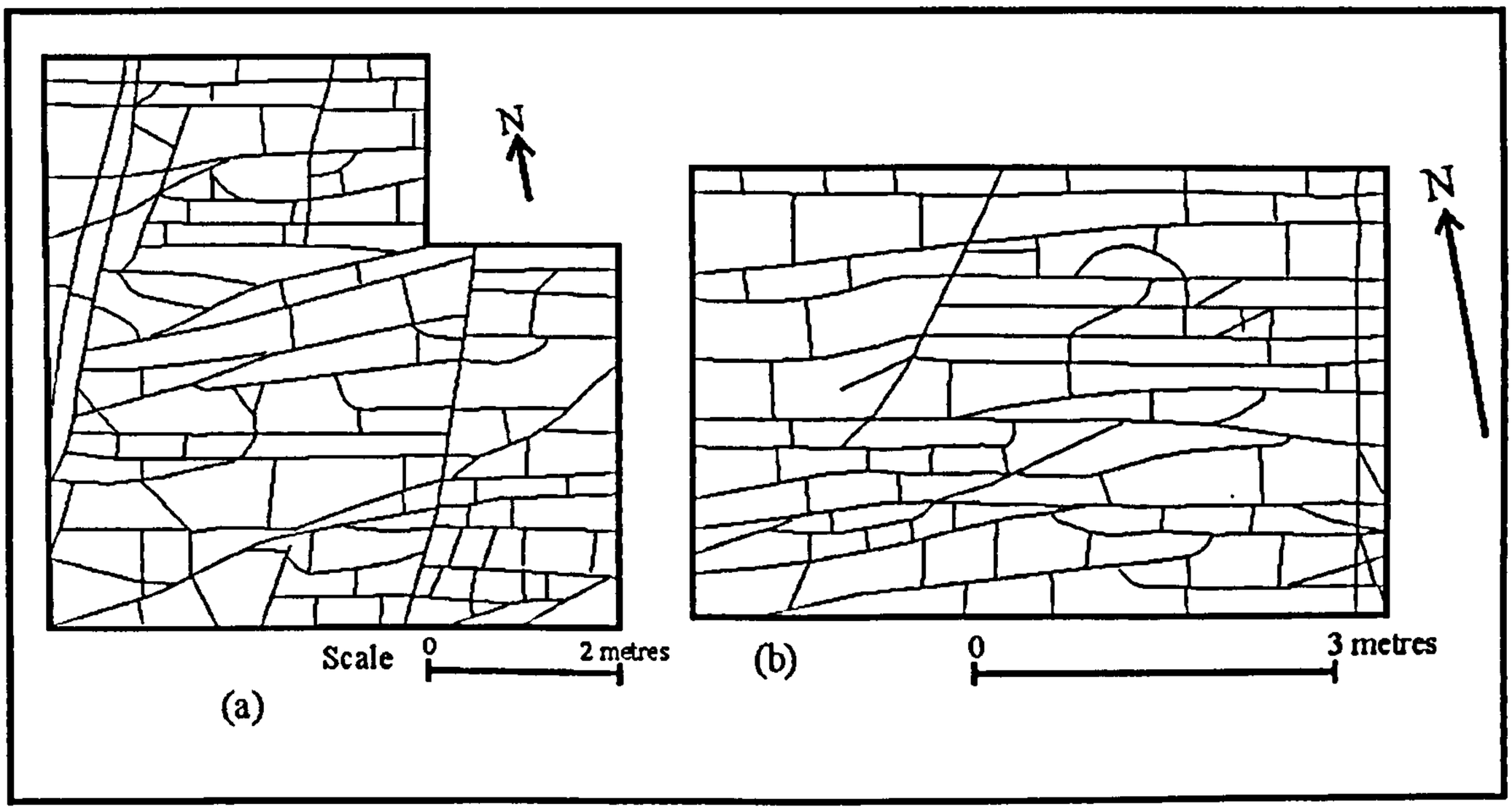


***Figure 4.26** Joint trace maps of two limestone beds on the hanging-wall of a normal fault east of Lilstock.*

4.4.3 Lilstock

This area was chosen because of the excellent exposure on wave cut platforms and cliff sections of alternating limestone and shale beds of the Lias. This area is probably one of the best exposed fractured limestone beds in the world. The major structures in this area include a series of WNW-ESE striking basin bounding normal faults, most of which dip to the north and were reactivated during Alpine inversion, a major asymmetric fold with an axis striking WNW-ESE, and NE-SW striking sinistral strike-slip faults (Fig. 4.27). Joints of different sets are abundant, varying in strike, spacing and abutting and crosscutting relationships from one bed to the next. The location of the beds on the Lilstock rollover anticline is shown in Fig. 4.27. The joint patterns and density obtained by 2D joint trace mapping and joint orientation obtained by scan line sampling are described in the following sections.

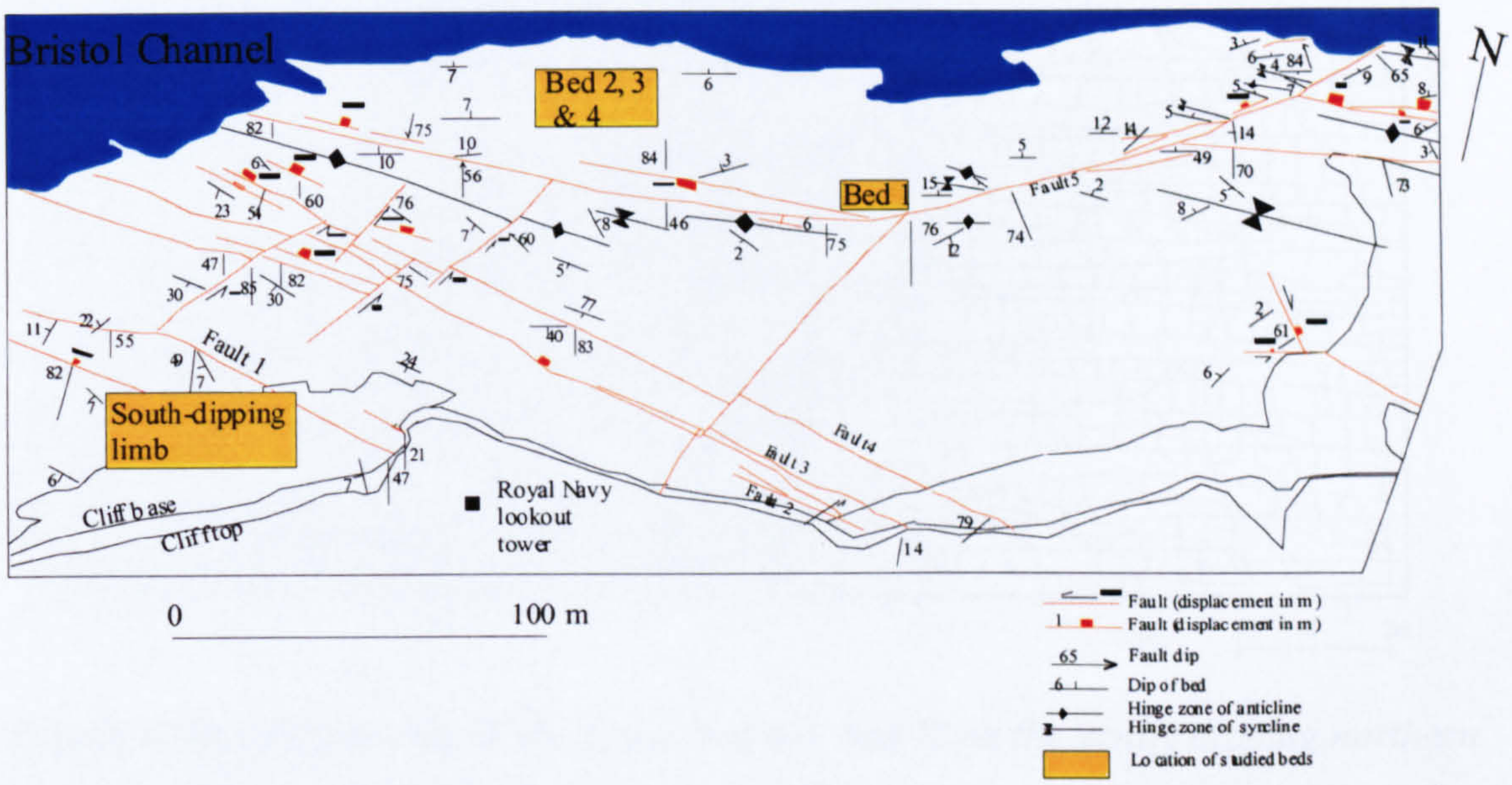


Figure 4.27 *Simplified structural map of Lilstock on the southern margin of the Bristol Channel Basin (from Rawnsley et al., 1998).*

4.4.3.1 Bed 1

The sampled window in bed 1 (Fig. 4.27) is located in the proximity of the E-W and ENE-WSW striking reverse reactivated normal fault. Limestone bed 1 is 10cm thick and has a dip/dip direction of 05°/008°. The thicknesses of the overlying and underlying shales are 90cm and 19cm respectively. In the unperturbed region (*i.e.* away from the fault), there are two joint sets: an early set of long E-W striking master joints (J_1) and the second set (J_2) made up of short joints which abut against them at approximately 90° to form ladder patterns (Fig. 4.28). A progressive change in joint strike is seen when moving from unperturbed regions away from the faults towards the strongly perturbed zones at the inflection of Fault 5 (Fig. 4.27) of Rawnsley *et al.* (1998). Curving of the joints is most pronounced approaching the inflection of the two segments of the fault (Fig. 4.29).

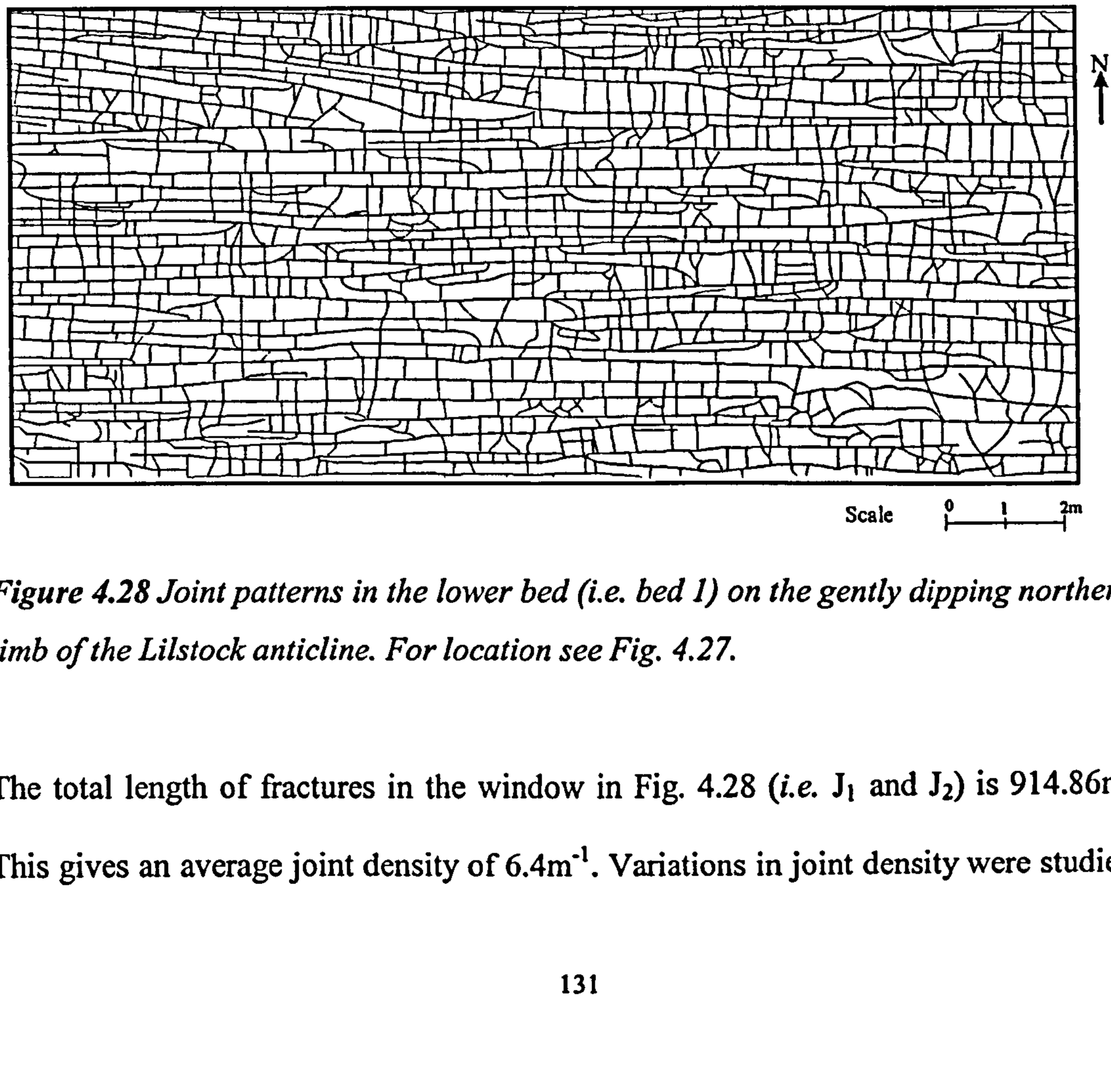


***Figure 4.28** Joint patterns in the lower bed (i.e. bed 1) on the gently dipping northern limb of the Lilstock anticline. For location see Fig. 4.27.*

The total length of fractures in the window in Fig. 4.28 (*i.e.* J_1 and J_2) is 914.86m. This gives an average joint density of $6.4m^{-1}$. Variations in joint density were studied

by using square and circular windows in cubic and rhombic packing arrangements. Both joint spacing and density remain constant in moving towards the fault. This implies that the effect of fault on joint density is low except around the inflection between the two fault segments. Peacock (2001) examined the relationship between faulting and jointing and demonstrated that joints that predate the fault tend to have experienced dilation, shear or affected by pressure solution during faulting, depending on their orientation in relation to the stress system. Joints that form either syn- or post-faulting may curve into the fault, reflecting stress perturbation, as proposed by Rawnsley *et al.* (1992). The change in the strike of the joints probably indicate that the joints were formed either synchronously or post-date the reactivation of the normal fault to reverse fault.



Figure 4.29 *Joints that propagated in the perturbed stress field around an inverted normal fault at Lilstock. Systematic joints gradually converge towards sticking points along the fault plane, which is made up of two segments.*

Square windows of 1, 4, 9 and 16m^2 were generated on the joint trace maps. Circular windows in cubic and rhombic packing with the same area as those of square windows were also studied. As can be seen from Fig. 4.30, the fluctuation of joint density around the mean is large when small windows of both geometric shapes are used. For areas that are greater than 4m^2, the curve approaches the mean from both sides. The joint density for square and circular and square windows is almost identical.

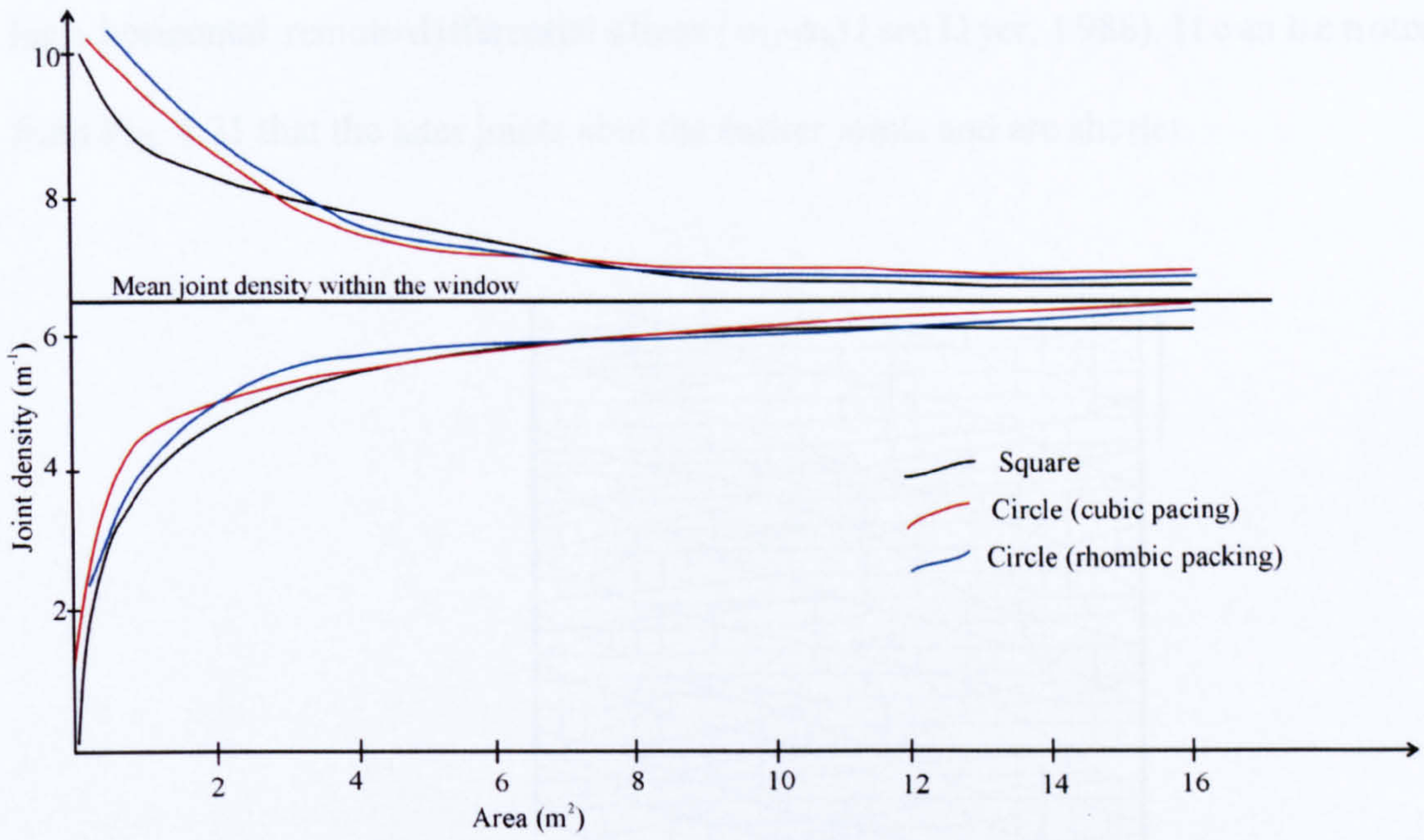


Figure 4.30 *Variation of joint density as a function of window size and shape in bed 1 from Lilstock generated using Densityinfo.*

4.4.3.2 Bed 2

The thickness of this limestone bed is 16cm and it has a dip/dip direction of 12°/004°. The thicknesses of the overlying and underlying shale beds are 32cm and 23cm respectively. Excluding burial joints, six joint sets were identified based on their abutting relationships (Fig. 4.31). Joints that were formed during the burial history of

the basin can be distinguished from Alpine joints because they are either partly healed or filled by calcite veins.

The earliest joint set is made up of long straight joints striking between 125°-130°. The average spacing of the joints in this set is 3.5m. The subsequent joint sets abut against this set. The greater length of these joints compared to subsequent sets probably reflects the fact that they propagated in an unperturbed stress field under a high horizontal remote differential stress (σ_H-σ_h) (see Dyer, 1988). It can be noted from Fig. 4.31 that the later joints abut the earlier joints and are shorter.

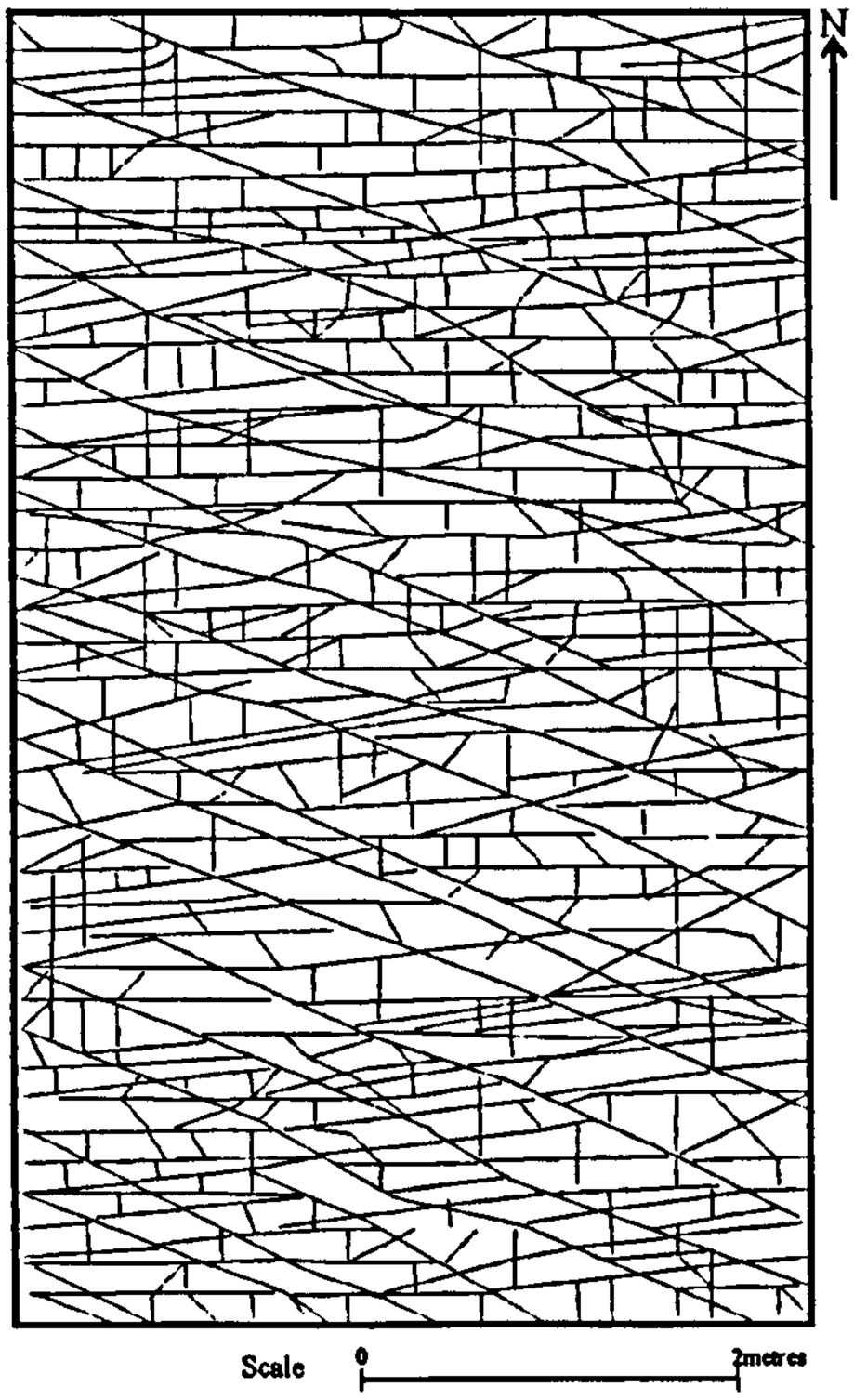


Figure 4.31 *Joint patterns in bed 2 from the gently dipping northern limb of the Lilstock buttress anticline. With the exception of burial joints locally observed, six joint sets were identified in this bed.*

The second joint set (Fig. 4.31) strikes between 110° and 115°. Curving of this set as it approaches the earlier set is commonly observed. This suggests that the first fracture set provided a low traction surface during the propagation of the second set. The propagation of the second joint set indicates that the local stress field may have rotated by about 15° in an anticlockwise sense since the formation of the first set. Some joints of the second set curve towards each other to form hook geometry (tip-to-plane junctions) and some form tip-to-tip junctions with joints of the first set. Fracture mechanics arguments indicate that it is easier to propagate a joint from a pre-existing joint within a rock than to initiate a completely new joint. Field observation in this locality shows that initiation and propagation of a joint of the second set commonly occurs at the tip of a joint from the first set. The width of the perturbed stress field around a joint that causes deflection of a later joint has been examined by Peacock (in prep.) Peacock shows that joints curve to abut the earlier joints over a metre-scale distance, implying that joints do not interact over large distances. The distance over which the oblique joint curves (*i.e.* the width of the stress disturbance zone) appears to show a log-normal distribution. He concludes that joints in a particular bed perturb the stress field throughout a zone of characteristic width (0.2m to 0.5m). The palaeo-stress significance of curving joints has been discussed by Dyer (1988) who argues that curving perpendicular joints (tip-to-plane) are indicative of low compressive horizontal stress ratios during propagation.

The third joint set (Fig. 4.31) strikes between 085° and 095° and is approximately sub-parallel to the burial joints or veins (*i.e.* those developed during basin opening). This third set abuts obliquely against the earlier joint sets, indicating that they had low but not zero interfacial shear strengths when the third set propagated. The first three joint

sets form 'oblique ladder' and 'oblique ladder within ladder' geometries. There is a similarity between the first three joint sets in this bed and the fractures generated by non-cylindrical folding in the analogue model shown in Fig. 4.32 in which torsion was applied before shortening (Rives and Petit, 1990). During the formation of the first three sets in bed 2, the least principal stress rotated in an anticlockwise direction from approximately 040° to roughly N-S (*e.g.* Rawnsley *et al.*, 1992).

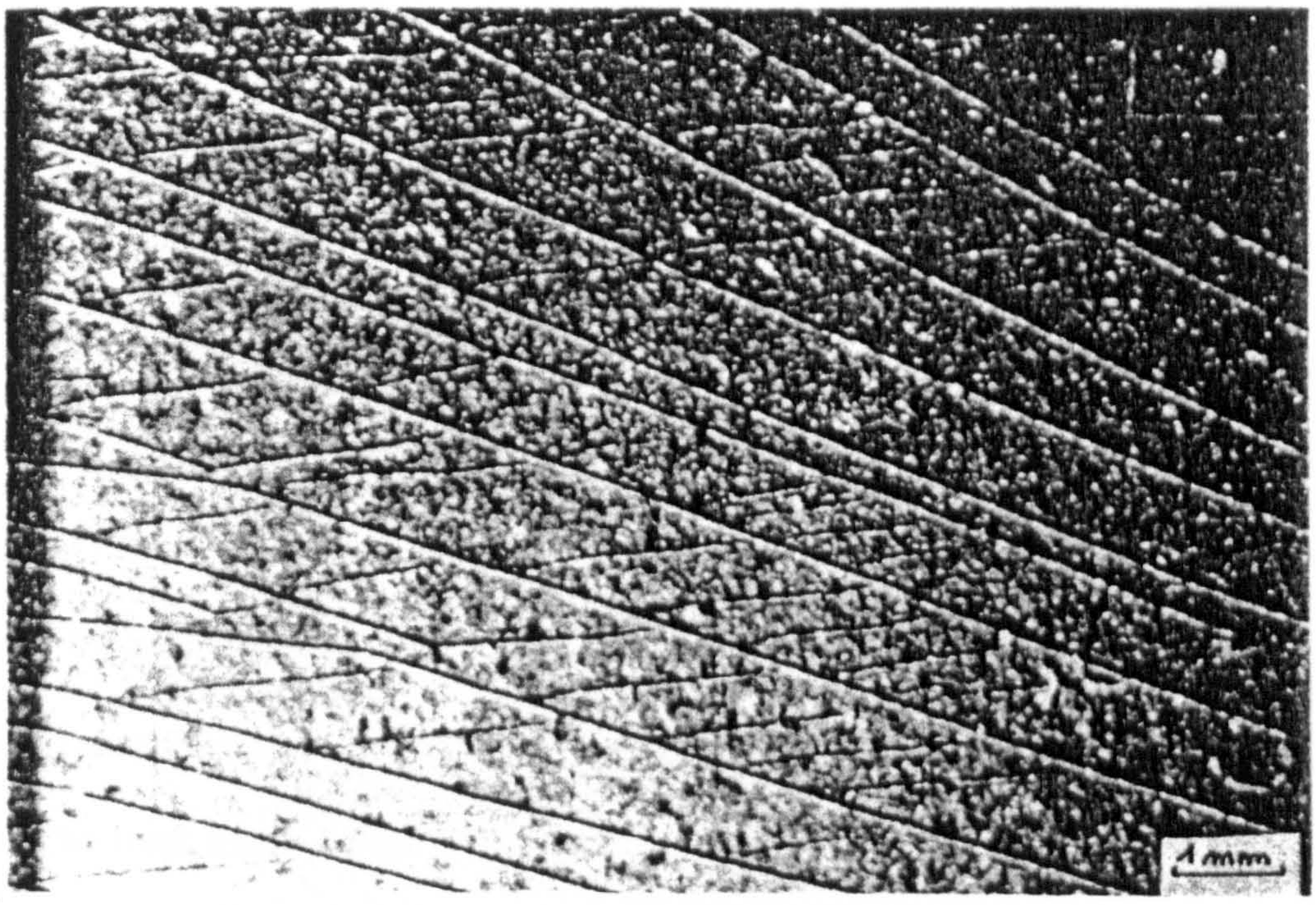


Figure 4.32 *Joint produced by bending of a PVC plate coated with brittle varnish during non-cylindrical folding (from Rives and Petit, 1990).*

The fourth joint set is poorly developed and strikes between 065° and 070°. It commonly shows a right-stepping *en-echelon* arrangement. This set mostly abuts the third set and crosscuts the first and second sets, implying either that they were filled

by secondary minerals that have subsequently been removed, or that a high normal stress was applied across the joints.

The fifth set strikes between 335° and 345° and the sixth set is between 350° and 010°. These two sets were formed probably relate to uplift and exhumation of the whole basin and the release of residual stresses locked-in at depth. The majority of the joints in the fifth set abut against the third set (>70%) and second set (~25%). A few examples were observed where the joints curve into an orientation either parallel to the third joint set or perpendicular to the second joint set.

The sixth set shows variation in strike; 75% of the joints abut against the third set and 15% against the second set. A few of the joints (~3-4%) curve into an orientation perpendicular to the first set and may link with members of the same set; ~2-3% curve into an orientation parallel to the first, second and third sets and about 2-3% show end to end linkage with the second and third sets. The two latest joint sets have a high aspect ratios (the ratio of opening to the length of the joint) compared to the earlier sets. The total length of all joints within the window is 337.4m giving an average fracture density of $12m^{-1}$.

4.4.3.3 Bed 3

This limestone bed (see Fig. 4.27 for location) has a thickness of 10cm and dip/dip direction of 8°/360°. The thicknesses of the overlying and underlying shale beds are 15cm and 32cm respectively. Based on abutting relationships, four joint sets were identified in this bed (Fig. 4.33). The first and third joint sets are sub-parallel and strike NW-SE. The second set is approximately N-S. The fourth set is made up of

short N-S striking joints, which probably formed during uplift. Non-systematic joints were also commonly observed in this bed. The total length of joints within the window is 383.7m with an average joint density of $5.35m^{-1}$. To check the reproducibility of this result, a separate rectangular window with the same area was mapped in the same bed. The average joint density being $4.37m^{-1}$. The difference in joint density between the two windows may be caused by lateral changes in the mechanical properties of the layer.

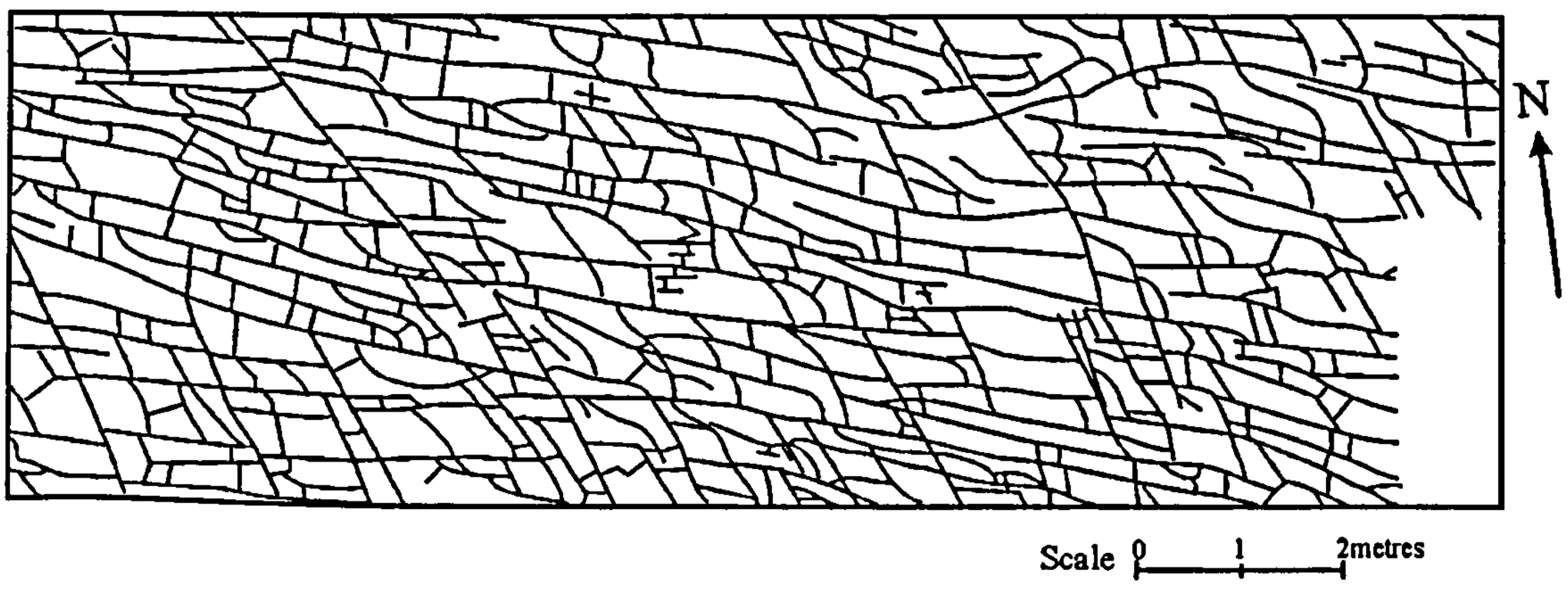


Figure 4.33 Joints pattern in bed 3 on the northern, gently dipping limb of Lilstock anticline.

4.4.3.4 Bed 4

This bed is the uppermost exposed fractured limestone bed on the gently dipping northern limb of the anticline and has a thickness of 15cm. The underlying shale is 8cm and the overlying shale is not exposed. Based on joint interactions, three joint sets are identified in this bed (Fig. 4.34). The strike of the first joint set is 320°. The second set strikes 300°. The first set consists of long straight joints with apertures up to 3cm. The second set curves into parallelism as it approaches the earlier set. This, according to Dyer (1988), relates to the horizontal differential stresses falling in the

range of $-3 < \sigma_H^{\infty}/\sigma_h^{\infty} < -1/3$. The last joints to form in this bed are short joints with approximately orientations. They may be related to later uplift.

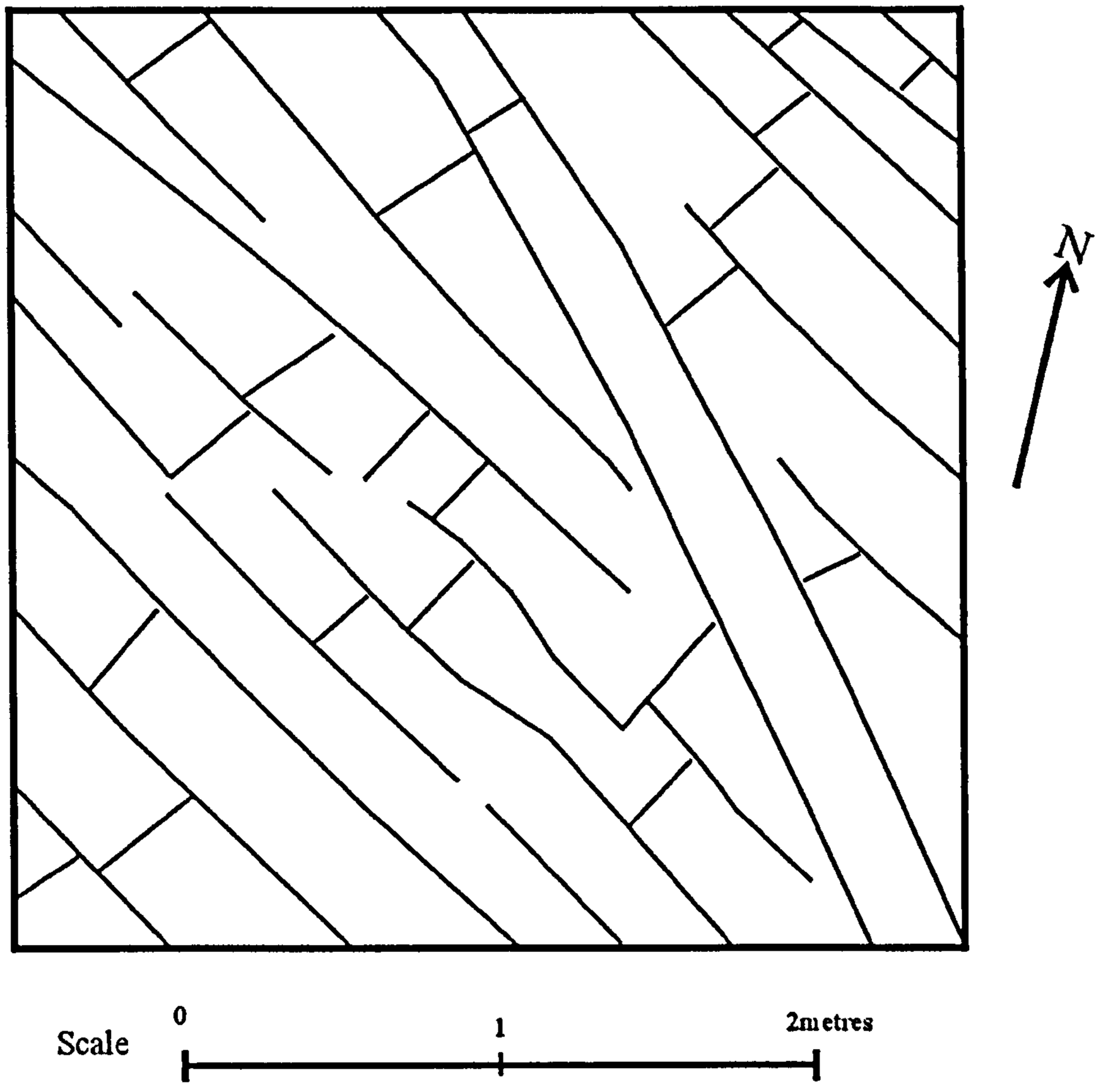


***Figure 4.34** Joint trace maps in bed 4 on the trailing limb of the Lilstock rollover anticline. Note that the second joint set is deflected as it approaches the earlier set.*

Measurements made along three scan lines with lengths of 92m trending 100° in bed 2, 51.5m trending 75° in bed 3 and 55.22m trending 70° in bed 4 are summarised in Fig. 4.35 and Table 4.1. As can be seen from Fig. 4.35 and Table 4.1, joint orientations in the three beds are different, which suggests that the limestone beds were mechanically decoupled during jointing.

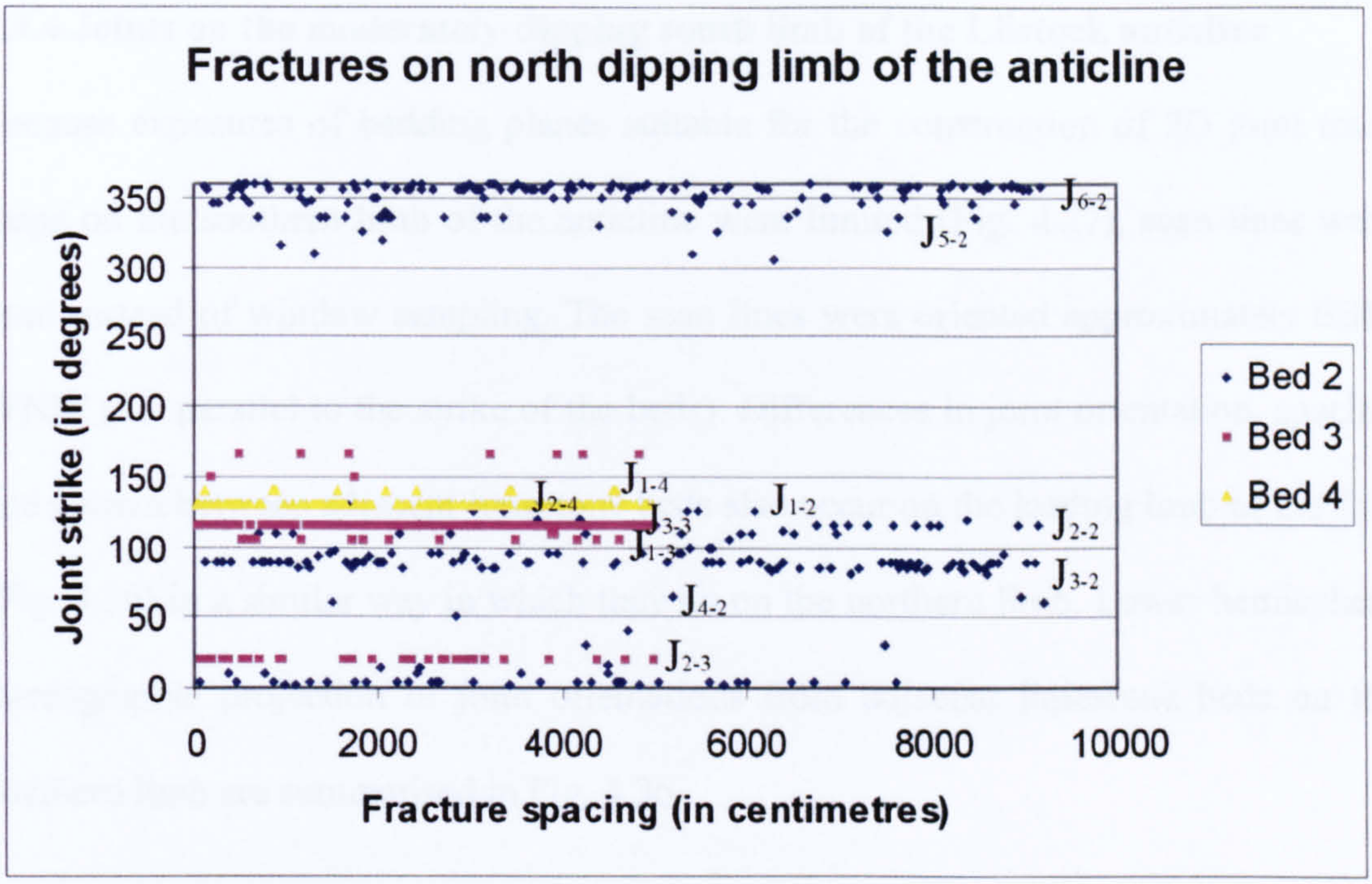


Figure 4.35 *Strike of the joints measured along three scan lines in bed 2, 3 and 4 on the northern, gently-dipping limb of the Lilstock anticline. Note that the first subscript shows the joint set number and the second indicates bed number.*

Table 4.1 *Summary of scan line sampling of joints on the northern limb of the Lilstock anticline.*

Bed number	Bed thickness	Joint set	Joint strike	Remark
1	10cm	J_1	090°	Post-Alpine
		J_2	N-S	
2	16cm	J_1	125-130°	
		J_2	110-115°	
		J_3	085-095°	
		J_4	065-070°	
		J_5	360°	Post-Alpine
		J_6	335-345°	Post-Alpine
3	10cm	J_1	105°	
		J_2	165°	
		J_3	115°	
		J_4	020°	
4	15cm	J_1	140°	
		J_2	130°	
		J_3	360°	Post-Alpine

4.4.4 Joints on the moderately-dipping south limb of the Lilstock anticline

Because exposures of bedding planes suitable for the construction of 2D joint trace maps on the southern limb of the anticline were limited (Fig. 4.27), scan lines were used instead of window sampling. The scan lines were oriented approximately ESE-WNW (*i.e.* parallel to the strike of the beds). Differences in joint orientation, spacing and pattern between adjacent limestone beds also occur on the leading limb of the fold (Fig. 4.36) in a similar way in which they do on the northern limb. Lower hemisphere stereographic projection of joint orientations from adjacent limestone beds on the southern limb are summarised in Fig. 4.36.

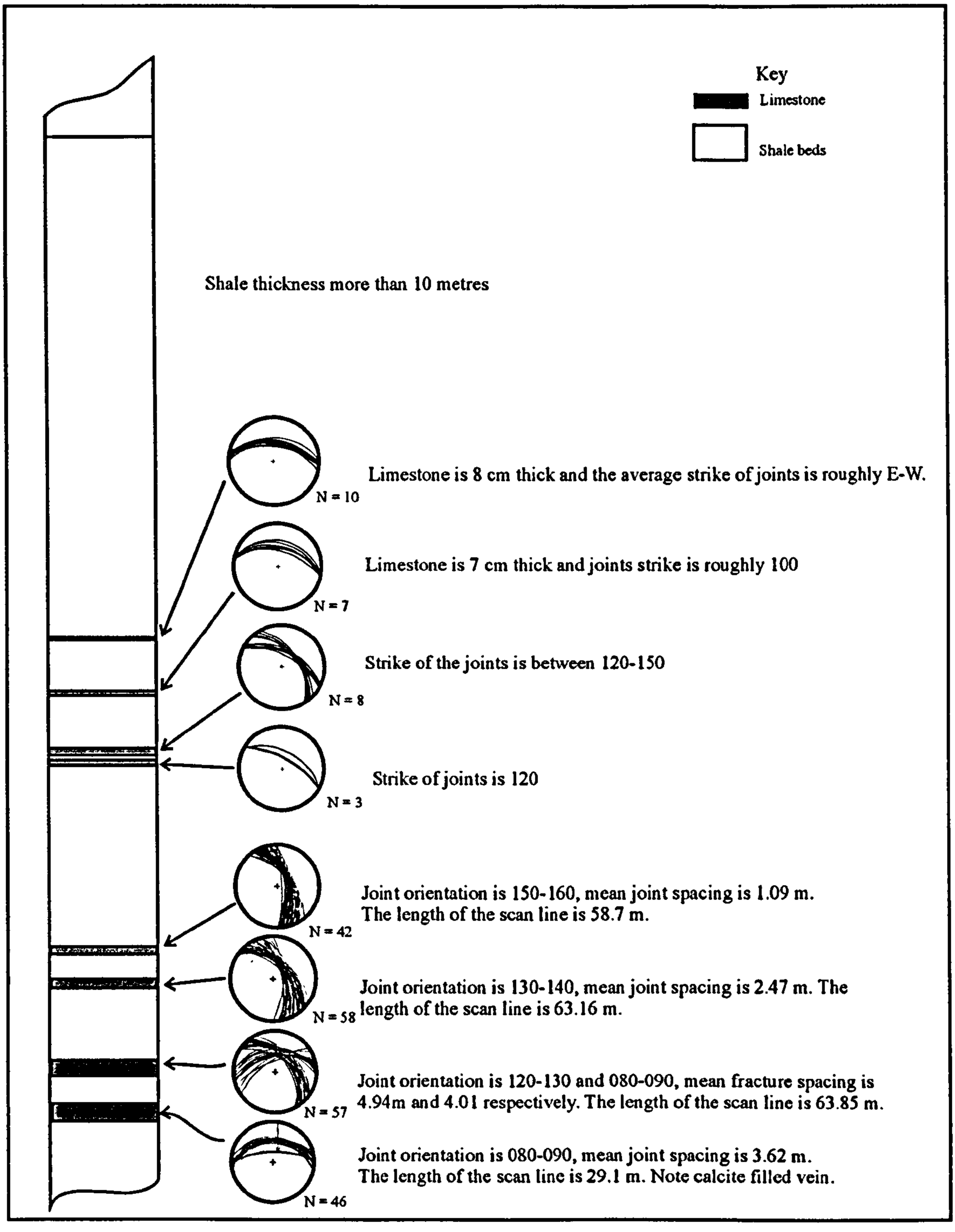


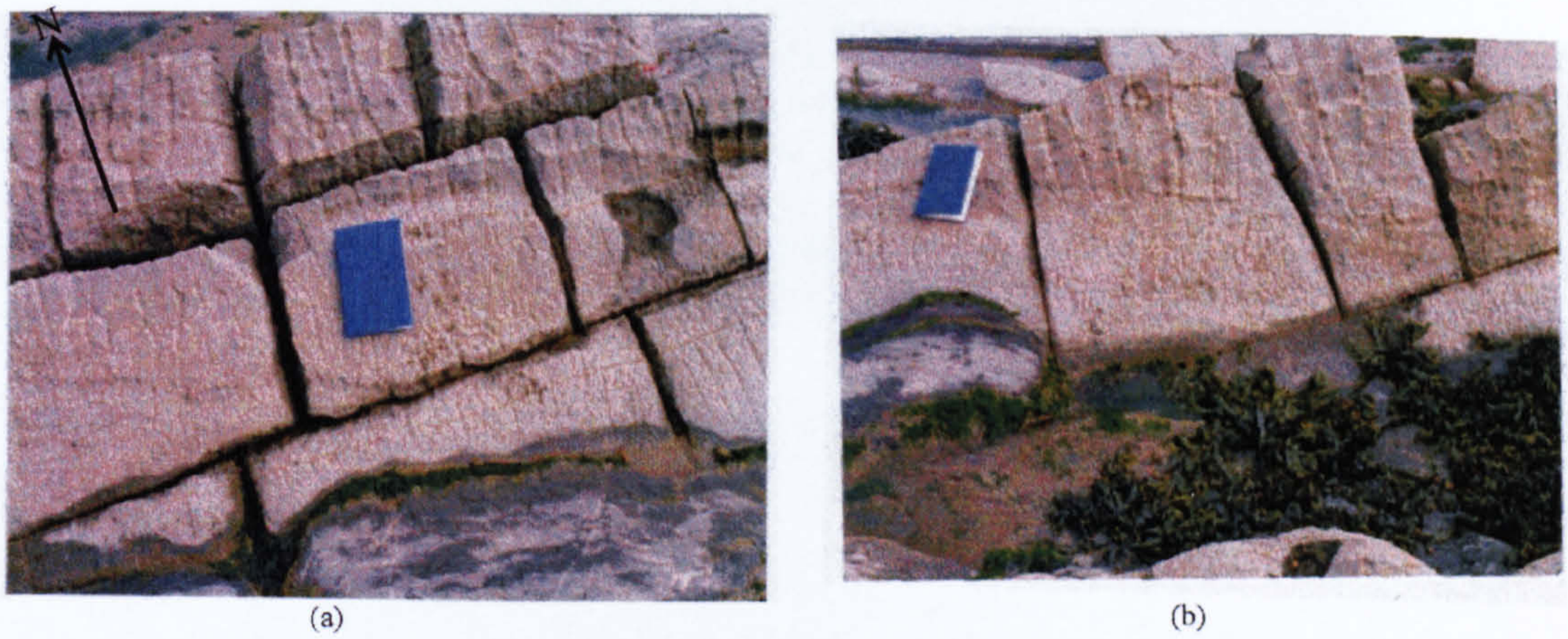
***Figure 4.36** Stratigraphic column showing stereographic projection of dominant joint sets on moderately southern dipping limb of Lilstock anticline. It appears that there was no mechanical communication between adjacent limestone beds and each limestone bed fractured totally independently of the overlying and underlying limestone beds.*



Figure 4.37 *An aerial view of joint patterns on the moderately dipping southern limb of the Lilstock rollover fold. View from the Royal Navy lookout (see Fig. 427) towards WNW.*

As can be seen in Fig. 4.36, the strike of joints in adjacent competent beds is highly variable. An oblique view of alternating limestone and shale beds in the leading limb of the Lilstock anticline is shown in Fig. 4.37. The most common joint pattern on this limb is a ladder pattern. A *ladder pattern* forms when the initial set of long parallel joints and associated non-crosscutting joints of the second set intersect at a high angle or normal to each other (Fig. 4.38). This pattern is produced when the shear strength of the initial joint set is very low (Rives *et al.*, 1994). A *grid pattern*, though not common, forms when the two joint sets are mutually at right angles to each other and where both sets cut across one another (Fig. 4 .39). S uch r elationships c an d evelop when the shear strength of the initial joint set is high, possibly related to high applied normal stress or healing (Rives *et al.*, 1994). The grid patterns result from two

independent stress events. *Oblique ladder* and *ladder-within-ladder* patterns form when the second set of fractures is oblique to and do not cross the earlier joints. In this case, the fractures of each newly formed set are shorter in length than the previous set (Fig. 4.40).



(a) (b)

Figure 4.38 *(a) and (b) show ladder patterns observed on the moderately dipping southern limb of the Lilstock anticline (notebook for scale on both photos).*



Figure 4.39 *Grid patterns formed by two mutually orthogonal crosscutting joint sets. The bottom edge of the photo is approximately 2.3m.*



Figure 4.40 *Oblique ladder and ladder-within-ladder patterns observed in moderately-dipping southern limb of Lilstock anticline. Note the compass on the centre right for scale.*

4.4.5 Joints around the hinge zone of the Lilstock rollover anticline

The hinge region of the Lilstock rollover anticline also shows minor variation in joint patterns but in this locality, variation in joint pattern between adjacent limestone beds is less compared with that found on the limbs. Fig. 4.41 shows an oblique field photograph (uncorrected for distortion) of a 5cm thick fractured limestone bed from the hinge zone of the anticline showing a ladder pattern. Calcite veins strike 095° and are probably related to basin opening. The Alpine joints in the hinge region strike parallel to the fold axis. A general observation at Lilstock is that thin limestone beds generally show smaller joint spacing than thicker beds. However, the variation is not systematic. Another pattern observed around the hinge region of the anticline is similar to the *irregular ladder* pattern of Rives *et al.* (1994) (Fig. 4.42).

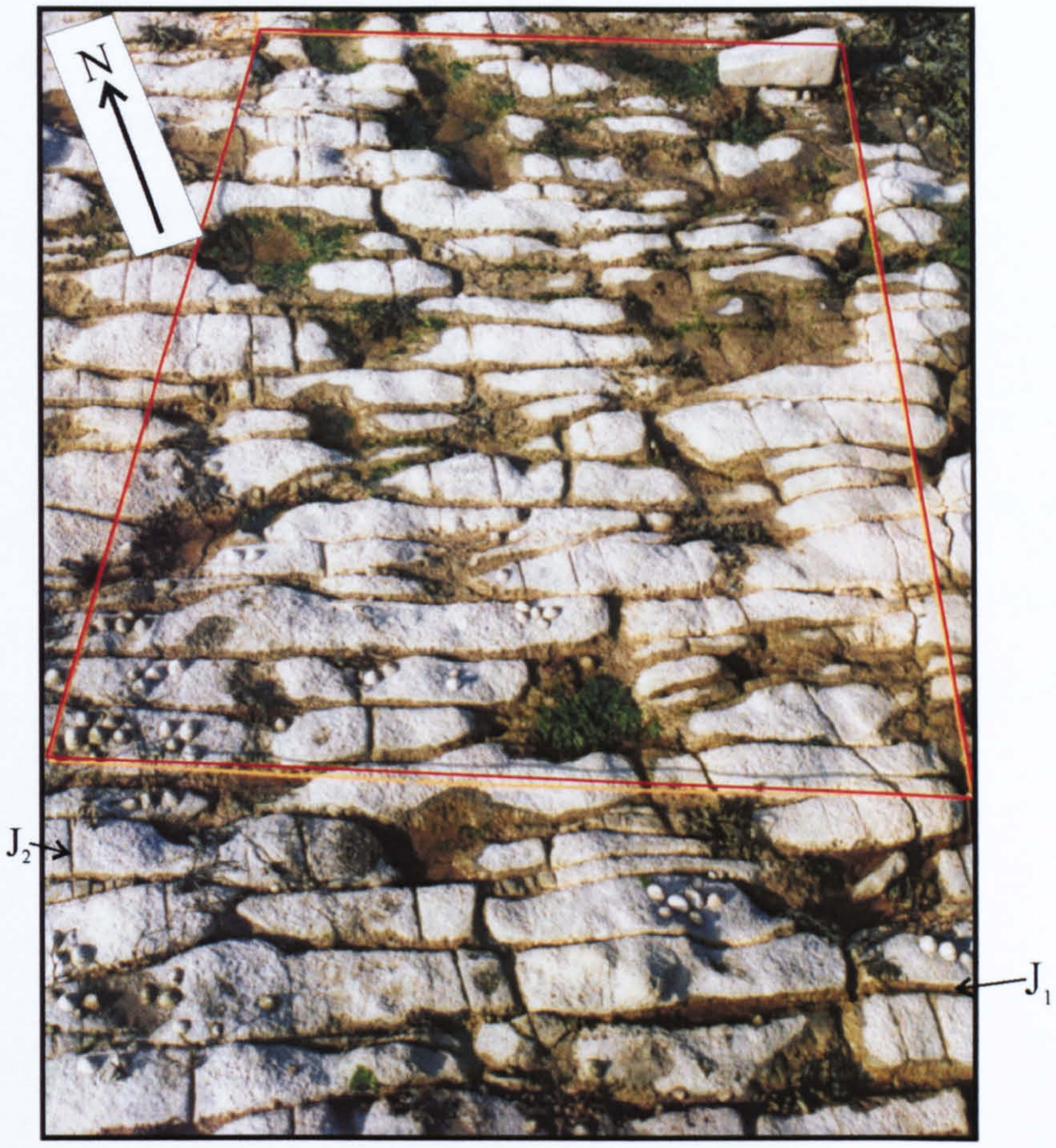


Figure 4.41 *Oblique field photograph of joints from a 5cm thick limestone bed in the hinge zone of the Lilstock anticline: The first joint (J_1) strikes 100°, which is approximately parallel to the fold axis and basin bounding faults. The second joint set (J_2) is a non-crosscutting joint set. Together they form a ladder pattern. The outlined area is 1.5 by 2.20m.*



Figure 4.42 *The joint pattern commonly observed on the hinge zone of the fold (similar to the irregular ladder pattern of Rives et al., 1994). The notebook on the far left of the photo is for scale.*

4.4.6 Kilve

In this section, fracture patterns related to folding are described using field photograph and joint trace maps. In places where 2D joint trace mapping was not possible because of limited exposure, scan lines were run to examine the relationship between bed thickness and joint spacing and to compare the number of joints along a particular direction in adjacent limestone beds. The results are expressed graphically.

At Kilve, 2.5km west of Lilstock (GR 152448), a gentle upright fold with a horizontal fold axis trending 110° occurs in the alternating limestone and shale beds (Fig. 4.43). The fold has a wavelength of over 50m and has an exposed strike length of more than 80m. The fold is exposed during low tides. The joints around the hinge zone of the Kilve anticline strike approximately parallel to the fold axis and are thought to be Alpine in age. These joints are not mineralised. The fold axis has been displaced by a NE-SW striking sinistral strike-slip fault with a horizontal displacement of about 30m (Fig. 4.44). 2D joint trace mapping in the hinge zone of the fold in a window of $44m^2$ (see Fig. 4.45) showed a total joint length of 160.15m.



Figure 4.43 *Joints around the hinge zone of the Kilve anticline viewed looking ESE. Note that the joints are sub-parallel to the fold axis, indicating synchronous development of jointing and folding.*

Where the fold is asymmetric on the far right hand side of the photograph shown in Fig. 4.43, the joint strike begins to deviate from being parallel to the fold axis and becomes oblique (Fig. 4.46). The early joints strike oblique to the axis and gradually change towards parallelism as new joints form. Each set of newly formed joints is shorter than joints of the previous set and the pattern produced is similar to the

oblique ladder patterns produced in analogue models by Rives and Petit (1990) and to the exposures at Lilstock (Figs. 4.31, 4.32 and 4.40).

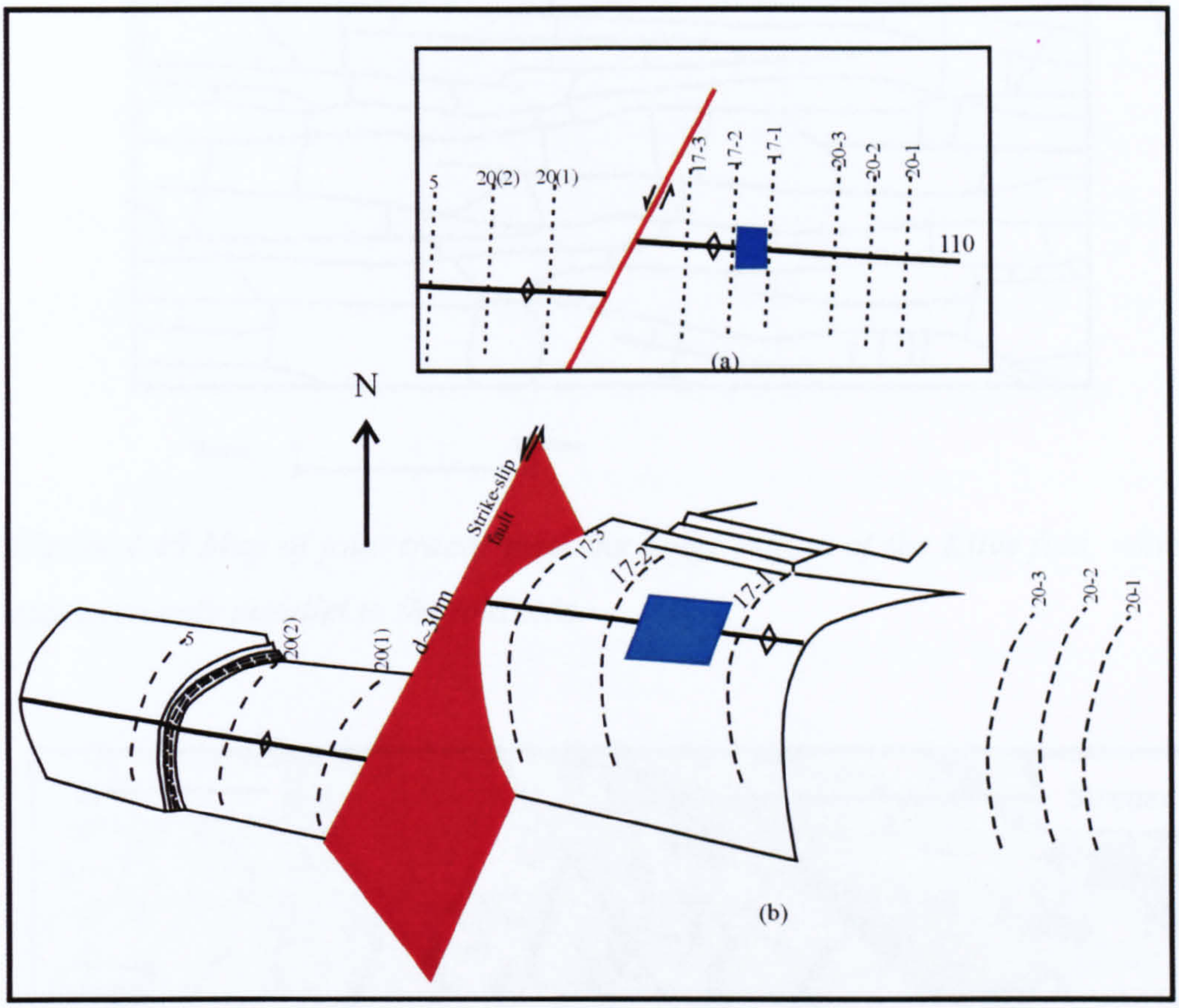


Figure 4.44 *(a) Plan view of the relationship between the fold and strike-slip fault and the layout of the scan line and window sample. (b) Schematic diagram of the Kilve anticline and the position and orientation of the scan lines and window samples. Refer text for explanation.*

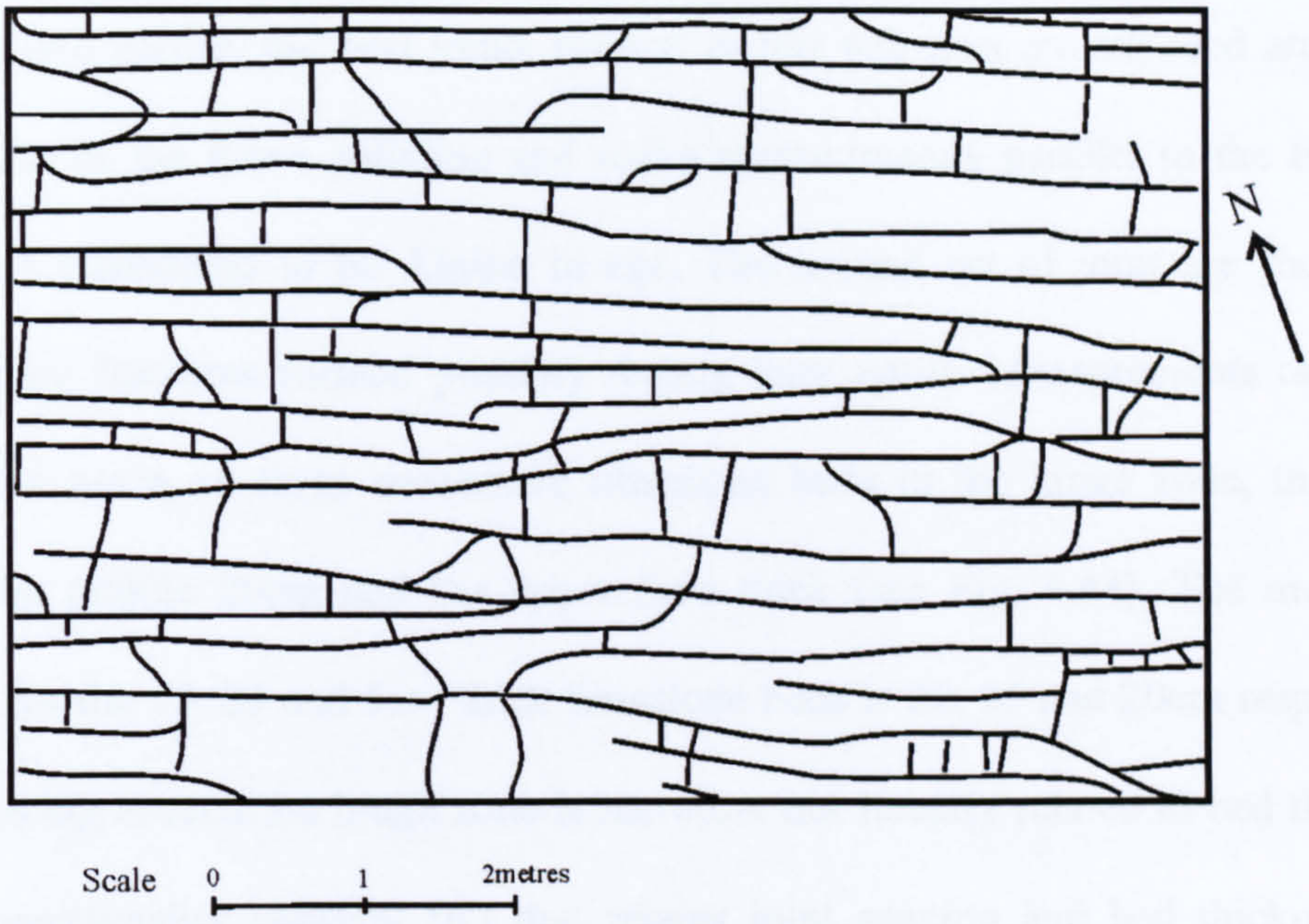


Figure 4.45 *Map of joint traces from the hinge region of the Kilve fold, which strike approximately parallel to the fold axis.*

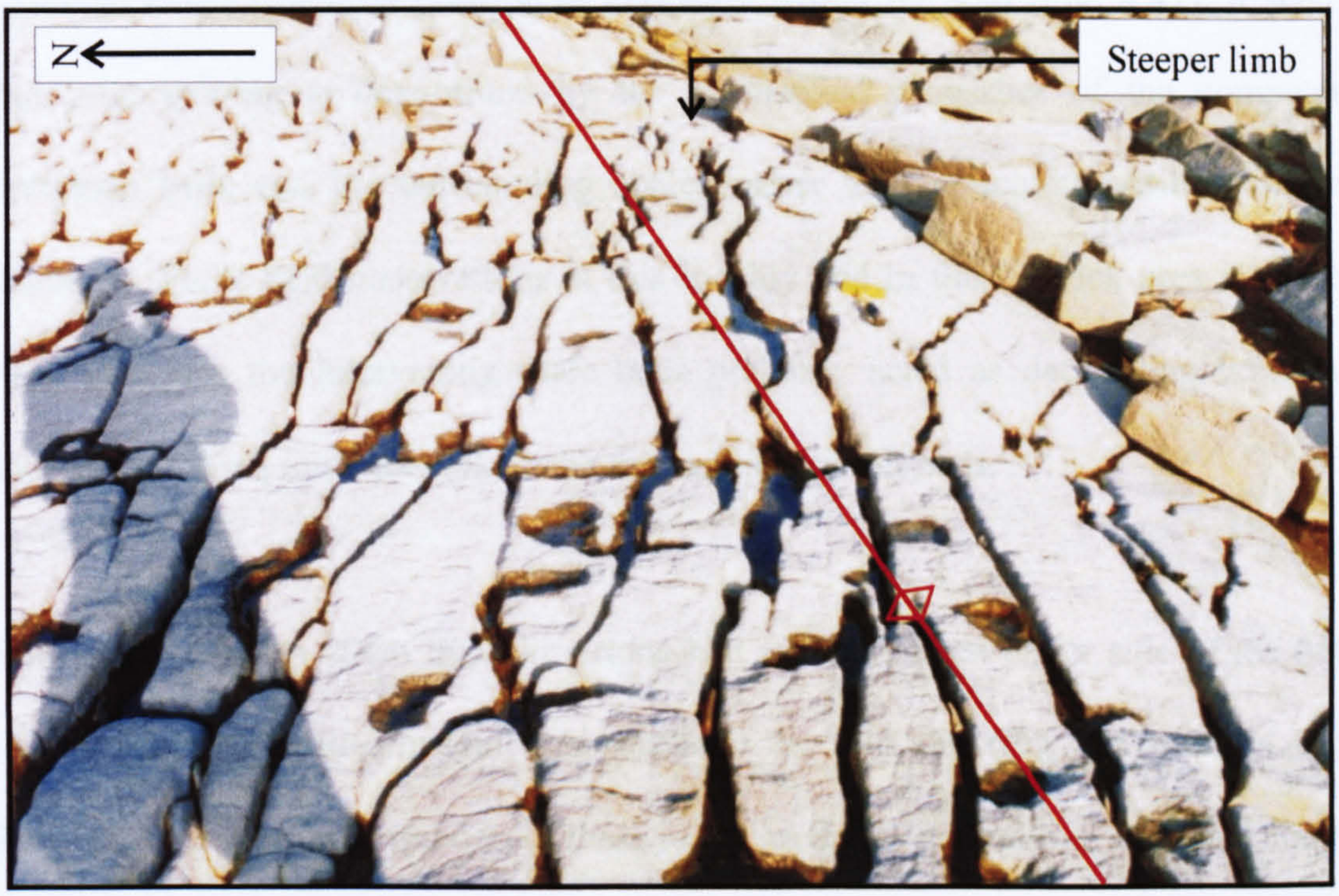


Figure 4.46 *Joint strike variations around the hinge of the asymmetric Kilve fold (viewed looking ESE). Note that the joints are oblique to the fold axis (shown in red) and that this pattern forms when the fold is asymmetric. Hammer in the right centre of the photograph is for scale.*

As discussed earlier, the first joints formed in this sub-area are exposed around the hinge zone of the Kilve anticline and strike approximately parallel to the fold axis. These are considered to be Alpine in age. The second set of joint are short, non-crosscutting fractures formed possibly during later uplift. Measurements on 9 scan lines were made on three successive limestone beds in the hinge zone, the lowest 17cm, the middle 20cm and the upper 5cm thick (see Fig. 4.44). The mean joint spacing for the 17, 20 and 5cm thick limestone beds is 22, 25 and 20cm respectively. Joint spacing around the hinge zone is therefore not linearly related to bed thickness. The proportionality constant (K) that relates joint spacing and bed thickness (*e.g.* Ladeira and Price, 1981; Price and Cosgrove 1990) is 1.3 for the lower bed, 1.25 for the middle bed and 4 for the upper bed. In this locality, joint spacing is not directly linked to either structural position or curvature within the fold (Fig. 4.47). It seems that joint spacing is determined by the mechanical properties of the competent limestone beds and the surrounding shales rather than structural position or bed thickness. From field observations at this locality and in the Lilstock area it can be concluded that the intervening shale beds probably acted as decoupling horizons, enabling different joint networks to be formed in adjacent beds.

Joint spacing in the 20cm thick limestone bed is identical on either side of the 040° striking sinistral strike-slip fault that displaces the fold axis (Fig. 4.47b and 4.47c). This indicates that the formation of these joints predated the faulting. As noted above, they are parallel to the fold axis suggesting that the development of these joints was associated with the folding.

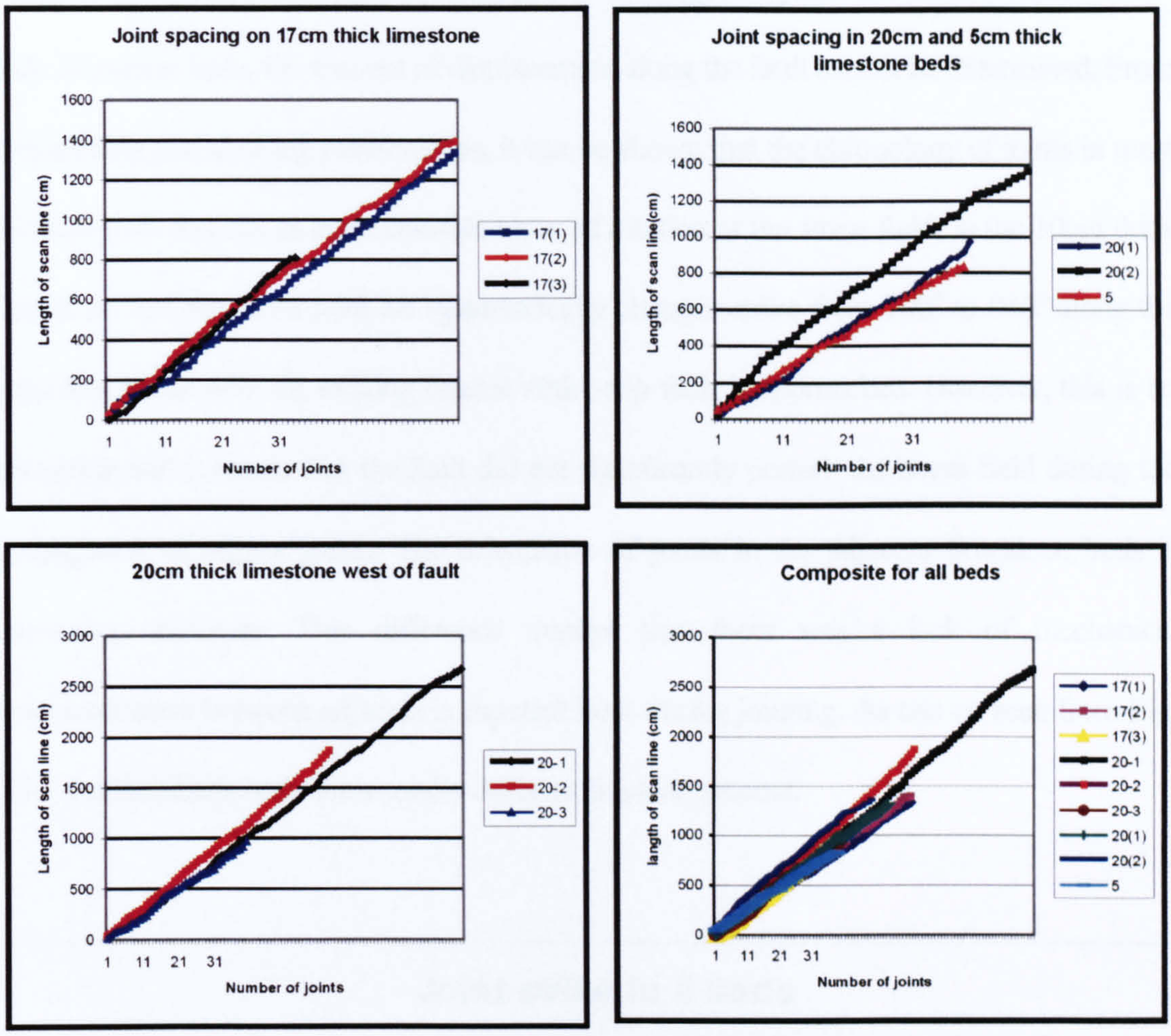


Figure 4.47 *Joint spacing in the hinge zone of Kilve fold (17cm (b) 20cm and 5cm (c) 20cm and (d) composite graph showing the number of joints along the scan line. For the position of each scan line refer to Fig. 4.44 and text for explanation. Note that the slope for all beds remains approximately the same despite their thickness variations.*

Approximately 200m ESE of the Kilve anticline, fractured limestone beds alternating with shale beds are exposed along Kilve Beach. 2D mapping of the joint traces was not possible because of limited exposure of the limestone beds. Scan lines were run parallel to the strike of the beds. There are five adjacent limestone beds having thicknesses of 20, 28, 33, 17 and 10cm (Fig. 4.48). All the beds dip between 18° - 22° to the S or SSW. NW-SE striking dextral strike-slip fault with horizontal offsets occurs in the vicinity, the sense of movement

4.4.7 East Quantoxhead and Blue Ben

This area is located approximately 3km west of Lilstock. A 25cm thick limestone bed dipping gently to the north was studied at this locality (grid reference 137443, see Fig. 2.7). There are three sets of joints. The oldest joints in this bed strike NW-SE, the second set ESE-WNW (110°) and the later exhumation joints strike approximately NNE-SSW (Fig. 4.49). Some of the second set tend to curve as they approach the first set to link with it at 90° (*i.e.* tip-to-plane junctions) and others abut against the early joint sets without any significant deflection (*i.e.* cracks propagate along a straight trajectory). The total length of joints within the window studied on this bed is 308.95m.

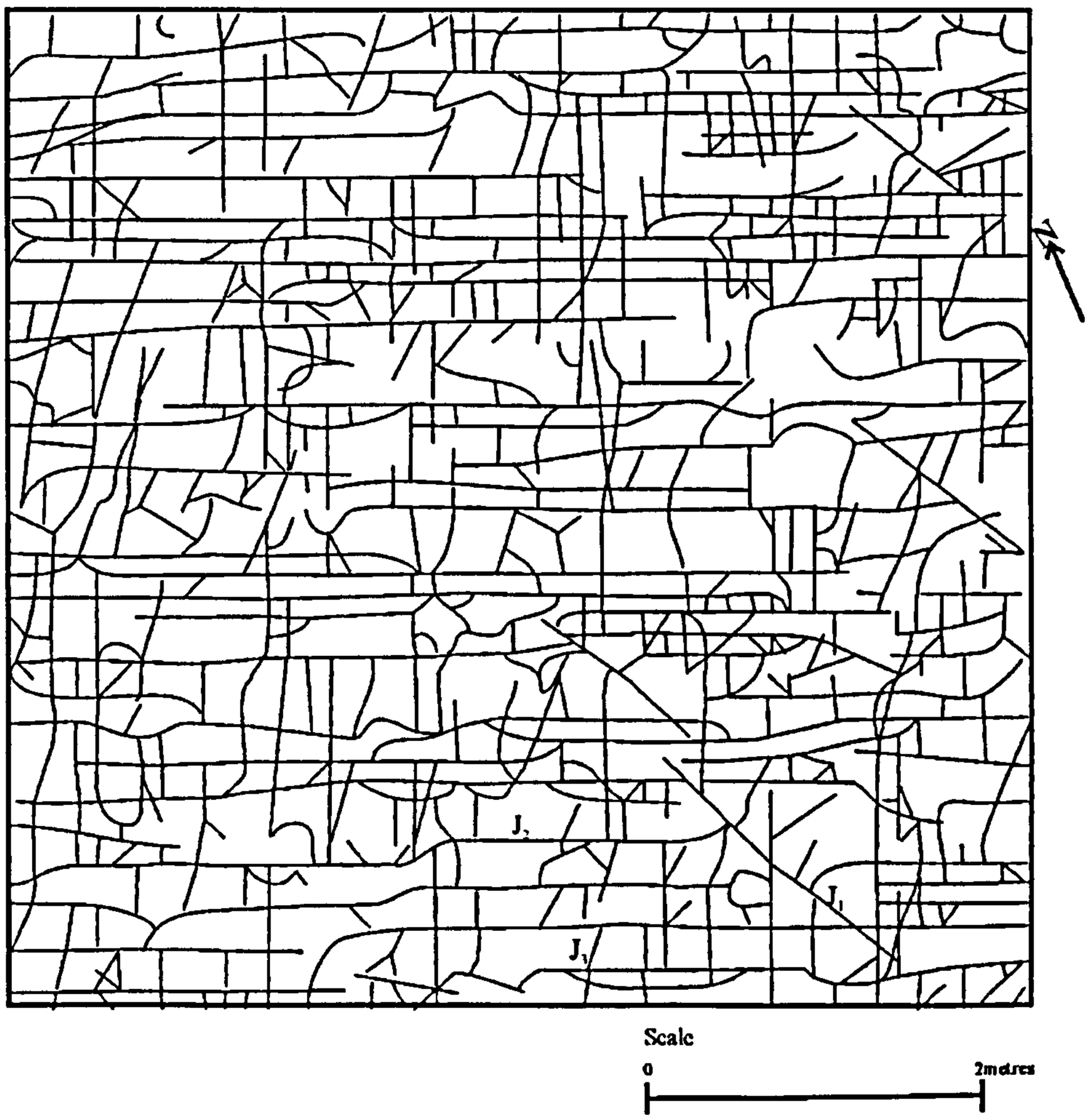


Figure 4.49 Map of joint traces on a 25cm thick limestone bed from East Quantoxhead. Note there are three joint sets labelled in this bed.

being deduced from the way the beds have been dragged against the fault. Because of the lack of marker beds, the amount of displacement along the fault cannot be determined. From crosscutting and abutting relationships, it can be shown that the chronology of joints in most of these beds records an anticlockwise sense of rotation of the stress field. In the 10cm thick limestone bed the same joint set systematically changes strike from 100° to 040° along the scan-line as the NW-SE striking dextral strike-slip fault is approached. However, this is an exception and it seems that the fault did not significantly perturb the stress field during the propagation of Alpine joints. The orientation of joints in the adjacent limestone beds is commonly different. This difference implies that there was a lack of mechanical communication between adjacent competent beds during jointing. As can be seen from Fig. 4.48, the limestone beds show totally different fracture patterns.

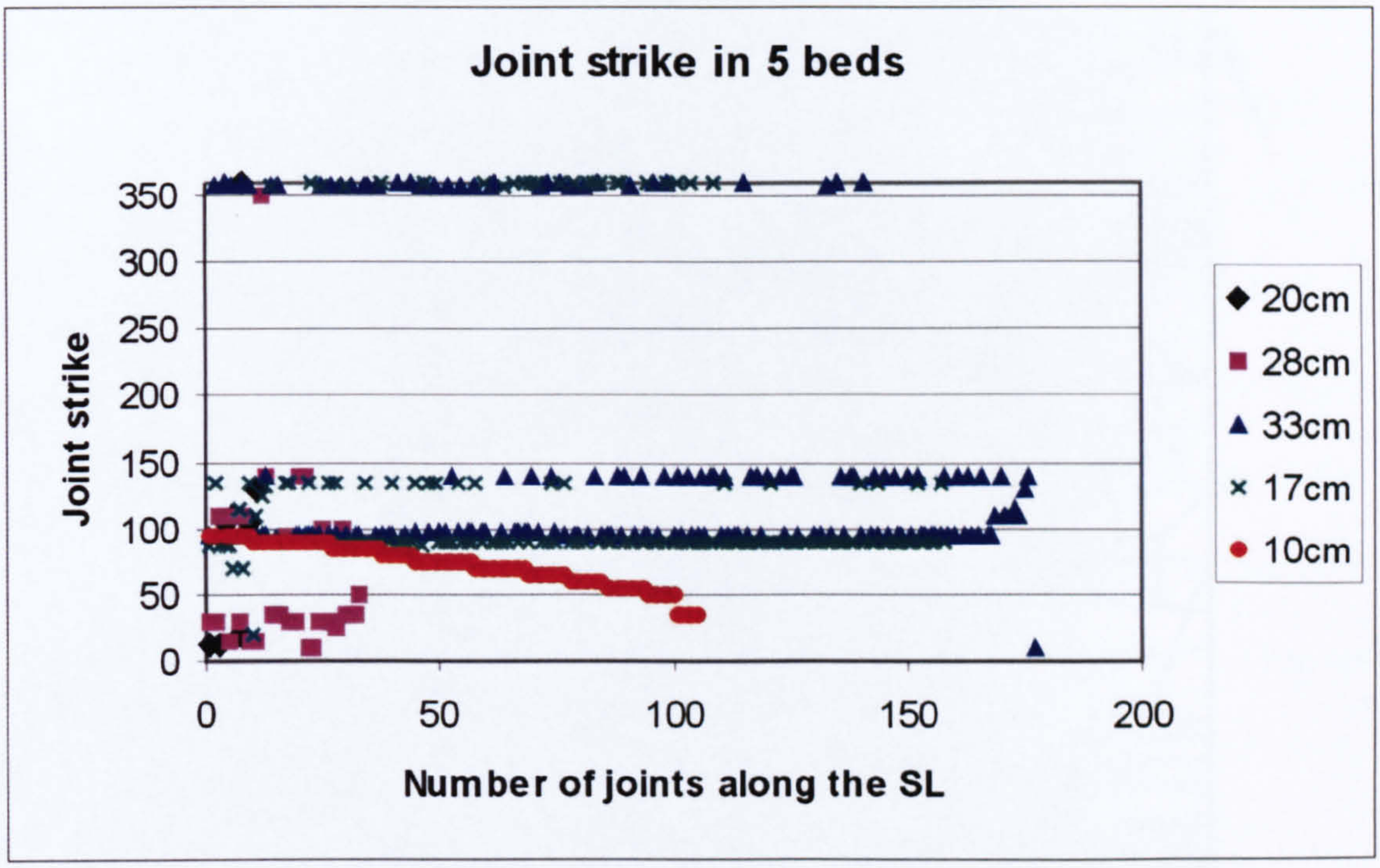


Figure 4.48 *Strike of joints versus number of joints along the scan line on 5 limestone beds in the vicinity of the NW-SE striking fault at Kilve Beach. The numbers on the right show bed thickness.*

Approximately 50m north of the previous area of observation, a 33cm thick limestone bed occurs containing two sets of Alpine joints: the first joint set (J_1) and the second set (J_2) striking 160° and 110° respectively (Figs. 4.50a and b). These joints have been displaced by a NE-SW striking wrench fault. The fault is made up of an array of N-S extensional veins linked by NE-SW striking unfilled fractures. The N-S Alpine compression created linkage between extensional joints by oblique fractures and the formation of dilational jogs. Although the oblique fractures did not dilate, fluids were channelled through them and left a lining of calcite along the joint walls. The reason why the Alpine joints did not dilate can be explained reasonably well. Delaney *et al.* (1986) analysed the orientation of Tertiary mafic dykes intruding sedimentary rocks in the Colorado Plateau. They argued that magma can invade older joints if the magma pressure exceeds the normal stress acting on the fracture wall. The WNW-ESE to E-W striking Alpine joints strike at a high angle to the maximum remote horizontal compression and remained closed, whereas those that strike sub-parallel to the remote stress dilated. By comparing the joint density on both sides of the strike-slip fault and the displacement of the joints by the fault, it can be argued that the joints predated the faulting. East Quantoxhead and west of Blue Ben, pressure solution cleavages strike 060°, 320° and the majority are E-W postdating the joints. These structures provide further evidence that the remote compression was constantly oriented approximately in N-S direction. Window samples in the rectangular windows shown in Figs. 4.51(a, and b) east and west of the fault contain total joint lengths of 87.27m and 86.7m respectively. The average joint density on both sides of the fault is $4.8m^{-1}$.

Below this bed is another 32cm thick limestone bed separated from it by an 80cm thick shale. The first joint set (J_1) in this bed strike 155°, the second joint se (J_2) strike

120° and the J_3 joints strike 65° (where J_1 is older than J_2 which is older than J_3). This pattern indicates an anticlockwise sense of stress rotation. The average joint density for the window shown in Fig. 4.51(c) (3.69m^{-1}) is very low compared to that in the overlying limestone bed. There are two veins with a strike of 020° filled with coarse-grained calcite cutting across the entire limestone and shale section in the exposure. The chronology of joints in the two beds is the same, but the joint density is different, even though the two limestone beds have approximately the same thickness. This implies that the number of joints and network properties, such as joint density, is more strongly dependent on the mechanical properties of the rock than the bed thickness.

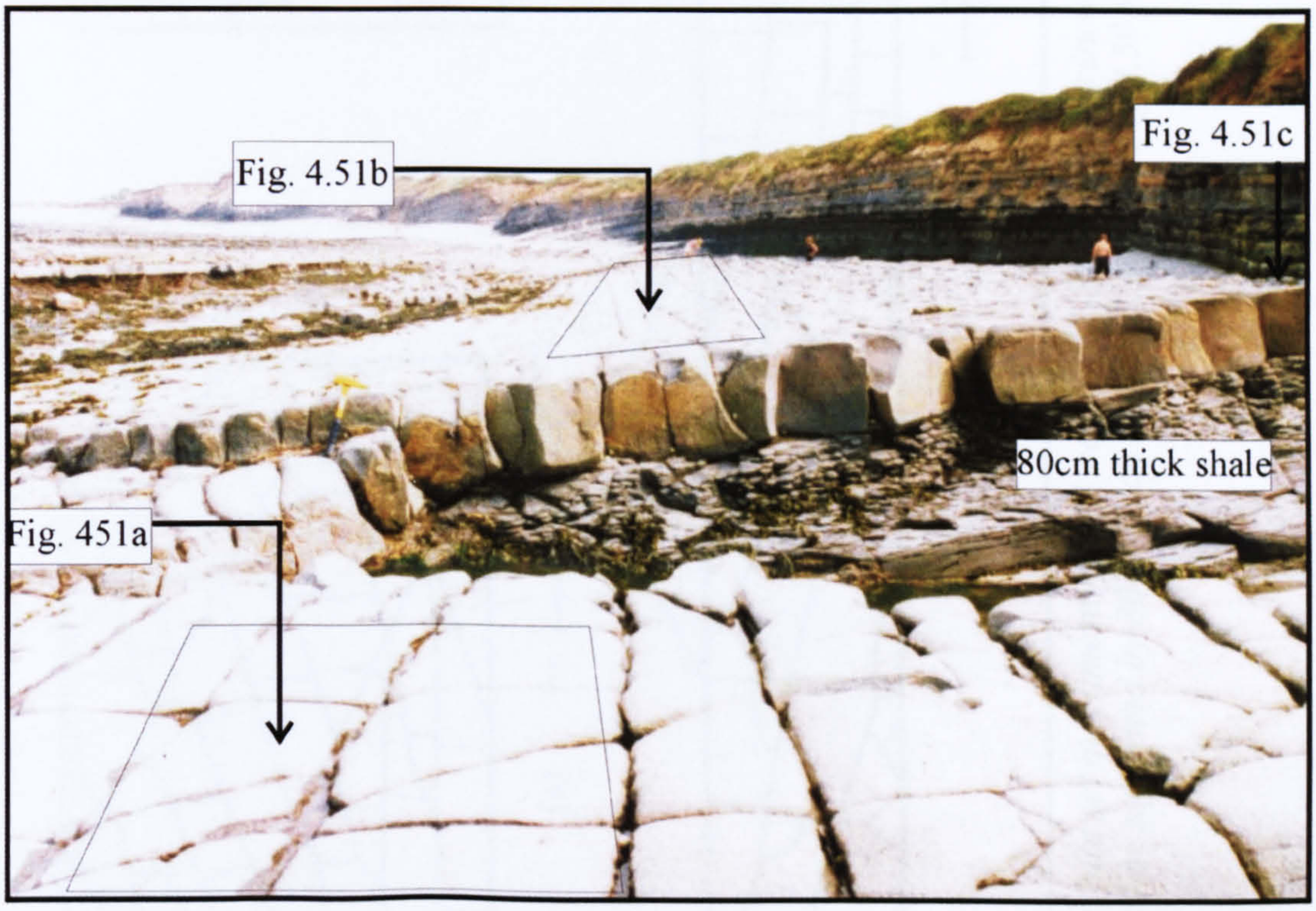


Figure 4.50 *The second joint set (J_2) strikes 110° in 33cm thick limestone bed dipping gently towards NNW at East Quantoxhead. View looking towards ESE. Note the fault displaces the joints. Hammer to the left of centre for scale.*

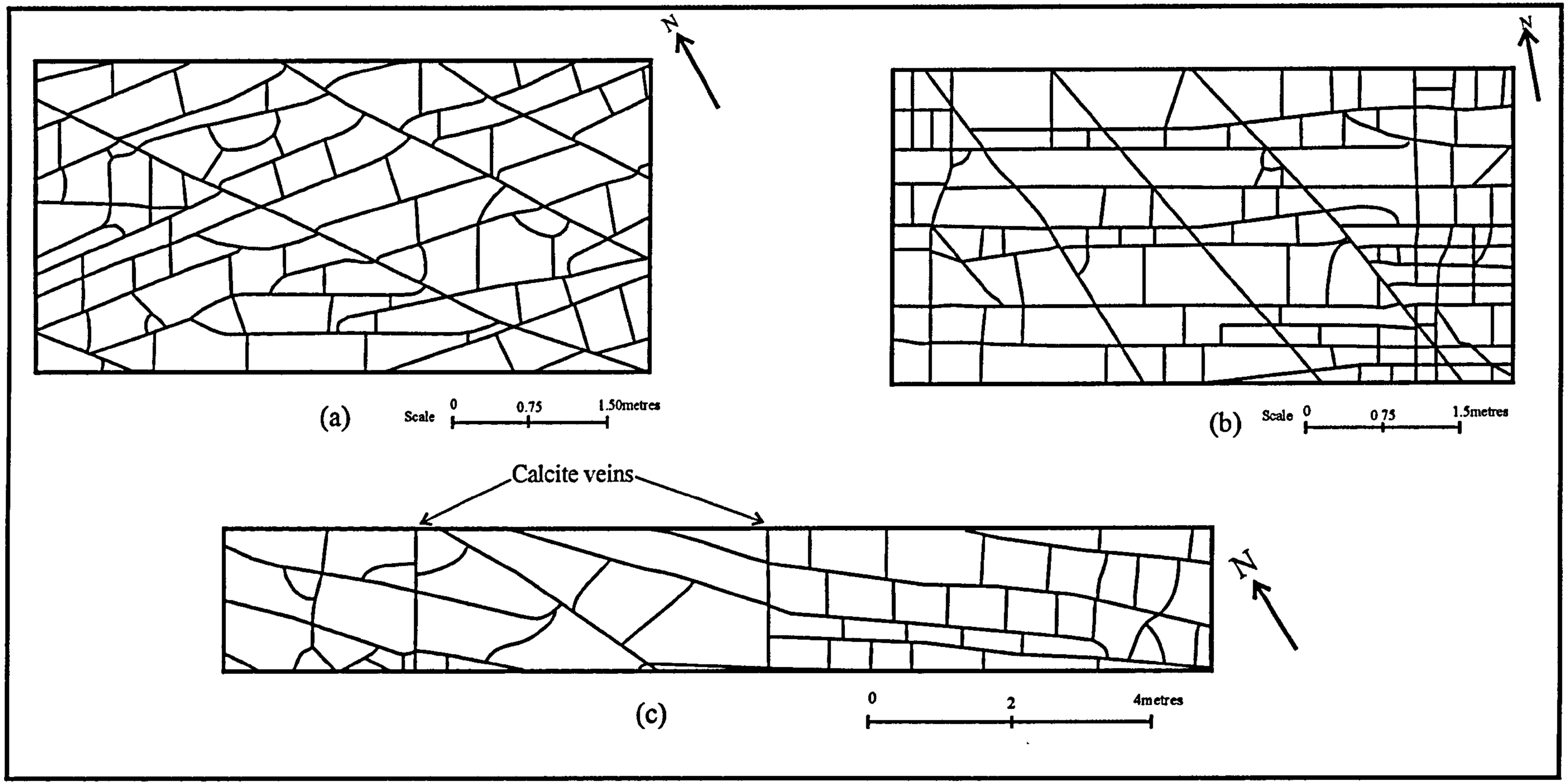


Figure 4.51 *(a) Three joint set in a limestone bed west of NE-SW striking wrench fault, (b) joints east of the fault and (c) joints below the above limestone separated by 80cm thick shale bed. Refer to Fig 4.50 for their location and text for explanation.*

The last window sample measured on the southern margin of the Bristol Channel Basin was located on a 25cm limestone bed dipping 05° to the north, west of the Blue Ben fault (grid reference 120439) (Fig. 4.52). The earliest Alpine joints (J_1) strike 090°. The second joint set (J_2) are non-crosscutting joints normal to the first set with which they form a ladder pattern. Other structures in the area include intense fracturing associated with veining in places leading to formation of breccia textures. Pressure solution seams strike between 060° and 090°. The total length of joints within the window is 320.87m and an average joint density of $3.21m^{-1}$.

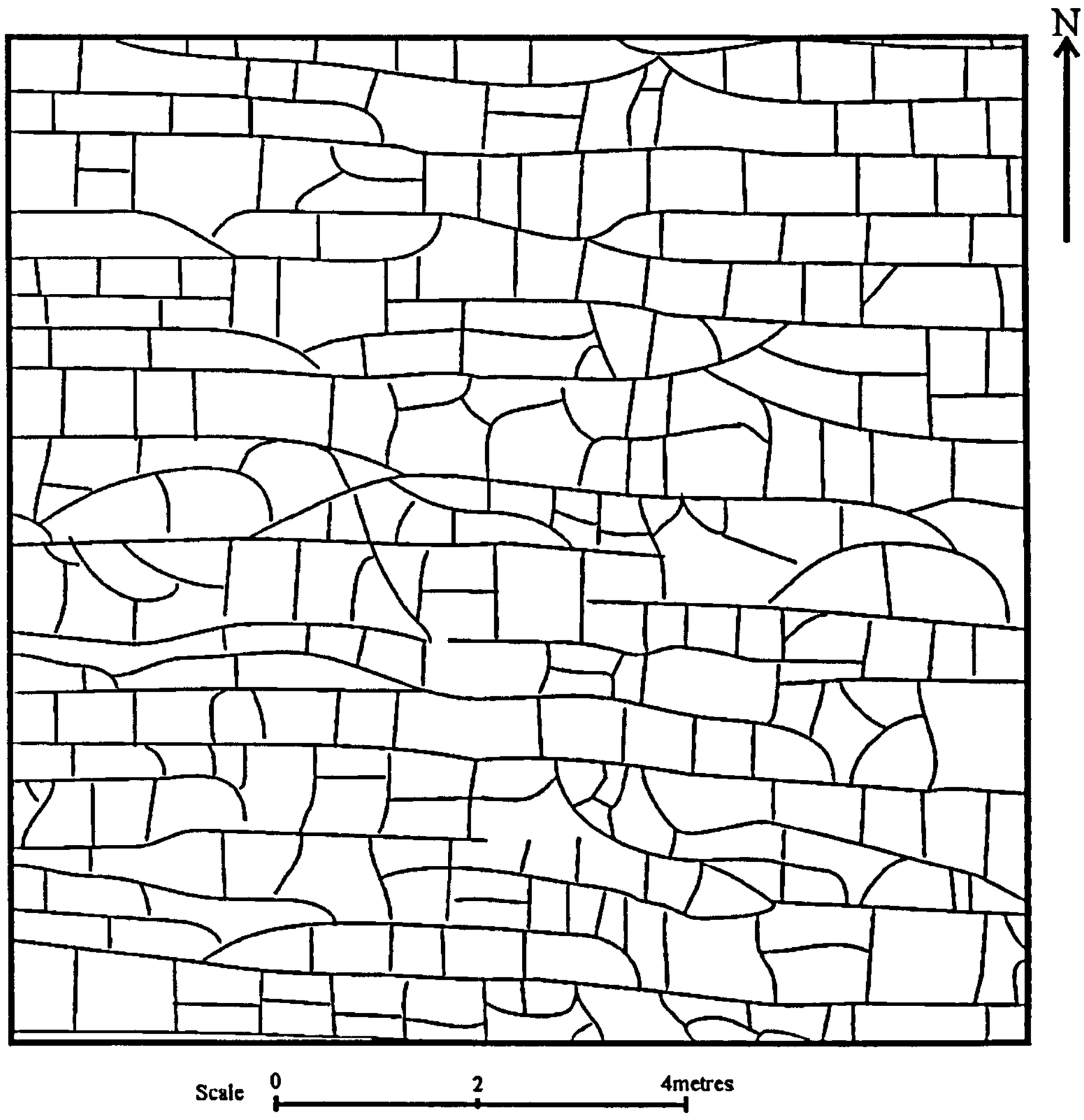


***Figure 4.52** Joint traces on a 25cm thick limestone west of Blue Ben fault. Early joints strike E-W and non-crosscutting joints form between them to form a ladder pattern.*

4.5 Post-Alpine joints

Post Alpine, exhumation joints are the most abundant of all structures in Somerset. They are short unmineralised fractures with wide apertures compared to the Alpine joints. Their orientation and length are highly variable and depend on the orientation and spacing of the pre-existing joints. Post-Alpine joints are sometimes difficult to differentiate from non-systematic fractures of unknown age. Mostly they abut the pre-existing joints to form a variety of reticular patterns on the bedding planes. Non-crosscutting joints, referred to here as uplift joints, probably formed by one or a combination of the following mechanisms:

(i) Strain relaxation: Based on the bending of a PVC plate coated by brittle varnish, Rives and Petit (1990) and Rives *et al.* (1994) proposed that joints form normal to the extension direction. Unloading the plates induces strain relaxation whereby the layers eventually return to the initial form. In so doing, tension in the direction normal to the earlier systematic fractures is produced. They argue that such a visco-elastic strain relaxation effect could be invoked where adjacent layers of contrasting mechanical properties such as alternating limestone and shale beds occur. Branches perpendicular to the primary fractures may also develop due to local stress relaxation at low strain-rates (Wu and Pollard, 1993).

(ii) Cooling: Engelder (1993) points out that uniaxial strain models of cooling during removal of the overburden (due to uplift and erosion) predict that, under elastic conditions, large tensile stresses are produced, sometimes at depths in excess of 1km. Engelder argues that an abrupt cooling of granite in which ΔT involves a change from initial T_o to T_s, with a Young's Modulus E = 100GPa, a Poisson's ratio $\nu = 0.25$ and a coefficient of thermal expansion $\alpha_T = 7 \times 10^{-6}\ C^{-1}$ will reduce the horizontal stress σ_h by 93MPa. This temperature drop causes tensile stresses by

reducing σ_h. If the tensile stresses are enough to overcome the confining stress and the tensile strength of the rocks, then the conditions will favour the propagation of tensile cracks. The effect of temperature changes on the reference state is beyond the scope of this work and the reader is referred to Engelder (1993) and references therein. Similarly, when alternating limestone and shale beds in the Bristol Channel were brought to the surface from a depth of about 1km, they cooled. If the temperature drop was enough to generate tensile stress sufficient to overcome the strength of the rock, tensile fractures would have been generated.

(iii) Effect of earlier joints: An initial set of parallel open joints may cut a layer into very long and narrow bands that are very sensitive to bending or warping (Rives *et al.*, 1994). Any warping of the bands by inhomogeneous settling of the overburden could introduce stress and lead to the formation of non-crosscutting joints.

(iv) Effect of joint formation: Reversals of the stress field involving a 90° switch can be caused by regional fluctuations of the far-field stresses (Hancock, 1994). This may have been the case during inversion of the Bristol Channel Basin. Such fluctuations could also occur during relaxation of rocks caused by uplift and erosion as release of locked-in stresses are relieved (Freidman, 1972).

Based on field observations and numerical analysis using a Poly3D numerical code, Bai *et al.* (2002) demonstrated that in a triaxial stress system in which the maximum and intermediate remote stresses are horizontal and the least principal stress is vertical (under the sign convention of positive for tensile stresses) the maximum principal stress is first perpendicular to, and then changes to become parallel to the strike of systematic fractures. They noted that as the ratio of the two horizontal stresses exceeds the threshold value of approximately 0.2, and the ratio of fracture spacing to

the height of the fractures changes from greater than to less than the critical value (discussed in section 3.5.1), then the fracturing process changes from infilling to the formation of orthogonal non-crosscutting joints. This does not require a 90° rotation of the remote stress field, and they argued that this provides an alternative mechanism for the formation of orthogonal joints. This model fails to explain circumstances in which abundant non-crosscutting fractures are observed in outcrops where the value of the fracture spacing to thickness ratio does not attain the critical condition of saturation.

4.6 Statistical analysis of joint spacing within the two study areas

In this chapter, joint patterns and their variation in the vicinity of various folds and fault structures at various locations on the Bristol Channel coastline and in the Pennines, North Yorkshire, have been described. In this section these joints are analysed using standard statistical curves described in section 3.3.

As discussed in section 3.3, joint spacing generally evolves from an initially negative exponential distribution through log-normal and normal distributions with increasing joint development and/or degree of deformation (Rives *et al.*, 1992). In this section patterns of joint spacing in the two field areas will be analysed by comparing the field data with standard statistical curves to determine whether they follow the evolution described above. This should reveal whether or not the spacing is controlled by random process. The evolution of joint spacing remains a subject of active debate. The same data can often be matched to a both a negative exponential and a log-normal distribution with the same degree of correlation. A normal distribution is taken by Rives *et al.* (1992) to characterise an advanced stage of joint development indicative

of a saturated state. Wu and Pollard (1995) also considers the condition of saturation and point out that joint spacing remains nearly constant once this stage has been reached. Bai and Pollard (2000b) presented an analysis that predicts the ratio of joint spacing to fractured layer thickness approaches one at saturation under conditions of pure tension unless fracturing is being driven by a hydraulic mechanism. In a companion paper (Bai and Pollard, 2000a) used finite element analysis to demonstrate that if there are flaws in the medium, fractures can propagate and further infilling is possible.

4.6.1 Analysis of joint spacing in the Pennines area

The joints in the Pennine study area are developed in massive to well-bedded limestone beds and, as a result, are through-going joints. The joint spacing in the Pennines fits statistical distributions. 90% of the data fits either to a negative exponential (Fig. 4.53) or a log-normal distribution (Fig. 4.54). Only one data set shows quasi-normal distribution and this is probably because of the superposition of younger sets of joints.

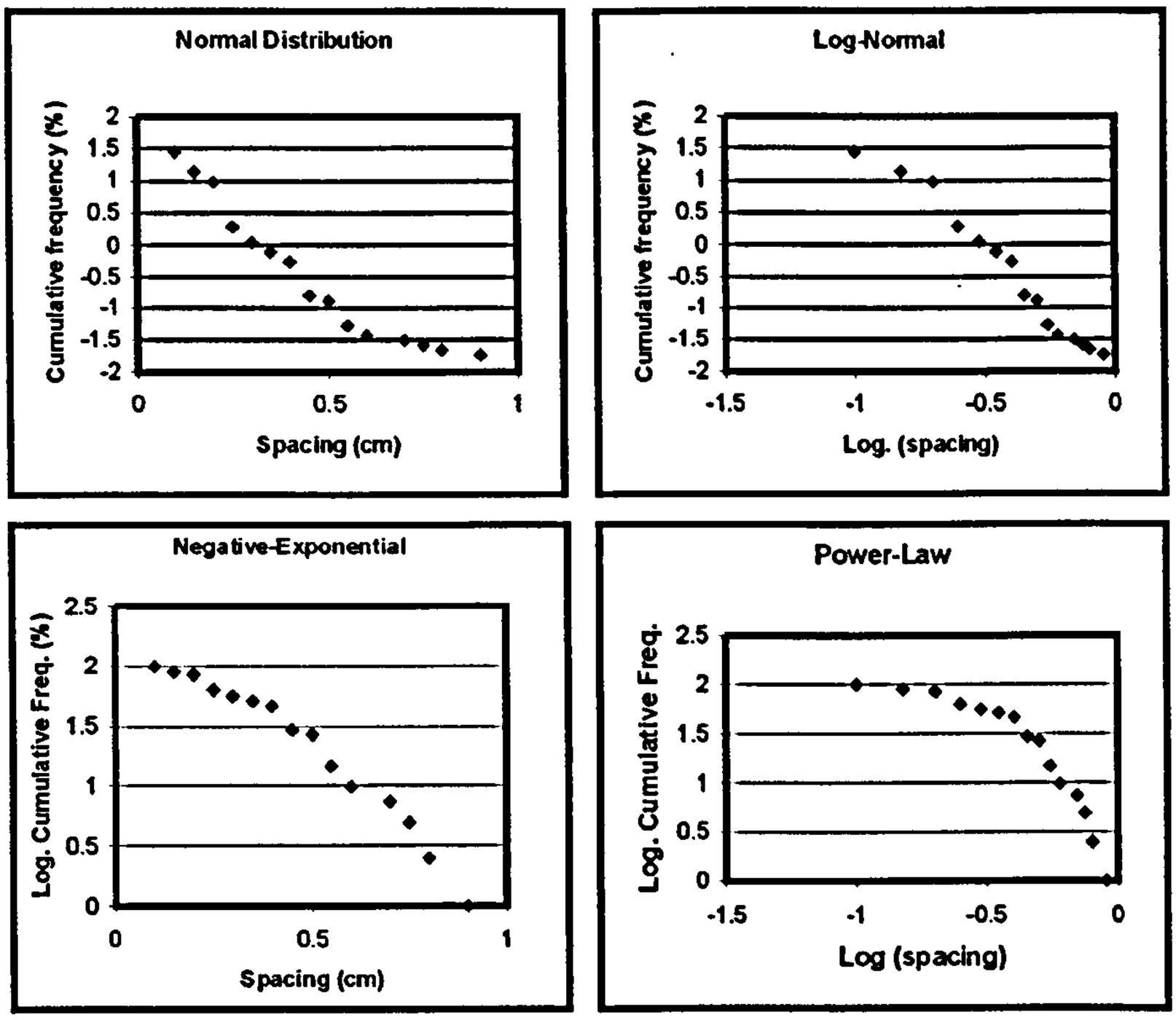


Figure 4.53 Joint spacing from the Gordale Limestone at Langcliffe that best fits a negative exponential distribution.

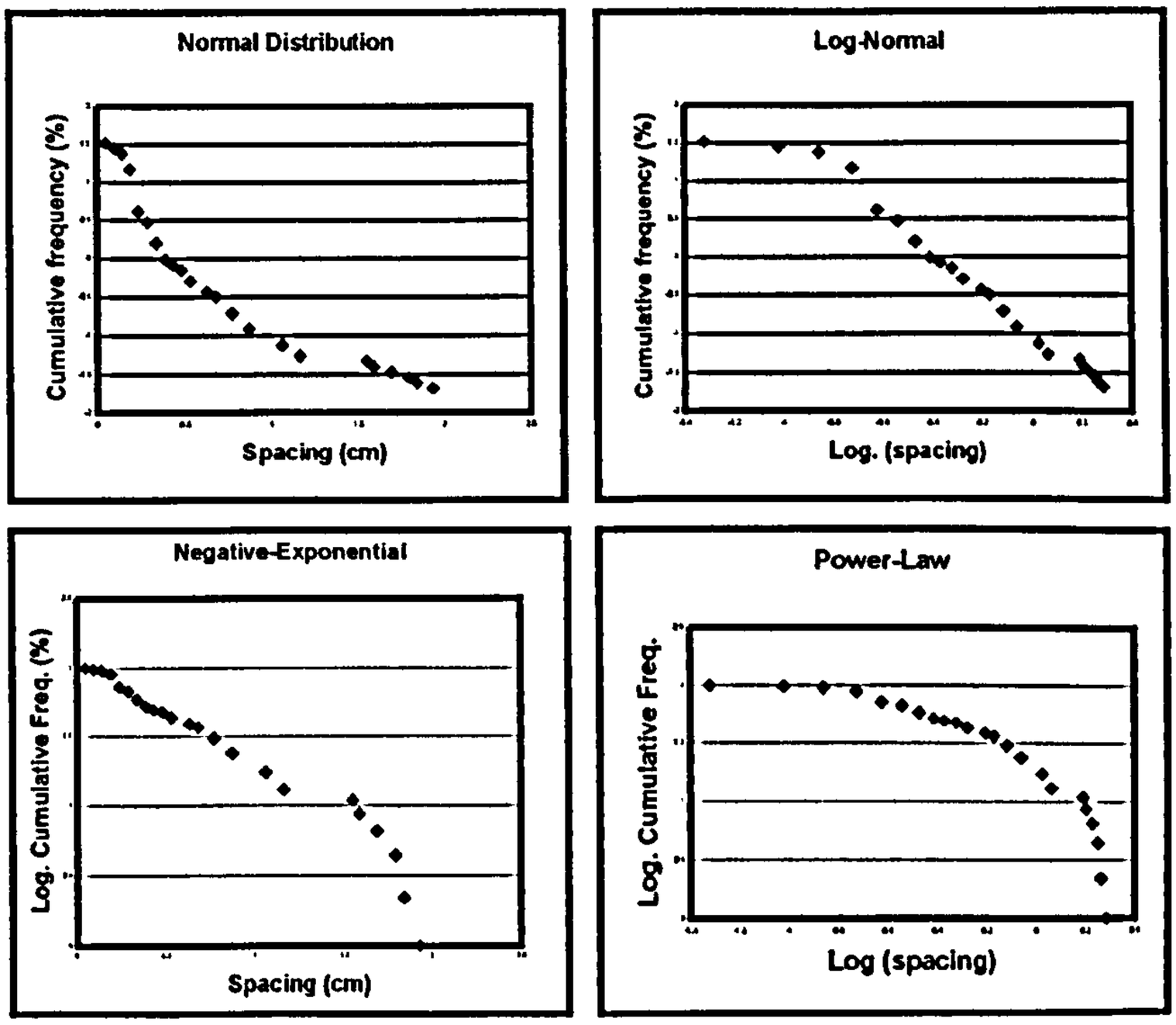


Figure 4.54 Joint spacing showing a best-fit to a log-normal distribution.

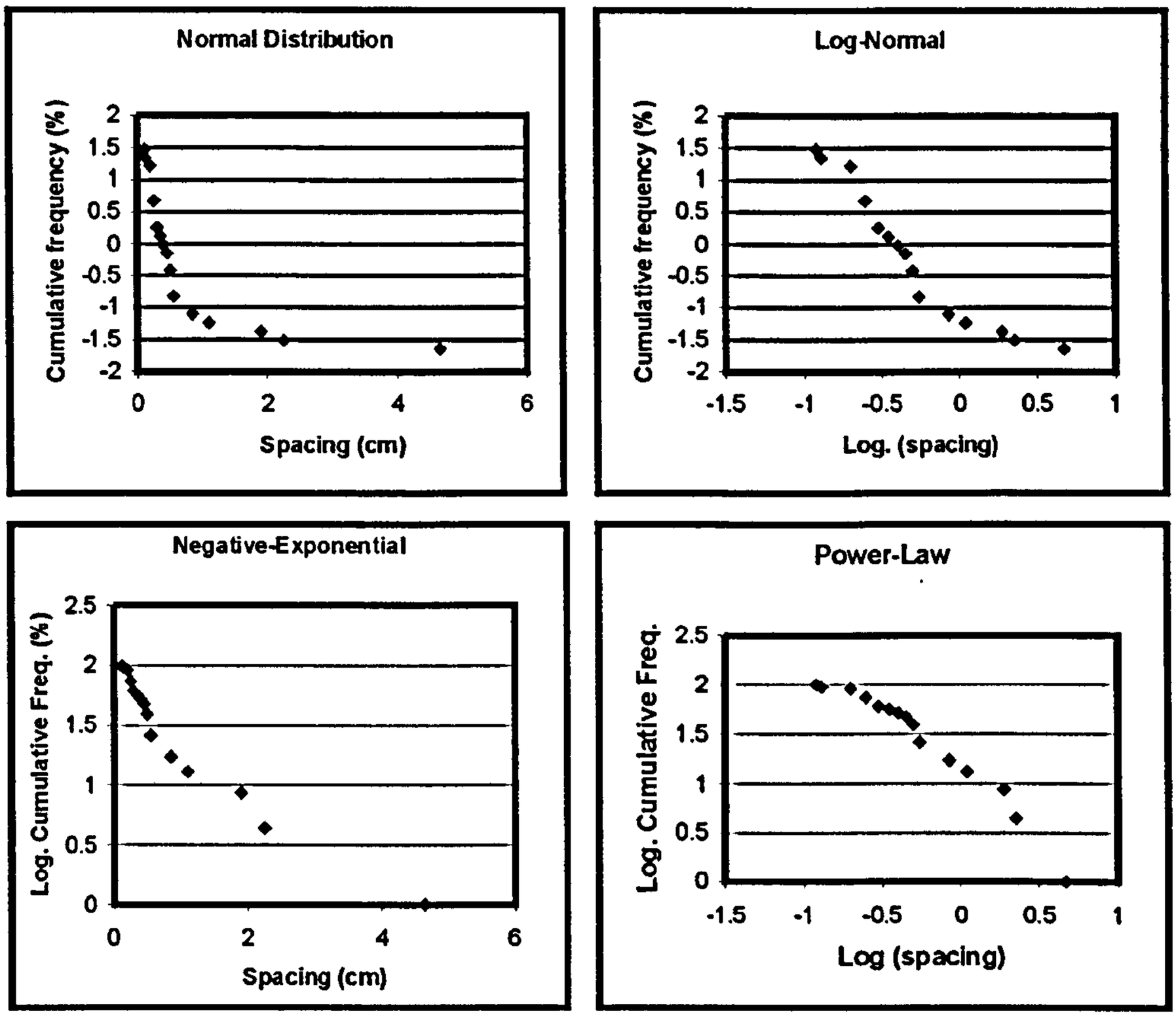


***Figure 4.55** Joint spacing from Malham Cove showing a best fit to a power-law distribution.*

4.6.2 Results of the analysis of joint spacing from the Bristol Channel

The spacing of veins (*i.e.* the earliest formed joints) on the southern margin of the Bristol Channel Basin has not been analysed because of their very limited occurrence in the study areas *i.e.* in the vicinity of faults and on the outer arcs of rollover folds. Alpine joints in the studied beds generally show a negative exponential distribution (Fig. 4.56). Some of the E-W striking joint sets show exponential spacing distribution (slightly bimodal), which is suggested by the writer to be a result of their superposition onto burial (syn-sedimentary) joints with a similar orientation (*e.g.* E-W striking joints in the second bed at Lilstock described in section 4.4.3.2 and Fig. 4.31).

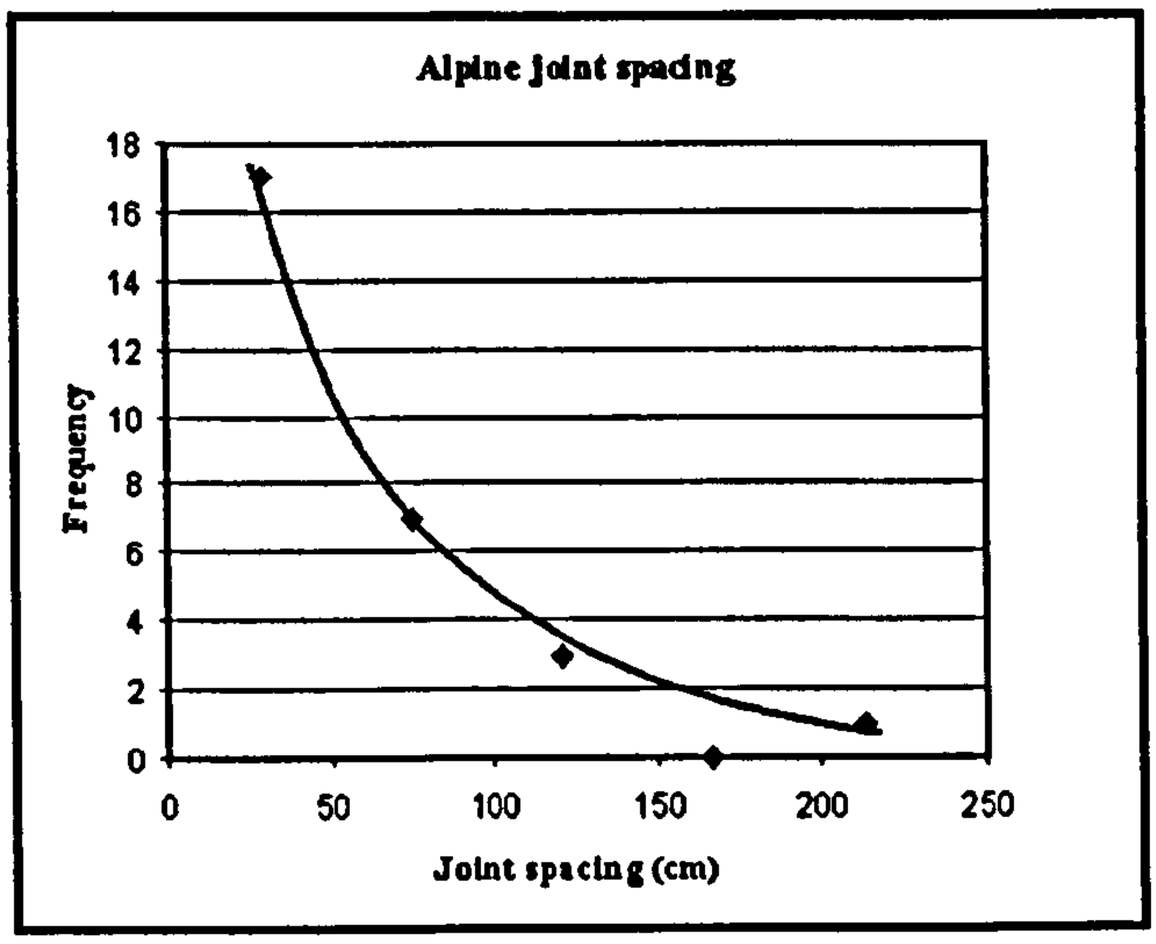


Figure 4.56 Alpine joint spacing at Lilstock (i.e. joint set 2 in bed 2) showing a negative exponential distribution.

Exhumation (post-Alpine) joints are the most common of all geological structures on the southern margin of the Bristol Channel and their spacing best fits a log-normal distribution (Fig. 4.57).

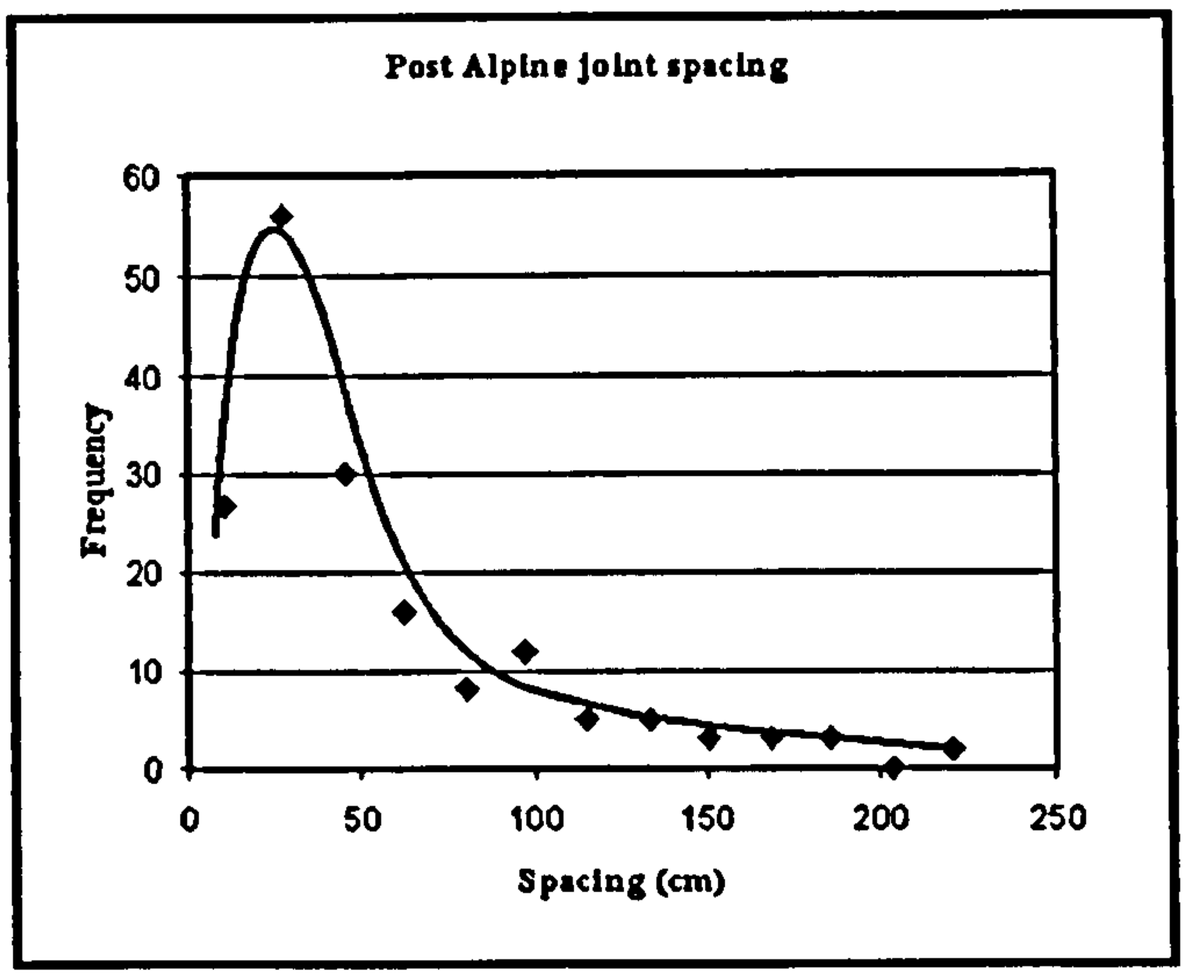


Figure 4.57 Graph of the spacing of the post-Alpine joints at Lilstock, which shows a log-normal distribution.

4.7 Summary

In the Pennines, the NE-SW to NNE-SSW and NW-SE joints form a conjugate set generated by σ_H that lay in the ESE-WNW direction. The variation in the acute angle from 60° to 90° is probably related to the differences in the mechanical properties of the rocks (N.B. $\theta = 45 - \Phi/2$ where $\Phi = \tan^{-1}\mu$ and μ is coefficient of sliding friction). In a few examples the angle 2θ exceeds 90° *i.e.* the theoretically predicted maximum value. It is suggested that this probably relates to shortening by pressure solution, as suggested by Ramsay and Huber (1987). Pressure solution also occurred in the Pennines, in response to a vertical maximum compression that was operating during burial and diagenesis. The pressure solution produced stylolites along the bedding planes. Bedding in both the Cove and Gordale limestones is defined by stylolites that increased the resistance to shear along the bedding and prevented slip. This, coupled with a large overburden stress, promoted the propagation of through-going joints in the Pennines. Although the development of stylolites along the bedding destroys some porosity, Hudson and Harrison (1997) note that permeability along a stylolite surface is slightly higher than through adjacent intact rocks.

The joints in the area were formed at a greater depth than those in the Bristol Channel area. The presence of mechanically identical competent layers, the absence of intervening shale beds between competent carbonate beds, and the definition of bedding by stylolitic surfaces promoted the through-going propagation of joints in the Pennines.

The main joints in the North Yorkshire study area strike NW-SE to NNW-SSE and NE-SW to ENE-WSW. Joints trending N-S and E-W occur, but are rare. Early

investigations in the region (Doughty, 1968), suggest that the two major joint sets form a conjugate pair that formed as a result of Varsican deformation during the Upper Carboniferous. The orientation of the Variscan stress field is highly variable, as can be seen in Fig. 2.2, which shows conditions in the Craven Basin south of the study area. The variation in stress field in the Craven Basin is mainly caused by the position of the granite-cored Askrigg and Alston Blocks to the north. The stress field deduced for the folds formed during Variscan contraction in the Craven Basin and for the conjugate fractures in the southern margin of the Askrigg Block are compatible.

The majority of the patterns of joint spacing measured in the Pennines fit best to either an exponential or log-normal distribution (Figs. 4.56 and 4.57). These two different distributions within the same rock type represent two different stages in evolution of a rock saturated with joint from an un-jointed state. The occurrence of these different stages may be the result of variation in the degree of deformation, either because of minor differences in stress levels and/or differences in rock properties. Some joints (<10%) show a power-law distribution of spacing and, because such a distribution is scale independent, it is possible to predict how the pattern will appear at different scales.

The study of joint density using windows of various shape and size gives an insight into the minimum size and shape of window required to obtain a measurement of '*average joint density*' that will be reasonably close to the mean. As the window size decreases, the frequency of joints becomes less predictable and may vary from a large number to zero. As the window area is increased, this fluctuation decreases, becoming more and more representative of the population as a whole (Figs. 4.13, 4.14b and

4.16). This fluctuation vanishes when the window size is sufficiently large.

Joint density can be used to examine the variation in fracture length relative to window size and shape in an area of interest, but it is not influenced by the organisation of the fractures and therefore tells me little about the connectivity which has a dramatic effect on fluid flow. This study demonstrates that fracture density is very sensitive to window size and shape. The advantage of using circular windows is that bias in orientation that can occur when using rectangular and square windows is minimised or avoided. The reason why no data on measurements of natural fracture traces made using circular windows have been published is because of the impracticality of using this shape in the field. The sensitivity of joint density values to window size raises questions regarding values of fracture density values obtained from borehole. The sample size is very small compared to the volume of the fractured rock mass and, in addition, where if the majority of fractures are vertical, and borehole is vertical will tend to be missed.

Some examples of the spacing of Alpine joints from the Bristol Channel fit best to a negative exponential distribution. Similar results were obtained by Loosveld and Franssen (1992). In contrast, the majority of joint spacing data for the exhumation joints measured in the Bristol Channel show fit best to a log-normal distribution. If the joint spacing evolves from an initial negative exponential to a normal distribution through a log-normal distribution with increasing degree of deformation (and joint saturation) as suggested by Rives *et al.* (1992), then it can be argued that the exhumation joints are more evolved (*i.e.* closer to saturation) compared to the Alpine joints. This may be explained by the uplift of the whole rock mass during and

following the inversion of the Bristol Channel Basin. These results from both of the areas of study show that the joint spacing fits statistically uni-modal laws. This indicates that a deterministic rather than random process controlled their evolution.

In the Bristol Channel, the majority of the veins strike ESE-WNW and contain calcite fibres growing normal to the joint walls, indicating that opening was consistently in NNE-SSW direction. High density veins (Rawnsley *et al.*, 1998) or micro-veins (Caputo and Hancock, 1999) were probably formed by a cracking and simultaneous sealing process or a crack jump mechanism (Caputo and Hancock, 1999). The presence of an open fracture deflects and suppresses the propagation of a new joint within a certain limited distance on either side of the fracture (*i.e.* the zone of interaction). Stress modifications in the vicinity of a traction-free surface or unsealed crack have been examined using numerical models (*e.g.* Pollard and Segal, 1987; Al-Mahruqi, 2001). Such analysis shows that the local stress within the interaction zone becomes compressive rather than tensile. The perturbed stress around the crack has to be restored before the stress field is appropriate for the opening of another crack close to the first takes place. The simultaneous opening and sealing process proposed by Caputo and Hancock (1999) would allow this to occur. Depending on the relative strength of the host rock and the sealing vein, the next crack will form either within the newly-formed vein by crack sealing mechanism as proposed by Ramsay (1980) or in the adjacent country rock by the crack-jump mechanism of Caputo and Hancock (1999).

The present investigation along the southern margin of the Bristol Channel has resulted in a general three-fold classification of joints in the area, *i.e.* joints formed during:

(1) **Opening of the basin:** Opening of the basin occurred in a NNE-SSW direction. The pore pressures in the sediments were high enough to cause mud volcanoes and, later, the formation of micro-veins. This was followed by linkage of the vertical veins (earlier formed as joints) and the development of the normal faults with associated rollover folds. The normal faults formed by the oblique linkage of extensional joints in the adjacent competent beds. Any movement on the fault produced pull-apart gaps in the limestone into which calcite fibres grew.

(2a) **Inversion of the basin:** Inversion of the basin led to the amplification of the pre-existing rollover folds, reactivation of the normal faults as reverse faults, and the development of fold-related Alpine joints. The joint patterns in different competent beds are different and that a mechanical decoupling of adjacent limestone beds occurred because of the intervening shale or marl horizon.

(2b) **Continued compression:** Continued compression caused the rocks to be displaced by NW-SE striking dextral and NE-SW striking sinistral strike-slip faults. In addition Al-Mahruqi (2001) reported N-S striking right-stepping strike-slip fault offsetting E-W striking joints. The strike-slip faults in the area do not significantly affect the fracture spacing or density of the Alpine joints and this is taken to indicate that the joints predated the faults. In deed, in places, the NE-SW striking sinistral strike-slip faults can be seen displacing the Alpine joints (Fig. 4.50).

(3) **Post-Alpine joints:** are the last structures to form in the study area.

CHAPTER FIVE

FRACTURE MECHANICS AND FRACTOGRAPHY

5.1 Introduction

The regional geological setting of the two studied areas, a review of the factors governing joint spacing, and the results of the scan line and window sampling of joint spacing/density in the two areas have been discussed in Chapters 2, 3 and 4 respectively. Now it is apposite to highlight the principles of fracture mechanics useful to explain the modes of joint propagation and general fractographic features. These surface features are very delicate and because limestones are prone to chemical solution, they are often removed by weathering. If preserved, important information can be obtained concerning joint initiation, the direction of joint propagation and the interaction between the remote and local stresses. The exposed joint surfaces in the Pennines have been subject to attack by acid ground water and glaciokarstic activity that have removed all the surface features. Consequently, the observations described in this chapter relate to joints in the limestone from the Bristol Channel Basin.

In this chapter, features such as plumose structures and twist hackle fringes observed on joint surfaces from the southern margin of the Bristol Channel are described and analysed. The results are used to challenge the generally accepted model of an anticlockwise rotation of the stress field (see *e.g.* Rawnsley *et al.*, 1998).

'Discontinuity' is the general term used to describe a break of continuity in a mass of rock. These breaks occur on all scales from the microscopic to the regional. They begin to form in a rock mass as soon as it is capable of brittle failure, whether near surface or

deeply buried. These processes take place in all types of igneous, sedimentary and metamorphic rocks. As a result of early lithification, limestone beds are particularly susceptible to brittle deformation by fracturing which can continue throughout their history. Joints initiate from flaws in the rock. These are sites where geochemical, thermal and mechanical processes all tend to be active during the geological evolution of a rock (Gabrielsen, 1990). From an economic point of view, joints are often important sites of mineralization and serve as pathways which allow the local build-up of hydrocarbons and the deposition of mineral lodes. Accurate data on the density of joints and their connectivity is essential for engineering and mining projects because poor understanding of fracture networks in rocks can lead to financial losses and social risks. From an engineering and geotechnical point of view, it is important to know how different fractures and fracture sets affect the rock properties. The initial properties of a coherent block of rock are very different to those of a fractured rock mass. For example fractures may act as hydraulic conductors or as barriers to fluid flow through a rock and can also cause a dramatic reduction in rock strength. Despite the ubiquity of fractures, their economic importance and the fact that they are one of the most studied of all geological structures in the earth's crust (*e.g.* Price, 1966; Bahat, 1991), fracture analysis remains one of the most difficult tasks facing structural geologists.

There are two principal approaches to joint description. The first is fractography which deals with the surface morphology of individual joints. The second approach deals with generalised attributes such as dominant orientation and styles and takes into account large populations of joints throughout a region (Hancock, 1994). In the latter approach, joints are described quantitatively by defining their spacing, length, orientation and distribution,

continuity or extent, thickness of the fractured layer (height of the joint), nature of any infill, aperture, roughness and the age relationship between different sets in the network. The history of displacement across a joint may be difficult to determine because of the small amount of movement involved, the lack of kinematic indicators such as slickensides on the fracture surface, and the infilling of joints by dykes or veins.

There is no simple and universally accepted definition of a joint. Some define joints as those "*fractures with field evidence for dominantly opening displacements*" (Pollard and Aydin, 1988). This definition implies that joints are the result of extensional failure. Others define joints in terms of "*a surface along which there has been no appreciable displacement*" regardless of the mode of origin of the fracture (Price, 1966; Blés and Feuga, 1986; Hancock, 1994). Most workers accept that joints are fractures across or along which very little displacement has occurred and Pollard and Aydin (1988) point out that even if a joint closes after formation, the existence of the two surfaces demonstrates that some displacement remains. Faults are defined as shear failure planes in which the two surfaces are displaced relative to each other along a direction parallel to that plane. Pollard and Segall (1987) argued that joints and faults are mechanically different because they have unique stress, strain and displacement fields.

From the point of view of fracture mechanics, joints have been related to the three modes of failure (Lawn, 1975) (Fig. 5.1a, b, c), namely extensional or mode I fractures, and shear fractures of modes II and III. A crack may propagate by any one of these modes of surface displacement:

Mode I (opening mode): In this mode the crack tip is subjected to a normal stress (σ_n) and the crack faces separate at the crack front so that the displacement of the crack surfaces is perpendicular to the crack plane (Fig. 5.1a). Pure mode I loading produces the maximum propagation energy for an increment of crack growth oriented in the plane of the joint leading to 'in-plane propagation'. A joint oriented normal to σ_3 satisfies this condition. If the principal stress direction remains the same throughout the extent of the joint plane, in-plane propagation will produce a planar crack.

Mode II (*sliding or in-plane-shear*): This mode of failure occurs when the crack tip is subjected to an *in-plane-shear* stress (τ) and the crack faces slide past one another so that the displacement of the crack faces lies in the crack plane and is perpendicular to the crack front (Fig. 5.1b).

Mode III (tearing or *out-of-plane shear cracks*): In this mode of failure the crack tip is subjected to an *out-of-plane-shear* stress (τ). The crack faces move relative to one another so that the displacement and the crack front are parallel. This mode of crack displacement is not very common in rocks (Fig. 5.1c).

Mixed mode failure involves a combination of any of the above three modes of crack displacement. Joints formed by mixed mode propagation lead to displacements in both tensile mode and by shear failure (Fig. 5.2). If the principal stress direction changes as the joint propagates, shear stresses are generated at the joint tip. The shear stress generated in mixed mode failure can be resolved in two orientations (*i.e.* in-plane and out-of-plane)

and this will then correspond to either mixed modes I + II or I + III loading. In both cases the preferred joint propagation path is out-of-plane and tends to be oriented perpendicular to the local maximum tensile stress thereby reducing the resolved shear.

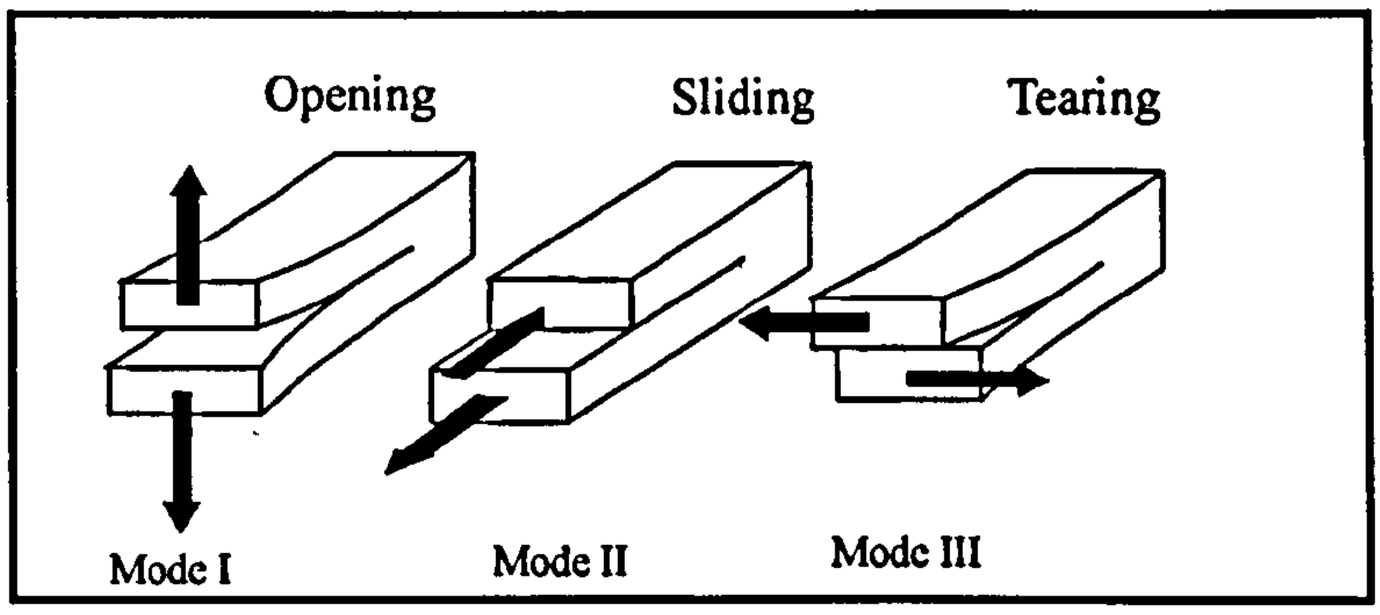


***Figure 5.1** The three modes of crack displacement (after Lawn, 1975). Note that the arrow indicates the direction of displacement of the blocks.*

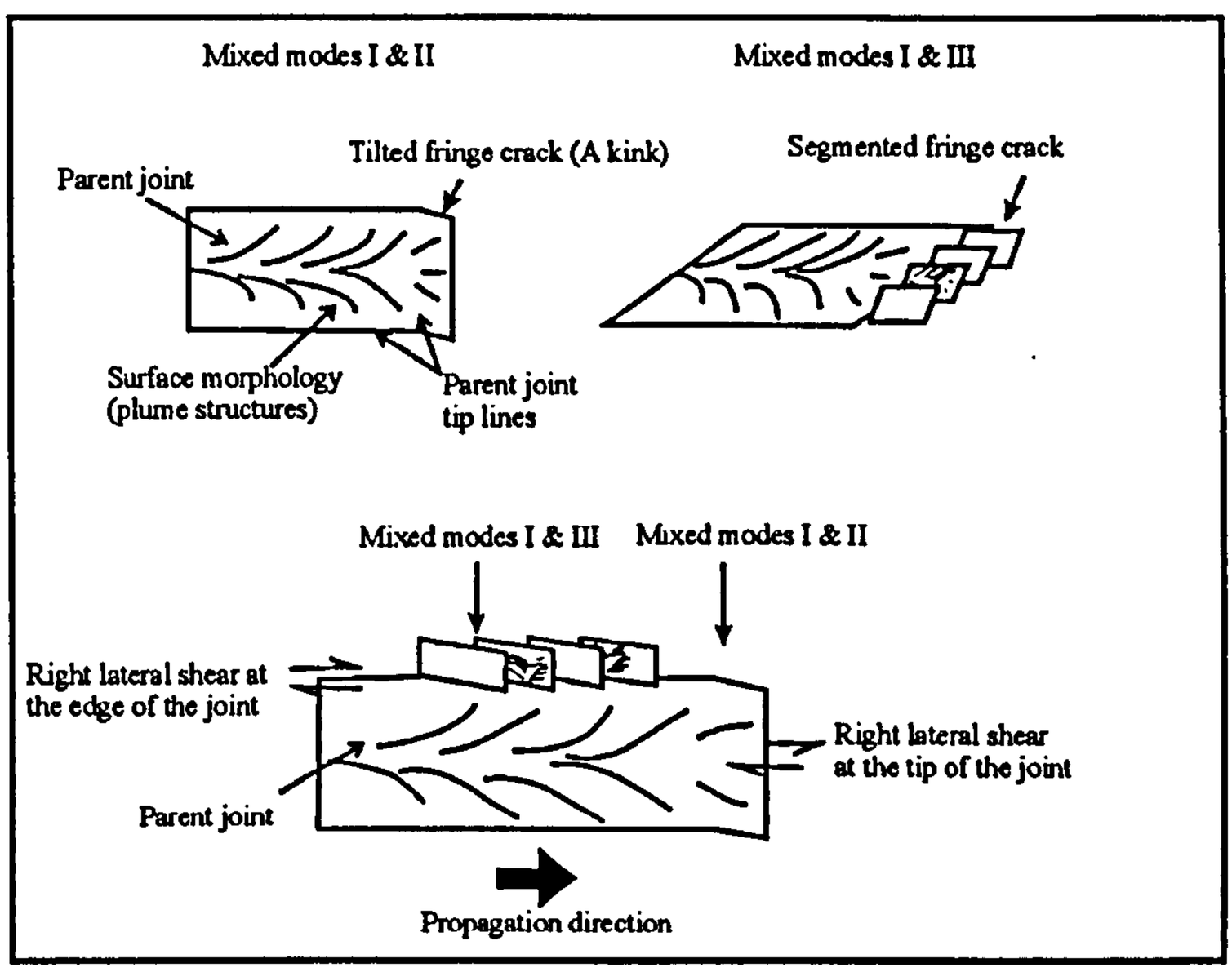


***Figure 5.2** Joint propagation in mixed-mode loading (from Younes and Engelder, 1999).*

5.2 Fracture mechanics

The fundamentals of fracture mechanics as applied to fractography are briefly reviewed in this section. The discipline of fracture mechanics is broad and can be applied to brittle fracture of all materials. Several research groups around the world are engaged in the application of fracture mechanics principles to rock engineering problems. In the following sections, some geological examples of crack initiation and propagation will be considered. Even prior to the initiation of joints, rock is a discontinuous medium at both small and large scales because it contains pores, micro-cracks and bedding planes. Engelder (1993) points out that the initiation of a joint requires some heterogeneity such as a void, micro-crack, fossil or some other inclusion within a rock, the presence of which modifies the stress distribution within the rock. The presence of joints fundamentally changes the properties of rocks, making them anisotropic, discontinuous and inhomogeneous. The problems of fracture initiation and propagation are now considered.

5.2.1 Fracture initiation

Kirsch (1898) devised an equation relating stress concentration about a circular hole in a uniformly stressed plate to the imposed stress. He found that the concentration or magnification of the stress ($-S_t$) around a circular hole was three times the remote or far-field applied stress ($-S_h$). Inglis (1913) and Griffith (1921) extended the concept (Fig. 5.3) and demonstrated that the stress concentration about an elliptical crack is related to the remote stress as follows:

$$-S_t = -S_h\,(1+2c/b) \qquad (5.1)$$

where c and b are the major and minor axes of the ellipse. Engelder (1993) explains the details of stress magnification as follows: (i) stress at the edge of an elliptical hole can

become larger than the average stress to which the layer is subjected. (ii) stress concentration depends on the shape of the flaw, not the size. (iii) maximum stress perturbation is found at a distance c from the centre of the circle or the ellipse. (iv) stress magnification increases in inverse proportion to the radius of curvature, r_c, and at the narrow end of the ellipse (*i.e.* the crack tip), the radius of curvature is given by:

$$r_c = b^2/c \qquad (5.2)$$

It follows from equations 5.1 and 5.2 that stress concentration at the tip of an elliptical hole is given by:

$$-S_t = -S_h(1 + 2\sqrt{[c/r_c]} \qquad (5.3)$$

rearranging equation 5.3 gives $S_t/S_h = 1 + 2\sqrt{c/r_c}$ (5.4)

For b<<c, Engelder (*op. cit.*) argues that the above equation approximates to:

$$S_t/S_h = 2c/b = 2\sqrt{c/r_c} \qquad (5.5)$$

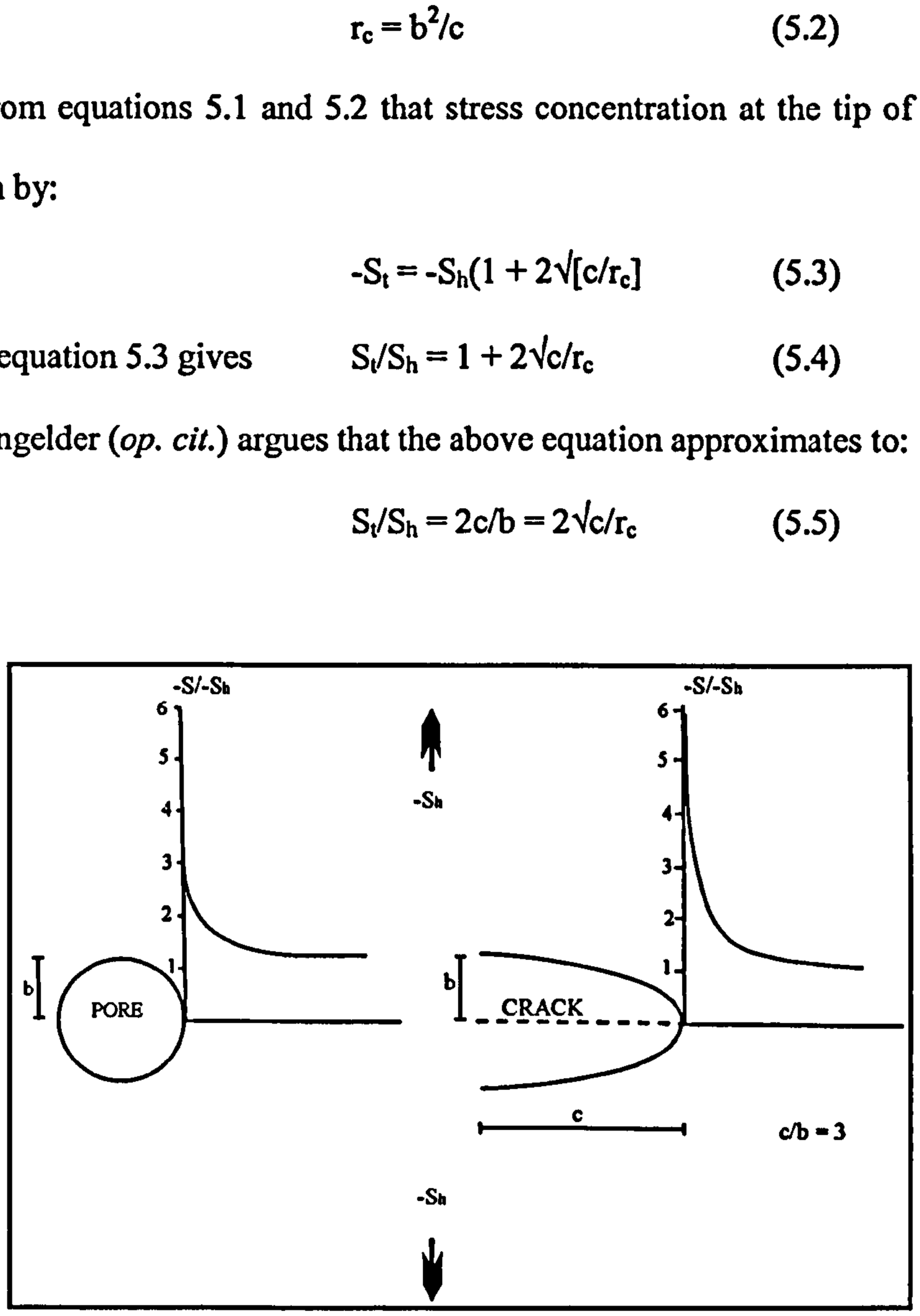


***Figure 5.3** Stress magnification (a) around a circular pore and (b) around an elliptical crack (from Engelder, 1993).*

This relationship expressed in equation 5.2 shows that r_c is inversely proportional to c. As c goes to infinity, r_c approaches 0 and the term *'crack'* can be mathematically defined as an infinitesimally narrow ellipse (Whittaker *et al.*, 1992, p.47). The stress condition described by the above equation is only valid at the moment when the crack initiates from the flaws and it is therefore necessary to consider mechanisms governing fracture propagation. If it is assumed that the tensile strength of a material is determined by inter-atomic bond strength then calculated values of the strength are several orders of magnitude greater than values measured experimentally on the real material.

5.2.1.1Griffith energy balance theory

The reason for the low tensile strength of real brittle material was not understood until Griffith (1921) applied the analysis of crack initiation of Inglis (1913) based on an *'energy balance'* approach. This approach later became the foundation of fracture mechanics. In his analysis of tensile failure, he qualitatively explained why brittle materials fail at much lower far-field stresses than the theoretically predicted values based on inter-atom bond strength. He argued that, as a result of stress concentration at the tip of the micro-flaws, very large stresses could be generated at fracture tips and these were capable of rupturing the bonds. He assumed the flaws to be elliptical with high eccentricity and proposed that failure of the material by extension is caused by the absorption of externally applied mechanical energy or the release of stored strain energy or by a combination of these two. Whittaker *et al.* (1992) gave an expression for the total energy U for an infinite, isotropic, linearly elastic material containing an elliptical crack based on the Griffith energy balance approach which is given by equation 5.6:

$$U = U_t + U_c - W + U_s = U_p + U_s \qquad (5.6)$$

where U is the total energy of an infinite cracked plate, U_t is the total initial elastic strain energy of the stressed but uncracked material, U_c is the elastic strain energy release caused by the introduction of a crack of length 2c and the relaxation of the material, U_s is the change in elastic strain energy caused by the creation of new surfaces, U_p is the change in the potential energy (*i.e.* $U_p = U_t + U_c - W$) and W is the work done by external sources. Detailed expressions for the above terms are beyond the scope of the present work and the reader is referred to the original publications.

Engelder (1993) considers that Griffith's analysis of crack propagation using Inglis' solution is unsatisfactory because the stress field in the vicinity of the crack tip and the radius of the crack tip are poorly defined. He argues that crack propagation in a rock is a complex problem that requires a more careful and detailed solution. Subsequent to Griffith work it was found out that for failure of a stressed solid, two necessary conditions have to be met: (i) the stress requirement (*i.e.* the local stress must be high enough to overcome molecular cohesive strength and has to be achieved by stress concentration due to the existence of Griffith flaws). (ii) the energy requirement (*i.e.* sufficient potential energy must be released to overcome the resistance to extension) and this can be achieved by increasing the work done by external force. In the Griffith theory, based on the energy balance approach, the crack is assumed to propagate in its own plane and difficulty arises when a more complicated stress field involving compression is applied. Thus the Griffith theory based on the energy balance approach is more applicable to the condition of tensile failure.

5.2.1.2 Griffith fracture stress criterion

Griffith (1924) proposed a critical maximum local tensile stress criterion for extension of an open crack from a crack tip. The fracture stress criterion is based on the fact that cracks initiate when tensile stress is induced at or near the tip of an open crack and exceeds the molecular cohesive strength of the material. He obtained values for the critical stress (σ) which were in agreement with the measured values for the tensile strength of glass. He showed that even when the applied far-field stresses are compressive, the crack-tip stress would be tensile. For an elliptical crack subjected to biaxial compression, and under the conditions in which $\sigma_1 \neq \sigma_3$, he demonstrated that the Griffith fracture stress criterion can be given in terms of the principal stresses by equations 5.7 and 5.8:

$$(\sigma_1 - \sigma_3)^2 + 8\sigma_t(\sigma_1 + \sigma_3) = 0 \text{ if } \sigma_1 + 3\sigma_3 \geq 0 \qquad (5.7)$$

$$\sigma_3 = \sigma_t \text{ if } \sigma_1 + 3\sigma_3 < 0 \qquad (5.8)$$

Where σ_1 and σ_3 are the maximum and least principal stresses respectively and σ_t is the uniaxial tensile strength of the material. The stress intensity factor approach has been used extensively in most rock mechanics and fracture mechanics problems and paved the way for the development of linear elastic fracture mechanics (LEFM) which can be applied to linearly elastic materials. The theory of linear elasticity is based on the assumption that the material is linearly elastic, isotropic and homogeneous and therefore the elastic properties are fully described by two mutually independent constants. These are the Young's Modulus (E) and Poisson ratio (ν). Deformation before the onset of brittle failure is assumed to be perfectly elastic. A body is said to be perfectly elastic if when a load is applied to the body, it starts to deform and when the load is removed it

recovers instantly. Elastic theory is valid for strains which are small and stresses which are low relative to those that occur in rocks. If the applied remote stress is not low, then stress magnification occurs at the tips of micro-flaws and rocks fail by brittle fracturing either extensional or shear depending on the magnitude of differential stress.

Fracture mechanics is a branch of material science which seeks to quantify the critical combinations of stress and crack size for cracks during propagation. The conditions for initiation and propagation of a crack of a given size can be obtained by the use of the stress intensity factor (K). This method has provided a more universal approach for analysis of fractures in materials. Whittaker *et al.* (1992) points out that the stress intensity approach uniquely predicts the crack tip stress and displacement fields and defines the magnitude or the strength of the stress intensity of a crack tip. K also shows the distribution of stress in the vicinity of a crack tip caused by the introduction of the crack. For a cracked body, under a certain type and magnitude of loading, K is known, and the stress and displacements can be determined accordingly. Crack initiation takes place if K reaches its critical value called K_C. Olson and Pollard (1988) define K as a measure of stress concentration at the crack-tip that depends on the crack loading and geometry. These authors show that the stress intensity factors for an isolated straight crack in an infinite, homogenous, isotropic elastic body that propagates in mode I and II are given by:

$$K_I = (\sigma^{\infty}_{11} + P)\sqrt{c} \qquad (5.9)$$

$$K_{II} = (\sigma^{\infty}_{12} - \sigma^{c}_{12})\sqrt{c} \qquad (5.10)$$

where K_I is the stress intensity factor for mode I and K_{II} is the stress intensity factor for mode II joint propagations described under section 5.1 (Fig. 5.1), c is the half crack

length, P is the fluid pressure inside the crack, superscripts ∞ and c denote the remote and crack tip stresses respectively. The quantity σ^{∞}_{11} + P in equation 5.9 is called the driving pressure for a mode I crack. Olson and Pollard (*op. cit.*) showed that the crack driving force, G (named in the honour of Griffith), which is the measure of mechanical energy available for an increment of crack growth, can be related to the stress intensity factors by:

$$G = \pi(1 - \nu)/E(K_I^2 + K_{II}^2) \qquad (5.11)$$

Where ν is Poisson's ratio, E is Young's Modulus. Olson and Pollard (*op. cit.*) argue that the critical stress intensity factor for mode I cracks (K_{IC}) can be substituted for G_{IC} provided the material under consideration is linearly elastic.

5.3 Factors controlling crack paths

Another powerful tool for investigating the mode of propagation of joints is the study of their surface morphology (fractography) (see section 5.4). As will be shown, interpretation of these features can be used to demonstrate the interaction between the local and remote stresses. The local heterogeneities within a rock mass can produce shear stresses at the front of a propagating joint and this leads either to the twisting of the parent joint from the ideal path to minimize the shear stress imposed on it, or to the breakdown of the main joint into incipient *en-echelon* cracks. In addition, pre-existing planes of weakness in rocks may favour deviation of the fracture paths from straight paths, even though they are not perpendicular to the least principal stress. In this case, joint propagation is of mixed mode and the opening displacement is oblique to the joint surface. Changes in the orientation of the crack surface can be sharp (kinking) or smooth

(gradual). Before attempting to discuss fractography and presenting field observations from the area of study in the Bristol Channel Basin, some reasons why fractures deviate from straight paths are given and some examples are described.

Cracks rarely occur in isolation and their presence in rocks perturbs the local stress field. This is demonstrated by the deflection of fractures as they approach one another (see tip-to-plane junctions discussed in sections 4.4.2 and 4.4.3.2 of Chapter 4 illustrated in Figs. 4.24 and 4.31). Pollard *et al.* (1982) studied the breakdown of a parent joint into multiple *en-echelon* crack segments when a parent crack propagating in a principal stress plane enters a region in which the remote principal stresses have rotated. According to their work, mixed mode cracks result in a path that twists about an axis parallel to the direction of fracture propagation. When this occurs, the fracture does not twist to maintain its continuity, but breaks down by increments into *en-echelon* segments. From energetic considerations, they argue that the breakdown of the parent joint is favoured because the surface area of multiple *en-echelon* segments is less than that of a single twisted surface. The sense of twist (*i.e.* clockwise or anticlockwise) depends on the sense of shearing. The tendency for breakdown increases with an increase in mode III and II stress intensity factors relative to mode I stress intensity.

Olson and Pollard (1988) employed a 2D displacement discontinuity boundary element computer code to model the behaviour of curved crack propagation under various loading conditions. They also carried out uniaxial crack propagation experiments on *en-echelon* crack arrays in PMMA sheets to examine the states of stress, fluid pressure and mechanical interaction governing joint propagation paths, crack lengths and

interconnectivity. Their work compares crack interaction at various spacing and differential stresses. Increasing crack-parallel differential stress resulted in both decrease in crack path deviation (convergence and divergence with respect to other fractures) and an increase in overlap of interacting cracks. The amount of overlap of *en-echelon* cracks depends on spacing. It increases for large spacing compared to smaller spacing because of the decreased interaction. It follows that when fractures are closely spaced, the propagation of one joint impedes the growth of the neighbouring joint. The propagation force, G (defined as the amount of energy available for an increment of crack growth) was also studied for *en-echelon* cracks under constant internal fluid pressure. When compared to the crack propagation force for an isolated crack with the same internal pressure and length, the propagation forces for *en-echelon* cracks first exceed that for an isolated crack as the crack tips approach one another, reaching a maximum value of 6 times the initial force when the overlap is zero for a spacing to total array length ratio of 0.1. As the overlap increases, G drops below that for an isolated crack, suggesting that propagation will cease unless the driving stress increases. Thus *en-echelon* cracks should impede one another's propagation after overlap (Olson and Pollard, 1988).

Based on fieldwork in the Colorado Plateau, Utah and numerical studies, Olson and Pollard (1989) argue that the curving paths of the overlapping *en-echelon* cracks suggest the dominance of local crack-induced stresses over remote stress. Their work suggests that nearly straight crack paths imply the dominance of remote compressive stress over local crack-induced stress. They obtained an initial divergence followed by convergence for closely spaced *en-echelon* cracks growing in an isotropic stress field. They also found that large differential stresses produced an almost straight path (Fig. 5.4).

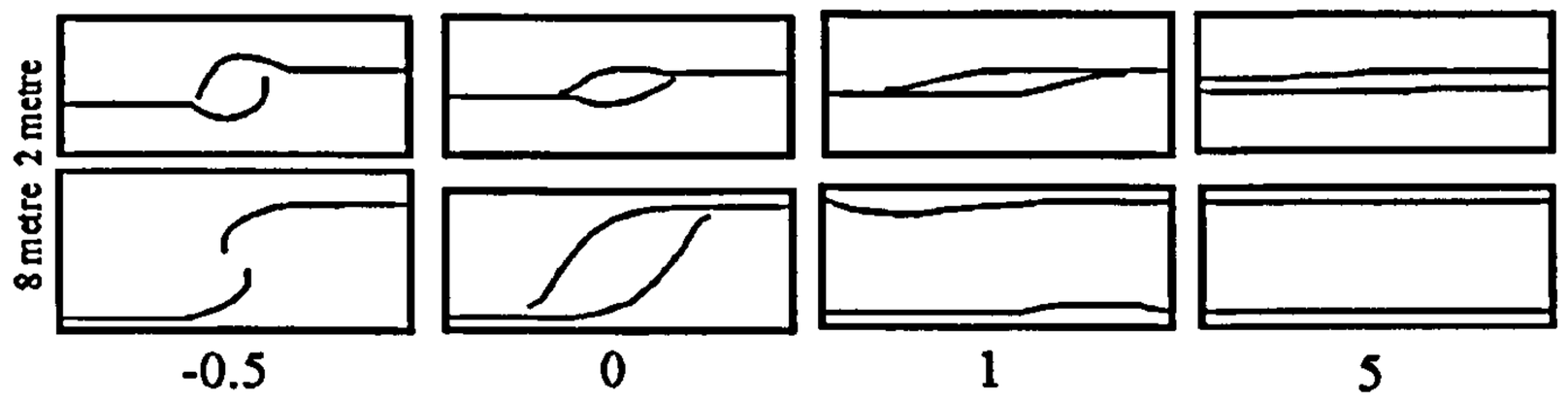


***Figure 5.4** Crack-paths of vertical en-echelon cracks at different spacing and differential stresses. S_x and S_y denote crack parallel and perpendicular stresses (from Olson and Pollard, 1989 and compiled by Engelder 1993).*

Systematic changes in the propagation direction of younger joints in the proximity of through-going joints under different horizontal remote differential stresses in the Salt Valley Anticline of the Arches National Park, southern Utah, have been discussed by Dyer (1988) and are discussed in section 3.6.3 of Chapter 3.

It is important to determine whether or not straight crack paths always indicate propagation under high differential stress. Renshaw and Pollard's (1994) numerical modelling demonstrates that the degree of fracture curvature between two mechanically interacting fractures depends not only on the ratio of remote differential stresses and the fracture driving stress, but also on the growth mechanism, such as sub-critical fracture growth, and on fracture surface roughness. They argue that sub-critical fracture propagation limits the fracture driving stress needed for propagation (*i.e.* the sub-critical stress intensity factor) and fracture surface roughness limits the magnitude of shear displacement that can be accommodated along the fracture. They introduce heterogeneity into their model around the crack tip (Fig. 5.5a). Whether the deviated fracture tip returns

to the projected straight path or continues to curve is controlled by the transverse stress or the T-stress which is defined by the differential stress, *i.e.* σ_3^{∞} - σ_1^{∞} using the sign convention of tension as positive. If T > 0 the shear stress induced by the *T-stress* and that of the local heterogeneity will have the same sign. The crack will continue to curve. If T < 0, the shearing induced by the *T-stress* will have an opposite sign to the local heterogeneity and the signs of the stress intensity factors will be different. If K_{II} due to the remote stress exceeds K_{II} caused by local heterogeneity, the crack path will be straight.

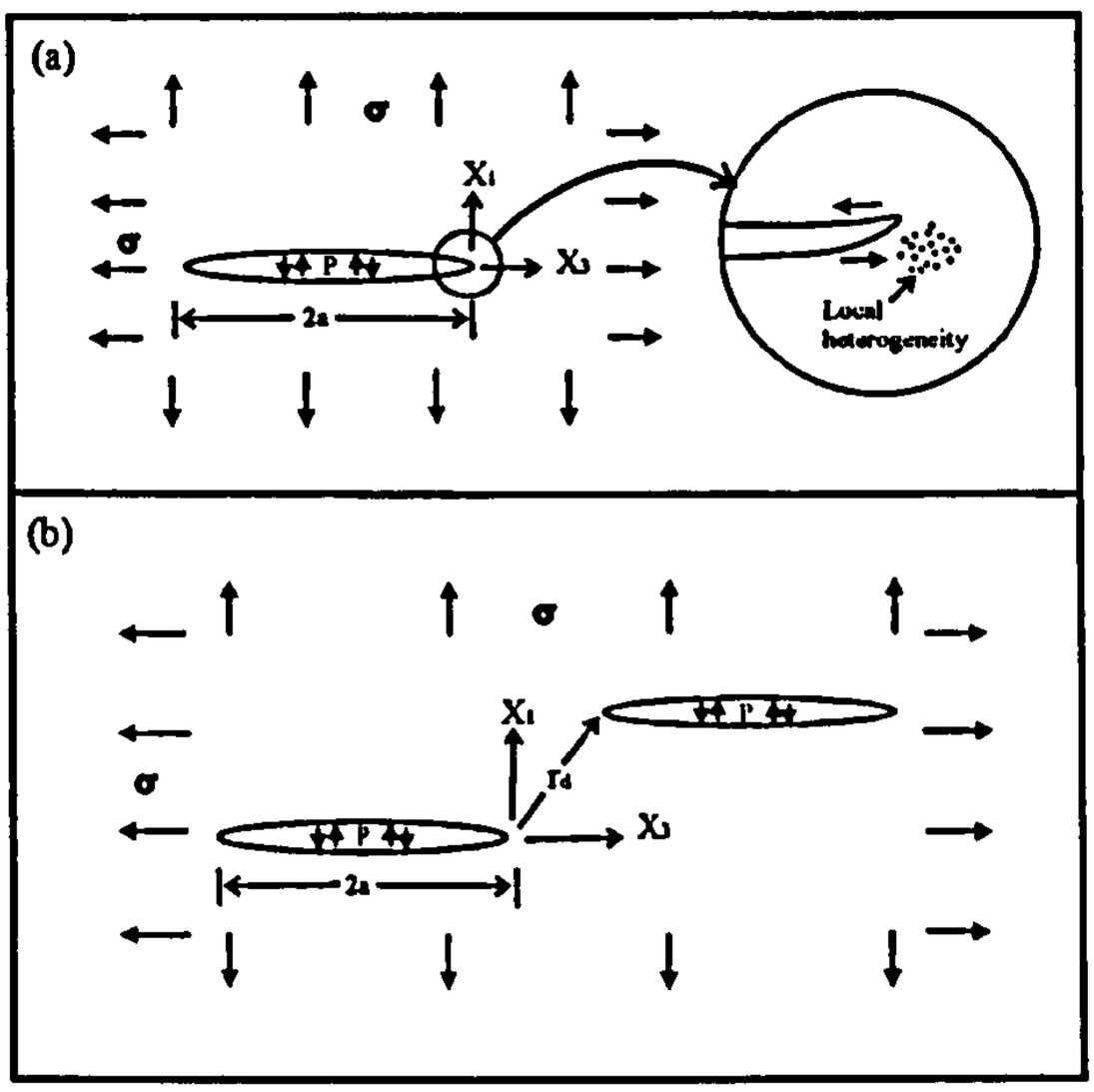


***Figure 5.5** (a) Inhomogeneities in a rock causing deviations from straight crack paths and (b) interaction between neighbouring joints (from Renshaw and Pollard, 1994).*

The interaction stress (*I-stress*) is a measure of the stress perturbation around one fracture caused by the presence of a second fracture (Renshaw and Pollard, *op. cit.*). They derived an expression for two mechanically interacting fractures as shown in Fig. 5.5b, the interaction stress (I) is given by:

$$I = C_g(\sigma_1^{\infty} + P) \qquad (5.12)$$

C_g depends only on the geometry of fractures, $\sigma_1^{\infty} + P$ is the driving stress for mode I crack growth. For a very close spacing of cracks, (*i.e.* $r_d << c$ where r_d is the tip separation and c is half crack length), C_g is approximated by:

$$C_g \approx O\,[\sqrt{c/r_d}] \qquad (5.13)$$

where O[] indicates the order of magnitude. For very wide spacing ($r_d > 1.5a$), the maximum value of C_g is in the order:

$$C_g = O\,[(c/r_d)^2] \qquad (5.14)$$

Natural crack surfaces have a roughness because of the granular nature of rocks and because of growth features such as hackle marks and hesitation lines (Renshaw and Pollard, 1994). Using a boundary element propagation model, they note that if the ratio of shear (S) to normal (N) displacement along the fracture is large (*i.e.* $S/N \leq 0.15$), the propagation path will curve. As S/N is decreased (*i.e.* $S/N \leq 0.04$ and $S/N \leq 0.01$) the propagation path becomes more and more straight.

Some of the exposures that contain the Alpine joints in the Bristol Channel area show a right- stepping *en-echelon* array in which the individual fractures are closely spaced and follow straight propagation paths (Fig. 5.6). However, close inspection shows that at the tip-region of the middle joint within the *en-echelon* array, the propagation diverges slightly away from the next joint, suggesting that the presence of one joint in the vicinity of a propagating joint influences the path of the new one. In general, most Alpine joints are long and tend to intersect the neighbouring joints tip-to-plane (Fig. 5.7). The

propagation path of individual Alpine joints which trend approximately E-W is highly variable and depends on many factors indicating the presence of pre-existing discontinuities such as folds, faults, joints and local heterogeneities. The presence of local heterogeneities in rocks commonly causes fractures to deviate from an ideal straight path during their propagation. However, this does not affect behaviour at the large-scale (Thomas and Pollard, 1993). Fig. 5.7 shows local heterogeneities causing the crack path to deviate from an ideal straight path and follow one governed by both the local conditions and the remote stresses. Post-Alpine joints are short and are less likely than Alpine joints to encounter heterogeneities during propagation. In addition, joint lengths are greater than their respective spacing and they are therefore less deflected from straight paths by the neighbouring joints of the same set during their propagation.

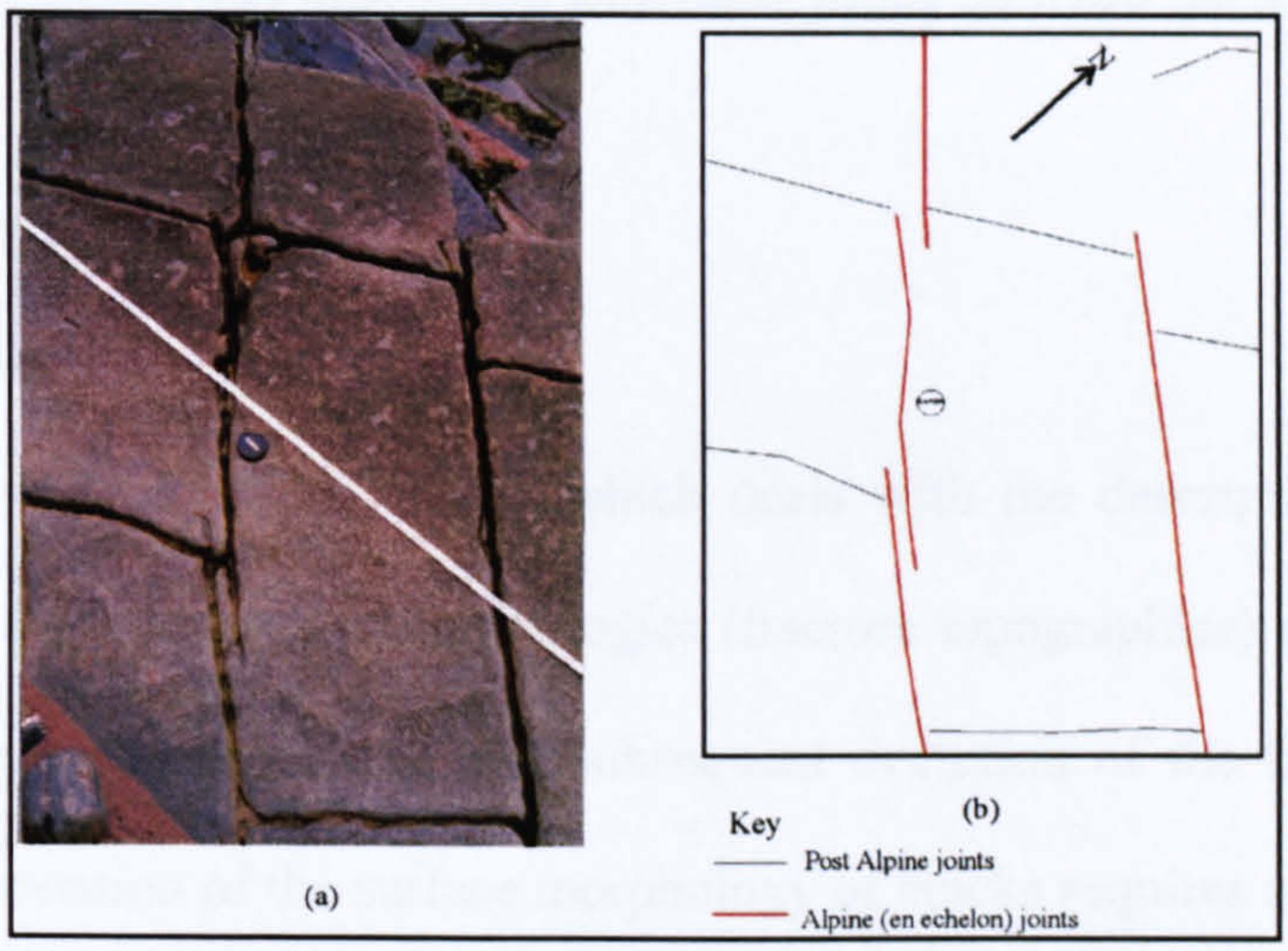


Figure 5.6 *(a) Photograph and (b) line drawing of right-stepping, closely spaced, en-echelon joints on the leading limb of the Lilstock buttress anticline. See Fig. 4.27 for the location of this Figure.*



Figure 5.7 *Variation in joint propagation paths East of Lilstock caused by local heterogeneity and interaction with adjacent joints of the same set. The result is a curving perpendicular or tip-to-plane geometry (highlighted by red circles). Note that the post-Alpine joints are relatively short and straight and the propagation paths are much less affected by heterogeneity and interaction with other joints than are the Alpine joints.*

5.4 Fractography

5.4.1 Introduction

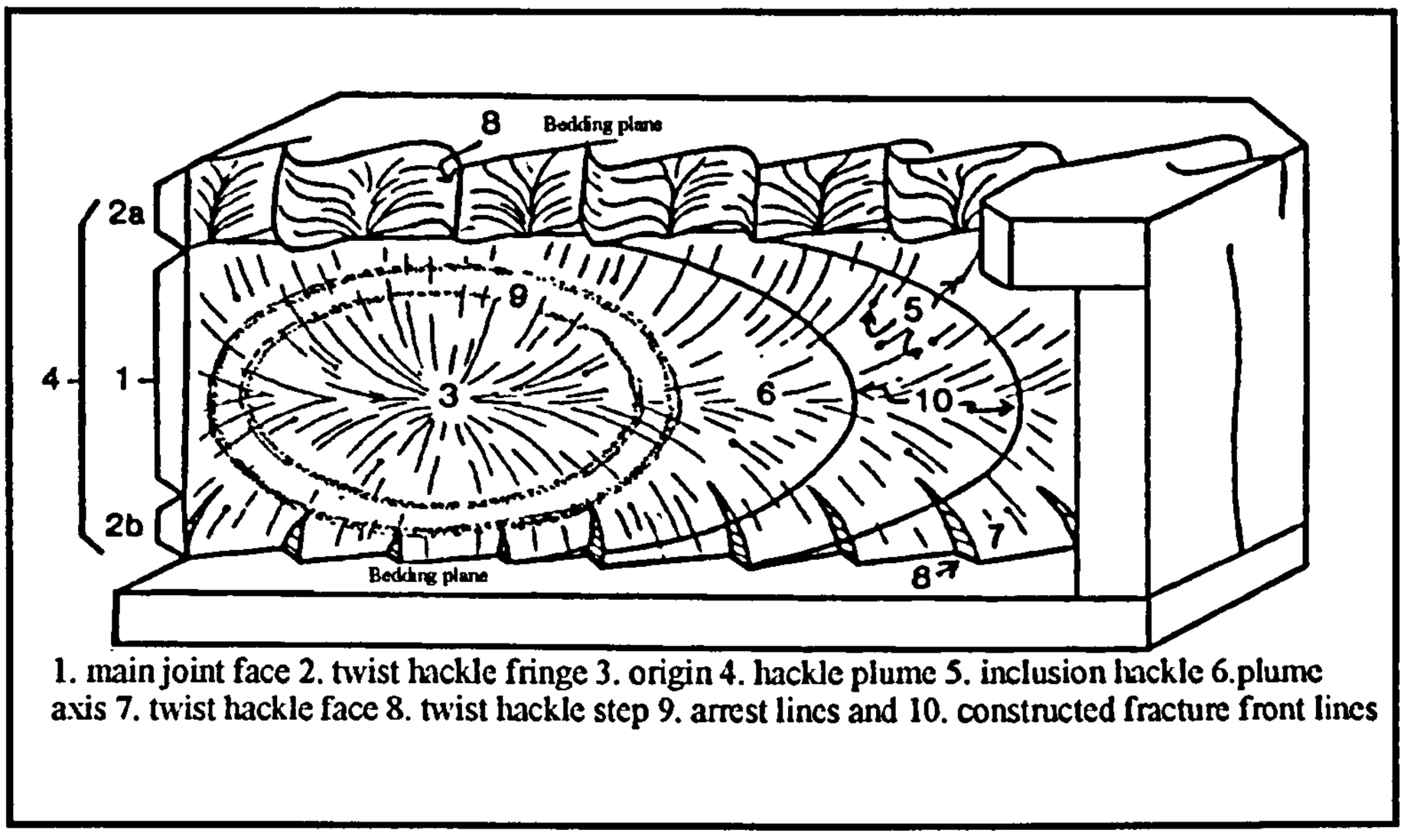
Fractography is defined as the science which deals with the description, analysis and interpretation of fracture surface morphologies (fracture topographies) and links them to the causative stresses, mechanisms and subsequent evolution of the fractures (Ameen, 1995). The interpretation of the surface morphology of cracks requires a good knowledge of fracture mechanics and has a wide application in material science, engineering and the geosciences. Fractography has been extensively used to study brittle failure in materials. Significant contributions have been made by Bahat (1991) who discusses fracture processes in glass, ceramics and rocks. He describes fracture surface morphology as ''the

fingerprint of fractography''. A detailed account of fractography as a tool in fracture mechanics and stress analysis has been given by Ameen (1995).

The rate at which cracks propagate during earthquakes is supersonic, a fact that is also evident from seismicity accompanying rock failure incurred during blasting. It is extremely difficult to determine the age of a single crack in a rock mass. Caputo and Hancock (1999) argue that the lifetime of each joint propagation event is not very long. Extension fractures do not form instantaneously, but incrementally and repeatedly over a time span of 10^5 to 10^6 years. This is mainly because joint propagation depends on many factors such as the degree of deformation, the strain rate and the mechanical properties of the jointed rocks. In addition, younger joints with the same orientation could be superimposed on pre-existing joints, making the interpretation extremely difficult. These joints inherit remarkable surface markings or ornamentations from which vital information regarding joint initiation, direction of propagation and arrest can be gathered. Fractography is a powerful tool that can be used to better understand the relationship between the remote and local stresses and the mode and direction of crack propagation.

Woodworth (1896) was one of the first to recognise and report the delicate fracture surface morphologies such as plumose structures on joint faces (Fig. 5.8). He suggested that the joints are opening mode fractures (*i.e.* mode I). Features which occurred on joint faces were carefully documented and described by Woodworth and interpreted as inherent characteristics of joints that fail by extension. He described joint initiation at a point and outward propagation to form plumose structures. Several other investigators later applied fractographic principles (*e.g.* Corte and Higashi, 1960; Hodgson, 1961;

Bahat and Engelder, 1984; Pollard and Aydin, 1988; Helgeson and Aydin, 1991; Bahat, 1991; Bankwitz and Bankwitz 1995; Younes and Engelder, 1999; Müller and Dahm, 2000 and 2001; Bahat *et al.*, 2001; Belayneh, in prep.) to the analysis of delicate structures on joint surfaces in order to deduce the points from which joints initiated, the direction of propagation and stages of arrest. Kulander and Dean (1995) suggest that fractographic features can be used in any material to determine the origin of the failure plane, changes in propagation velocities, stress directions and stress magnitudes at the crack tip during failure. Well-preserved fracture surface morphologies in the limestones of the Bristol Channel are comparatively rare and difficult to find but they can be extremely informative. However, in carbonates these various ornamentations can be eroded very easily as is the case in the North Yorkshire study area (section 4.3 of Chapter 4). Fortunately the limestones of the Bristol Channel Basin do have some preserved surface markings.



1. main joint face 2. twist hackle fringe 3. origin 4. hackle plume 5. inclusion hackle 6.plume axis 7. twist hackle face 8. twist hackle step 9. arrest lines and 10. constructed fracture front lines

***Figure 5.8** Surface features typical of a joint surface (from Hodgson, 1961).*

5.4.2 Types of fracture surface morphology

The suite of surface features displayed by joint surfaces is summarised in Fig. 5.8. In the Bristol Channel area studied by the present author, the most common fracture surface markings are plumose structures and twist hackles fringes. *'Plumose structure'* is the name given to the feather-like markings that appear to radiate from some central point (3 in Fig. 5.8), which is the point of fracture initiation. They are the result of mode I failure and the direction of propagation is parallel to the plumose lineation. The position of the fracture front at different times in the fracture history can be obtained by studying fracture front lines normal to the plumes (10 in Fig 5.8). These lines are often present on the face as arrest lines *i.e.* lines which mark the position of the fracture front when the fracture temporarily stopped propagating or the fracture front decelerated. The fracture shown in Fig. 5.8 is bounded by a *'Twist hackle fringe'* with a systematic morphology, the topographic amplitude of which is usually much higher than that of the central zone (or plume) of the joint (Pollard and Aydin, 1988; Bahat, 1997; Younes and Engelder, 1999; Müller and Dahm, 2000). Younes and Engelder define the twist hackles (twist hackle fringes in this work) as a series of *en-echelon* fringe cracks that initiate from the plane of the parent joint and twist out of the plane by propagating normal to the overall lateral propagation direction of the parent joint. When it forms, a twist hackle twists away from the parent joint (either gradually to form a twist hackle or abruptly to form an abrupt twist hackle or kink). Experiments on analogue models such as starch-water mixtures (Müller and Dahm, 2000) indicate that in a twist hackle fringe zone, joints propagate more slowly than in the central zone. They argue that a similar process will operate in a rock layer in which the fringe zone forms along the layer interface (Fig. 5.8).

The mechanisms by which plumose hackle structures and twist hackle fringes form are well understood. A specific feature of fracture surface markings, namely the border plane, or twist-hackle fringe, has been used to determine the orientation of stresses under which the twist-hackle structures develop. Plumose structures indicate mode I failure (opening) and the twist hackle fringe (border planes) indicate the propagation out-of-plane from the main joint. They form in response to a twist imposed by the influence of the remote stress field (Pollard *et al.*, 1982; Roberts, 1995; Younes and Engelder, 1999). The recognition of twist-hackle planes is important because they form when a propagating fracture abruptly enters a region of different stress orientation (Pollard *et al.*, 1982.). The fracture breaks (twists) into a series of individual *en-echelon* lance-like twist-hackle faces forming in steps, each perpendicular to the resultant tension, that are generally more closely spaced than the adjacent main joint planes (Roberts, 1995; Kulander and Dean, 1995). Breakdown of the crack into *en-echelon* segments is indicative of different mode III/mode I or mode II/mode I ratios (Cooke and Pollard, 1996; Bahat *et al.*, 2001). The conditions under which this occurs have been discussed earlier in section 5.3 of this chapter.

Younes and Engelder (1999) argue that fringe cracks originate when an advancing joint encounters a shear couple. They propose that if the propagating crack enters a volume of rock subject to a stress field misaligned in relation to that guiding the parent joint, transverse adjustments will occur due to mixed mode crack propagation, thus causing the joint to break down into fringe cracks. They classify fringe cracks into gradual twist hackles, abrupt twist hackles and kinks. These hackles and kinks form as follows. Gradual twist hackles are curvi-planar *en-echelon* fringe cracks that result from the continuous breakdown of the parent joint so that the fringe cracks twist out of the plane by

propagating normal to the original direction of propagation (*i.e.* vertically). Individual *en-echelon* cracks that are planar and that emanate abruptly from the edge of a parent joint are known as abrupt twist hackles. In map view they appear to grow across the edge of the parent joint. Kinks occur as mode I cracks and the tilt in the crack path is driven by shear traction superimposed on the parent joint after arrest following a finite amount of mode I propagation. Kinks occur at the termination of a straight joint, adopting a strike which is abruptly different from that of the initial joint. A kink that turns clockwise with respect to the direction of the main joint is the result of right lateral shear, whereas a kink that turns counter-clockwise is the result of left lateral shear (Cruikshank *et al.*, 1991).

A crack subjected only to the opening mode deformation will dilate and propagate in its own plane (Pollard *et al.*, 1982). The breakdown of a parent joint into *en-echelon* fringe cracks is initiated by parallel shear at the crack tip, that is, mode III deformation (Pollard *et al.*, 1982; Bahat, 1991; Younes and Engelder, 1999). The tendency for breakdown increases with increase in stress intensity ratio (K_{III}/K_I). The twist angle between the parent joint and the fringe crack (β) is a function of stress ratio (R), the angular change of the remote stress (α) and Poisson's ratio (ν) (Pollard *et al.*, 1982):

$$\beta = \frac{0.5\tan^{-1}[\sin 2\alpha]}{(R + \cos 2\alpha)(0.5 - \nu)} \qquad (5.15)$$

For a small angular change in the remote stress, ($\alpha \leq 10^{o}$), the fringe cracks form perpendicular to the rotated least compressive stress when:

$$R = \frac{0.5 + \nu}{0.5 - \nu} \qquad (5.16)$$

Younes and Engelder (1999) argue that the twist angle β of the crack relative to the parent joint will differ from the stress rotation angle α. The discrepancy between the stress rotation angle α and the angle between the twist hackle fringe and the parent joint (β) may be caused by the interaction of neighbouring fractures and local heterogeneities within the rock mass.

Müller and Dahm (2000) studied fracture surface morphology, mainly plumose structures on tensile cracks, and the rupture velocity of cracks formed by desiccation of starch-water mixtures. Based on rupture velocity they distinguished joints, which they argued were spontaneously nucleating dynamic cracks, from quasi-static cracks. They deduced that plumose structures are indicative of rupture direction and drew an analogy between plumose structures and rupture direction on one hand and seismic rays and seismic wave velocity on the other.

Bankwitz and Bankwitz (2001) have made significant contributions in the application of the science of fractography to geology. They used fractographic features on early fracture sets in granite plutons as evidence of the cooling stages and, in some cases, the conditions operating in the crust at the time of joint formation. They argue that the fractographic features of joints formed at depth are not a typical reflection of simple thermoelastic contraction in the granite. They present evidence that joints are fluid driven and estimate the depth of formation of these early fractures to lie between 7 to 15kms.

5.5 Present work

A study of surface features on joints was carried out at Lilstock, Kilve, East Quantoxhead and Blue Ben. Although there are millions of joints in the area, joints decorated with plumose structures and fringe cracks are rare. Excellent exposures can be seen on some of the wave cut platforms and in the cliffs. The plumose structures along the southern margin of the Bristol Channel indicate that joints were initiated from points in the middle of the limestone beds (Fig. 5.9). Many thick limestone beds (thickness generally > 20cm) show plume axes approximately parallel to the bedding plane, indicating that joint propagation was bed-parallel. However, some of the beds have multiple initiation points and show complex plumose structures (Fig. 5.10). As the joint propagates towards the bedding plane with the shales above and below, it encounters a stress field that is neither normal nor parallel to the joint plane. The incompatibility between the remote and local stresses imposes a twist on the crack front of a propagating joint. The interaction between the remote and local stresses causes the joints to breakdown into twist hackle fringes. The mixed modes I and II propagation (or an in-plane shear mode) of the twist hackle is controlled by the local stress field, which is not necessarily in the same orientation as the remote stress field. The position of the plume axis is usually offset from the central position in the bed as if searching for a portion of the bed with ideal elastic properties (Engelder and Savalli, 2001).



Figure 5.9 *Plumose structures indicating the initiation of a joint from a point source in the middle of a 17cm thick limestone bed at Kilve. Note that the plume axis is approximately symmetrical with respect to the edge of the bed. The upper fringe zone has been weathered back from the joint face shown because of the enhanced weathering (chemical and mechanical) resulting from the higher intensity of fracturing.*



Figure 5.10 *Photograph of multiple initiation points showing complex propagation directions on a joint face at Lilstock. The black marker on the lower side is for scale.*

The parent joints in limestone beds thicker than 20cm are commonly planar and persistent in their central part. As the joint propagates and approaches the bedding planes, the stress intensity factor at the crack tip drops and joint propagation is impeded. Joint propagation will then be arrested at the limestone-shale interfaces. In thin limestone beds, the parent joints are most commonly made up of several *en-echelon* cracks linked together. In plan view, depending on the strike of the parent joint with which they are associated, they show a clockwise (CW) or anticlockwise (ACW) sense of rotation. Joints whose strike is between 0° - 090° show a left-stepping (clockwise) sense of rotation; joints striking 090° - 180° show right-stepping (anticlockwise) sense of rotation (Fig. 5.11). The length of the twist hackle (fringes) depends on the angle of deviation of the parent joint from the general E-W direction. If the strike of the parent joint deviates from the general E-W direction, the length of the fringe becomes shorter and the longest fringes form when the angle of twist from the parent joint is smallest. The length of the fringe crack varies from a few mm to 3cm.

The twist angle, *i.e.* the angle between the parent joint and the fringe crack, ranges from 0° to 80° (Table 5.1). As discussed earlier (in sections 4.4.2 to 4.4.7) the Alpine joints were formed during the Alpine compression that caused the amplification of the pre-existing rollover folds such as the Lilstock and Kilve anticlines. At both localities, in the hinge region of these folds, the joints are sub-parallel to the fold axes and are therefore fold-related. Twist-hackle fringes (Figs. 5.11) strike approximately E-W regardless of the orientation of parent joints, probably indicating a consistent N-S orientation of the local least principal compressive stress along the hinge zone of the fold at the time of joint formation. The local stress was determined by the position relative to pre-existing structures such as folds, faults and fractures.

Table 5.1 *Twist hackle fringes measured on joints from Lilstock.*

Strike of parent joint in degrees	Twist angle	Sense of rotation	Steps
360	81	CW	Left stepping
12	65	CW	Left stepping
14	80	CW	Left stepping
85	Sub-parallel	Difficult to determine	?
102	Sub-parallel	Difficult to determine	?
105	11	ACW	Right stepping
115	35	ACW	Right stepping
116	20	ACW	?

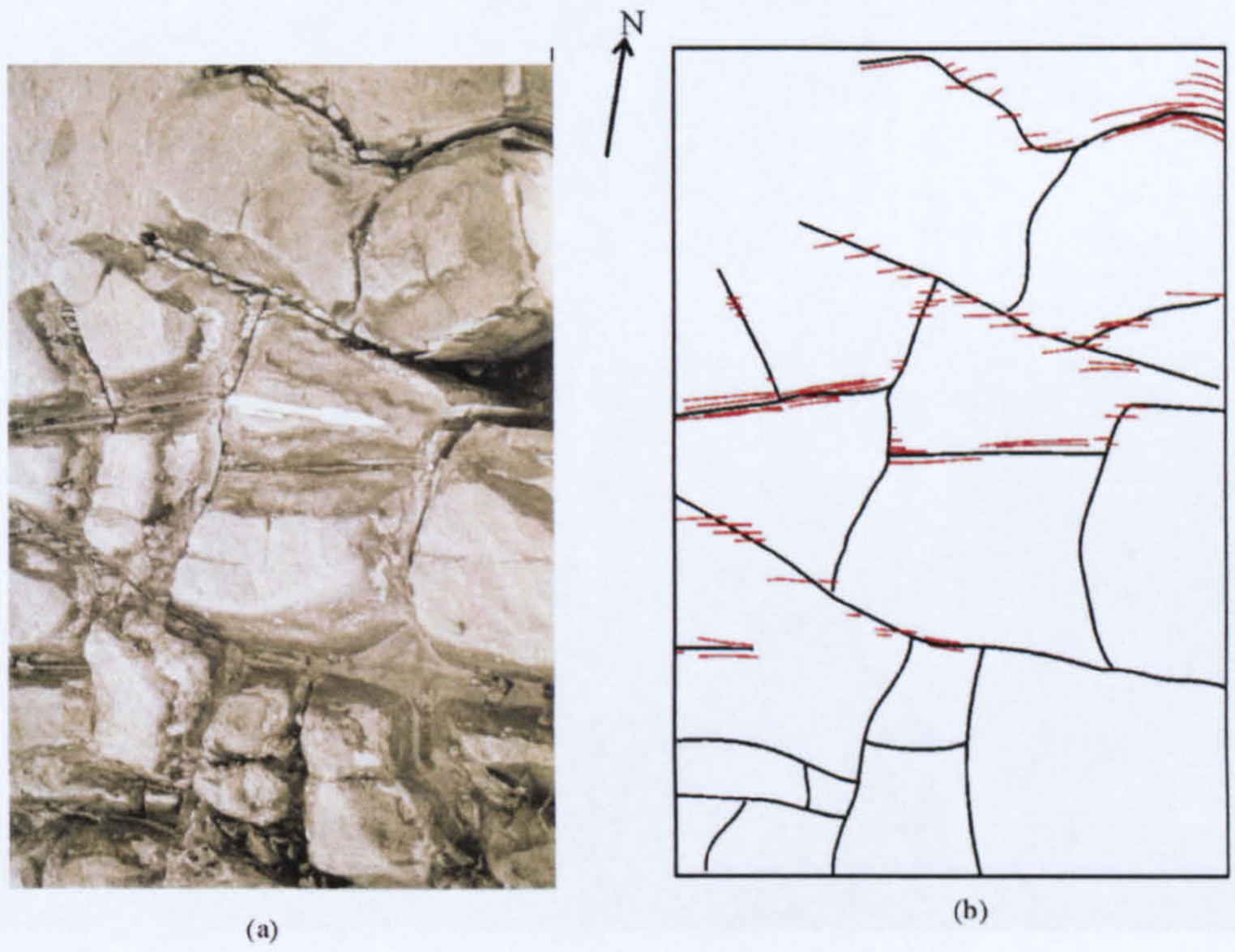


Figure 5.11 *(a) Photograph and (b) line drawing showing a plan view of twist hackle fringe observed at Lilstock. Note that the orientation of fringes remains roughly E-W regardless of the strike of the parent joint confirming constant N-S orientation of the remote stress field during Alpine inversion of the Bristol Channel Basin. The size of the photo is 42.5 by 62.5cm.*

The fringe zones are mostly asymmetric *i.e.* narrower along one margin of the parent joint than on the other (Fig. 5.12). The contact between the fractured limestone and the

adjacent shale bed is highly variable and ranges from sharp to gradational (*i.e.* grading from mudstone to marls or marly limestone). If the contact between the fractured limestone and the adjacent shale bed is sharp, the width of the fringe zone is broad. Alternatively if the contrast in mechanical properties between the limestone and the adjacent bed is either low or gradational, the width of the fringe zone is narrow. This

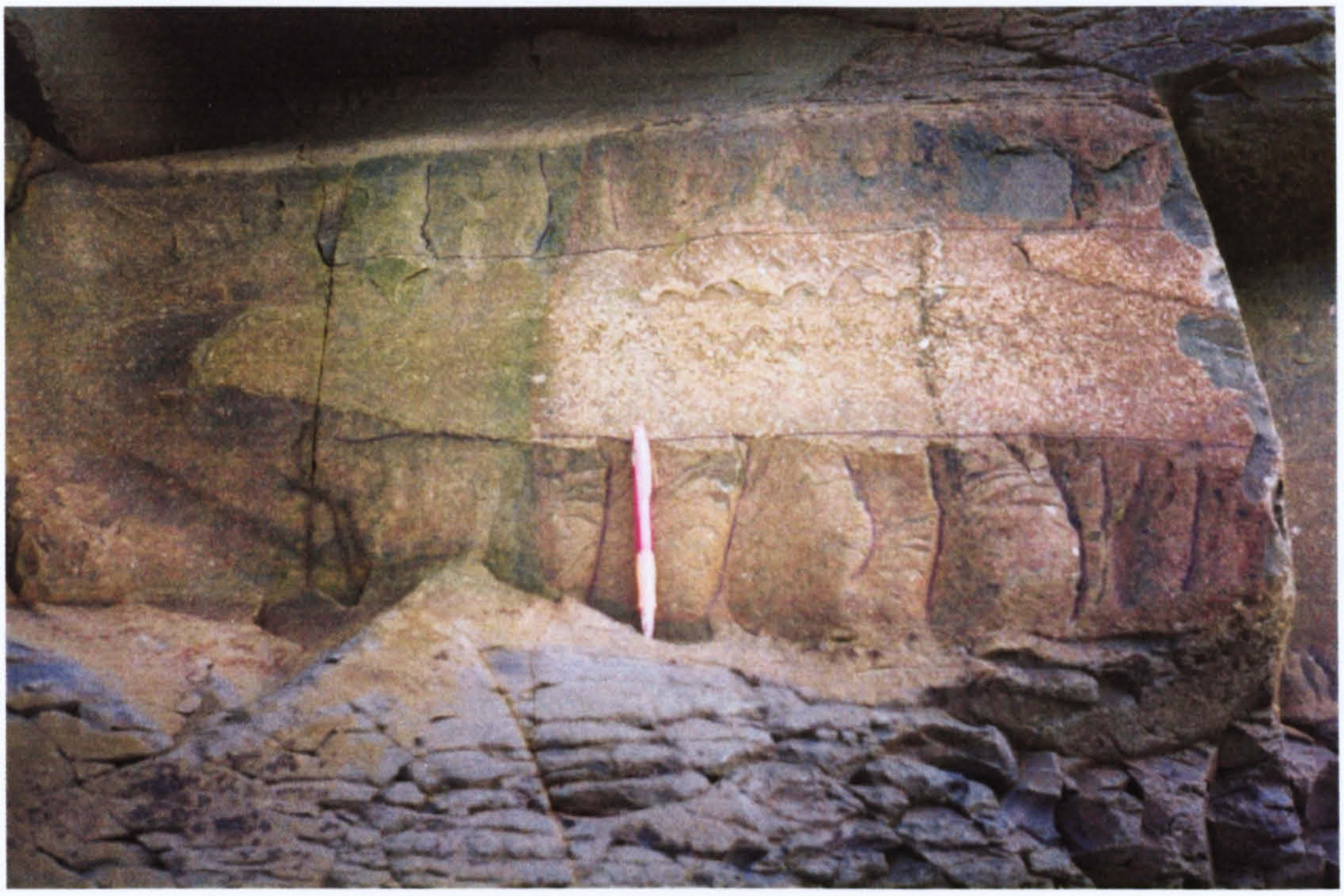


Figure 5.12 *Asymmetrical twist hackle fringe from Kilve. Note the different width of the fringe zone at the top and bottom of the bed. The top part is made up of more compact shaly limestone than the remainder of the bed and has different mechanical properties. The twist angle is also higher along the lower portion of the bed.*

shows that the width of the fringe zone depends on the properties of the interface between the limestone and shale beds and indicates that the difference in material properties on either side of the interface is an important factor in determining the width of the fringe zones. In general,

the thickness of the plumose structure is approximately twice the thickness of the twist hackle fringe zone on one edge of a limestone bed (Fig. 5.13 and Table 5.2).



Figure 5.13 *Photograph of plumose structure with an approximately symmetrical twist hackle fringe at Blue Ben. Note that the plumose structure approximately in the middle is twice the width of the twist hackle fringe. The propagation direction of the joint is from right to left as deduced from the feather on the fracture surface.*

In thinly bedded limestones, the fringe zones commonly occupy the whole thickness of the fractured layer. If the thickness of the competent bed is less than 15 to 20cm, a plumose structure is not commonly observed. The fringe zone extends from top to bottom of the bedding plane. The master joint is formed by a series of right- or left-stepping interconnected *en-echelon* cracks (Fig. 5.14). The angle between the parent joint and the fringe crack (*i.e.* β) shows either a clockwise or anticlockwise sense of rotation when the twist hackle fringe is viewed in relation to the parent joint. The twist hackle fringe in the jointed rock becomes a penetrative feature in thin micritic limestone beds.

***Table 5.2** Thickness of the plumose structure and twist hackle fringe (i.e. the combined lower and upper fringes) in limestone beds from the Bristol Channel Basin.*

Thickness of the limestone bed (cm)	Twist hackle fringe (cm)	Width of plumose structure (cm)	Locality
45	27	18	Lilstock
42	20	22	Lilstock
47	30	17	Lilstock
40	20	20	Lilstock
40	17	23	Lilstock
45	19	26	Lilstock
44	25	19	Lilstock
48	25	23	Lilstock
50	26	24	Kilve-Lilstock
42	19	23	Kilve-Lilstock
39	14	25	Kilve-Lilstock
45	19	26	Kilve-Lilstock
26	6	20	Kilve-Lilstock
40	20	20	Kilve-Lilstock
38	16	22	Kilve-Lilstock
40	19	21	Kilve
37	17	20	Kilve
37	21	16	West of Kilve
44	26	18	East Quantoxhead
39	18	21	East Quantoxhead
40	22	18	East Quantoxhead
41	18	23	East Quantoxhead
41	20.5	20.5	East Quantoxhead
41	25	16	East Quantoxhead
44	20	24	Kilve
42	17	25	East of Blue Ben
44	24	20	W of Blue Ben
42	26	16	W of Blue Ben



Figure 5.14 *Twist hackle fringe extending from one side of the bedding plane to the other in a thin limestone bed at Kilve. Coin is 2.2cm in diameter.*

5.6 Summary

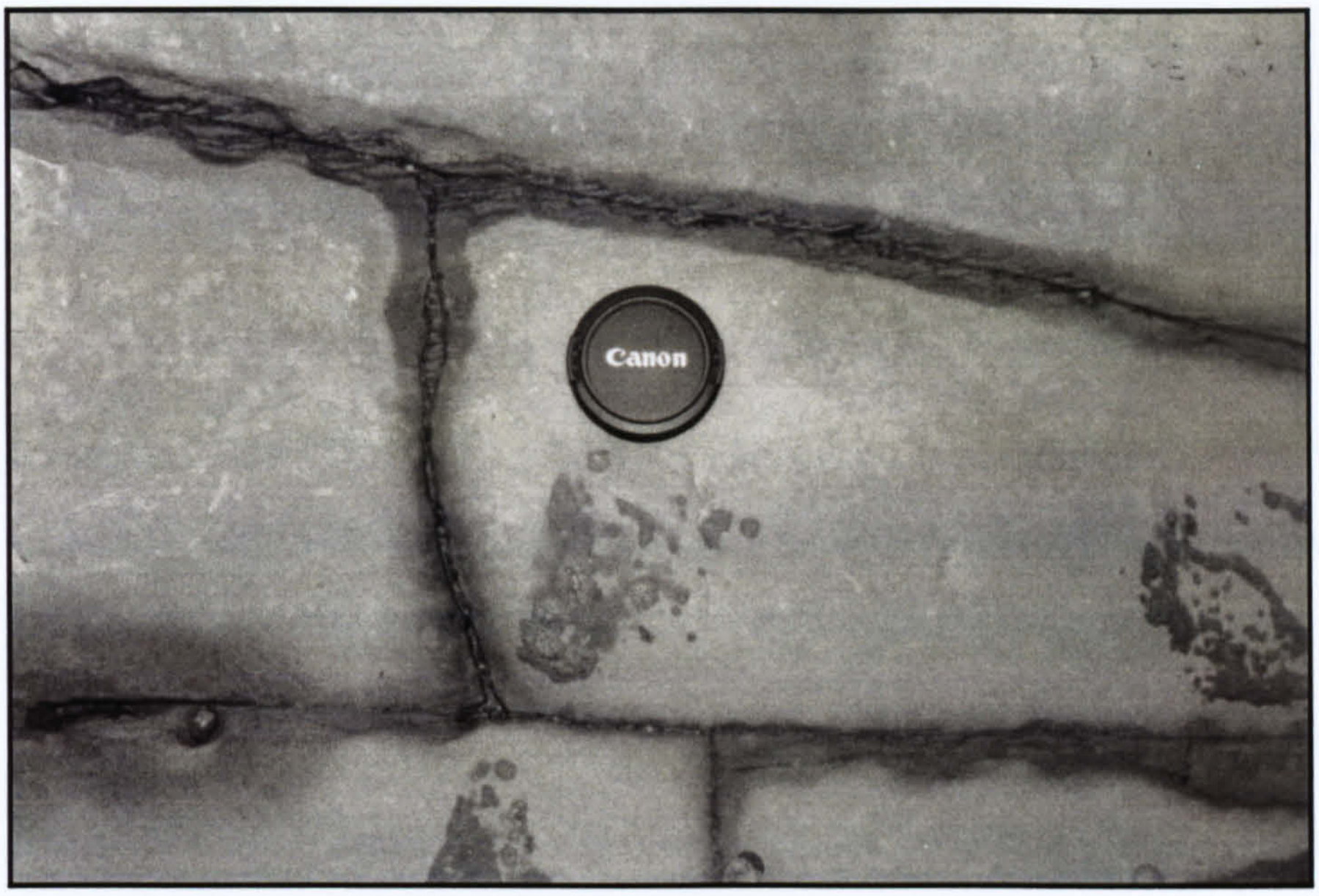
Based on Dart *et al.* (1995) and the present work, the tectonic evolution of the North Somerset coast can be divided into three stages: (1) the development of an E-W extensional fault system in response to N-S directed extension. (2a) N-S compression leading to formation of folds and thrusts and also causing the reactivation of pre-existing normal faults. This deformation event also resulted in brittle fracturing in the limestone beds and the formation of Alpine joints. As noted in sections 2.4.2.2 (Fig. 2.15b) and 3.6 3 (Fig. 3.3a), the maximum principal stress was N-S and horizontal and intermediate stress was E-w and horizontal during folding and thrusting, the least compressive stress being vertical. Buckling of the limestone and shale successions in the study area of the Bristol Channel caused layer-parallel shortening and thickening in the vertical direction. This created the ideal configuration for strike-slip faults to form when the intermediate and the least principal stresses swapped. Stage (2b) followed with the formation of NW-SE striking dextral and NE-SW striking sinistral strike-slip faults during continued N-S compression.

The interaction between N-S directed remote compression and local stresses that were governed by the local structures such as anticlines in the limestone-shale succession, and local heterogeneities in the rock mass, led to incompatibilities that resulted in the breakdown of the main joints into a series of *en-echelon* fractures during propagation. The configuration of the *en-echelon* fractures, whether right-stepping or left-stepping, depends on the strike of the parent joints. It is found that, regardless of the orientation of the parent joints with which they are associated, the strike of the fringe zones is always E-W. Thus for joints striking between 0° to 090° the sense of rotation is clockwise and for joints striking 090° to 180° the sense of rotation is anticlockwise.

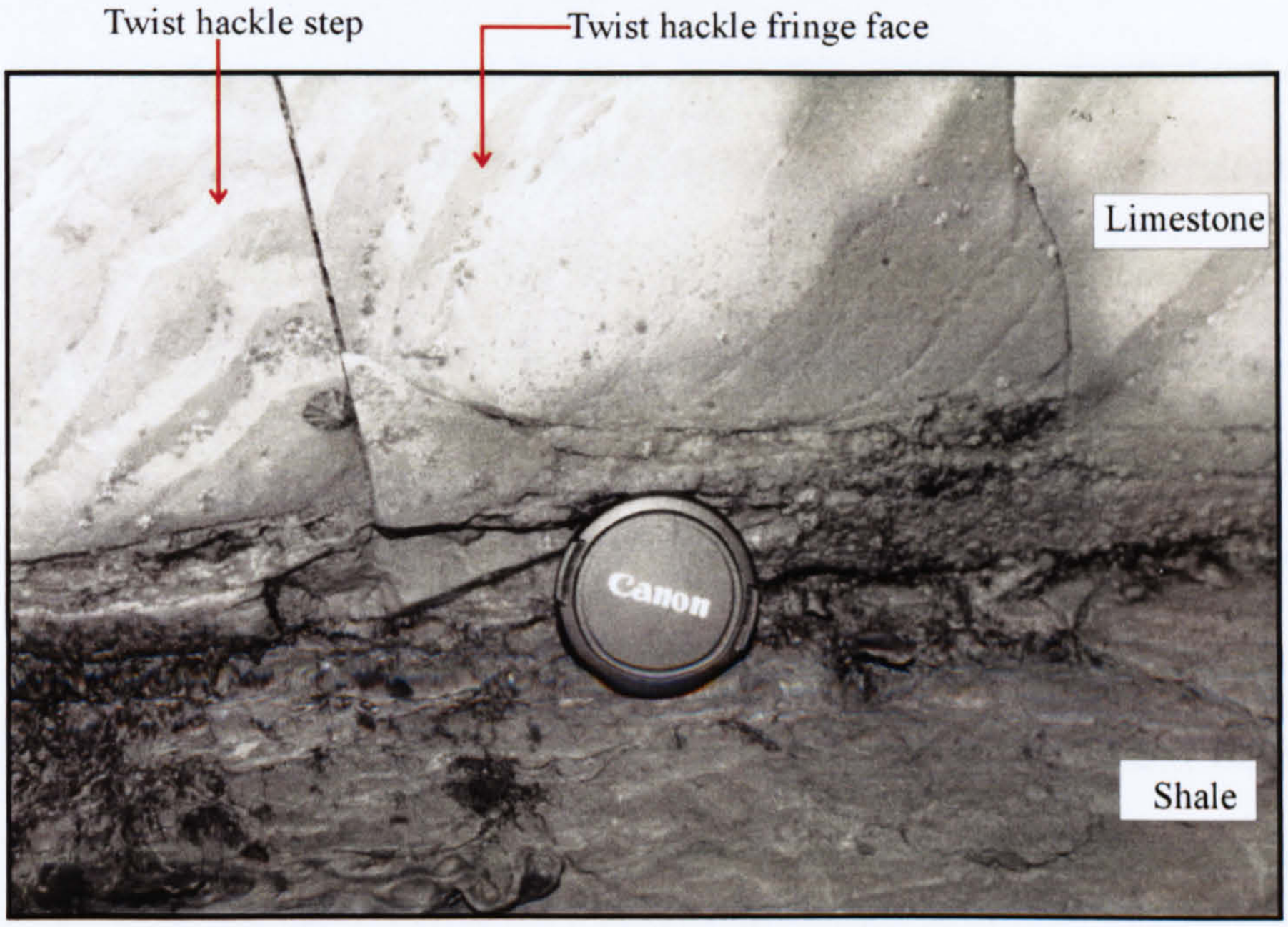
Field evidence presented by Younes and Engelder (1999), based on their study of the Ithaca Formation of the Genesee Group in the Finger Lakes area of New York State suggest that the competent beds (siltstones) fracture at an earlier time and shale beds later. The evidence gathered by me indicates that the Liassic succession of the Bristol Channel behaved in a similar way. Joints formed initially in the limestone beds and later linked to one another through the intervening shale beds. Based on the interaction between the joints in the shale and in the adjacent limestones, which show hook junctions and kinking similar to the abrupt fringes of Younes and Engelder (1999), it is argued that these joints are younger and propagated across the shale interfaces possibly during uplift. It is known from field observation and numerical models that joint propagation is often arrested at the boundary between a competent and an incompetent layer (see Al-Mahruqi, 2001). The joint becomes discontinuous across the shale layers and in addition it can be seen that the joints above and below the shale bed are not in the same plane (Heldgeson and Aydin, 1991).

Al-Mahruqi (2001) studied fracture propagation across a layered interface using the finite element method. He noted that the stress intensity factor (K), which is a measure of stress intensity at the crack tip within competent layer, increases as the fracture propagates from the centre of the layer until the fracture encounters the interface. He demonstrates that as soon as the fracture enters the incompetent layer, K drops sharply and becomes less than the critical value K_C needed to drive the fracture across the incompetent layer between the competent beds. The breakdown of the parent joint into a twist hackle fringe indicates misalignment between the consistently oriented N-S remote stress and the locally variable stress fields in the different competent limestone beds separated by shales. The crack path factor, (*i.e.* ratio of the stress intensity factor for mode II and mode I fracturing) increases as the fracture propagates from the centre of the limestone beds towards the bedding interface (Dov Bahat, personal communication). Bahat also argues that the middle of the limestone layer is subject to plane strain conditions (mode I) and the zone close to the bedding plane interface (twist hackle fringe zone) is mainly subject to mode II failure. The study of fringe zones gives an insight into (i) the possible modes of joint propagation and (ii) the interaction between the remote and local stresses.

The micro-veins or high-density veins of Rawnsley *et al.* (1998) between Lilstock and Kilve are sub-parallel to the basin bounding faults. They predate the normal faults and probably formed as a result of a rupture and seal process during diagenesis. The joints in the area are synchronous with the Alpine Orogeny. This is contrary to the interpretation of Rawnsley *et al.* (1998) who regard the joints in the area as post-dating other structures such as folds and faults.



(a)



(b)

Figure 5.15 *(a) planar view and (b) section view of twist hackle fringes on a 16cm thick limestone (Bed 2) at Lilstock. Note that the twist hackle fringes link by tip-to-plane intersections leaving a step on the major joint surfaces.*

Based on abutting relationships, it has been suggested by Rawnsley *et al.* (1998) that joints in the area were formed by an opening mode and provide evidence of an anticlockwise stress rotation. Although the right-stepping twist hackle fringes at Lilstock (Fig. 5.15) suggest anticlockwise stress rotation for joints whose strike is between 90° and 180°, nevertheless this conclusion is contradicted by a number of observations made in the study area: for example (i) most Alpine joints, with very few exceptions, strike approximately E-W. (ii) Left-stepping twist hackle fringes (clockwise sense of stress rotation) can be observed on parent joints striking between 0° and 090° which is not compatible with an anticlockwise sense of rotation of the stress field. In addition, Al-Mahruqi (2001) has described a local clockwise rotation of the stress field deduced from the chronology of joints at Lilstock, a fact confirmed by my observations at east Lilstock. (iii) E-W striking pressure solution cleavage post-dates the joint development in the area such as at Kilve, Blue Ben and East Quantoxhead (Fig. 5.16), suggesting that the remote maximum principal compressive stress was approximately N-S during inversion of the Bristol Channel Basin. (iv) I have observed N-S striking extensional veins at Kilve and East Quantoxhead postdating Alpine joints. In addition, strike-slip faults displacing the joints at Lilstock have been described by Al-Mahruqi (2001) and also observed by me at Kilve and Lilstock. (v) Chadwick (1993), in his study of the Wessex Basin, confirms that the mid-Tertiary compressive stress was approximately N-S. (vi) The joint set formed around the hinge zone of symmetric folds in the area (*e.g.* Kilve anticline) is consistent with the folding with outer arc extension during N-S compression. The second set that formed during uplift is associated with uplift (referred as post-Alpine joints in this work) and the process of their formation is discussed in section 4.5. The Alpine joints and post-Alpine joints in the hinge region of the folds display a characteristic ladder pattern. (vii)

Palaeo-stress determinations based on observations of fracture surface markings in the interbedded limestones and mudstones of Liassic age between Lavernock Point and Saint Mary's Well Bay at Penarth, South Wales, (Roberts, 1995) suggest that σ_1 was oriented approximately N-S at the time of joint propagation. Roberts (1995) deduced the stress from joint traces striking 010° (show anticlockwise sense) and 335° (show clockwise sense) and twist hackle fringes and concluded that σ_1 was approximately N-S during the propagation of both joints.



Figure 5.16 *Pressure solution cleavage striking approximately E-W and post-dating joint development in the area is evidence that the remote stress remained N-S during basin inversion. Pencil is aligned N-S.*

CHAPTER SIX

MODELS OF FLUID FLOW IN LIMESTONE USING REALISTIC JOINT NETWORKS

6.1 Introduction

In this chapter the way in which joints localise fluid flow in a fractured medium is investigated using the techniques of numerical modelling. Interest in the study of the conductivity of natural fractures has increased dramatically in recent years, mainly because of the need to increase production and efficiency of recovery from oil and gas wells and for risk assessments and engineering applications. Fractures are the primary water bearing openings in aquifers that govern fluid flow and transport in subsurface systems. Initial fractures may subsequently be altered by dissolution and/or mineralised. This may either have a positive or a negative effect on the permeability of a rock mass (Nelson, 1985). Thus, fractures may either enhance or obstruct permeability depending on their aperture, orientation and spatial organisation. This chapter examines fluid flow in connected joint networks using finite element/finite volume numerical modelling techniques in order to understand how the geometry of these natural fracture networks influences flow.

6.2 Overview of flow in porous and fractured media

Darcy (1856) carried out experiments on the movement of water through sands for filtering water. Darcy found that the rate of water flow or the discharge (Q) through the sediments is proportional to the difference in the height of the water columns called the hydraulic head (dh) and inversely proportional to the length of the flow path (dl). Darcy also determined the proportionality constant (K) that depends on the intrinsic properties

of the porous medium. Flow through a cross-section of area A can be expressed using Darcy's law as follows:

$$Q = -KA(dh/dl) \qquad (6.1)$$

The negative sign indicates that flow is in the direction of decreasing hydraulic head. For flow to occur in a medium there must be a hydraulic gradient. Darcy velocity or specific discharge (q) (sometimes designated as v) is given by the volumetric flow rate per unit area and is expressed as:

$$q = Q/A = -Kdh/dl \qquad (6.2)$$

Hydraulic conductivity (K) is obtained by:

$$K = -(Q/A)/(dh/dl) \qquad (6.3)$$

K is a function of both the property of the porous medium and the fluid passing through the medium. Typical ranges of intrinsic permeability k_i, (*i.e.* the permeability governed by the intrinsic properties of the rock) and hydraulic conductivity for unconsolidated sediments are shown in Table 6.1.

***Table 6.1** Range of intrinsic permeability and hydraulic conductivity for unconsolidated sediments (from Fetter, 2001).*

Material	Intrinsic permeability (dar)	Hydraulic conductivity (cm/s)
Clay	1.00e-06 - 1.00e-03	1.00e-09 - 1.00e-06
Silty, sandy silt, clayey sand and till	1.00e-03 - 1.00e-01	1.00e-06 - 1.00e-04
Silty sand, fine sand, well-sorted sand	1.00e-02 - 1	1.00e-05 - 1.00e-03
Glacial outwash	1 - 1.00e02	1.00e-03 - 1.00e-01
Well-sorted gravel	10 - 1.00e03	1.00e-02 - 1

The relationship between conductivity (K) and intrinsic permeability (k_i) is given by:

$$K = k_i (\gamma/\mu) \text{ or } K = k_i(\rho g/\mu) \qquad (6.4)$$

Where γ represents the specific weight (*i.e.* the force exerted by gravity on a unit volume of a fluid) and μ is its dynamic viscosity. Permeability is an intrinsic property of a porous medium that depends on the size of the interconnected pores.

6.2.1 The role of fluids during deformation: effective stress

The first important steps towards an understanding of the mechanical role of fluid pressure in the deformation of rocks were taken by Terzaghi (1923), who introduced the concept of *effective stress*. He showed experimentally that it is not the total stress resulting from the forces applied to a rock mass that controls its behaviour. Terzaghi argued, on the contrary, that there is an '*effective stress*', which he defined as the difference between the total confining stress and the pore pressure in the rock. These ideas were later developed by Hubbert and Rubey (1959) and Rubey and Hubbert (1959) to solve the mechanical problem of moving large overthrust blocks at geologically realistic stress levels. Their work showed that under sufficiently high fluid pressures, large blocks can be thrust over a nearly horizontal plane or can be moved down gentle slopes at stresses much lower than would be required in the absence of fluid pressure. They argued that interstitial fluid pressures greater than the lithostatic pressure exist in many parts of the Earth's crust such as the Basin of the Gulf Coast of Mexico. Here abnormal fluid pressure was caused by rapid burial and compaction of thick shale beds or mudstones. An essential step in their analysis was to argue that the fluid pressure in the rock pores opposed the overburden and tectonic stress and that the actual or effective stress available to deform the rock is given by:

$$\sigma_{eff} = \sigma - P \qquad (6.5)$$

where σ is the lithostatic stress, P the pore fluid pressure and σ_{eff} the effective stress respectively.

Joints abound in the crust despite the stress state generally being all three principal stresses are compressive. Secor (1965) considered this anomaly in the light of the fluid pressure ideas developed by Hubbert and Rubey (1959). He argued that the Griffith theory of extension failure, when expressed in terms of '*effective stress,*' should be the appropriate failure criterion for rocks and argued that extension fractures can develop at increasingly greater depths as the ratio of fluid pressure to the overburden pressure approaches one. Secor argued that an even hydrostatic fluid pressure distribution permits the development of tension fractures and concluded that previously formed fractures could be opened by fluid pressure, even at considerable depths in the Earth's crust, thus facilitating the migration of groundwater, hydrocarbons and the formation of ore deposits.

The effect of pore fluid pressure on the stress state in a rock can be illustrated graphically by representing the lithostathic and effective stress in a Mohr diagram (Fig. 6.1). The fluid pressure P counteracts the normal stress applied on any plane moving the Mohr stress circle to the left by an amount equal to the fluid pressure (P). If the circle comes into contact with the failure envelope, failure will occur. Such fluid pressure induced failure is known as hydraulic fracturing.

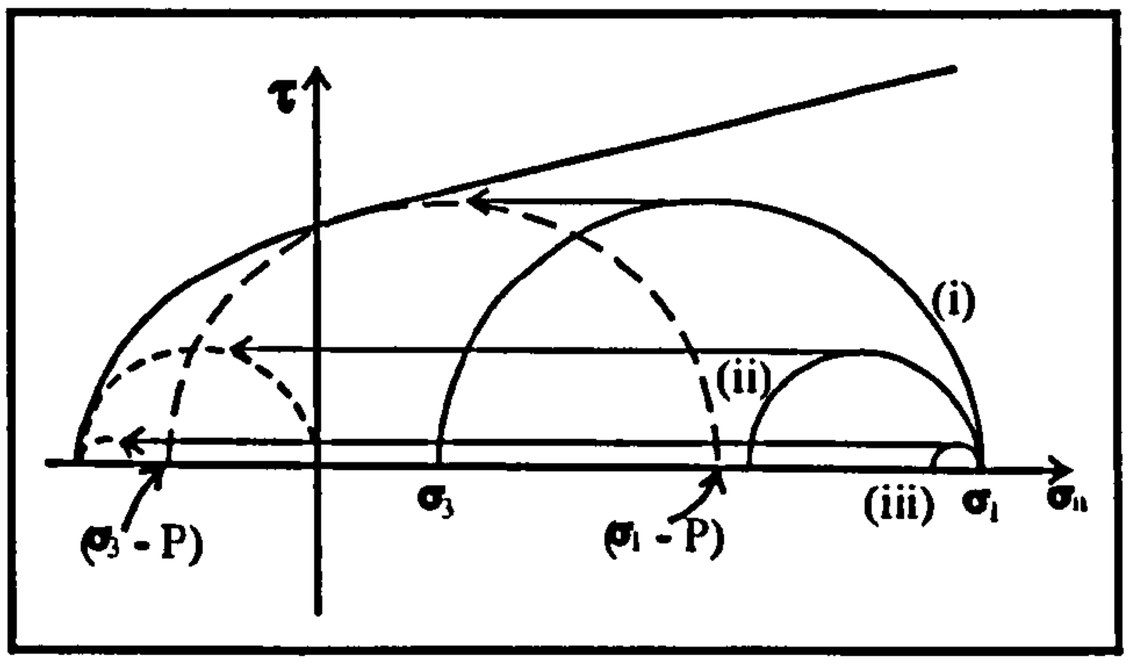


***Figure 6.1** The influence of an increase of fluid pressure on stable stress states represented by circles (i), (ii) and (iii) is to cause a shift to the left by an amount equal to P so that they touch the failure envelope (from Price and Cosgrove, 1990).*

Nelson (1985) asserts that both fracture permeability (k_f) and fracture porosity (ϕ_f) can be expressed as a function of fracture aperture (e) and fracture spacing (s). He argued that the combined effects of both fracture spacing and aperture will have a dramatic effect on fracture porosity and permeability. The shortcoming of this model is that the fractures are assumed to be planar and parallel sided and flow through the fractures is taken to obey a cubic law, which will be discussed later. However, Renshaw (1995) and Taylor *et al.* (1999) indicate that fractures are non-planar and non-parallel sided and it is therefore necessary to separate the 'mechanical' and 'hydraulic' aperture.

Renshaw (1995) showed how flow characteristics are strongly-controlled by the fracture apertures and argued that flow through rough-walled fractures is approximated by a cubic law as long as the concept of an '*average fracture aperture*' is used. Many studies however (*e.g.* Taylor *et al.*, 1999) indicate that flow through fractures occurs along preferential paths. These are the effective hydraulic apertures which comprise <30% of the mechanical aperture. For rough-walled joints, the 'hydraulic aperture' is the measure

of aperture that when used the cubic law produces the observed flow rate (Q) (Taylor *et al.*, 1999). The 'mechanical aperture' is the perpendicular distance between the opposing fracture surfaces. For perfectly planar joint walls, the mechanical and hydraulic apertures are the same.

The influence of fracture aperture on fluid flow has been extensively investigated using the steady-state solution of the Navier-Stokes equations for laminar viscous flow between two planar parallel plates (*see e.g.* Renshaw and Dadakis, 2000). For laminar flow through the fractures, the cubic law states that the volumetric flux (Q) is proportional to the hydraulic gradient (dh), fluid density (ρ), the dynamic viscosity (μ) and the cube of the hydraulic aperture b_h

$$Q = -b_h^3 \rho g dh / 12\mu \qquad (6.6)$$

where g is the acceleration due to gravity. For the cubic law to be valid, the fracture walls are assumed to be parallel and smooth. In rough-walled fractures where the aperture is variable, flow paths may be quite complex due to inertia (*i.e.* the fluid will follow a tortuous path).

As the fracture aperture decreases an increase in mechanical aperture does not necessarily increase the effective hydraulic aperture (Witherspoon *et al.* 1980 referenced in Renshaw 1995; Cook *et al.* 1990 referenced in USNCRM, 1996). According to these authors, fracture permeability decreases more rapidly than predicted by the cubic law in which the variable *b* (equation 6.6) is assigned the value of mechanical aperture. Witherspoon *et al.* (1980) from induced fracture in marble reported that there is a linear relationship between

hydraulic and mechanical apertures above a critical value of 0.007mm for the mechanical aperture.

Sanderson and Zhang (1999) investigated fluid flow in fractured rock masses using numerical modelling. In their work, three types of fracture networks are considered: (i) A network in which fractures are randomly oriented and therefore tend to define polygons. (ii) A network of two equally developed sets of regular fractures and (iii) a network consisting of one principal set and cross-joints. The results show that at low differential stresses and low fluid pressures, small openings and closures occur in almost all fractures and that flow is approximately uniformly distributed. For each fracture network geometry and loading scheme, they determined the critical stress state under which the fractured mass yields by slip on parts of the fracture and openings are generated at some of the intersections. Above the critical stress, flow is more localised within the network. Sanderson and Zhang conclude that the critical differential stress is dependent on the orientation of the principal stress with respect to the strike of the joints.

Taylor *et al.* (1999) demonstrate that complex joint patterns may either enhance or reduce flow depending on the geometric arrangement of fractures and the hydraulic properties of both joints and porous matrix. They argue that when the permeability ratio (k_r), defined as the ratio of joint permeability to matrix permeability, is < 3.0, all the joints are only connected indirectly and as a result considerable flow occurs through the matrix. Their work indicates that as joint conductivity increases, flow becomes more localised along the fractures and when k_r is greater than 6.5, flow is dominantly through the connected

fractures. They conclude that when the joint aperture is 2.3mm and when the permeability ratio is 5, 32% of the joints conduct significant volumes of fluid.

The study of the Mercia mudstones in North Somerset by Cosgrove (2001), shows that the formation of hydraulic fractures was controlled mainly by the magnitude of the differential stress and the intrinsic properties of the rock. Cosgrove suggests that various mechanisms account for the build-up of fluid pressure within the sedimentary succession. These include: (i) compaction of low permeability sediments during burial or during tectonism resulting in reduction of void volume and an accompanying increase in fluid pressure (ii) aquathermal pressuring due to phase changes involving dehydration during diagenesis, (iii) hydrocarbon generation and fluid flow. Cosgrove concludes that the main process for the build up of fluid pressure in the Mercia mudstone was compaction during diagenesis and tectonism.

6.3 Evidence of high fluid pressure in the Lower Lias of the Bristol Channel

The study area is situated on the southern margin of the Bristol Channel Basin. This rift basin formed by extensional failure of the Palaeozoic basement during the post-Variscan break up of Pangaea. The basin has a general E-W trend, is 155km long and 30km across from N to S. Basin opening was initiated in the Permian (Kamerling, 1979; Nemčok *et al.*, 1995; Rawnsley *et al.*, 1998) and rifting continued throughout the Jurassic with the formation of E-W striking normal faults (Nemčok and Gayer, 1996). The Bristol Channel region is an excellent area for studying the various folds, faults, joints and veins that formed during the evolution of a basin and for examining the role of fluids during both the extensional phase of basin opening during the Permian to Cretaceous, and basin

inversion during the Tertiary. As the basin opened, fluids were expelled from the accumulating sediments as a result of loading and diagenesis and vertical extensional calcite veins formed in the competent limestone beds. These are observed in the cliff sections in the vicinity of the listric normal faults and as tension gashes in the hinge zones of the rollover folds which form against these faults.

East of Lilstock (Fig. 4.23) some of the burial joints are filled by a limestone/mudstone mixture derived from the surrounding beds, providing strong evidence of soft sediment injection and therefore of the early age of these fractures. Extensional veins filled either by idiomorphic calcite crystals or fibrous calcite oriented normal to the burial joint walls have also been reported from the northern part of the Bristol Channel basin by Nemčok *et al.* (1995) and Nemčok and Gayer (1996). They argue that calcite-filled veins associated with normal faulting in the Lower Jurassic rocks indicate that fluid overpressure prevented these sediments from compacting until the end of the Early Jurassic, when rifting opened fractures that allowed fluids to escape. To support this idea they point out that the normally bed parallel fabric of the underlying shale is tightly "folded" into the base of the joints in the adjacent overlying limestone, suggesting that the cusp originated as soft sediment injection structures. Nemčok and Gayer estimated the vertical shortening caused by compaction using folded veins as strain markers and obtained shortening values between 50 and 75%. At Kilve, porosity caused by fracturing during rifting event was calculated to be up to 20.3%. The shale layers accommodated this stretching by ductile deformation without the formation of discrete visible planes. The limestone beds underwent a significant rotation about a horizontal axis and in some cases were separated into lozenge-shaped blocks (Nemčok and Gayer, 1996).

Nemčok and Gayer (1996) suggested that an array of bed-parallel décollements within the shale layers developed with the rollover fold forming as a result of layer parallel displacements. For example, at Rhoose in the northern part of the Bristol Channel Basin, they reported calcite growth by a crack-seal mechanism within these décollements and argued that this was possible evidence of multiple reactivations of slip. They describe extensional veins and Riedel shear arrays that have been rotated about a horizontal axis by approximately 30° towards the south in the southerly-dipping limb of a rollover anticline.



Figure 6.2 *7cm thick horizontal veins of vertical calcite fibres growing normal to the bedding plane at Kilve, suggesting a build up of high fluid pressure during the inversion of the basin. In this area, evidences have been found for normal faults serving as transient fluid channels during the whole history of the Bristol Channel. Note slivers of shale within calcite fibre vein.*

I found evidence that the pre-existing normal faults have served as transient fluid pathway during both the opening and inversion of the basin. At Kilve Beach, a 7cm thick horizontal composite vein consisting of fibrous calcite units with a direction of opening normal to the bedding surface was observed (Fig. 6.2). Slivers of the shale country rocks lie parallel to the veins, indicating multiple hydraulic fracturing events caused by episodic build up of fluid pressure leading to fracturing, injection and filling by the crack-seal mechanism of Ramsay (1980). These veins thin and die out when traced laterally away from the normal fault (Fig. 6.2) suggesting that the fault was the source of fluid pressure and was a major conduit for fluid flow during inversion.

6.4 Numerical modelling

As was briefly discussed in section 6.1 fluids are abundant in the Earth's crust. They occupy pores and fractures in aquifers and reservoirs and play a fundamental role in controlling various geological processes within the Earth's crust. Fractures frequently act as conduits that significantly determine fluid pathways in rocks. The joint patterns carefully mapped and photographed in the field were rectified to enable the construction of undistorted 2D joint trace maps (see section 1.3.2). Fluid flow through fractured rock masses has been modelled using the natural fracture patterns mapped in the two field areas *i.e.* north Yorkshire and the southern margin of the Bristol Channel coast. The numerical code used was written by Matthäi and Roberts (1996) and Roberts and Matthäi (1996). Before the behaviour of the fracture systems sampled in individual 'windows' from the two study areas are described, it is necessary to discuss the steps, methodology and the numerical method used in the investigation.

To address the influence of joints in localising flow, a combination of finite element and finite volume numerical simulations were carried out by the present author using the Complex Systems Platform (CSP) (Geiger *et al.*, 2001; Matthäi *et al.*, 2001). The simulations presented employ an implicit for pressure and explicit for saturation approximation (IMPES) (Helmig, 1997; Geiger *et al.*, 2001). In this method, fluid pressure is computed using the finite element method by solving the partial differential equation (PDE) (equation 6.7) at the nodes. The interstitial velocities and saturation are then extrapolated explicitly from the pressure using the finite volume method via Darcy's Law based on mass balance of the fluid phase(s). Application of the finite element methods requires:

(i) The discretization of a continuous geometrical domain, such as a fractured limestone beds in the Bristol Channel, into a finite number of sub-domains (finite elements) connected to each other at specified points (nodes).

(ii) The identification of a set of physical variables such as porosity and permeability that represent the properties in the real domain.

(iii) A knowledge of the spatial and temporal coupling mechanisms that relate dependent variables.

(iv) The equations describing the interrelations between the variables. The PDE for steady state analysis based on conservation of volume is given by:

$$\nabla u = Q \qquad (6.7)$$

where u is the source term for incompressible to slightly compressible fluids and Q is flux. Using Darcy's Law, equation 6.7 can be written as:

$$\nabla(k/\mu\nabla P) = k/\mu\nabla^2 P = Q \qquad (6.8)$$

where P, k, μ and Q are fluid pressure gradient, permeability, dynamic viscosity and flux respectively.

(v) The setting of essential and initial values including time of computation.

(vi) Outputs (described under sections 6.4.1.3 and 6.4.1.4) that are retrieved in the form of pressure distribution maps (pressure contours), output to JPEG file formats, velocity histograms and charts.

A detailed discussion of the algorithms used in each code is given by Matthäi *et al.* (2001) and Geiger *et al.* (2001 and references therein).

6.4.1 Methodology

As the initial step, 2D joint trace maps of the bedding planes are saved in 'CorelDraw' or some other graphics package. This file is saved in 'AutoCad' as **my file.dxf** or in 'Adobe Illustrator' as **my file.ai**. These are then imported to the Rhinoceros2.0™ commercial software package. In the 'properties' dialogue box, initial settings are set before proceeding to the next step. Unless otherwise stated, all measurements are in SI units.

(i) **Model units** in metres

(ii) **Absolute tolerance** (0.0001) in metres is one order of magnitude smaller than the smallest feature in the model. The smallest feature in the model is 1mm by default.

(iii) **Relative tolerance** (0.01) is the ratio of the smallest to the largest feature expressed as a percentage. If the largest and smallest features in the model have magnitudes of 10m and 0.001m, the relative tolerance will be 0.01.

(iv) **Angle tolerance** is set to 0.01 determining the quality of the meshes used.

The **'grid spacing'** dialogue box shows **snap spacing, grid spacing, major lines every,** and **grid extents.** These properties are dependent on the size of the 2D map under consideration. After setting the above properties, the joint/fracture trace maps can be imported to Rhinoceros. Converting to the required scale is achieved by clicking on the **transform** dialogue box and then selecting **scale 2D.** The lower left co-ordinates in all models start at the origin (0, 0) and extend up and to the right.

To assign an aperture for each joint trace map, each joint has to be offset by the magnitude of the joint aperture (*e.g.* 0.003 and 0.005m for Alpine and post Alpine joints in the Bristol Channel). Joint aperture is the distance measured perpendicular to the plane between the opposite walls of a joint. Joint surfaces are far from being planar and the distance between the two varies along the fracture. The boundary object that bounds the fracture trace map on the **default layer** is carefully redrawn. The fracture traces are drawn as poly-lines. The poly-lines in the middle of the model are closed poly-lines whereas the ones adjoining the boundary object are open. All points along the boundary lines intersecting the boundary object should be precisely snapped.

On a different drawing layer, each region has to be defined by material points. Each fracture bounded block is bounded by a poly-line defined by material points with co-ordinates (x,y) in the 2D plane and (x,y,z) in 3D space. These points serve to uniquely identify fracture bounded blocks (matrix) and fractures within the model, as shown in Table 6.2. The assignment of the material points shown in Table 6.2 can be done using Microsoft Excel and saved as a tab-delimited text document.

Table 6.2 Material points assigned to joints and joint bounded blocks (matrix).

1	x_1	y_1	z_1	k_1	A_1 (all columns are tab-delimited)
2	x_2	y_2	z_2	k_2	A_2
.	.	.	.	.	.
.	.	.	.	.	.
n	x_n	y_n	z_n	k_n	A_n

where n represents the number of the material point within the model. The first column is a positive integer ranging from 1 to n allocated to each data point, the second to the fourth column represent the position in the 2D plane or 3D space, the fifth column represents permeability and the last column is the maximum area of the largest finite element allowed in the mesh of this region of the finite element model. Because of their different sizes, fractures and matrix will have different mesh sizes. This adaptation to size gives a unique possibility of representing and analysing the smallest features in the model. In this model, joints and matrix have permeability (k) values of 1.00e-12m^2 and 1.00e-15m^2 respectively. If the joints are interconnected, a single value of permeability will define the property of the network. To distinguish each block so that it can later be addressed individually, permeability variation of 1.00e-10m^2 has been added in order to simulate a realistic variation of permeability that would be found in rocks. This artificially enhances the permeability and enables the variations encountered in naturally fractured rock masses to be represented. In this work the specified apertures are large enough to ensure that joint permeability is always greater than the permeability of the matrix unless otherwise stated. The complete view of the joint trace map drawn using Rhinoceros commercial software with the material points assigned is shown in Fig. 6.3.

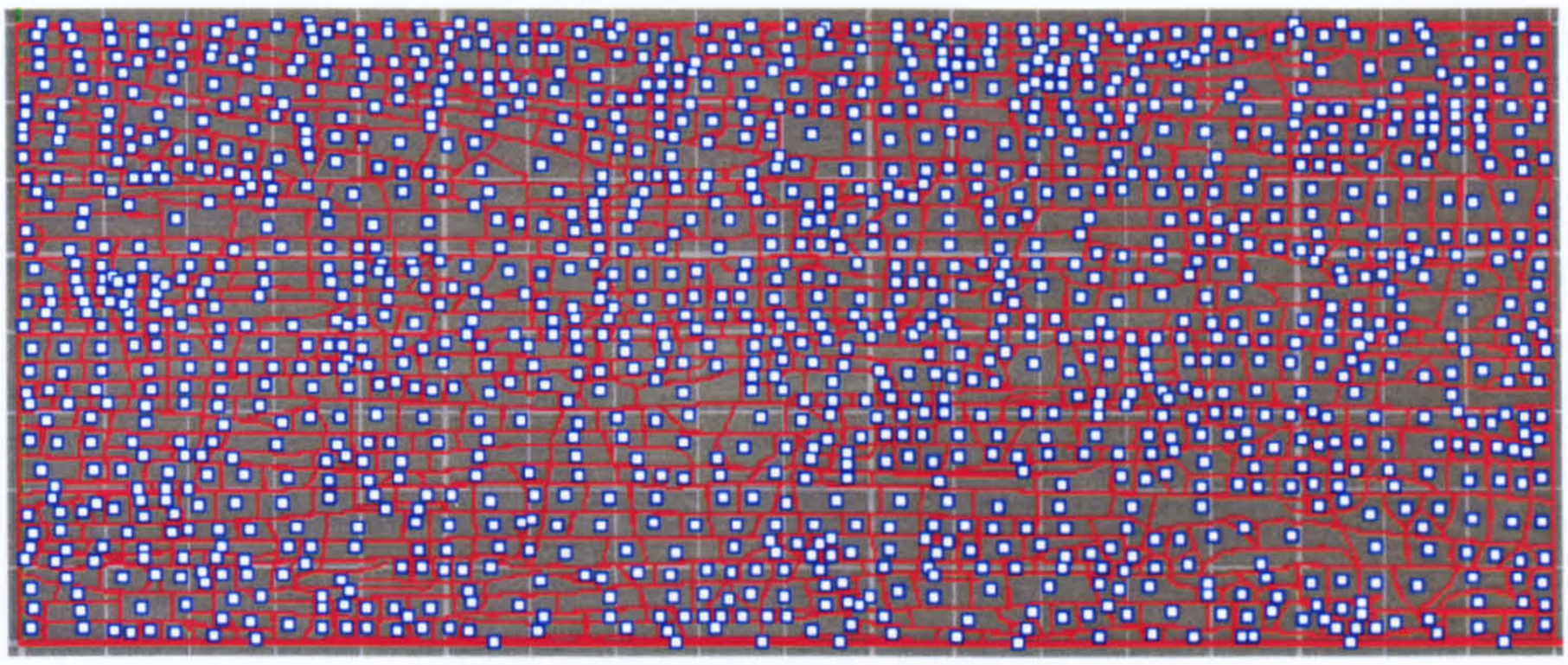


Figure 6.3 *The joint trace map from the lowest bed on the trailing limb of the Lilstock rollover anticline (Fig. 4.27). Red lines are traces of joints with apertures of 0.003 and 0.005m for Alpine and post Alpine joints respectively. Blue squares represent material points defined by fracture-bounded blocks. In the model 1369 material points, 1375 curves and 23,579 curve points are depicted. White lines indicate metre grids.*

The default layer is saved in 'Rhinoceros' as **my file.3dm** and **my file.dxf** in AutoCad release 12. The dialogue box appears and the settings **entities only, polyline maximum angle** (0.01), **polyline chord height** (0.001) and **polyline segment length** are selected. The layer containing the material points will be saved as **my file.csv** and then the extension converted to **my file.txt**.

6.4.1.1 Run a GeometryPreprocessor .exe program.

This program is an input file for triangleMesher and helps to identify faulty input geometries such as those violating the angle limit of 20°, which will be discussed section 6.4.1.2. To run this command, type 1 and press enter. **Main: enter the name of the dxf file**: type the file name without the extension and press enter. **Please enter the number of the drawing layers to be read from file**: type 1 and press enter. **Please enter the name of the desired layer**: type **DEFAULT** all in upper case letters. This program reads

polygon(s) and lines from **AutoCad.dxf** format and converts polylines to triangleMesher input such as **my file.poly** and **my file.vtk** files. Open **my file.poly** and type the number of material points described in Table 6.2 and type 1 separated by a tab. Then copy and paste the five columns from Microsoft Excel saved as tab delimited ***.txt** format from Table 6.2 in **my file.poly** created by the GeometricPreprocessor.exe program.

6.4.1.2 triangleMesher (window)

Go to (change directory) the directory where the triangle mesher is located and type **csp-etc\meshing\triangleMesher -aAnepCVq20. my file.poly**. The combination of letters signifies a range of options available through -help. The number 20 denotes the minimum angle criterion in the triangle mesh (*i.e.* that the angle between two poly-lines within the mesh should be greater than or equal to 20). The mesher creates five output files with the extensions ***.1.poly, *.1.ele, *.1.node, *.1.neigh** and ***.1.edge**. The maximum number of points, triangles, segments, encroached segments and bad triangles will be displayed on the screen. In the example shown (Fig. 6.3) 623,975 nodes, 1,897,141 segment faces and 1,264,167 triangles are allocated. In addition to this information the mesher shows the minimum area of individual triangles in the mesh which should be greater than 1.00e-06 in this analysis.

6.4.1.3 Run CSP3D_Mesh_to_VTK.exe

Type **my file.1** without extension. In this analysis the main element width range, element area range and model dimensions (x,y) 0-x and 0-y in metres will be displayed on the screen. The program checks the existing files and creates the files **mesh0.vtk** and **log10-permeability-node.vtk** which will later be displayed in the viewing directory. It also shows

SMALL_ELEMENTS-mesh.vtk when the areas of the finite elements are less than or equal to 1.00e-06 and **ZERO_ELEMENTS_mesh.vtk** when there are regions in which material points are absent. Small elements will be created if extremely small regions (less than the value in the default) accidentally exist in the model or when the poly-lines (traces of joints) are not properly snapped to boundaries in 'Rhinoceros'. Before proceeding to the next step, regions with no material point should be assigned one, and small areas need to be removed. The mesh can be displayed by copying and pasting **mesh0.vtk** and **log10-permeability-node.vtk** files into the VTK examples directory as shown in Fig. 6.4.

Compared to the 'finite grid difference methods' in which all objects are discretized with equal resolution, the unstructured grids of the combined finite element and finite volume methods have the advantage of flexibility in grid size and are therefore capable of representing the smallest features, such as fractures, reasonably well (Fig. 6.5). In finite difference methods, the properties of the material are assumed to be continuous and uniform. A continuous material within the model can be represented as a set of discrete points arranged as an equally spaced grid. The unknown variables in the equation are solved at the nodes. Associated with each node or block are the known values. There are two types of nodal representations: (i) '*block centred grid*' where the nodes are placed at the centre of the grid and (ii) '*mesh centred grid*' where the nodes are placed at the intersection of the grids. The finite difference method is commonly employed in hydrogeology where mesh- and grid-centred methods are most convenient in situations where head and flux are specified respectively (Fetter, 2001). The grid is regular with the rows and columns representing small increments in x (*i.e.* Δx) and y (*i.e.* Δy) directions respectively from the reference point.

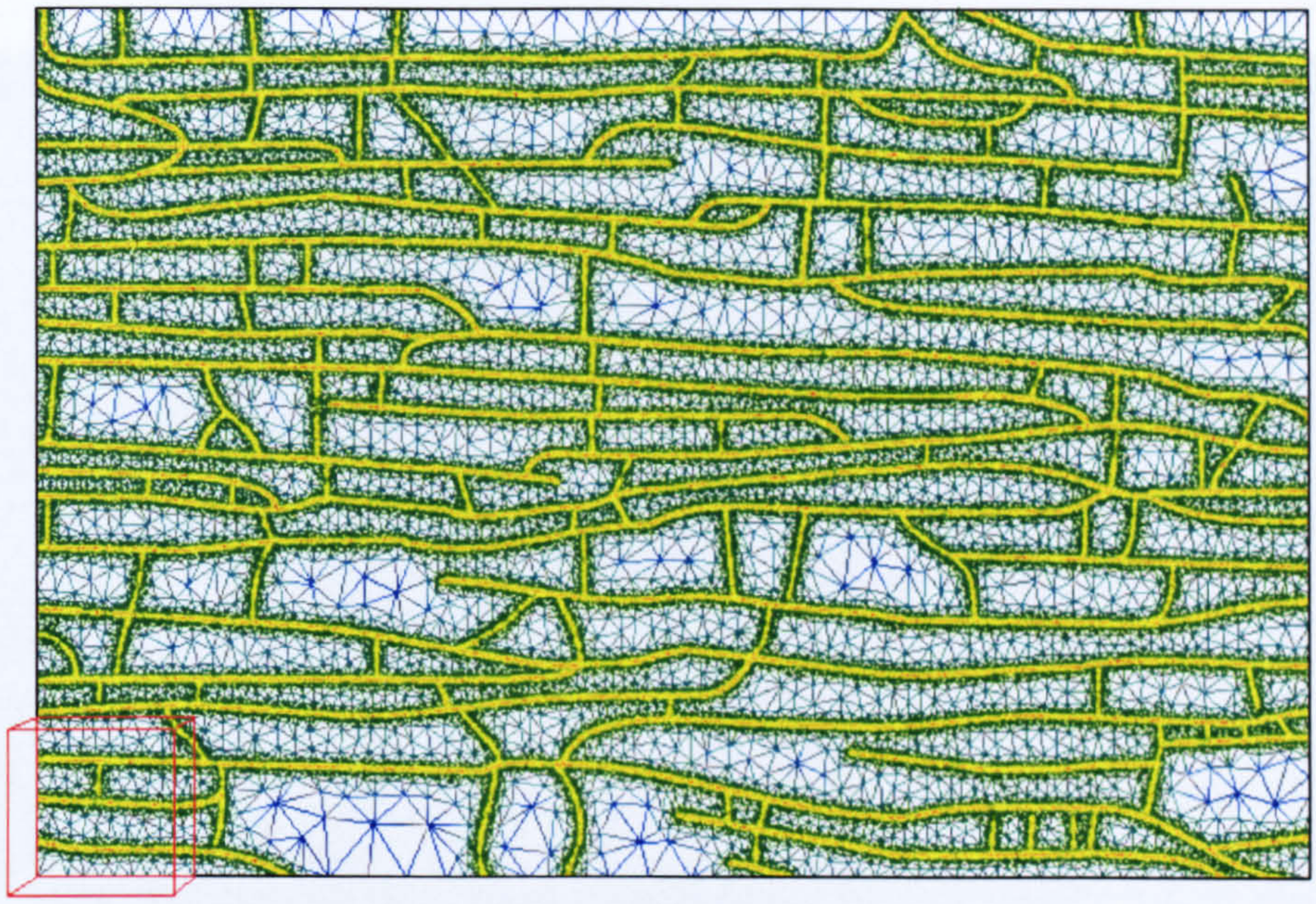


Figure 6.4 *Example of a triangular mesh of fractured limestone at Kilve. In contrast to the 'finite difference grid methods' based on uniform grids, in the smallest regions of the model the mesh is very fine so that joints are adequately represented.*

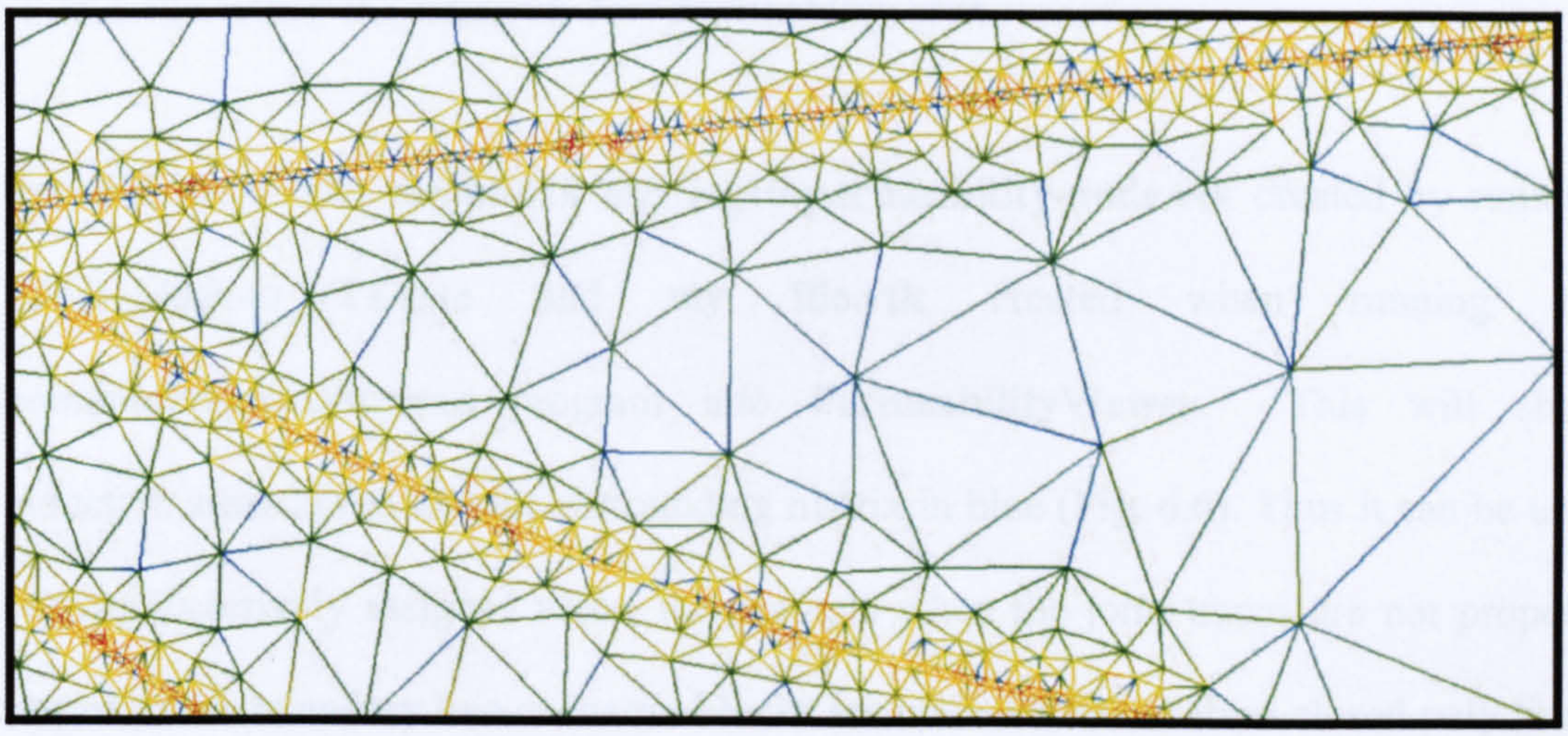


Figure 6.5 *An enlargement of the lower right hand corner of Figure 6.3. The two lines represent joint traces projected onto a horizontal plane. The highly variable size of triangles inside the fractures and within the surrounding matrix enables fractures to be represented with adequate resolution.*

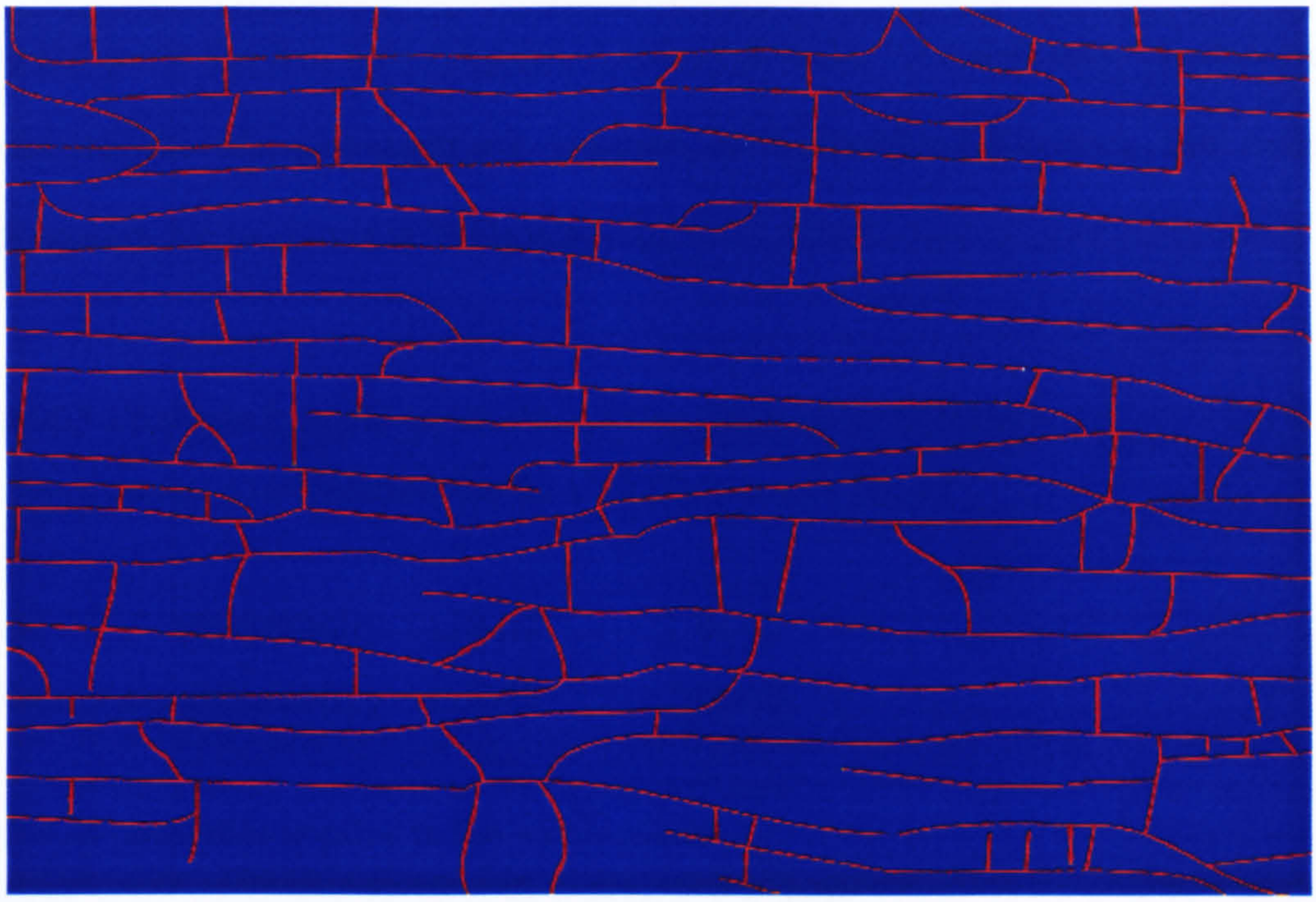


Figure 6.6 *Interconnected networks of joints from the hinge zone of the Kilve fold viewed in 'PermeabilityViewer'. The red colour shows high conductivity (i.e. along the fracture) and blue represents the relatively low permeability of the matrix.*

Copy and paste both **mesh0.vtk** and **log10-permeability-node.vtk** created by running CSP3D_Mesh-to_VTK.exe and **my file.vtk** created when running the GeometricPreprocessor.exe program into **PermeabilityViewer.** This will show conductive areas in red and the surrounding matrix in blue (Fig. 6.6). Thus it can be used to detect incorrectly assigned areas, for example when the joint traces are not properly snapped to the boundary line or matrix blocks are not constructed from closed poly lines. In the latter case, the model will flood with red indicating that the matrix has the same permeability as the fractures.

6.4.1.4 Run CSP3D_linear_flow_analysis.exe

Copy and paste the five files ***.1.poly, *.1.ele, *.1.node, *.1.neigh** and ***.1.edge** created by running the triangleMesher.exe program in the working directory and write the configuration file as shown in Table 6.3.

Table 6.3 Configuration file for the linear flow analysis in CSP3D.

'my file.1' model configuration file for CSP3D example file set

joints	permeability	1.0e-12	1.0e-12
matrix	permeability	1.0e-15	1.0e-15

# material properties applied to the whole model				
porosity			0.25	
storativity			1.0e-9	
fluid volume source			0.0	
fluid pressure			0.0	
# property assignment to model subregions				
joints	complete	porosity	1.0	
joints	complete	permeability	1.0e-9	
# global essential conditions (in this case boundary conditions)				
LEFT	Dirichlet	fluid pressure	1.0e+7	1.0e+7
RIGHT	Dirichlet	fluid pressure	0.0e+0	0.0e+0

CSP3D_linear_flow_analysis.exe reads ***.1.node, *.1.ele, *.1.neigh** and this configuration file displays the properties of the model described in Table 6.3. The permeability at each nodal point, each finite element and neighbouring elements will be

computed. The user will then be prompted to indicate whether he/she (i) requires the output in the form of JPEG images of the pressure and velocity distribution or (ii) if the user would like to group integral by group volume or if he/she (iii) would like to vary permeability in a single group or if he/she (iv) would like to model transient flow.

The output from the linear flow analysis is a series of files for the visualisation toolkit (VTK, Kitware.com) such as **fluid-pressure0.vtk, nvelocity0.vtk, nvolume-flux0.vtk, volume-flux0.vtk, velocity0.vtk,** CSP-monitored regions in text format, and a flow velocity histogram for the model. **Fluid-pressure0.vtk** depicts the pressure distribution within the model for a given far-field pressure. The output file **velocity** shows the fluid flow velocity in the finite elements and **nvolume flux** shows the nodal volume flux within the model. Flux is extrapolated to the nodes so that it can be visualised using rainbow colour shading. **Flux_histogram.bins** creates **joints-volume_flux.txt** and **matrix-volume_flux.txt** which are the velocities of fluid within the joints and matrix repectively, computed as a range of normalised frequency versus velocity (as class intervals) which will later be opened with Microsoft Excel™ or notepad. The results can be plotted as histograms to determine the characteristic velocity of fluid flow either within the joints or within the matrix.

A hydrostatic far-field fluid pressure gradient has been assigned to the models in order to give flow velocities a physical meaning. A fixed (Dirichlet) fluid pressure is applied on the two opposing edges of the model. The other two edges are treated as no flow boundaries. In the model, this makes the fractures impermeable on the no-flow boundary region.

6.5 Validation of FE/FV numerical models

To verify the simulation, the same pressure was applied to the model where the fractures and the matrix were assigned the same permeability i.e. the model was assumed to have a uniform permeability. The velocity displayed on the screen during computation for Fig. 6.15 is 6.129e-09ms^{-1}. The specific discharge (q) over a distance can be computed from:

$$q = k/\mu \nabla P \qquad (6.9)$$

where μ is the dynamic fluid viscosity (1.6e-03), k is the permeability within the model (1.0e-15m^2) and ∇P is the pressure gradient. The fluid density (ρ) = 1000kgm^{-3}, g = 9.80665ms^{-2} and the horizontal distance (z) is 1m. As noted in section 6.2, the Darcy velocity derived using equation 6.2 is 6.129e-09ms^{-1}. Values obtained in the numerical analysis were identical to those obtained by using equation 6.9, thus validating the numerical analysis. In addition, the numerical code has already been used by Matthäi and Roberts (1996) to study flow across faults and by Taylor *et al.* (1999) to examine alteration haloes around joints now exposed at the Earth's surface.

In the following sections, the results of the CSP numerical simulations for realistic joint networks are presented. This includes pressure distribution maps, pressure contours and normalised fluid velocity histograms for both the matrix and the joints. The majority of the results presented are for models from the southern margin of the Bristol Channel and only one example is taken from North Yorkshire (section 6.6.1). These systems show dual porosity with unfilled joints (ϕ_j = 1.0) and the pore spaces of the matrix (ϕ_m = 0.25). The joints from the Bristol Channel fall into two categories: Alpine joints with apertures of 0.003m and post-Alpine joints with apertures of 0.005m. The bulk porosity based on the

contribution of both matrix and joints is approximately 0.25 in the Bristol Channel. In the area of North Yorkshire that was studied, the joints were all assigned a uniform aperture of 0.005m. The values of the porosity for the rock and the joints are approximately the same as on the southern margin of the Bristol Channel.

The detailed study of the natural fracture networks from the Bristol Channel and Yorkshire and the estimation of the joint aperture and bulk porosity of the system enables fluid flow and hydrologic properties of these networks to be modelled (the procedures are described in section 6.4.1.4). In the majority of the illustrations, the far-field fluid pressure gradient is applied from left to right; high pressure is represented by red and low is blue. Exceptions occurred when the dominant joints were oriented at a high angle to this pressure gradient or when the 'windows' were too narrow (*e.g.* Figs. 6.24 and 6.36).

6.6 Results of the simulation

6.6.1 North Yorkshire

The geometry and spatial organisation of fracture networks in the Carboniferous Limestone of North Yorkshire are discussed in detail in section 4.3. In order to determine the effect of this network on fluid flow, a square window of 225m^2 was constructed from rectified field photographs taken in the Ingleton area and this is shown in Fig. 6.7. The fractures are generally through-going, dominated by long NNW-SSE to NW-SE and short ENE-WSW to NE-SW striking joints. N-S and E-W joints are subordinate. The total length of joints within the window is 465.33m and the average fracture density (defined as length of fractures over area of window) is 2.1m^{-1}.

A fluid pressure gradient was applied across the 'window' with a high value at the top and a low value at the bottom. The result of fluid flow simulation across this fracture network is shown in Fig. 6.7. It can be seen that there are fractures in the right-hand side that extend from the top boundary of the map almost to the lower right corner. In contrast there are no similar long fractures on the left hand side of the map. On the right hand side the flow profile is considerably more advanced than on the left hand side.

The joints have been assigned a relatively large aperture and therefore act as channels selectively governing flow. This fact, combined with the relatively long length of the joints and their orientation with respect to pressure gradient results in a large perturbation of the flow regime. The resulting spectrum of velocities is shown in the histogram in Fig. 6.8.

The model consists of numerous finite elements, some representing the fractures and others the rock matrix. The output from the analysis includes the flow velocity in each element and these are represented on the histogram in Fig. 6.8. The difference in flow velocity in the fracture and matrix is apparent from this figure.

In the remaining part of this chapter the author presents some of the results of the numerical analyses of flow pattern through several of the natural fracture networks measured by the author and discussed in this thesis (sections 4.4.2 to 4.4.7). For each study the fracture networks and the results of the analyses are presented (i) as pressure distribution maps which also show the fracture network and the direction of pressure gradient during fluid flow and (ii) as a histogram of flow velocities (*e.g.* Figs. 6.7 and 6.8). After presenting the results of each study an attempt is made to relate the pattern of

flow velocity histograms to the properties of the fracture network and to the fluid transfer between the fracture and the surrounding rock.

It can be seen from Fig. 6.8 that the normalised velocity histogram for the matrix has a long tail of low values whereas that for the joints is skewed to the right *i.e.* towards high values. In addition the two groups of data that relate to flow in the matrix and fractures are made up of subpopulations with different average values. Interpretation of these statistical distributions is not straightforward.

The results show that in porous, fractured rock, one cannot expect the fluid to flow with the same velocity throughout the fracture network. There is a clear separation between the flow regime in the fracture and that in the matrix where, not surprisingly, flow velocities are much lower. As noted above the two groups of data on the histogram are made up of subpopulations and one way of interpreting departures from the mean is by separating the distribution into different populations each with its own mean and standard deviation. From the velocity histogram for the joints, three superimposed populations can be recognised. This may reflect flow within the three sets of joints, most apparently oriented with respect to the pressure gradient. These are striking ENE-WSW, the set striking NNW-SSE and the set striking WNW-ESE. Note that the north arrow is oblique to the boundary of the window.

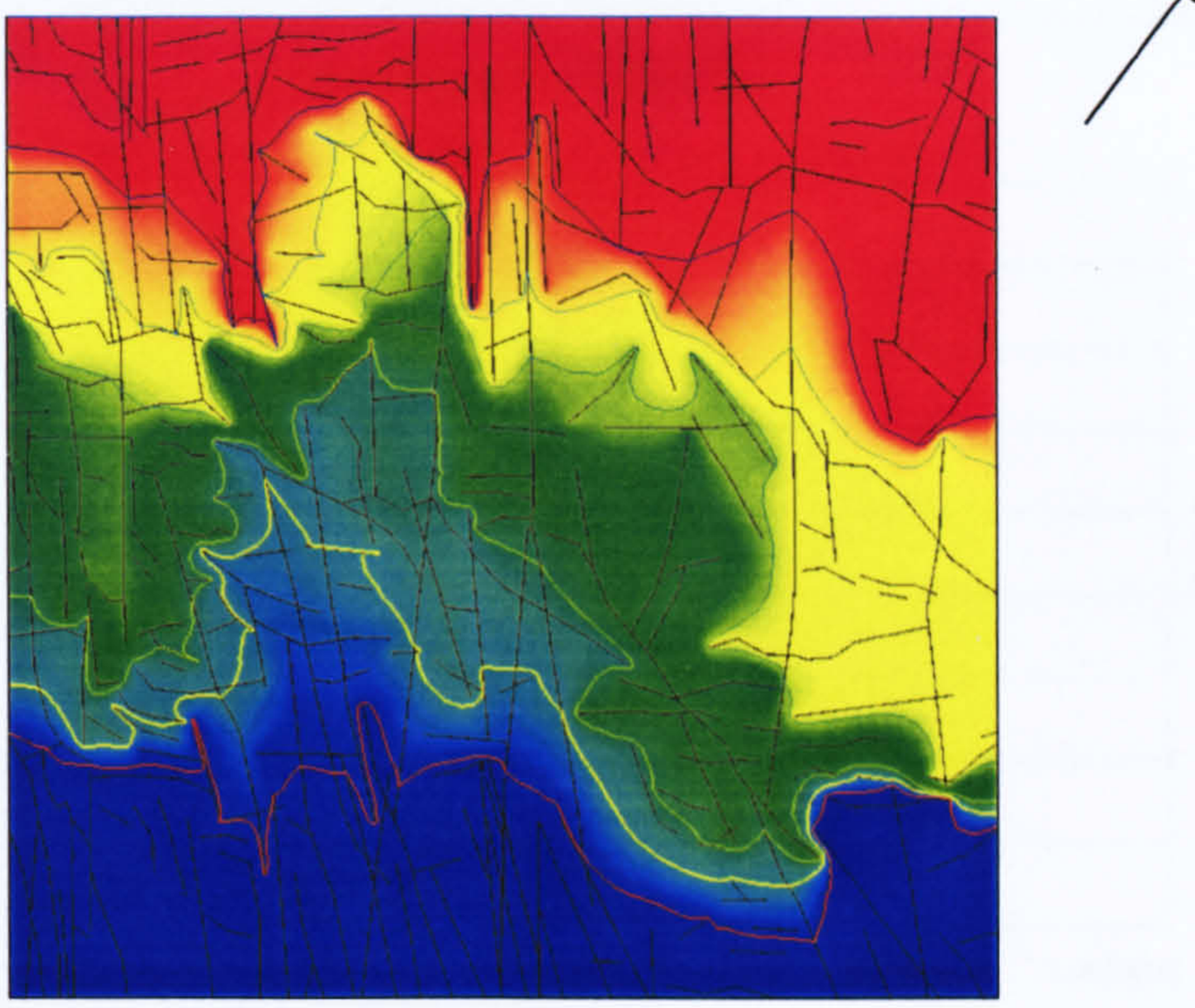


Figure 6.7 *Pressure distribution map in a model of fractured Carboniferous Limestone from Ingleton. Note that the pressure contours are strongly perturbed around long and systematic joints. Pressure distribution in rainbow colour scheme shows red for high and blue for low. Arrow indicates north.*

The two histograms in Fig. 6.8 overlap. In this region of overlap the fluid velocities in the matrix and joints are comparable. This reduction of fluid velocity in the fracture and increase in the matrix is related to the phenomenon of enhanced velocity within the matrix where flow converges into a joint. A reduced fluid velocity within some of the joints is probably caused by their unfavourable orientation *i.e.* when they lie at a high angle to the applied far-field fluid pressure gradient. This has been discussed by Taylor *et al.* (1999) who point out that the geometric arrangement of joints creates regions of enhanced and reduced fluid flow.

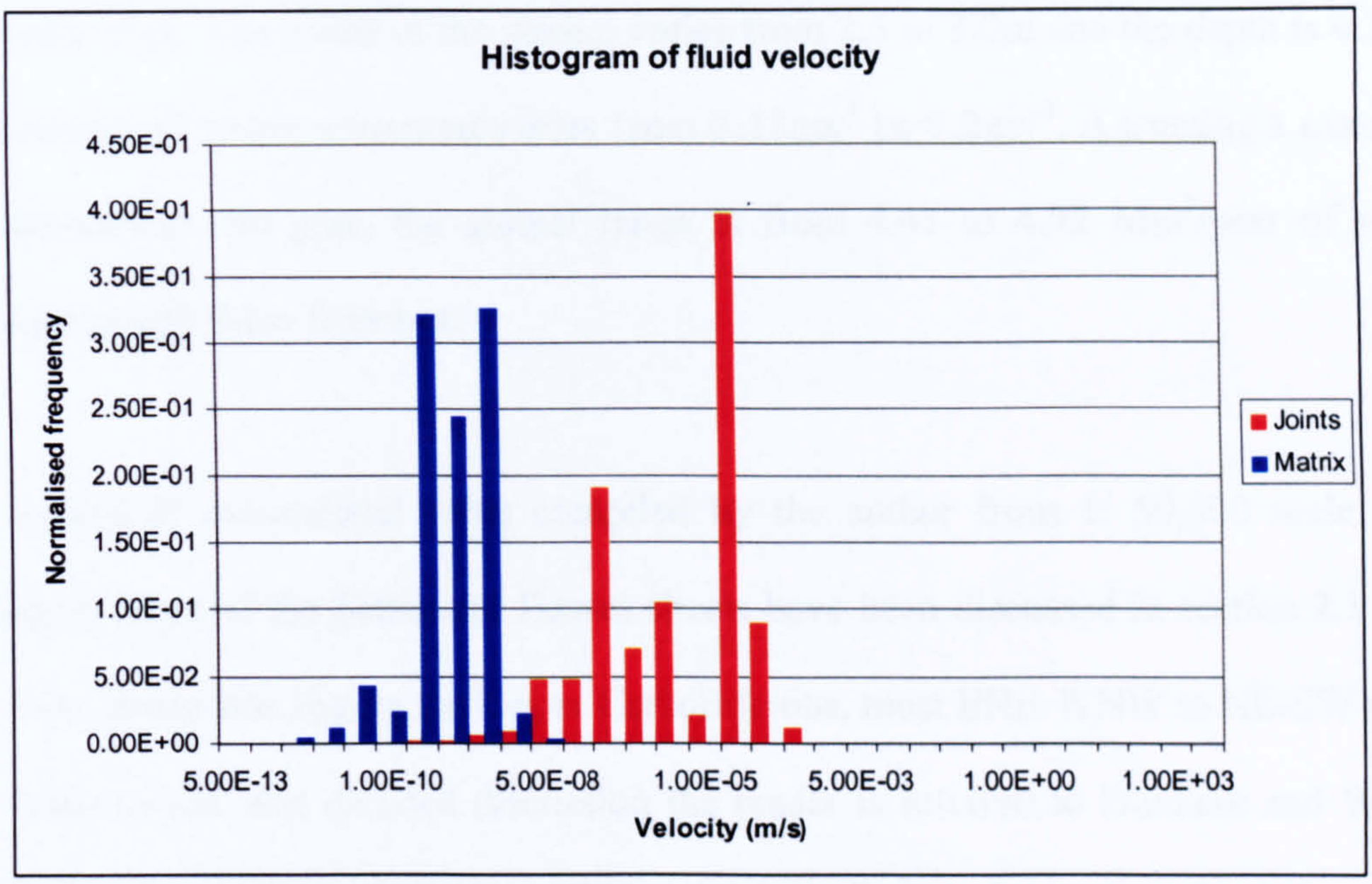


Figure 6.8 *Histogram of normalised fluid velocity within the fractures and matrix from massive bedded limestone beds at Ingleton shown in Fig. 6.7.*

In addition to studying flow through natural fracture networks using the numerical code, I have also examined flow in the field. A small lake, Malham Tarn, discharges into fractures in the Carboniferous Limestone before emerging 3 km SSE at Malham Cove. The water flows subsurface for 3km along the fracture network exploiting one of the major fracture sets. An attempt was made to estimate the fluid flow along the fracture set by measuring the volume of flow where the stream emerges at Malham Cove.

Water flowing in a stream is subject to friction at its contact with the river bank and to wind resistance at the surface. Many field studies have shown that the flow velocity at a depth of 0.6 times the total depth is close to the average velocity (Fetter, 2001). To obtain an estimate of how much water is flowing through the fractures, (*i.e.* recharging the stream) a straight portion of stream with a fairly smooth bank was chosen to estimate the

volumetric flux. The width of the stream varies from 2.5 to 3.0m and the depth is 0.30m. The velocity of water measured varies from 0.13ms^{-1} to 0.2ms^{-1}. Assuming a constant flux throughout the year, the annual range is from 4.41 to 4.92 Mm^3/year of water gushing through these fractures.

The pattern of mineralised veins compiled by the author from 1: 50,000 scale BGS geological maps of the Settle and Hawes sheets have been discussed in section 2.1 (Fig. 6.9). This shows that during the Upper Carboniferous, most ENE-WNW to NE-SW joints were mineralised. For detailed discussion the reader is referred to Dunham and Wilson (1985). In contrast the contribution of these joints to flow at the present day is low. This means that joints that were conductive during the period of Upper Carboniferous mineralisation have changed their hydrologic properties. This may be explained by (i) mineralisation along the fractures, which reduced permeability (ii) the removal of supporting asperities from the fracture walls by pressure solution resulting in loss of permeability, or (iii) a change in the stress fields so that the maximum principal stress (σ_1) is now at a high angle to the fractures thus reducing their permeability. In their detailed study of mineralization in Yorkshire, Dunham and Wilson (1985) argued that joints with small displacements provided the most effective channels for circulation of mineralising fluids (Fig. 6.9).

As discussed above, flow is now highly focused along the NW-SE fractures. This focusing of flow along the dominant joint set at Malham Cove is compatible with the results of the simulation shown in Fig. 6.7. This shows the rapid propagation of the pressure front along the NW-SE joints in the Ingleton area.

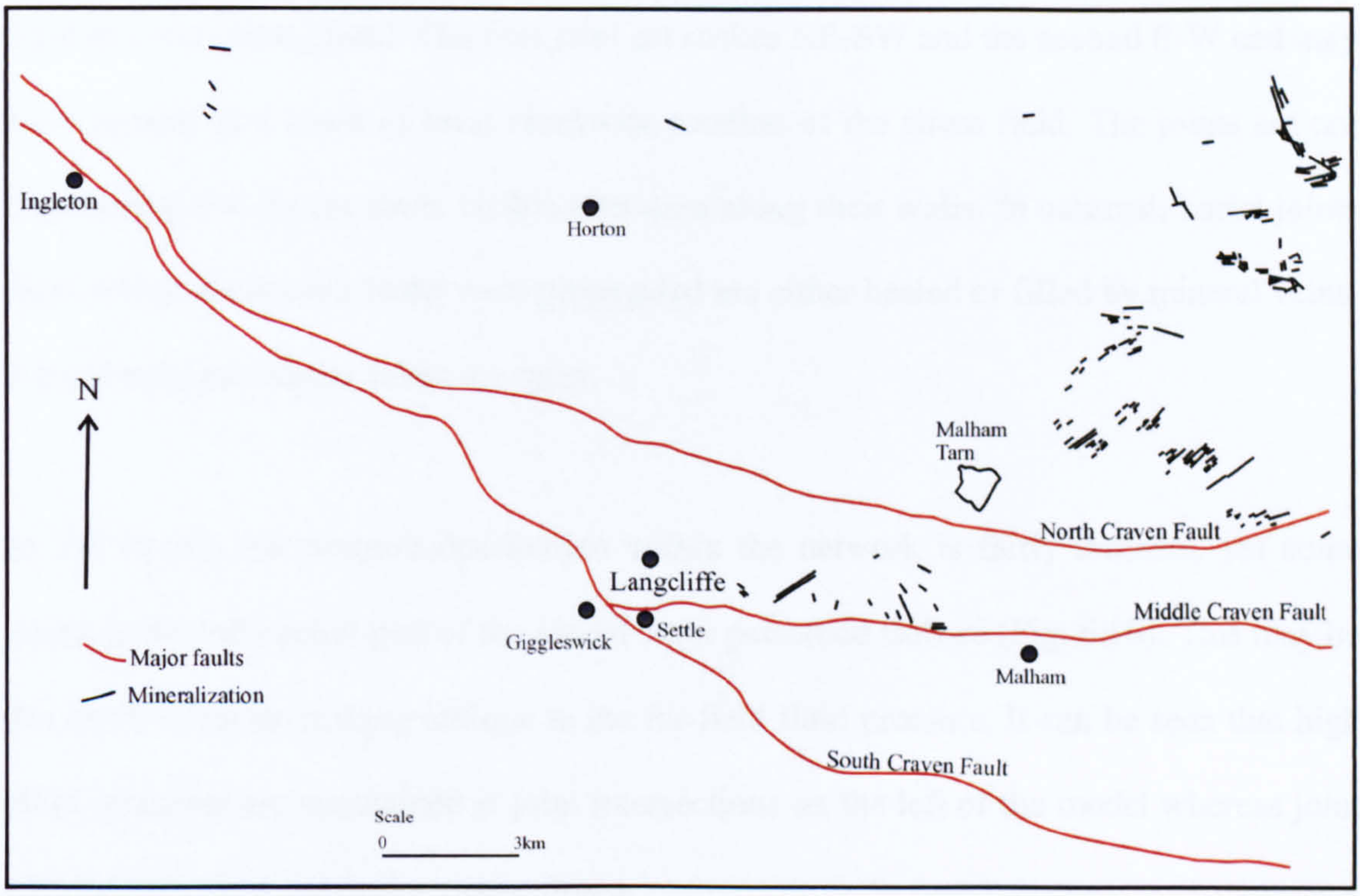


Figure 6.9 *The Craven Faults and the distribution of mineralised veins in the region compiled from 1:50,000 scale maps of sheets 50 and 60. Note that the Upper Carboniferous mineralisation was controlled by the joints. The length of mineralized veins is slightly exaggerated for clarity.*

6.6.2 East of Lilstock

In this section the results of numerical simulation of fluid flow through joint networks from the southern margin of the Bristol Channel described in Chapter 4 (sections 4.4.2 to 4.4.7) are presented and discussed. The order of description is from east to west.

The fracture network shown in Fig. 6.10 is from east of Lilstock. The 'window' has an area of $72m^2$. The total length of the joints within the 'window' is 248.42m giving an average joint density of $3.45m^{-1}$. The joint network was mapped 2m into the hanging-wall of an E-W striking, north-dipping normal fault. Based on abutting relationships, three

joint sets were recognised. The first joint set strikes NE-SW and the second E-W and may have formed as a result of local clockwise rotation of the stress field. The joints are not mineralised and do not show visible alteration along their walls. In contrast, burial joints from which the normal faults were propagated are either healed or filled by mineral veins. Alpine and post-Alpine joints are open.

In the model, the pressure distribution within the network is fairly uniform, yet some zones in the left central part of the model show perturbed isobars (Fig. 6.10). This may be the result of joints striking oblique to the far-field fluid pressure. It can be seen that high fluid pressures are maintained at joint intersections on the left of the model whereas joint bifurcations show marked pressure drops.

The normalised velocity histogram for the joints is skewed to the left *i.e.* the low velocity end and fluid velocity within the matrix is skewed to the right (Fig. 6.11). This may be related to the presence of enhanced flow within the matrix adjacent to the conductive joints or to the fact that some joints are not hydrologically active (*e.g.* joints at high angles or normal to the fluid pressure gradient). If joints strike at an unfavourable orientation to the far-field fluid pressure gradient, fluid can flow from the fractures into the surrounding matrix. In contrast if the joints strike parallel to the fluid gradient and have wide apertures *i.e.* two factors that will increase fluid flow, fluid pressure eases inside the fracture and fluid will tend to drain from the matrix into the closest joint. In this case flow velocity within the matrix will be enhanced.

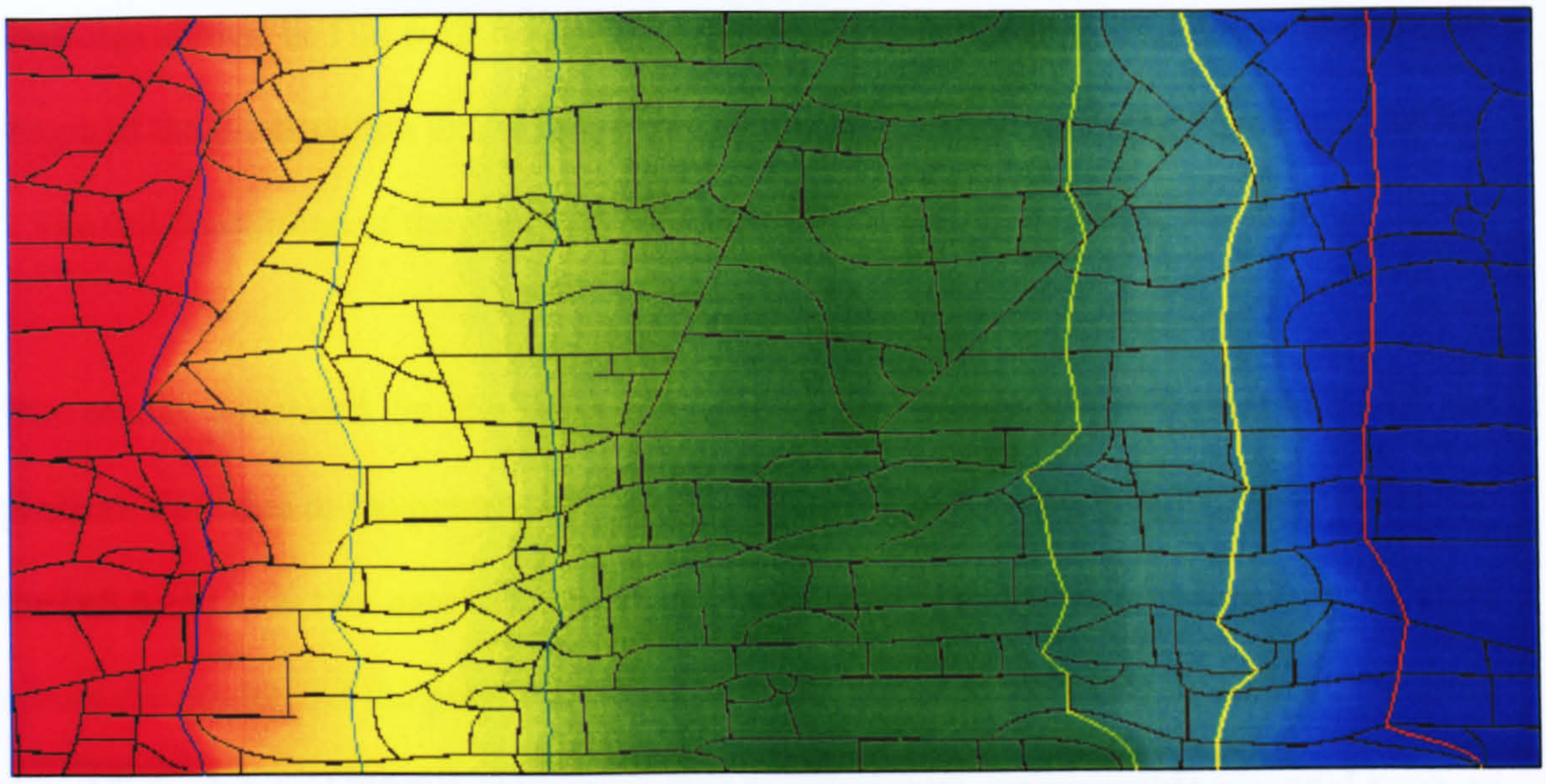


Figure 6.10 *Pressure distribution map for approximately uniformly distributed joint network. The gradient is almost linear. The black lines are joint traces with apertures of 0.003 for long and 0.005m for short fractures. The coloured lines are the isobars.*

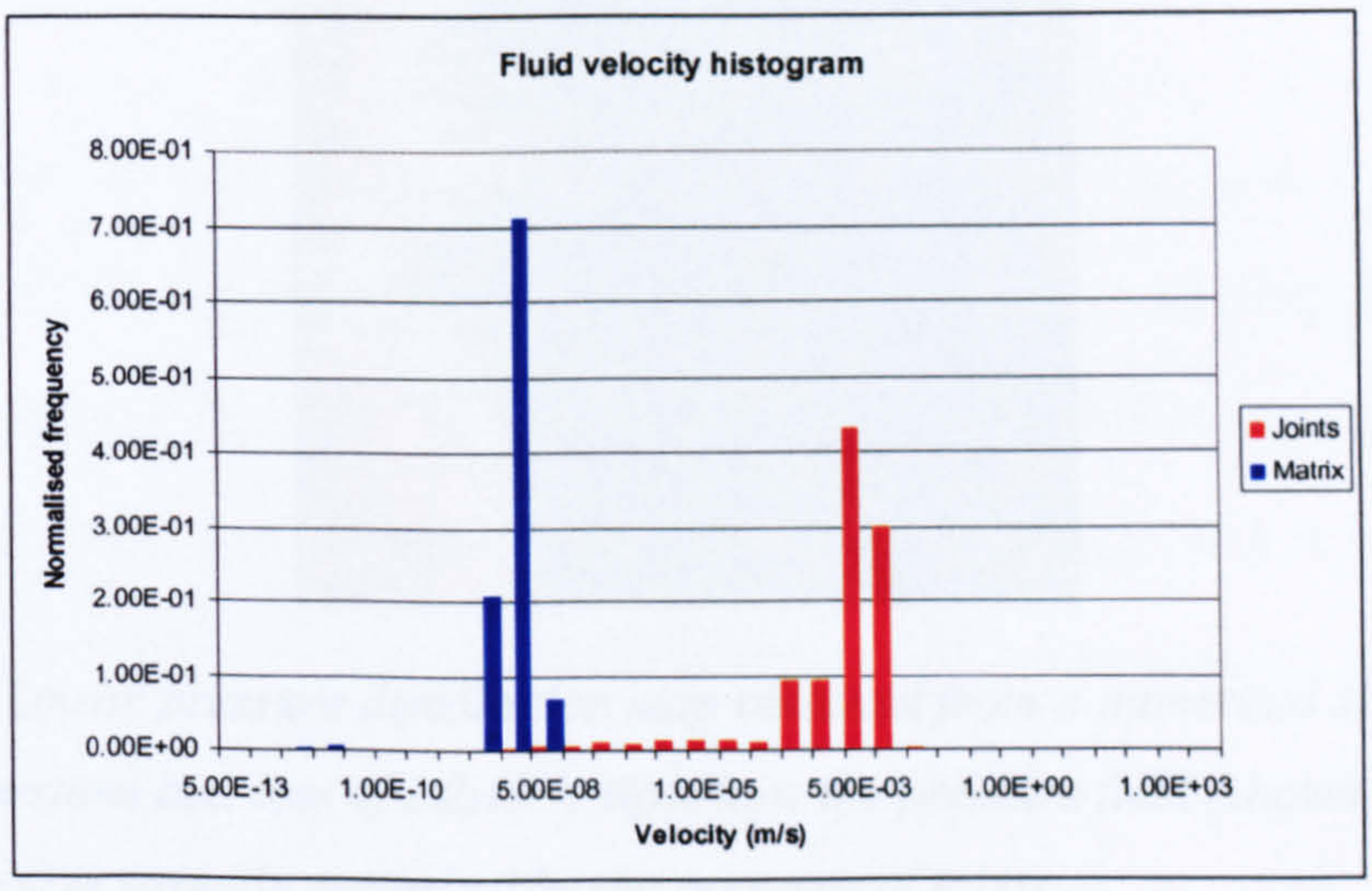


Figure 6.11 *Normalised velocity histogram of fluid flow through the joints and matrix obtained from numerical simulation illustrated in Fig. 6.10.*

The map shown in Fig. 6.12 has an area of $36m^2$ and contains three joint sets. The total length of the joints within the 'window' is 128.8m giving an average joint density of $3.57m^{-1}$. The full description of the joint networks is given in section 4.4.2 (see Fig. 4.26a).

The model generated by the numerical simulation shows strong perturbation of the pressure field due to the presence of joints oblique to the pressure gradient (Fig. 6.12). On the left hand side the map, oblique joints behave as a barrier preventing flow of fluid across the model and the pressure field is strongly perturbed. Fluid flow trajectories cross the oblique joints. If these oblique joints are filled with impermeable material such as clay, veins or dykes, they would behave as a barrier to fluid flow across them.

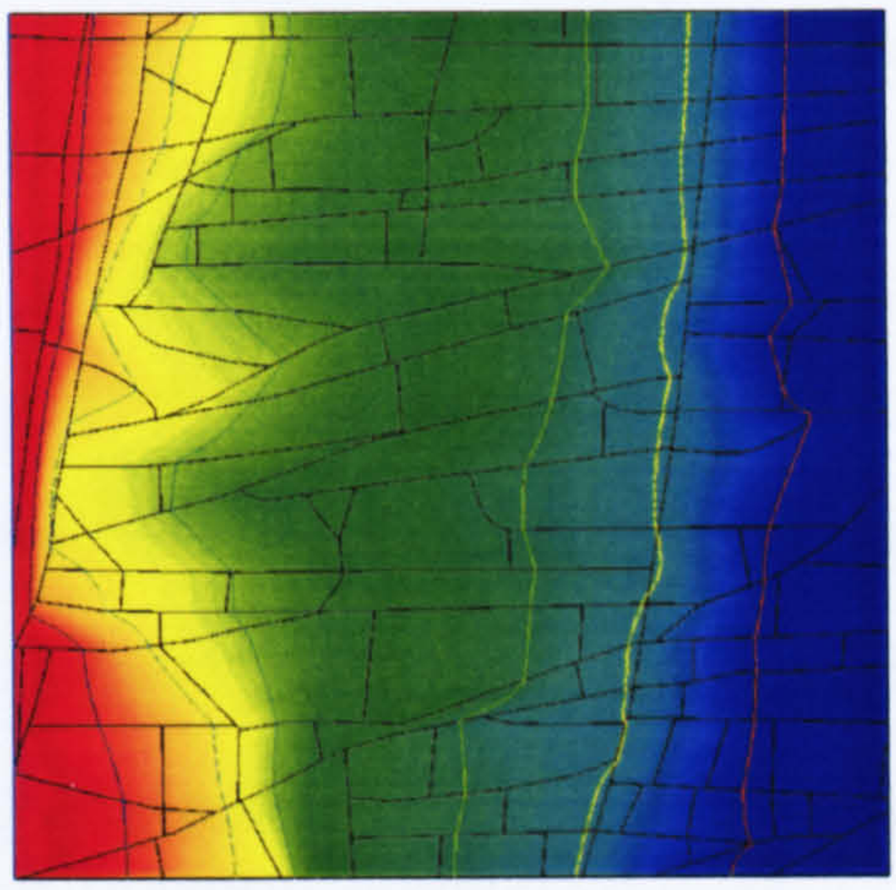


Figure 6.12 *Linear pressure distribution map obtained from a numerical simulation of a fractured limestone bed east of Lilstock. Note how the pressure field (shown by a rainbow colour scheme) is strongly perturbed by the presence of joints.*

The normalised fluid velocity within the matrix (Fig. 6.13) shows a log-normal distribution skewed to high values, whereas within the joints the distribution is skewed in the opposite sense and there is a tail of low values. As discussed earlier in connection

with the histogram shown in Fig. 6.11, skewing of the histogram is believed to be the result of hydraulic communication between the joints and the surrounding matrix.

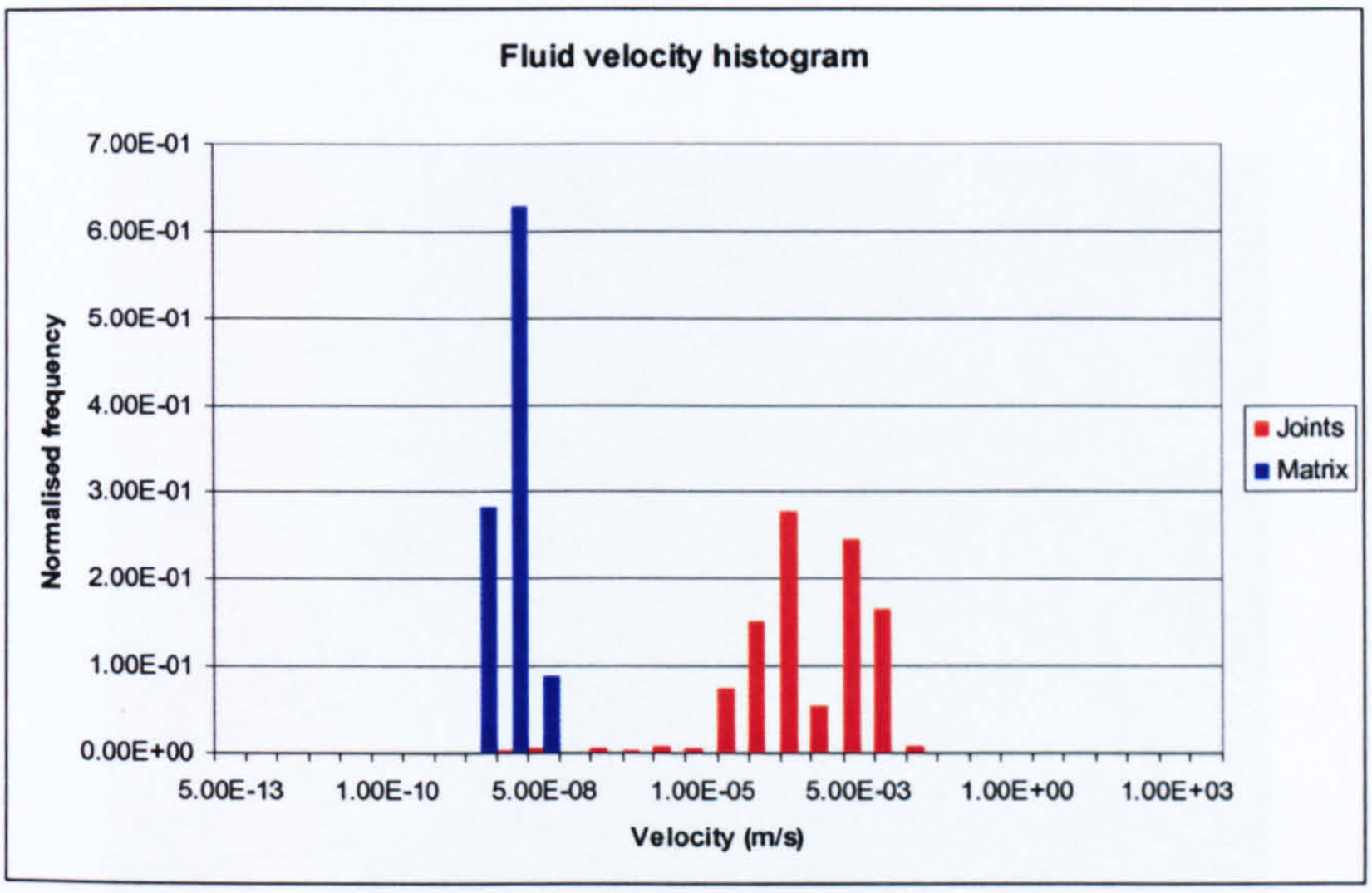


Figure 6.13 *Normalised velocity histogram of fluid flow within the joints and matrix obtained from the numerical simulation of the fracture network shown in Fig. 6.12.*

Another window from the outcrop in East Lilstock is shown in Fig. 6.14. The area of the window is $24m^2$ with a total length of the joints of 102.42m giving an average joint density is $4.26m^{-1}$. The Alpine joints strike 020° and 095°. Fluid flow simulation shows a highly perturbed pressure field (Fig. 6.14). The full description of the joint networks is given in section 4.4.2 of Chapter 4 (Fig. 4.26b). In the left central part of the model it can be observed that fluids have been drained from the matrix into a joint which is not connected to the far-field fluid pressure. The pattern of the isobars shows large variations caused by the conductive joints.

As in the previous example, fluid flow velocity within the matrix is skewed to the right whereas for the joints it is skewed to the left (Fig. 6.15). In addition fluid velocity within

the matrix overlaps the fluid velocity within some of joints indicating that flow in some of the joints is very low and comparable to that in the matrix. These data probably relate to the joints oriented at a high angle or normal to the far-field fluid pressure or short fractures.

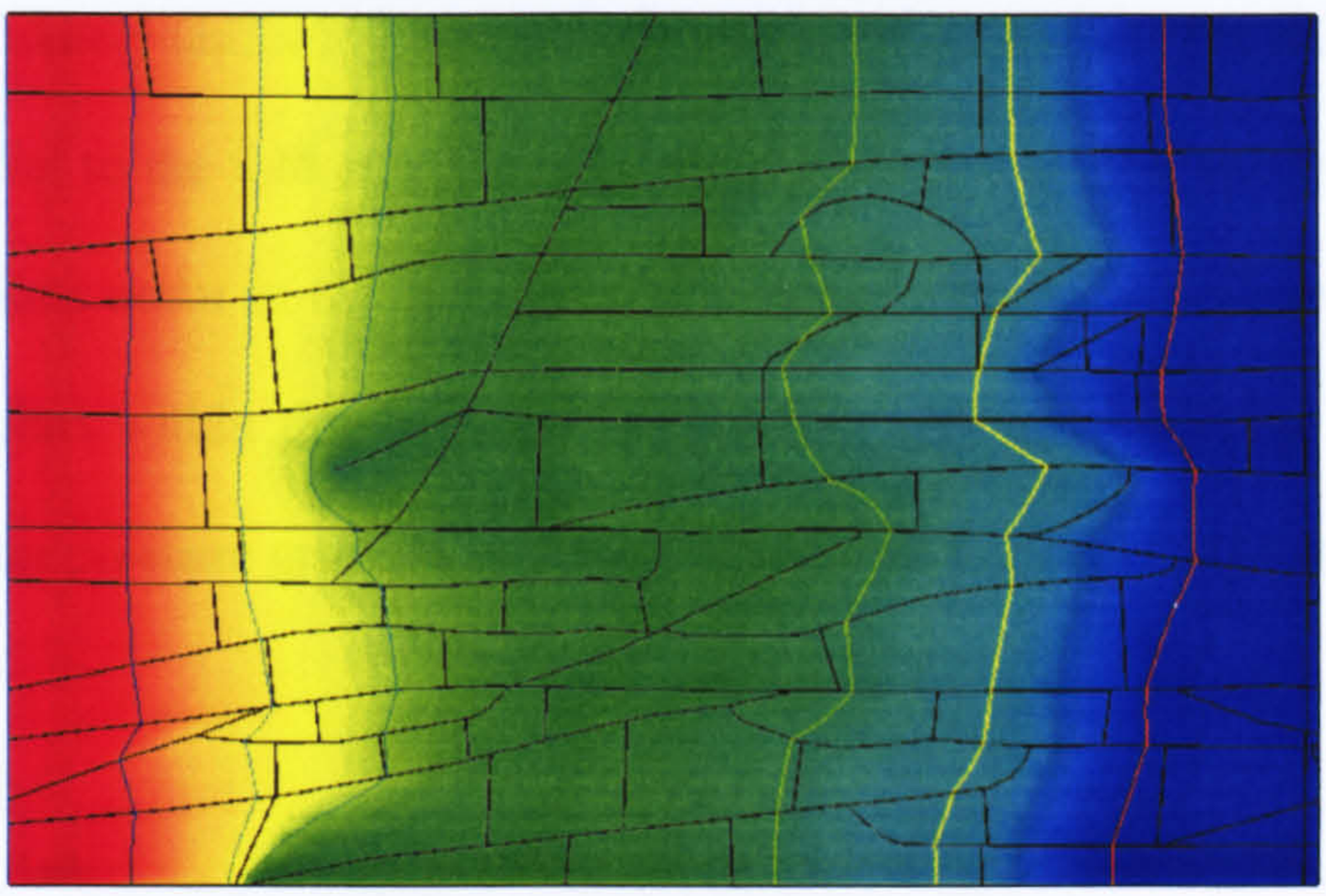


Figure 6.14 *Linear pressure map of jointed limestone bed from East of Lilstock. Note the upstream end of the fracture unconnected to the far-field fluid pressure gradient in the left central part of the model increases flow from matrix to fracture and the isobars are deflected.*

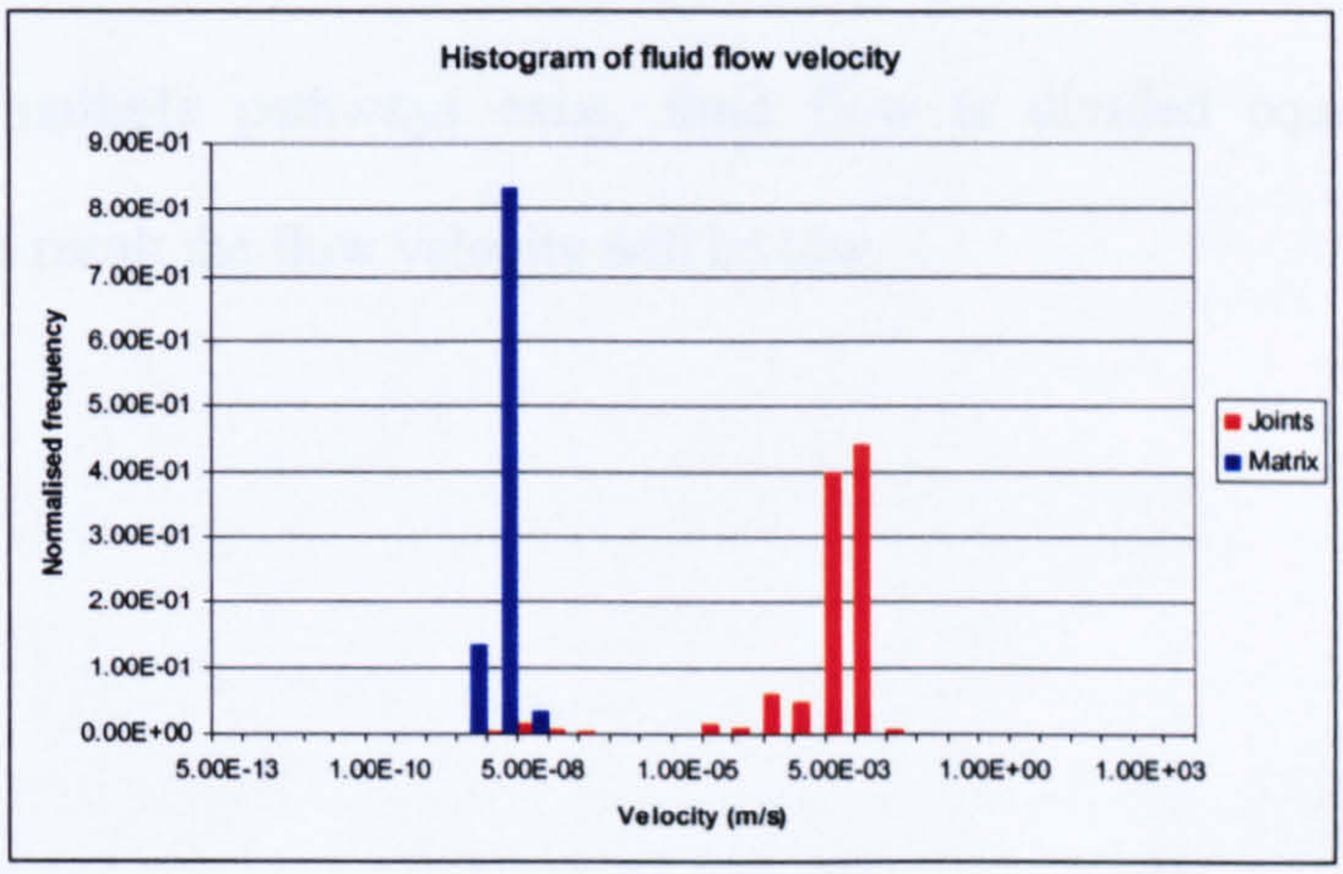


Figure 6.15 *Normalised velocity histogram of flow in the joints and matrix shown in Fig. 6.14 obtained by numerical simulation. Note that fluid flow within the matrix is skewed to the right and within the joints to the left.*

6.6.3 Lilstock

Lilstock is situated approximately 3km northeast of Kilve (Fig. 2.7). The lowest exposed bed at this locality is described in section 4.4.3.1 and occurs on the trailing (north-dipping) limb of the Lilstock anticline (Fig. 6.16). It contains two orthogonal sets of joints. The joint sets are approximately uniformly distributed throughout the model. The earliest joint set in this bed is parallel to the fold axis of the Lilstock rollover anticline, except in areas where stress perturbations occur in the vicinity of a fault (see Fig. 4.29 in Chapter 4). The total length of the joints within this 'window' is 914.86m, giving an average joint density of $6.4m^{-1}$. The linear pressure gradient in the model shows a uniform distribution pattern (Fig. 6.16).

The histogram of velocity of fluid flow in the joints is broad and skewed to the left (Fig. 6.17). The histogram of matrix velocity is uniform with a distribution only slightly skewed to the right. As discussed above the skewed distribution of flow velocity of the two histograms reflects the communication between the fractures and the surrounding matrix. Where multiple pathways exist, fluid flow is divided equally between the fractures and as a result the flow velocity will be low.

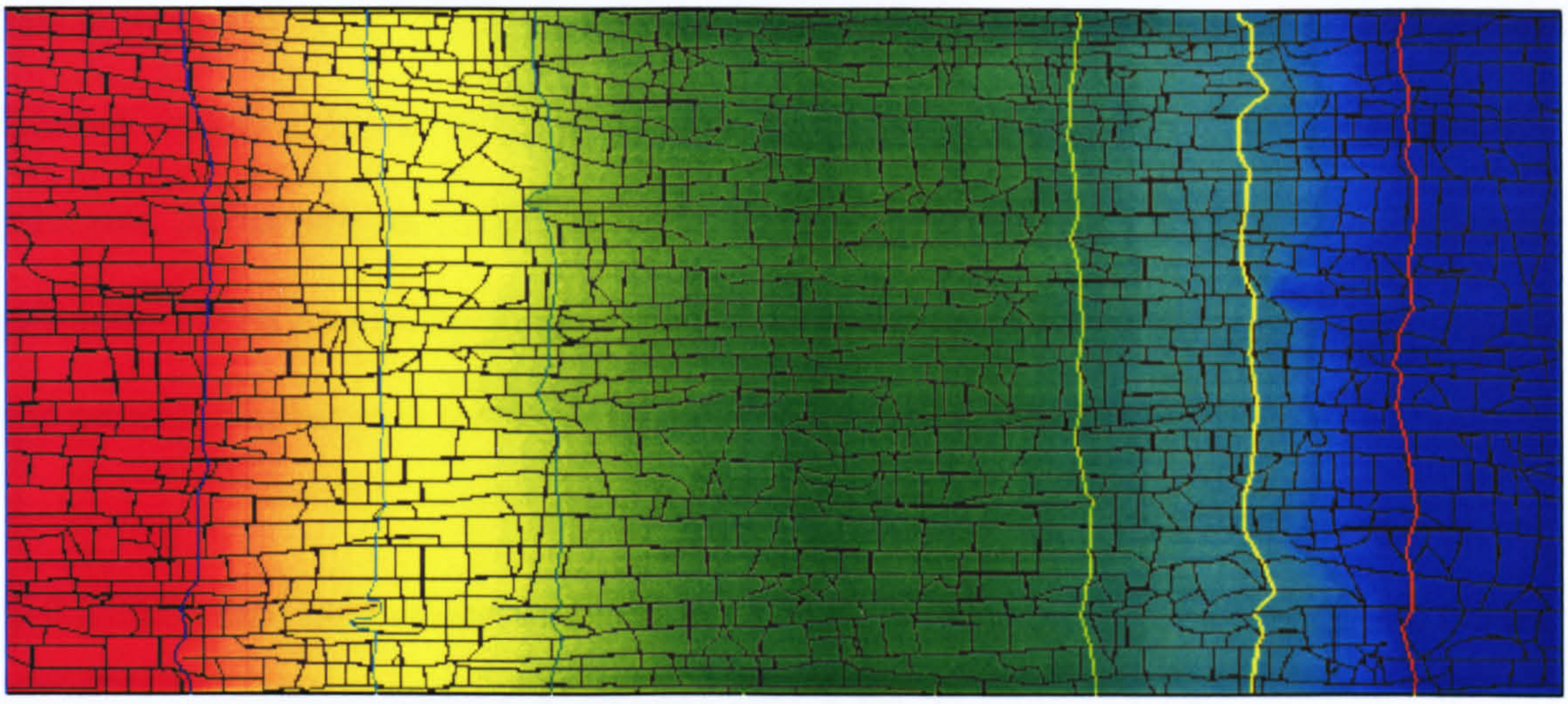


Figure 6.16 *Linear pressure distribution map of fractured limestone from the lowest exposed trailing limb of Lilstock rollover anticline.*

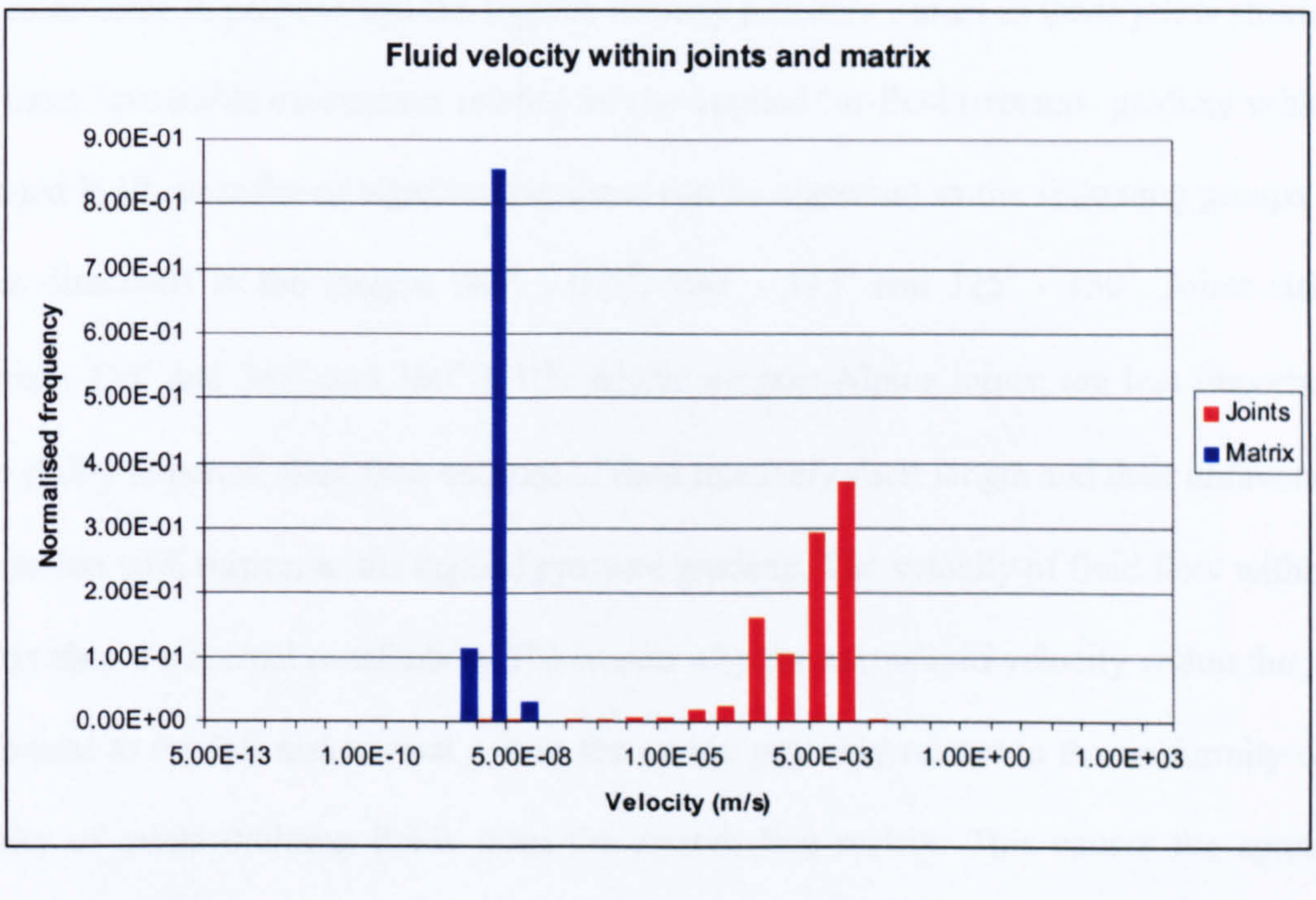


Figure 6.17 *Flow velocity histograms for the joints and matrix of the lowest exposed limestone bed of the Lilstock anticline (Fig. 6.16). Note that the matrix velocity is well defined and the joint velocity is diffuse which may be explained by the orientation of joints to the far-field pressure.*

The map in Fig. 6.18 shows a fractured limestone from the north-dipping limb of the Lilstock anticline. It was fully described in section 4.4.3.2 (see Fig. 4.31). It contains six joint sets, the earliest set striking NW-SE and the younger joints having strikes that rotate progressively in an anticlockwise sense. The pressure contour map is highly contorted and perturbed because of the presence of joints in various orientations.

In this study fluid flow velocities in the matrix obtained from the numerical model and plotted on a histogram show a normal distribution (Fig. 6.19). In contrast the frequency distribution histogram of velocity for the joints shows a distribution skewed to the left. Although it is very difficult to separate the velocities of fluid in such a well-connected system of fractured beds, it is reasonable to propose that the highest velocity probably occurs in those joints striking in the most favourable orientation relative to the applied far-field pressure gradient which is oriented E-W. In order of significance, these can be classified in the following groups with strike directions in the ranges: 085° - 095°, 100° - 115° and 125° - 130°. Joints striking between 335° and 345° and 360° ± 10°, which are post-Alpine joints, are less important in their ability to permit fluid flow because of their relatively short length and their unfavourable orientation with respect to the applied pressure gradient. The velocity of fluid flow within the matrix shows a normal distribution. The reason why the normalised velocity within the joints is skewed to the left and normal within the matrix probably relates to the uniformity of the density of joints draining fluids from the surrounding matrix. This causes the spread of velocity around the mean within the matrix to be uniform.

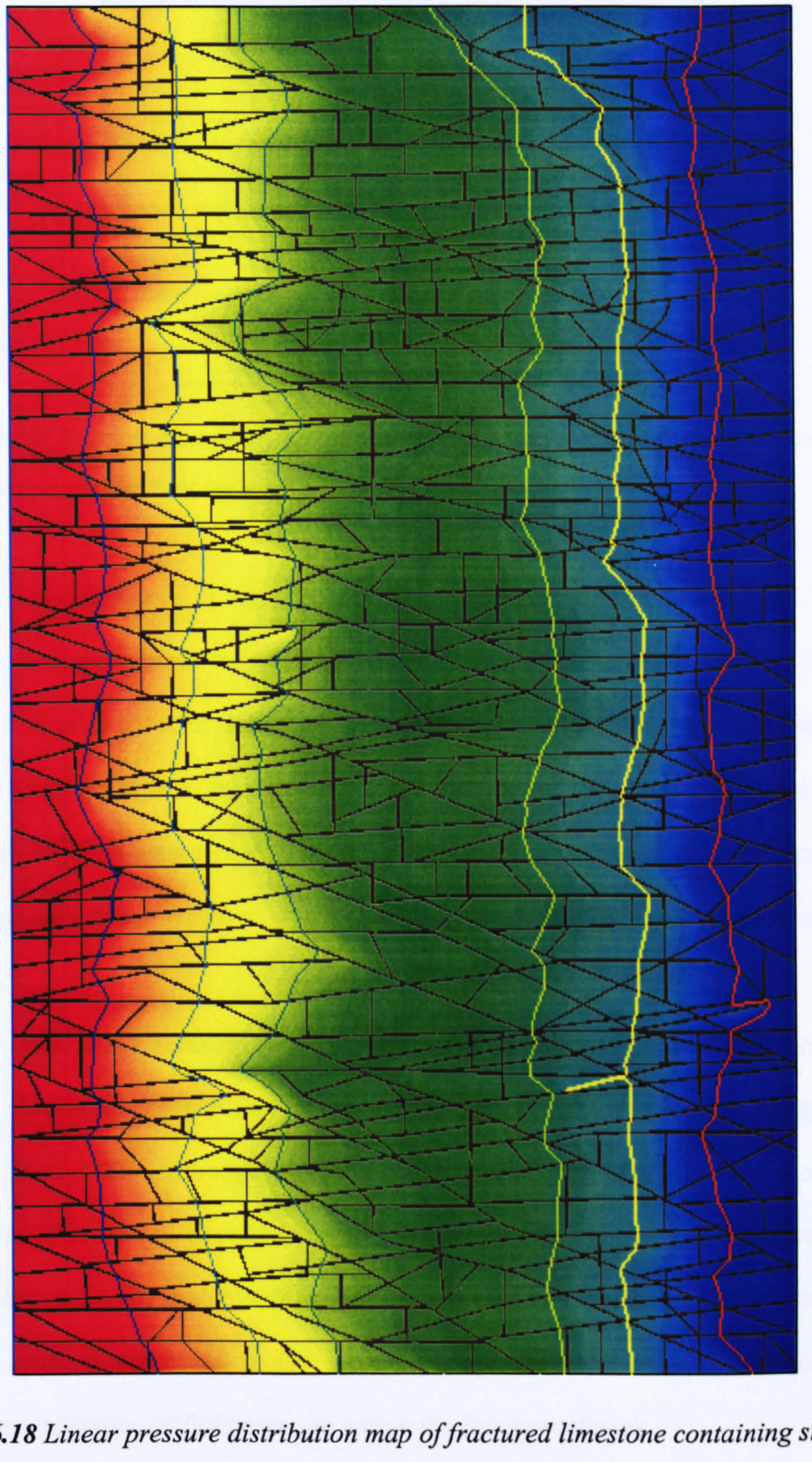


Figure 6.18 *Linear pressure distribution map of fractured limestone containing six joint sets from the trailing limb of Lilstock rollover anticline.*

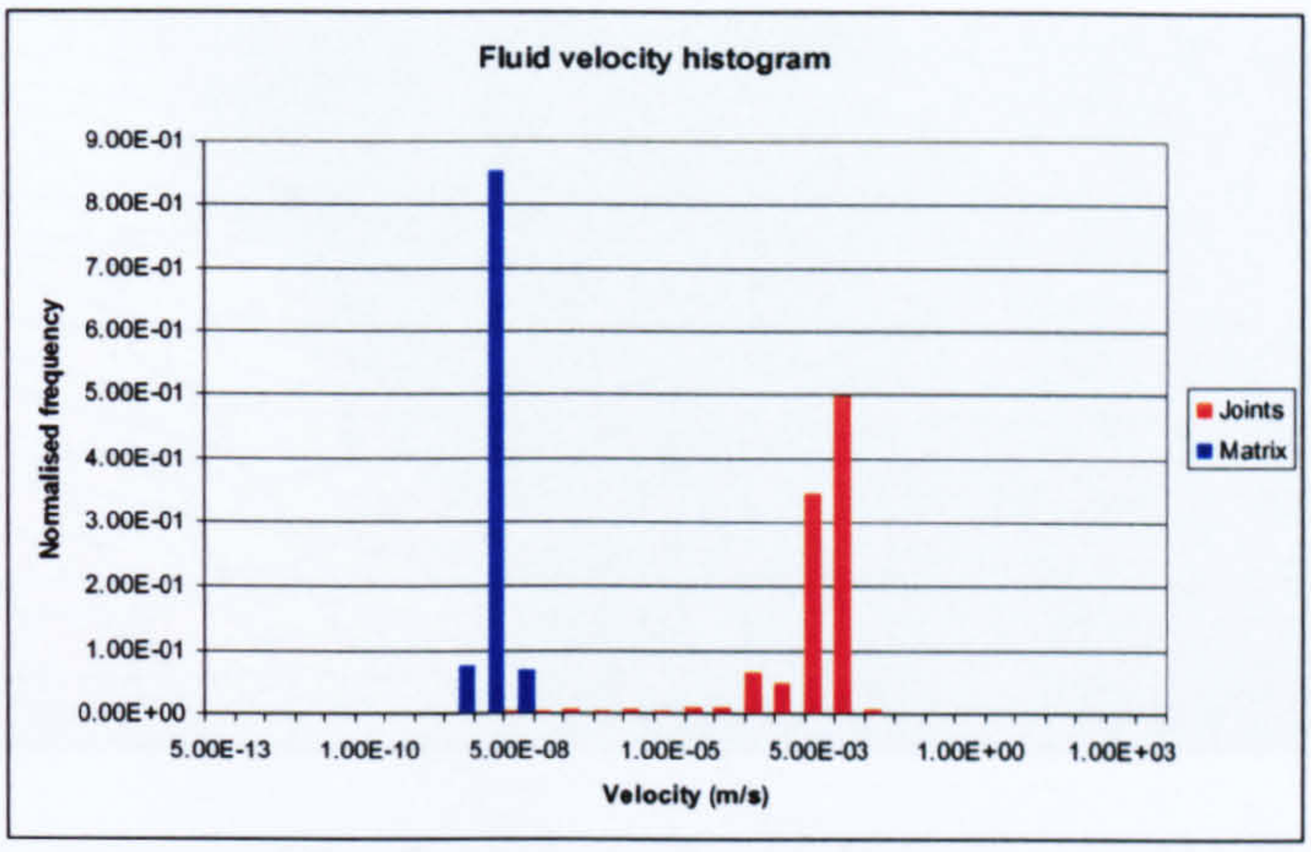


Figure 6.19 *Velocity histogram of the joints and matrix obtained from the numerical simulations in the fracture network shown in Fig. 6.18.*

The joint network shown in Fig. 6.20 was described in detail in section 4.4.3.3. The total length of fractures within the 'window' is 383.7m and the average fracture density is $5.35m^{-1}$. The joint network shown in Fig. 6.22 is from another locality on the same bed. The total joint length is 473m and the average joint density is $4.37m^{-1}$. This bed contains joints with two dominant strikes. As can be seen the first set is approximately parallel to the longest side of the 'window' whereas the second set is oblique to the former set.

When a linear fluid pressure gradient is applied to this model, the contours on the pressure distribution map rotate to become parallel to the strike of the oblique joints (Figs. 6.20 and 22). Although the joint patterns from the two localities show slight differences, there is an overall similarity in the pressure maps. The pressure map is strongly influenced by the oblique strike of the joints, with respect to the direction of the pressure gradient especially in the second example. These oblique joints govern the compartmentalisation of fluid pressure within the fracture network.

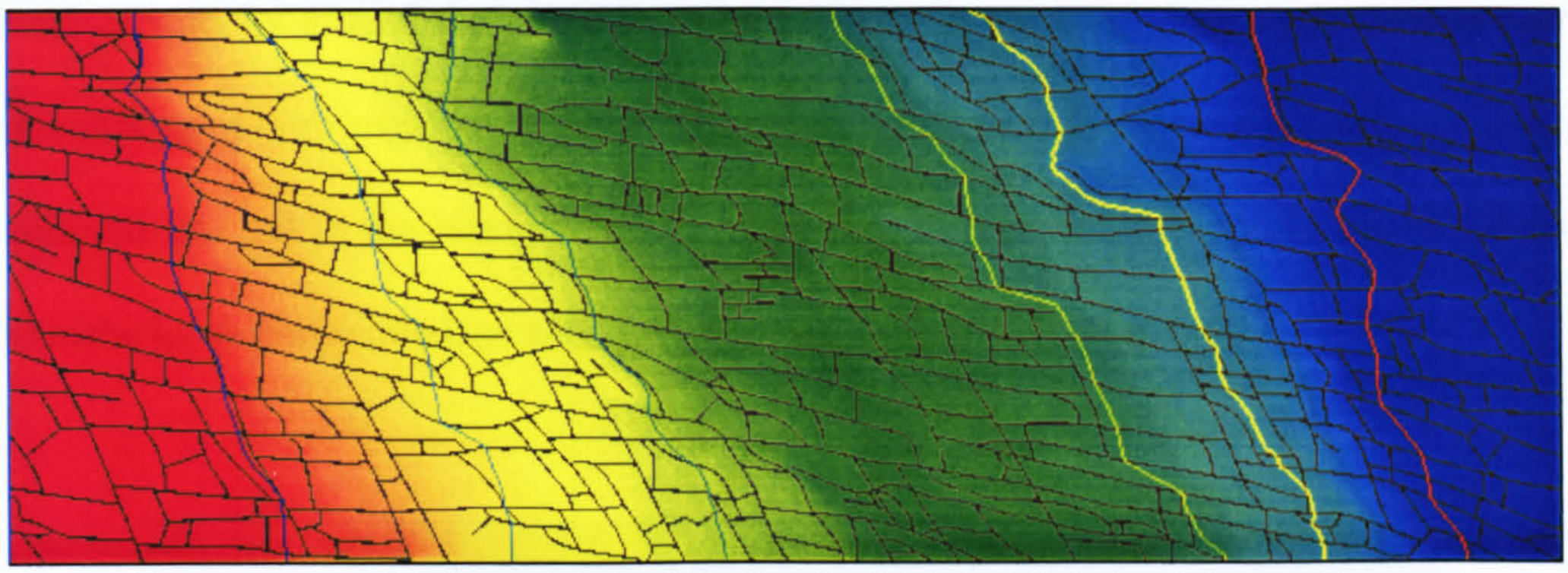


Figure 6.20 *The trajectory of the fluid pressure gradient expressed as a rainbow colour scheme is strongly perturbed by the oblique pattern of connected fractures in the bed.*

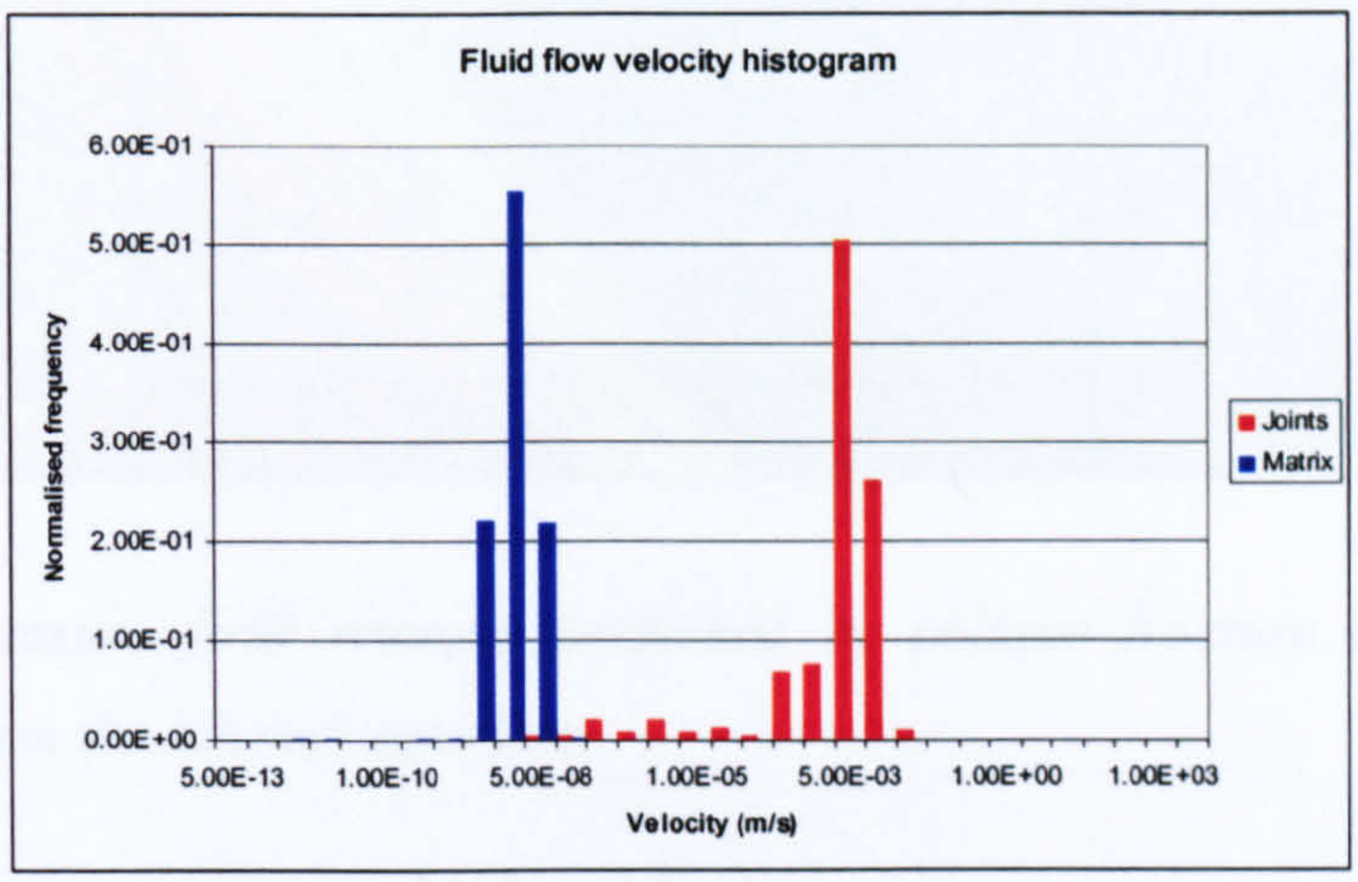


Figure 6.21 *Velocity histogram of fluid flow within the joints and the matrix in the fracture network shown in Fig. 6.20.*

The normalised fluid velocity through the matrix for the fracture network shown in Fig. 6.20 (Fig. 6.21) is normal whereas for the fracture network shown in Fig. 6.22 it is skewed to the left. The velocity histogram of flow through the joints is skew to the left for both networks (Figs. 6.21 and 6.23). The slight differences in the shape of the velocity histograms are considered to be related to the interaction between the joints and the surrounding matrix. In the former example the joints drain the surrounding matrix approximately uniformly and therefore the

spread of velocity around the mode remains uniform. In the second example there are some joints striking at high angle to the pressure gradient which tend to reduce fluid velocity and plot within the low tail in the histogram. It is interesting to note that the population of velocities within the joints partly overlaps with the velocities in the matrix (Fig. 6. 23).

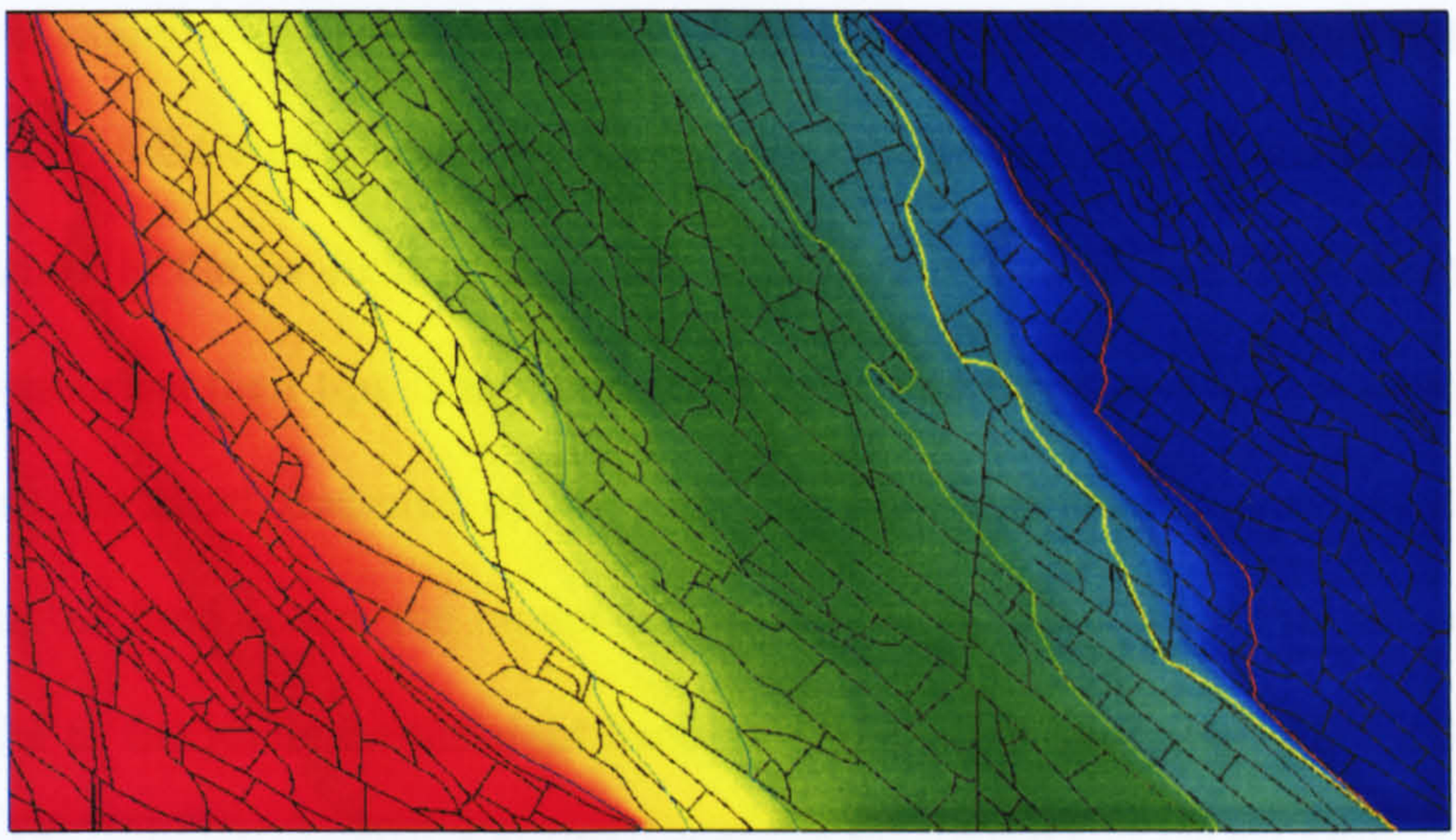


Figure 6.22 *Pressure field strongly perturbed by oblique fracture distribution in a limestone bed from the Lilstock anticline.*

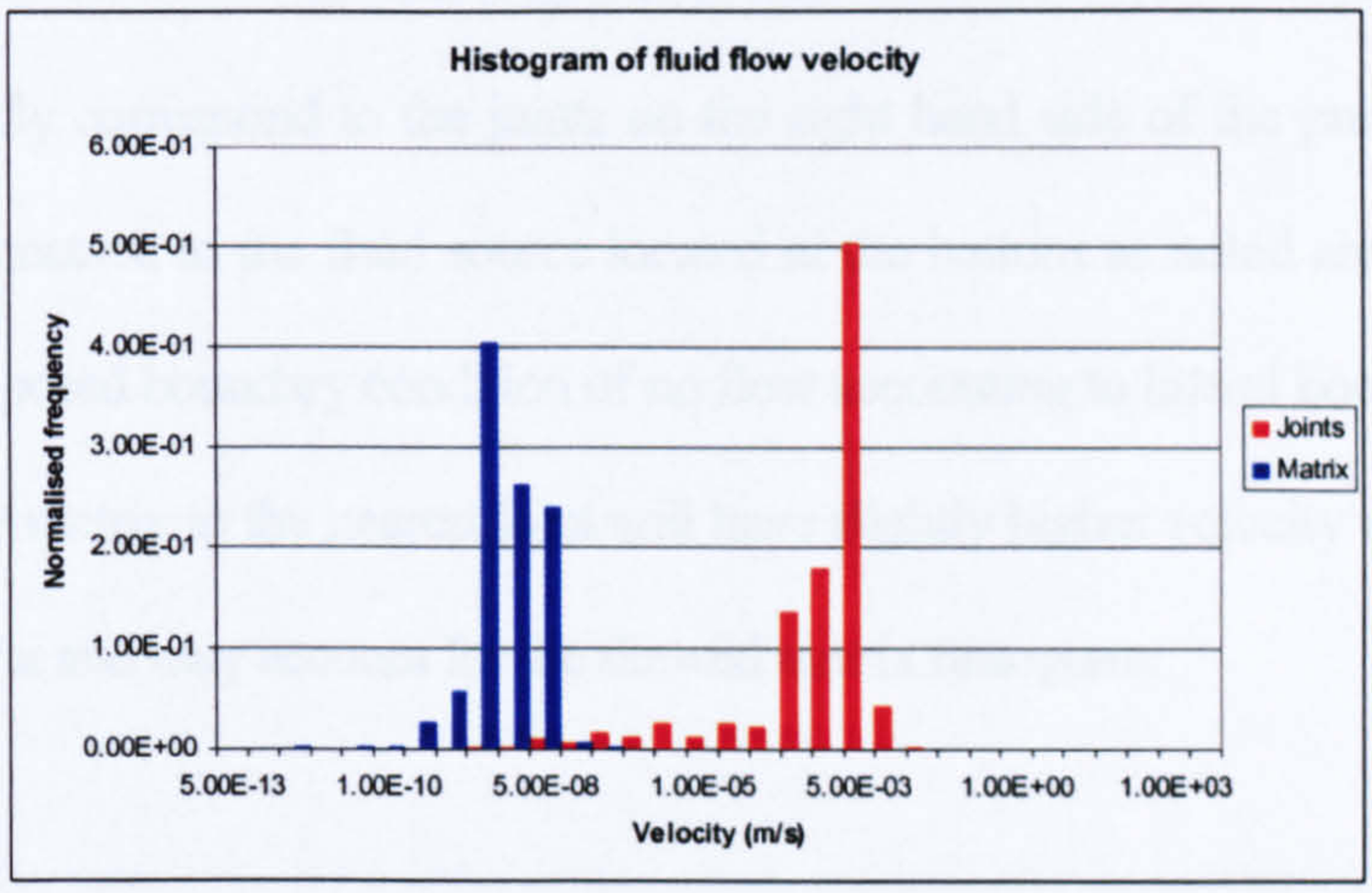


Figure 6.23 *Normalised velocity histogram of flow through the joints and surrounding matrix. Note that some of the joints have the same velocity as the matrix.*

The 'window' shown in Fig. 6.24 contains joint sets striking 320° and 300°, together with non-crosscutting joints of post-Alpine age. The total length of joints within the window is 91.41m giving an average joint density of $3.05m^{-1}$.

In order to examine the role of joints as fluid conduits, the fluid source in the model shown in Fig. 6.24 was placed along the bottom boundary. As can be seen, the joints which connect to the far-field pressure and terminate within the 'window' show build-up of fluid pressure at their tips. The joints that transect the entire area do not show the same pressure as the short fractures of the same set. This can be explained as a result of channelling of fluid across the model boundary. It should be noted that the isobars are sub-parallel to the joints on the right hand side of the pressure map. This is an artefact introduced by setting a no flow boundary at the right and left hand sides of the model.

The flow velocity histogram for the matrix shows a slightly skew to the right whereas the velocity within the joints is skewed to the left (Fig. 6.25). Low velocities within the joints shown in the histogram probably correspond to the joints on the right hand side of the pressure map. These joints are not connected to the fluid source located at the bottom as noted above and this is an artefact of the imposed boundary condition of no flow accounting to lateral boundaries. The fluid draining from the matrix to the nearest joint will have slightly higher velocity with respect to the surrounding matrix and may account for the skewed matrix histogram.

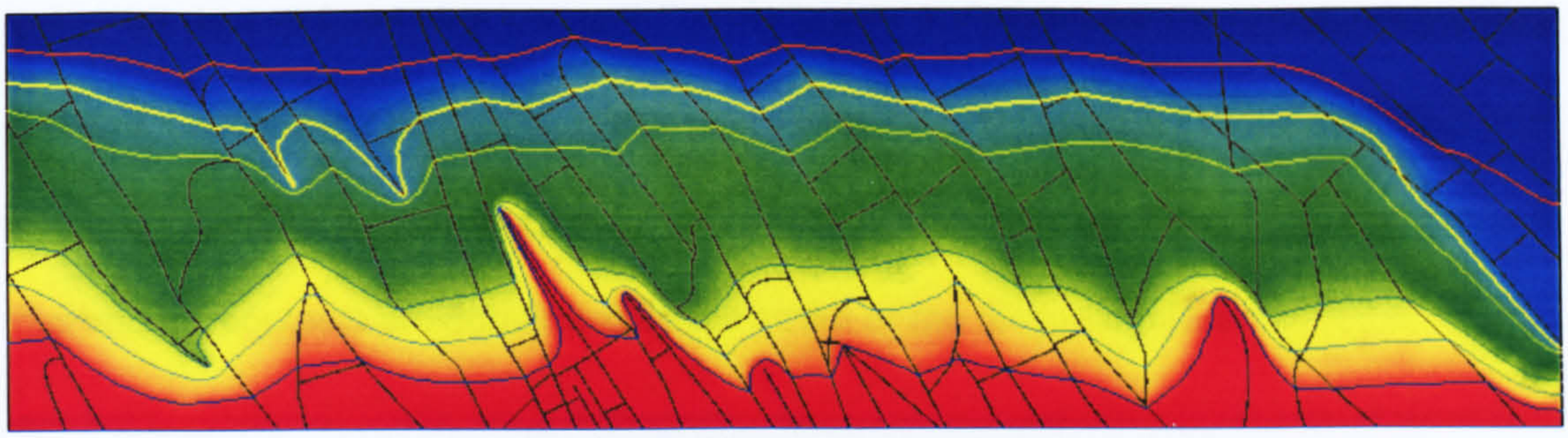


Figure 6.24 *This model shows how the pressure is distributed when the pressure gradient originates from the lower boundary of the model. Note how the joints modify the uniformly applied pressure.*

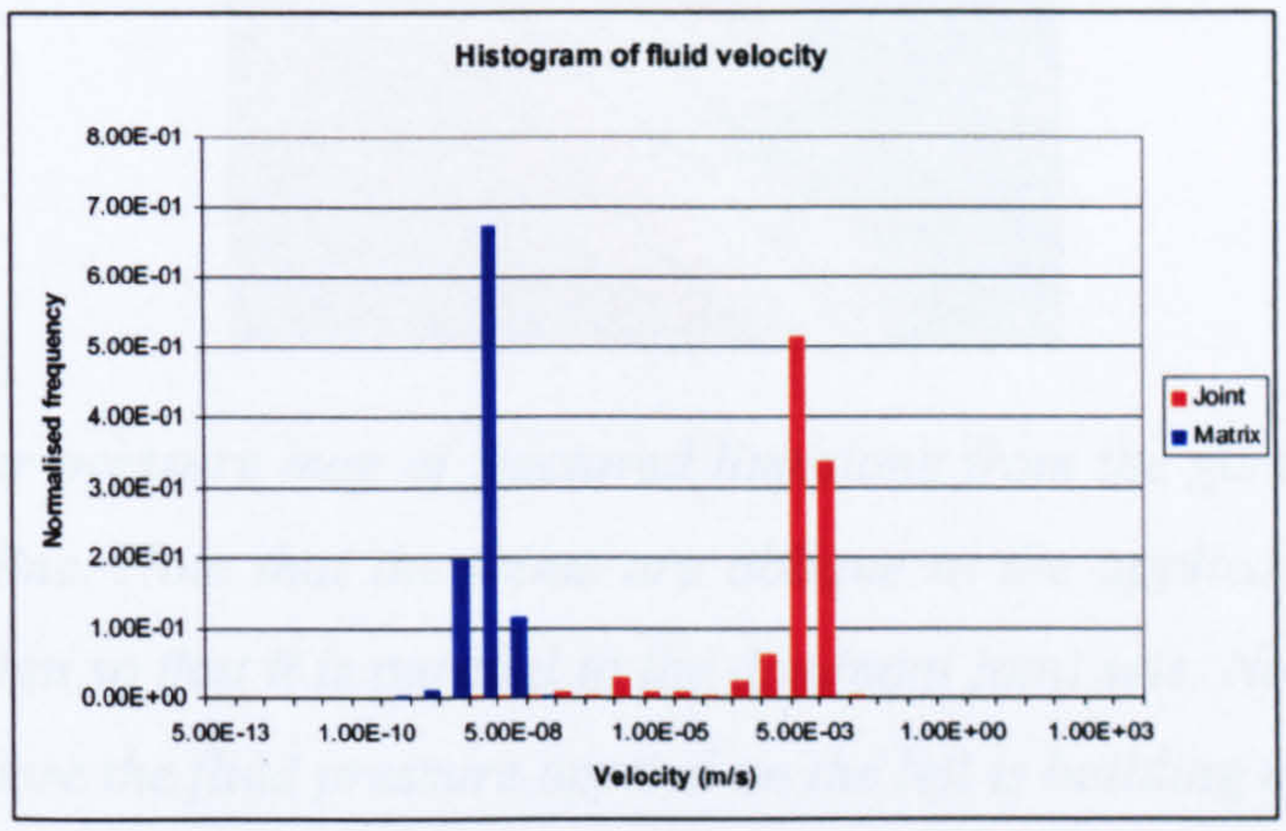


Figure 6.25 *Normalised velocity histogram of fluid flow within the joints and matrix for the fracture network shown in Fig. 6.24.*

The joint pattern shown in Fig. 6.26 is from a different area of the same bed discussed above (see Fig. 6.24). The 'window' was fully described in section 4.4.3.4 (see Fig. 4.34). The total joint length within the 'window' is 35.76m and the average joint density is $3.97m^{-1}$. As discussed above, three joint sets occur within this 'window'. Fluid pressure is applied on the left hand side of the model. The applied linear far-field fluid pressure is perturbed by the oblique joints (Fig. 6.26). As can be seen, joints extending from the fluid

source on the left hand side and terminating inside the model locally develop high fluid pressure. On the right hand side, the pressure contour is sub-parallel to the dominant joint which is probably related to an artefact caused by the no flow boundary. The pressure map and the contours are dominated by the strike of the diagonal joints.

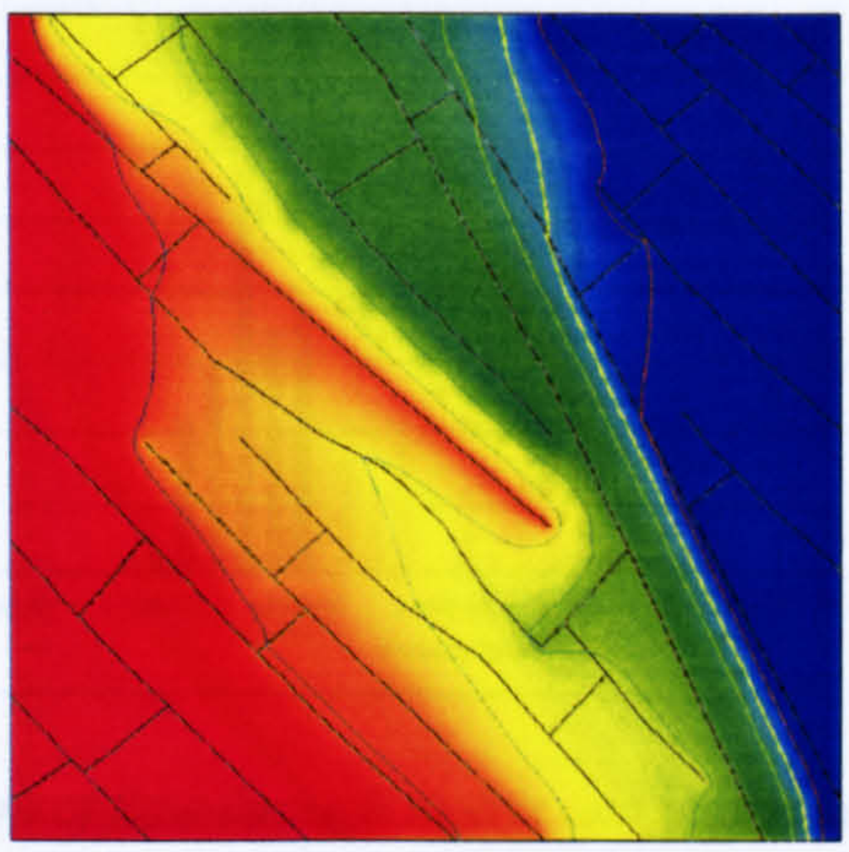


Figure 6.26 *Linear pressure map of fractured limestone from the gently-dipping limb of the Lilstock anticline. Note that the joints are oblique to the applied pressure gradient that tends to re-align so that it is parallel to the dominant joint sets. Note the downstream end of the joint where the fluid pressure applied on the left is building up.*

Inspection of the fluid velocity histogram for the joints (Fig. 6.27) shows it is made up of several populations. These are high, intermediate and low velocity and a similar pattern is seen in the velocity histogram for the matrix. High velocities computed in the analysis correspond to those in long joints that channel fluid from the source and out of the system. The intermediate velocity may correspond to the joints that do not extend as far as the fluid source but still allow flow to occur. The low velocity may be related to low velocity flow in the post-Alpine joints because of their short length or flow in those joints that are not connected to the fluid source. As discussed previously the variation of

velocity within the matrix may also be related to the perturbation of flow caused by the existence of fractures. This example illustrates clearly the role joint and length in governing flow through the fractured medium.

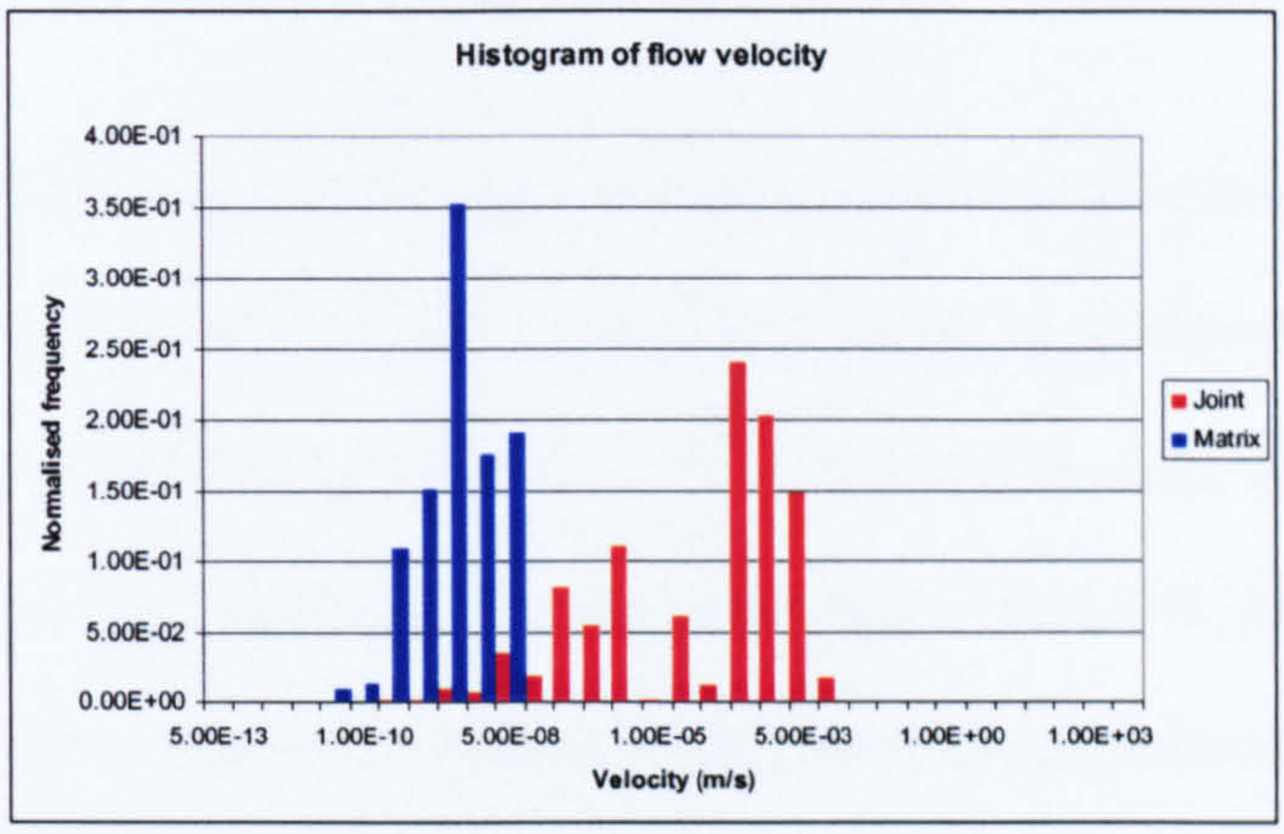


Figure 6.27 *Velocity histogram of flow through matrix and joints shown in Fig. 6.26. Note that the joints with a low flow velocity (i.e. the post-Alpine joints) have the same flow velocity as the matrix.*

6.6.4 Kilve, East Quantoxhead and Blue Ben

The joint trace map shown in Fig. 6.28 was described in detail in sections 4.4.6 (Fig. 4.45). The 'window' has an area of $44m^2$ and contains joints with a total length of 170.4m giving an average joint density is $4.00m^{-1}$. The joints are parallel to the axis of the Kilve fold and contain two joint sets that together form a ladder pattern (*i.e.* formed by long early joints and later non-crosscutting joints).

In order to study the hydraulic properties of the joints, the fluid pressure was applied parallel to the systematic joint set, *i.e.* from the left to the right hand side of the model (Fig. 6.28a). On the right hand side of the map (highlighted in the circle) a high fluid pressure is shown at the confluence of the two joints within the fracture. Flow trajectories around the

resulting joint indicate that this joint also feeds fluid through the matrix to the closest unconnected joint tip (Fig. 6.28b). This constitutes an indirect hydraulic connection. Another interesting aspect of this model is that it shows that where the joints bifurcate downstream along the fluid pressure gradient, pressure within the joints drops dramatically.

The velocity histogram for the matrix is skewed to right and that for the joints is skewed to the left (Fig. 6.29). As noted earlier this is taken by the present author to indicate that there is hydraulic communication between the joints and the matrix. The velocity histogram of flow within the joints is well defined showing a characteristic velocity which is the result of systematic joints striking parallel to the pressure gradient. Low pressure zones are observed in the upstream portions of the joint tips which are not connected to the fluid source as shown in the left central, lower and middle right side of the pressure map (Fig. 6.28). In these areas fluid will be drained from the matrix to the joints.

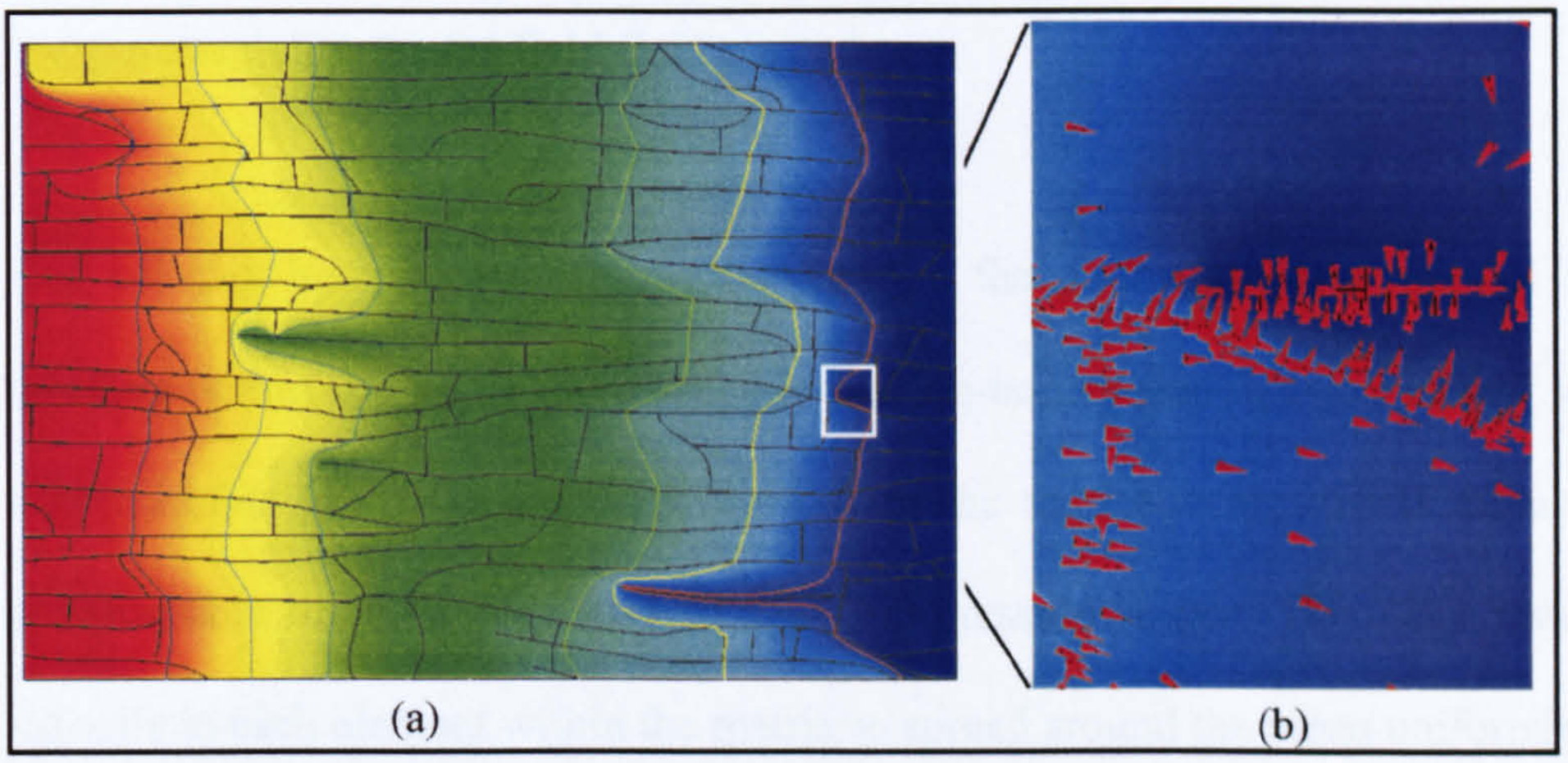


Figure 6.28 *(a) Pressure distribution map of fracture network in limestone from the hinge zone of the Kilve fold. (b) Enlargement of the highlighted area showing communication between the matrix and joints. Note the upstream end of unconnected joints in the left central and lower right corner of the model (a) showing strongly perturb pressure field. Red arrows in model (b) show direction of fluid movement.*

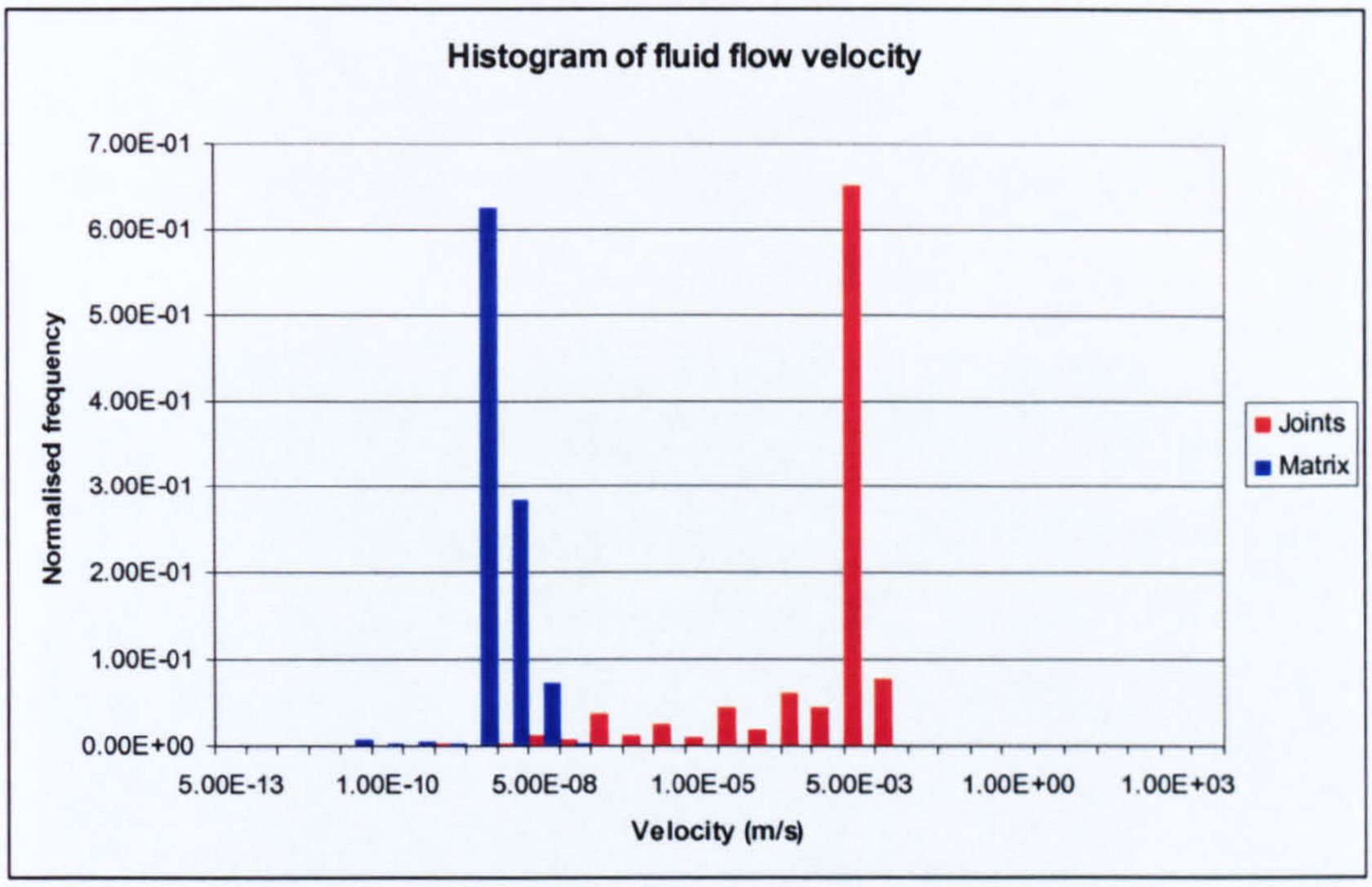


Figure 6.29 *Velocity histogram of fluid flow through the joints and matrix.*

The model shown in Fig. 6.28 was reanalysed with the fluid pressure source rotated through 90° (Fig. 6.30). The pressure gradient runs from top to bottom of the model and it is clear that the isobars are approximately parallel to the joints and that these joints compartmentalise the far-field fluid pressure.

The velocity histogram of fluid flow through the matrix shows a normal distribution whereas within the joints the distribution is log-normal and skewed to low values (Fig. 6.31). Alpine joints do not drain fluid from the neighbouring matrix because of their unfavourable orientation relative to the fluid pressure source. This may result the fluid velocity in each element within the matrix to spread around the mean uniformly.

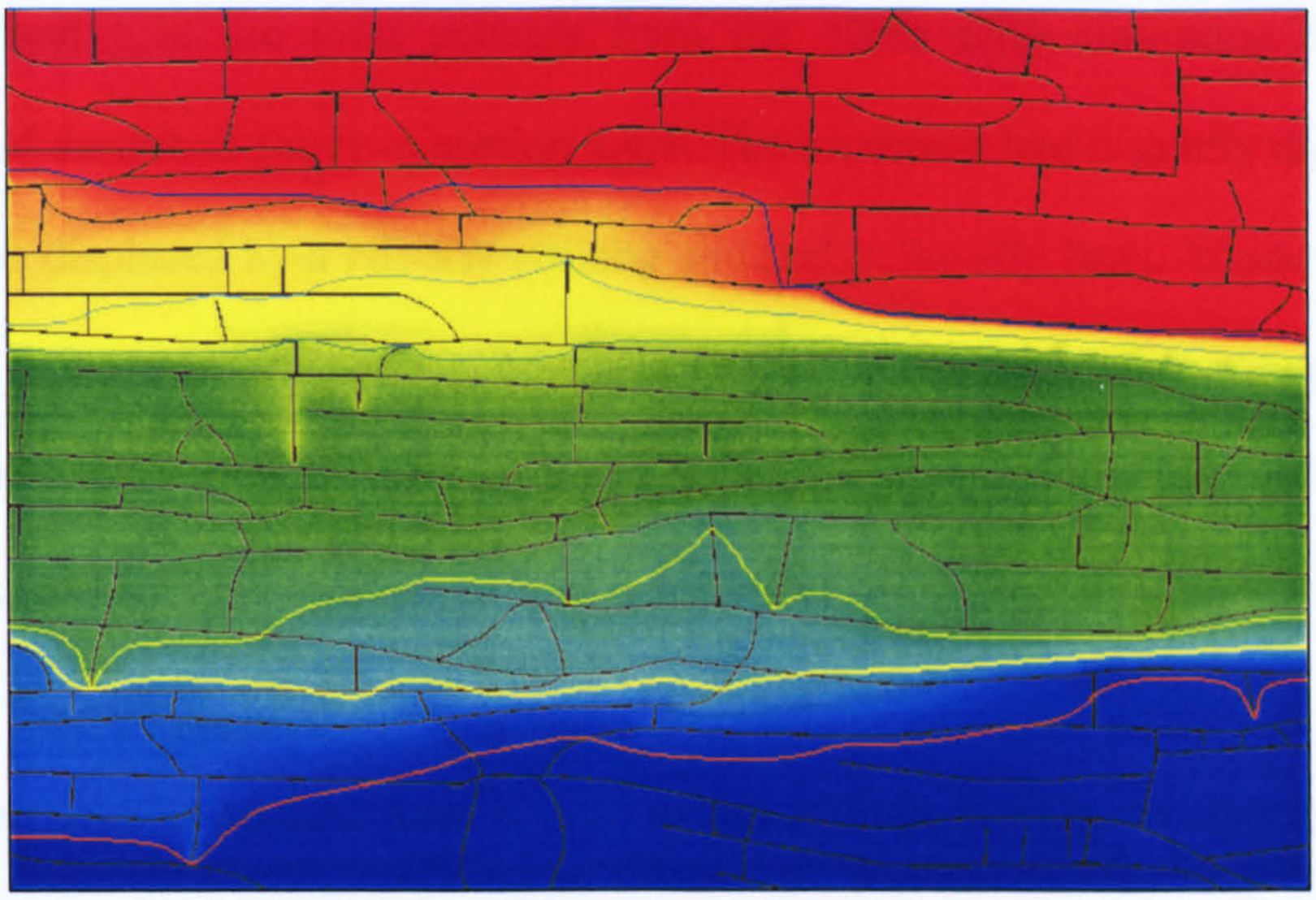


Figure 6.30 *The same model as shown in Fig. 6.28 but with the fluid pressure applied normal to the strike of the dominant joint set striking 110°. These joints acted as a barrier to the far-field fluid pressure. Note how the joints compartmentalise the pressure field.*

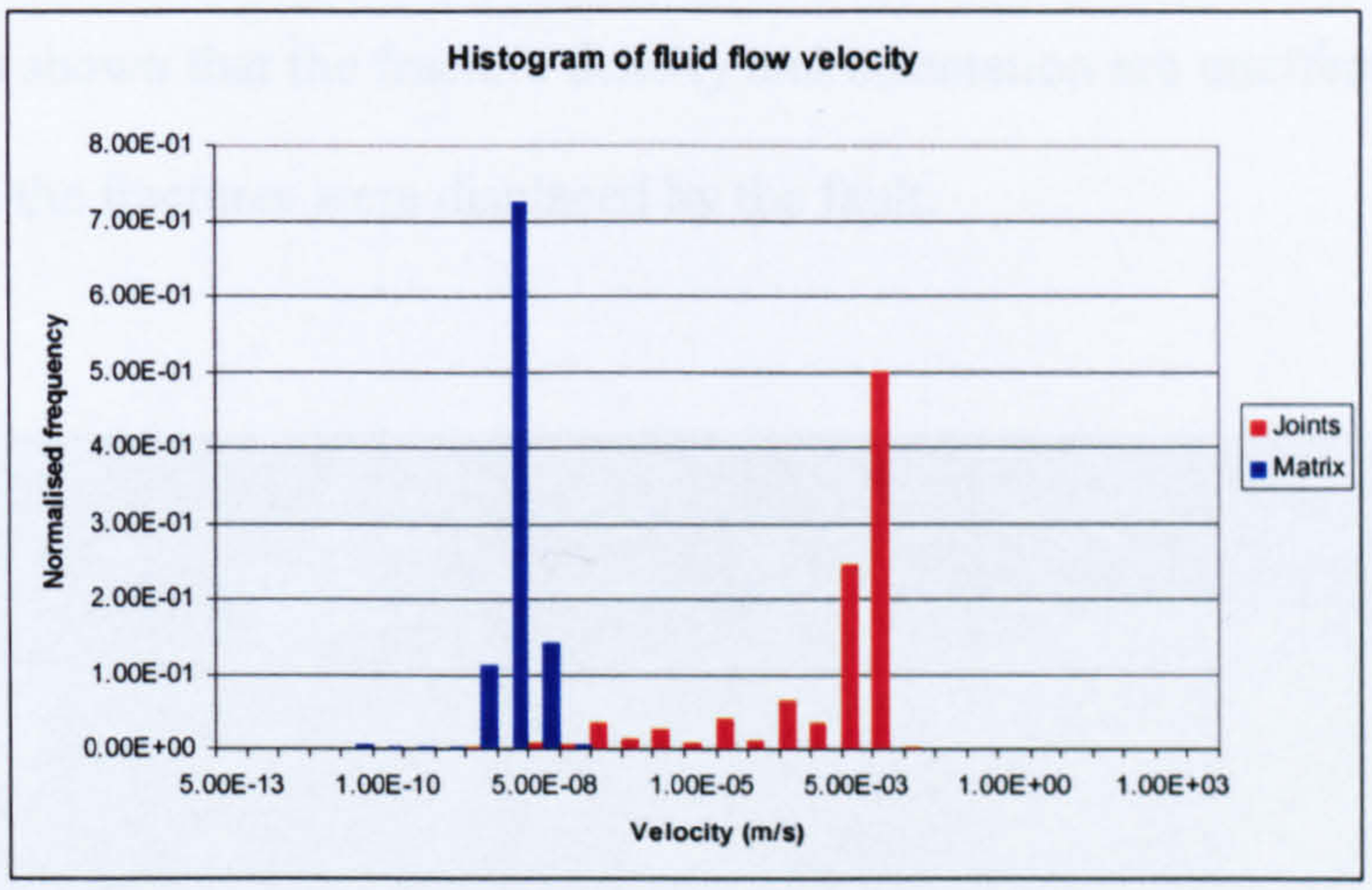


Figure 6.31 *Left skewed velocity histogram of fluid flow through joints and approximately normal through the matrix. It can be seen in this case that the highest velocity in the joints is low compared to the situation in which fluid flow is parallel to the major joints.*

Figs. 6.32 and 6.34 are joint patterns from the 32cm thick limestone bed at East Quantoxhead described above in section 4.4.6. The limestone bed is gently dipping to the NNW and is displaced by a NE-SW striking sinistral strike-slip fault. Window shown in Fig. 6.32 is to the west whereas Fig. 6.34 is to the east of the fault. The northern tip of this fault is a few metres from the bed (see Fig. 4.50 in Chapter 4). The 'windows' which each have an area of $18m^2$ and an average joint densities of approximately $4.8m^{-1}$.

The fluid pressure is applied from bottom to top of both models. In addition, the joint trace maps are wider in the x-direction and provide a better opportunity to model fluid flow during the N-S compression that accompanied the strike-slip faulting. The pressure distribution maps are shown in Figs. 6.32 and 6.34 and are identical. This simulation of pressure distribution supports the suggestion given above that the joints predate the faulting. It was shown that the fracture density and orientation are unaffected by the fault and in addition the fractures were displaced by the fault.

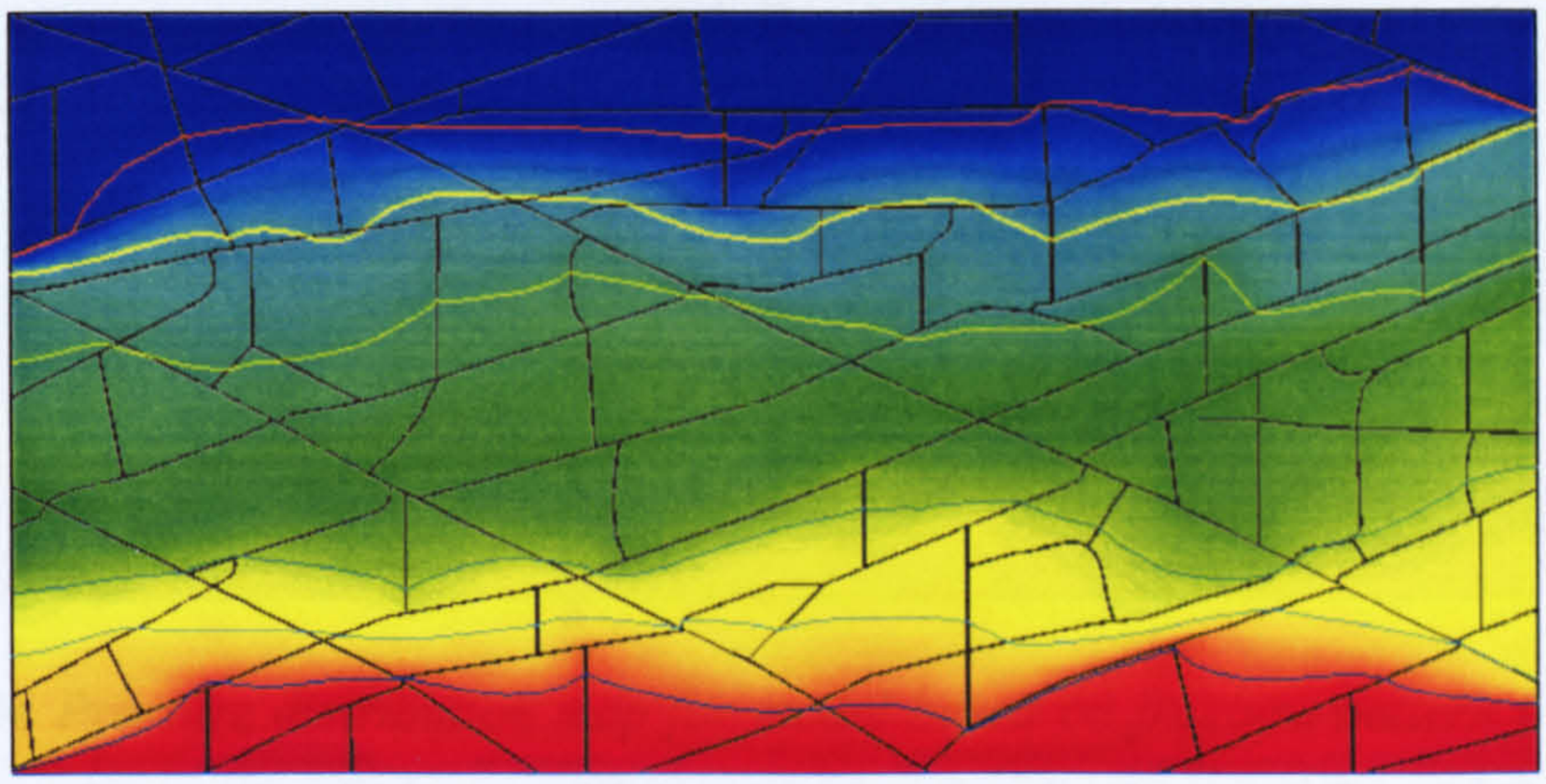


Figure 6.32 *Pressure distribution map in the model based on the joint network in the 32cm thick limestone bed west of the sinistral strike-slip fault at East Quantoxhead (cf. Fig. 6.34).*

In both maps the histogram of fluid flow velocity within the matrix shows skewed to the right whereas the histograms of fluid flow velocities through the joints are skewed to the left (Figs. 6.33 and 6.35).

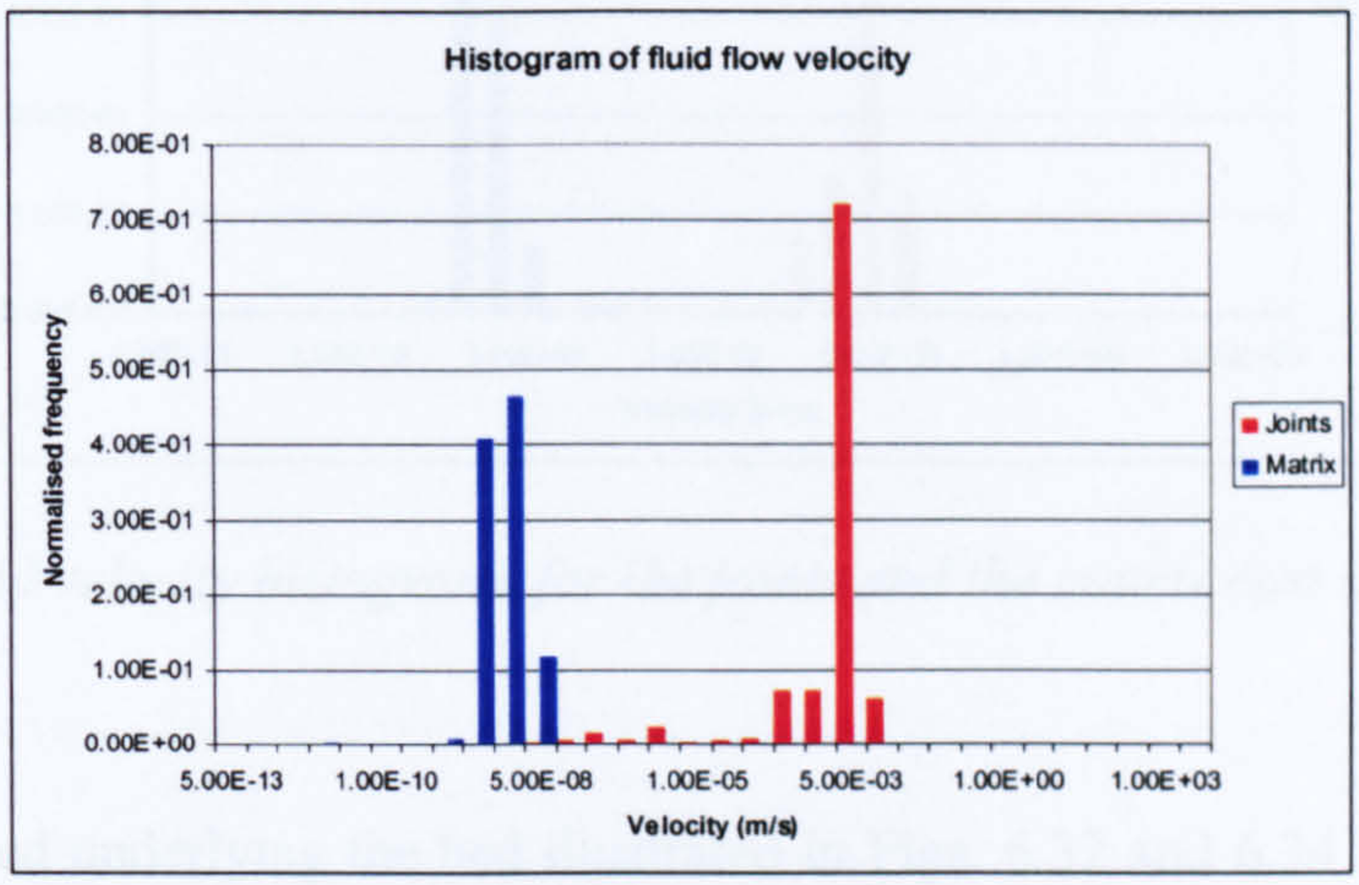


Figure 6.33 *Histogram of fluid flow velocity through the matrix and through the joints west of the fault.*

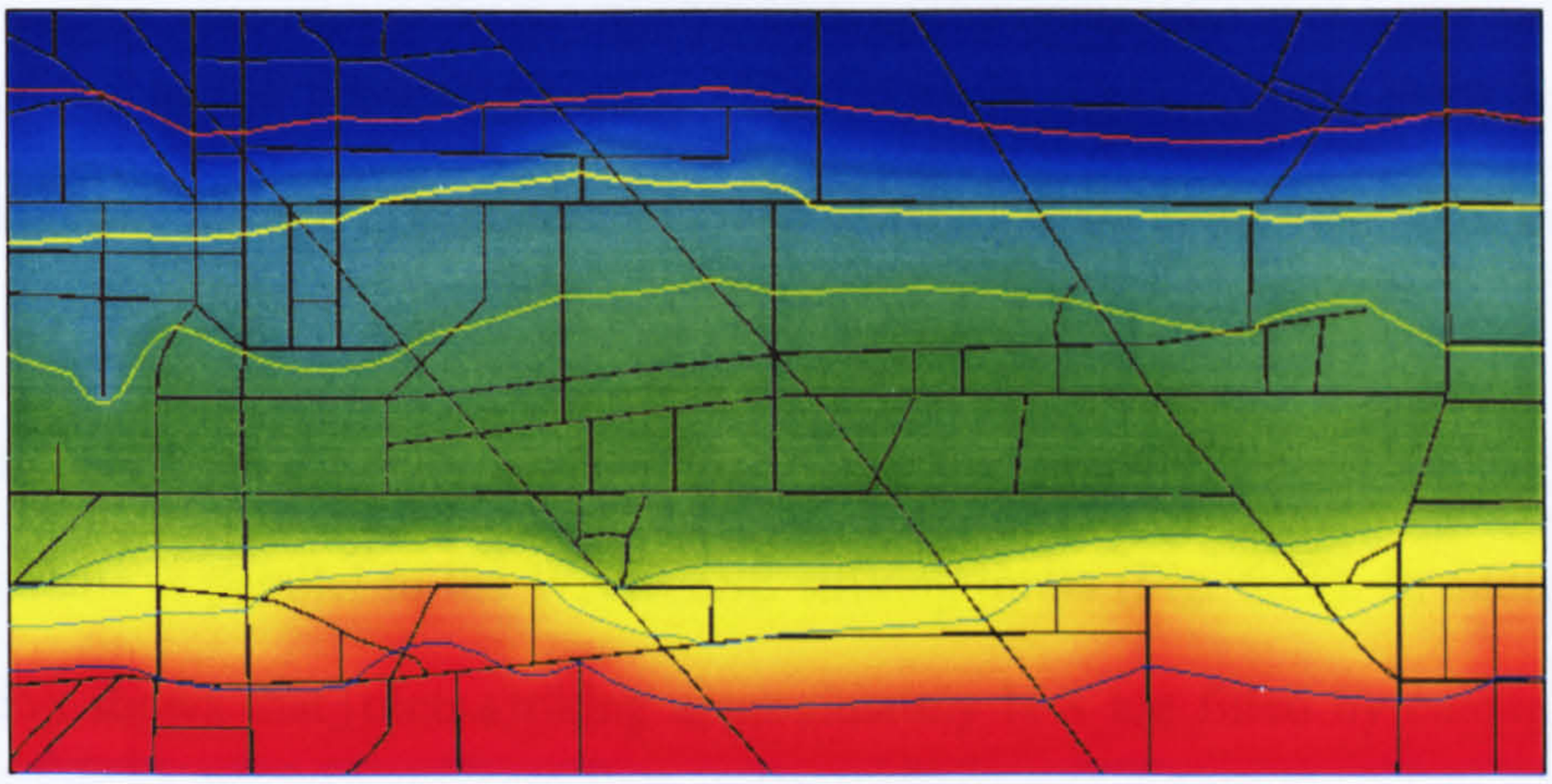


Figure 6.34 *Pressure distribution map for model based on fracture pattern in the 32cm thick fractured limestone bed east of the sinistral strike-slip fault (cf. Fig. 6.32).*

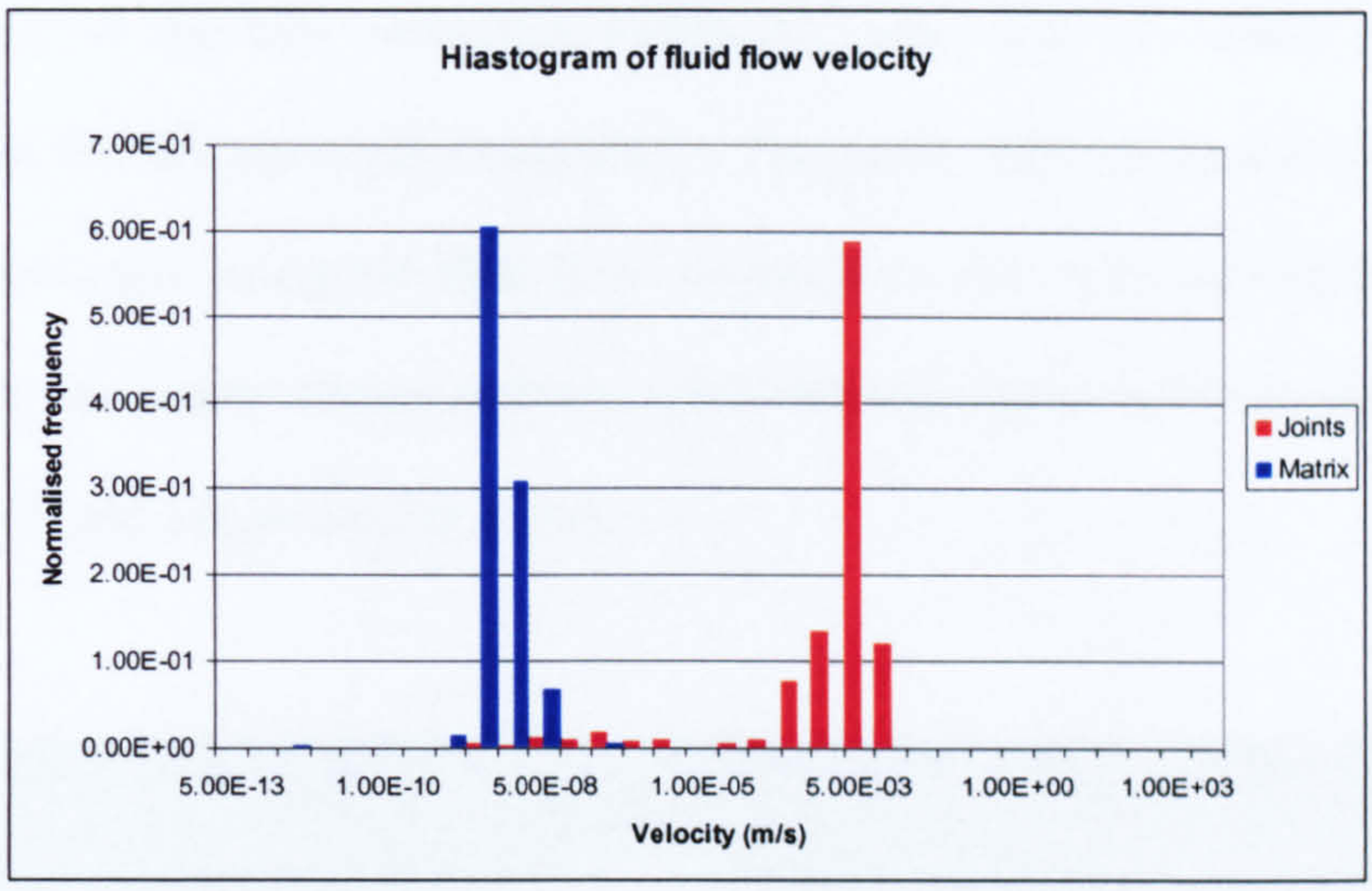


Figure 6.35 *Fluid velocity histograms for the joints and the matrix east of the fault.*

The limestone bed underlying the bed illustrated in Figs. 6.32 and 6.34 is separated from it by a bed of shale 80cm thick. It has a thickness of 33cm and the exposed width of the outcrop is between 1.5m and 2m. The joint length within the 'window' of $15m^2$ is 50.59m giving an average joint density of $3.69m^{-1}$. This bed is less well jointed than the overlying bed described in the preceding section (Figs. 6.32 to 6.35). Calcite veins have been observed cutting the two limestones and the intervening shale in the vicinity of the fault.

It can be noted from the pressure distribution map that pressure represented by different colour scheme is parallel to the WNW-ESE striking joints (Fig. 6.36). In addition, field observation shows that joints striking approximately N-S are filled by calcite. Coarse-grained calcite grew normal to the N-S striking joints. Close inspection of the joints striking NNE-SSW shows that they have been partly utilised to channel mineralized fluid from one segment to another in the N-S striking vein but may have been prevented from opening because of their unfavourable orientation with respect to the pressure gradient.

The histogram of the flow velocities within the joints and the matrix show skewed distribution to the left and right respectively. The joints striking parallel to the far-field pressure tend to open and guide fluid flow. As has been shown by the previous results of the numerical simulation discussed above, the histogram shows hydraulic communication between matrix and the joints (Fig. 6.37).

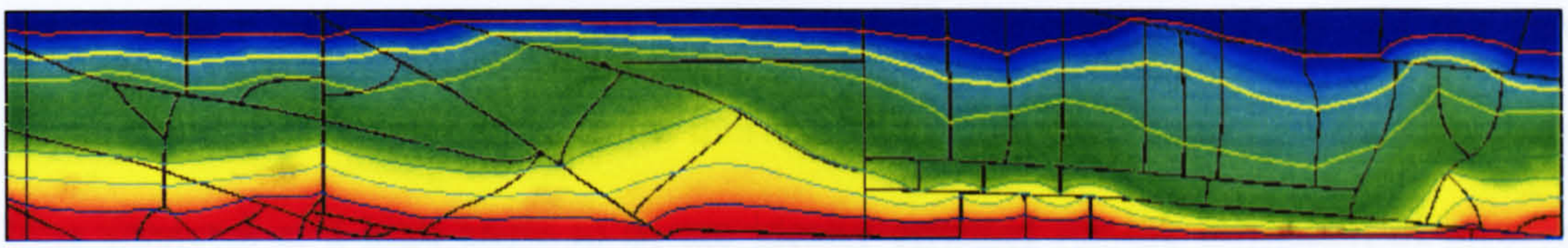


Figure 6.36 *Pressure distribution map of fractured limestone underlying the beds shown in Figs. 6.30 and 6.32.*

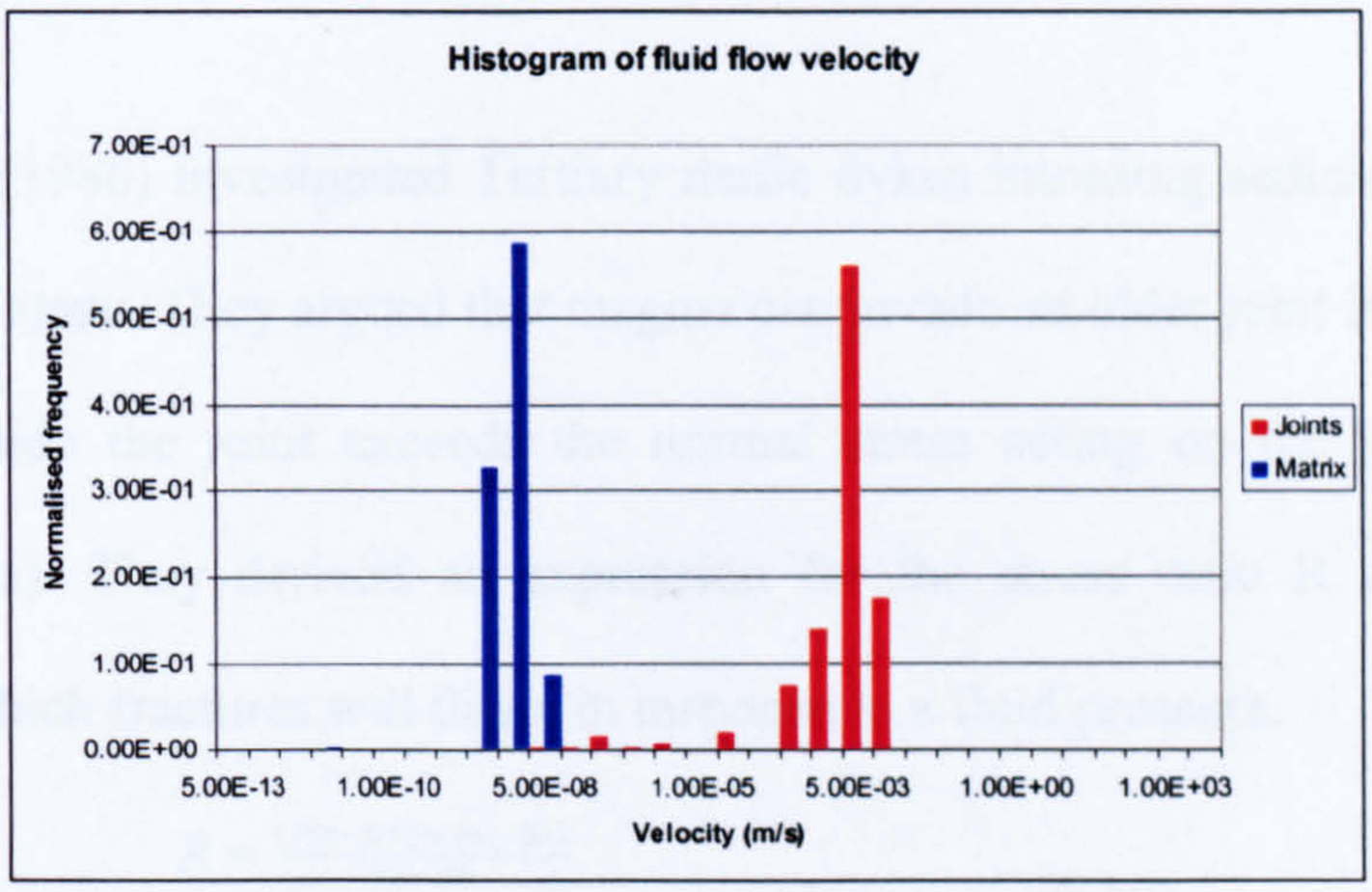


Figure 6.37 *Right skewed histogram of velocity within the matrix and left skewed histograms of velocity within joints obtained by numerical modelling of the fractures shown in Fig. 6.36.*

Joints strike approximately N-S and are exposed around the fault at East Quantoxhead. They are localized around the fault. They are mineralised with coarse-grained calcite and may have propagated during faulting. The majority of Alpine joints are barren, strike at a

high angle to the maximum principal stress and are displaced by the fault. Despite this, earlier workers in the area (Rawnsley *et al.*, 1998; Peacock, 2001) have argued that these joints are the last structures to have formed in the Bristol Channel. The fluid flow models generated in this study, together with field observations, show that the joints that are sub-parallel to the far-field fluid pressure gradient (which is parallel to the maximum principal horizontal stress) will tend to dilate and act as channels of fluid flow. If the joints strike normal or at a high angle to the pressure gradient, they tend to close and the flow direction and the velocity field show that the fluids are not channelled through them. These fractures at a high angle to σ_1 are ideally oriented for the formation of pressure solution cleavage. The strike of the pressure solution cleavage observed at East Quantoxhead and Blue Ben is compatible with the N-S orientation of σ_1.

Delaney *et al.* (1986) investigated Tertiary mafic dykes intruding sedimentary rocks on the Colorado Plateau. They argued that magma can invade an older joint if the pressure of the magma inside the joint exceeds the normal stress acting on the joint plane (*i.e.* confining stress). They derived an expression for the stress ratio R which gives an indication of which fractures will dilate in response to a fluid pressure.

$$R = \frac{(Pm - SH) + (Pm - Sh)}{SH - Sh} \qquad (6.10)$$

where S_H and S_h are the maximum and minimum principal horizontal stresses, P_m is the magma pressure (fluid pressure). When R is plotted against the angle α, (the angle made in the horizontal plane between the vertical fracture and the direction of the least principal stress), four regions can be defined: (Fig. 6.38a): (i) when the stress ratio R is < -1, no fractures are able to dilate (ii) when $R > 1$, joints of all orientations are able to dilate (iii)

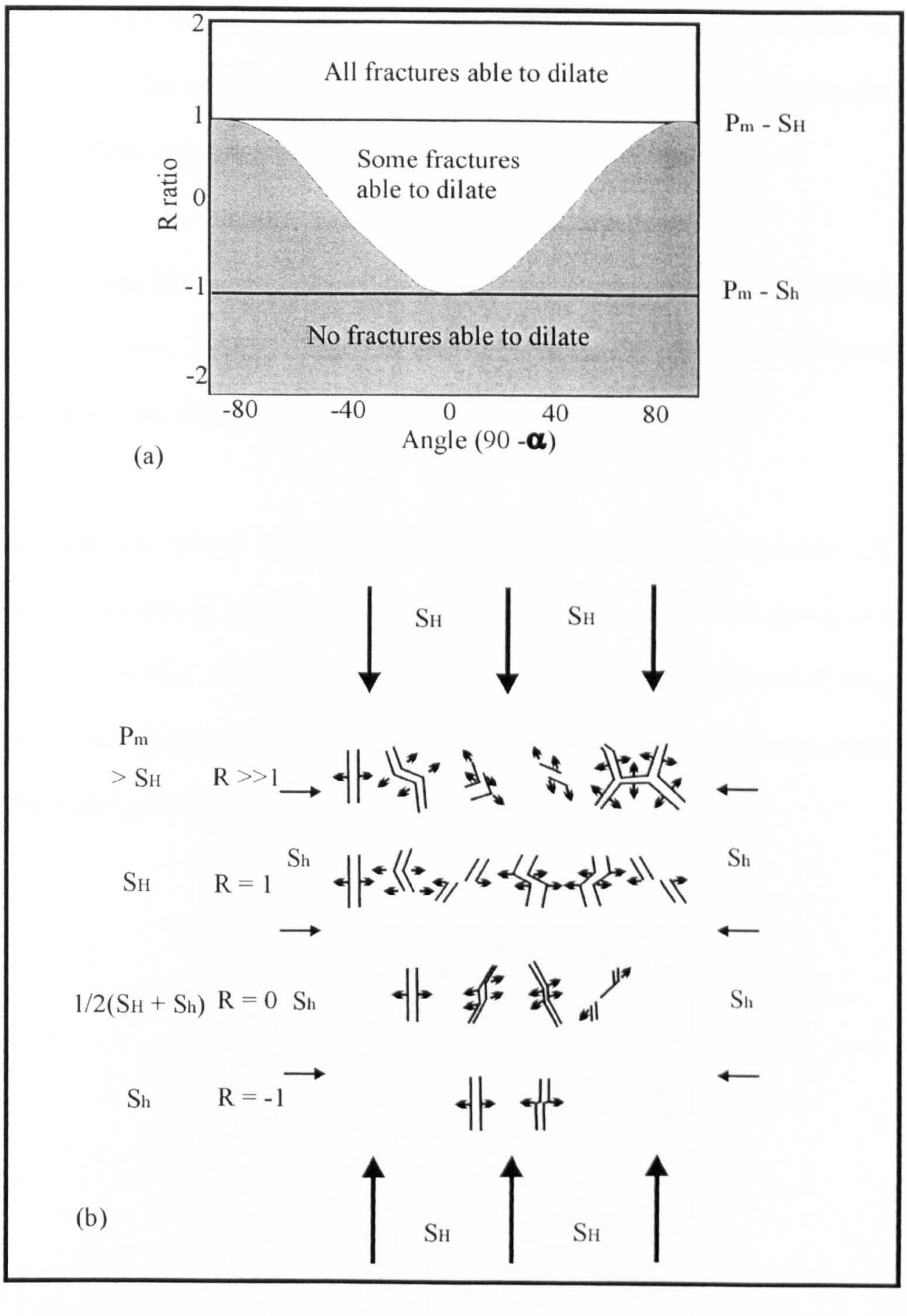


Figure 6.38 *(a) Plot of stress ratio R, magma pressure and the angle between minimum principal stress and joint wall (from Delaney et al., 1986), (b) Range of orientation of joints that are likely to dilate for different stress ratios. Arrows indicate the direction of opening of the joint or dyke (from Jolly and Sanderson, 1995).*

if $-1 < R < 1$, there are two fields in the middle region of the diagram. One lies above the curve defined by the above equation and one below. Above the curve magma pressure is sufficient to dilate suitably oriented joints.

The link between the fluid pressure, the principal stress and the range of fractures that will dilate is shown in Fig. 6.38b. This concept was also applied to the intrusion of igneous dykes in the Mull swarm, Scotland (Jolly and Sanderson, 1995).

The joint network shown in Fig. 6.39 was discussed in detail in section 4.4.7. The 'window' has an area of $36m^2$ and the total length of joints is 308.95m giving an average joint density of $8.58m^{-1}$. The joint sets are made up of an early-formed set of long master joints and a second set consisting of abutting and crosscutting joints. Unsystematic joints which form polygons also occur, but are much fewer.

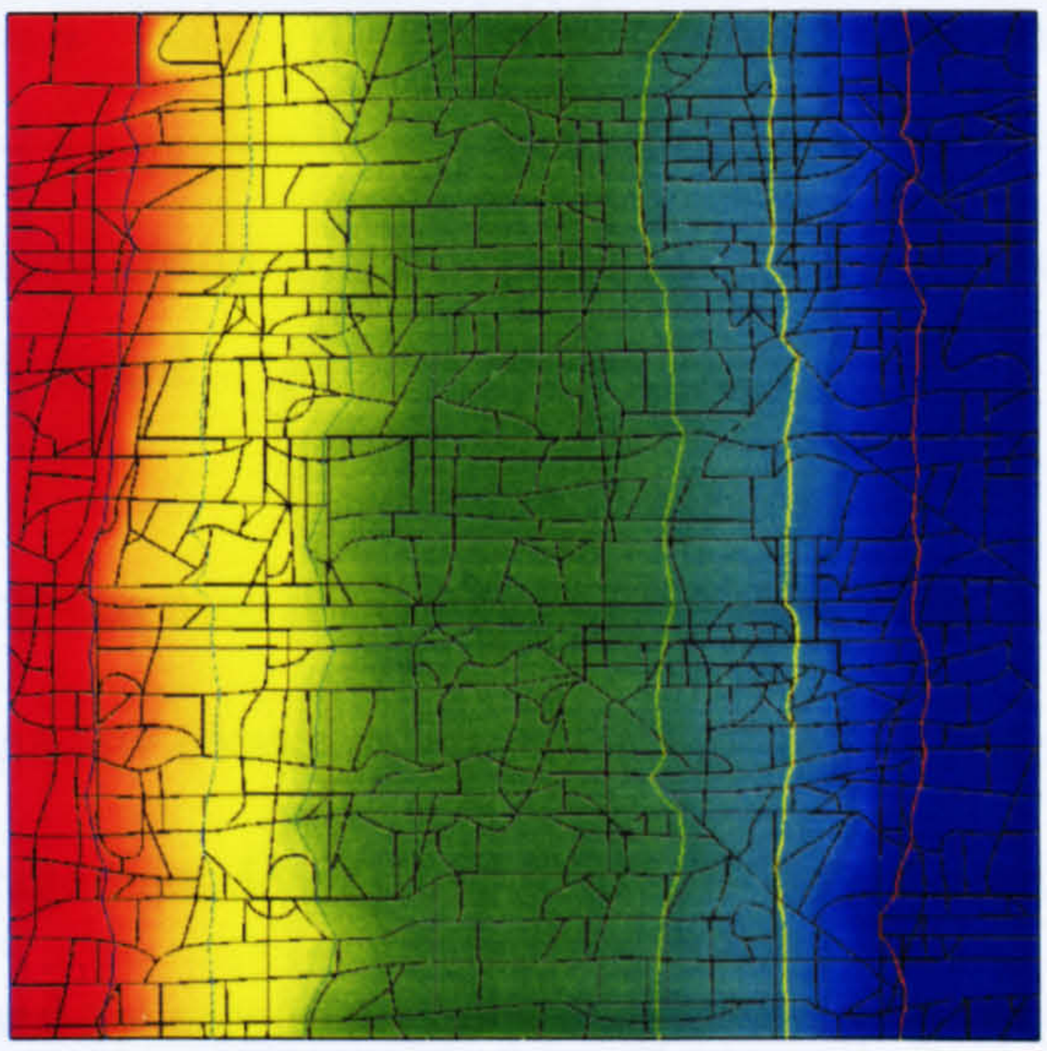


Figure 6.39 *Pressure map of well connected and approximately uniform distribution of joints from the limestone bed at East Quantoxhead.*

The pressure gradient was applied from left hand side and shows some local perturbations at joint intersections *e.g.* where there is confluence or bifurcation of joints in the direction of the pressure gradient (Fig. 6.39). It can be seen from the histogram of flow velocity (Fig. 6.40) that fluid flow velocity through the matrix is skewed to the right whereas that within the joints it is skewed to the left. As can be seen from the histogram of fluid flow, the range of velocity within the joints is high. This is probably the result of joints striking parallel, oblique and normal or at high angle to the pressure gradient.

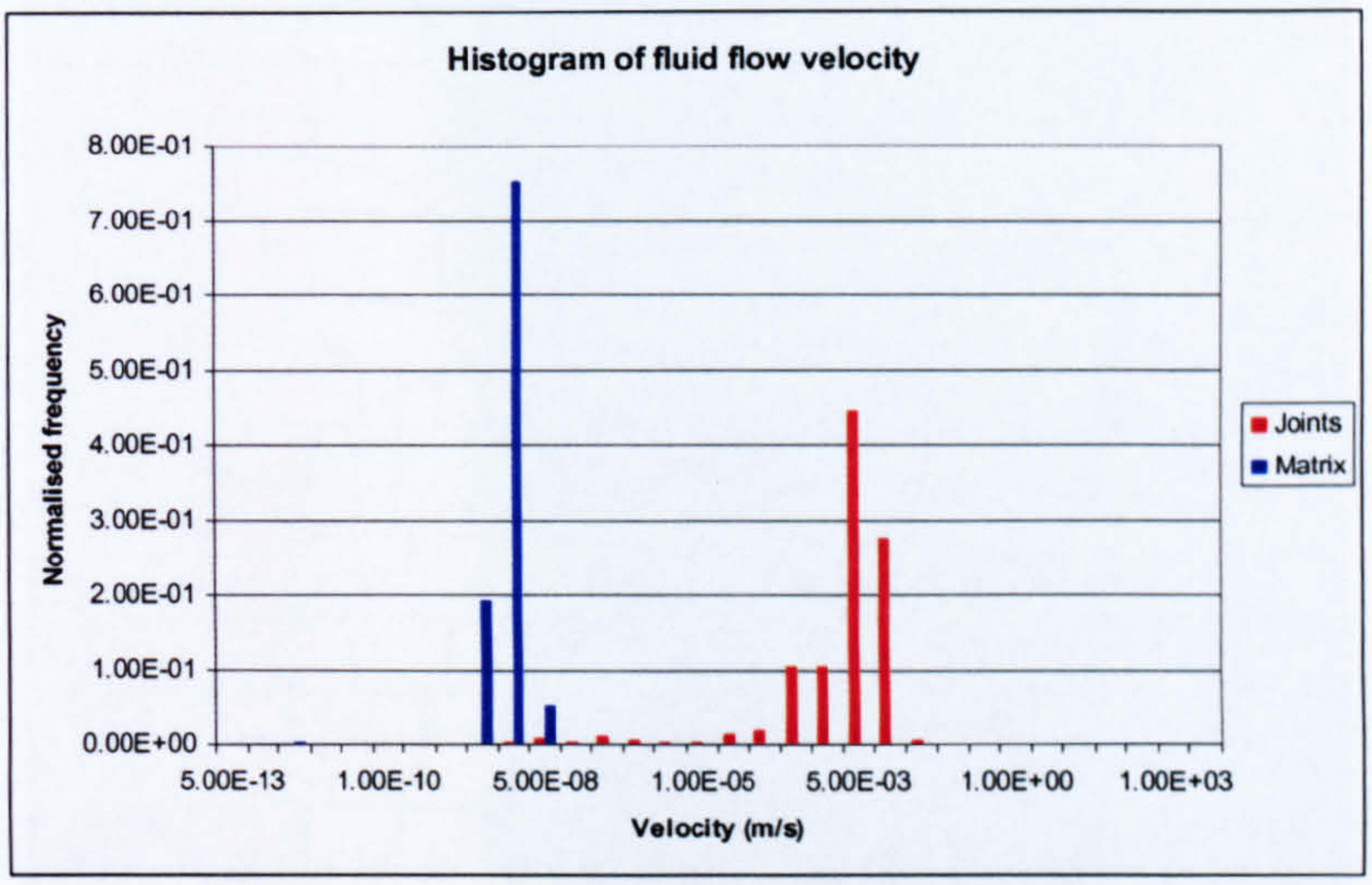


Figure 6.40 *Fluid velocity histogram obtained from numerical models for the joints and matrix from East Quantoxhead.*

The limestone bed which was used to construct the model in Fig. 6.41 is described in detail in section 4.4.7. This window covers an area of $100m^2$ and contains a total joint length of 320.87m giving an average joint density of $3.21m^{-1}$. As can be seen the joint set is made up of an early formed set and the second set consisting of abutting and crosscutting joints. The pressure contours are locally perturbed at the intersections of the joints (Fig. 6.41).

The fluid velocity histogram within the matrix shows a log-normal distribution skewed to the right (Fig. 6.42) and the histogram of fluid velocity within the joints best fits a log-normal distribution skewed to the left. As can be seen from the histogram, fluid velocity within the joints is dispersed and this is probably as a result of the presence of numerous joints with the same strike. This results in neighbouring joints competing to channel fluids.

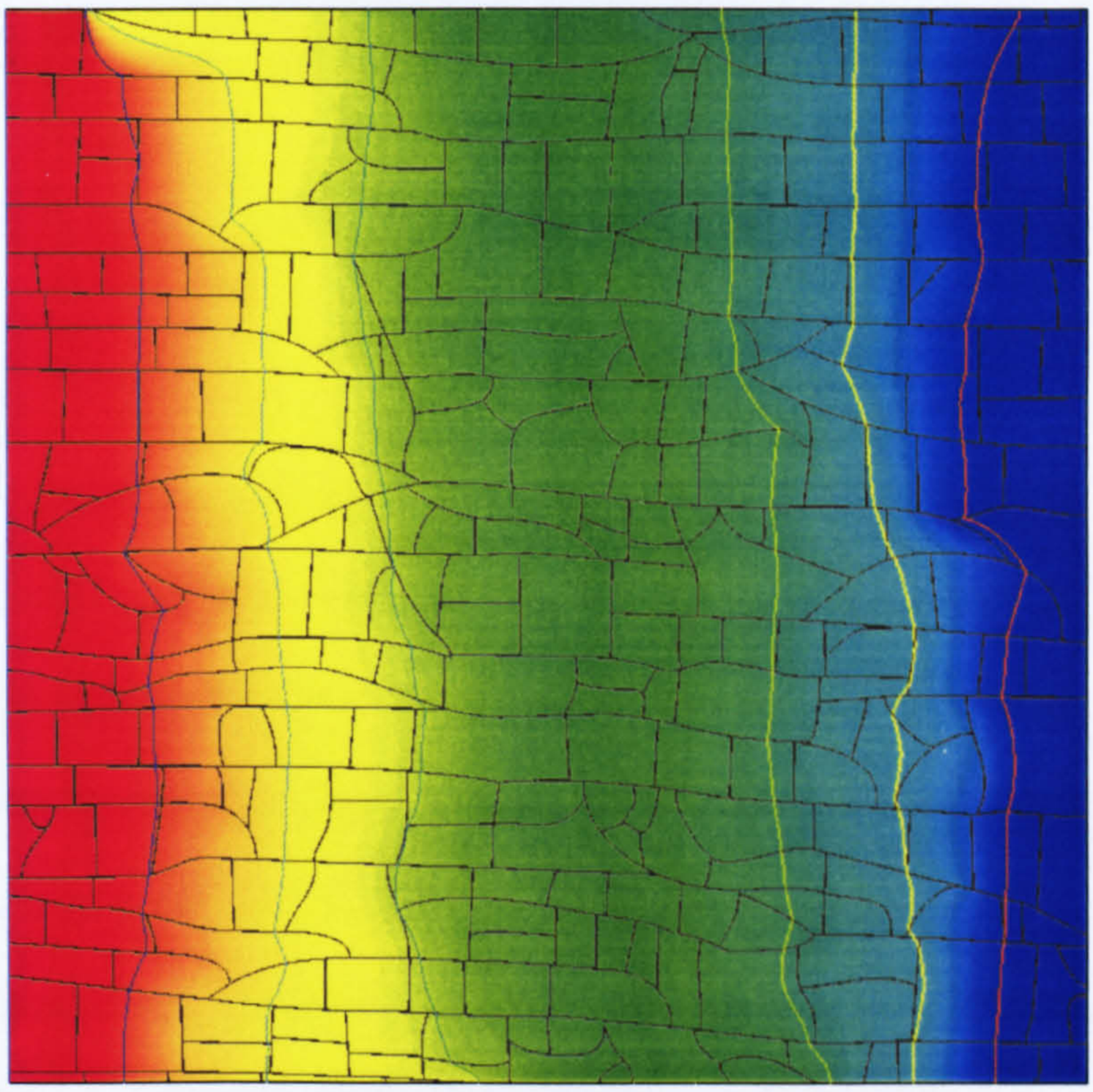


Figure 6.41 *Pressure distributions for uniformly distributed joint network from Blue Ben.*

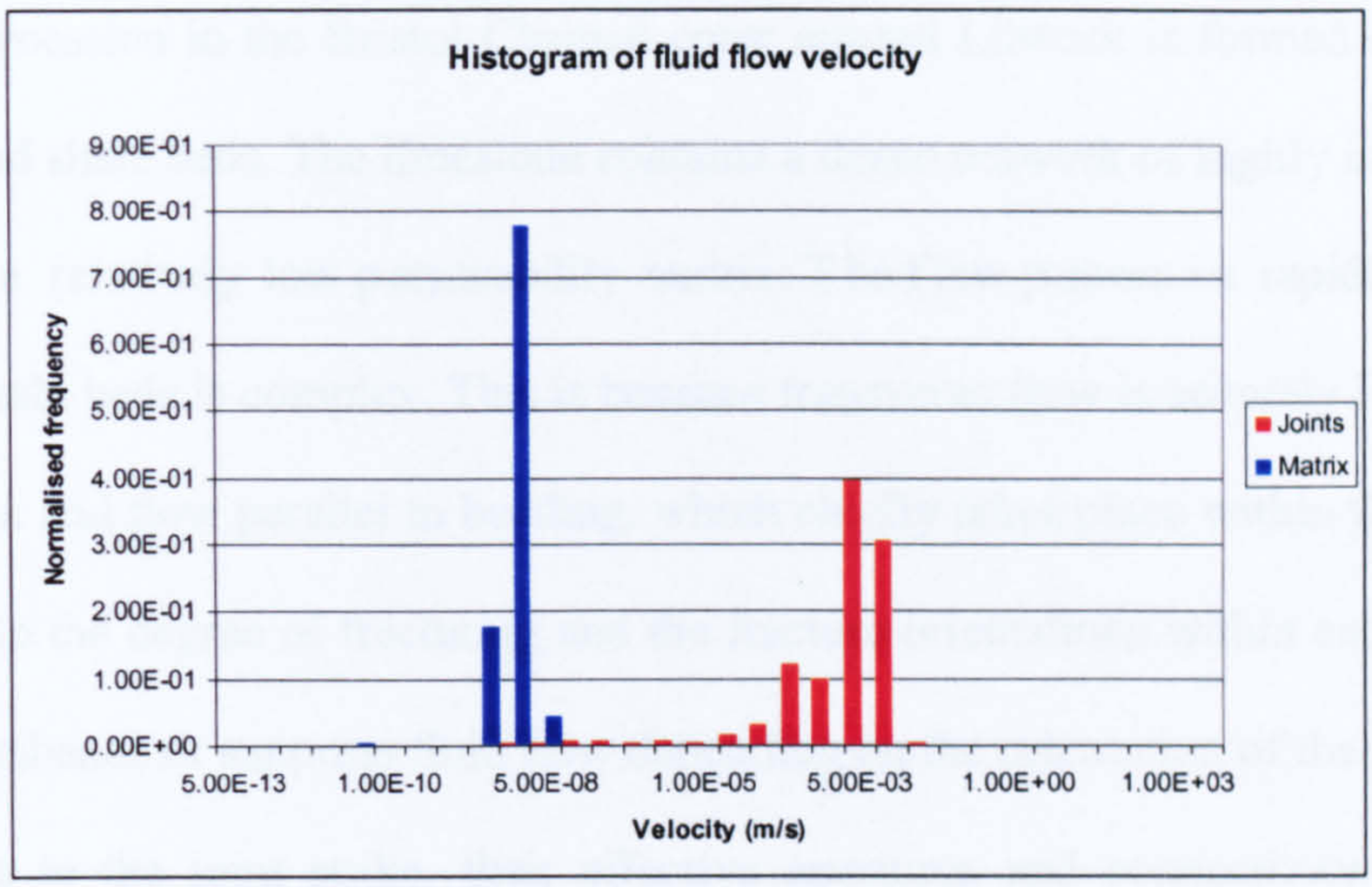


Figure 6.42 *Velocity histogram for the joint and the matrix in a limestone bed of Blue Ben.*

6.7 Discussion

Field observations of fracture networks in limestones combined with the results of the numerical modelling of flow through the networks suggest that the limestone beds in Yorkshire have a strong directional permeability. Flow paths are strongly controlled by the strike of the fractures. Various projects in this area, including engineering projects and hydrogeological projects (*i.e.* the selection of waste disposal sites in the region) require that any major, currently conductive fracture in the area be identified together with the present orientation of the stress field. This study has demonstrated that the flow patterns within fractures have changed with time. For example the ENE-WSW striking joints were the major channels for mineralizing fluids during Upper Carboniferous (see Fig. 6.9) whereas the present day flow in the region (both surface and subsurface) is dominantly along the NNW- SSE trending fractures.

The rock succession in the Bristol Channel coast around Lilstock is formed of alternating limestone and shale beds. The limestone contains a dense network of highly interconnected fractures in a relatively low permeability matrix. The flow pattern in rapidly alternating limestone-shale beds is complex. This is because transverse flow is severely limited by the shale horizon and flow parallel to bedding, which chiefly takes place within the limestones is sensitive to the degree of fracturing and the fracture orientations within each bed. Joints may either enhance or suppress fluid flow depending on the orientation of the flow gradient with respect to the joint strike, their effective apertures and connectivity. In addition, USNCRM (1996) argue that if the rock is fractured the hydraulic properties of rock masses are likely to be very heterogeneous, even within single lithological units.

Although it is mainly the fractures that control permeability in the limestones of the Bristol Channel area, the matrix is also permeable. Flow in dual permeability media, either alternating beds of different permeability or a permeable rock containing fractures, has been studied by numerous authors and it is known that fluid flow trajectories will be deflected when fluids pass from one medium to another with a different permeability (see *e.g.* Taylor *et al.*, 1999). Taylor *et al.* (1999) argue that this deflection (refraction) of fluid particles is similar the refraction of light travelling from one medium to another and will be governed by Snell's Law. The fluid flow in the rocks of the Bristol Channel is mainly bedding parallel and this is a result of the contrast in permeability between the shale and the limestones. The shales are intrinsically impermeable and contain relatively few fractures.

In a system containing multiple joint sets, as for example the limestone beds in the Bristol Channel, the flow path is even more complex. A joint belonging to a particular set may

cause a reduction in flow in adjacent joints of the same set because of their efficiency as fluid pathways. Around such a fracture, a region of reduced fluid pressure will be generated and any joint falling in that region will experience a drop in pressure which will tend to increase flow. Alternatively, if the joints link with each other, they might generate a local zone of high hydraulic conductivity with a correspondingly high flow (see Taylor *et al.*, 1999). In a bed containing a fracture network made up of several fracture sets, the orientation of a joint with respect to the existing fluid pressure gradient and regional stress field will strongly influence its ability to act as a channel of fluid flow. To maximise its permeability, the ideal attitude for the joint is to be parallel to both the maximum principal compressive stress and the fluid pressure gradient. In addition, it should be noted that because joints show widening and narrowing, the joint surface irregularities can generate tortuous flow within the system, thus changing the flow velocity and trajectories.

Any system that contains joints cutting a porous matrix must be treated as a dual porosity or dual permeability system. Flow through both the fractures and the matrix may be good however, if the joints are mineralized or sealed with low permeability materials such as clays, flow through the fractures will be severely impeded. As Nelson (1985) points out, if the presence of an impervious lining on the fractures is not recognised, erroneous estimates of the partitioning of flow within the system are inevitable.

The numerical code used to examine fluid flow through naturally occurring fracture networks in the limestone beds of the Bristol Channel Basin does model dual permeability. The numerical models show that flow velocities in both the matrix and the fractures are variable. For example in areas where two joints converge in the direction of

flow, a local build-up of fluid pressure occurs inside the fracture. This causes flow from the joint into the adjacent matrix or to the nearest neighbouring joint by an indirect hydraulic connection (*e.g.* Fig. 6.28). Conversely when a joint bifurcates in the direction of flow, the numerical model studies show that there is a decrease of fluid pressure inside the joint which tends to increase flow from the matrix into the joints.

Regarding the chronology of the joints, three major joint sets have been recognised in the Bristol Channel Basin. These are burial joints, Alpine joints and post-Alpine joints formed during basin opening, basin inversion and uplift of the basin respectively. Field observation, combined with numerical simulation, show that the Alpine joints predate the NE-SW striking sinistral and NW-SE striking dextral wrench faults. The reasons for this conclusion are as follows:

(i) Joint spacing, joint density, joint patterns, joint strike and the number of joint sets on both sides of the fault are identical.

(ii) The pressure distribution maps and the histograms of fluid velocity through the joints and matrix on either side of the fault as determined using the numerical code described in section 6.4 and 6.5 are remarkably similar (see Figs. 6.32 to 6.35).

(iii) The Alpine joints are clearly displaced by the fault (Fig. 4.27 and 4.50 in Chapter 4)

(iv) If the joints had post-dated the strike slip faults, either the stress field around faults during joint propagation would have been perturbed (*cf.* Rawnsley *et al.*, 1998) with the resulting modification of the joint orientation as the fault is

approached or the joint frequency would have tended to increase as the fault is approached (*e.g.* Peacock, 2001).

It will be recalled from sections 2.4.2.2 (Fig. 2.15b), section 3.6 (Fig. 3.3a) and section 5.6, during thrust faulting, the maximum and intermediate principal stresses were horizontal and the least compressive stress imposed by the overburden was vertical. During buckling of the limestone and shale beds in the study area of the Bristol Channel, layer-parallel shortening and thickening in the vertical direction took place. This gradual increase in the vertical stress leads to a change over between the intermediate and the least principal stresses and creating ideal stress configuration for the formation of strike-slip faults. The condition for the strike-slip faults occurred late in the inversion and it is therefore not surprising that they postdate the Alpine joints.

It has been noted that the fault-related joints that strike ±15° either side of north are mineralised and the E-W striking Alpine joints in the area are barren. As pointed out by Delaney *et al.* (1986) and Jolly and Sanderson (1995), if the joint strike is greater than ±45° to the direction of the maximum principal compressive stress and the stress ratio R is low (equation 6.10 and Fig. 6.38) and these joints tend to remain closed.

CHAPTER SEVEN

DISCUSSION AND CONCLUSION

Massive- to well-bedded Lower Carboniferous Limestones exposed in the Pennines of North Yorkshire, and the Liassic sequence of alternating beds of limestone and shale that crop out on the southern shore of the Bristol Channel Basin, were examined in order to determine and understand the joint orientation, spacing and density pattern within them. They form end members of spectrum of carbonate rocks ranging from massive limestones to alternations of limestone and shale. The regional geological settings of the two areas are briefly discussed in Chapter 2. Controls on joint spacing, mechanisms of joint initiation, joint propagation and evolution of joint spacing are discussed in Chapter 3. In addition, because of the intimate relationship between joints and other structures, particularly folds and faults, an overview of previous work on this topic is presented at the end of Chapter 3. Field observations and a detailed statistical analysis of joint spacing, orientation and density in the two field areas are discussed in great detail in Chapter 4. In order to complement these field observations, an examination of the surface morphology of joints (fractography) is used to infer the palaeo-stress field that generated the Alpine joints in the Bristol Channel study area (see Chapter 5). Because of the abundance of fluids in the Earth's crust and because fractures create anisotropy in rocks so that flow of mineral and hydrocarbon-bearing fluids is focussed along particular pathways, it is essential to consider the hydraulic properties of these fractures. This is discussed in Chapter 6 where an analysis of the 2D joint trace maps measured in the field are analysed using the CSP numerical code.

7.1 The study area in the Pennines

As discussed in section 2.1, the Cove and Gordale Limestones consist of massive- and well-bedded limestones that were deposited the Lower Carboniferous. Joints in these rocks were probably formed during the Upper Carboniferous. The age of the North-, the Middle and the South-Craven Faults, which are the major structures in the study area, is contentious. They are thought by some authors (*e.g.* Dunham and Wilson, 1985; Soper, 2001) to predate the development of joints and to have probably initiated during Ordovician-Silurian times. These faults were active towards the end of the Dinantian, prior to the unconformable progradation of Namurian clastic deposits across the Askrigg block and basin, and also later in the Carboniferous, possibly in dextrally transpressive mode, causing en echelon folding of the basinal rocks to form the Ribblesdale fold belt (Soper, 2001). In contrast, Moseley and Ahmed (1967) argued that the joints are older than the faults. Odling (1992) and Odling *et al.* (1999) suggest that the reason why the joints are mineralised and the faults not may be related to the fact that the joints tend to be more connected to each other than the faults. Dunham and Wilson (1985), in their detailed study of mineralisation in the region, noted that joints with small displacements provided the most effective channels for the mineralising fluids during the Upper Carboniferous. The orientation of σ_1 during joint formation was inferred to lie in an E-W to WNW-ESE direction, which is compatible with the stress field responsible for the Variscan folds in the Craven Basin to the south of the study area.

Renshaw and Pollard (1995) argued that the opening of a vertical joint crossing a horizontal discontinuity such as a bedding plane has to be accommodated by sliding of the adjacent layer along the bedding plane. If sliding along the interface is not possible

and the tensile stress at the tip of the propagating crack exceeds that of the tensile strength of the rock in front of the propagating crack, then the condition will favour propagation across the interface. This stress increases with depth and it follows that fracture propagation across the interface is more likely at greater depth where sliding is inhibited by the increase in layer-normal load. Gillespie *et al.* (2001) also suggest that vertically persistent, through-going joints will tend to form at a greater depth than impersistent layer-bound joints. In addition a strongly-bonded interface between similar layers favours joint propagation across the interface (Helgeson and Aydin, 1991), whereas a joint approaching an interface between two weakly bonded different materials would tend not to propagate across the interface.

There are three important factors that influenced the propagation of through-going joints in the Pennines: (i) many of the bedding planes are defined by stylolites that locked the beds together (ii) the rocks on both sides of the interface are the same, and (iii) the magnitude of overburden stress that assisted joint propagation across the bedding plane boundary. The thickness of sediments that covered the structural highs such as the Askrigg and the Alston Blocks on which the study area is located, is uncertain.

Zones of closely spaced fractures are called fracture corridors common, and these are in the limestones of the Yorkshire study area. They form as a result of strain localisation (Peter Connolly, personal communication) and are briefly discussed in Chapter 4. As pointed out in section 4.3.2, these closely spaced fractures may be formed by the process called crack-tip-shielding (see Olson, 1993 and references therein). This means that regions in front of a long propagating crack have relatively

high driving stresses that are capable of causing smaller cracks to start propagating. However, immediately after the propagating crack by passes these fractures, they stop propagation because they lie within the shadow zone of the main fracture.

As pointed out in section 3.3 and section 4.6, joints evolve from randomly positioned flaws within the rock masses and the histograms of joint spacing initially best fits a negative exponential distribution. With increasing degree of deformation (*i.e.* formation of more fractures) the spacing evolves towards a log-normal distribution. The final stage in joint spacing evolution corresponds to a joint saturation. At this stage joint spacing fits a normal or Gaussian distribution. In the parts of the Pennines of North Yorkshire which were studied, joint spacing ranges between a negative exponential and to a log-normal distribution. Fracture spacing along some of the scan lines fits equally to both negative exponential and log-normal distributions. It is important to consider why the two distributions occur in the same area as they show different stages in fracture spacing evolution. This may be the result of variation in degree of deformation, which resulted from the differences in the mechanical properties of the rocks.

Fracture density data were analysed using a computer programme *Densityinfo*. Joint density values for the through-going fractures of this study area are highly dependent on the window size and shape. As window size increases, the variation in fracture density decreases and focuses in on a representation value. For this reason it is desirable to know the optimum size of the window that samples the fractures representatively and that therefore gives a representative fracture density value. Size for size, rectangular windows gave the most variation in fracture density values.

Fracture density is found to depend on both size and orientation of the window. For example fracture density is different depending on whether the longest side of the rectangle is parallel to or perpendicular to the dominant fracture direction. Using square and circular windows, for the through-going fractures it was found that the variation in fracture density became acceptable *i.e.* fracture density approximates to the mean in windows with areas of more than $20m^2$. Circular windows are found to be the most effective geometry because orientation bias is minimised. Although this window shape gives a more representative measurement of fracture density, it is time consuming and/or impractical to construct such windows in the field. They can however be generated by computer from rectified photographic images.

As discussed in Chapter 4, mineralisation in the study area was mainly controlled by ENE-WSW to NE-SW trending fractures (Fig. 6.9). Some of the NW-SE striking joints are also mineralised. The present-day flow (both surface and subsurface) is mostly along the NW-SE fractures. This indicates that the hydrological effect of a fracture can change with time. This may be a result of change of permeability of fractures caused by pressure solution, deposition of minerals to form veins, or because of a change in the stress field that alters the normal stress across different fracture sets.

7.2 The Bristol Channel study area

As discussed in section 2.4, the Bristol Channel Basin is an exhumed E-W trending basin that was formed in the Palaeozoic basement during the Permo-Triassic and continued throughout the Jurassic to Early Cretaceous. Basin inversion occurred during the Cretaceous-Tertiary. Joints are classified into three main categories,

namely: burial joints associated with basin subsidence, Alpine joints related to Alpine compression and basin inversion, and post-Alpine joints that are related to uplift.

7.2.1 The role of the normal faults

Micro-veins formed during Permo-Triassic basin opening, when the limestone layers were subjected to layer-parallel extension. An abundance of fluid charged with $CaCO_3$ was drawn into these 'open' spaces and the process of infilling and rupture by a crack-jump mechanism (Caputo and Hancock, 1999) continued until the strain became sufficiently focussed for the formation of vertical veins. At this stage, the rate of mineral infilling did not match the rate of opening of the rupture and empty spaces were created (Fig. 4.20). Some of the vertical veins in the limestone beds were later linked to the adjacent limestone bed by the formation of an oblique fractures in the intervening shale (Peacock and Sanderson, 1991) (see Fig. 4.20). It can be seen from Fig. 4.20 that the normal fault is made up of a series of offset vertical extensional fractures in the limestone beds linked by oblique fractures in the shales. Slip on this stepped fracture results in the formation of pull-aparts. The formation of vertical veins in the limestone beds is therefore precursor for the formation of normal faults. Micro-veins terminate at the limestone-shale contacts, indicating that lithological control was significant. Coeval vertical extensional and oblique shear fractures were seen in an 80cm thick marly layer at Kilve Beach, suggesting that the differential stress was around four times the tensile strength of the rock during the formation of these fractures.

Alpine joint spacing, orientation and density have been studied on the hanging-walls of the normal faults (Figs. 4.26a, b and 4.28). The normal faults predate the Alpine

joints. However, the normal faults are also partly filled by calcite veins and as a result did not have a significant mechanical role during the development of Alpine joints as neither the joint density nor joint spacing increases as these faults are approached.

7.2.2 The relationship between joints and folds

Alpine joints in the hinge region strike parallel to the fold axis. These joints were formed synchronously with folding. Thin limestone beds generally show a smaller spacing than thicker beds, but a systematic relationship between joint spacing and bed thicknesses is difficult to establish. In addition joint spacing is not found to depend on structural position *i.e.* on the degree of deformation.

Scan line measurements and window sampling on adjacent competent limestone beds on both the northern, gently dipping limb of the Lilstock anticline (Fig. 4.35), and on the south-dipping limb (Fig. 4.36) show great variations in the strike of Alpine joints. Despite excellent exposures of fractured limestone beds in the Lilstock and Kilve areas, it is extremely difficult to determine any systematic geometrical relationships between either a particular fracture set within the same bed or between fracture patterns in different beds and structural position. Despite the simple structural evolution of basin opening and closure, the fracture patterns, orientation and spacing are extremely variable. The anticlines described at Lilstock and Kilve are small-scale examples of structural traps that are targeted for hydrocarbons and that are typical of this type of sedimentary basin. The variability in fracture orientation and density within a single bed and the very different fracture networks that occur in adjacent limestone beds because of the decoupling effect of the intervening shales, revealed by

this study, highlight some of the difficulties that are likely to be encountered in the prediction of fracturing in these potential reservoirs.

7.2.3 Reverse faults

The effect of reverse faults (*i.e.* inversion of normal faults during the Alpine phase of basin inversion) on Alpine joints was not observable in the study area. At Lilstock, the strikes of Alpine joints converge at the intersection of the two fault segments striking ENE-WSW and WNW-ESE (see Figs. 4.27 and 4.29). This is interpreted to have been caused by stress concentration at sticking points along the faults (see Rawnsley *et al.*, 1998).

7.2.4 Strike-slip faults

As was discussed in sections 2.4 and 2.5, and in Chapters 4, 5 and 6, under the stress regime associated with folding and thrusting (*i.e.* basin inversion), σ_1 and σ_2 were horizontal (N-S and E-W respectively) with σ_3 being vertical. This caused layer-parallel shortening and thickening that led to a swap of the intermediate and least principal stresses and the onset of the conditions appropriate for formation of wrench faults. At Lilstock (Fig. 4.27), at Kilve (Fig. 4.43) and at East Quantoxhead (Fig. 4.50), the Alpine joints are clearly displaced by the resulting NE-SW striking sinistral strike-slip faults. One exception has been seen at Kilve Beach where the strike of Alpine joints in a 10cm thick limestone changes systematically from ESE-WNW through E-W to NE-SW to intersect a dextral strike-slip fault at right angles. The reason for this is not clear but it indicates this fault predated the fractures.

The fracture patterns on the southern margin of the Bristol Channel coast are determined by several factors including the position within a fold, the mechanical

properties of the competent and the intervening shale beds and the interaction between the remote and local stresses. The field observations discussed in Chapter 4 show that the joint patterns in the limestone beds of the Bristol Channel area vary from one bed to another. This suggests that fracturing of each bed occurs totally independently of the others *i.e.* that there was a decoupling across the intervening shales. In one particular example (Fig. 4.24) where the intervening shale is very thin (*i.e.* not visible to the naked eye), fractures propagated either vertically upwards or downwards from the two adjacent limestones without significant offsets. In areas where the shale beds are thin, the degree of offset between fractures in successive limestone beds is not very significant. This indicates that the degree of offset depends in part on the thickness and mechanical properties of the shale beds and indicates that the thicker shale beds did act as decoupling horizons allowing stress/strain partitioning during the formation of the Alpine joints.

7.2.5 Joint spacing and bed thicknesses

As noted above, analysis of data collected on the southern margin of the Bristol Channel shows that joint spacing and bed thicknesses are not simply related. Alpine joints are only parallel to the fold axis in the hinge region of the fold, as for example in the Lilstock and Kilve anticlines. As one moves away from the hinge region towards the limbs, the variation in joint orientation increases.

7.2.6 Joint spacing as a function of structural position

As pointed out in Chapter 3, the value of joint frequency depends on the degree of deformation. Scan line sampling of the Alpine joints around the hinge of the Kilve fold and to the east of Lilstock (Fig. 4.25) suggests that joint spacing varies neither

with the structural position nor bed thickness. It may be more dependent on the mechanical properties of the fractured competent beds and the intervening incompetent layers. Joint spacing for Alpine joints has been discussed in section 4.6.2, and fits best to a negative exponential distribution *i.e.* a distribution characteristic of the early stage of joint evolution. Conversely, post-Alpine joints fit best to a log-normal distribution indicating a more advanced stage in joint spacing evolution.

The relationship between folds and fractures has been discussed in section 3.6.2. A comparison of the complex joint patterns around the folds on the southern margin of the Bristol Channel coast with those predicted to form in conceptual fold models taken from the literature, show that none of the models match the joint networks in the area. The predicted strain distribution in the flexural slip fold models (see *e.g.* Ramsay, 1967; Couples *et al.*, 1998) best approximates the complexity of the strain (expressed as fractures) seen in the joint networks of the Bristol Channel area.

Depending on the thickness and mechanical properties of the intervening shale beds, varying degrees of mechanical communication between joints in adjacent competent beds has occurred. Thus, depending on the thickness of the shales composite joints (*i.e.* through-going joints) may form or the two layers may fracture independently. The thickness of the incompetent shale beds in the southern margin of the Bristol Channel is mostly greater than that of the competent limestone beds and so the shales served as major decoupling horizons that controlled the partitioning of stress and strain during the formation of joints associated with the Alpine Orogeny. Both low overburden pressure and the presence of shale between the limestone beds assisted the containment of joints within individual competent limestone beds. Some joints do

communicate through the shale horizon. These through-going or multilayer joints (Al-Mahruqi, 2001) may have formed by the linkage of two or more favourably positioned Alpine joints within the adjacent limestone rather than by the propagation of a joint from one limestone to the next through the intervening shale.

7.2.7 Fractographic evidence seen on joint faces

A study of plumose structures and twist hackle fringes on joints from the southern margin of the Bristol Channel has been used to determine where joints initiated, the direction of joint propagation, and the palaeo-stress orientation during the Alpine deformation. It was found that regardless of the strike of the parent joints in which they are contained, twist hackle fringes strike approximately E-W. In the hinge region joints are sub-parallel to the fold axis and they are dynamically stable in the N-S stress field. The plumose structures in these fractures propagate E-W and both the twist hackles and the axial joint sets indicate that the remote compression was N-S. Initiation points of the joints are mostly in the middle of the bed. Field study of plumose structures on joint surfaces show that propagation radiates from the point of initiation until it encounters regions with different material properties. Thus, the joints are arrested by the shales that overlie and underlie the limestone bed but propagate considerable distance in a direction parallel to bedding.

7.2.8 Fluid flow modelling

The geologically realistic fracture networks obtained from the field studies in the Pennines and the Bristol Channel Basin have been used to study fluid pressures, fluid velocity and fluid flow pattern within the joints and the surrounding matrix. The numerical code used in this analysis utilises the traditional finite element method to

calculate the pressure variation implicitly and the finite volume method to determine the volume flux explicitly (IMPES) (Helmig, 1997; Geiger *et al.*, 2001).

When the fracture system is dominated by long fractures, the fluid pressure is highly perturbed (Fig. 6.7). A high pressure front advances parallel to these fractures from the fluid source areas from where the fractures extend. The flow velocity within the matrix and fractures is complex and the fluid flow trajectories follow tortuous paths. Regions of enhanced and reduced fluid flow are created within the matrix and inside the fractures. The enhanced fluid velocity within the matrix that occurs in the proximity of fractures is caused by flow from the matrix to the neighbouring joint.

In well-connected fracture systems such as those that occur in the competent limestone beds in the Bristol Channel area, the fluid pressure and thus the flow velocity within the fractures can be correlated with the orientation of fractures with respect to the direction of the remote pressure gradient applied to the system. The outputs from the numerical analyses include the flow velocity histograms for both the matrix and the joints. In the majority of the histograms, the matrix velocity is skewed to the right and that of the velocity within the joints skewed to the left. It is argued that this includes hydraulic communication between the matrix and the joints. Odling (1992) concludes that fracture induced permeability is a function of the number of fracture sets, and the number of fracture intersections (connectivity) as well as fracture density. The results in this work suggest that the different plateaux on the histograms correspond to the highest velocities along the most hydraulically conducting joint sets. These are generally the relatively long joints sub-parallel to the applied fluid pressure gradient. In areas where two joints converge in the direction of the fluid pressure

gradient, the fluid pressure inside the fractures increases. This causes flow from the joint to the neighbouring matrix or to the nearest joint through an indirect hydraulic connection (Fig. 6.28). Conversely, if the joints bifurcate in the direction of the fluid pressure gradient, the pressure inside the fracture decreases. This may lead to flow from the matrix into the joint. If the joints strike at a high angle to the fluid pressure gradient, the flow trajectories cross the joints rather than running parallel to them. In Fig. 6.30, the flow trajectories cross the Alpine joints. A study of the pressure map from the analysis (Fig. 6.30) shows how the main joints compartmentalise the fluid pressure.

When the joint strike is oblique to the fluid pressure gradient (Figs. 6.20, 6.22 and 6.26), the gradient locally rotates. As can be seen from these figures, the pressure map is strongly controlled by the strike of oblique joints. As noted above, the skewing of the normalised fluid velocity histogram for the matrix to the right and for the joints to the left is taken to indicate that hydraulic communication occurs between the matrix and the fractures.

The numerical studies show large variations in fluid flow velocity within the fracture networks and that fluid flow is tortuous in a fractured system. In a fractured rocks, flow can be approximated by the cubic law that states that flow rate is proportional to the cube of the aperture and to the pressure gradient across the model (cross sectional area) and is inversely proportional to the dynamic viscosity. Recent investigations, however, have shown that it is appropriate to use the effective hydraulic aperture of the fracture in this law and that this is less than the mechanical aperture (Odling, 1992; Renshaw, 1995; Taylor *et al.*, 1999).

Layer-bound (strata-bound) and through-going joints represent the end members of a spectrum of joint type. As discussed in section 4.1, persistency across a bedding plane is determined by the resistance to slip. This is determined not only by the intrinsic cohesion but also by any subsequent modification of this during diagenesis (*e.g.* the formation of stylolites will increase the resistance to slip on bedding), and by the normal stress acting across the bedding.

7.3 Conclusions

- The orientation of the stress field responsible for the folds in the Craven Basin south of the area of study, and that determined by interpretation of the fractures in the field area are the same. This indicates fracturing took place at the same time with Variscan Orogeny.
- Joints in the Pennines were formed at a greater depth compared to the joints in the Bristol Channel Basin. This relatively high lithostatic load, together with bedding plane irregularities such as stylolites, and the identical mechanical properties of adjacent beds of limestone (no intervening shale) in the Pennines all assisted fracture propagation across the bedding interface and explains the dominance of through-going joints in the region.
- In both the Pennines and the Bristol Channel, spacing of joints in both through-going and layer-bound joints fit a statistical unimodal distribution. This may indicate that a deterministic process operated during the propagation of joints.
- Based on field work and numerical models, the following chronology of events is proposed for the Bristol Channel coast. Different parts of this chronology are also supported by work carried out by previous investigation as indicated below.

1) Basin opening took place during the Permo-Triassic with the deposition of continental sediments. This gave way to marine conditions at the Triassic-Jurassic boundary (*i.e.* Liassic) and led to the deposition of a shale-limestone sequence. Diagenesis and lithification of the sediments resulted in the formation of vertical high density veins (Rawnsley *et al.*, 1998) or micro-veins (Caputo and Hancock, 1999) and vein networks formed around the embryonic normal faults at an early stage. Vertical strata-bound extensional joints then formed and those appropriately positioned linked obliquely to form the normal faults (*e.g.* Peacock and Sanderson, 1991); some of which had a listric geometry.

2a) Inversion took place during the Cretaceous-Tertiary Alpine Orogeny. Structures that formed in response to the associated N-S compression were thrust faults and minor reverse displacements on the normal faults, outcrop scale folds with associated weakly developed incipient cleavage and Alpine joints.

2b) NNW-SSE dextral and NNE-SSW sinistral strike-slip faults formed at the end of Alpine compression. Uplift took place during which the post-Alpine joints were formed.

- From field observations of joint orientations and from fractographic evidence, it is concluded that the Alpine compression was consistently N-S throughout the deformation.
- In the Bristol Channel Basin where the rocks show a contrast in mechanical properties, adjacent competent limestone beds are separated from each other by intervening shale and as a result may contain different fracture patterns. The shale allows the adjacent limestone beds to become mechanically decoupled, which results

in partitioning of strain along the bedding plane interfaces.

- Fluid flow in fractured rock masses is strongly controlled by orientation and spatial organisation (connectivity) of fractures, direction of fluid source and stresses. Fluid flow is mainly governed by joints that are suitably oriented with relationship to the pressure gradient to allow selective channelling of the fluid flow.
- Preliminary studies show that the contribution to porosity of 3D blocks and their associated fractures the fracture is around $1/20^{th}$ of that of the pores. Nevertheless, the numerical studies described earlier show that the fracture totally dominates the movement of fluids through the rock medium.

7.4 Recommendations for future work

The southern margin of the Bristol Channel Basin is an area in which the various structures formed during the extension and inversion of an evolving sedimentary basin can be studied. An important aspect of future work will be the detailed study of micro-veins (Caputo and Hancock, 1999) or high-density veins (Rawnsley *et al.*, 1998). The view expressed in this thesis is that micro-veins were formed during basin opening and represent the earliest expression of brittle failure in the competent limestone beds. After their formation the stress field was locally perturbed in the region around the fractures but a gradual restoration of the stress field took place with the infilling of the fractures by fine-grained sparry calcite. The veins are the result of series of such rupture and seal events. A detailed study of the textures of these veins allows the various stages in their evolution to be identified. It is suggested that to achieve a fuller understanding detailed field study and numerical modelling should be undertaken so as to obtain an insight into the mechanical processes and resulting structures that form during the incipient stages of extension of a sedimentary basin.

Using the Complex Systems Platform (CSP) numerical code (Matthäi *et al.*, 2001) the 2D fluid flow in fractured and porous media has been modelled in fractured limestone beds and encouraging results have been obtained. This work demonstrates that the existence of fractures within rock masses imposes a mechanical anisotropy on the rock that can dramatically influence the fluid pressure and flow velocity distribution. It is planned to extend this work to examine patterns of 3D flow in single layer and multilayer sequences made up of rocks with contrasting mechanical properties such as porosity, permeability, existence or absence of fractures and differences in the spatial organisation of the fractures.

Fracture density is defined differently depending on the technique used to measure it. When measuring using a scan line (1D), it is defined simply as the number of fractures per unit length of the scan line. When working on fracture windows (2D), the fracture density is defined as the length of fracture trace in the window divided by the area. Fracture can also be defined in 3D as the total fracture surface area to the volume of rock mass. The study of fracture density described in this thesis is related to either scan line or window studies. However, because the thickness of the limestone beds containing the fractures are known it is possible to adapt the 2D window into 3D analysis. From the analysis it would be possible to calculate the void ratio (defined as the volume of voids to the total volume of rock mass) and to establish the percentage contribution of the pores and fractures to the total porosity. Previous studies by the author show that the volume of the pores is approximately20 times greater than tht of the fracture. Nevertheless, as indicated by the analysis and fluid flow through the dual porosity media outlined in the thesis, it is clear that it is the fractures that control the movement of fluids in the rock mass.

The 3D study of the fracture networks will enable the aspect ratios of individual fracture bounded blocks (*i.e.* the ratio of the shortest to the longest axes of the blocks) to be determined. This is very useful in quarrying as it permits the calculation of the maximum surface area (2D) and volume (3D) of blocks that can be obtained from a fractured rock mass. The formation of different sizes and shapes of individual blocks in a quarry results from the mutual intersection of discontinuity sets (most important being joints and bedding) with different spacing and orientation. Both the spacing and persistence of discontinuities greatly influence the size of individual blocks in fractured rocks. The mutual orientation of joints determines the shape of the individual blocks within the rock mass. The number of discontinuity sets also influences the appearance of the rock mass. Block sizes and shapes are the direct results of the joint spacing, persistence of discontinuities and the number of discontinuity sets.

The models of fluid flow within the fractured rock masses discussed in this thesis have been constrained to those using single fluid. Geological problems related to flow through such system are often complicated by the fact that more than one fluid is involved (*e.g.* oil, water, gas). The numerical analysis is capable of incorporating such multiphase flow problem and it is suggested that a study of fluid flow of multiphase fluids through the natural fracture networks described in Chapters 4 and 6 be carryout. For example the output from these enables one to determine the relative permeability curves for the fractured limestones for two liquids with different properties and examine the sweep efficiency, a factor of critical interest to the oil industry and reservoir engineering. In addition, the study would help to identify the degree of saturation within the matrix where the magnitude and direction of specific discharge and saturation changes with time.

The numerical analyses described in the thesis have all involved a constant pressure being applied along one side of the model. It can be argued that a geologically more realistic situation is one of several transient pressure pulses and the CSP numerical code is able to cope with this. In the following section some examples are shown of snapshots of transient flow analysis. The fracture pattern shown in Fig. 7.1 was described in detail in section 4.4.3.1 (Fig. 4.27) and its response to a fluid pressure in Chapter 6 (see Fig. 6.16). In the experiment shown in Fig. 7.1, the fluid pressure was applied on the left hand side and released after 2 hours.

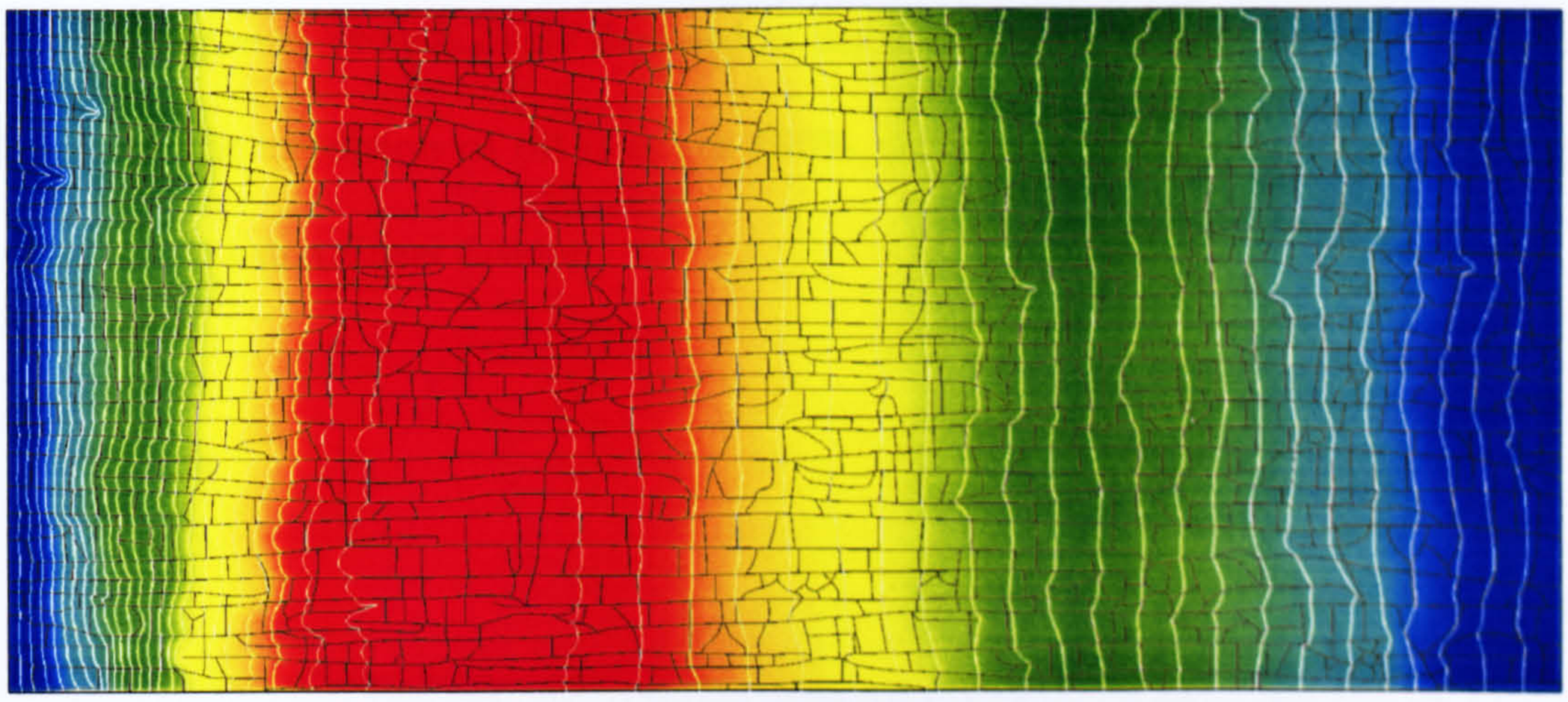


Figure 7.1 *Pressurised 2D window model with gradient decreasing from left to right. Pressure on the left-hand side was released after 2 hours. Note the strong perturbation of pressure contours around the main joints.*

The fracture trace maps shown in Figs. 7.2 to 7.5 were discussed in section 4.4.3.2 (see Fig. 4.31) and Fig. 6.18 where their responses to a constant fluid pressure on a single-phase fluid was considered. The model was saturated with oil to examine the sweep of oil by water from the fractures and matrix.

For the transient flow analysis shown in Figs. 7.2, 7.3, 7.4, 7.5 and 7.6, water injected for enhanced oil recovery was examined using the following boundary conditions: (i) The water pressure P_f applied to the left hand side of the model in an attempt to displace the wetting phase (oil) was 10^6Pa. (ii) The matrix porosity is 25%. (iii) The oil/water viscosity ratio is taken to be 1. (iv) The Brooks-Corey parameter is 2. The Brooks-Corey parameter designated by λ usually lies between 0.2 and 3.0 (Helmig, 1997). According to Helmig (1997) a very small λ-parameter values describes a single grain-size material whereas a very large value indicates a highly non-uniform material. The preliminary results show how each fracture-bounded block of the network becomes progressively depleted as the waterfront migrates across the model. However, the expulsion of oil is never 100% and the original oil saturation change with time in a non-linear fashion.

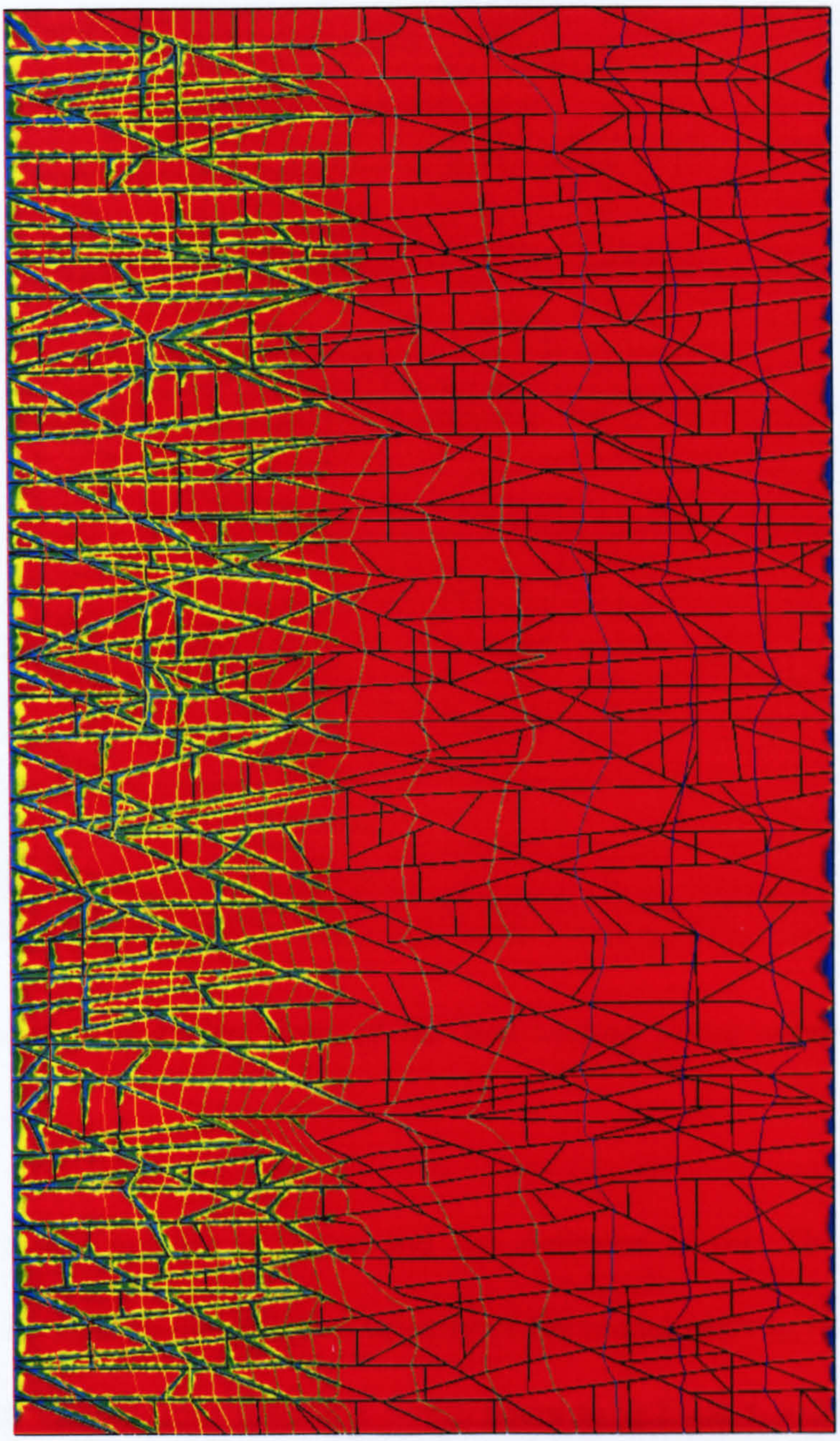


Figure 7.2 *After 5.2 hours the non-wetting front advances at approximately the same speed along most fractures. This may be caused by a uniform distribution of fractures within the window.* $dx/v_{max} = 0.46$

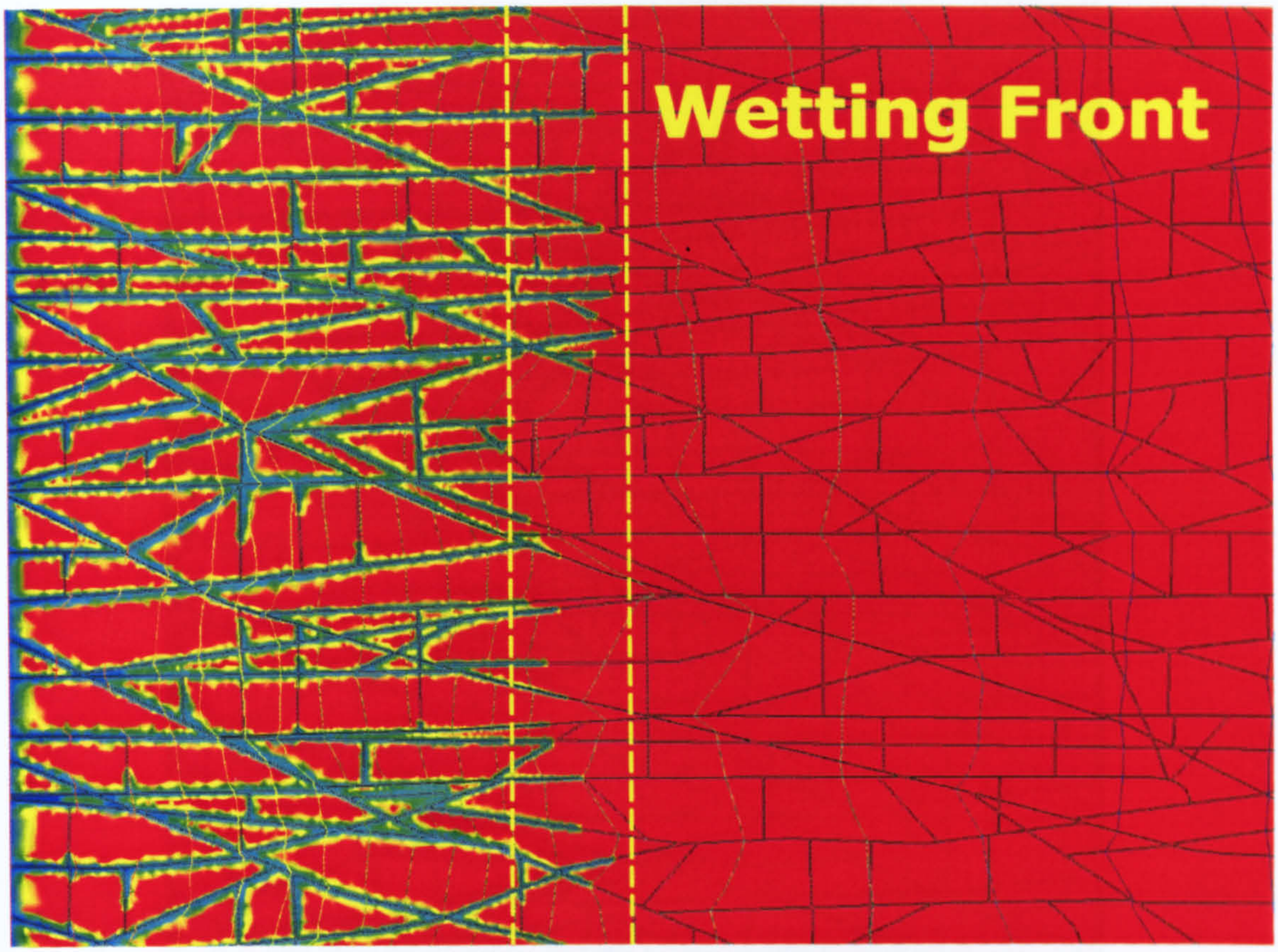


Figure 7.3 *shows advancing front of the non-wetting phase occurs along some fractures.*

In the models the invader is water and the defender is oil. The increment of displacement divided by the effective velocity of the model (dx/v_{max}) as noted above, decreases non-linearly from 0.46 at t = 5.2 hours to 0.23 at t = 21.6 hours. The significance of these numerical analyses is that they enable the production planning and reservoir management in natural analogues of fractured reservoirs such the Bristol Channel Basin or elsewhere in the World such as the carbonate reservoirs in the Zagros Fold-Thrust belt, to be planned more carefully and efficiently.

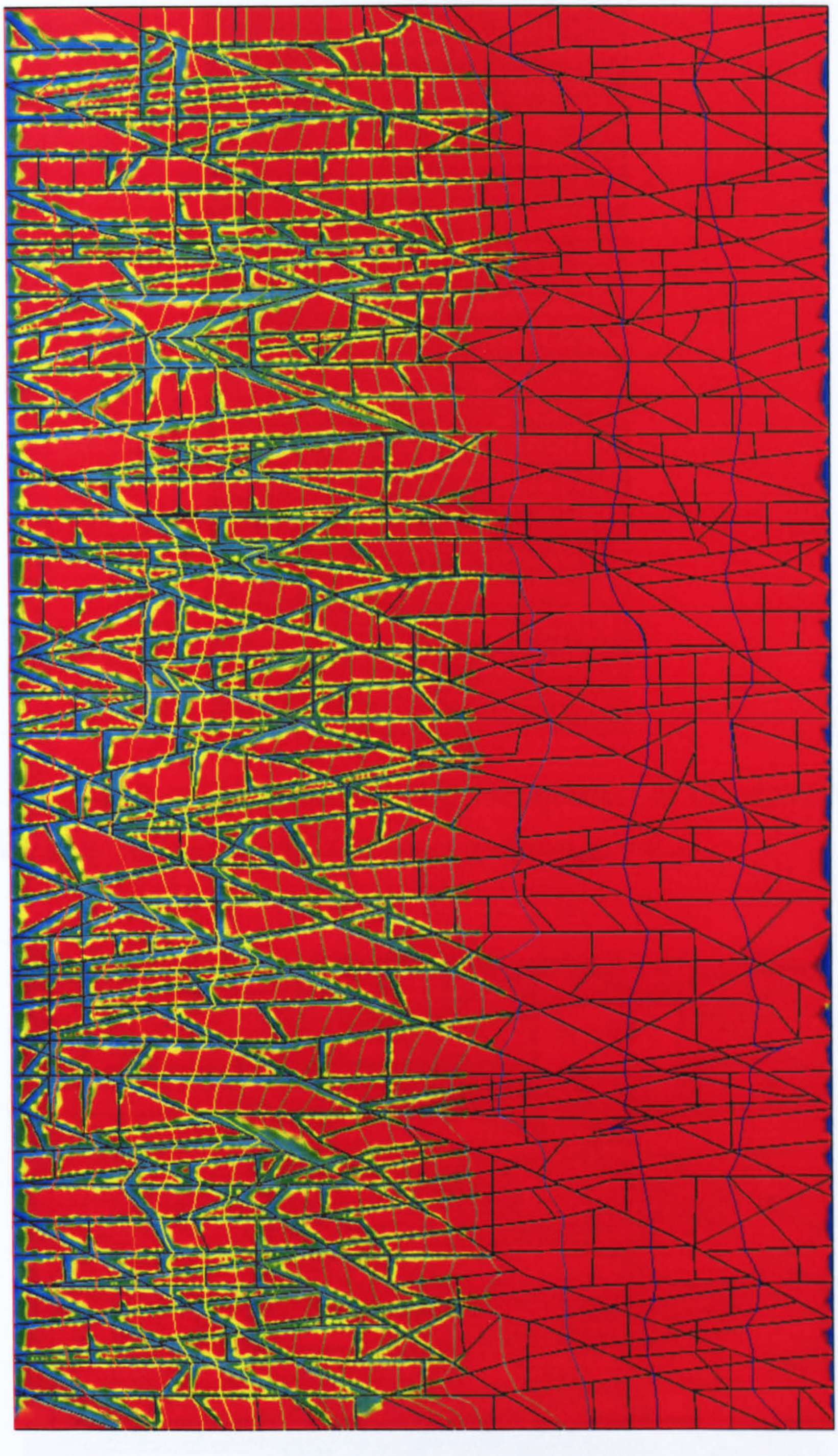


Figure 7.4 *Sweeping of oil from the matrix and from the fractures after 9.8 hours. Note the perturbation of pressure contours around the joints.* $dx/v_{max} = 0.36$

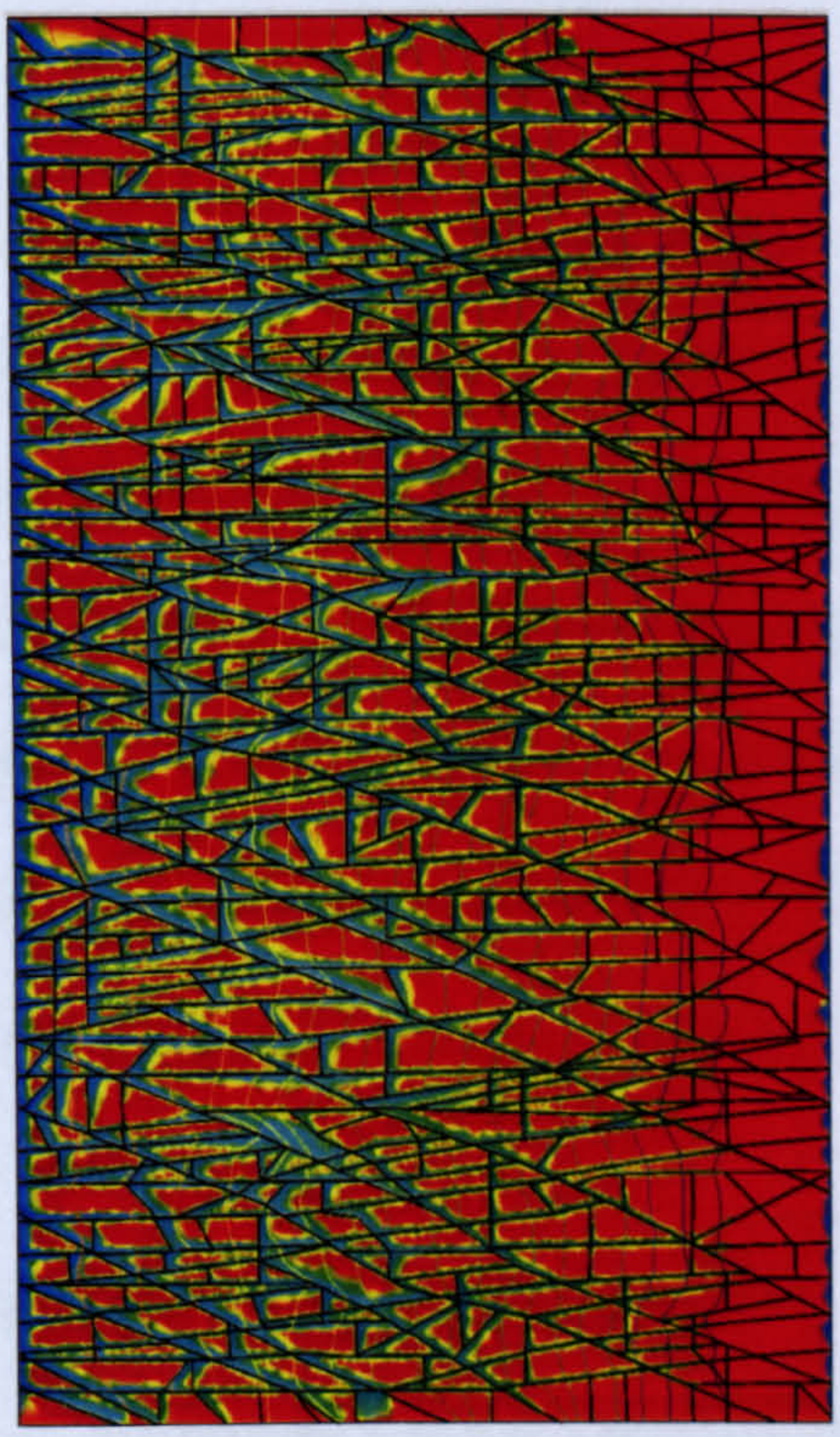


Figure 7.5 *Snapshot of the model showing the advance of the water front after running the numerical analysis for 21.6 hours and* $dx/v_{max} = 0.23$

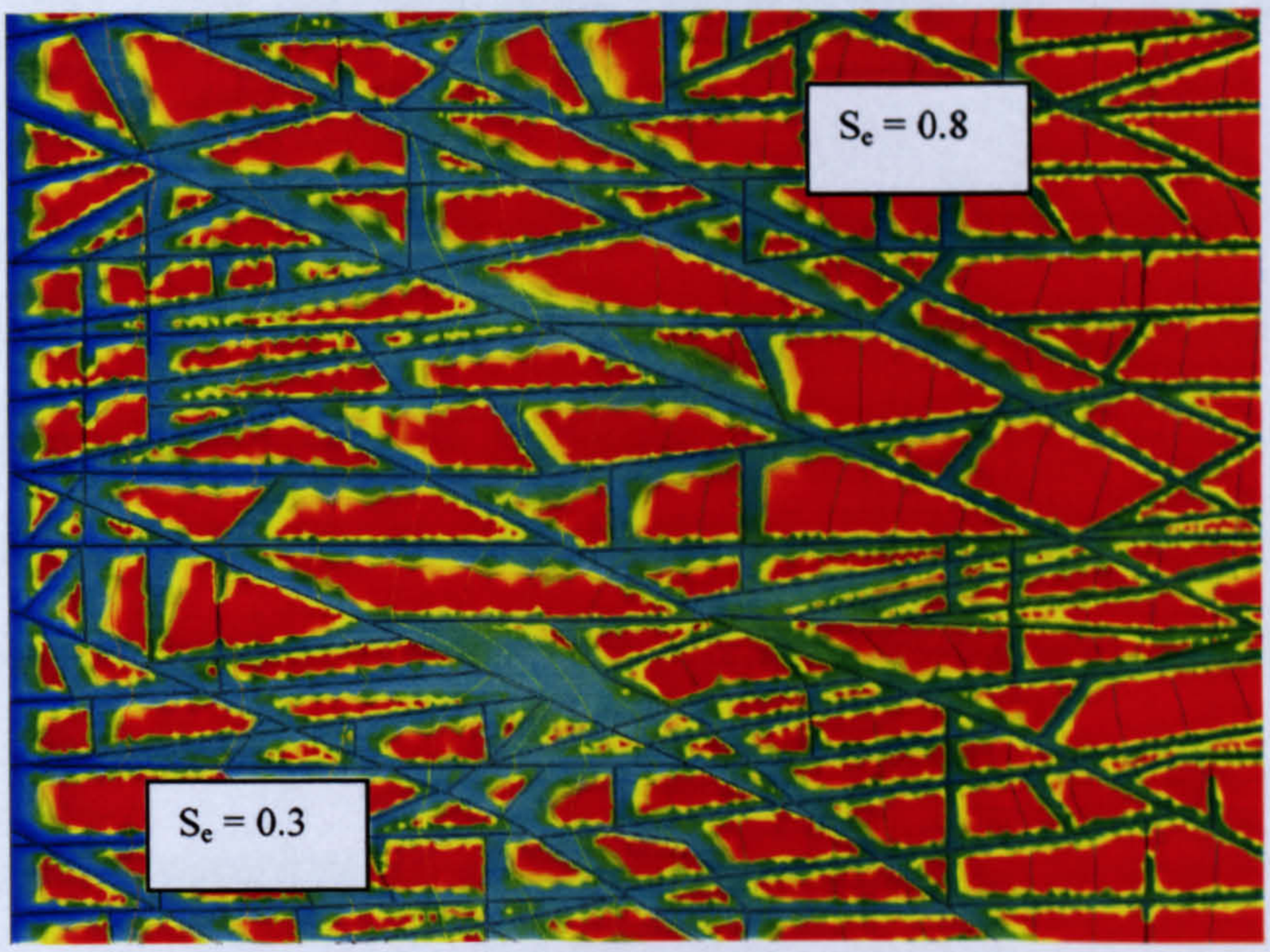


Figure 7.6 *Snapshot of the lower left section of the model simulations showing water breakthrough in the fractured system. The water sweeps some of the oil within the fracture-bound limestone blocks. Note the variation in oil saturation* (S_e) *where the water in the fractures bypasses the oil-saturated blocks and oil within matrix will be trapped.*

References

Al-Mahruqi, S. A. S. (2001). Fracture patterns and fracture propagation as a function of lithology. PhD thesis, Imperial College, University of London, UK. pp288.

Ameen, M. S., ed. (1995). Fractography: fracture topography as a tool in fracture mechanics and stress analysis. Geological Society Special Publication, **92**.

Anderson, E. M. (1951). The dynamics of faulting. Edinburgh, Oliver and Boyd.

Aydin, A., DeGraff, M. (1988). Evolution of polygonal fracture patterns in lava flows. Science **239**, 471-476.

Bahat, D. (1991). Tectonofractography. Springer-Verlag, Berlin.

Bahat, D. (1997). Mechanisms of dilatant *en-echelon* crack formation in jointed layered chalks. Journal of Structural Geology **19**, 1375-1392.

Bahat, D. (1999). Single-layer burial joints vs single-layer uplift joints in Eocene chalk from the Beer Sheva syncline in Israel. Journal of Structural Geology **21**, 293-303.

Bahat, D., Bankwitz, P., Bankwitz, E. (2001). Changes of crack velocities at the transition from the parent joint through *en-echelon* to secondary mirror plane. Journal of Structural Geology **23**, 1215-1221.

Bahat, D., Engelder, T. (1984). Surface morphology on cross-fold joints of the Appalachian Plateau, New York and Pennsylvania. Tectonophysics **104**, 299-313.

Bai, T., Maerten, L., Gross, M. R., Aydin, A. (2002). Orthogonal cross joints: do they imply a regional stress rotation? Journal of Structural Geology **24**, 77-88.

Bai, T., Pollard, D. D. (2000a). Fracture spacing in layered rocks: a new explanation based on stress transition. Journal of Structural Geology **22**, 43-57.

Bai, T., Pollard, D. D. (2000b). Closely spaced fractures in layered rocks: initiation mechanism and propagation kinematics. Journal of Structural Geology **22**, 1409-1425.

Bankwitz, P., Bankwitz, E. (1995). Fractographic features on joints of KTB drill cores (Bavaria, Germany). In: Ameen, M. S. (ed). Fractography: fracture topography as a tool in fracture mechanics and stress analysis. Geological Society Special Publication, **92**, 39-58.

Bankwitz, P., Bankwitz, E. (2001). Differences of mirror and fringe pattern of primary joints in granitic plutons. Mechanisms of jointing in the crust. Paul L. Hancock memorial meeting. 1-4th August 2001. Program and Abstracts, 27-30.

Belayneh, M., (in prep.). Palaeostress orientation inferred from surface morphology of joints from the southern margin of the Bristol Channel Basin. Special Volume of the Geological Society of London.

Biddle, K. T., Christe-Blick, N. (1985). Glossary - strike-slip deformation, basin formation and sedimentation. The Society of Economic Paleontologists and Mineralogists **3913**, 375-386.

Blés, J. L., Feuga, B. (1986). The fracture of rocks, North Oxford Academic, 127pp.

Bogdanov, A. (1947). The intensity of cleavage as related to the thickness of the bed (in Russian). Soviet Geology **16**.

Brooks, M., Al-Saadi, R. H. (1977). Seismic refraction studies of geological structures in the inner part of the Bristol Channel area, UK. Journal of the Geological Society **145**, 439-444.

Brooks, M., Trayner, P. M., Trimble, T. J. (1988). Mesozoic reactivation of Variscan thrusting in the Bristol Channel area, UK. Journal of the Geological Society **145**, 439-444.

Caputo, R., Hancock, P. L. (1999). Crack-jump mechanism and its implications for stress cyclicity during extension fracturing. Geodynamics **27**, 45-60.

Chadwick, R. A. (1993). Aspects of basin inversion in southern Britain. Journal of the Geological Society **150**, 311-322.

Chadwick, R. A. (1986). Extension tectonics in the Wessex Basin, southern England. Journal of the Geological Society **143**, 465-488.

Cobbold, P. R., Ferguson, C. C. (1979). Description and origin of spatial periodicity in tectonic structures: report on a Tectonic Studies Group conference held at Nottingham University. Journal of Structural Geology **1**, 93-97.

Cook, A. M., Myer, L. R., Cook, N. G. W., Doyle, F. M. (1990). The effects of tortuosity on flow through a natural fracture. Proceedings of the 31st U. S. Symposium on Rock Mechanics, Rotterdam, Balkema.

Cooke, M. L., Pollard, D. D. (1996). Fracture propagation paths under mixed mode loading within rectangular blocks of polymethyl methacrylate. Journal of Geophysical Research **101**, 3387-3400.

Corte, A., Higashi, A. (1960). Experimental research on desiccation cracks in soils. SIPRE (Snow, Ice and Permafrost Research Establishment). **1-71.**

Cosgrove, J. W. (1997). The influence of mechanical anisotropy on the behaviour of the lower crust. Tectonophysics **280, 1-14.**

Cosgrove, J. W., Ameen, M. S., eds. (2000). Forced folds and fractures. Geological Society specil publication, 169, 7-21.

Cosgrove, J. W. (2001). Hydraulic fracturing during the formation and deformation of a basin: a factor in the dewatering of low-permeability sediments. The American Association of Petroleum Geologists 85, 737-748.

Couples, G. D., Lewis, H., Tanner, P. W. G. (1998). Strain partitioning during flexural-slip folding. In: Coward, M. P., Daltaban, T. S., Johnson, H. (eds), Structural Geology in Reservoir Characterization. Geological Society Special Publication. 127, 149-165.

Cox, D. R., Lewis, P. A. W. (1966). The statistical analysis of series of events., Methuen, London.

Cruikshank, K. M., Zhao, G., Johnson, A. D. (1991). "Analysis of minor fractures associated with joints and faulted joints. Journal of Structural Geology 13, 865-886.

Darcy, H. (1856). Les fontaines publiques de la ville de Dijon. Paris, Victor Dalmont.

Dart, C. J., McClay, K, Hollings, P. N. (1995). 3D analysis of inverted extensional fault systems, southern Bristol Channel Basin, UK. In: Buchanan, J. G., Buchanan, P. G., (eds), Basin inversion. Geological Society Special Publication, 88, 393-413.

DeGraff, J. M., Aydin, A. (1987). Surface morphology of columnar joints and its significance to mechanics and direction of joint growth. Geological Society of America 99, 605-617.

Delaney, P. T., Pollard, D. D., Ziony, J. I., McKee, E. H. (1986). Field relations between dikes and joints: emplacement processes and paleostress analysis. Journal of Geophysical Research **91**, 4920-4938.

Dewey, J. F. (1982). Plate tectonics and the evolution of the British Isles." Journal of the Geological Society **139**, 371-412.

Doughty, P. S. (1968). Joint densities and their relation to lithology in the Great Scar Limestone. Proceedings of the Yorkshire Geological Society **36**, 497-512.

Dunham, K. C., Wilson, A. A. (1985). Geology of the northern Pennine orefield: volume 2 Stainmore to Craven. London, British Geological Survey.

Dyer, R. (1988). Using joint interactions to estimate paleostress ratios. Journal of Structural Geology **10**, 685-699.

Edwards, W., Trotter, F. M., Wray, D. A. (1954). The Pennines and adjacent areas. British Geological Survey.

Engelder, T. (1993). Stress regimes in the lithosphere. Princeton, Princeton University Press.

Engelder, T., Peacock, D. C. P. (2001). Joint development normal to regional compression during flexural-flow folding: the Lilstock buttress anticline, Somerset, England. Journal of Structural Geology **23**, 259-277.

Engelder, T., Savalli, L (2001). Some of the peculiar characteristics of joint surface morphology: question that they raise about the mechanical conditions for in-plane propagation joints. Mechanisms of jointing in the crust. Paul L. Hancock memorial meeting, 1-4th August 2001. Program and Abstracts, 31-35.

Erdogan, F., Biricikoglu, V. (1973). Two bonded half planes with a crack going through the interface. International Journal of Engineering Science **11**, 745-766.

Fetter, C. W. (2001). Applied hydrogeology. New Jersey, Prentice Hall, 598pp.

Freidman, M. (1972). Residual elastic strain in rocks. Tectonophysics **15**, 297-330.

Gabrielsen, R. H. (1990). Characteristics of joints and faults. In: Barton and Stephansson, (eds), Rock joints. Balkema, 11-17.

Geiger, S., Roberts, S., Matthai, S. K., Zoppou, C. (2001). Combining Finite Volume and Finite Element methods to simulate flow in geologic media. Submitted to the Australian and New Zealand Industrial and Applied Mathematics Journal.

Gibbs, A. D. (1984). "Structural evolution of extensional basin margins. Journal of the Geological Society **141**, 609-620.

Gillespie, P. A., Howard, C. B., Walsh, J. J., Watterson, J. (1993). "Measurement and Characterisation of spatial distributions of fractures." Tectonophysics **226**, 113-141.

Gillespie, P. A., Johnston, J. D., Loriga, M. A., McCaffrey, K. J. W., Walsh, J. J., Watterson, J. (1999). Influence of layering on vein systematics in line samples. In: McCaffrey, K. J. W., Lonergan, L., Wilkinson, J. J. (eds), Fractures, fluid flow and mineralization. Geological Society Special Publication. **155**, 35-56.

Gillespie, P. A., Walsh, J. J., Watterson, J., Bonson, C. G., Manzocchi, T. (2001). Scaling relationships of joint and vein arrays from the Burren, Co. Clare, Ireland. Journal of Structural Geology **23**, 183-201.

Griffith, A. A. (1924). The theory of rupture. Proceedings of the 1st Internantional Congress on Applied Mechanics.

Griffith, A. A. (1921). The phenomon of rupture and flow in solids. Phil. Transaction of Royal Society of London Series A **221**, 163-198.

Gross, M. R., Fischer, M. P., Engelder, T., Greenfield, R. J. (1995). Factors controlling joint spacing in interbedded sedimentary rocks: integrating numerical models with field observations from the Monterey Formation. In: M. S., Ameen, (ed), Fractography, fracture topography as a tool in fracture mechanics and stress analysis. Geological Society Special Publication, **92**, 215-233.

Gross, M. R. (1993). "The origin and spacing of cross joints: examples from the Monterey Formation, Santa Barbara Coastline, California. Journal of Structural Geology **15**, 737-751.

Guion, P. D., Gutteridge, P., Davies, S. J. (2000). Carboniferous sedimentation and volcanism on the Laurussian margin. In: Woodcock, N., Strachan, R., (eds), Geological history of Britain and Ireland. Blackwell Science, 227-270.

Hancock, P. L. (1994). From joints to paleostress. In: Roure, F. (ed), Peri-Tethyan platforms. Editions Technip, 145-158.

Hancock, P. L. (1985). Brittle microtectonics: principles and practice. Journal of Structural Geology **7**, 437-457.

Hancock, P. L. (1969). Jointing in the Jurassic limestones of the Cotswold Hills. Proceedings of the Geological Association **80**, 219-241.

Helgeson, D. E., Aydin, A. (1991). "Characterstics of joint propagation across layer interfaces in sedimentary rocks." Journal of Structural Geology **13**, 897-911.

Helmig, R. (1997). Multiphase flow and transport processes in the subsurface. Berlin, Springer.

Hesselbo, S. P. (2000). Late Triassic and Jurassic: dissentegrating Pangaea. In: Woodcock, N., Strachan, R., (eds), Geological history of Britain and Ireland. Blackwell Science, 314-338.

Hobbs, D. W. (1967). The formation of tension joints in sedimentary rocks: an explanation. Geological Magazine **104**, 550-556.

Hodgson, R. A. (1961). Regional study of jointing in Comb Ridge-Navajo mountain area, Arizona and Utah. Bulletin of the American Association of Petroleum Geologists **45**, 1-38.

Holliday, D. W. (1993). Mesozoic cover over northern England: interpretation of apatite fission track data. Journal of the Geological Society **150**, 657-660.

Holloway, S., Chadwick, R. A. (1986). The Sticklepath-Lustleigh fault zone: Tertiary sinistral reactivation of a Variscan dextral strike-slip fault. Journal of the Geological Society **143**: 447-452.

Huang, Q., Angelier, J. (1989). Fracture spacing and its relation to bed thickness. Geological Magazine **126**, 355-362.

Hubbert, M. K., Rubey, W. W. (1959). Role of fluid pressure in mechanics of overthrust faulting. Bulletin of the Geological Society of America **70**, 115-166.

Hudleston, P. J., Treagus, S. H., Lan, L. (1996). Flexural flow folding: does it occur in nature? Geology **24**, 203-206.

Hudson, J. A., Harrison, J. P. (1997). Engineering rock mechanics: an introduction to the principles. Amestrdam, Elsevier Science.

Hudson, J. A., Priest, S. D. (1979). Discontinuities and rock mass geometry. International Journal of Rock Mechanics, Mining Science and Geomechanics **16**, 339-362.

Hudson, J. A., Priest, S. D. (1983). Discontinuity frequency in rock masses. International Journal of Rock Mechanics, Mining Science and Geomechanics. **20**, 73-89.

Inglis, C. E. (1913). Stresses in a plate due to the presence of cracks and sharp corners. Transactions **55**, 219.

Jackson, J. A., King, G., Vita-Finzi, C. (1982). The neotectonics of the Aegean: an alternative view. Earth and Planetary Science Letters **61**, 303-318.

Ji, S., Saruwatari, K. (1998). A revised model for the relationship between joint spacing and layer thickness. Journal of Structural Geology **20**, 1495-1508.

Jolly, R. J. H., Sanderson, D. J. (1995). Variation in the form and distribution of dykes in the Mull swarm, Scotland. Journal of Structural Geology **17**, 1543-1557.

Kamerling, P. (1979). "The geology and the hydrocarbon habitat of the Bristol Channel Basin." Journal of Petroleum Geology **2**, 75-93.

Kidan, T. W., Cosgrove, J. W. (1996). The deformation of multilayers by layer-normal compression; an experimental investigation. Journal of Structural Geology **18**, 461-474.

Kidan, T. W. (1982). Deformation of multilayers compressed normal to the layering. PhD thesis, Imperial College, University of London, UK, 253pp.

Kirillova, I. V. (1949). Some problems of folding (in Russian).

Kirsch, G. (1898). Die Theorie der Elastizitat und die Bedurfnisse der Festigheitslehre. Zeitschrift des Vereines Deutscher Ingenieure **42**, 797.

Kulander, B. R., Dean, S. L. (1995). Observation on fractography with laboratory experiments for geologists. In: Ameen, M. S. (ed), Fractography: fracture

topography as a tool if fracture mechanics and stress analysis., Geological Society Special Publication, 92, 59-82.

Kulander, B. R., Barton, C. C., Dean, S. L. (1979). The application of fractography to core and outcrop fracture investigation. Springfield, US Department of Commerce Technical Report METC/SP-79/3.

La Pointe, P. R. (1988). A method to characterize fracture density and connectivity through fractal geometry. International Journal of Rock Mechanics, Mining Science and Geomechanics **Abstr. 25**: 421-429.

La Pointe, P. R., Hudson, J. A. (1985). Characterization and interpretation of rock mass joint patterns. Geological Society of America Special Paper **199, 1-25.**

Lachenbruch, A. H. (1961). Depth and spacing of tension cracks. Journal of Geophysical Research. **66**, 4273-4292.

Ladeira, F. L., Price, N. J. (1981). Relationship between fracture spacing and bed thickness. Journal of Structural Geology **3**, 179-183.

Lawn, B. (1975). Fracture of brittle solids. Cambridge, Cambridge University Press.

Le Pichon, X. (1981). Passive margins: a model of formation. Journal of Geophysical Research. **86**, 3708-3720.

Leslie, A. B., Spiro, B., Tucker, M. E. (1993). Geochemical and mineralogical variations in the upper Mercia Mudstone Group (Late Triassic), southwest Britain: correlation of outcrop sequences with borehole geophysical logs. Journal of the Geological Society, **150**, 67-75.

Lloyd, G. E., Ferguson, C. C., Reading, K. (1982). A stress-transfer model for the development of extension fracture boudinage. Journal of Structural Geology 4, 355-372.

Loosveld, R. J. H., Franssen, R. C. M. W. (1992). Extensional vs. shear fractures: implications for r eservoir c haracterisation. Society of Petroleum Engineers. 23-30.

Mandal, N., Debb, K. S., Khan, D. (1994). Evidence of a non-linear relationship between fracture spacing and layer thickness. Journal of Structural Geology 16, 1275-1281.

Masuda, T., Kuriyama, M. (1988). Successive mid-point fracturing during microboudinage: an estimate of the stress-strain relation during a natural deformation. Tectonophysics 147, 171-177.

Matthäi, S. K., Roberts, S. G. (1996). The influence of fault permeability on single-phase fluid flow near fault-sand intersections: results from steady-state high-resolution models of pressure driven flow. American Association of Petroleum Geologists Bulletin 80, 1763-1779.

Matthäi, S. K., Geiger, S., Roberts, S. G. (2001). Complex Systems Platform CSP3D.0 User's Guide.

Mauldon, M., Dunne, W. M., Rohrbaugh, M. B. (2001). Circular scanlines and circular windows: new tools for characterizing the geometry of fracture traces. Journal of Structural Geology 23, 247-258.

McKenzie, D. P. (1978). Some remarks on the development of sedimentary basins." Earth and Planetary Science Letters 40, 25-32.

McQuillan, H. (1973). Small-scale fracture density in Asmari Formation of southwest Iran and its relation to bed thickness and structural setting. The American Association of Petroleum Geologists Bulletin **57**, 2367-2385.

Moseley, F., Ahmed, S. M. (1967). Carboniferous joints in the north of England and their relation to earlier and later structures. Proceedings of the Yorkshire Geological Society **36**, 61-90.

Müller, G. (1998a). Starch column: analog model for basalt columns. Journal of Geophysical Research **103**, 15239-15253.

Müller, G. (1998b). Experimental simulation of basalt columns. Journal of Volcanology and Geothermal Research **86**, 93-96.

Müller, G. (2001). Experimental simulation of joint morphology. Journal of Structural Geology **23**, 45-49.

Müller, G., Dahm, T. (2000). Fracture morphology of tensile cracks and rupture velocity. Journal of Geophysical Research **105**, 723-738.

Narr, W. (1996). Estimating average fracture spacing in subsurface rock. American Association of Petroleum Geologists Bulletin **80**, 1565-1586.

Narr, W., Suppe, J. (1991). Joint spacing in sedimentary rocks. Journal of Structural Geology **13**, 1037-1048.

Nelson, R. A. (1985). Geologic analysis of naturally fractured reservoirs. Houston, Gulf Publishing Company.

Nemčok, M., Gayer, R. (1996). Modelling palaeostress magnitude and age in extensional basins: a case study from the Mesozoic Bristol Channel Basin, UK. Journal of Structural Geology **18**, 1301-1314.

Nemčok, M., Gayer, R., Miliorizos, M. (1995). Structural analysis of the inverted Bristol Channel Basin: implications for the geometry and timing of fracture porosity. In: Buchanan, J. G., Buchanan, P. G. (eds), Basin inversion. Geological Society Special Publication, 88, 355-392.

Nickelson, R. P., Hough, V. N. D. (1967). Jointing in the Appalachian Plateau of Pennsylvania. Geological Society of American Bulletin 78, 609-630.

Norris, D. K. (1966). The mesoscopic fabric of rock masses about some Canadian coal mines. Proceedings of International Congress on Rock Mechanics 1, 191-198.

Novikova, A. C. (1947). The intensity of cleavage as related to bed thickness (in Russian). Soviet Geology 16.

Odling, N. E. (1992). Permeability of natural and simulated fracture patterns. In: Larsen, R. M., Brekke, H., Larsen, B. T., Talleraas, E. (eds) Structural and tectonic modelling and its application to petroleum geology. NPF Special Publication, 1, 365-380.

Odling, N. E., Gillespie, P., Bourgine, B., Castaing, C., Chiles, J-P., Christensen, N. P., Fillion, E., Genter, A., Olsen, C., Thrane, L., Trice, R., Aarseth, E., Walsh, J. J., Watterson, J. (1999). Variations on fracture system geometry and their implications for fluid flow in fractured hydrocarbon reservoirs. Petroleum Geoscience 5, 373-384.

Olson, J., Pollard, D. D. (1988). Inferring stress states from detailed joint geometry. In: Cundall, P. A., Sterling, R. L., Starfield, A. M., (eds), Key questions in rock mechanics. Proceedings of U. S. Symposium on Rock Mechanics, Balkema, 159-167.

Olson, J., Pollard, D. D. (1989). Inferring paleostress from natural fracture patterns: a new method. Geology 17, 345-348.

Olson, L. E. (1993). Joint pattern development: effects of subcritical crack growth and mechanical crack interaction. Journal of Geophysical Research 98, 12251-12265.

Peacock, D. C. P. (in prep.). Scaling of fault transfer zones and interacting joints.

Peacock, D. C. P. (2001). The temporal relationship between joints and faults. Journal of Structural Geology 23, 329-341.

Peacock, D. C. P., Sanderson, D. J. (1995). Strike-slip relay ramps. Journal of Structural Geology 17, 1351-1360.

Peacock, D. C. P., Sanderson, D. J. (1992). Effects of layering and anisotropy on fault geometry. Journal of the Geological Society of London 149, 793-802.

Peacock, D. C. P., Sanderson, D. J. (1991). Displacement, segment linkage and relay ramps in normal fault zones. Journal of Structural Geology 13, 721-733.

Pollard, D. D., Aydin, A. (1988). Progress in understanding jointing in the last century. Geological Society of American Bulletin 100, 1181-1204.

Pollard, D. D., Segall, P. (1987). Theoretical displacements and stresses near fractures in rocks, with applications to faults, joints, veins, dikes and solution surfaces. In: Atkinson, B. K. (ed), Fracture mechanics in rock. Academic Press.

Pollard, D. D., Segall, P., Delaney, P. T. (1982). Formation and interpretation of dilatant echelon cracks. Geological Society of American Bulletin 93, 1291-1303.

Price, N. J. (1966). Fault and joint development in brittle and semi-brittle rocks. Pergamon Press, 171pp.

Price, N. J., Cosgrove, J. W. (1990). Analysis of geological structures. Cambridge University Press, 502pp.

Priest, S. D. (1993). Discontinuity analysis for rock engineering. Chapman and Hall.

Priest, S. D., Hudson, J. A. (1976). Discontinuity spacings in rock. International Journal of Rock Mechanics, Mining Science and Geomechanics.13, 135-148.

Ramberg, H. (1955). Natural and experimental boudinage and pinch-and-swell structures. Journal of Geology 63, 512-526.

Ramsay, J. G. (1967). Folding and fracturing of rocks. New York, McGraw-Hill.

Ramsay, J. G. (1980). The crack-seal mechanism of rock deformation. Nature 284, 135-139.

Ramsay, J. G., Huber, M. I. (1987). The techniques of modern structural geology volume 2: folds and fractures. London, Academic Press.

Rawnsley, K. D., Rives, T., Petit, J-P., Hencher, S. R., Lumsden, A. C. (1992). Joint development in perturbed stress fields near faults. Journal of Structural Geology 14, 939-951.

Rawnsley, K. D., Peacock, D. C. P., Rives, T., Petit, J-P. (1998). Joints in the Mesozoic sediments around the Bristol Channel Basin. Journal of Structural Geology 20, 1641-1661.

Renshaw, C. E. (1995). On the relationship between mechanical and hydraulic apertures in rough-walled fractures. Journal of Geophysical Research 100, 24629-24636.

Renshaw, C. E., Pollard, D. D. (1995). An experimentally verified criterion for propagation across unbounded frictional interface in brittle, linear elastic

materials. International Journal of Rock Mechanics, Mining Science and Geomechanics. 32, 237-249.

Renshaw, C. E., Dadakis, J. S. (2000). Measuring fracture apertures: a comparison of methods. Geophysical Research Letters 27, 289-292.

Renshaw, C. E., Pollard, D. D. (1994). Are large differential stresses required for straight fracture propagation paths? Journal of Structural Geology 16, 817-822.

Richard, P. (1990). Champs de Failles Audessus d'un Decrochement de Socle: Modelisation Experimentale, PhD thesis, University of Rennes, France.

Rives, T., Petit, J-P. (1990). Experimental study of jointing during cylindrical and non-cylindrical folding. In: Rossmanith, H. P. (ed), Mechanics of jointed and faulted rock. Balkema, Rotterdam, 205-211.

Rives, T., Razak, M., Petit, J-P., Rawnsley, K. D. (1992). Joint spacing: analogue and numerical simulations. Journal of Structural Geology 14, 925-937.

Rives, T., Rawnsley, K. D., Petit, J-P. (1994). Analogue simulation of natural orthogonal joint set formation in brittle varnish. Journal of Structural Geology 16, 419-429.

Roberts, J. C. (1995). Fracture surface markings in Liassic limestone at Lavernock Point, South Wales. In: Ameen, M. S. (ed), Fractography: fracture topography as a tool in fracture mechanics and stress analysis. Geological Society Special Publication, 92, 175-186.

Roberts, S. G., Matthäi, S. K. (1996). High-resolution potential flow methods in oil exploration. Canberra, Centre for Mathematics and its Applications, School of Mathematical Sciences, Australian National University: 9p.

Royden, L., Schlater, J. G., Von-Herzen, R. P. (1980). Continental margin subsidence and heat flow: important parameters in formation of petroleum hydrocarbons. Bulletin of the American Association of Petroleum Geologists **64**, 173-187.

Rubey, W. W., Hubbert, M. K. (1959). Role of fluid pressure in the mechanics of overthrust faulting. Bulletin of the Geological Society of America **70**, 167-206.

Sanderson, D. J., Zhang, X. (1999). Critical stress localization of flow associated with deformation of well-fractured rock masses, with implications for mineral deposits. In: McCaffrey, K. J. W., Lonergan, L., Wilkinson, J. J. (eds), Fractures, fluid flow and mineralisation. Geological Society Special Publication, **155**, 69-81.

Secor, D. T. (1965). Role of fluid pressure in jointing. American Journal of Science **263**, 633-646.

Segall, P., Pollard, D. D. (1983). Joint formation in granitic rock of the Sierra Nevada. Geological Society of America Bulletin **94**, 563-575.

Sen, Z., Kazi, A. (1984). Discontinuity spacing and RQD estimates from finite length scanlines. International Journal of Rock Mechanics, Mining Science and Geomechanics. **21**, 203-212.

Sibson, R. H. (1985). A note on fault reactivation. Journal of Structural Geology **7**, 751-754.

Soper, J. (2001). Tectonic Studies Group Eield Excursion Guide. Tectonic Studies Group Annual Meeting. 3-6th January 2001. Leeds.

Stearns, D. W. (1967). Certain aspects of fracture in naturally deformed rocks. In: Riecker, R. E., (ed) Rock Mechanics Seminar: US Air Force Cambridge Research Laboratories. 97-118.

Taylor, W. L., Pollard, D. D., Aydin, A. (1999). Fluid flow in discrete joint sets: field observations and numerical simulation. Journal of Geophysical Research **104**, 28983-29006.

Terzaghi, K. V. (1923). Die Berechnung der Durchlassigkeitziffer des Tones aus dem Verlauf der hydrodynamischen Spannungerscheinungen. Sber. Akad. Wiss.

Terzaghi, R. D. (1965). "Sources of errors in joint surveys." Geotechnique **5**, 287-304.

Teufel, L. W., Clark, J. A. (1984). Hydraulic fracture propagation in layered rock: experimental studies of fracture containment. Society of Petroleum Engineers Journal. 19-32.

Thomas, A. L., Pollard, D. D. (1993). The geometry of echelon fractures in rock: implications from laboratory and numerical experiments. Journal of Structural Geology **15**, 323-334.

Twiss, R. J., Moores, E. M. (1992). Structural geology. New York, W. H. Freeman and Company.

USNCRM. (1996). Rock fractures and fluid flow: contemporary understanding and applications/committee on fracture characterization and fluid flow, U. S. National Committee for Rock Mechanics. Washington, National Academic Press.

Van Djik, J. P., Bello, M., Toscano, C., Bersani, A., Nardon, S. (2000). Tectonic model and three-dimensional fracture network analysis of Monte Alpi (southern Apennines). Tectonophysics **324**, 203-237.

Wang, H. (1992). Prediction of in-situ and blastpile block size distributions of rock masses with special reference to coastal requirements. PhD thesis, Queen Marry and Westfield College, University of London, UK.

Wang, H., Latham, J-P, Matheson, G. D. (1992). Design of fragmentation blasting in surface rock excavation. Proceedings of the ISRM Symposium: EUROCK '92.

Wang, H., Latham, J-P, Poole, A. B. (1991). In-situ block size distribution for quarrying. Quarterly Journal of Engineering Geology **24**, 91-99.

Warr, L. N. (2000). The Variscan Orogeny: the welding of Pangaea. In: Woodcock, N., Strachan, R. (eds), Geological history of Britain and Ireland. Blackwell and Science, 271-296.

Waters, R. A., Lawrence, D. J. D, Ivimey-Cook, H. C., Mitchel, M., Worthington, G. White, D. E., Lewis, M. A. (1987). Geology of South Wales coalfield, part II, the country around Cardiff. British Geological Survey.

Weinberger, R. (1999). "Initiation and growth of cracks during desiccation of stratified muddy sediments." Journal of Structural Geology **21**, 379-386.

Weinberger, R. (2001). Joint nucleation in layered rocks with non-uniform distribution cavities. Journal of Structural Geology **23**, 1241-1254.

Whitherspoon, P. A., Wang, J. S. Y., Iwai, K., Gale, J. E. (1980). "Validity of cubic law for fluid flow in a deformable rock fracture. Water Resources Research **16**, 1016.

Whittaker, A., Green, G. W (1983). Geology of the Country around Weston-Super-Mare, Mem. Geological Survey of Great Britain Sheet 279 and parts of 263 and 295. HMSO.

Whittaker, B. N., Singh, R. N., Sun, G. (1992). Rock fracture mechanics principles, design and applications. Development in Geotechnical Engineering, **71**, Elsevier, 570pp.

Whittaker, R. (1972). The Watchet fault - post-Liassic transcurrent reverse fault. Bulletin of the Geological Survey **41**, 75-80.

Wilson, A. (1997). Geology of the Yorkshire Dales National Park. Smith and Sons.

Woodcock, N., Strachan, R. (2000). Regional geological history: why and how? In: Woodcock, N., Strachan, R. (eds), Geological history of Britain and Ireland. Cambridge, Blackwell Science, 3-18.

Woodworth, J. (1896). On the fracture system of joints, with remarks on certain great fractures. Boston Society of Natural History Proceedings. **27**, 163-184.

Wu, H., Pollard, D. D. (1993). Effects of strain rate on a set of fractures. International Journal of Rock Mechanics, Mining Science and Geomechanics. **30**, 869-872.

Wu, H., Pollard, D. D. (1995). An experimental study of the relationship between joint spacing and layer thickness. Journal of Structural Geology **17**, 887-905.

Xiao, H., Suppe, J. (1992). Origin of rollover. The American Association of Petroleum Geologists Bulletin **76**, 509-529.

Younes, A. I., Engelder, E. (1999). Fringe cracks: key structures for the interpretation of the progressive Alleghanian deformation of the Appalachian Plateau. Geological Society of American Bulletin **111**, 219-239.

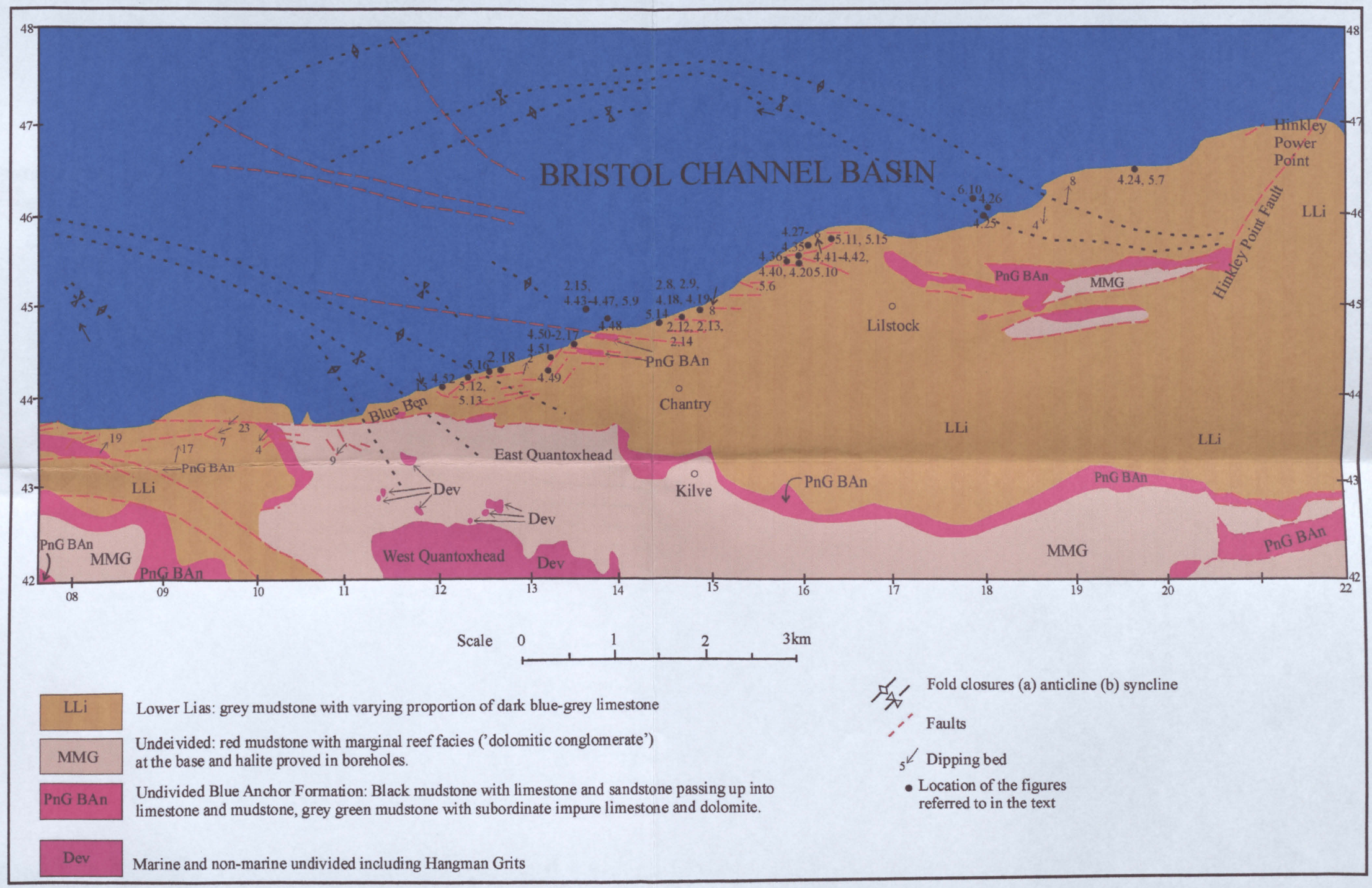


***Figure 2.7** Geology and major structures in Lilstock-Kilve areas on the southern margin of the Bristol Channel Basin (modified from 1: 50,000 scale geological maps of England and Wales sheets 263, 279 and part of 295). Note the locations of the figures referred to in the text.*